Citrus maxima (Burm.) Merr. fruit juice and peel extract mediated synthesis of silver nanoparticles (AgNPs) and their applications as antimicrobial agents and plant growth enhancers

Indukalpa Das[1], Abhijit Sonowal[1], Bhaskarjyoti Gogoi[1], Bidisha Sharma[2], Kaustuvmani Patowary[3], Debajit Borah[1]*

[1]*Dept. of Biotechnology, The Assam Royal Global University, Guwahati-781035, India*
[2]*Dept. of Botany, Cotton University, Guwahati- 781001, India*
[3]*Institute of Advanced Study in Science and Technology, Guwahati;*
Present address:
University of Science and Technology, Meghalaya-793101

**Corresponding author: dborah89@gmail.com*

Abstract

Green synthesis of metal nanoparticles (NP) has emerged as a recent trend in green chemistry. However, their potential in the field of agriculture is yet underexplored. In this study, silver nanoparticles (Ag NPs) were synthesized by using the fruit juice and peel extract of *Citrus maxima* (Burm.) Merr.as a reducing and capping agent. The nano-primed seeds of *Zea mays*, *Glycine max*, and *Cicerarietinum*showed enhanced germination rate up to 90% as compared to the respective control (30-60%) and also enhanced plant growth. The HRTEM images of fruit-mediated Ag NPs showed well-dispersed particles. The XRD diffraction pattern confirmed the crystalline nature of Ag NPs with fcc lattice points of 101, 111, 200, 220, and 311 with an average crystal size of 19.1275±1.73 nm. On the other hand, the peel-mediated Ag NPs exhibited a size range of 10-20 nm with average crystal size of 19.09±1.71 nm. The FTIR spectra confirmed the presence of $\upsilon_{C=C-H}$, υ_{CH2}, $\upsilon_{C=O}$ (stretch), $\upsilon_{C=C}$ (stretch), υ_{C-H} (bend), υ_{C-O} (bend) in the Ag NPs synthesized by the fruit and peel extract. The Ag NPs also showed potential antimicrobial effects against both Gram-positive (*Staphylococcus aureus*) and negative bacteria (*Klebsiella pneumonia*).

Keywords: Antimicrobial activity; green synthesis; plant growth; seed germination; silver nanoparticles.

1. Introduction

In the last few years, researchers are attracted to the exploration of scopes of nano-materials in agricultural sectors to meet the increasing global food crisis through the enhancement of crop yield and quality (Soliman *et al*., 2020). The metallic nanoparticles have also shown their potential to reduce nutrient loss and improvement of plant augmentation (Dimkpa *et al*. 2017). In order to maintain economic stability and increase the commercial production of agricultural resources, the foremost concern should be on expeditious and consistent germination of seeds (Acharya *et al*., 2020). Hence, it is very crucial to undergo treatment of the seeds before sowing under certain controlled conditions to improve the quality and production of some commercially vital crops. The process of treating the seeds before sowing

is called seed priming, which has exhibited the potential to solve diverse agricultural problems and thereby benefit the farmers as such it reduces the time of germination, enhances growth, increases the activity of various enzymes, and acts as biofertilizer (Acharya *et al*., 2020).

The basic reason behind the rapid growth of nano-primed seeds may be enhancing the activity of some vital enzymes such as amylases, proteases, and lipases that are involved in the germination process of seeds (Acharya *et al*., 2020). Moreover, nano-primed seeds are also mitigated from stress, and as a result of which the rate of emergence of seedlings increases (Acharya *et al*., 2020). As a result of which, nano-priming is thought to have the potential to enhance the rate of seedling emergence, yield, and quality of the crop (Mahakham *et al*., 2017; Acharya *et al*., 2020).

Both physical and chemical methods of synthesis have their disadvantages as they are capital intensive, require high energy, produce unstable nanoparticles with reduced target activity, and release toxic substances (Kiran *et al*., 2011). Therefore, researchers are trying to substitute the physical and chemical methods with an eco-friendly, non-toxic, highly stable, and cost-effective mode of nanoparticle synthesis. As a result, research on the biological mode of synthesis is gaining importance in recent times (El-Chaghaby *et al*., 2022).

A series of literature has revealed that plant extracts, fungi, algae, cyanobacteria, bacteria, yeasts, actinomycetes, viruses, standalone biomolecules such as proteins, amino acids, enzymes, glucose, biosurfactants, *etc*. (Jayabalan *et al*., 2019; Selvan *et al*., 2018; Tomer *et al.*, 2019; Sowbarnika *et al*., 2018; Nabila & Kannabiran, 2018) have the potential to act as a reducing and stabilizing agent that is essential to synthesize nanoparticles of varied shapes and sizes (Jayabalan *et al*., 2019). Plant extracts of *Tagetes* sp., *Rosa* sp., *Achillea wilhelmsii*, *Piper sarmentosum*, *Mentha piperita*, *Ipomoea digitata*, *Pelargonium graveolens*, *Azadirachta indica*, *Cymbopogon flexuosus*, *Tamarindus indica*, *Aloe vera*, *Coriandrum sativum*, *Cinnamomum camphora*, *Capsicum annuum*, and *Calendula officinalis etc*. have been extensively studied for their potential to reduce various metal salts into the respective metal nanoparticles with excellent antimicrobial activity against several phytopathogens (Hernández-Díaz *et al*., 2021).

Citrus maxima (Burm.) Merr. is a tropical fruiting plant, widely available throughout the sub-Himalayan foothill regions which includes the North-eastern region of India (Ani *et al*., 2020). It is widely known as a rich source of various phytochemicals such as flavonoids, alkaloids, saponins, phenolics, *etc*., and is known to have the potential to act as a reducing agent for the synthesis of metal nanoparticles (Ali *et al*., 2020). Considering the above facts, the potential of *Citrus maxima* (Burm.) Merr. fruit juice and peel extract were explored for the synthesis of Ag NPs as they are known to have unique abilities to fight against pathogenic microbesand some recent studies also reveals their potential in the agricultural sector (Almutairi & Alharbi, 2015).

These bio-inspired Ag NPs were used for enhancing the germination and growth of soybean, maize, and chickpea seed. Further, the antimicrobial effect of Ag NPs was also explored. It may be noted that maize (*Zea mays*), soybean (*Glycine max*), and chickpea (*Cicerarietinum*) are among the most commonly grown and economically important food crops in the world (Afzal, 2021). According to the Food and Agriculture Organization (FAO), 44% of the total soybean produced in the world is used for the production of oil (Radočaj *et*

al., 2020). Chickpea is a major leguminous crop that is extensively distributed in various parts of the globe (Afzal, 2021). However, the production of economically important food crops needs to be increased in response to the rising demands of the growing world population and to cope with the challenges faced by drastic climatic changes (Pereira, 2017). Therefore, there is a need to increase the yield of such economically important crops by using some recent smart nano-based agricultural methods.

2. Materials and Methods

2.1 Extraction of juice and peel extract from *C. grandis* (Burm.) Merr. Fruit

The juice was extracted from the fruit and filtered through a strainer to remove the pulp followed by filtration using Whatman no.1 filter paper to remove the unwanted residues. The peel extract was prepared by boiling small pieces of peel (10 g) in distilled water (100 mL) for 20 min followed by filtration through Whatman no.1 filter paper. These were then kept at 4°C for further use.

2.2 Synthesis of Silver nanoparticles

For the synthesis of Ag NPs, 10 mM AgNO3 solution was prepared in distilled water. A hundred milliliters for such solution was reduced to Ag NPs by adding 40 mL of *C. grandis* (Burm.) Merr.fruit juice and 0.3% soluble starch (w/v) with constant stirring followed by autoclaving at 121°C, 15 lbs pressure for 15 min. Similarly, the second set was reduced by 40 mL of peel extract. After this, the solution was brought back to room temperature followed by centrifugation at 10,000 rpm for 10min. The precipitate was dried and kept for further use.

2.3 Characterization of Ag NPs

The synthesized Ag NPs were extensively characterized by UV-Vis spectrophotometry (Shimadzu UV-1800 spectrophotometer, Tokyo, Japan), X-ray Diffraction (Bruker D8 Advance Powder XRD, Karlsruhe, Germany), FTIR (Bruker Corporation, Germany) and HRTEM (JEOL-JEM2100F, Japan).

2.4 Evaluation of antimicrobial activity

The antimicrobial potential of Ag NPs was evaluated against both Gram-positive (*Staphylococcus aureus*) and Gram-negative (*Klebsiella pneumonia*) bacterial pathogens by the standard agar well diffusion method (Khalid *et al*., 2021). Overnight microbial cultures ($O.D._{600}$=1.0) were inoculated by spread plating method on Mullar-Hinton agar and 50 µL of 1 mg/mL Ag NPs suspension in distilled water was loaded in the respective well taking suitable controls for the experiment. The cultured plates were then incubated for 24 h at 37°C. The diameter of the clear zone around the respective well (zone of inhibition) confirming the antimicrobial activity of Ag NPs was recorded.

2.5 Seed germination assay

Thoroughly cleaned seeds of maize, chickpea, soybean, and wheat were soaked in distilled water (control), 0.3% (w/v) soluble starch, Ag NPs suspension of 10 mg/L and 20 mg/L for

24 h followed by placing the primed seeds on top of the humid cotton bed and allowed to germinate. Weight of the seeds after nano-priming was recorded at the end of day-1 and day-3. The total length of the germinated seeds was also recorded after 5 days of treatment.

2.6 Statistical analysis

The experiments were performed in triplicate for the reliability of the data and the results were expressed in mean ± S.D. Student's *t*-test was performed by using GraphPad™ online statistical tool to analyse the significance of the results.

3. Results

Change in colour of the solution from pale yellow to dark brown confirms the formation Ag NPs after reducing by both fruit juice and peel extract. The UV-Vis spectrophotometric analysis also showed a broad peak at a wavelength of 418 nm also confirms the formation of Ag NPs in both solutions. TEM image shows well-dispersed Ag NPs synthesized by reducing with *C. grandis* (Burm.) Merr.fruit juice (figure 1a and b). The average particle size distribution shows the majority of NPs within the range of ~50-60 nm.

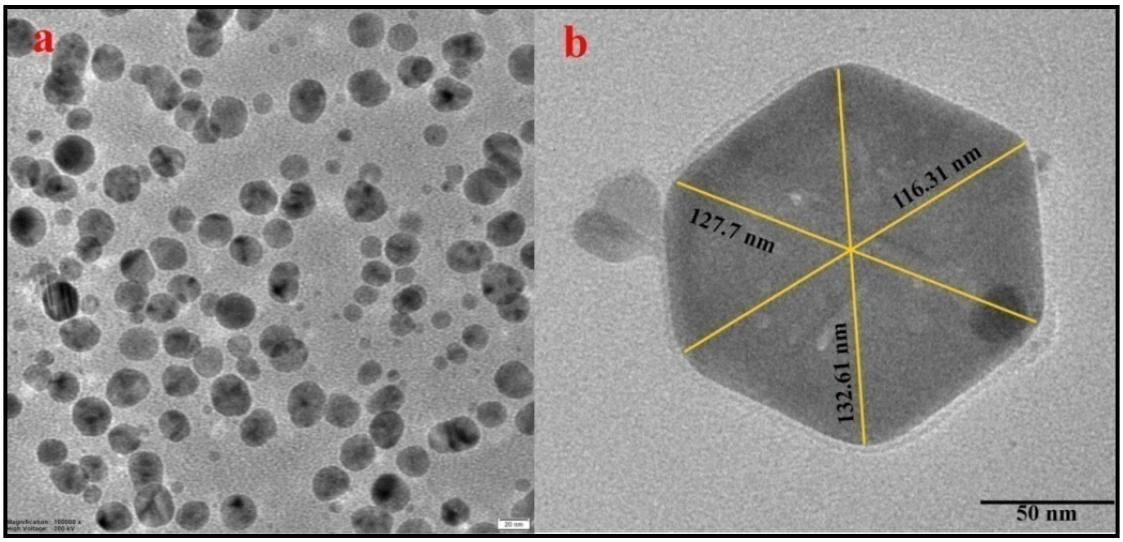

Fig. 1. TEM images of *C. grandis* (Burm.) Merr. fruit juice mediated Ag NPs at (a) low magnification, and (b) high magnification.

The X-ray diffraction analysis of the synthesized Ag NPs has shown distinct peaks attributed 2θ values of approximately 32.5°, 38°, 44.5°, 64.5°, and 77°corresponds to fcc lattice points of 101, 111, 200, 220, and 311 respectively confirm the crystalline structure of the NPs with an average crystal size of 19.1275±1.73 nm based on Scherrer's equation (figure 2). These were further confirmed by selected area diffraction (SAED) analysis using HR-TEM (figure 2). On the other hand, more dispersed Ag NPs with a size range of 10-20 nm were formed when synthesized by using the peel extract of *C. grandis* (Burm.) Merr. as a reducing agent (figure 3). However, the XRD analysis of peel-mediated Ag NPs showed similar lattice fringes when compared to juice-mediated Ag NPs with average crystal size of 19.09±1.71 nm (figure 3).

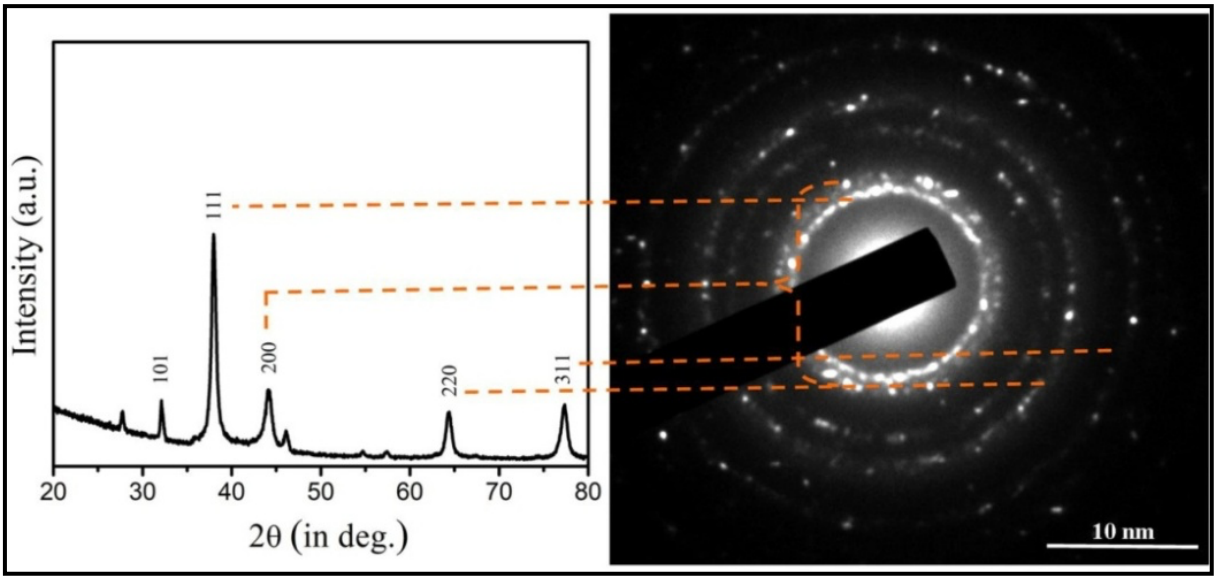

Fig. 2. XRD (left) and SAED (right) images of *C. grandis* (Burm.) Merr. fruit juice mediated Ag NPs.

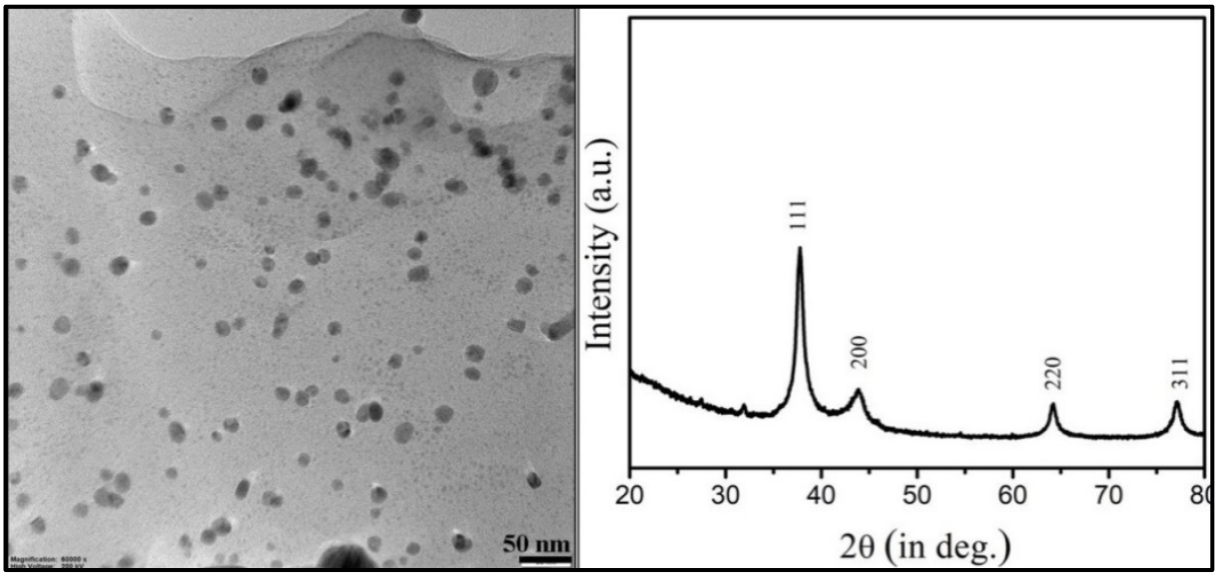

Fig 3. TEM (left) and XRD (right) images of *C. grandis* (Burm.) Merr. peel-mediated Ag NPs.

The FTIR spectra of juice mediated Ag NPs showed distinct peaks in the regions 2922.90, 2851.85 1633.63, 1384.24, 1237.25, 1151.95, 1076.74, 1026.17, 668.89 and 573.77 cm^{-1} (figure 4a). Similarly, peel-mediated Ag NPs showed peaks in the regions 2923.41, 2852.94, 1743.05, 1641.93, 1541.09, 1383.91, 1238.75, 1153.38, 1078.16, 1025.21, 669.19, 576.03, 523.18 cm^{-1} (figure 4b). Both the FTIR spectra have shown the presence of $\upsilon_{C=C-H}$, υ_{CH2}, $\upsilon_{C=O}$ (stretch), $\upsilon_{C=C}$ (stretch), υ_{C-H} (bend), υ_{C-O} (bend) in the synthesized NPs.

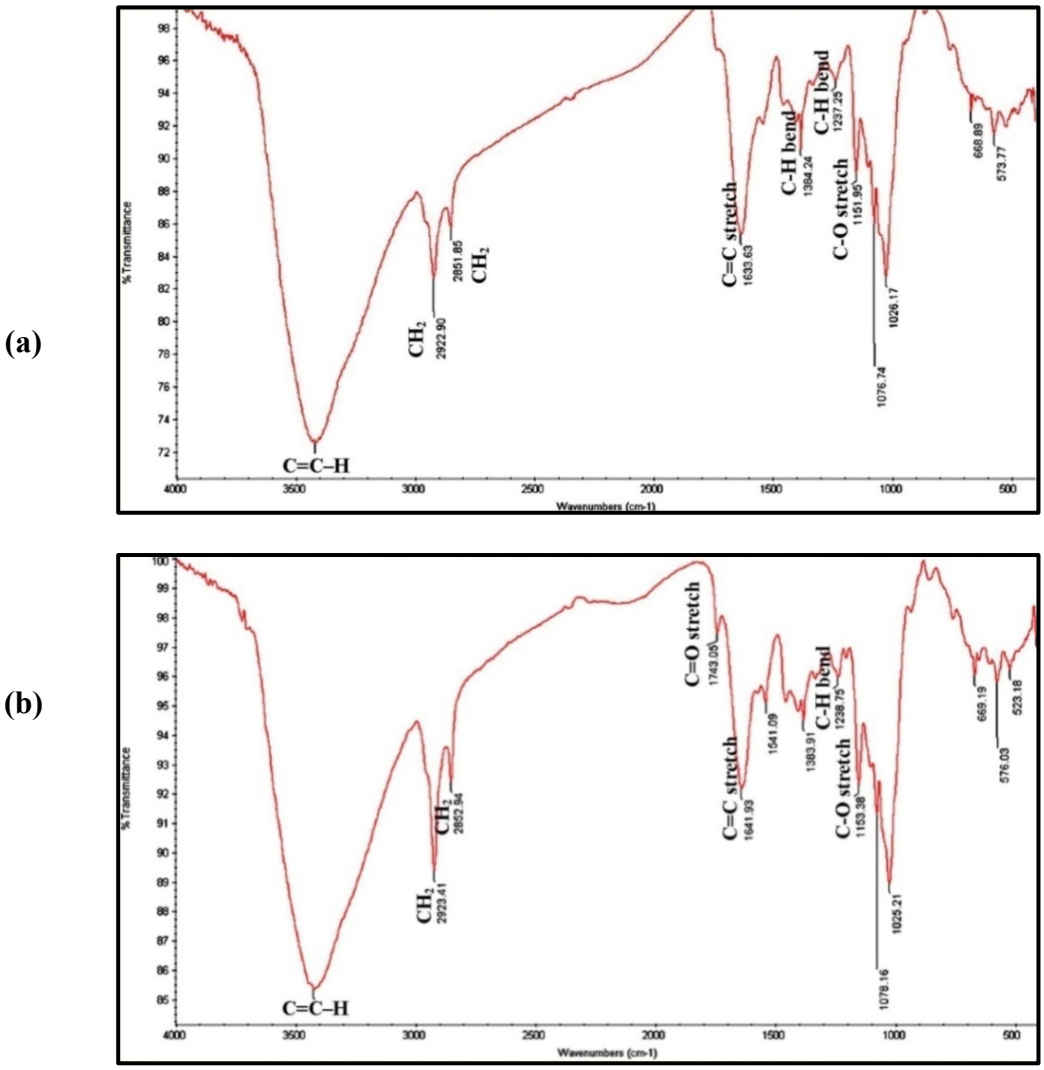

Fig. 4. FTIR spectra of juice mediated (a) and peel extract mediated (b) Ag NPs.

The Ag NPs synthesized by both the methods were tested against Gram-positive (*S. aureus*) and negative bacteria (*K. pneumonia*) by the agar well diffusion method. Both of these NPs exerted similar antimicrobial potential against both the microbes ($p = 0.86$) (table 1 and figure 5).

Table 1. Diameter of zone of inhibition of Ag NPs against test microbes

Test microbes	**Zone of inhibition (in mm) exerted by**			
	Juice mediated Ag NPs	**Peel-mediated Ag NPs**	**Juice (control)**	**Peel extract (control)**
S. aureus	19.7±2	20±2	-	-
K. pneumonia	15±2	15±2	-	-

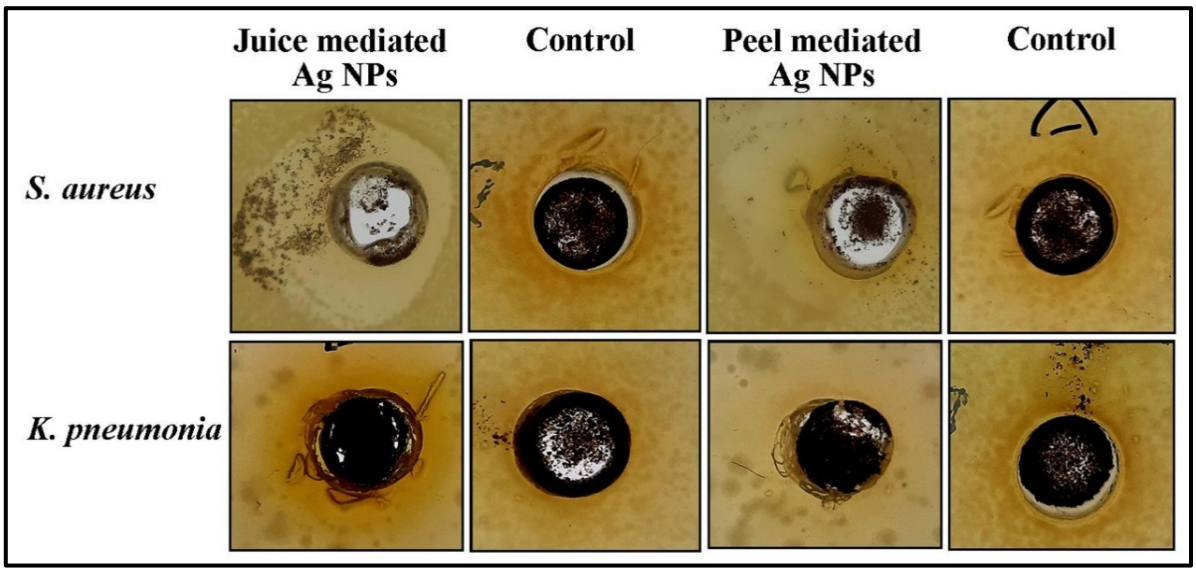

Fig. 5. Zone of inhibition exerted by Ag NPs against bacterial pathogens

Seeds of maize, chickpea, soybean, and wheat were primed with Ag NPs synthesized by both methods. Figure 6 depicts the significant increase in the average weight of each type of seed after the 3rdday of treatment as compared to the end of the 1stday. When chickpeas were primed with starch solution and distilled water considered as positive and negative controls respectively, the germination percentage was 52% and 60% respectively. The rate of germination was increased to 88% and 92% when chickpea was primed with 10 mg/L of fruit-mediated Ag NPs and 10 mg/L of peel-mediated Ag NPs respectively but comparatively decreased to 76% and 84% when primed with 20 mg/L Ag NPs. Similarly, the germination rate of maize seeds increased to 80% and 88% as compared to control (44%) when primed with 10 mg/L of fruit and peel-mediated Ag NPs respectively but decreased to 64% and 76% at a concentration of 20 mg/L (fig 7). The rate of germination of soybean seeds was increased up to 84% and 88% respectively when primedwith10mg/L concentration of fruit and peel-mediated Ag NPs as compared to control (32-52%) but decreased to 72% and 80% when primed with 20 mg/L of Ag NPs (figure 7).

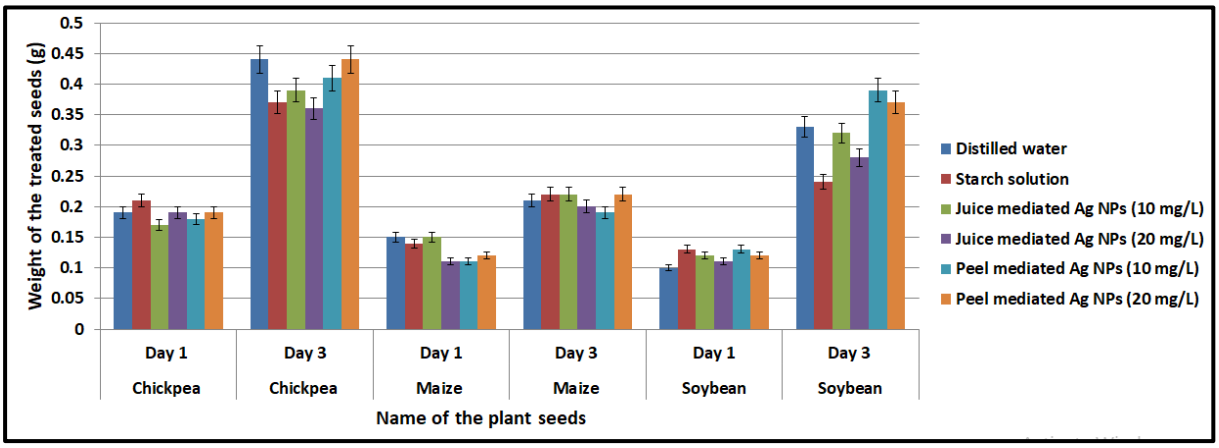

Fig. 6. Weight of the nano-primed seeds on day-1 and 3 before germination

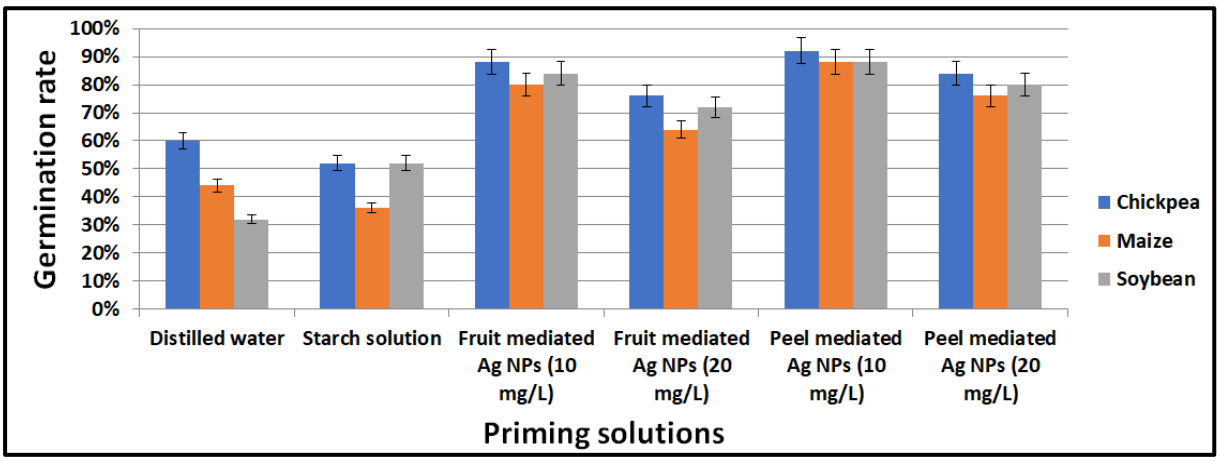

Fig. 7. Germination rates data of at least 25 seeds of each type

Priming of seeds with different solutions also showed variations in the total length of the sprouted seedlings (figure 8). When distilled water and the starch solution were used as priming solution, the total length of chickpea seedlings was 4.5 and 4.8 cm respectively. The length increased to 8.73 and 8.18 cm when primed with 10mg/L of fruit and peel-mediated Ag NPs respectively. On the contrary, the seedling length decreased to 4.43±0.5 and 4.6±0.5 cm when primed with 20mg/L of fruit-mediated and peel-mediated Ag NPs respectively (figure 8). Similarly, the total length of maize seedlings was increased to 2.68 and 4.33 cm but decreased length to 1.78±0.2 and 1.1±0.2 cm respectively when treated with 20 mg/L of fruit and peel-mediated Ag NPs individually. Length of nano-primed soybean seedlings was increased to 3.68±0.4 and 3.88±0.4 when primed with 10 mg/L and decreased to 1.98±0.2 cm and 0.88±0.2 cm when primed with 20 mg/L of fruit and peel-mediated Ag NPs respectively. Fig 9 represents the germinated seed of chickpea, maize, and soybean under the influence of AgNPs.

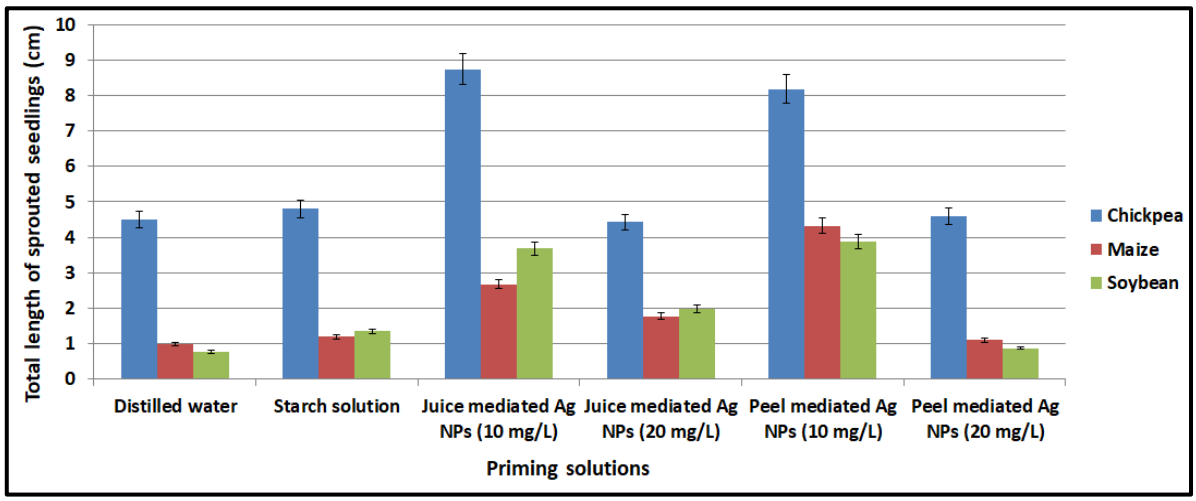

Fig. 8. Total length of the sprouted seedlings after nano-priming.

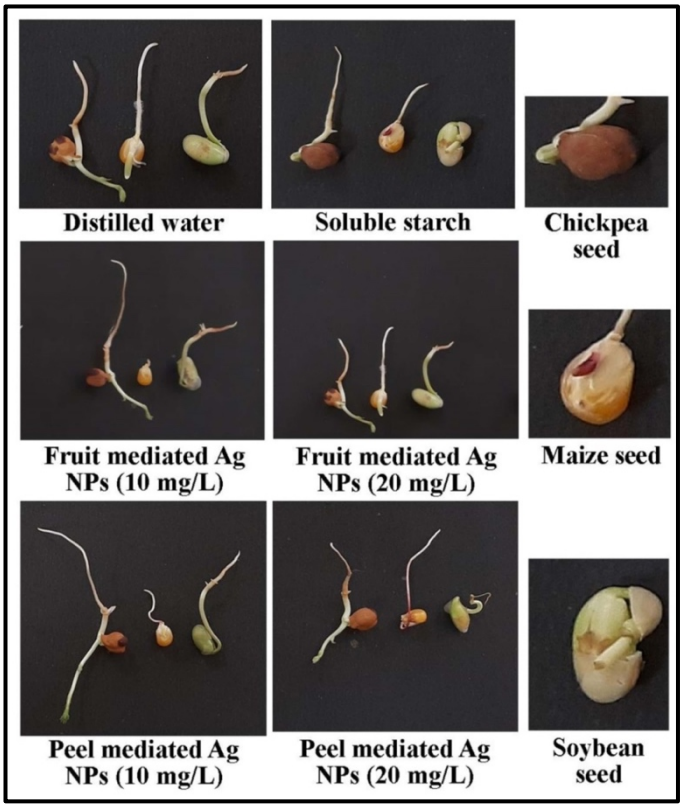

Fig. 9. Effect of fruit and peel-mediated AgNPs on seed germination.

Discussions

Green synthesis of Ag NPs using plant, microbial, or animal extracts has now become a new trend in green chemistry as such mode of synthesis is cost-effective and eco-friendly (Salem & Fouda *et al*., 2021). *Citrus maxima* is a citrus fruiting plant that is rich in citric acid and phytochemicals such as flavonoids, alkaloids, saponins, and phenolics *etc*. and is widely distributed throughout the Himalayan foothill regions which include the North-eastern region of India and south-east Asian countries (Khan *et al*., 2018). These phytochemicals are known to have a reducing potential to reduce metallic salt into metal nanoparticles and also act as capping agent to provide better stability (Muthuvel *et al*., 2020). The Ag NPs synthesized by both methods have shown similar potential in terms of their antimicrobial activity against both Gram-positive and negative test bacterial strains which is following the finding of some concurrent studies (Jomehzadeh *et al*., 2021; Shirzadi-Ahodashti *et al*., 2021; Jyoti *et al*., 2021).Both the Ag NPs exhibited lesser antimicrobial activity against *K. pneumonia* as compared to *S. aureus*. This may be due to the fact that the overall thickness of *K. pneumonia* cell wall is more as compared to that of *S. aureus*. *Klebsiella pneumonia* has an overall cell wall thickness of approximately 160 nm as compared to the cell wall thickness of *S. aureus* which is approximately 20 to 40 nm only (Giesbrecht *et al*., 1998; Amako *et al*., 1988).

Applications of NPs in the field of agriculture as plant growth promoter has been least explored as compared to their pharmaceutical and medical applications (Ahmed *et al*., 2021; Rai-Kalal & Jajoo, 2021; Rafique *et al*., 2022; Ali *et al*., 2021). And also the interactions of metal nanomaterials with plants have still not been fully elucidated. The process of germination starts with the uptake of water by dry seeds through a process called imbibitions

(Mahakham *et al.*, 2017). But the impact of Ag NPs on plant growth largely varies based on several factors *viz*., species of the plant, size of NPs, the concentration of the NPs, experimental conditions which include temperature, duration of treatment, and method of exposure *etc* (Almutairi & Alharbi, 2015).

One of the vital enzymes involved in the degradation of starch during germination of cereal seeds and the subsequent emergence of the seedling is α-amylase (Mahakham *et al*., 2017). In addition, metal NPs such as Ag NPs are also known to exhibit catalytic activities hence it may also be assumed that NPs may catalyze the activity of α-amylase by entering through the cellular pores of the seeds by taking the advantage of their nanoscale size and thus enhancing the seed germination rate (Mahakham *et al*., 2017). It is also hypothesized by many researchers that the treatment of seeds with metal NPs may also boost the expression levels of aquaporin genes which are responsible for the absorption of water in germinating seeds (Mahakham *et al*., 2017). Literature also shows that nano-priming of seeds may fuel up the superoxide dismutase and other reactive oxygen species scavenging enzyme activity in seeds (Govindaraj *et al*., 2017). Nano-priming of chickpea, maize, and soybean seeds with 10 and 20 mg/L concentration Ag NPs synthesized by both methods showed variations in terms of seed germination rate and plant growth. However, the germination rate and also the plant growth was found maximum at 10 mg/L concentration of Ag NPs and found to decline at 20 mg/L concentration. On the other hand, the control study showed no significant results when treated with starch solution and distilled water as alone. It can be seen that the average growth rate of nano-primed seeds was faster compared to the control (Zhou *et al*., 2022). This thereby shows that enhancement of seed germination depends on the dosage of Ag NPs used for seed priming (Almutairi &Alharbi, 2015).The size of Ag NPs also plays an important role in Ag NP effectiveness (Syu *et al*., 2014). A number of studies have indicated that the cellular uptake of nanoparticles is dependent on their size, charge and surface properties (Syu *et al*., 2014).It was observed that peel-mediated Ag NPs showed somewhat better activities in terms of seed germination rate which may be due to the fact that peel-mediated NPs were much smaller as compared to that of fruit-mediated counterparts which helps is defying the cellular barrier. Furthermore, this study opens up the possibility for the application of Ag NPs to be used in enhancing crop productivity in the future.

Conclusion

We reported a rapid green method for the synthesis of Ag NPs using fruit juice and peel extract of *Citrus maxima* (Burm.) Merr. The XRD analysis confirmed the crystalline nature of the NPs. The Ag NPs exhibited similar antimicrobial activities against both the bacterial samples irrespective of their mode of synthesis. Recently, it has been explored that, in order to fulfil the high agricultural and food demands, there is a need to improve the quality of seeds. Therefore, it is important to treat the seeds and enhance the rate of seed germination by using recently developed technologies. Among the other methods of seed quality improvement, the most commonly used method is the priming of seeds. The nano-primed test seeds of the selected economically important crop species under this study showed enhanced seed germination rate and plant growth as compared to the respective controls which advocate their future application in the field of agricultural science. However, the mode of

action of Ag NPs on seed germination and plant growth *i.e*., the interaction with plants in detail is to be studied.

Conflict of interest

The authors declare that there is no conflict of interest.

References

Acharya P, Jayaprakasha, GK, Crosby KM, Jifon JL, & Patil BS (2020): Nanoparticle-mediated seed priming improves germination, growth, yield, and quality of watermelons (*Citrullus lanatus*) at multi-locations in Texas. *Sci Rep*, 10(1): 1-16.

Afzal MK (2021): Economic value of chickpea production consumption and world trade. *AFS-Adv Food Sci*, 211.

Ahmed B, Syed A, Rizvi A, Shahid M, Bahkali AH, Khan MS, & Musarrat J (2021): Impact of metal-oxide nanoparticles on growth, physiology and yield of tomato (*Solanum lycopersicum* L.) modulated by *Azotobacter salinestris* strain ASM. *Environ Pollut*, 269: 116218.

Ali KA, Yao R, Wu W, Masum MMI, Luo J, Wang Y, Zhang Y, An Q , Sun G,& Li B (2020): Biosynthesis of silver nanoparticle from pomelo (*Citrus maxima*) and their antibacterial activity against *Acidovorax oryzae* RS-2. *Mater Res Express*, *7*(1): 015097.

Ali S, Mehmood A, & Khan N (2021): Uptake, translocation, and consequences of nanomaterials on plant growth and stress adaptation. *J Nanomater.* DOI: https://doi.org/10.1155/2021/6677616

Almutairi ZM, & Alharbi A (2015): Effect of silver nanoparticles on seed germination of crop plants. *J Adv Agric*, 4(1): 283-288.

Amako K, Meno Y, & Takade A (1988): Fine structures of the capsules of *Klebsiella pneumoniae* and *Escherichia coli* K1. *J Bacteriol*, 170(10): 4960-4962.

Ani PN, & Ochu KE (2020): Anti-diabetic, anti-hyperlipidemic and hepatoprotective potential of shaddock (*Citrus maxima*) peel extract. *ActaSci Pol Technol Aliment*, 19(3): 271-278.

Dimkpa CO, White JC, Elmer WH, & Gardea-Torresdey J (2017): Nanoparticle and ionic Zn promote nutrient loading of sorghum grain under low NPK fertilization. *J Agric Food Chem*, 65(39): 8552-8559.

El-Chaghaby G, Rashad S, &Eid H (2022): Antioxidant, antimicrobial and anti-cancer properties of silver nanoparticles biosynthesized using artichoke waste extract. *Kuwait J Sci*DOI: https://doi.org/10.48129/kjs.10012

Giesbrecht P, Kersten T, Maidhof H, & Wecke J (1998): Staphylococcal cell wall: morphogenesis and fatal variations in the presence of penicillin. *Microbio and Mol Bio Rev*, 62(4): 1371-1414.

Govindaraj M, Masilamani P, Albert VA, & Bhaskaran M (2017): Role of antioxidant in seed quality-A review. *Agric Rev*, 38(3): 180-190.

Hernández-Díaz JA, Garza-García JJ, Zamudio-Ojeda A, León-Morales JM, López-Velázquez JC, & García-Morales S (2021): Plant-mediated synthesis of nanoparticles and their antimicrobial activity against phytopathogens. *J Sci Food Agric*, 101(4): 1270-1287.

Jayabalan J, Mani G, Krishnan N, Pernabas J, Devadoss JM, & Jang HT (2019): Green biogenic synthesis of zinc oxide nanoparticles using *Pseudomonas putida* culture and its In vitro antibacterial and anti-biofilm activity. *Biocatal Agric Biotechnol*, 21: 101327.

Jomehzadeh N, Koolivand Z, Dahdouh E, Akbari A, Zahedi A, & Chamkouri N (2021): Investigating *in-vitro* antimicrobial activity, biosynthesis, and characterization of silver nanoparticles, zinc oxide nanoparticles, and silver-zinc oxide nanocomposites using *Pistacia atlantica* resin. *Mater Today Commun*, 27: 102457.

Jyoti K, Arora D, Fekete G, Lendvai L, Dogossy G, & Singh T (2021): Antibacterial and anti-inflammatory activities of Cassia fistula fungal broth-capped silver nanoparticles. *Mater Technol*, 36(14): 883-893.

Khalid A, Ahmad P, Alharthi AI, Muhammad S, Khandaker MU, Faruque MRI, Din IU, Alotaibi MA, & Khan A (2021): Synergistic effects of Cu-doped ZnO nanoantibiotic against Gram-positive bacterial strains. *Plos one*, 16(5): e0251082.

Khan NH, Qian CJ, & Perveen N (2018): Phytochemical screening, antimicrobial and antioxidant activity determination of citrus maxima peel. *Pharm Pharmacol Int J*, 6(4): 279-285.

Kiran GS, Selvin J, Manilal A, & Sujith S (2011): Biosurfactants as green stabilizers for the biological synthesis of nanoparticles. *Crit Rev Biotechnol*, 31(4): 354-364.

Mahakham W, Sarmah AK, Maensiri S, & Theerakulpisut P (2017): Nanopriming technology for enhancing germination and starch metabolism of aged rice seeds using phytosynthesized silver nanoparticles. *Sci Rep*, 7(1): 1-21.

Muthuvel A, Jothibas M, Manoharan C, & Jayakumar SJ (2020): Synthesis of CeO2-NPs by chemical and biological methods and their photocatalytic, antibacterial and in vitro antioxidant activity. *Res Chem Intermed*, 46(5): 2705-2729.

Nabila MI, & Kannabiran K (2018): Biosynthesis, characterization and antibacterial activity of copper oxide nanoparticles (CuO NPs) from actinomycetes. *Biocatal Agricul Biotechnol*, 15: 56-62.

Pereira LS (2017): Water, agriculture and food: challenges and issues. *Water Resour Manag*, 31(10): 2985-2999.

Radočaj D, Jurišić M, Gašparović M, & Plaščak I (2020): Optimal soybean (*Glycine max* L.) land suitability using GIS-based multicriteria analysis and Sentinel-2 multitemporal images. *Remote Sens*, 12(9): 1463.

Rafique M, Tahir R, Gillani SSA, Tahir MB, Shakil M, Iqbal T, & Abdellahi MO (2022): Plant-mediated green synthesis of zinc oxide nanoparticles from *Syzygium cumini* for seed germination and wastewater purification. *Int J Environ Anal Chem*, 102(1): 23-38.

Rai-Kalal P, & Jajoo A (2021): Priming with zinc oxide nanoparticles improve germination and photosynthetic performance in wheat. *Plant Physiol Biochem*, 160: 341-351.

Salem SS, & Fouda A (2021): Green synthesis of metallic nanoparticles and their prospective biotechnological applications: an overview. *Biol Trace Elem Res*, 199(1): 344-370.

Selvan DA, Mahendiran D, Kumar RS, & Rahiman AK (2018): Garlic, green tea and turmeric extracts-mediated green synthesis of silver nanoparticles: Phytochemical, antioxidant and in vitro cytotoxicity studies. *J Photochem and Photobiol B, Biol*, 180: 243-252.

Shirzadi-Ahodashti M, Mizwari ZM, Hashemi Z, Rajabalipour S, Ghoreishi SM, Mortazavi-Derazkola S, & Ebrahimzadeh MA (2021): Discovery of high antibacterial and catalytic activities of biosynthesized silver nanoparticles using *C. fruticosus* (CF-Ag NPs) against multi-drug resistant clinical strains and hazardous pollutants. *Environ Technol & Innov*, 23: 101607.

Soliman M, Qari SH, Abu-Elsaoud A, El-Esawi M, Alhaithloul H, & Elkelish A (2020): Rapid green synthesis of silver nanoparticles from blue gum augment growth and performance of maize, fenugreek, and onion by modulating plants cellular antioxidant machinery and genes expression. *Acta Physiol Plant*, 42(9): 1-16.

Sowbarnika R, Anhuradha S, &Preetha B (2018): Enhanced antimicrobial effect of yeast mediated silver nanoparticles synthesized from baker's yeast. *Int J Nanosci Nanotechnol*, 14(1): 33-42.

Syu YY, Hung JH, Chen JC, & Chuang HW (2014): Impacts of size and shape of silver nanoparticles on Arabidopsis plant growth and gene expression. *Plant Physiol and Biochem*, 83: 57-64.

Tomer AK, Rahi T, Neelam DK, & Dadheech PK (2019): Cyanobacterial extract-mediated synthesis of silver nanoparticles and their application in ammonia sensing. *Int Microbiol*, 22(1): 49-58.

Zhou X, Jia X, Zhang Z, Chen K, Wang L, Chen H, Yang Z, Li C, & Zhao L (2022): Ag NPs seed priming accelerated germination speed and altered nutritional profile of Chinese cabbage. *Sci Total Environ*, 808: 151896.

Submitted: 03/04/2022
Revised: 15/06/2022
Accepted: 19/06/2022
DOI: 10.48129/kjs.19889

Kuwait J.Sci., Vol.50, No.(1B),January.2023,pp(14-26)

Cloning and molecular modeling of free fatty acid receptor GPCR 43 with dietary flavonoids as novel ligands

*Arooma Ihtsham[1], Rida Hayat[1], Fariha Khan[1,] **

[1]Dept. of Biosciences, Functional Genomics Laboratory,
COMSATS University Islamabad,
45550 Islamabad, Pakistan

**Corresponding author: farihakhan2031@gmail.com*

Abstract

G-protein couple receptors (GPCRs) are considered as the largest membrane protein family involved in the regulation of body homeostasis in health and disease. GPCR43 or FFA2 (free fatty acid receptor 2) is implicated in diabetes. Efficient methods are needed to express GPCRs for structural studies. Small GPCR fragments consisting of 1-2 transmembrane domains are routinely used in NMR studies. In the present study, the first three transmembrane segments 1-3 of GPCR43 (GPCR43-TM1-3) were cloned and expressed with expression enhancement tag, AT4 and His tag at the C and N termini respectively into pET23b(+). The plant compounds, flavonoids, with reported beneficial effects in diabetes mellitus type 2 (T2DM) were subjected to docking against the target, GPCR43. Our results revealed that the ligands exhibited better binding interaction to GPCR43. Diosmin was predicted to be the best ligand with good binding affinity than the other ligands. Hence, we concluded that Diosmin may become a potential drug candidate for T2DM via GPCR43 pathway. However, studies are warranted to confirm its efficacy in animal models of T2DM.

Keywords: Cloning; Diabetes type 2; Diosmin; Flavonoids; G-protein coupled receptors (GPCRs).

1. Introduction

G-protein coupled receptors (GPCRs) generally regarded as seven transmembrane (7TM) receptors, is the largest family of the cell surface receptors with more than eight hundred GPCRs identified in the human genome. GPCRs based on sequence homology and functional similarities have been categorized into A-F classes (Fredriksson *et al.,* 2003). Class A rhodopsin like receptors is the largest family with about 80 % GPCRs belonging to this class, contains many hormones, neurotransmitters and light receptors representing interesting targets for drug discovery (Hu *et al.,* 2017). GPCR43 or FFAR2, a member of class A GPCR, is highly expressed in the adipose tissue, gastrointestinal tract (GI), and immune cells (Kimura *et al.,* 2014). GPCR43 reportedly functions in regulation of glucose metabolism by acting at the beta cells and adipose tissues as well as mitigates inflammation (Villa *et al.,* 2017; Xu *et al.,* 2019). Several reports show that the activation of GPCR43 by short chain fatty acids regulates insulin secretion besides protective effects on β

cells in response to insulin resistance highlighting the significance of GPCR43 in T2DM and obesity (Tolhurst *et al.,* 2012; Forbes *et al.,* 2015; Priyadarshini *et al.,* 2015; McNelis *et al.,* 2015; Tang *et al.,* 2015). For instance, Gαq/11-biased agonists of GPCR43 with 100-fold increased potency were identified causing an increase in glucose stimulated insulin secretion (GSIS) and growth of beta cells (Villa *et al.,* 2017). Recently, exercise induced improvement in T2DM was hindered by inhibiting GPCR43 in mice models (Yang *et al.,* 2020).

Diabetes mellitus is considered among the oldest diseases of humankind. A chronic condition with estimated 415 million people worldwide and the number of patients is increasing steadily. More than 90% of diabetics have T2DM which results in microvascular and macrovascular complications resulting in physical deficiencies as well as financial losses with an enormous burden on health systems (Olokoba *et al.,* 2012; Chatterjee *et al.*, 2017). No treatments have been found yet. The disease is managed by adopting healthy lifestyle, exercise and medications including antihyperglycaemic, antihypertensive agents, cholesterol lowering and antiplatelet drugs (Stumvoll *et al.,* 2005).

Plants contain a tremendous wealth of bioactive compounds with healthcare benefits including terpenes, flavonoids, alkaloids and sterols (Kris-Etherton *et al.,* 2002). Many flavonoids such as disosmin, rutin, catechin and EGCG have been reported for therapeutic effects in diabetes (Nagao *et al.,* 2009; Gothai *et al.,* 2016; Eng *et al.,* 2018; Gosslau *et al.,* 2019; Unuofin & Lebelo*,* 2020).

It is estimated that almost one third of the drugs act via GPCRs. Structure elucidation is a key area for the drug designing which requires cloning and expression studies. The current work is focused on GPCR43 as a T2DM target. First three transmembrane segments of GPCR43 (GPCR43-TM1-3) were cloned and expressed in *E. coli.* GPCR43 was modeled and docking studies were carried out by using plant-based compounds with therapeutic effects on T2DM.

2. Materials and Methods

2.1 Plasmid construction and cloning

The expression vector pET23(b+) containing strong T7 promoter with IPTG inducible expression system was used to design expression construct. The bacterial codon-optimized gene for full-length GPCR43 was synthesized and cloned into pET-23b(+) vector (Gene Universal, USA) with N-terminal expression enhancement AT-rich gene tag, AT4 (AAATATTATAAA) (Pandey *et al.,* 2014). The plasmid construct hence obtained had an N-terminal AT4 tag and a hexahistidine-tag (6xHis-tag) at the C-terminus. First three transmembrane segments of GPCR43 (GPCR43-TM1-3) were expressed by subcloning the cDNA encoding transmembrane segments (315bp) into pET-23b (+) using NdeI and XhoI restriction sites. Forward (ATACTACATATGAAATATTATAAAATGCTGCCTGACTGGAAGTCC) and reverse primers (ACTAGCCTCGAGTTAATGGTGATGGTGATGGTGAATGCTAATGCCGGCCAGCAG) were designed to amplify GPCR43-TM1-3.

2.2 Protein expression

E coli strains have been reported to produce high protein yield. Recombinant proteins were expressed using IPTG inducer. Briefly, a few colonies were inoculated in 5 mL LB media with chloramphenicol (34 μg/mL) and ampicillin (100 μg/mL) antibiotics. The cultures were incubated overnight at 37℃. The next day cultures were shifted to 15 mL media with antibiotics and incubated for almost 3-4 hours until the optical density (OD_{600}) reached 0.5-0.7. Cultures were induced with IPTG and 1 mL culture was taken as un-induced (centrifuged at 10,000 rpm for 2 minutes). After induction, the cells were grown for 3 h at 37 °C and harvested by centrifugation (10000 rpm at 4 °C for 10 minutes). Protein expression was observed on 12 % SDS-PAGE (Schägger, 2006). Western blotting was performed by transferring the gel onto PVDF membrane and blot was detected by using anti-His antibody (Invitrogen).

2.3 Structure prediction and docking

The full-length sequence of GPCR43 (Uniprot ID: O15552) protein was used as query in I-TASSER to predict three-dimensional structure model. Images of the model were generated using Chimera. The predicted models were refined by Galaxy and ModRefiner and further validated by SAVES server which is composed of several online servers such as Procheck, ERRAT, Verify3D, whatcheck and Ramachandran plot. The binding pockets were identified by CASTp.

Four active compounds of plant origin, catechin, diosmin, rutin and EGCG, reportedly involved in T2DM were selected. Molecular docking was performed by PyRx, a software for computational drug discovery. In AutoDock4, 50 conformations were analyzed for GPCR43 and Ligands interactions and best conformation was selected on the basis of binding energy, number of hydrogen bonds and maximum number of residues. Further, the best selected conformations were studied through LigPlus.

3. Results

3.1 Cloning and expression of GPCR43-TM1-3 in *E.coli*

GPCR43-TM1-3 was successfully cloned with small tags, N-terminal AT4 tag and C-terminal His tag into pET23b(+) (Figure. 1a-d). The cloned insert was confirmed by PCR amplification with gene specific primers by using the recombinant plasmid (pET23b(+)-GPCR43-TM1-3) as template (Figure 1d). Expression of recombinant GPCR43-TM1-3 (12kDa) was induced with 1mM IPTG in *E. coli* BL21 (DE3) which was confirmed by western blotting (Figure 2).

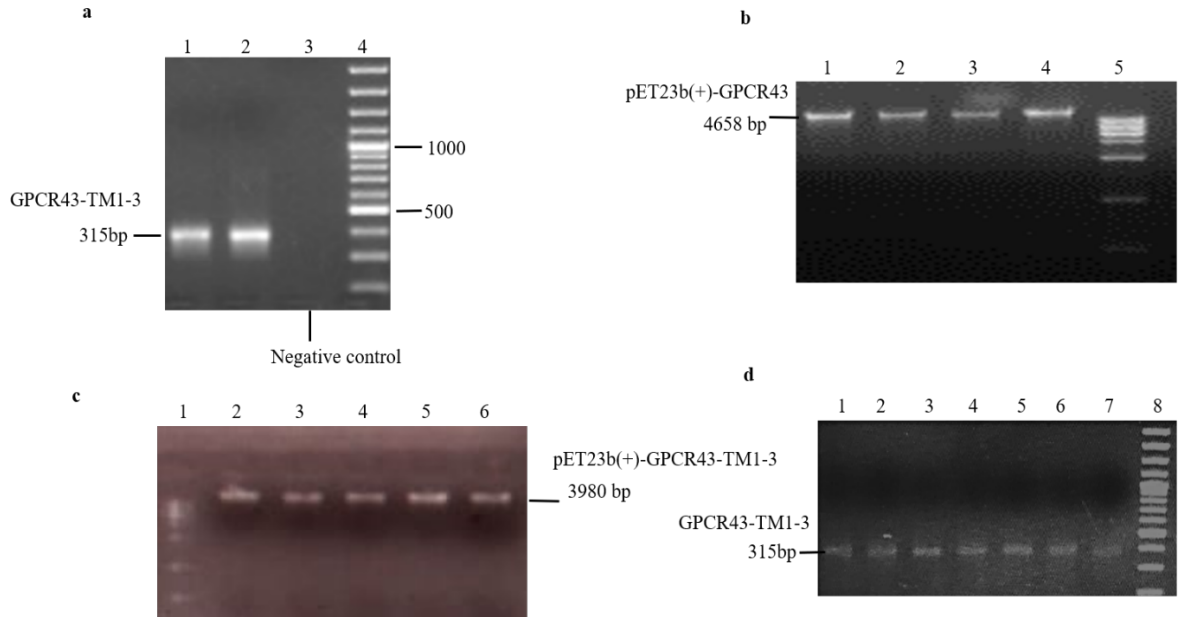

Fig. 1. cDNA Cloning of the first three transmembrane segments of GPCR 43 (GPCR43-TM1-3) in pET23b(+). (a) PCR amplification of cDNA encoding GPCR43-TM1-3. Lane 1-2, PCR products showing 315bp of GPCR43-TM1-3, Lane3, Negative control, Lane 4, 100bp DNA marker. (b) Transformation of *E. coli* with the designed vector construct, pET23b(+)-GPCR43 which contains full length cDNA of GPCR43 and plasmid isolation. Lane 1-4, pET23b(+)-GPCR43, Lane 5, 1 Kb DNA marker. (c) Subcloning the cDNA encoding transmembrane segments (315 bp) into pET-23b (+) using NdeI and XhoI pET23b(+)-GPCR43 yielded 3980bp of recombinant pET23b(+)-GPCR43-TM1-3. Lane 1, DNA marker, Lane 2-6, Extracted pET23b(+)-GPCR43-TM1-3. (d) Confirmation of the insert by using pET23b(+)-GPCR43-TM1-3 as DNA template in PCR. Lane 1-7, PCR amplification of the insert of 315bp, Lane 8, DNA marker.

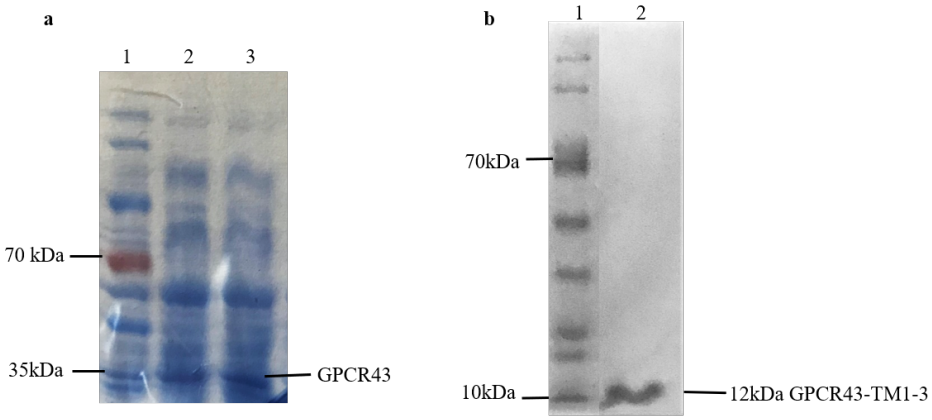

Fig. 2. Protein expression of recombinant GPCR43 in *E. coli* BL21(DE3) pLysS strain. (a). Lane 1, Pre-stained protein marker, Lane 2, uninduced sample, Lane 3, Induced protein sample. (b) Expression of GPCR43-TM1-3 by western blotting. Labe 1, Pre-stained protein marker, Lane 2, 12kDa fragment corresponds to GPCR43-TM1-3.

3.2 Molecular Docking Analysis

The best GPCR43 model was selected on the basis of C score and RMSD value. Molecular docking was carried out to understand the molecular interactions between the active sites of protein target and the natural products (catechin, diosmin, rutin and EGCG) (Table 1, Figure 3-Figure 6).

Table 1. Docking studies of GPCR43 with plant-based ligands scores.

Ligand	Binding Scores	Active Residues
Catechin	-7.3	Pro3, Lys6, Ser7, Ile10, Lys65, Glu68, Ala69, Ala70, Ser71, Asn72, Phe73, Pro252, Arg255, Ser256, Val259
Diosmin	-9.5	Pro3, Asp4, Ser7, Lys65, Ala69, Asn72, Phe73, Thr153, Glu154
Rutin	-8.4	Pro3, Ala69, Asn72, Phe73, Pro252, Ser256
EGCG	-7.5	Lys6, Ser7, Ala69, Asn72, Pro252, Arg255

CASTp calculated the active site, pocket area, and binding pocket volume of the protein. The residues which occupy the active site for GPCR43 are PRO3, LYS6, SER7, ILE10, TYR14, LYS65, LEU62, ALA69, ALA70, ASN72, TRP75, PHE73, CYS82, THR85, SER86, PHE89, TYR90, PRO252 and ARG255. (Figure 3). The docking pose was ranked by energy, the more negative the value, the better the interactions. The best interaction was nominated based on binding affinity values (Table 1). Analysis with Lig+ indicated the hydrogen bonds and hydrophobic interactions of both ligand and receptor, binding energy and binding residues (Figure 3b, 4b, 5b, 6b).

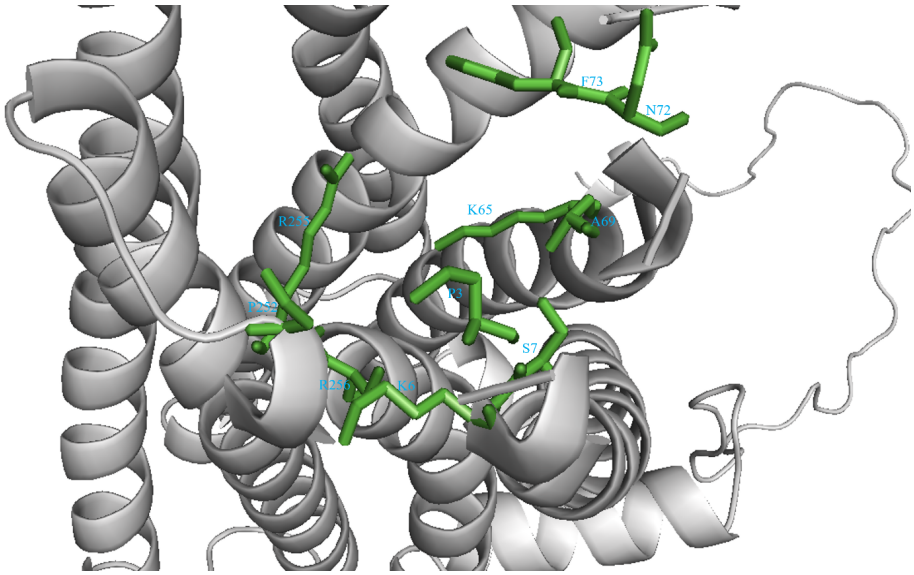

Fig. 3. Binding pocket of GPCR43**.** The amino acids involved in the binding pocket were predicted by CASTp. The side chains of the important residues are highlighted.

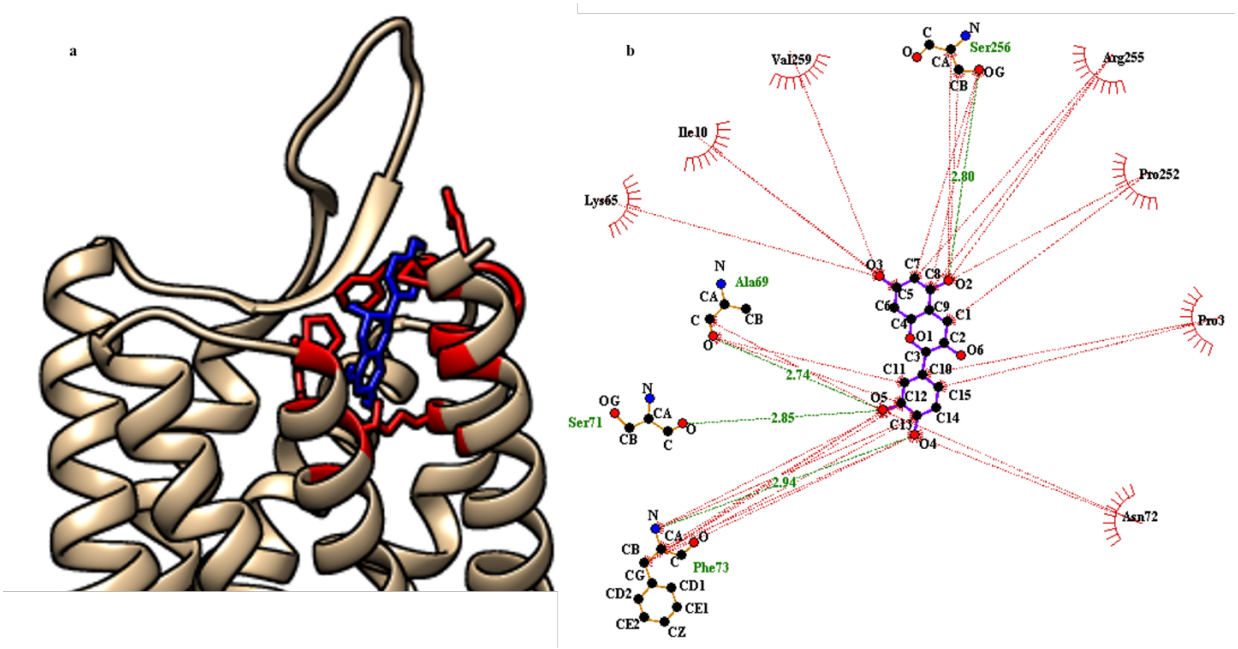

Fig. 4. Docking of GPCR43 with catechin. (a) GPCR43 with catechin docked in the active site. (b) Interactions between GPCR43 and catechin, the residues in the binding sites are highlighted. Visualization of interactions between receptor (brown edges) with ligand (purple edges) in LigPlot along with hydrophobic interactions (red lashes) and hydrogen bond (green).

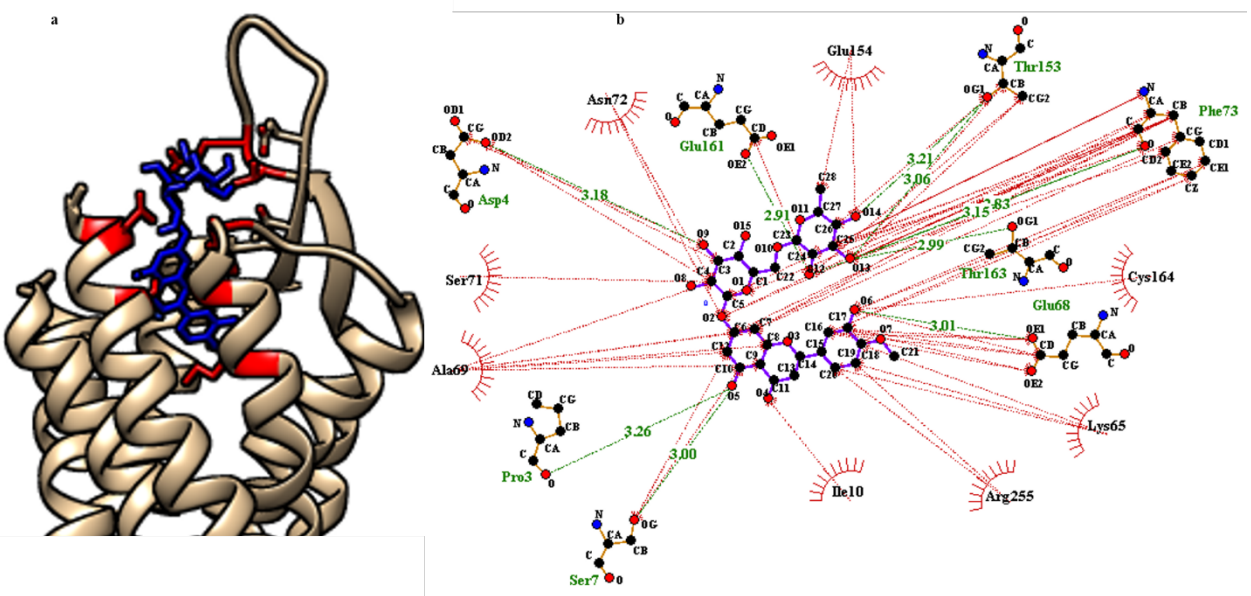

Fig. 5. Docking of GPCR43 with diosmin. (a) A docking pose of GPCR43 with diosmin. (b) Interactions between GPCR43 and diosmin, the residues in the binding sites are highlighted.

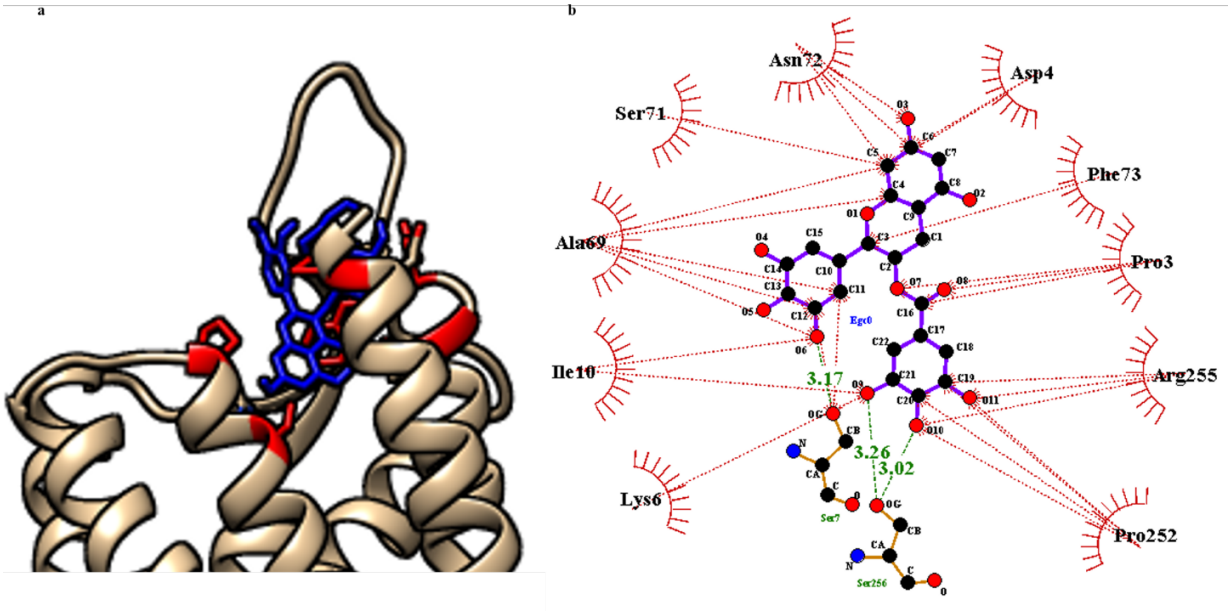

Fig. 6. Docking of GPCR43 with rutin. (a) GPCR43 with rutin docked in the active site. (b) Interactions between GPCR43 and rutin, the residues in the binding sites are highlighted.

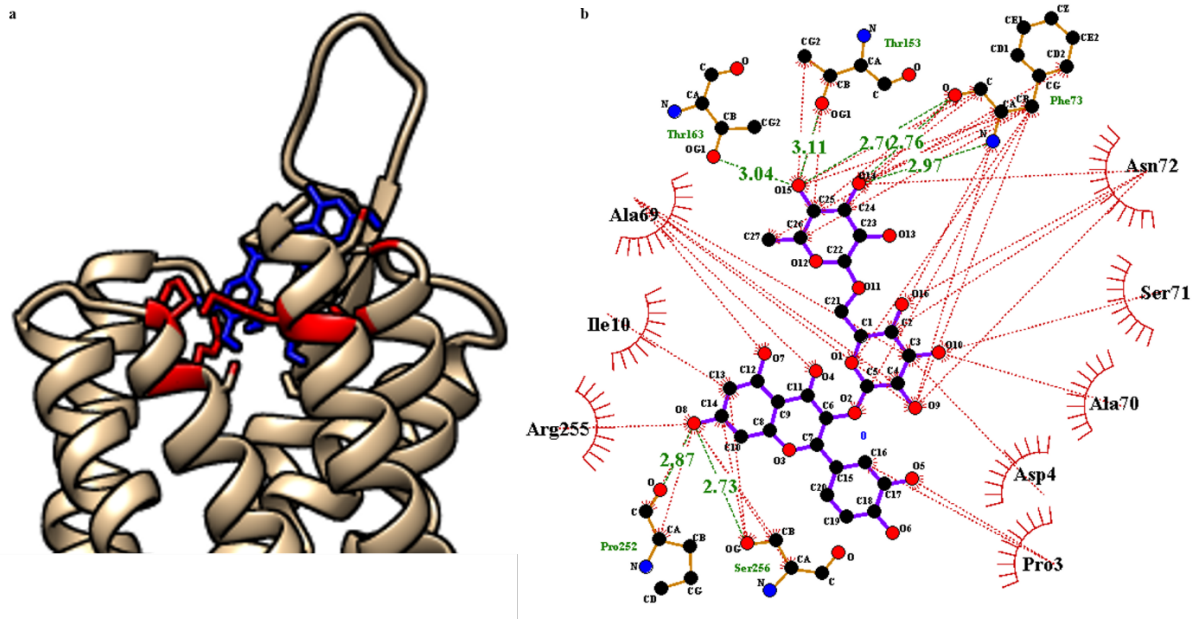

Fig. 7. Docking of GPCR43 with EGCG. (a) A docking pose of GPCR43 with EGCG docked in the active site. (b) Interactions between GPCR43 and EGCG, the residues in the binding sites are highlighted.

The plant-based ligands were docked successfully with good docking scores and interactions. The binding residues such as PRO3, LYS6, SER7, ALA69, ASN72, PHE73, PRO252, ARG255, are predominantly involved in interaction with the ligands (Table 1). According to the docking results, Diosmin and rutin were predicted to be the best ligands with binding score of -9.5 and -8.4 respectively.

4. Discussion

GPCRs are the key players in a multitude of physiological processes and hence, regarded as the promising drug targets (Wiseman *et al.,* 2020). The structure-aided drug design requires purified proteins to obtain three dimensional structures. Recombinant protein production lies at the heart of structural biology. Obtaining high quantities of purified membrane proteins is certainly a challenging task for which scientists have been developing protocols for optimization of protein expres sion. Expression of membrane proteins like GPCRs is difficult owing to the big size, poor stability, and low expression. Herein, we report the successful expression of first three transmembrane domains of GPCR43 by using a small expression tag, AT4. AT rich gene tags next to the translation start site were reported to enhance cell free expression previously (Haberstock *et al.,* 2012). AT rich small gene tags were used to successfully express first three transmembrane segments of apelin receptor which could not be expressed without AT tag (Pandey *et al.,* 2014). Fusion protein tags have greatly facilitated the expression and purification of soluble proteins (Esposito & Chatterjee, 2006; Ki & Pack, 2020). Large tags such as glutathione S-transferase (Harper & Speicher ,2011) and maltose-binding protein (Khan *et al.,* 2014) enhance expression and aid in purification but needs to be cleaved off using an appropriate protease before subsequent analysis due to their large sizes. However, protease digestion gets quite difficult as the fusion protein is insoluble under the conditions needed for protease activity due to the high hydrophobicity of membrane proteins. Therefore, using small tags like AT4 which does not require removal can be highly advantageous in membrane proteins especially involving the structural studies by NMR spectroscopy (Zhou *et al.,* 2010).

Structure modeling and docking studies have become instrumental in structure-aided drug discovery (Gschwend *et al.,* 1996; Meng *et al.,* 2011, Pinzi & Rastelli, 2019). The docking and virtual screening methods have provided various ways to target GPCRs for therapy (Evers & Klabunde, 2005; Chen *et al.,* 2007; Michino *et al.,* 2009; Kooistra *et al.,* 2013; Beuming *et al.,* 2015; Kooistra *et al.,* 2016). Plants contain an inexhaustible array of natural products which can be exploited for drug discovery. For instance, 40 percent of the drugs in the market of western countries originate from plants (USDA website). Plants have been widely used for the treatment of DM (Modak *et al.,* 2007; Rizvi & Mishra, 2013; Kooti *et al.,* 2016; Farzaei *et al.,* 2017).

In the present study, the docking of GPCR43 was conducted with the plant-derived ligands reported with beneficial effects in diabetes. Our results indicate that the selected plant-based ligands were capable of binding to the active site of GPCR43 with good binding scores especially diosmin and rutin.

Rutin and diosmin, two polyhydroxyflavone glycosides found in citrus peel and present in the pulp of various citrus species show diverse pharmacological effects in diseases associated with chronic inflammation (Gosslau *et al.,* 2019). Studies provided evidence that rutin was able to reduce serum glucose levels in animal models of T2DM (Niture *et al.,* 2014; Lee *et al.,* 2016; Liang *et al.,* 2018). Diosmin possess antiplatelet activity and is shown to have preventive effects on various diseases such as hyperglycemia, hyperlipidemia, ulcer, chronic venous insufficiency and hemorrhoids (Zaragozá *et al.,* 2021).

Our group plans to conduct the further investigation of these candidate compounds in animal models to be used in the drug discovery of T2DM.

ACKNOWLEDGEMENTS

The project was funded by the Higher Education Commission (HEC) Pakistan (National Research Program for Universities (NRPU) research grant, No: 9105/Balochistan/NRPU/R&D/HEC/2017). FK is the recipient of the grant.

References

Beuming, T., Lenselink, B., Pala, D., McRobb, F., Repasky, M. and Sherman, W., 2015. Docking and virtual screening strategies for GPCR drug discovery. G Protein-Coupled Receptors in Drug Discovery, pp.251-276.

Chatterjee, S., Khunti, K. and Davies, M.J., 2017. Type 2 diabetes. The lancet, 389(10085), pp.2239-2251.

Chen, J.Z., Wang, J. and Xie, X.Q., 2007. GPCR structure-based virtual screening approach for CB2 antagonist search. Journal of chemical information and modeling, 47(4), pp.1626-1637.
Eng, Q.Y., Thanikachalam, P.V. and Ramamurthy, S., 2018. Molecular understanding of Epigallocatechin gallate (EGCG) in cardiovascular and metabolic diseases. Journal of ethnopharmacology, 210, pp.296-310.

Esposito, D. and Chatterjee, D.K., 2006. Enhancement of soluble protein expression through the use of fusion tags. Current opinion in biotechnology, 17(4), pp.353-358.

Evers, A. and Klabunde, T., 2005. Structure-based drug discovery using GPCR homology modeling: successful virtual screening for antagonists of the alpha1A adrenergic receptor. Journal of medicinal chemistry, 48(4), pp.1088-1097.

Farzaei, F., Morovati, M.R., Farjadmand, F. and Farzaei, M.H., 2017. A mechanistic review on medicinal plants used for diabetes mellitus in traditional Persian medicine. Journal of evidence-based complementary & alternative medicine, 22(4), pp.944-955.

Fredriksson, R., Lagerström, M.C., Lundin, L.G. and Schiöth, H.B., 2003. The G-protein-coupled receptors in the human genome form five main families. Phylogenetic analysis, paralogon groups, and fingerprints. Molecular pharmacology, 63(6), pp.1256-1272.

Gosslau, A., Ho, C.T. and Li, S., 2019. The role of rutin and diosmin, two citrus polyhydroxyflavones in disease prevention and treatment. Journal of Food Bioactives, 5, pp.43-56.

Gschwend, D.A., Good, A.C. and Kuntz, I.D., 1996. Molecular docking towards drug discovery. Journal of Molecular Recognition: An Interdisciplinary Journal, 9(2), pp.175-186.

Gothai, S., Ganesan, P., Park, S.Y., Fakurazi, S., Choi, D.K. and Arulselvan, P., 2016. Natural phyto-bioactive compounds for the treatment of type 2 diabetes: inflammation as a target. Nutrients, 8(8), p.461.

Haberstock, S., Roos, C., Hoevels, Y., Dötsch, V., Schnapp, G., Pautsch, A. and Bernhard, F., 2012. A systematic approach to increase the efficiency of membrane protein production in cell-free expression systems. Protein expression and purification, 82(2), pp.308-316.

Harper, S. and Speicher, D.W., 2011. Purification of proteins fused to glutathione S-transferase. In Protein chromatography (pp. 259-280). Humana Press.

Hu, G.M., Mai, T.L. and Chen, C.M., 2017. Visualizing the GPCR network: classification and evolution. Scientific reports, 7(1), pp.1-15.

Khan, F., Daniëls, M.A., Folkers, G.E., Boelens, R., Saqlan Naqvi, S.M. and Van Ingen, H., 2014. Structural basis of nucleic acid binding by Nicotiana tabacum glycine-rich RNA-binding protein: implications for its RNA chaperone function. Nucleic Acids Research, 42(13), pp.8705-8718.

Ki, M.R. and Pack, S.P., 2020. Fusion tags to enhance heterologous protein expression. Applied microbiology and biotechnology, 104(6), pp.2411-2425.

Kimura, I., Inoue, D., Hirano, K. and Tsujimoto, G., 2014. The SCFA receptor GPR43 and energy metabolism. Frontiers in endocrinology, 5, p.85.

Kooistra, A.J., Roumen, L., Leurs, R., de Esch, I.J. and de Graaf, C., 2013. From heptahelical bundle to hits from the Haystack: structure-based virtual screening for GPCR ligands. Methods in enzymology, 522, pp.279-336.

Kooistra, A.J., Vischer, H.F., McNaught-Flores, D., Leurs, R., De Esch, I.J. and De Graaf, C., 2016. Function-specific virtual screening for GPCR ligands using a combined scoring method. Scientific reports, 6(1), pp.1-21.

Kooti, W., Farokhipour, M., Asadzadeh, Z., Ashtary-Larky, D. and Asadi-Samani, M., 2016. The role of medicinal plants in the treatment of diabetes: a systematic review. Electronic physician, 8(1), p.1832.

Kris-Etherton, P.M., Hecker, K.D., Bonanome, A., Coval, S.M., Binkoski, A.E., Hilpert, K.F., Griel, A.E. and Etherton, T.D., 2002. Bioactive compounds in foods: their role in the prevention of cardiovascular disease and cancer. The American journal of medicine, 113(9), pp.71-88.

Lee, D.G., Jang, I.S., Yang, K.E., Yoon, S.J., Baek, S., Lee, J.Y., Suzuki, T., Chung, K.Y., Woo, S.H. and Choi, J.S., 2016. Effect of rutin from tartary buckwheat sprout on serum glucose-lowering in animal model of type 2 diabetes. Acta Pharmaceutica, 66(2), pp.297-302.

Liang, W., Zhang, D., Kang, J., Meng, X., Yang, J., Yang, L., Xue, N., Gao, Q., Han, S. and Gou, X., 2018. Protective effects of rutin on liver injury in type 2 diabetic db/db mice. Biomedicine & Pharmacotherapy, 107, pp.721-728.

McNelis, J.C., Lee, Y.S., Mayoral, R., van der Kant, R., Johnson, A.M., Wollam, J. and Olefsky, J.M., 2015. GPR43 potentiates β-cell function in obesity. Diabetes, 64(9), pp.3203-3217.

Meng, X.Y., Zhang, H.X., Mezei, M. and Cui, M., 2011. Molecular docking: a powerful approach for structure-based drug discovery. Current computer-aided drug design, 7(2), pp.146-157.

Michino, M., Abola, E., Brooks, C.L., Dixon, J.S., Moult, J. and Stevens, R.C., 2009. Community-wide assessment of GPCR structure modelling and ligand docking: GPCR Dock 2008. Nature Reviews Drug Discovery, 8(6), pp.455-463.

Modak, M., Dixit, P., Londhe, J., Ghaskadbi, S. and Devasagayam, T.P.A., 2007. Indian herbs and herbal drugs used for the treatment of diabetes. Journal of clinical biochemistry and nutrition, 40(3), pp.163-173.

Nagao, T., Meguro, S., Hase, T., Otsuka, K., Komikado, M., Tokimitsu, I., Yamamoto, T. and Yamamoto, K., 2009. A catechin-rich beverage improves obesity and blood glucose control in patients with type 2 diabetes. Obesity, 17(2), pp.310-317.

Niture, N.T., Ansari, A.A. and Naik, S.R., 2014. Anti-hyperglycemic activity of rutin in streptozotocin-induced diabetic rats: an effect mediated through cytokines, antioxidants and lipid biomarkers. Indian Journal of Experimental Biology, 52, pp.720-727.

Olokoba, A.B., Obateru, O.A. and Olokoba, L.B., 2012. Type 2 diabetes mellitus: a review of current trends. Oman medical journal, 27(4), p.269.

Pandey, A., Sarker, M., Liu, X.Q. and Rainey, J.K., 2014. Small expression tags enhance bacterial expression of the first three transmembrane segments of the apelin receptor. Biochemistry and Cell Biology, 92(4), pp.269-278.

Pinzi, L. and Rastelli, G., 2019. Molecular docking: shifting paradigms in drug discovery. International journal of molecular sciences, 20(18), p.4331.

Priyadarshini, M., Villa, S.R., Fuller, M., Wicksteed, B., Mackay, C.R., Alquier, T., Poitout, V., Mancebo, H., Mirmira, R.G., Gilchrist, A. and Layden, B.T., 2015. An acetate-specific GPCR, FFAR2, regulates insulin secretion. Molecular endocrinology, 29(7), pp.1055-1066.

Rizvi, S.I. and Mishra, N., 2013. Traditional Indian medicines used for the management of diabetes mellitus. Journal of diabetes research, pp.1-11.

Schägger, H., 2006. Tricine–sds-page. Nature protocols, 1(1), pp.16-22.

Stumvoll, M., Goldstein, B.J. and Van Haeften, T.W., 2005. Type 2 diabetes: principles of pathogenesis and therapy. The Lancet, 365(9467), pp.1333-1346.

Tang, C., Ahmed, K., Gille, A., Lu, S., Gröne, H.J., Tunaru, S. and Offermanns, S., 2015. Loss of FFA2 and FFA3 increases insulin secretion and improves glucose tolerance in type 2 diabetes. Nature medicine, 21(2), pp.173-177.

Tolhurst, G., Heffron, H., Lam, Y.S., Parker, H.E., Habib, A.M., Diakogiannaki, E., Cameron, J., Grosse, J., Reimann, F. and Gribble, F.M., 2012. Short-chain fatty acids stimulate glucagon-like peptide-1 secretion via the G-protein–coupled receptor FFAR2. Diabetes, 61(2), pp.364-371.

Unuofin, J.O. and Lebelo, S.L., 2020. Antioxidant effects and mechanisms of medicinal plants and their bioactive compounds for the prevention and treatment of type 2 diabetes: an updated review. Oxidative medicine and cellular longevity, pp.1-36.

Villa, S.R., Mishra, R.K., Zapater, J.L., Priyadarshini, M., Gilchrist, A., Mancebo, H., Schiltz, G.E. and Layden, B.T., 2017. Homology modeling of FFA2 identifies novel agonists that potentiate insulin secretion. Journal of Investigative Medicine, 65(8), pp.1116-1124.

Wiseman, D.N., Otchere, A., Patel, J.H., Uddin, R., Pollock, N.L., Routledge, S.J., Rothnie, A.J., Slack, C., Poyner, D.R., Bill, R.M. and Goddard, A.D., 2020. Expression and purification of recombinant G protein-coupled receptors: A review. Protein expression and purification, 167, p.105524.

Xu, M., Jiang, Z., Wang, C., Li, N., Bo, L., Zha, Y., Bian, J., Zhang, Y. and Deng, X., 2019. Acetate attenuates inflammasome activation through GPR43-mediated Ca2+-dependent NLRP3 ubiquitination. Experimental & molecular medicine, 51(7), pp.1-13.

Yang, L., Lin, H., Lin, W. and Xu, X., 2020. Exercise ameliorates insulin resistance of type 2 diabetes through motivating short-chain fatty acid-mediated skeletal muscle cell autophagy. Biology, 9(8), p.203.

Zaragozá, C., Monserrat, J., Mantecón, C., Villaescusa, L., Álvarez-Mon, M.Á., Zaragozá, F. and Álvarez-Mon, M., 2021. Binding and antiplatelet activity of quercetin, rutin, diosmetin, and diosmin flavonoids. Biomedicine & Pharmacotherapy, 141, p.111867.

Zhou, P. and Wagner, G., 2010. Overcoming the solubility limit with solubility-enhancement tags: successful applications in biomolecular NMR studies. Journal of biomolecular NMR, 46(1), pp.23-31.

Submitted: 21/02/2022
Revised: 08/06/2022
Accepted: 06/07/2022
DOI: 10.48129/kjs.19029

Congruent assessment of human hypoglycemic effect through STZ-induced diabetic rats fed Dromedary Camel (*Camelus dromedarius*) milk

Amal M. Al-Saffar[1*], Sirar A. Baker[1], Mona A. Al-sughayer[1]

Dept. of Biological Sciences, Faculty of Science, Kuwait University, PO Box 5969, Safat (13060), Kuwait

**Corresponding author: amal.alsaffar@ku.edu.kw*

Abstract

Diabetes mellitus (DM), a heterogeneous metabolic disorder, affect people at any point of their lives. Globally, a wide variation in the prevalence of diabetes was observed but, showed zero percent within people that regularly consume camel milk because of their highly nutritional and therapeutic potentials to treat many metabolic and autoimmune diseases. The present study validated the efficacy of camel milk by investigating the differential hypoglycemic effects in concurrence with related biochemical tests in rats fed with raw and pasteurized milk of the one-humped Arabian camel (*Camelus dromedarius*). Male Sprague-Dawley rats (60mg.Kg^{-1} body weight) fed separately with raw and pasteurized camel milk for three weeks and injected with streptozotocin induced DM besides the investigation on the levels of blood glucose, cholesterol, triacylglycerol (TAG), and insulin. Results showed a significant hypoglycemic effect with both raw and pasteurized camel milk but, more prominent with the raw milk. Three weeks consumption of raw camel milk significantly increased blood cholesterol levels while consumption of pasteurized camel milk caused the reverse. Both types of camel milk revealed significant decrease in the blood TAG levels and were statistically validated. Thus, the present study recommends the choice of camel milk consumption especially in diabetic patients as well, as an immunity booster in the wake of the present environmental health issues.

Keywords: Camel milk; diabetes mellitus; hypoglycemic effect; streptozotocin; triacylglycerol.

1. Introduction

The incidence of Diabetes mellitus (DM) is increasing worldwide. World Health Organization (WHO) reported more than 420 million diabetic individuals in the world, an estimate that could rise to 570 million by 2030 and to 700 million by 2045 (WHO 2021). Type II DM is a major chronic disease in the population of Kuwait. The prevalence in the adult population is 14.8% (Al-Kandari *et al.,* 2019), and among children aged 0-14 years old, the incidence is 34.9 in every 100,000 children (Shaltout *et al.,* 2017). In addition, the occurrence of type I DM in Kuwait is high compared to other countries and the incidence is 20.1 in every 100,000 children under the age of 14 (Costa-Gouveia *et al.,* 2017; Shaltout *et al.,* 2017). Increasing interest in the constituents of camel milk has developed from the fact that it is a major part of human diet in many arid lands around the world (Hattem 2017). Although most of the camel milk is consumed

raw by nomads and desert inhabitants, pasteurized camel milk became available for populations in many African, Asian, and most recently, in some European countries. However, heat treatments have direct influences on the nutritional, biological and functional properties of milk proteins (Hattem 2017; Shori 2015; Atakan *et al.,* 2016). Additionally, the impact of regional and seasonal differences on camel milk composition has been widely suggested, which includes species and breeds, feeding conditions, and seasonal and physiological variations (Bouhaddaoui *et al.,* 2019) as well, the stage of lactation and genetic differences within the species (Pak *et al.,* 2019). The main composition of camel milk (g/100 ml) obtained from meta-analysis of literature data revealed 3.82 of fat, 3.35 total protein, 4.46 of lactose, 12.47 of dry matter and 0.79 for ash (Bouhaddaoui *et al.,* 2019). Camel milk composition is highly affected by water content which ranges from 86% to 91% depending on the accessibility of camels to water (Zibaee *et al.,* 2015). Few regional studies revealed the seasonal effect of camel milk composition with significant variations (Othman 2016). The mean components of camel milk are protein (3.1%), lipid (3.5%), lactose (4.4%), ash (0.79%), and total solids (11.9%) besides, rich source of vitamins (A, E, D, B) (Zibae *et al*., 2015). Casein is the predominant protein (whey protein/casein 0.31) in camel milk (Boughellout *et al.,* 2016). Camel milk whey contains higher contents of some protective antibacterial proteins such as lysozyme, lactoferrin, lactoperoxidase, peptidoglycan, serum albumin, and immunoglobulins (Rasheed, 2017; Koc & Atasever 2016; Nascimento *et al.,* 2016; Sakandar *et al.,* 2018). The average amount of components of camel milk is protein 3.1%; fat 3.5%; lactose 4.4%; ash 0.79%, and total solids 11.9% β-Lactoglobulin protein is however absent suggesting minimal hypersensitivity reactions for camel milk (Nascimento *et al.,* 2016). Moreover, camel milk whey protein is found to contain a small protein that is rich in cystine/half-cystine (Yasmin *et al.,* 2020). In general, camel milk proteins contain an adequate and balanced content of essential amino acids like the cow's milk (Jilo & Tegegne 2016; Rahmeh *et al.,* 2019). Triacylglycerols accounted for 96% of the total lipids in milk. Short chain fatty acids (4:0-12:0) are present in very small amounts in camel milk fat and lower than that of cow milk fat. Camel milk fat showed a higher content of 16:1, 18:0, 18:1 and 18:2*n*-6 but comparable level of 18:3*n*-3 to that of cow milk (Konuspayeva *et al.,* 2009; Karaman *et al.,* 2021; Pak *et al.,* 2019). Although camel milk fat has a higher unsaturated/saturated ratio, the high content of unsaturated fatty acids and the appreciable amount of essential fatty acids contributes to the overall nutritional value of camel milk (Boughellout *et al.,* 2016; Jilo & Tegegene 2016; Bouhaddaoui *et al.,* 2019). Additionally, camel milk contains considerably higher content of manganese, iron (Konuspayeva *et al.,* 2009; Brezovečki *et al.,* 2015), vitamin C and niacin (Costa-Gouveia *et al.,* 2017) than cow's milk. In addition to its nutritional potential, camel milk is also known to have medicinal properties that facilitates the treatment of many metabolic and autoimmune diseases (Urazakov & Baînazarov 1974; Yagil 1982; Agrawal *et al.,* 2005; Agrawal *et al.,* 2007; Aida *et al.,* 2019; Kamlesh & Asha 2020; Karaman *et al.,* 2021) in addition to their role in the prevention and management of DM. Researchers reported that the consumption of camel milk had a hypoglycemic effect in diabetic rats (Shah *et al.,* 2019; Aida *et al*., 2019; Agrawal *et al*., 2005). Similarly, a study performed on streptozotocin (STZ)-induced diabetic rats has reported a significant hypoglycemic effect upon consumption of raw camel milk for three

weeks, an effect which was not as significantly observed for raw cattle milk (Agarwal *et al.,* 2007; Ejtahed *et al.,* 2015). They also established that pasteurization has reduced the hypoglycemic effect suggesting that heating the milk may have affected the biological factors that produced this hypoglycemic effect (Hattem 2017; Kamlesh & Asha 2020). The prevalence of DM is zero among people in the rural Raica community (State of Rajasthan, India), who regularly consume camel milk, as compared to a 5.5% prevalence of the disease among non-Raica subjects from the same area (Urazakov & Baînazarov 1974).

In randomized studies on human subjects, observations revealed improvement of glycemic control in type I DM by standard therapy using camel milk supplementation (Al-Amin *et al.,* 2006; Kappeler *et al.,* 2006). There was a significant reduction (30-35%) in daily doses of insulin in type I diabetic patients fed raw camel milk. In addition, a marked improvement in diabetes quality control of life score (satisfaction score, impact score and worry score) was observed after three months of camel milk treatment. Based on these findings, the present study investigated the differential biochemical effects of feeding raw and pasteurized camel milk to STZ-induced and non-induced diabetic rats on blood levels of glucose, cholesterol, and TAG. This study will pave way not only to researchers in validate the effect of camel milk but, also will facilitate animal husbandry and health sector to promote the yield and consumption of camel milk for better immunity to humans especially, during this pandemic health issues.

2. Materials and methods

2.1. Feeding trials and regime

Raw and pasteurized camel milk were obtained from the local farms of Kuwait. Milk samples were transported in polypropylene containers and stored at 4°C. The feeding bottles of the rats were cleaned and refilled with fresh camel milk daily to encourage the rats to drink it. After acclimation with water and camel milk the following regime of milk and water was given to the rats: (a) non-diabetic and diabetic rats (control) were supplied with 300ml water/d, (b) from 1d to 21d, two groups of diabetic induced rats were provided 300ml/d raw and pasteurized camel milk, respectively. The diabetic induced rats were never given water since, this study revealed rats fed with water abstained from consuming camel milk.

2.2 Treatment of rats

Male Sprague-Dawley rats (a strain of *Rattus norvegicus* at F1 generation), bred in our animal house (Life Science Department, Kuwait University). These rats were four weeks old, weighing 145g and maintained on normal pellet diet (VRF1) that followed the standard and validated regime described by Special Diet Services, Essex, UK (SDS, 2022). The ingredients in this feed were fat (2.7%), crude protein (14.4%), crude fiber (4.7%), and Vitamin-A (8000 IU/Kg), D3 (600 IU/Kg), Vitamin-E (62 IU/Kg), Copper (11mg/Kg), and Calcium (0.73%). They were also provided with sufficient filtered water in the experiment. Standard animal care and handling was applied throughout the experiment. The rats were injected with a single dose of 0.5 ml STZ (streptozotocin) intraperitoneally (IP) in saline solution (0.9% NaCl) @ 60 mg/kg body weight to

induce diabetes. These concentrations were standardized in this study after deducing the optimum and non-lethal dose that neither induced stress nor disproportioned the dose against the body weight of the rats. These rats with blood glucose levels higher than 350 mg/dL were selected as severely diabetic rats (Agrawal *et al.,* 2007).

2.3 Biochemical analysis

Blood samples were collected from fasting rats before treatment and after 7, 14, and 21 days (Week 1-3) of treatment. The serum was prepared and stored for later analysis. Serum glucose and cholesterol levels were determined by the glucose oxidase assay and the cholesterol oxidase assay, respectively, using kits provided by WAKO Company, USA. Serum TAG levels were determined using a kit provided by WAKO Company, USA.

2.4 Statistical analysis

Statistical analyses were performed using the ANOVA tests to determine the significance between and within each group. Results were represented with mean and ± standard error. *P* value <0.05 was considered statistically the threshold level for significance.

3. Results

Figure 1 represents mean values of serum levels of glucose, cholesterol, and triacylglycerol (TAG) of the control and experimental rat groups throughout the experiment; normal non-diabetic control group (Ct *n* 7) as a normal baseline, untreated STZ-induced diabetic control group (D-Ct *n* 5) as a diabetic baseline, raw camel milk-treated STZ-induced diabetic group (DT-R *n*5) and pasteurized camel milk-treated STZ-induced diabetic group (DT-P *n*5). In establishing the diabetic status, mean values for D-Ct group were statistically compared to Ct group (Figure 1). It is to note that the results were transformed to logarithmic values to show the wide-ranged differential units and reduce the dispersed numerical data values to visualize or respond to skewness towards large values and express the figure (Figure 1) in compactness. Additionally, analysis of variance (ANOVA) tested the significant differences between the variables and the samples (Table 1).

The significance of changes in blood parameters for every group were calculated by comparing the mean values obtained in each week to the previous week within the same group (Figure 1). In addition, significant changes were also observed for the mean values of DT-R and DT-P groups in comparison to D-Ct (Figure 1).

Treatment with STZ led to several alterations in some of the blood parameters. The mean blood glucose level of Ct rats was 121.00 ±13.12mg/dL (log 2.08) initially, and constantly maintained throughout the duration of the experiment (Figure 1). On the other hand, the D-Ct rats showed significant increase in their mean blood glucose level to 455.21 ±20.21 mg/dL (log 2.66) compared to the Ct rats. Treatment with raw (DT-R) and pasteurized (DT-P) camel milk resulted in a significant reduction in blood glucose levels after the first week and throughout the duration of the experiment (Figure 1).

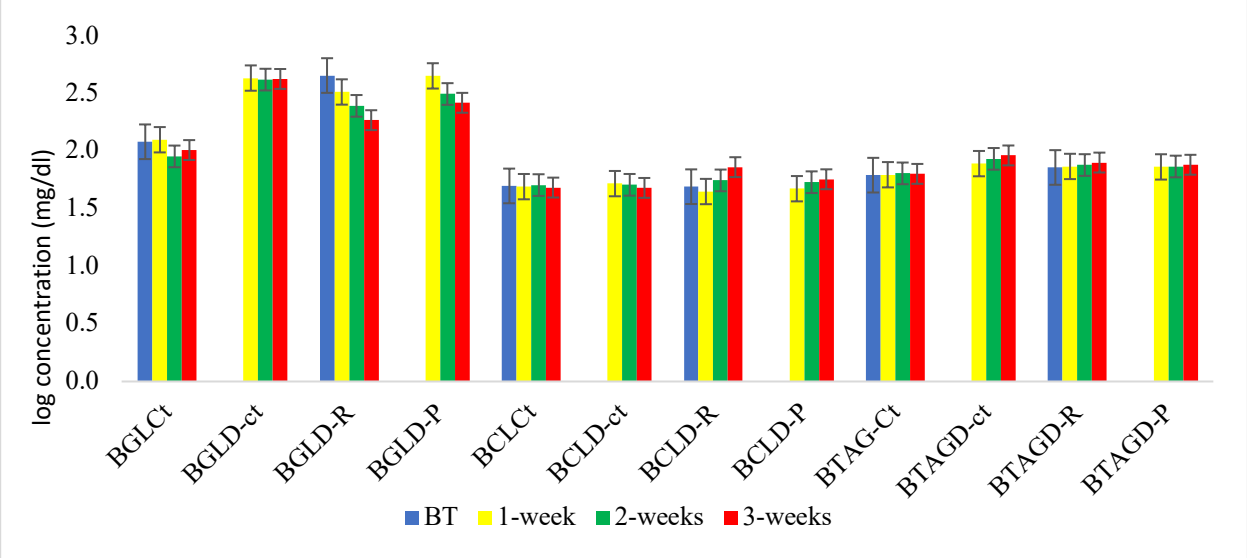

Fig .1. Serum levels of glucose, cholesterol, triacylglycerol (TAG) and control group in rats treated with raw and pasteurized camel milk Ct: control, D-Ct: STZ-induced diabetic rats, DT-R and DT-P: STZ-induced diabetic rats treated with raw and pasteurized camel milk, BCL: blood cholesterol level, BGL: blood glucose level, B-TAG: blood triglyceride, BT: before treatment

Initially, the mean blood cholesterol levels of Ct and D-Ct rats were 50 ±7.32 mg/dL (log 1.70) and 49.25±5.92 mg/dL (log 1.69) respectively and there were no significant changes in these levels throughout the duration of the experiment (Figure 1). In the case of the DT-R and DT-P groups, noticeably there were no significant changes in the mean blood cholesterol levels (p=0.424 and p=0.29 respectively) after one week of treatment. However, by the end of the third week of treatment, DT-R showed a significant increase in the mean blood cholesterol levels while DT-P showed insignificant increase (p=0.117). By the end of the experiment, treatment with raw camel milk resulted in 47% elevation in blood cholesterol compared to 16% exerted by pasteurized camel milk. A significant increase was also observed when the mean blood cholesterol levels of DT-R rats were compared to that of the D-Ct rats (Figure 1).

The mean blood TAG level of Ct rats was 62.02 ± 0.96 mg/dL (log 1.79) at the beginning of the experiment. There were no significant changes in this level throughout the duration of the experiment (Figure 1). However, diabetic status induced by STZ has caused a significant increase in blood TAG level seen for D-Ct rats up to 72.35 ±1.13 mg/dL (log 1.86). The mean blood TAG levels of the D-Ct group remained at significant levels compared to the Ct rats throughout the duration of the experiment. In the first and second weeks of treatment, there were no significant changes in the blood TAG levels of STZ-induced diabetic rats treated with raw camel milk (DT-R) or with pasteurized camel milk (DT-P). However, after the third week of treatment observations revealed significant increase in TAG levels of both DT-R and DT-P rats. Noticeably, the blood TAG levels of both treated groups (DT-R and DT-P) were lower than the diabetic control group (D-Ct) throughout the three weeks of treatment.

Table 1. ANOVA test on serum levels of glucose, cholesterol and triacylglycerol (TAG) in rats fed with untreated and treated group camel's milk

SUMMARY	*Count*	*Sum*	*Average*	*Variance*		
BGL:Ct	3	318.81	106.27	329.47		
BGL:D-ct	3	1277.59	425.86	43.54		
BGL:DT-R	3	762.14	254.05	5010.53		
BGL:DT-P	3	1030.58	343.53	9485.42		
BCL:Ct	3	148.55	49.52	1.55		
BCL:D-ct	3	151.58	50.53	4.90		
BCL:DT-R	3	173.37	57.79	200.34		
BCL:DT-P	3	158.33	52.78	25.14		
BTAG:Ct	3	190.51	63.50	0.77		
BTAG:D-ct	3	256.14	85.38	48.75		
BTAG:DT-R	3	229.63	76.54	9.19		
BTAG:DT-P	3	223.31	74.44	2.95		
After one week	12	1819.8	151.65	24465.63		
After two weeks	12	1584.42	132.04	15415.35		
After three weeks	12	1516.32	126.36	12911.46		
Source of Variation	*SS*	*df*	*MS*	*F*	*P-value*	*F crit*
Rows	554617.97	11	50419.81	42.50	<0.0001	2.25852
Columns	4226.15	2	2113.07	1.78	0.19	3.44336
Error	26098.95	22	1186.31			
Total	584943.07	35				

* Statistically significant $p<0.05$; Control rats (Ct), control STZ-induced diabetic rats (D-Ct), STZ-induced diabetic rats treated with raw camel milk (DT-R), STZ-induced diabetic rats treated with pasteurized camel milk (DT-P), TAG: triglyceride, B: blood

4. Discussion

Studies (Urazakov & Baînazarov 1974; Shori 2015) revealed DM is very uncommon in communities that consume camel milk, and this knowledge has led to an interest in studying the beneficial health and therapeutic effects of camel milk consumption to protect from DM. Previous studies in camel milk on diabetic patients as well as rats with induced diabetes proved that daily consumption of camel milk can lower the blood glucose levels considerably (Shori, 2015; Shah *et al.,* 2019; Kamlesh & Asha 2020). Additionally, it was shown that patients who consumed camel milk had to lower their daily insulin requirement to achieve a balanced blood glucose level. However, observations showed the reverse of glycemic control when camel milk consumption was discontinued (Ejtahed *et al.,* 2015; Shori, 2015; Shaltout *et al*., 2016; Shah *et*

al., 2019). In the present study, the blood glucose, cholesterol, and TAG levels of the normal, non- diabetic rats (Ct) were used as a normal baseline, while those of the diabetic, untreated rats (D-Ct) were used as a diabetic baseline. The D-Ct group maintained a diabetic status throughout the duration of the experiment, and any changes in blood levels of glucose, cholesterol, and TAG of the DT-R and DT-P groups were observed from the treatment with raw or pasteurized camel milk and not from other unrelated factors.

The present study on the hypoglycemic effect while consuming the local dromedary camel milk was found comparatively in line with the effect observed with other camel milk elsewhere the globe (Al-Amin 2006; Shori, 2015; Costa- Gouveia *et al*., 2017; Kamlesh & Asha 2020). Treatment with camel milk, whether raw or pasteurized, showed apparent and significant hypoglycemic effects in STZ-induced diabetic rats. Comparatively, the raw camel milk indicated prominent effect than pasteurized camel milk. During the three weeks experimental study, the reduction of blood glucose levels in DT-R and DT-P rats were 59% and 42% respectively and were in line with the earlier findings (Shori 2015; Kamlesh & Asha 2020). The reduced hypoglycemic activity of the pasteurized camel milk could be because of heating on the bioactive component(s) of the camel milk that facilitates the hypoglycemic effect.

The hypoglycemic activity of camel milk attributes to several factors. Few studies suggest that camel milk does not coagulate in the acidic media of the stomach (Othman 2016; Aida *et al*., 2019). Milk coagulation in the stomach takes place when the acid stable peptidases act on a sensitive sequence in the κ-casein proteins in the milk (Sakandar *et al*., 2018; Nascimento *et al*., 2016; Ejtahed *et al*., 2015; Al-Amin, 2006). Camel milk coagulates two to three times slower than cow milk (Shori, 2015). There is only a small quantity of κ-casein in camel milk (Konuspayeva *et al*., 2009) and it has structural differences from other species. Hence, it is not sensitive to coagulation (Konuspayeva *et al.*, 2009; Eitahed *et al.,* 2015; Shori 2015; Hattem, 2017; Kasmlesh & Asha 2020). Moreover, calcium plays an important role in the coagulation of proteins. Casein (65%) are linked to calcium in many dairy products while camel milk indicates 35% of the casein link with calcium (Brezovečki *et al*., 2015). Furthermore, one among the contributing factor is that of the moisture richness in camel milk during the summer season with fewer solids constituents that were observed to prevent earlier and complete coagulation (Brezovečki *et al.,* 2015). This also suggested the faster mobility of camel milk into the small intestine. Additionally, camel milk was found to have a high content of insulin (45-128 units/l) that reaches the intestinal mucosa unharmed with minimal digestion. Such diabetes can either be obtained as insulin present in camel milk or by beta cells stimulation through secretion. Earlier studies showed that camel milk augment insulin absorption and act within the body in a similarly to that of the endogenous insulin (Kamlesh 2020, Aida *et al.*, 2019; Shah *et al.,* 2019). Likewise, the high levels of antioxidants, especially vitamin C present in camel milk is found to improve insulin sensitivity to insulin receptors (Agrawal 2007).

Figure 1 showed seldom effect of STZ on blood cholesterol levels throughout the three weeks after induction of diabetes. Observations on the blood cholesterol levels in camel milk-treated groups (DT-R and DT-P) indicated significantly increase blood cholesterol levels when raw camel milk for three weeks was consumed while, this was not observed with the treatment

with pasteurized camel milk. Although this study has shown that the raw camel milk has more prominent hypoglycemic effect than the pasteurized camel milk, it could be a preferred option of diabetic patients to consume pasteurized rather raw camel milk to avoid the unwanted increase in blood cholesterol levels. Shori *et al.* (2015) revealed the consumption of camel milk does not affect total blood cholesterol levels in humans. However, the present study showed an increase in total cholesterol that was significant for raw camel milk. The possible attributes for these results could be related to the free form of cholesterol in the camel milk which makes it easier for the absorption in the intestine (Al-Amin *et al.,* 2006; Zibaee *et al.*, 2015). Camel milk is relatively high in cholesterol (31.32 mg/100 g) when compared to other kinds of milk, such as cow milk (25.63 mg/100 g), goat milk (13.0 mg/100 g), sheep milk (23.0 mg/100 g), and human milk (20mg/100g) (Brezovečki *et al*., 2015; Bouhaddaoui *et al*., 2019). Furthermore, there are many seasonal and regional differences that may reflect different concentrations of cholesterol and fatty acids in the camel milk (Bouhaddaoui *et al.*, 2019; Rahmeh *et al.*, 2019).

Conclusion

In the present study, both the raw and pasteurized camel milk has favorable TAG-lowering (hypotriglyceridemic) effect on DT-R and DT-P rat groups. Statistical comparison between these two treated groups revealed no significant differences between the impacts of the two camel milk types on blood TAG levels of the diabetic rats. Such TAG-lowering effects of consumption of camel milk may be attributed to the regulation of metabolism and improvised body functions (Kamlesh & Asha 2020). Thus, this study recommends the consumption of camel milk since, it not only increases the general body immunity but also a preferable option to diabetic patients due to their low glucose levels when compared to the cow or goat milk.

ACKNOWLEDGEMENTS

We express our profound gratitude for the support rendered by Kuwait University grant number YS06/07 and the College of Graduate Studies, Kuwait University, Kuwait.

References

Agrawal, R.P., Budania, S., Sharma, P., Gupta, R., Kochar, D.K., Panwar, R.B. *et al*., (2007) Zero prevalence of diabetes in camel milk consuming Raica community of north-west Rajasthan, India. Diabetes Research Clinic Practices, 76 **(2):** 290–296.

Agrawal, R.P., Sahani, M.S., Tuteja, F.C., Ghouri, S.K., Sena, D.S., Gupta, R. & Kochar, D.K. (2005) Hypoglycemic activity of camel milk in chemically pancreatectomized rats-An experimental study. International Journal of Diabetes in Developing Countries, 25:75-79.

Aida, A.K., Abdel, G.M., Abdel, G. & Abdulqader, A.A. (2019) Comparison of the hypoglycemic and antithrombotic (anticoagulant) actions of whole bovine and camel milk in streptozotocin-induced diabetes mellitus in rats. Journal of Dairy Science, 103 **(1):** 30-41.

Al-Amin, Z.M., Thomson, M., Al-Qattan, K.K., Shalaby, R.P. & Ali, M. (2006) Anti-diabetic and hypolipidemic properties of ginger (*Zingiber officinale*) in streptozotocin-induced diabetic rats. British Journal of Nutrition, 96: 660-666.

Al-Kandari, H., Al-Abdulrazzaq, D., Davidsson, L., Sharma, P., Al-Tararwa, A., Mandani, F. *et al.,* (2019) Incidence of Type 2 Diabetes in Kuwaiti children and adolescents: Results from the childhood-onset diabetes electronic registry (CODeR). Frontiers in Endocrinology, 10:836.

Boughellout, H., Choiset, Y., Rabesona, H, Chobert, J.M., Haertlé, T. & Zidoune, M.N. (2016) Camel's milk: A new source of proteins for children with cow's milk allergy? Revue francaise d'allergologie, Elsevier, 56 **(4)**:344-348.

Bouhaddaoui, S., Chabir, R., Errachidi, F., El-Ghadraoui, L., El-Khalfi, B., Benjelloun, M. & Soukri, A. (2019) Study of the biochemical biodiversity of camel milk. The Science World Journal, 2019: 1–7.

Brezovečki, A., Čagalj, M., DZrinka, F., Mikulec, N., Bendelja, L.D. & Antunac, N. (2015) Camel milk and milk products. Mljekarstvo, 65 **(2)**: 81-90.

Costa-Gouveia, J., Pancani, E., Machelart, J.S.A., Delorme, V., Salzano, G., Iantomasi, R., *et al.,* (2017) Combination therapy for tuberculosis treatment: pulmonary administration of ethionamide and booster co-loaded nanoparticles. Scientific Reports, 7:5390.

Ejtahed, H.S., Naslaji, A.N., Mirmiran, P., Yeganeh, M.Z., Hedayati, M., Azizi, F. *et al*., (2015) Effect of camel milk on blood sugar and lipid profile of patients with type 2 diabetes: a pilot clinical trial. International Journal of Endocrinology and Metabolism, 13**(1):** e21160.

Hattem, H.E. (2017) Effect of heat treatments and seasons of the year on the protective proteins in milk of different animals. Egyptian Journal of Agriculture Research, 95 **(1)**: 287-297.

Jilo, K. & Tegegne, D. (2016) Chemical composition and medicinal values of camel milk. International Journal of Research Studies & Biosciences, 4**(4):**13-25.

Kamlesh, P. & Asha, A. (2020) In-Silico comparative study of camel milk protein and insulin secondary structure. IOSR Journal of Pharmacy & Biological Sciences, 15**(4):**18-26.

Kappeler, SR., van den Brink, H.M., Rahbek-Nielsen, H., Farah, Z., Puhan, Z., Hansen, E.B. & Johansen, E. (2006) Characterization of recombinant camel chymosin reveals superior

properties for the coagulation of bovine and camel milk. Biochem Biophys Res Commun 342 **(2):** 647–654

Karaman, A.D., Yildiz, A., Öğüt, F., Seçilmiş, C.S.H. & Alvarez, V. (2021) Gross composition of raw camel's milk produced in Turkey. Food Science & Technology, E-pub 1-8. 2021.

Konuspayeva, G., Faye, B. & Loiseau, G. (2009) The composition of camel milk: A meta-analysis of the literature data. Journal of Food Composition & Analysis, 22: 95–101.

Koc, A. & Atasever, S. (2016) Production and characteristics of camel milk. Conference: I. International Selçuk-Ephesus symposium on culture of camel-dealing and camel wrestling at: Selçuk/İzmir/Turkey 1-14.

Nascimento, R.A.H., Cavalcanti, S., Urbano, S., Júnior, G., Bezerra, J.G., Neto, A. *et al*., (2016) Lactose intolerance and cow's milk protein allergy. Food Science & Technology, 36**(2):** 179-187.

Othman, A.S. (2016) Detection of bactericidal activity of camel's milk compared with raw and processed cow's milk against pathogenic bacteria. Egyptian Pharmaceuticals Journal, 15:31-7.

Pak, V.V., Khojimatov, O.K., Abdiniyazova, G.J., Elena, B. & Magay (2019) Composition of camel milk and evaluation of food supply for camels in Uzbekistan. Journal of Ethnic Food, 6:20.

Rahmeh, R., Alomirah, H., Akbar, A. & Sidhu, J. (2019) Composition and properties of camel milk, milk production, processing, and marketing. Khalid Javed Intech Open, 10.5772/intechopen.82592.

Rasheed Z. (2017) Medicinal values of bioactive constituents of camel milk: A concise report. International Journal of Health Science (Qassim), 11(**5**): 1–2.

Sakandar, H.A., Ahmad, S., Perveen, R., Aslam, H.K.W., Shakeel, A., Sadiq, F.A. & Imran, M. (2018) Camel milk and its allied health claims: a review. Progress Nutrition, 20 **(1):** 15-29.

SDS (2022) World of research diets, products and data sheets. efaidnbmnnnibpcajpcglclefindmkaj/https://sdsdiets.com/wpcontent/uploads/2021/02/vrf1-p.pdf

Shah, K., Yasobant, S. & Saxena, D. (2019) Camel milk for reduction of diabetes risk: Are we heading toward the right direction? Journal of Family Medicine & Primary Care, 8 (10): 3083-3085.

Shaltout, A.A., Wake, D., Thanaraj, T.A., Omar, D.M., Al-AbdulRazzaq, D., Channanath, A. *et al.,* (2017) Incidence of type 1 diabetes has doubled in Kuwaiti children 0-14 years over the last 20 years. Pediatric Diabetes, 18**(8)**:761–766.

Shori, A.B. (2015) Camel milk as a potential therapy for controlling diabetes and its complications: A review of in vivo studies. Journal of Food Drug Analysis, 23 **(4)**: 609-618.

Urazakov, N.U. & Baînazarov, S.H. (1974) The 1st clinic in history for the treatment of pulmonary tuberculosis with camel's sour milk. Problemy Tuberkuleza, 2: 89-90.

WHO (2021) World Health Organization. Draft recommendations to strengthen and monitor diabetes responses within national noncommunicable disease programmes, including potential targets.https://cdn.who.int/media/docs/default-source/searo/eb150---annex-2-diabetes)pdf?sfvrsn=b 01fa62_12 &download=true

Yagil R (1982) Camels and camel milk no. 26. Rome: Food and Agriculture Organization of the United Nations.

Yasmin, I., Iqbal, R., Liaqat, A., Khan, W.A., Nadeem, M., Iqbal, A. *et al*., (2020) Characterization and comparative evaluation of milk protein variants from Pakistani dairy breeds. Food Science & Animal Research, 40**(5):** 689–698.

Zibaee, S., Hosseini, S.M., Yousefi, M., Taghipour, A., Kiani, M.A. & Noras, M.R. (2015) Nutritional and therapeutic characteristics of camel milk in children: a systematic review. Electronic Physician, 7**(7)**: 1523–1528.

Submitted: 17/10/2021
Revised: 27/06/2022
Accepted: 03/07/2022
DOI: 10.48129/kjs.16777

Determination of antimicrobial resistance profiles and molecular detection of carbapenemases in Gram negative bacilli isolated from different sources in Mosul city, Iraq

Dr. Mahmood Zeki Al-Hasso*

Dept. of Biophysics College of Science, Mosul University, Mosul, Iraq

**Corresponding author: mahmoodalhasso@uomosul.edu.iq*

Abstract

The objectives of the present study were to determine the antimicrobial resistance profiles and evaluate the occurrence of metallo-β-lactamase and other carbapenemases in Gram-negative bacilli isolated from different sources in Mosul city. Bacterial isolates were recovered from clinical, veterinary, and environmental specimens and samples. Pure isolates were identified and tested for determination of their antimicrobial resistance profiles using disk diffusion method. Phenotypic detection of metallo-carbapenemase-producing bacteria was conducted using combined disk method. Imipenem-resistant strains were subjected to molecular detection of carbapenemase genes (*bla* $_{VIM}$, *bla* $_{KPC}$, *bla* $_{NDM}$, *bla* $_{OXA-48}$, *bla* $_{IMP}$) using multiplex PCR. Three hundred and ninety three bacterial isolates were recovered from (365) specimens and samples, 246 isolates (62.6%) were multi-drug resistant (MDR). The isolates were highly resistant to amoxicillin-clavulanic acid, tetracycline, cefotaxime, sulfamethoxazole, and ceftriaxone (96.7%, 65.1%, 64.1% and 63.6%, and 63.1% respectively). Carbapenems were the most effective antimicrobials used, the percentages of isolates resistant to imipenem and meropenem were (12.5%), and (10.7%), respectively. The study found that (7.4%) of the isolates were metallo-carbapenemase producers, phenotypically. Multiplex PCR results revealed that 47/49 (95.5%) imipenem-resistant isolates were positive for PCR detection test, isolates with double genes (*bla* $_{KPC}$ + *bla* $_{VIM}$ and *bla* $_{KPC}$ + *bla* $_{NDM}$) were the most prevalent (n=9; 18.4% for each), followed by *bla* $_{KPC}$ and *bla* $_{NDM}$ (n=8; 16.3% for each), and *bla* $_{VIM}$ (n=6; 12.2%). Three isolates (6.1%) were positive for *bla* $_{IMP}$ and two others (4.1%) were positive for each of *bla* $_{OXA-48}$ and *bla* $_{KPC}$ + *bla* $_{OXA-48}$, while two isolates (4.1%) gave a negative result for the test. In conclusion, carbapenemase genes were detected in the environmental isolates as well as in the clinical and veterinary ones, which might suggest the transmission of carbapenemase-producing bacteria and /or resistance determinants from clinical and veterinary settings to the environment.

Keywords: Carbapenemase genes; gram-negative bacilli; metallo-carbapenemase; Mosul (Iraq); multiplex PCR

1. Introduction

Carbapenems are the most powerful antimicrobial agents used nowadays for treating bacterial infections (Jean *at al.*, 2015; Livermore & Woodford 2000). Unfortunately, with the extensive use of these drugs, the occurrence of carbapenems-resistant Gram negative bacilli (GNB) has increased significantly representing a serious challenge facing the use of antimicrobials in all aspects (Ali *et al.,* 2021; Jean *at al.*, 2015; Nordmann *et al*., 2011). However, carbapenemase production is considered as the most prevalent mechanism used by the resistant bacteria to overcome the cidal action of carbapenems (Queenan & Bush 2007).

β-lactamases are classified based on the functional classification into four groups (1-4), or according to Ambler molecular classification into four classes (A-D) (Bush and Jacoby 2010; Ambler *at al*., 1980). Carbapenemases are currently located within the functional groups 2d, 2f, 3, and according to the molecular classification their types fall within the classes A, B, and D (Jean *at al.*, 2015; Queenan & Bush 2007; Ambler *at al*., 1980). The emergence of carbapenemases in Gram-negative bacilli is rapidly increasing especially during the past years (Loqman *et al*., 2021; Karabay *et al*., 2016), consequently these enzymes reduce the effectiveness of carbapenems which are the last resort against severe bacterial infections that are resistant to treatment in hospitals and various health institutions (Jean *at al.*, 2015; Nordmann *et al*., 2011; Queenan & Bush 2007).

Class A carbapenemases are one of the serine β-lactamases characterized by their sensitivity to clavulanic acid and other traditional β-lactamase inhibitors, they include: Guiana Extended Spectrum enzymes (GES), *S. marcescens* enzymes (SME), Imipenem- hydrolyzing β-lactamase (IMI), *K.pneumoniae* Carbapenemases (KPC), and Non-Metallo Carbapenemases (NMC) (Jean *at al.*, 2015; Queenan & Bush 2007).

Class B carbapenemases are metallo enzymes with expanded capabilities to degrade almost all β-lactams without being affected by traditional β-lactamase inhibitors (Bush and Jacoby 2010). They have zinc divalent cations in their active sites crucial for the enzymatic activity (Bush and Jacoby 2010; Ambler *at al*., 1980). Metallo-carbapenemases are usually inhibited by chelator compounds such as EDTA. Among metallo β-lactamases, Verone integron mediated metallo enzymes (VIM), Imipenemase (IMPs), and New Delhi metallo enzymes (NDM) are the most prevalence, whereas Sao Paulo metallo enzymes (SPM), Seoul Imipenemase (SIM), German Imipenemase (GIM) are nearly endemic (Bush and Jacoby 2010; Queenan & Bush 2007; Ambler *at al*., 1980).

Class D carbapenemases (also known as OXA enzymes) are specifically present in the MDR- *Acinetobacter baumannii* and have been responsible for many hospital's outbreaks associated with high mortality rates. Isolates of GNB other than *A. baumannii* carrying $bla_{\text{OXA-48}}$ genes were also reported (Loqman *et al*., 2021; Carrër *et al*., 2008). These enzymes are distinguished by their lack of inhibition by both clavulanic acid and EDTA (Bush & Jacoby 2010; Queenan & Bush 2007). Among the most important enzymatic types of this group are: OXA-48, OXA-58, OXA-23, and OXA-24 (Bush & Jacoby 2010).

The occurrence and global spread of carbapenemase-producing bacteria (CPB) represent an urgent concern worldwide, with the growing sources for these resistant strains not only in the health and veterinary settings but even in the environment and the community as well (Guerra *et al*., 2014; Nordmann *et al*., 2011; Queenan & Bush 2007). The real prevalence of CPB in Mosul city is not well understood. Therefore, it is essential to conduct a surveillance studies investigating the occurrence of CPB in Mosul and use the collected data in the formulation of control measures that assist in the prevention of their spread. Since the detection of β-lactamases, including carbapenemases, represents the first most important step in evaluating their dissemination and prevalence (Elbadawi *et al*., 2021; Al-Hasso & Khalaf 2020; Cui *et al*., 2019), the present work aimed to screen different bacterial species isolated from various sources in Mosul city for the presence of metallo-β-lactamases (class B) and determine the prevalent carbapenemase genes.

2. Materials and Methods

The study was conducted in Mosul city, Iraq for the period from April 2019 to October 2020. The study included 365 specimens and samples (clinical, veterinary, and environmental). The clinical specimens (n=120) were varied between pus, sputum, urine, and diarrhea taken from patients who visited several Mosul hospitals, while the veterinary specimens (n=135) represented by rectal swabs of infected chicken with diarrhea from poultry farms in Mosul. Environmental samples (n=110) were taken from different sources (soil and water bodies) and different sites of the city. The study and data accumulation were carried out with the approval of Biophysics Dept. Board No. 28c on 27/3/2019.

2.1. Bacterial Isolation and Identification

For the isolation and the identification of bacteria, all specimens and samples were treated with the standard bacteriological methods. Briefly, the samples were grown on special culture media, which included MacConkey agar, blood agar, and nutrient agar (Himedia Co., India). The pure isolates were subjected to microscopic examination after staining with Gram's stain, in addition to biochemical tests (IMViC, oxidase, nitrate reduction, DNase, carbohydrate fermentation, TSI, gelatin liquefaction, phenylalanine deaminase, and urease). Bacterial isolates were identified presumptively based on their morphological shapes, cultural characteristics, and biochemical tests (Procop *et al*., 2017; MacFaddin 1980).

2.2. Antimicrobial Susceptibility Testing (AST)

AST was conducted for all bacterial isolates against different groups of antimicrobials (Bioanalyse Co., Turkey) using Kirby-Bauer disc diffusion method. Briefly, Mueller-Hinton agar plates were inoculated with fresh bacterial inoculums equivalent to 0.5 McFarland standards and incubated at 35^{o}C for 16-18 hrs. after applying antimicrobial disks. The results were interpreted based on CLSI recommendations (CLSI 2021). Standard strains *P. aeruginosa* ATCC 27853 and *E.coli* ATCC 25922 were used as qualitative control. Bacterial

isolates resistant to three or more different classes of antimicrobials were considered as Multi-Drug Resistant strains (CLSI 2021; Thapa *et al*., 2017).

2.3. Phenotypic Detection of Metallo-Carbapenemase-Producing Strains

A suspension of the fresh bacterial culture equivalent in turbidity to 0.5 McFarland standard tube was used, the suspension was diluted (1:10), and inoculated on a Mueller-Hinton Agar plate. Two discs of meropenem, one with 10 µl of (0.5 M) EDTA and another without EDTA, were placed on the medium (25mm apart). An increase in the diameter of the inhibition zone equal to 7 mm or more in the case of the EDTA-containing disc compared with the other disc was considered as a positive result of the screening test (Thapa *et al*., 2017; Franklin *et al*., 2006).

2.4. Molecular Detection of Carbapenemase-Producing Strains

Carbapenem resistant isolates were molecularly tested for the presence of carbapenemase genes (*bla*$_{VIM}$, *bla*$_{KPC}$, *bla*$_{NDM}$, *bla*$_{OXA-48}$, *bla*$_{IMP}$) using multiplex PCR technique. Preparation of DNA template was performed according to Presto Mini gDNA Bacteria Kit from Geneaid Biotech Ltd. (www.geneaid.com). Molecular detection was conducted using 96-well thermal cycler Optimus 96G, England. The reaction mixture (50 µl) composed of (25 µl) master mix (Bioneer co.) and (1 µl) DNA template. The concentrations of each of the forward and reverse primers used in a single PCR tube were as follows: 15 pmoles/µl for *bla*$_{KPC}$, *bla*$_{IMP}$, and *bla*$_{VIM}$; 20 pmoles/µl for *bla*$_{NDM}$; and 25 pmoles/µl for *bla*$_{OXA-48}$. The PCR program performed was as follows; an initial denaturation step at 95°C for 5 min, then 35 cycles of DNA denaturation at 95°C for 45 s, and primer annealing at 60°C for 45 s. Primer extension was at 72°C for 1 min, and final extension at 72°C for 8 min (Amer *et al*., 2016; Doyle *et al*., 2012). PCR products were examined by agarose gel electrophoresis with 1.5% agarose in 0.5x Tris-borate-EDTA (TBE) buffer. Gene bands were visualized and confirmed with the aid of a UV transilluminator. Table (I) summarizes the amplicon sizes and the primer sequences used in the study.

Table 1. Primers used for the detection of carbapenemase genes.

Carbapenemase gene	Amplicon size (bp)	Primer sequences*
*bla*KPC	900	5'-TGTCACTGTATCGCCGTC-3' 5'-CTCAGTGCTCTACAGAAAACC-3'
*bla*IMP	587	5'-GAAGGCGTTTATGTTCATAC-3' 5'-GTACGTTTCAAGAGTGATGC-3'
*bla*VIM	389	5'-GTTTGGTCGCATATCGCAAC-3' 5'-AATGCGCAGCACCAGGATAG-3'
*bla*NDM	782	5'-GCAGCTTGTCGGCCATGCGGGC-3' 5'-GGTCGCGAAGCTGAGCACCGCAT-3'
*bla*OXA-48-like	438	5'-GCGTGGTTAAGGATGAACAC-3' 5'-CATCAAGTTCAACCCAACCG-3'

* The first and second primers for each gene are forward and reverse primers, respectively.

2.5. Statistical Analysis

Data was statistically analyzed using one-way ANOVA (SPSS software ver. 21) for the comparison of categorical data, p-values of ≤ 0.05 and ≤ 0.01 were considered as significant and highly significant, respectively. Additionally, percentages were used for the expression of antimicrobial resistance profiles and phenotypic metallo-β-lactamase detection results.

3. Results

From the total of 365 specimens and samples collected in the study, 393 bacterial strains were isolated (Figure 1). The isolation rates varied according to the bacterial species and the source of the isolation. *E.coli* isolates had the highest percentage (n=109, 27.7%), while *Serratia marcescens* was the lowest (n=21, 5.4%). The number and percentage of bacteria that were isolated from environmental samples were the highest (n=156, 39.7%) with a highly significant difference at p-value ≤ 0.01 in comparison to that isolated from clinical specimens (n=109, 27.7%). On the other hand, the number of bacteria isolated from veterinary specimens (n=128, 32.6%) has a significant difference at p-value ≤ 0.05 in comparison to clinical specimens. There was no significant difference between bacterial numbers isolated from veterinary specimens and environmental samples (Figure 1).

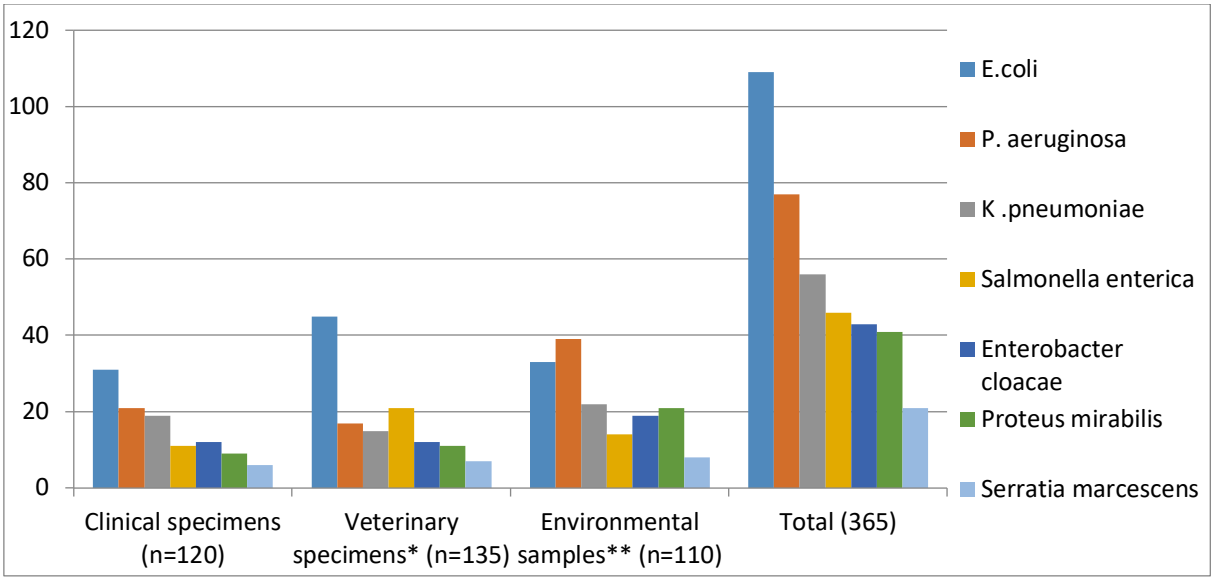

* Significant difference between total bacterial number isolated from veterinary and clinical specimens at p≤ 0.05.
** Highly significant difference between total bacterial number isolated from environmental samples and clinical specimens at p≤ 0.01.

Fig. 1. Number and sources of bacterial isolates used in the study.

Of the total 393 bacterial isolates recovered in the study, 380 (96.7%) were resistant to amoxicillin-clavulanic acid, which proved to be ineffective against the vast majority of the studied isolates. The percentage of resistance to ceftazidime, cefotaxime and ceftriaxone was (57%), (64.1%) and (63.1%) respectively (Table 3). The isolates showed high resistance to tetracycline and sulfamethoxazole (65.1% and 63.6%, respectively), their resistance to

ciprofloxacin was (20.6%). Carbapenems were the most effective antimicrobials used, the percentages of isolates resistant to imipenem and meropenem were (12.5%), and (10.7%), respectively (Table 2). The results showed that 246 out of 393 isolates (62.6%) were Multi-Drug Resistant (MDR) where *P. aeruginosa*, *S.enterica* , and *K.pneumoniae* isolates represented the most MDR strains. The most antimicrobial-resistant isolates were from clinical specimens followed by veterinary specimens, while isolates from environmental samples were the least resistant to antimicrobials (Figure 2).

Table 2. Number and percentage (%) of antimicrobial resistant isolates.

Bacterial species	Antimicrobials tested *										
	CTX	CAZ	IPM	MEM	CRO	AMC	FOX	CIP	TET	SXT	GEN
E.coli (n=109)	60(55)	49(45)	13(11.9)	10(9.2)	59(54.1)	99(90.8)	68(62.4)	22(20.2)	68(62.4)	61(56)	45(4.3)
P. aeruginosa (n=77)	59(76.6)	52(67.5)	18(23.4)	15(19.5)	49(63.6)	77(100)	67(87)	26(33.8)	63(81.8)	63(81.8)	65(84.4)
K .pneumoniae (n=56)	47(83.3)	47(83.9)	10(17.9)	9(16.1)	(80.3)45	56(100)	38(67.9)	17(30.6)	47(83.9)	(80.3)45	39(69.6)
S. enterica (n=46)	33(71.7)	30(65.2)	8(17.4)	8(17.4)	39(84.8)	46(100)	29(63)	8(17.4)	36(78.3)	37(80.4)	27(58.7)
E. cloacae (n=43)	6(60.5)2	20(46.5)	0(0)	0(0)	26(60.5)	43(100)	14(32.6)	3(7)	15(34.9)	17(39.5)	6(14)
P. mirabilis (n=41)	10(24.4)	9(22)	0(0)	0(0)	15(36.6)	39(95.1)	(51.2) 21	3(7.3)	16(39)	18(43.9)	6(14.6)
S. marcescens (n=21)	17(81)	17(81)	0(0)	0(0)	15(71.4)	20(95.2)	11(52.4)	2(9.5)	11(52.4)	9(42.8)	3(14.3)
Total (n=393)	252(64.1)	224(57)	49(12.5)	42(10.7)	248(63.1)	380(96.7)	248(63.1)	81(20.6)	256(65.1)	250(63.6)	191(48.6)

* CXT: cefotaxime, CAZ: ceftazidime, IPM: imipenem, MEM: meropenem, CRO: ceftriaxone, AMC: amoxicillin-clavulanic acid , FOX: cefoxitin, CIP: ciprofloxacin, TET: tetracycline, SXT: sulfamethoxazole, GEN: gentamicin

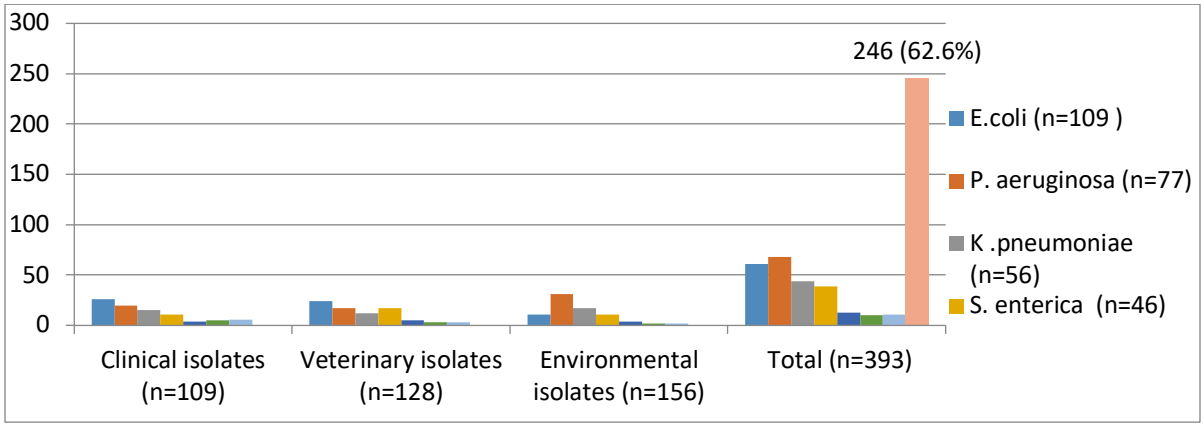

Fig. 2. Number, percentage (%), and sources of Multi-Drug Resistant (MDR) isolates.

Among the 393 bacterial isolates of Gram-negative bacilli recovered in the study, 29 isolates (7.4%) gave a positive result for the detection test of metallo-carbapenemase production according to the compound disc method used (Figure 3). *P. aeruginosa* isolates were the most producing species compared to the rest of the isolates (n=14, 18.2%), followed by *E.coli*, *K. pneumoniae* and *Salmonella enterica* (7.3%, 7.1%, and 6.5%, respectively) (Figure 4). It is noteworthy that 13 isolates out of 109 (11.9%) were from clinical specimens, 10/128 isolates (7.8%) were from veterinary specimens, and 6/156 isolates (3.8%) were from environmental samples (Figure 4).

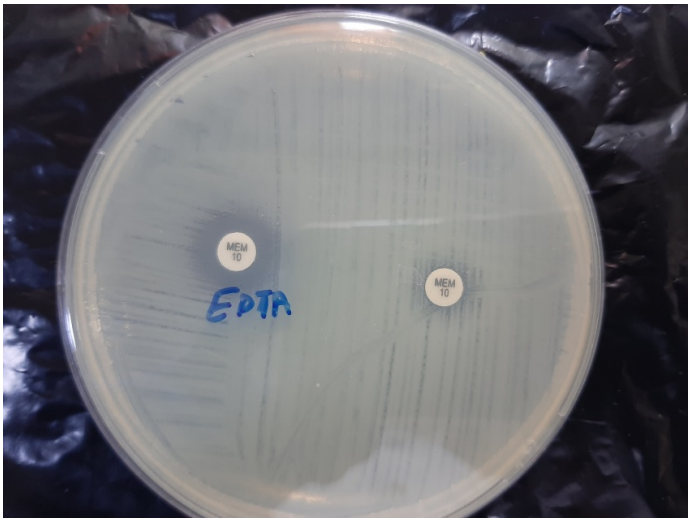

Fig. 3. Phenotypic metallo-carbapenemase detection by combined disk method.

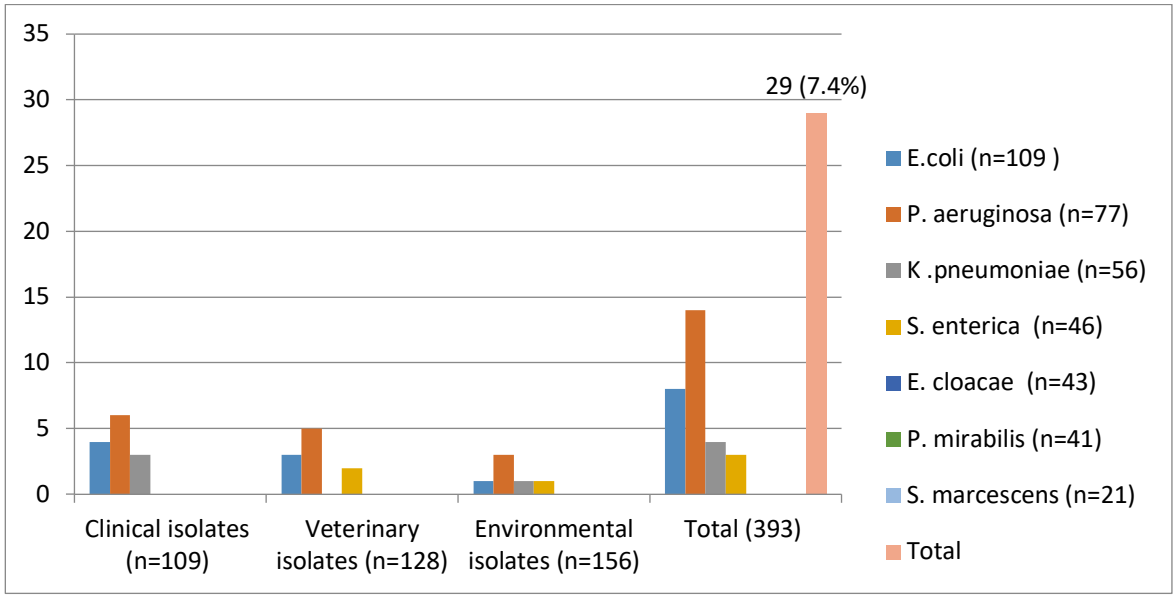

Fig. 4. Number and percentage (%) of phenotypically metallo-carbapenemase positive isolates.

Out of 49 imipenem resistant isolates, 47 isolates (95.5%) were positive for the molecular detection by multiplex PCR. The most prevalent genes detected were bla_{KPC} + bla_{VIM} and bla_{KPC} + bla_{NDM} (n=9; 18.4% for each), followed by bla_{KPC} and bla_{NDM} (n=8; 16.3% for each), and bla_{VIM} (n=6; 12.2%). Three isolates (6.1%) were positive for bla_{IMP} and two others (4.1%) were positive for each of bla_{OXA-48} and bla_{KPC} + bla_{OXA-48}, while two isolates (4.1%) gave a negative result for the PCR molecular detection test (Table 3).

Table 3. Distribution of carbapenemase genes among bacterial isolates.

Carbapenemase gene	*P. aeruginosa* (n=18)			*E.coli* (n=13)			*K .pneumoniae* (n= 10)			*S. enterica* (n=8)			Total (n= 49)
	C*	V	E	C	V	E	C	V	E	C	V	E	
bla_{KPC}	2			2	1	1	-		2	-			8(16.3%)
bla_{IMP}	2			1			-			-			3(6.1%)
bla_{VIM}	2	1	1	-			1			1			6(12.2%)
bla_{NDM}	1	1		-	1		-	1		1	1	2	8(16.3%)
$bla_{OXA-48-like}$	-			1			1			-			2(4.1%)
bla_{KPC} + bla_{VIM}	2	2	1	1			1		1	1			9 (18.4%)
bla_{KPC} + bla_{NDM}	3			1	1		-	2		1		1	9 (18.4%)
bla_{KPC} + $bla_{OXA-48-like}$	-			1			1			-			2 (4.1%)
PCR negative	-					2	-			-			2(4.1%)
Total genes detected													**47 (95.9%)**

* C: clinical isolates ; V: veterinary isolates ; E: environmental isolates

4. Discussion

In this study (393) Gram-negative bacilli were isolated from (365) clinical, veterinary, and environmental specimens and samples. The isolated species included: *K. pneumoniae, E.coli*, *P. aeruginosa*, *S. marcescens, S. enterica*, *E. cloacae*, and *P. mirabilis* with various isolation rates (Figure 1). The isolates showed variable antimicrobial resistance patterns ranged between high resistance rates to amoxicillin-clavulanic acid, tetracycline, cefotaxime and sulfamethoxazole (96.7%, 65.1%, 64.1% and 63.6% respectively) and low resistance rates to ciprofloxacin, imipenem and meropenem (20.6%, 12.5% and 10.7%, respectively as shown in Table 2). Our results revealed that (246) isolates (62.6%) were MDR strains (Figure 2). These findings are lower than the results reported by Thapa *et al*. (2017) in their study conducted on clinical Gram negative bacteria isolated in Nepal where resistance rates to cefotaxime, ciprofloxacin, ceftazidime, imipenem, sulfamethoxazole and gentamicin were 89%, 76%, 43.9%, 8.3%, 72% and 65% respectively. Loqman *et al*. (2021) also reported, in their study conducted in Morocco on clinical *Enterobacteriaceae* isolates, higher rates in comparison to our results (ciprofloxacin 87%, sulfamethoxazole 87.8% and gentamicin 100%). In China, Zhang *et al*. (2018) found that 26.8%, 36.6% and 43.9% of carbapenem-resistant clinical *K .pneumoniae* isolates were resistant to ciprofloxacin, sulfamethoxazole, and gentamicin, respectively and these results were lower than ours (30.6%, 80.3% and

69.6%, respectively), however their resistance rates to ceftazidime and ceftriaxone were 100% for each antibiotic compared to 83.9% and 80.3% reported in the present study. Our results were close to the findings of an Iranian study (Rahbar *et al*., 2008) as they reported 40% and 30% resistance rates for *K. pneumoniae* and *P. aeruginosa* clinical isolates to ciprofloxacin (we reported 30.6% and 33.8%, respectively), as well they reported 80% and 73% resistance rates to ceftazidime, respectively for both species in comparison to 83.9% and 67.5% in our study. In the study of Loqman *et al*. (2021) they reported the occurrence of carbapenems resistance in 131/1603 (8.2%) clinical strains of *Enterobacteriaceae* and this result was close to ours (Table 2). As for MDR *P. aeruginosa* and *K. pneumoniae*, our results were higher (88.3% and 78.6% respectively) in comparison to (44.4% and 38.7%, respectively) that reported by Thapa *et al*. (2017) but similar for MDR *E.coli* (56%) and lower than MDR *Enterobacter* and *P. mirabilis* (30.2% and 24.4%, respectively). Our results showed that 62.6% of the isolates were MDR, as 246 isolates out of 393 were resistant to three basic groups of antimicrobials (clinical isolates gave the largest rate (79.8%), followed by veterinary (63.3%), and environmental (50%) isolates as illustrated in figure 2. This indicates the occurrence and the prevalence of MDR strains even in the environmental samples which are supposed to be low in rates, this may be attributed to the misuse, irresponsible, and often unmonitored use of antimicrobials, specifically β-lactams, as discussed later.

As illustrated in figure 4, among 393 isolates recovered in the present study, only 29 isolates (7.4%) were found to be metallo-carbapenemase producing bacteria by EDTA Combined Disk (CD) method. The positive isolates include *P.aeruginosa* (n=14), *E.coli* (n=8), *K.pneumoniae* (n=4), and *S.enterica* (n=3). Thirteen of them were isolated from clinical specimens, 10 were isolated from veterinary specimens while the other six were from environmental samples (Figure 4). Our results were close to the findings of Thapa *et al*. (2017) who reported a detection rate of 5.8% among 362 Gram negative isolates, but higher than that reported by Mishra *et al*. (2012) which was 1.3% of GNB isolated from lower respiratory tract infections in Nepal and that reported by Al-Charrakh *et al*. (2016) which was 5.3% of *P.aeruginosa* isolates recovered from clinical specimens in Baghdad (Iraq). On the other hand, our findings were lower than that reported by Amer *et al*. (2016) which was 19.1% of clinical *Enterobacteriaceae* isolated in Egypt, and Jamal *et al*. (2020) in their study conducted in Iraq as they found that (17.1%) of *K.pneumoniae* clinical isolates were positive for metallo-β-lactamases (MBLs) detection test. Elbadawi *et al*. (2021) also reported a phenotypic detection rate for (MBLs) of 50.9% among Carbapenem-Resistant *Enterobacteriaceae* (CRE) isolated from hospitalized patients in Sudan, while Loqman *et al*. (2021) found that 25.9% of CRE were positive for metallo- carbapenemase CD detection test. Also, Anoar *et al*. (2014) reported in their study conducted in Sulaimani city (Iraq) that 46/177 isolates (25.9%) of the clinical Gram negative bacteria tested were MBLs positive. Moreover, in the studies of Bhat *et al.* (2013) in India and Hussein *et al*. (2018) in Wasit city (Iraq) they found that (37% and 31%, respectively) of *Pseudomonas* clinical isolates were

MBLs positive by EDTA double-disc test, these result are almost double than ours as we reported 18.2% of *P. aeruginosa* isolates with positive detection test (Figure 4).

Molecular detection of carbapenemase genes by multiplex PCR revealed that 20 isolates out of 49 tested (40.8%) have double genes (bla_{KPC} + bla_{VIM} 9/49, bla_{KPC} + bla_{NDM} 9/49, bla_{KPC} + bla_{OXA-48}- 2/49). As single genes, bla_{KPC} and bla_{NDM} were the most prevalent genes (8/49, 16.3% for each) followed by bla_{VIM} (6/49, 12.2%). The total detection rate was 95.9% as two isolates were negative for the detection test (Table 3). These findings are in consistence with the results of Amer *et al*. (2016) and Kazi *et al*. (2015) who reported a detection rate of carbapenemase genes of 97.7% and 98.2% respectively, but higher than the results of Elbadawi *et al*. (2021) and Jamal *et al.* (2020) who reported a molecular detection rate of 58.7% and 50%, respectively with bla_{NDM} being the most prevalent gene in comparison to other genes. The gene bla_{KPC} was most frequently detected in *P. aeruginosa* isolates followed by *E.coli*, *K. pneumoniae*, and *S. enterica* isolates, this finding was in contrast to what Amer *et al*. (2016) found in their study as they reported the occurrence of bla_{KPC} in *K. pneumoniae* more frequently in comparison to other species. This may be attributed to the differences in the number of isolates and source of isolation in both studies. Interestingly, carbapenemase genes were detected in environmental isolates as well as in clinical and veterinary ones, which might suggest the existence of interplay between the three ecologies (clinical, veterinary, and environmental) in the transmission of resistant strains.

The results of the present study indicate the occurrence and the dissemination of CPB among bacterial isolates recovered from various specimens and samples in Mosul city. These findings represent a preliminary evidence of the existence of a relationship between the different sources of isolation. This is probably attributed to the wide use of antimicrobials in medical and veterinary aspects which contributes, as a selective factor, in accelerating the emergence of resistant strains possessing these enzymes (Ali *et al*., 2022; Bonardi & Pitino 2019; Zurfluh *et al*., 2017; Bhat *et al*., 2013). Furthermore, the resistance genes mediated by transmissible elements such as plasmids, transposons, and integrons play a great role in increasing the frequency of dissemination of these enzymes through horizontal genetic transfer between bacterial species (Ali *et al*., 2022; Le Terrier *et al*., 2020; Kazi *et al*., 2015).

The presence of CPB among environmental strains as well as among clinical and veterinary ones may suggest the possibility of clonal or strain dissemination from other sources which might be hospitals, or veterinary farms in which antimicrobials are used a lot whether as a therapy, a prophylaxis or as a growth promotors (Le Terrier *et al*., 2020; Bonardi & Pitino 2019; Zurfluh *et al*., 2017; Hamza *et al*., 2016). The resistant strains as a consequence of the selective pressure imposed by these drugs will flourish and dominate in these establishments and reach the environment through the effluent water, wastewater, discharged patients and poultry products. Thus, the environment will become an emergence source for the dissemination of these strains added to the existing ones (Hamza *et al*., 2016; EFSA 2013 ; Pesapane *et al*., 2013). The similarity between the environmental and the clinical CPB has been reported by Khan *et al*. (2018) who suggested the dispersion of these

strains from hospitals to aquatic environment and the probability of their presence in the community.

The detection of carbapenemase genes in 95.5% of the carbapenem resistant strains raises the alarm when taking into account the fact that carbapenems are the most effective and powerful agents currently available for treating bacterial infections and they represent our last line of defense in the face of resistant microorganisms. These results also shed light on the fact that such mechanism used by bacteria to resist carbapenems are present within the arsenal of local isolates in Mosul city, including environmental isolates and it is undoubtedly increasing with the continued use of carbapenems in hospitals and other health institutions in Mosul city recently.

5. Conclusion

The current study aimed primarily to detect the occurrence and the prevalence of carbapenemase genes in Gram-negative bacilli isolated from clinical, veterinary, and environmental sources in Mosul city. The results showed the presence of these enzymes in the environmental strains as well as in the clinical and veterinary ones, which indicates the emergence and the spread of such strains in the city's environments as well, rendering them to a new source for the dissemination of carbapenemase producing bacteria in the future with the growing use of carbapenems in the city. The outputs of the study concentrate mainly on the necessity of taking measures to control and monitor carbapenems usage in order to prevent the dissemination of CPB from health and veterinary settings to the environment.

ACKNOWLEDGMENT

The present work was supported by: Biophysics Department\ College of Science\ Mosul University\ Mosul \ Iraq.

References

Al-Charrakh A.H., Al-Awadi S.J. & Mohammed A.S. (2016) Detection of metallo-β-lactamase producing *Pseudomonas aeruginosa* isolated from public and private hospitals in Baghdad, Iraq. Acta Medica Iranica, 54 (2): 108-113

Al-Hasso M.Z. & Khalaf S.H. (2020) Comparison of five methods for detection of extended spectrum β-lactamases in Gram negative enteric bacteria. Karbala International Journal of Modern Sciences, **6** : 62-67.

Ali F., Shakeela Q., Uzma B., Bibi A., Najeeb B., Rahman A., Shah M. & Ahmed, S. (2022) Antimicrobial resistance pattern and phenotypic detection of ESBL-and MBL-producing *Pseudomonas aeruginosa* isolated from indoor-patients suffering ear discharge. Kuwait Journal of Science, **49**: 1-9.

Ali F., Kamal S., Shakeela Q. & Ahmed S. (2021) Extended-spectrum and Metallo-beta lactamase enzymes mediated resistance in *Pseudomonas aeruginosa* in clinically isolated specimens. Kuwait Journal of Science, **48**: 1-9.

Anoar K.A., Ali F.A., & Omer S.A. (2014). Detection of metallo-β-lactamase enzyme in some Gram negative bacteria isolated from burn patients in Sulaimani city, Iraq. European Scientific journal, **10** (3). 485-496.

Ambler R.P. (1980) The structure of β-lactamases. Philosophical Transactions of Royal Society London B Biological Sciences, **289**: 321–331.

Amer W.H., Khalil H.S. & Abd Elwahab M.A.A. (2016) Characterization of carbapenem resistant *Enterobacteriaceae* in risk factors , phenotypic and genotypic characterization of carbapenem resistant *Enterobacteriaceae* in Tanta University Hospitals , Egypt. International Journal of Infection Control, **12**: 1–11.

Bhat S., Sharma R. & Euphemia Z. (2013) Carbapenem resistance in clinically significant non fermenting Gram negative bacilli. Journal of Evolution Medical and Dental Sciences, **2** : 9131-9134.

Bonardi S. & Pitino R. (2019) Carbapenemase-producing bacteria in food-producing animals, wildlife and environment: A challenge for human health. Italian Journal of food safety, **8** : 77-92.

Bush K. & Jacoby G.A. (2010) Updated functional classification of β-lactamases. Antimicrobial Agents and Chemotherapy, **54**: 969–976.

Carrër A., Poirel L., Eraksoy H., Cagatay A.A., Badur S. *et al.,* (2008) Spread of OXA-48-positive carbapenem-resistant *Klebsiella pneumoniae* isolates in Istanbul, Turkey. Antimicrobial Agents and Chemotherapy, **52**: 2950–4.

Clinical and Laboratory Standards Institute CLSI. (2021) Performance standards for antimicrobial susceptibility testing. Thirty first informational supplement update. CLSI document M100, M02, M07, and M11 Clinical and Laboratory Standards Institute, Wayne, PA, USA

Cui X., Zhang H. & Du H. (2019) Carbapenemases in *Enterobacteriaceae*: detection and antimicrobial therapy. Frontiers in Microbiology, **10**: 1823.

Doyle D., Peirano G., Lascols C., Lloyd T., Church D. *et al.,* (2012) Laboratory detection of *Enterobacteriaceae* that produce carbapenemases. Journal of Clinical Microbiology, **50** (12): 3877-3880.

EFSA Panel on Biological Hazards (BIOHAZ). (2013) Scientific opinion on carbapenem resistance in food animal ecosystems. EFSA Journal, **11**: 3501.

Elbadawi H.S., Elhag K.M. & Mahgoub E. (2021) Detection and characterization of carbapenem resistant Gram-negative bacilli isolates recovered from hospitalized patients at Soba University Hospital, Sudan. BMC Microbiology, **21:** 136.

Franklin C., Liolios L. & Peleg A.Y. (2006) Phenotypic detection of carbapenem-susceptible metallo-β-lactamase-producing Gram-negative bacilli in the clinical laboratory. Journal of Clinical Microbiology, **44**: 3139- 3144.

Guerra B., Fischer J. & Helmuth R. (2014) An emerging public health problem: acquired carbapenemase-producing microorganisms are present in food-producing animals, their environment, companion animals and wild birds. Veterinary Microbiology, **171**: 290-297.

Hamza E., Dorgham S.M. & Hamza D.A. (2016) Carbapenemase-producing *Klebsiella pneumoniae* in broiler poultry farming in Egypt. Journal Global Antimicrobial Resistance, **7**: 8-10.

Hussein Z.K., Kadhim H.S. & Hassan J. S. (2018) Detection of New Delhi metallo-beta-lactamase-1 ($bla_{\text{NDM-1}}$) in carbapenem-resistant pseudomonas aeruginosa isolated from clinical samples in Wasit hospitals. Iraqi JMS, **16** (3): 239-246.

Jamal N. A., AL-Khafaf M. N. & Abdulazeez S. M. (2020) Detection of Metallo β-lactamase in *Klebsiella pneumoniae* isolated from upper respiratory tract of carrier individuals in Iraq. Systematic Reviews in Pharmacy, 11(12): 1896-1900.

Jean S.S., Lee W.S., Lam C., Hsu C.W., Chen R.J. *et al.,* (2015) Carbapenemase-producing Gram-negative bacteria: current epidemics, antimicrobial susceptibility and treatment options. Future Microbiology, **10**: 407-25.

Karabay O., Altindis M., Koroglu M., Karatuna O., & Aydemir Ö.A. (2016) The carbapenem - resistant *Enterobacteriaceae* threat is growing : NDM - 1 epidemic at a training hospital in Turkey. Annals Clinical Microbiology Antimicrobials, **15**: 1–6.

Kazi M., Drego L., Nikam C., Ajbani K., Soman R., *et al.,* (2015) Molecular characterization of carbapenem-resistant *Enterobacteriaceae* at a tertiary care laboratory in Mumbai. European Journal of Clinical Microbiology & Infectious Diseases, **34 (3**): 467-472.

Khan F.A., Hellmark B., Ehricht R., Söderquist B. & Jass J. (2018) Related carbapenemase-producing Klebsiella isolates detected in both a hospital and associated aquatic environment in Sweden. European Journal of Clinical Microbiology & Infectious Diseases, **37**: 2241-2251.

Le Terrier C., Masseron A., Uwaezuoke N.S., Edwin C.P., Ekuma A.E. *et al.,* (2020) Wide spread of carbapenemase-producing bacterial isolates in a Nigerian environment. Journal Global Antimicrobial Resistance , **21**: 321-323.

Livermore D.M. & Woodford N. (2000) Carbapenemases: a problem in waiting? Current Opinion in Microbiology, **3**: 489-495.

Loqman S., Soraa N., Diene S.M. & Rolain J.M. (2021) Dissemination of carbapenemases (OXA-48, NDM and VIM) producing *Enterobacteriaceae* isolated from the Mohamed VI University hospital in Marrakech, Morocco. Antibiotics, **10**: 492.

MacFaddin J.F.M. (1980) Biochemical tests for identification of medical bacteria. Williams & Willkins Inc., Baltimor. Pp: 156.

Mishra S.K., Acharya J., Kattel H.P., Koirala J., Rijal B.P. *et al.,* (2012) Metallo-β -lactamase producing Gram-negative bacterial isolates. Journal of Nepal Health Research Council, **10**: 208-213.

Nordmann P., Naas T. & Poirel L. (2011). Global spread of Carbapenemase producing *Enterobacteriaceae*. Emerging Infectious Diseases, **17**: 1791–1798.

Pesapane R., Ponder M. & Alexander K.A. (2013) Tracking pathogen transmission at the human–wildlife interface: banded mongoose and *Escherichia coli*. Ecohealth, **10** : 115-128.

Procop G.W., Church D.L., Hall G.S., Janda W.M. & Koneman E.W. (2017) Koneman's color atlas and textbook of diagnostic microbiology. 7th ed. Wolters Kluwer, Philadelphia PA, USA, Pp: 238

Queenan A.M. and Bush K. (2007) Carbapenemases: the versatile β-lactamases. Clinical Microbiology Review, **20**: 440–58.

Rahbar M., Monnavar M., Vatan K.K., Haqi A.F. & Shakerian F. (2008) Carbapenem resistance in Gram-negative bacilli isolates in an Iranian 1000-bed Tertiary Hospital. Pakistani Journal of Medical Sciences, **24**: 537-540

Thapa P., Bhandari D., Shrestha D., Parajuli H., Chaudhary P. *et al.,* (2017) A hospital based surveillance of metallo-beta-lactamase producing gram negative bacteria in Nepal by imipenem-EDTA disk method. BMC research notes, **10**: 1-6.

Zhang X., Chen D., Xu G., Huang W. & Wang X. (2018) Molecular epidemiology and drug resistant mechanism in carbapenem-resistant *Klebsiella pneumoniae* isolated from pediatric patients in Shanghai, China. PLoS One, **20**: 1–10.

Zurfluh K., Bagutti C., Brodmann P., Alt M., Schulze J. *et al*., (2017) Wastewater is a reservoir for clinically relevant carbapenemase-and 16s rRNA methylase-producing *Enterobacteriaceae*. International Journal of Antimicrobial Agents, **50**: 436-440.

Submitted: 06/11/2021
Revised: 03/04/2022
Accepted: 04/04/2022
DOI: 10.48129/kjs.17079

Diagnosing and Mitigating the Risks of Lambs' Mortality in the Sheep Farms of Kuwait

Hana'a Burezq*; Faten Khalil

Desert Agriculture and Ecosystems Program
Environment and Life Sciences Research Centre,
Kuwait Institute for Scientific Research, P.O. 24885, Safat 13109

**Corresponding Author: haborizq@kisr.edu.kw*

Abstract

A survey was carried out to diagnose the rates of mortality of lambs in the sheep farms of Kuwait. The survey results helped determine that the cause of high mortality rate in Kuwait of newborn lambs (≈35%) during the first three weeks of age is the certain infectious diseases affecting the sheep. Following the survey, a field experiment was carried out using a modified vaccination protocol (vaccination during pregnancy) to improve the immune status of the secreted colostrum. This new protocol has improved the immunity of newborn lambs after suckling the hyperimmune colostrum, and reduced mortality rate significantly, compared to the conventional protocol (vaccination before pregnancy). The results have proved the efficiency of the modified vaccination protocol. The experiment concluded that the vaccination during pregnancy has shown great promise to reduce the mortality rate of newborn lambs in sheep farms of Kuwait. Upscaling the tested vaccination protocol may set the scene for the betterment of sheep industry of Kuwait.

Keywords: Diseases; infection; lamb; mortality; newborn lambs; survey.

1. Introduction

Arabian Gulf region is known for its hot arid climate. Fat-tailed sheep in this region are well adapted to such harsh climatic conditions, and provide abundance of lean meat (Razzaque & Abbas, 2010). In Kuwait, Naeemi sheep breed represents 65 to 70% of the total sheep population, which are widely adapted to the harsh arid local climate (Mohammed *et al*., 2009; Razzaque & Abbas, 2010). The highly nutritious and tasty meat of the Naeemi sheep motivates the farmers to increase the local production. However, high disease incidences have led to high mortality rate in lambs, which has resulted in livestock producers suffering significant losses in their Naeemi sheep production. To address these losses and to set a way forward to improve the sheep industry in Kuwait, a field survey was carried out to diagnose the causes of high mortality rates lambs in both the private and public farms. Vaccination is considered a standard practice to reduce the incidence of various diseases affecting the sheep flocks. After completing the survey, a field experiment was carried out in the selected farms to compare vaccination protocols to control lambs' mortality rates. It was hypothesized that compared to conventional vaccination of ewes before pregnancy period, the vaccination during the pregnancy controls the newly born lambs' mortality through improving the quality of the colostrum secreted.

1.1 A. Survey Study

A farm survey was conducted in nine sheep farms in Kuwait and information was collected. The information was recorded using a scientifically designed questionnaire to establish the baseline data on lambs' mortality in Kuwait. The aim of the survey was to evaluate the rate of mortality in young lambs, especially during the first three weeks of age (Appendix-I) and make efforts to mitigate these losses. The selected farms were categorized into small (10-150 heads), medium (151-750) and large (751-1,000 heads) categories (Figure 1). The team visited the small and medium farms once and large farms twice a week to collect the information. The project leader coordinated with the farm managers to confirm the date and times to facilitate the survey and to assure that the farm staff is available to help fill the questionnaire. Data was collected during the peak lambing time of ewes.

1.2 B. Field Experiment

After completing the farm survey, a field experiment was carried out in the selected farms. The main objectives of the field experiment are: (1) to investigate the mortality rate (%) of lambs and causes of mortality; (2) to investigate and compare the effectiveness of the vaccination protocols used in the selected farms; and (3) to investigate the effect of the newly introduced vaccination protocol on the quality of secreted colostrum of ewes.

2. Materials and Methods

2.1 Experimental Design for the Field Experiment

Three flocks (F#1, F#2, F#3) were separated from each farm. A total of 27 flocks were used in the field experiment. Each flock was comprised of 6 ewes (27 flocks X 6 ewes =162 ewes), and the ear tags were used for the selected ewes to identify and monitor their performance. All selected ewes belong to Naeemi sheep breed (12-18 months old, live weight 38 ± 2.89 kg). During the field experiment, two vaccination protocols were used:

1) Conventional vaccination protocol used by the farmers, i.e., the ewes were vaccinated once before pregnancy and then a straight breeding program of mating Naeemi rams with Naeemi ewes.
2) KISR's vaccination protocol (ewes were vaccinated twice during the pregnancy period).

2.2 Vaccination Protocol Used in the Selected Farms

Ewes at Fuad Al-Ghanim, Al-Reham, Al-Terkeet, Al-Redab, Al-Hamaeid farms, and PAAFR, DEGTC, and BDTC's farms were vaccinated according to the vaccination protocol recommended by PAAFR. Thus, the flocks were vaccinated with 1. *Clostridial sp.*, which consists of seven species of the antigen [(*Cl. Septicum; Cl. Perfringens Types A, C, and D; Cl. Sordellii; and Cl. novy, Type B toxoids* (CZ Veterinaria S. A, Spain)]; 2. *Pasteurella sp.* (CZ Veterinaria S. A, Spain); 3. *PPR* (CZ Veterinaria S.A, Spain) and 4. *FMD* (CZ Veterinaria S.A, Spain) before pregnancy period and no intervention measures were taken during the pregnancy period. In contrast, ewes from KISR's farm were vaccinated with the

same vaccines as mentioned before, but ewes were vaccinated twice during the pregnancy period. The first vaccination was at the beginning of the pregnancy period, and the second booster dose was given four weeks prior to lambing. Ewes were given selenium and vitamin E as supplements during the pregnancy period.

2.3 Mortality Rate (MR) of Lambs

The MR is defined as the percentage of lambs died at the age between 1 and 21 days after birth. The mortality rate of lambs is calculated using the standard equatuion: MR=[(A-B)/A] X 100 (Hashemi *et al*., 2008), where A = Total number of born lambs, and B = number of survived lambs.

2.4 Collection of Blood Samples

Blood samples were collected before the morning feeding from the jugular vein in 10–ml vacutainer tubes (Moore *et al*., 2005). Blood samples were incubated at room temperature for 2 hours (h), and then centrifuged at 2000 × *g* for 10 min at 4 °C (Universal 32 R, Hettich–Zentrifugen, Tuttlingen, Germany) to separate and collect the serum samples. The collected serum samples were stored at –20 °C until analysis.

2.5 Collection of Colostrum Samples

To collect the colostrum samples (6-12 hours after birth), teats were grasped between the thumb and forefinger and were gently squeezed to force the milk downward within the teat canal. Colostrum was collected in clean plastic screw-top containers. Colostrum samples were stored in a freezer at –20 °C until analysis by Enzyme-Linked Immunosorbent Assay (ELISA) kits.

2.6 Enzyme-Linked Immunosorbent Assay

The concentrations of immunoglobins (Ig's) in the colostrum and serum samples were determined by ELISA method using ELISA kits (SunLong, China), and the results were compared with purified sheep Ig's, as standard reference. Results were expressed as milligrams (mg) of Ig per milliliter (ml) of serum/ colostrum. Samples were individually analyzed in triplicate, and a valid result was considered when differences between obtained results were less than 10 % (Crowther, 2009).

2.7 Diagnosis of Diseases that Cause Lambs' Mortality

To diagnose the causes of lambs' mortality, tissue samples were collected from different organs of dead lambs by using Koch's Postulates. Koch postulated depends mainly on three rules: a) the isolated microorganism should be isolated from all animals infected with the same disease; b) the microorganism should be isolated from the infected animal and grown in pure culture; and c) this specific microorganism should be reproduced when inoculated into a healthy animal (Burezq *et al*., 2015**)**.

3. Results of Field Survey

The descriptive statistics for data collected from survey work are listed subsequently:

3.1 Housing System

The housing system used in all visited farms was confined (zero grazing) because of hot weather and scarce vegetation cover in the deserts, which is not enough to meet the grazing requirements of the animals. Each farm was managed by a supervisor and three to five laborers. The pens are cleaned on daily basis, but the bedding is changed annually and replaced with clean sand. The animals are given free access to freshwater for drinking. All farms were surrounded with a fence to protect the herd from diseases transmitted from any wild animal. In contrast, pens in KISR and PAAFR farms were cleaned daily, and bedding was changed weekly and replaced with clean sand.

3.2 Management Level

Management level was one of the criteria recorded during the survey study, since it significantly affects the mortality rate of lambs. The main difference between the private farm and KISR/PAAFR farms is hygene related. The management level in seven out of nine farms was very good, but at KISR and PAAFR farms the management level was excellent. All farms have separate pens for ewes and their lambs after lambing and until weaning, except Al-Terkeet farm, where ewes were kept in the same pen with the other animals. Total number of lambs and ewes in each farm is shown in Figure 1, and the summary of the data collected is given Table 1.

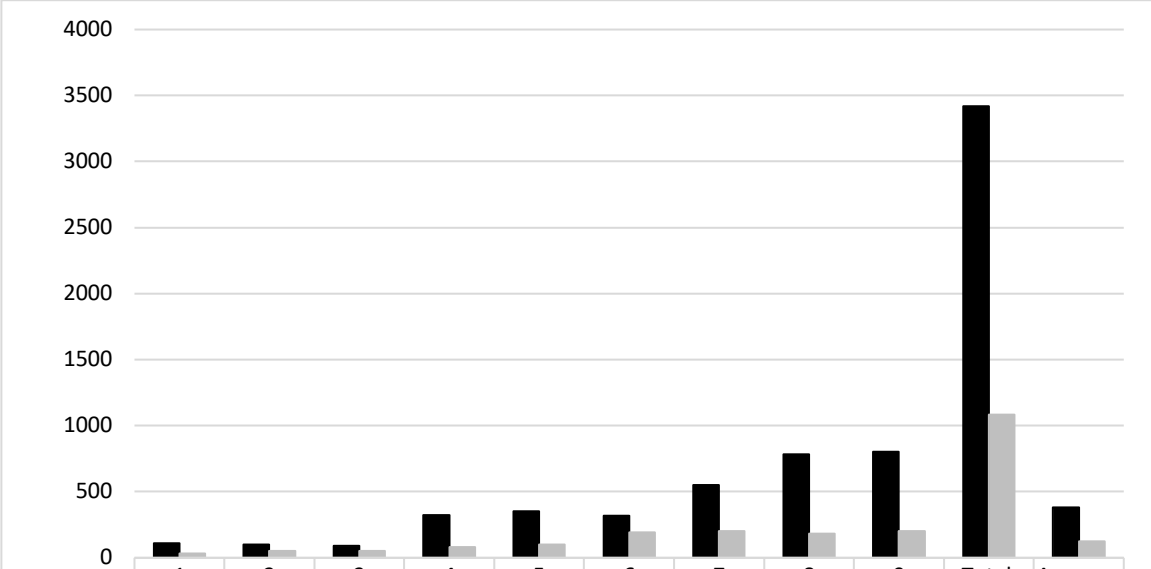

	1	2	3	4	5	6	7	8	9	Total	Average
Ewes	110	100	90	320	350	318	551	780	800	3419	379.89
Lamb	30	50	50	80	100	193	200	180	200	1083	120.33

1: Fuad Al-Ghanim Farm, 2: Al-Reham Farm, 3: Al-Terkeet Farm, 4: Al-Redab Farm, 5: Al-Hamaeid Farm, 6: KISR's Farm, 7: DEGTC's Farm, 8: PAAFR's Farm, 9: BGTC's Farm.

Fig. 1. Total number of lambs and ewes in sheep farms

Table 1. Summary of data collected from sheep farms of Kuwait

Farm's Name	Mortality Rate (%)	Still Birth (%)	Lambs Born Alive/ Year	Abortion Rate (%)	Weaned Lambs (3 months) (n)	C:R for Ewes and Rams	C:R for Lambs
Small Farms							
1	40	2	130	30	80	70:30	80:20
2	30	2	130	10	80	70:30	80:20
3	50	10	130	30	70	70:30	80:20
Medium							
4	50	2	130	2	110	70:30	80:20
5	35	2	180	2	120	70:30	80:20
6	0	0	193	2	193	70:30	80:20
Large Farms							
7	15	3	180	2	110	70:30	80:20
8	8	2	180	2	140	70:30	80:20
9	15	3	130	30	80	70:30	80:20

1: Fuad Al-Ghanim Farm, 2: Al-Reham Farm, 3: Al-Terkeet Farm, 4: Al-Redab Farm, 5: Al-Hamaeid Farm, 6: KISR's Farm, 7: DEGTC's Farm, 8: PAAFR's Farm, 9: BGTC's Farm, C: Concentrate, R: Roughages

3.3 Feeding and Nutrition

Table 2 presents the composition of rations for ewes and lambs. Each ration consists of: 1) roughages (i.e., alfalfa hay and wheat straw), and 2) concentrates (i.e., barely, wheat bran, corn, soya bean meal), vitamins, and minerals. Two different, concentrates: roughages (C: R) rations were used in the present study. Rams and ewes were fed with ration of C: R 70:30 and young lambs were given a ration of C: R 80:20 (Abbas *et al*., 2015). A daily feed rate of 1.0 kg/head was provided to rams and 1.25 kg/head was given two weeks before joining ewes. Dry ewes (i.e., not pregnant) were provided daily with 0.8 kg/head of the same feed to rams, which was amplified steadily during the last month of pregnancy to 1.25 kg/head/day (NRC, 2001, 2007; Razzaque, 1995). All the selected farms were using the aforementioned rations for ewes, rams, and young lambs (3 months and above).

Table 2. Ingredients of rations on dry basis, vitamin, and mineral composition

Ingredients	(70C:30R) (Used for Ewes and Rams in	(80C:20R) (Used for Young Lambs in
Concentrates		
Barley	40.5	51.0
Wheat bran	10.0	10.0
Corn	10.0	10.0
Soybean meal	6.5	6.0
*Premix (vitamins and	1.0	1.0
Limestone	1.0	1.0
Salt	1.0	1.0
Total A	**70.0**	**80.0**
Roughages		
Alfalfa Hay	15.0	10.0
Wheat Straw	15.0	10.0
Total B	**30.0**	**20.0**
Total A + B	**100**	**100**

*Premix (vitamins and minerals): Phosphorus (5.00 %), calcium (18.00 %), sodium (5.00 %), magnesium (5.00 %), manganese (500 mg/kg as manganese oxide), cobalt (100 mg/kg as cobaltous sulfate), zinc (2000 mg/kg as zinc oxide), iodine (125 mg/kg as calcium iodate), selenium (10 mg/kg as sodium selenite), vitamin A (400000 IUkg), vitamin D3 (100000 IU/kg), vitamin E (Alpha–Tocopherol) (400 IU/kg).

3.4 Mortality Rate (%) of Lambs (MRL).

Data collected on lambs' mortality was for two years (2017–2018). The mortality rate of newborn lambs (3 weeks of age) was determined. The highest mortality rate (50 %) of newborn lambs was recorded in both the Al-Redab and Al-Terkeet farms, following by 40% mortality rate in Fuad Al-Ghanim farm. The mortality rate in Al-Reham and Al-Hamaeid farms is lower than the aforementioned farms, but still it is high and reaches to 30% and 35%, respectively. The MRL of DEGTC'S and BGTC farms was significantly lower than that of the previous farms but still considered high (15%). The PAAFR farm has relatively lower mortality rate (8%), and the lowest was at KISR Research Station (2%) (Table 1).

3.5 Abortion Rate (%) of Ewes (AR).

The highest abortion rate was recoded in farm nos. 1, 3, and 9 (30%), other farms present 2% except farm no. 2 (10%) as shown in Table 1.

3.6 Stillbirth Rate (%) of Ewes (SBR)

The stillbirth rate reaches 2% in the Fuad Al-Ghanim, Al-Reham, Al-Redab, Al-Hamaeid, KISR, and PAAFR's farms, while it was slighty higher in the DEGTC and BGTC's farms reaching 3%. In contrast, SBR was apparently higher in Al-Terkeet farm and reaches 10% (Table 1).

4. Results and Discusion of Field Experiment

The concentration of Ig's in the blood samples of ewes in seven farms ranged between 18.343±0.052 and 23.31±0.058 (i.e., Fuad Al-Ghanim, Al-Reham, Al-Terkeet, Al-Redab, Al-Hamaeid, DEGTC's farm, and BGTC's farms). The serum Ig's in the blood samples collected from the ewes at PAAFR farm was recorded as 37.3 ± 0.058 mg/ml, whereas the highest Ig's was recorded in blood samples from ewes in KISR's farm (45.786 ± 0.01 mg/ml). The higher Ig's at KISR farm can be due to vaccination given twice during the pregnancy period, which is also supported by Gilbert *et al*. (2014). This concludes that the vaccination during pregnancy period can improve the immunity of ewes (Table 3).

Table 3. Concentration of Ig's in ewes' blood serum

	IgG mg/ml			
Farms' Name	**Flock–1**	**Flock–2**	**Flock–3**	**Mean ± Standard Deviation**
Fuad Al-Ghanim	19.963	20.198	17.862	19.341±0.013
Al-Reham	20.483	30.388	19.057	23.31±0.058
Al-Terkeet	19.115	18.033	17.883	18.343±0.052
Al-Redab	20.787	19.961	20.555	20.434±0.026
Al-Hamaeid	19.803	19.185	18.052	19.013±0.038
*KISR	46.136	45.138	46.083	45.786±0.01
****DEGTC	20.733	19.828	21.722	20.761±0.05
**PAAFR	37.495	36.607	37.747	37.3±0.058
***BGTC	19.999	19.095	18.411	19.168±0.026

*: Kuwait Institute for Scientific Research, **: Public Authority for Agricultural Affairs and Fish Resources, ***: Brand General Trading & Contracting Co., **** Diamond Expertise for General Trading and Contracting Co.

4.1 Ig's Concentration of Colostrum.

Concentration of Ig's in the colostrum samples collected from the ewes at eight farms (Fuad Al-Ghanim, Al-Reham, Al-Terkeet, Al-Redab, Al-Hamaeid, DEGTC, PAAFR, and BGTC's farms) ranged between 50.43±0.028 and 54.21 ±0.045 mg/ml. The highest concentrations (65.96±0.005 mg/ml) of Ig's in the colostrum samples in the ewes at KISR's farm was recorded. These results clearly showed that vaccinating the ewes at KISR's farm during pregnancy period increased the concentration of Ig's in the colostrum compared to the Ig's concentration in the colostrum samples collected from other farms. These results showed that improved immunity of the ewes by vaccinating twice during pregnancy period helped in elevating the concentration of Ig's both in the blood and secreted colostrum, which have led to increase in the survival rate of newborn lambs. Thus, the vaccination protocol used in KISR was found to be more efficient than that in PAAFR. The high concentration of Ig's in the colostrum would help in improving the immune status of lambs feeding on the colostrum; as a result, the lambs would have enough immunity especially in the first 3 weeks of lives, until their immune system becomes fully activated. Increasing the quality of the colostrum is crucial to increase the survival rate of newborn lamb because colostrum is the only source of both nutrition and antibodies (Martín–Gómez *et al*., 2006). Based on these results, it can be confidently stated that increasing the immunity status of colostrum as feed of newborn lambs not only decreases the mortality rate but may also improve the sheep industry in Kuwait and increase the livelihood of the farm owners (Table 4).

Table 4. Concentrations of Ig's in colostrum samples

Farms	**IgG mg/ml ± S.D.**			
	F#1 (n=6)	**F#2 (n=6)**	**F#3 (n=6)**	**Mean ± SD**
*KISR	65.15	66.76	65.97	65.96±0.005
**PAAFR	54.30	54.13	54.20	54.21±0.045
Al-Reham	53.01	54.04	52.14	53.06±0.051
Al-Redab	52.11	51.21	50.33	51.22±0.040
Al-Hamaeid	50.09	50.23	51.33	50.55±0.049
Fuad Al-Ghanim	51.45	52.53	51.88	51.95±0.043
***BGTC	50.33	50.98	51.06	50.79±0.018
****DEGT C	49.85	50.88	50.57	50.43±0.028
Al-Terkeet	50.54	52.07	51.77	51.46±0.011

*: Kuwait Institute for Scientific Research, **: Public Authority for Agricultural Affairs and Fish Resources, ***: Brand General Trading & Contracting Co., **** Diamond Expertise for General Trading and Contracting Co.

4.2 Mortality Rate of Newborn Lambs (MR)

The results in Table 5 shows that the mortality rate of newborn lambs at KISR's farm (born lambs n=23) was apparently lower than that in the rest of the farms. This is because no incidence of mortality of newborn lambs was recorded at KISR farm during the field experiment. Although the MR at PAAFR farm (born lambs n=25) was 4% was higher than

the MR of lambs in KISR, it was lower than the MR of all other farms. Only one lamb was recorded as dead in the field experiment due to the infection with FMD disease.

The number of newborn lambs was n=18 in the 4 farms (Fuad Al-Ghanim, Al-Reham, Al-Redab, and Al-Hamaeid farm), where the mortality rate was recorded as 22.23 %, for young lambs especially in the first 3 weeks of lives. In each of these farms, 4 lambs were dead due to different diseases. For example, in Fuad Al-Ghanim farm, the young lambs died due to the infection by *E. Coli* (2 lambs), *Pasteurella* (1 lamb), and *Salmonella* (1 lamb), while the cause of lambs' death in Al-Reham farm was the infection by *Salmonella* (2 lambs) and *E. Coli* (2 lambs). In contrast, the main cause of lambs' death in Al-Redab farm was the infection with *Clostridia* (3 lambs) and *Pasteurella* (1 lamb) diseases. The mortality of young lambs in Al-Hamaeid farm was due to the infection by *FMD* (4 lambs) disease. The main reason could be the similar management in these 4 farms. These farms were managed by the same owner, supervisor, and by the same management. Thus, animals in these farms have received the same type of vaccination (Table 4) and at same time; in these farms, the ewes were vaccinated before pregnancy and no intervention measures were taken during the pregnancy.

In addition, the mortality rates of newborn lambs in the Al-Terkeet farm (born lambs n=10) was higher than that in the aforementioned farms, where the MR reaches to 30%, which is significantly (P<0.05) higher than that in the other farms; the main reason of lambs' mortality was the infection of *PPR* disease. Finally, the highest MR of lambs was reported from DEGTC (n=17) and BGTC farms (n=23), where the MR reaches 41.5 % and 43.5 %, respectively. The main cause of lamb's mortality was the infection with *Pasteurella* and *Salmonella* in DEGTC farm, while the cause of death of young lambs in BDTC farm was the infection of *Coronaviruse*, *rotaviruse* (5 lambs), *E. coli* (3 lambs) and *Clostridia* (3 lambs). The MR in these two farms was significantly (P<0.05) higher, as compared to the aforementioned farms (Table 5).

Table 5 shows that the total number of born lambs in the selected farms was 170, from which 132 (77.6%) survived. The number of dead lambs due to the infection by *E. coli* is 7, same as *Salmonella* (n=7), and *Clostridia* (n=6). Collectively these three diseases caused the death of young lambs by 11.77 %. Furthermore, the percentages of the lambs' death due to the infection with *Pasteurella (n=5)* and *FMD* (n=5) were 2.9% each. In contrast, the percentages of lambs' death due to the infection with *PPR* (n=3) and corona/rotaviruses (n=5) were 1.76 % and 2.94 %, respectively. To conclude, for a total number of 170 newborn lambs, 22.35 % (n=38) of lambs died due to different diseases and only 77.6% remained alive during the field experiment and could reach weaning and adult stage.

These results show that vaccinating ewes during pregnancy period can help in boosting the immunity of ewes during pregnancy, and as a result improves the quality of the secreted colostrum. In addition, lambs feeding on the high-quality colostrum will have more chance for survival. Colostrum is the only source for antibodies and nutrition for the newborn lambs. Thus, improving the quality of colostrum through vaccination would help boost the immunity of young lambs and reduce the lambs' mortality rate (Burezq *et al*., 2015**)**. Thus, this may help mitigate the infections of diseases and improve the sheep industry in Kuwait, and bridge the gap between locally produced meat and the importation for food security.

4.3 Diagnosing the Causes of Lambs' Mortality

Biological samples were collected from the dead lambs (for example, tissues from liver, or spleen, or small intestine, or heart), and sent to PAAFR laboratories for disease diagnosis. The results showed that the mortality of the lambs at the age of less than one to seven days of age was commonly because of being infected with *enterotoxigenic Escherichia coli* from *enteric or septicemic* forms. The main symptoms observed in these lambs were fever, diarrhea and in some cases sudden death. Other diseases diagnosed to cause the death of lambs at 7–21 days of age include the following:

- *Clostridia. Clostridia* is a disease caused by the two different strains of bacteria, stains *C and D*, which are found in the gastrointestinal tract of the sheep. Lambs infected with *Clostridia* suffers from high fever, swollen areas, and death due to toxaemia (that is blood poisoning) caused by the bacteria (Scholes & Edwards, 2009).
- *Pasteurella.* This disease is caused by the bacteria that could move from tonsil to lung, and then to the blood. This disease can cause severe fibrin necrotic pneumonia, fever, listlessness, poor appetite, and sudden death.
- The *Foot–and–Mouth Disease (FMD).* Typical symptoms of the FMD are fever lasting two to three days, painful lesions in the mouth due to which the animal would eat less, weight loss, high mortality rate of new born lambs, and feet lesions.
- Infection with *Salmonella.* This is a disease caused by the proliferation of *Salmonella* bacteria in the gastrointestinal tract and other organs. The known symptoms of Salmonellosis are diarrhea, decreased appetite, fever, blood poisoning, and death.
- *PPR. PPR* is an acute and highly contagious viral disease that causes illness and mortality of the young lambs. The symptoms observed on the infected lambs are diarrhea, sores in mouth, pneumonia, and death (Aziz–Ul–Rahman *et al*., 2016; Wernike *et al*., 2016).
- *Coronavirus* and *Rotavirus*. The symptom observed on lambs infected with *Coronavirus* and *Rotavirus* is diarrhea, and in some cases, diarrhea is associated with some pathogens, for example, *Cryptosporidium* (Durham *et al*., 2011; Bjorkman *et al*., 2003).

Table 5 shows that the total number of newborn lambs in selected farms was 170; and only 132 lambs managed to survive and grow until reach weaning age. Thus, out of 170 born lambs, only 77.6% remained alive during the field experiment and reached weaning phase, which means that 22.35% of the lambs are dead.

4.4 Proximate Analysis and Calculation of Energy Values of Experimental Rations

A balanced feed ration is essential for normal health, growth and reproduction of the sheep. Nutrients in the feed are utilized by the sheep to meet their nutritional requirements. It is not the feed itself that meets these needs but the components (concentrates and roughages) that make up the feed. Nutrient requirements vary during the production cycle as the body has difference demands. Ewes, rams, and lambs and replacement all have varying nutritional needs. Testing the feed is important, as nutrient levels vary depending on the quality of the feed (Abbas *et al*., 2015).

Feed samples were collected for quantitative analysis to determine the percentages of the components including moisture, crude protein, crude fat, neutral detergent fiber, acid detergent fiber (ADF), and ash (%) (Table 6). The actual intake of DM (dry matter) is shown in Table 7 from both C and R, and it was calculated based on the analytical data of DM contents of total feeds intake (Table 7) for ewes, rams and lambs (Abbas *et al*., 2015). In the field study, two different R:C rations were used, according to KISRs' nutritional and feedlot recommendations (Abbas *et al*., 2015). Although the team used two different R:C rations, the concentrations of CP, NDF, ADF, and other minerals in the used rations were not significantly different (Table 7). The ration used for the ewes and rams was with a C:R ratio of 70:30, and was found to be the best feeding regime for complete production cycle of ewes, in Kuwait's feedlot system, irrespective of the season (Abbas *et al*., 2015). Using a ration with C: R 80:20 for lambs was reported to be the best for lambs during the pre-weaning, suckling and post-weaning periods, and for the best average daily gain (ADG) (i.e., the efficiency with which the bodies of livestock can convert feed into more body weight) and feed conversion ratio (FCR) for lambs (Abbas *et al*., 2015). ADG can be defined as the rate of weight gain per day over a specified period of time, and FCR is a ratio measuring the efficiency of the animals' body to convert the feed into the desired output (e.g., sheep raised for meat) (Abbas *et al*., 2015). It is the energy that provides fuel to enable the body to maintain normal functions. The energy can be derived from carbohydrates, fats, oils and protein, and is generally measured as total digestible nutrients (TDN) or as digestible energy (DE) (Abbas *et al*., 2015).

Therefore, carbohydrates, fats and excess proteins in the ration together contribute to provide the energy requirements of ewes. Concentrates are considered a rich source of energy, while forages contain high fibers instead, but low energy content (roughages). Meeting the energy requirements of sheep is one of the biggest challenges for sheep producers. Insufficient energy intake can lead to malnutrition, weight loss, reproductive failure, and decreased milk production, lower resistance to parasites and disease and increased mortality due to decreased efficiency of immune system.

Thus, animals become more susceptible to diseases, especially gastrointestinal worms, and eventually to death. In contrast, excess of energy consumption could cause obesity of sheep, impair reproductive function in both rams and ewes, and during late gestation, fat ewes become more likely to have ketosis (pregnancy toxemia). Energy could be quantified in the ration in many ways, by measuring the total digestible nutrients (TDN) or metabolizable energy (ME) and net energy (NE) (Table 8). The TDN was used to formulate rations for breeding animals, while the net energy system is usually used to calculate diets for growing lambs (Abbas *et al*., 2015).

5. Discussion

The idea of the present study came from the unpublished data of PAAFR about the mortality rate of newborn lambs in Kuwait farms. The PAAFR reports had highlighted that the mortality rate of the newborn lambs could be as high as 25 to 35% (PAAFR unpublished data). Therefore, the producers suffer from significant economic losses.

A survey study was carried out to diagnose the causes of high mortality of lambs in the representative small, medium and large sheep farms, and to mitigate these causes of death to improve the survival of the newly born lambs. The results from the survey confirmed that the sheep farms in Kuwait suffer from high mortality rate of newborn lambs, especially in the first three weeks of age, and it is a serious problem since the mortality rate ranges between 25 and 35%. At present, the number of lambs produced in sheep farms could meet about 11–12% of total red meat demands of the country. Therefore, controlling the mortality rate of young lambs could have a significant positive effect on the sheep industry in Kuwait (Burezq *et al*., 2015). In addition, the data collected from survey study recommend vaccinating animals during pregnancy period to improve the quality of secreted colostrum.

5. 1 Field Experiment

A field experiment was carried out where ewes from eight farms were vaccinated according to conventional PAAFR vaccination protocol, before pregnancy period, and no intervention measures were carried out during pregnancy. In contrast, the ewes from KISR's farm were vaccinated twice during pregnancy period. To study the effectiveness of KISR and PAAFR's vaccination protocols on lambs' mortality during the field experiment, some factors were unified, such as feeding/nutrition, care of lambs after lambing, age, and body condition score (BCS). After unifying these factors, the second step was to evaluate the vaccination protocol used in the selected farms, by measuring IgG in the blood and colostrum samples, and to find the causes of mortality and determine the mortality rates.

5.2 Impact of Vaccination of Pregnant Ewes on Ig's Concentration of Blood of Ewes.

The present study proves the efficiency of vaccinating ewes during pregnancy. Farms adopted the modified vaccination protocol to control the mortality of young lambs. (Gilbert *et al*., 2014; Hashemi *et al*., 2008).

5.3 Impact of Vaccination of Pregnant Ewes on Ig's Concentration of Colostrum

Vaccinating the ewes during pregnancy period in KISR's farm increased the concentration of Ig's in the colostrum significantly ($P<0.05$), as compared to the concentration of Ig's in colostrum samples collected from other farms. These results showed that improving the immunity of ewes by vaccinating them twice during pregnancy period would help elevate the concentration of Ig's in their blood and consequently in the secreted colostrum, which could have a significant effect in improving the survival rate of newborn lambs. Having high concentrations of Ig's in colostrum would help improve the immunity of newborn lambs significantly, especially in the first 3 weeks of lives, until their immune system becomes fully activated (Moore *et al*., 2005).

Table 5. Mortality and Weaning Rates of Young Lambs

Farms	Lambs Born Alive (n)	Weaned Lambs (n)	Weaning Rate (%) of Lambs at 2 months of Age	Mortality Rate (%) of Lambs at 1–21 days of Age	Number of Dead Lambs	Causes of Mortality of Newborn Lambs
Fuad Al-Ghanim	18	14	77.77	22.23	4	2 lambs by *E. coli,* 1 lamb by *Pasteurella*, 1 lamb by *Salmonella*
Al-Reham	18	14	77.7	22.23	4	2 lambs by *Salmonella*, 2 lambs by *E.coli,*
Al-Terkeet	10	7	70	30.00	3	3 lambs by *PPR*
Al-Redab	18	14	77.77	22.23	4	4 lambs by *Clostridia* 1 lamb by *Pasteurella*
Al-Hamaeid	18	14	77.77	22.23	4	4 lambs by *FMD*
*KISR	23	23	100	0	0	0
****DEGTC	17	10	58.82	41.18	7	3 lambs by *Pasteurella* 4 lambs by *Salmonella*
**PAAFR	25	24	96	4.0	1	1 lamb by *FMD*
***BGTC	23	12	52.17	47.83	11	5 lambs by *Corona virus* and *rotaviruse*, 3 lambs by *E. Coli*, 3 lambs by *Clostridia*
Total	**170**	**132**			**38**	

*: Kuwait Institute for Scientific Research, **: Public Authority for Agricultural Affairs and Fish Resources, ***: Brand General Trading & Contracting Co., **** Diamond Expertise for General Trading and Contracting Co. Data in Table 5 were collected during the field experiment (18 months)

Table 6. Proximate Analysis of Concentrate and Roughage Composition Used for Rations Formulation

*Parameters (%)	Barley	Wheat Bran	Soybean	Corn	Alfalfa	Wheat Straw
Moisture	6.07 ±0.14	8.95 ±0.15	8.5 ±0.09	7.83 ±0.17	5.67 ±0.06	–
Ash	2.32 ±0.2	3.93 ±0.07	9.33 ±0.07	1.14 ±0.06	11.99	8.3 ±0.34
CP	10.88 ±0.7	15.42 ±0.03	52.07 ±0.44	7.73 ±0.12	14.75 ±1.1	3.1 ±0.15
CF	–	7.45 ±0.37	5.87 ±0.47	1.64 ±0.06	32.3 ±0.12	–
NDF	24.5 ±0.7	16.8 ±0.6	13.2 ±0.43	40.8 ±0.53	45.2 ±0.28	47.5 ±0.09
ADF	5.6 ±0.06	2.4 ±0.8	9.6 ±0.03	11.9 ±0.11	35.3 ±0.3	44.5 ±0.05

*CP: crude protein; CF: crude fiber; NDF: neutral detergent fiber; ADF: acid detergent fiber.

Table 7. Composition of Experimental Rations (Combined Concentrate and Roughages)

Component (%)	Composition of Rations (70C:30R) (For Ewes and Rams)	Composition of Rations (80C:20R) (For Young Lambs)
Moisture	8.03 ±0.13	9.37 ±0.24
DM	90.98 ± 0.1	90.64 ±0.25
Ash*	5.48 ±0.18	2.64 ±0.07
CP*	13.32 ±0.29	12.45 ±0.12
EE*	1.56 ±0.84	2.85 ±01.61
NDF	20.11 ±0.56	19.86 ±0.30
ADF	4.95 ±0.28	4.55 ±0.45
Ca*	0.37 ±0.051	0.43 ±0.20
P*	1.26 ±0.04	–

*: % of dry matter; CP: crude protein; EE: ether extract; ADF: acid detergent fiber; NDF: neutral detergent fiber; Ca: calcium; P: phosphorous; –: not available.

Table 8. Calculated Energy Values of Experimental Rations (On DM Basis) *

	70C:30R (For Ewes and Rams)	80C:20R (For Young Lambs)
*DE MCal/kg	3.38 (14.150)	3.47 (14.528)
**ME MCal/kg	2.77 (11.597)	2.85 (11.932)
***TDN %	76.74	78.94

*DE: Digestible energy; **ME: Metabolizable energy; ***TDN: Total digestible nutrients were calculated according to (Linn & Martin, 1999). TDN% = 88.9 – (0.779 × ADF %), Values in parenthesis are MJ/kg. DE and ME values were calculated according to equations/program of the University of Minnesota and the Ontario Ministry of Agriculture, Canada.

Colostrum absorption usually occurs through the intestinal cells by the neonatal receptor FcRn and endocytosis using transport vacuoles (Smith & Foster, 2007). This absorptive capacity starts to decrease 6 to 12 h after birth and ends by 48 h after birth (Smith & Foster, 2007). The concentration of Ig's in serum increases significantly shortly after colostrum ingestion. Sometimes, lambs fail to get the sufficient amount of colostrum. They would get trace amounts of Ig's during the first three days of life; therefore, lambs become more susceptible to diseases and death. Lambs should get sufficient amount of good quality colostrum between 1 and 6 h of birth, because the gut ability to absorb the antibodies decreases significantly after this period. The quality of colostrum varies depending on the animal species; some can secrete better quality colostrum than the others. The amount needed for each lamb is about 100–200 ml per feeding, which is about 600 ml for three times feeding in the first 12 hours of life, and lambs should be fed for three to four days after lambing. In case the lambs cannot suckle the colostrum directly from the teat, colostrum could be collected and fed to them via a stomach tube (Smith & Foster, 2007). In some cases, such as ewes having weak twins, or in case of orphan lambs, dams having no milk, and in case of quadruplets and triplets, where lambs could not have enough colostrum, the only way is to establish a colostrum bank with high-quality colostrum. Feeding young lambs with high quality colostrum would help them get enough immunity especially in the first three weeks of life, and help increase their survival rate.

6. Conclusions

The survey study showed that the mortality rate of young lambs varies between 25 and 35% in 7 of the selected farms, while in KISR and PAAFR farms, the mortality rate of lambs was 2 and 8%, respectively. The field experiment showed that (1) Ig's concentration in the serum and the colostrum samples in the ewes of KISR farm were significantly higher (P<0.05) than that of the other farms. Also, the mortality rate of lamb ranges between 22.23 and 47.83% in other sheep farms, while there was no incidence of lambs' mortality reported in KISR's farm. In addition, the main cause of lambs' mortality was the infection with some diseases such as *Clostridia, Pasteurella, FMD, PPR, Salmonella, Coronavirus and Rotavirus sp*. It was concluded from the present study that vaccinating ewes during pregnancy period resulted in significantly higher (P<0.05) Ig's in ewes' blood and colostrum, which have a positive effect on decreasing the mortality rate of young lambs, and could be beneficial to livestock industry in Kuwait. Therefore, the hypothesis of improving the immune status through vaccinating during pregnancy is confirmed.

ACKNOWLEDGEMENTS

Special thanks and appreciation are extended to the Kuwait Foundation for Advancement of Science (KFAS) for funding the project and the management of the Kuwait Institute for Scientific Research (KISR) for the support.

References

Abbas, S. Razzaque, M. A., Elsaid, A., Albert, S., Gelan, A., Khalil, F., Al-Bahouh, M., Naseeb, A., Burezq, H. (2015) The effect of nutrition and season of breeding on reproductive performance of Naeemi ewes. Final Research Report, KISR No. 12848, Kuwait Institute for Scientific Research, Kuwait.

Aziz–Ul–Rahman, M., Abubakar, M.H., Rasool, S., Manzoor, M., Saqalein, M., Rizwan, M., Munir, Q., Ali, J., Wensman, J.J. (2016) Evaluation of risk factors for peste des petits ruminants virus in sheep and goats at the wildlife–livestock interface in Punjab province. BioMed Research International, 2016: 7826245.

Bjorkman, C., Svensson, C., Christensson, B., de Verdier, K. (2003) Cryptosporidium parvum and Giardia intestinalis in calf diarrhoea in Sweden. Acta Veterinaria Scandinavica. 44(3–4):145.

Burezq, H., Khalil, F., Razzaque, M., Albert, S., Ali, S., Al-Ballam, Z., Al-Qalaf, W. (2015) Biochemical and humoral evaluations of normal colostrum and hyperimmune colostrum of sheep and goats. Final Research Report for Project FA118K, KISR NO. 13466, Kuwait Institute for Scientific Research, Kuwait.

Crowther, J.R. (2009) The ELISA guidebook, 2nd Ed. Humana Press, Totowa (NJ).

Durham, P.J.K., Stevenson, B.J., Farquharson, B.C. (2011) Rotavirus and coronavirus associated diarrhea in domestic animals. New Zealand Veterinary Journal, 27(3): 30-32.

Gilbert, R.P., Gaskins, T.C., Hillers, J.K., Parker, C.F., McGuire, T.C. (2014) Genetic and environmental factors affecting immunoglobulin G concentrations in ewes' colostrum and lambs serum. Journal of Animal Sciences, 66: 863.

Hashemi, M., Zamiri, M.J., Safdarian, M. (2008) Effects of nutritional level during late pregnancy on clostral production and blood immunoglobulin levels of Karakul ewes and their lambs. Small Ruminants Research, 75: 209.

Linn, J.G., Martin, N.P. (1999) Forage quality tests and interpretations. http://www.extension.umn.edu/distribution/livestocksystems/D12637.html (Accessed August 28, 2008).

Martín–Gómez, S., Alvarez–Sánchez, M.A., Rojo–Vázquez, F.A. (2006) Obtaining hyperimmune anti–cryptosporidium parvum ovine colostrum. A study of the humoral immune response in immunized sheep. Parasitology Research, 98:129.

Mohammed, I. B., Nikhaila, A., Abdel Moneim, M. (2009) Effect of parity on the productivity of Taggar goats. International Journal of Arts and Science Research, 8: 278.

Moore, M., Tyler, J.W.M., Chigerwe, M.E., Dawes, M.E., Middleton, J.R. (2005) Effect of delayed colostrum collection on colostral IgG concentration in dairy cows. Journal of the American Medical informatics Association, 226: 1377.

NRC (2001) Nutrient requirements of dairy cattle, 7th ed. National Research Council. National Academy Press, Washington D.C.

NRC (2007) Nutrient Requirement of small ruminants. Washington, DC: The National Academic Press.

Razzaque, M.A. (1995) Intensive lamb production using local and imported sheep. Final Research Report. KISR No. 1763, Kuwait Institute for Scientific Research, Kuwait.

Razzaque, M.A., Abbas, S. (2010) Three-breeds of fat tail sheep: productive performance in Arabian Gulf Region. The Indian Journal of Small Ruminants, 16(2): 183-189.

Scholes, S. F., Edwards, G. T. (2009) Tyzzer's disease (Clostridium piliforme infection) and possible copper toxicity in a lamb. Veterinary Record, 164(15):470-471.

Smith, G.W., Foster, D.M. (2007) Short communication: Absorption of protein and immunoglobulin g in calves fed a colostrum replacer. Journal of Dairy Science, 90: 2908.

Wernike, K., Eschbaumer, M., Breithaupt, A., Maltzan, J., Wiesner, H., Beer, M., Hoffmann, B. (2014) Experimental infection of sheep and goats with a recent isolate of Peste des Petits ruminant's virus from Kurdistan. Veterinary Microbiology. 172(1–2):140-145.

Submitted: 07/06/2021
Revised: 04/12/2021
Accepted: 05/12/2021
DOI: 10.48129/kjs.14607

Enhanced phytase production by *Aspergillus niger* mutants in solid state fermentation

Shahzad Mahmood [1,2,*], Memuna G. Shahid[1], Muhammad Nadeem[2],
Rubina Nelofer[2], Muhammad Irfan[3]

[1] *Dept. of Botany, Government College University, Katchery Road, Lahore-54000, Pakistan*
[2] *Food and Biotechnology Research Centre (FBRC), Pakistan Council of Scientific and Industrial Research (PCSIR) Laboratories Complex, Ferozepur Road, Lahore-54600, Pakistan*
[3]*Dept. of Biotechnology, University of Sargodha, Sargodha-40100, Pakistan*

**Corresponding Author: shahzadbiology@gmail.com*

Abstract

The present research work was conducted to improve the phytase production by genetic alteration of *Aspergillus niger* with induced mutagenesis using solid state fermentation. Strain improvement was carried out in the presence of ultra violet (UV) irradiation and ethyl-methane sulphonate (EMS) [0.5% v/v] treatments for various time intervals. We reported an improved strain of *Aspergillus niger* designated as UV-3 mutant producing a zone of hydrolysis of about 40 mm, in comparison to wild strain (26 mm). The highest enzyme activity was found to be 547.64 IU/g for UV-3 mutant followed by EMS-4 mutant (492.23 IU/g) compared to wild strain which showed 406.45 IU/g of enzyme activity. There was 1.35-fold increase in phytase production after mutation studies of *Aspergillus niger*. Phytase was applied as poultry feed additive and given to broiler chickens for 5 weeks. The results exhibited that there was increase in body weight gain (BWG) of chicks for experimental group (2028 g) in comparison to control group (1903 g). Thus, physical and chemical mutagenesis was proved as an effective technique for the improvement of strain and ultimately for enhanced and economical phytase production for different industrial applications.

Keywords: *Aspergillus niger*; induced mutagenesis; phytase production; solid state fermentation; UV irradiation & EMS treatment.

1. Introduction

Phytic acid (*myo*-inositol hexakis-phosphate) is the major storage form of organic phosphorus. It is found in legume seeds, cereal grains, nuts and oilseeds. These seeds and grains are the major ingredients of commercial animal feeds (Shah *et al*., 2009; Sandhya *et al*., 2015; Kumar *et al*., 2017). Monogastric animals like poultry and fish, do not have adequate quantity of intrinsic phytases in their digestive tract to degrade the phytic acid complexes present in their feed. As a result, the undigested phytate phosphorus is released by these animals as waste material in their fecal matter which creates severe environmental pollution and eutrophication in water bodies (Singh & Satyanaryana, 2010; Yao *et al.,* 2011; Sandhya *et al*., 2015).

Moreover, phytic acid makes insoluble complexes with proteins and many important metal ions i.e. magnesium, calcium, iron and zinc and, thus reduces the bioavailability of these vital nutrients and acts as an anti-nutritional factor (Rao *et al*., 2009; Bakri *et al*., 2018).

Phytases (*myo*-inositol hexakis-phosphate phosphohydrolase) (EC 3.1.3.8 and 3.1.3.26) are the enzymes that belong to a sub-class of histidine acid phosphatases. Phytase produces different substances i.e. lower *myo*-inositol phosphate, free inorganic phosphate (Pi) and potentially chelated minerals, and in some cases, free *myo*-inositol by catalyzing the hydrolytic splitting of phytic acid in stepwise reactions. When phytase is added in poultry feed, more inorganic phosphorus and other vital minerals can become available. The amount of phosphorus, excreted through the manure can also be minimized (Rasul *et al*., 2019; Zaheer *et al*., 2019).

Phytases have very profound role in the animal feed and various food industries because these enzymes enhance the digestion and absorption of phosphorus and certain other poorly available nutrients including copper, manganese, iron and zinc in the monogastric diet supplements (Munir & Maqsood, 2013; Vasudevan *et al*., 2017) and play important role in increasing the body weight gain (BWG) and growth performance of these animals. Phytases also decrease the concentration of phosphorous in the animal's excrement, which can otherwise cause environmental pollution. Phytases as animals feed additive can thus be used as substitute for expensive di-calcium phosphate and reduce the cost of animal feed (Dahiya, 2016; Jatuwong *et al*., 2020).

Phytase has been obtained from different organisms like fungi, bacteria, yeasts, plants and animals. Among various fungi, filamentous fungi like *Aspergillus niger* is being investigated as an excellent source of phytase. It has ability to grow on different agro-wastes under solid state fermentation process and can produce cost effective phytases (Salmon *et al*., 2012; Singh *et al*., 2015; Ahmad *et al*., 2017; Bakri *et al*., 2018).

In the last few decades, there is an increasing demand of phytase in different fields particularly as an animal feed additive, therefore, the ultimate goal is the cost-effective production of phytase by hyper secretory strains (Shah *et al*., 2009). For this purpose, serious attentions are required towards qualitative and quantitative improvement methods. Quantitative enhancement methods include the exploitation of different mutagens for improvement of strain and optimization of fermentation conditions for the higher yield of enzyme, as the amount of enzyme produced by wild culture is low (Bhaskaran *et al*., 2018).

In view of industrial applications, the objective of current investigation was to enhance the phytase production by strain improvement of filamentous fungus *Aspergillus niger* through mutagenesis technique using two different mutagens (UV irradiation and Ethyl methane sulphonate).

2. Materials and methods

2.1. Procurement and maintenance of microbial cultures

Different microbial strains i.e. *Penicillium commune*, *Rhizopus oligosporus*, *Aspergillus niger*, *Trichoderma viride* and *Saccharomyces cerevisiae* were obtained from the Microbiology Laboratory, PCSIR Laboratories complex, Lahore. These microbes were preserved on Potato

Dextrose Agar (PDA) slants at 4°C. For culturing, a loop full of spores from pure microbial culture was transferred into each Potato Dextrose Agar (PDA) slant aseptically and incubated at 35ºC for 5-7 days in an incubator. The slants showing suitable growth of microbial strains were selected for subsequent studies.

2.2. Inoculum preparation

For preparing inoculum, sterilized distilled water (10 ml) was added into five days old culture slant and the fungal mycelia were scrapped with the help of inoculation loop, under aseptic conditions. To homogenize the spore suspension, it was agitated mildly for 2 minutes. A hemocytometer was used to adjust the number of spore (1×10^7 spores/ml).

2.3. Screening of microbial strains and fermentation media

For the screening purpose, five microbial strains i.e. *Penicillium commune*, *Rhizopus oligosporus*, *Aspergillus niger*, *Trichoderma viride* and *Saccharomyces cerevisiae* were cultured on ten different fermentation media (Table 1). The best microbial strain and fermentation medium were selected for maximum phytase production using solid state fermentation process.

Table 1. Composition of the different fermentation media (M) for phytase production

Ingredients (g)	**Fermentation medium (M) (g)**									
	M1	**M2**	**M3**	**M4**	**M5**	**M6**	**M7**	**M8**	**M9**	**M 10**
Wheat Bran	100	-	-	-	-	-	-	-	-	-
Rice Bran	-	100	-	-	-	-	-	-	-	-
Cotton Seed Meal	-	-	100	-	-	-	-	-	-	-
Wheat Straw	-	-	-	100	-	-	-	-	-	-
Rice Polish	-	-	-	-	100	-	-	-	-	-
Soybean Meal	-	-	-	-	-	100	-	-	-	-
Corn Cobs	-	-	-	-	-	-	100	-	-	-
Corn Husk	-	-	-	-	-	-	-	100	-	-
Rice Straw	-	-	-	-	-	-	-	-	100	-
Rice Husk	-	-	-	-	-	-	-	-	-	100
Urea	0.5	0.5	0.5	0.5	0.5	0.5	0.5	0.5	0.5	0.5
$MgSO_4.7H_2O$	0.1	0.1	0.1	0.1	0.1	0.1	0.1	0.1	0.1	0.1
KCl	0.1	0.1	0.1	0.1	0.1	0.1	0.1	0.1	0.1	0.1
$FeSO_4.7H_2O$	0.1	0.1	0.1	0.1	0.1	0.1	0.1	0.1	0.1	0.1

2.4. Conditions for UV and EMS Mutagenesis

Spore suspension of *Aspergillus niger* was prepared by serial dilution method from 5 days old fungal slant. From 7^{th} dilution (10^{-7}), 1 ml of the spore suspensions were poured in the uncontaminated petri plates and exposed to UV irradiation (240 nm) at a distance of 15 cm for

variable time durations i.e. 15, 30, 45, 60, 90 and 120 minutes in a UV chamber except for control (without UV irradiation treatment).

For chemical mutagenesis, a stock solution of 0.5% (V/V) Ethyl methane sulfonate (EMS) was prepared. 1 ml of spore suspension from 7th dilution (10^{-7}) and 1 ml of EMS (5 µl/ml) solution were mixed in various test tubes and incubated for various time intervals (3, 6, 9, 12 and 24 hrs) at room temperature. Potato Dextrose Agar (PDA) in molten form (45^{o}C) was then poured into each petri plate containing mutated spore suspensions under sterilized conditions and placed in an incubator at 37°C for five to seven days until sporulation of fungal culture. The petri plates showing least percentage of survival rates of fungal colonies were chosen for further studies.

2.5. Selection of best mutant strain for enhanced phytase production

All the selected colonies of *Aspergillus niger*, after various mutagenic treatments, were streaked on the phytase screening medium (PSM) plates. Composition of PSM is given in Table 2. These plates were incubated for three to five days at 37°C and zone of hydrolysis were observed after every 24 hours. The selection of hyper-secretory mutants was made on the basis of enhanced zone of hydrolysis after same incubation period and by analyzing enzyme activity after solid state fermentation batch.

Table 2. Composition of phytase screening medium (PSM)

Ingredients	Concentrations (g/L)	Ingredients	Concentrations (g/L)
Glucose	5	$FeSO_4.7H_2O$	0.01
Phytic acid	3	KCl	0.5
NH_4NO_3	5	$MnSO_4.4H_2O$	0.01
$MgSO_4.7H_2O$	0.5	Agar	20

2.6. Fermentation studies

The fermentation medium (10 g rice polish, 0.5% NH_4NO_3, 0.1% KCl, 0.1% $FeSO_4.7H_2O$ and 0.1% $MgSO_4.7H_2O$) was taken in 250 ml Erlenmeyer flask, after amended with 10 ml distilled water. The medium was autoclaved for sterilization at 121°C for 15 min. After cooling at room temperature, 10% (v/w) of fungal inoculum was added, and kept in an incubator at 37°C for five days.

After incubation, 0.2 M citrate buffer, 50 ml (pH 5.5) was poured to each fermented flask, placed in a water bath shaker at 37°C and shaken for 1.5 hours at 200 rpm. Double layered muslin cloth was used for filtration and centrifugation of filtrate was done at 10,000 rpm for 15 min in a centrifuge machine. Supernatant was collected as crude enzyme extract and phytase activity was measured.

2.7. Phytase assay

Phytase activity was measured by estimation of inorganic phosphorus released from substrate (sodium phytic acid solution), according to the modified methods of McKie & McCleary (2016). Reaction mixture, containing 1% (w/v) phytic acid solution (pH 5.5) and enzyme extract 0.2 ml each, was taken in a test tube and placed in a water bath for 15 min at 37°C.

Then, 0.4 ml of trichloroacetic acid (TCA) 15%, was added to stop the reaction. Afterwards, 2 ml colour reagent was added in the test tube containing above mixture (0.2 ml) and 1.8 ml double distilled water, and incubated at 50°C for 15 min. Absorbance of the liberated inorganic phosphorus was measured at 655 nm.

One-unit phytase activity is defined as the quantity of enzyme required to release 1 μ mole inorganic phosphorus per ml per min using the standard assay conditions.

2.8. Application of phytase as poultry feed additive

The phyatse was checked as poultry feed additive and its effect on the growth performance of broiler chickens was analyzed.

For this purpose, a 5-week feeding trial containing 30 chicks was undertaken with three dietary treatment groups i.e. T0 (control group) without any phytase in the basal diet**,** T1 with phytase @ 1000 IU/Kg diet, T2 with phytase @ 2000 IU/Kg diet. Composition of basal diets given to birds g/100 g, maize 65.65, soybean meal 24, corn gluten meal 3, soybean oil 3, lime stone 1.2, dicalcium phosphate 1.6, vitamin-mineral premix 1, salt 0.3, lysine 0.15, methionine 0.1. Phytase was mixed in liquid form in the feed. Phytase produced from *Aspergillus niger* using solid state fermentation was used as feed supplement for the better growth of chicks.

2.9. Statistical analysis

All the experiments were set up in a completely randomized design (CRD) with three replicates. Analysis of variance of all parameters were computed using COSTAT computer package (CoHort Software, 2003, Monterey, California).

3. Results

The present study includes the screening of microbial strains and fermentation media. It also includes mutational studies of *Aspergillus niger* for enhanced and cost-effective production of phytase using solid state fermentation. The outcome of this study revealed improved and economical production of enzyme by mutant strains compared to wild type.

3.1. Screening of microbial strains and fermentation media for phytase production

Different microbial strains and fermentation media were screened for maximum phytase production. Results shown in Figure 1 indicate that *Aspergillus niger* and M5 fermentation medium produced maximum phytase.

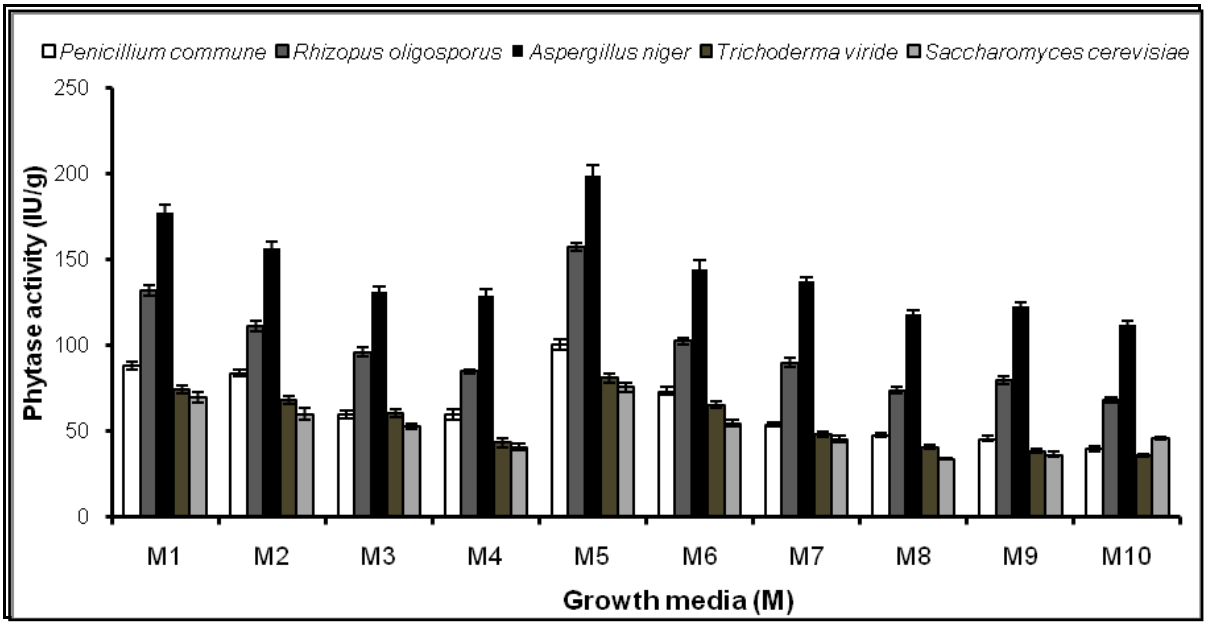

Fig. 1. Screening of microbial strains and fermentation media for phytase production

3.2. Mutagenesis by UV irradiations and EMS treatments

For physical and chemical mutagenesis, the wild strain of *Aspergillus niger* was characterized by exposing to different doses of resistance to UV irradiation i.e. 15-120 min and to EMS treatment for different duration of time i.e. 3-24 hrs, in separate experiments. The results indicated that the survival rate of fungus decreased gradually, it was 77.55% after 15 min and reduced to 8.16% and 2.04% after 90 min and 120 min of exposure time, respectively for UV irradiation (Figure 2 a), whereas for EMS treatment, a survival rate of 81.57% was achieved after 3 hrs, and it became 10.52% after 12 hrs and decreased to 0% after 24 hrs of exposure time (Figure 2 b).

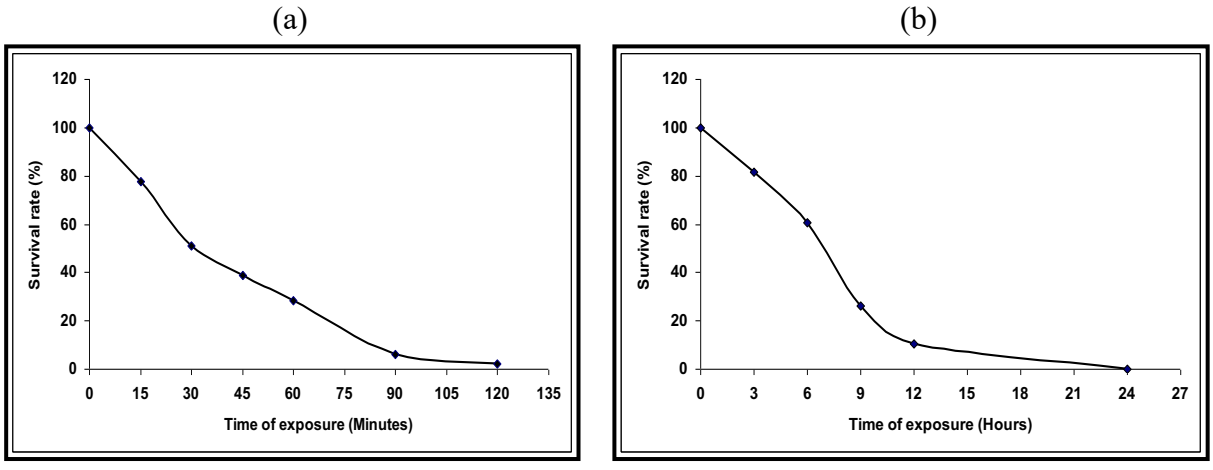

Fig. 2. Survival curves for colonies of *Aspergillus niger* at different exposure time of (a) UV radiations & (b) EMS treatment

3.3. Screening of best mutant strain of *Aspergillus niger* for best phytase production

All the selected colonies of *Aspergillus niger* with minimum rate of survival were streaked on the phytase screening medium (PSM) plates and put in the incubator for 3-5 days at 37°C. The selection of best mutants was carried out on the basis of large zones of hydrolysis. Among UV mutants, largest zone of hydrolysis of 40 mm was formed by UV-3 followed by UV-1 (34 mm) and UV-5 (30 mm) than control (26 mm) as shown in Table 3 & Figure 3. Among EMS mutants, EMS-4, EMS-2 and EMS-1 producing 37 mm, 32 nm and 27 mm zones of clearance, respectively (Table 3 & Figure 4).

Table 3. Comparison of zones of clearance produced by wild and UV & EMS mutant strains of *Aspergillus niger*

Sr. No.	Strains	Zones of clearance (mm)	Sr. No.	Strains	Zones of clearance (mm)
	Wild	26		Wild	26
1	UV-1	34	1	EMS-1	27
2	UV-2	29	2	EMS-2	32
3	UV-3	40	3	EMS-3	ND
4	UV-4	21	4	EMS-4	37
5	UV-5	30			

(UV: Ultra violet irradiations), (EMS = Ethyl methane sulphonate; ND: Not detectable)

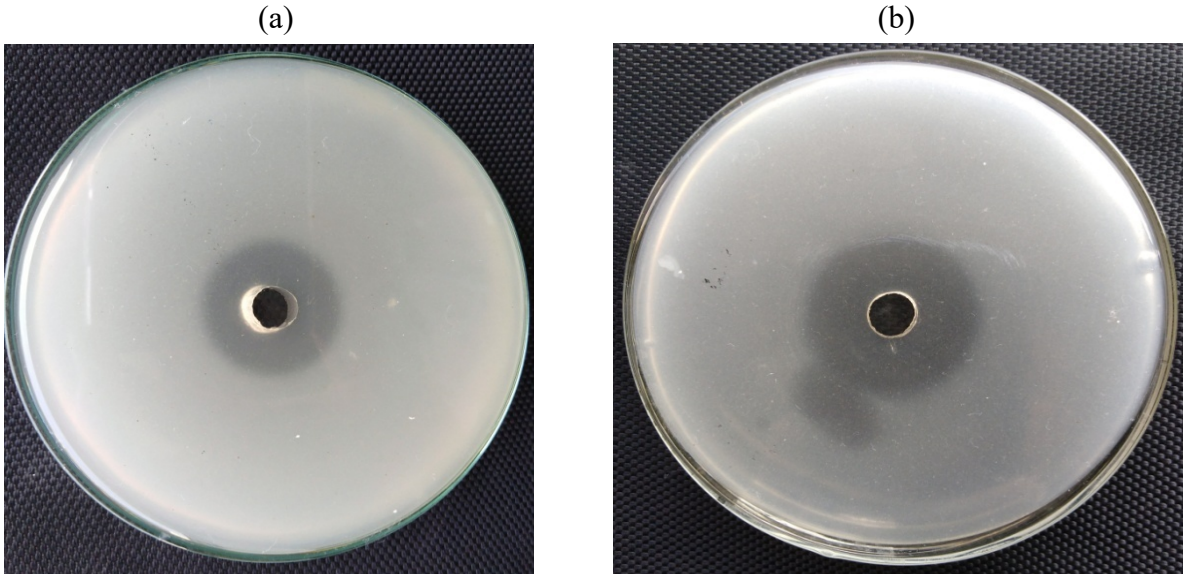

Fig. 3. Zones of clearances shown by (a) control (wild strain) and (b) UV-3 mutant on phytase screening medium after incubation at 37°C for 3-5 days

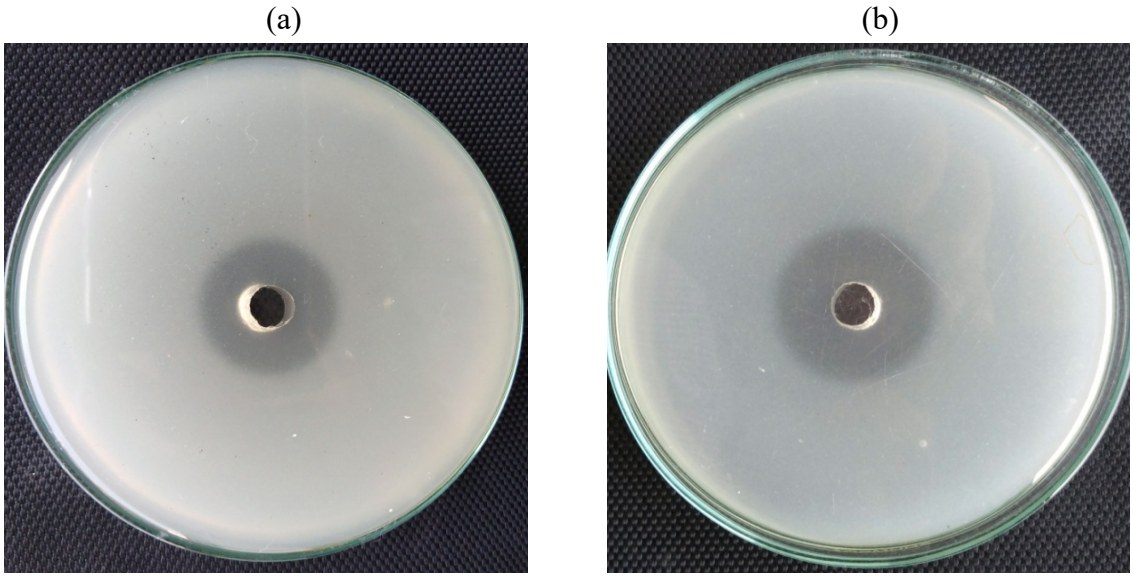

Fig. 4. Zones of clearances shown by (a) control (wild strain) and (b) EMS-4 mutant on phytase screening medium after incubation at 37°C for 3-5 days

3.4. Compararison of phytase production by wild and selected mutant strains of *Aspergillus niger*

All positive mutants (selected on the basis of large zones of hydrolysis on phytase screening medium) were further studied for their potential to produce maximum phytase enzyme by solid state fermentation process at pre-optimized culture conditions and best phytase producer was find out. Among the various positive mutants, the maximum production of phytase was (547.64±7.27 IU/g) given by UV-3 mutant followed by EMS-4 (492.23±5.59 IU/g) and UV-1 (481.54±7.14 IU/g) compared to wild strain (406.45±6.18 IU/g) (Figure 5).

Thus, UV-3 mutant designated as *Aspergillus niger* UV-3 was found to be most hyper secretory (547.64±7.27 IU/g) mutant strain amongst all mutated and wild strains (406.45±6.18 IU/g) as shown in Figure 5. It gave about 1.35-fold increased phytase production compared to the wild strain using similar fermentation conditions. A comparison of other mutagenesis reports with current study is given in Table 4.

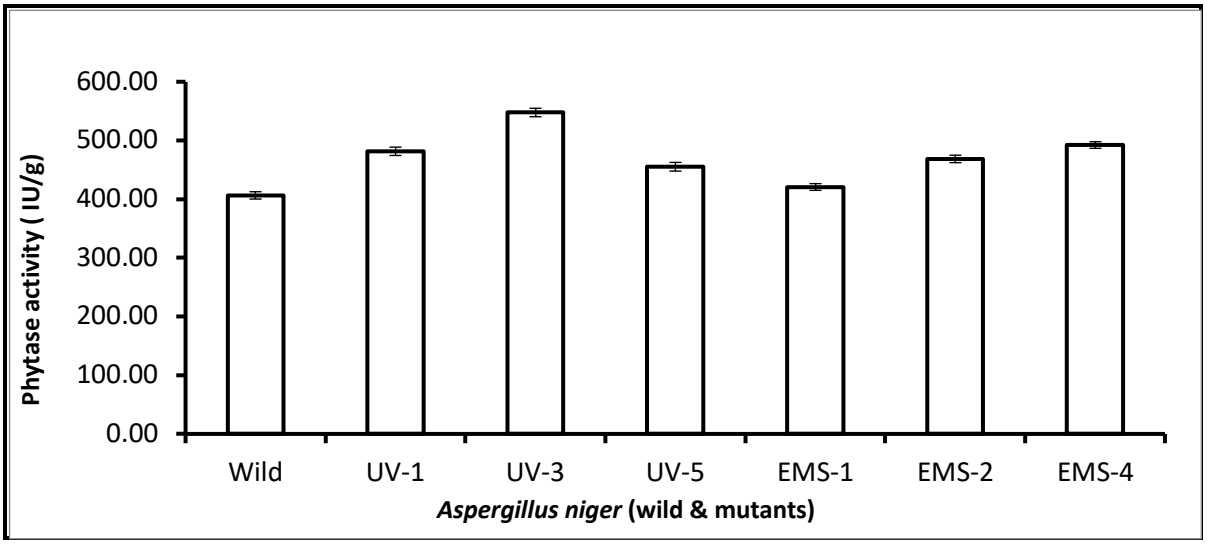

Fig. 5. Comparison of enzyme activities of wild and mutant strain of *Aspergillus niger*. Bars represent standard errors.

Table 4. Comparison of other mutagenesis reports with current study

Mutagens	Microorganisms	Phytase activity		References
		Wild	Mutant	
UV irradiation, Ethyl methyl sulfonate (EMS)	*Aspergillus niger*	406.45 IU/g	547.64 IU/g	Our current study
UV irradiation, Ethyl methyl sulfonate (EMS)	*Aspergillus niger*	6,181 IU/L/D	9,523 IU/L/D	Shah *et al*., 2009
UV irradiation, Ethyl methyl sulfonate (EMS)	*Rhizopus oligosporus*	6.2 U gds^{-1}	31.3 U gds^{-1}	Suresh & Radha (2016)
UV irradiation, Ethidium bromide, Hydroxyl amine	*Aspergillus niger* NCIM1359	254,500 U/l	407,200 U/l	Bhavsar *et al*., 2012
Gamma radiation and Ethyl methyl sulfonate (EMS)	*Sporotrichum thermophile*	6185 U/l/d	19875 U/l/d	Mehmood *et al*., 2019

3.5. Determination of the impact of phytase on the growth performance of broiler chickens

Body weight gain (BWG) of broiler chickens was recorded at weekly interval. Table 5 describes the average body weight gain of chicks after 5 weeks of their age. The results indicated that birds in group T3 had highest average body weight gain (2028 g) compared to other groups.

Table 5. Body weight gain (BWG) g/bird of broiler chickens after 5 weeks

T0	T1	T2
1868	1933	1984
1876	1941	1997
1885	1948	2010
1893	1960	2021
1905	1968	2025
1917	1977	2039
1911	1984	2047
1934	1993	2055
1922	2001	2067
1919	1995	2035
Average 1903	**1970**	**2028**

T0 = Control group (Basal feed without phytase), T1 = with phytase @ 1000 IU/Kg diet, T2 = with phytase @ 2000 IU/Kg diet

4. Discussion

Aspergillus niger was selected as the best strain amongst all the above-mentioned microbial strains for the maximum phytase production using solid state fermentation (SSF) process. Production of phyatse was also obtained by *Aspergillus ficuum* SGA and *Aspergillus niger* CFR 335 (Shivanna & Venkateswaran, 2014) and many other species of genus *Aspergillus* reported by Singh *et al*. (2015); Buddhiwant *et al*. (2016); Thakur *et al*. (2017); Neira-Vielma *et al*. (2018). In the present study, *Aspergillus niger* produced a highest amount of phytase when it was grown in M5 fermentation medium (Rice polish, 0.5% NH_4NO_3, 0.1% $MgSO_4.7H_2O$, 0.1% KCl, 0.1% $FeSO_4.7H_2O$).

In industrial biotechnology, microorganisms have become a major source for the primary and secondary metabolites production, as well as for the synthesis of enzymes and recombinant proteins. Extensive strain improvement studies were carried out, in the beginning by classical mutagenesis and at present by advanced genetic manipulation techniques.

In the current study, mutation of the wild strain of *Aspergillus niger* was carried out in an attempt to find out such an improved hyper-secretory strain which can produce more enzyme. For physical and chemical mutagenesis, different doses of UV irradiations and EMS treatments were given to the wild strain of *Aspergillus niger*. It was noted that the lethality was increased with the increase in dose of these mutagens, and there was decrease in the number of surviving fungal colonies. Several research workers reported that the number of fungal colonies decreases as UV irradiations exposure time increases (Irfan *et al*., 2011; Suresh & Radha, 2016; Castillo *et al*., 2017).

EL-Bondkly & Keera (2007) performed experiments for mutation of *P. roquefortii* and used different doses of EMS mutagen (100 µl/ml). The results indicated that as the mutagen dose increased, the lethality was also improved. They obtained 20.8% and 7% survival rate after 30 and 60 min of EMS exposure time, respectively.

The selected fungal colonies with lower survival rates were streaked on phyatse screening medium (PSM) plates and fungal strains with large zones of hydrolysis were selected and confirmed for enhanced phytase production in solid state fermentation conditions. In many mutation-based research works, the selection of mutants was carried out due to large zones of hydrolysis on sodium phytic acid medium compared to wild strain (Shah *et al*., 2009; Suresh & Radha, 2016).

Among all hyper secretory mutants, *Aspergillus niger* UV-3 mutant exhibited maximum phytase activity (547.64±7.27 IU/g) compared to wild strain (406.45±6.18 IU/g) and improved phytase yield of about 1.35-fold. A mutagenesis study was conducted using UV irradiation and EMS treatment by Suresh & Radha (2016) for obtaining hyper secretory fungal strain. The results showed that among all the mutant strains, *R. oligosporus* MTCC 1116 (0.3% EMS) depicted 31.3 gds^{-1} phytase activity at 116 hrs, and increased the yield of about 4 fold compared to the wild strain with ADT27 Rice bran variety. Shivana & Govindarajulu (2009) treated *Aspergillus niger* CRF 335 in physical and chemical mutagenesis and found improvement in phytase productivity of mutant strain from 0.85 to 1.26 U mg^{-1}.

Mehmood *et al*. (2019) carried out mutagenesis studies on a fungal strain *Sporotrichum thermophile* using gamma rays and EMS treatment for enhanced phytase production. They reported an improved fungal strain ST20, which showed maximum enzyme activity of 19875 U/l/d compared to wild (6185 U/l/d), with an increase in enzyme productivity of 3.2 time that of wild strain.

Biotechnological application of phytase was performed. Phyatse was used as poultry feed additive and its affect on body weight gain (BWG) of chicks was determined. For this purpose, one control group (T0) without phytase in the feed and two experimental groups (T1, T2) with varying concentrations of phytase in the feed were made (as mentioned in text 2.8). The experimental work was carried out for 5 weeks. The results shown in Table 5 revealed that average body weight gain (BWG) of chicks in experimental group T2 (2028 g) was highest compared to the control group (1903 g).

For biotechnological application of phytase, the effect of phytase was studied on the growth performance of broilers by pre-treating corn-soya diets with microbial phytase by Jatuwong *et al*. (2020). They reported that there was an increase of availability of 60% inorganic phosphorus when microbial phytase was given to broilers fed on low phosphorus diet and phosphorus concentration in the chicken manure was decreased by 50%. The results also indicated the 5.8-13.2% increase in body weight of chickens, after 21 days of phytase supplementation in their diet.

It is obvious from the above-mentioned results that phytase has positive effect on the growth performance of broiler chicken when it was supplemented as poultry feed additive. Where it improves the nutrient contents of the diet by degrading phytic acid and release inorganic phosphorous and important minerals in the poultry feed. Therefore, phytase produced by *Aspergillus niger* using solid state fermentation can be employed successfully as poultry feed supplement.

5. Conclusion

In the present research work, UV irradiation and EMS mutagenesis of *Aspergillus niger* was performed for enhanced and low cost phytase production. UV-3 mutant of *Aspergillus niger* was found as hyper secretory strain that could produce maximum enzymatic activity (547.64 IU/g) compared to wild strain (406.45 IU/g). Due to induced mutagenesis, there was about 1.35-fold of increase in phytase production. Growth performance of broiler chickens was improved (1903 g/bird to 2028 g/bird), when phytase was used as poultry feed additive. Thus, strain improvement strategies, using mutagens like UV irradiation and EMS, were proved to be competent techniques for cost effective and higher-level production of phytase by *Aspergillus niger* using solid state fermentation.

ACKNOWLEDGEMENT

The authors gratefully acknowledge the research assistance from the Microbiology Laboratory, Food and Biotechnology Research Centre (FBRC), PCSIR Laboratories complex, Lahore, to conduct this research work.

References

Ahmad, A., Anjum, A.A., Rabbani, M., Ashraf, K., Nawaz, M., *et al.* (2017) Diversity of phyatse producing non-toxigenic fungi isolated from soil. Journal of Animal and Plant Sciences. **27:** 1-8.

Bakri, Y., Ezzeldeen, H. & Akeed, Y. (2018) Screening of phytase producing fungi isolated from Syrian soil. Journal of Biological Innovation, **7:** 462-474.

Bhaskaran, B., Shankar, S. & Sonu, N. (2018) Genetic modification of *Aspergillus niger* by induced mutagenesis for lipase enzyme production. International Journal of Life Sciences, **11:** 91-96.

Buddhiwant, P., Bhavsar, K., Kumar, R. & Khire, V. (2016) Phytase production by solid state fermentation of groundnut oil cake by *Aspergillus niger*: a bioprocess optimization study for animal feedstock applications. Preparative Biochemistry and Biotechnology, **46:** 531-538.

Castillo, B.G., Díez-Municio, M., de la Cruz, J.C. & Moreno, J. (2017) Obtaining mutant fungal strains of *Aspergillus niger* with high production of fructo-oligosaccharides (FOS) using ultraviolet light irradiation. African Journal of Biotechnology**, 16:** 1810-1818.

CoHort Software (2003) CoStat version 6.303, 798 Lighthouse Ave. PMB 320, Monterey, CA, 93940, USA.

Dahiya, S. (2016) Industrial applications of phytases. International Journal of Applied Research, **2(2):** 95-98.

EL-Bondkly, A.M. & Keera, A.A. (2007) UV and EMS-induced mutations affecting synthesis of alkaloids and lipase in *Penicillium roquefortii*. Arab journal of Biotechnology, **10:** 241-248.

Irfan, M., Javed, J. & Syed, Q. (2011) UV mutagenesis of *Aspergillus niger* for enzyme production in submerged fermentation. Pakistan Journal of Biochemistry and Molecular Biology, **44:** 137-140.

Jatuwong, K., Suwannarach, N., Kumla, J., Penkhrue, W., Kakumyan, P. *et al.* (2020) Bioprocess for production, characteristics, and biotechnological applications of fungal phytases. Frontier Microbiology, **11(18):** 1-18.

Kumar, V., Yadav, A.N., Verma, P., Sangwan, P., Saxena, *et al.* (2017) β-Propeller phytases: Diversity, catalytic attributes, current developments and potential biotechnological applications. International Journal of Macromolecules, **98:** 595-609.

McKie, V.A. & McCleary, B.V. (2016) A novel and rapid colorimetric method for measuring total phosphorus and phytic acid in foods and animal feeds. Journal of AOAC International, **99:** 738-743.

Mehmood, A., Baneen, U., Zaheer, A., Sajid, M.W., Hussain, A. *et al.* (2019) Physical and chemical mutagens improved Sporotrichum thermophile, strain ST20 for enhanced Phytase activity. Saudi Journal of Biological Sciences, **26(7):** 1485-1491.

Munir, K. & Maqsood, S. (2013) A review on role of exogenous enzyme supplementation in poultry production. Emir. Journal of Food and Agriculture. **25:** 66-80.

Neira-Vielma, A.A., Aguilar, C.N., Ilyina, A., Contreras-Esquivel, J.C., Michelena-Alvarez, G. *et al.* (2018) Purification and biochemical characterization of an *Aspergillus niger* phytase produced by solid-state fermentation using triticale residues as substrate. Biotechnology reports, **17:** 49-54.

Rao, D.E., Rao, K.V., Reddy, T.P. & Reddy, V.D. (2009) Molecular characterization, physicochemical properties, known and potential applications of phytases: an overview. Critical Reviews in Biotechnology, **29:** 182-198.

Rasul, M., Yasmin, S., Suleman, M., Zaheer, A., Reitz, T., *et al.* (2019) Glucose dehydrogenase gene containing phosphobacteria for biofortification of Phosphorus with growth promotion of rice. Microbiological Research, **223:** 1-12.

Salmon, D.N.X., Piva, L.C., Binati, R.L., Rodrigues, C., Vandenberghe, L.P., *et al.* (2012) A bioprocess for the production of phytase from *Schizophyllum commune:* studies of its optimization, profile of fermentation parameters, characterization and stability. Bioprocess and Biosystems Engineering, **35**: 1067-1079.

Sandhya, A., Sridevi, A., Devi, S.P. & Narasimha, G. (2015) Potential fungal phytase producers from rhizosphere soils. International Journal of Advance Biotechnological Research, **6:** 227-23.

Shah, P., Bhavsar, K., Soni, S.K. & Khire, J.M. (2009) Strain improvement and up scaling of phytase production by *Aspergillus niger* NCIM 563 under submerged fermentation conditions. Journal of Industrial Microbiology and Biotechnology, **36:** 373-380.

Shivanna G.B. & Govindarajulu, V. (2009) Screening of asporogenic mutants of phytase producing *Aspergillus niger* CFR 335 strain. Microbial Ecology in Health and Disease, **21:** 57-63.

Shivanna, G.B. & Venkateswaran, G. (2014) Phytase production by *Aspergillus niger* CFR335 and *Aspergillus ficuum* SGA 01 through submerged and solid-state fermentation. The Scientific World Journal, Pp: 1-6.

Singh, B. & Satyanarayana, T. (2010) Plant growth promotion by an extracellular HAP-phytase of a thermophilic mold *Sporotrichum thermophile*. Applied Biochemistry and Biotechnology, **160:** 1267-1276.

Singh, N., Kumari, A., Gakhar, S. & Singh, B. (2015) Enhanced cost-effective phytase production by *Aspergillus niger* and its applicability in dephytinization of food ingredients. Microbiology, **84:** 219-226.

Suresh, S. & Radha, K.V. (2016) Statistical optimization and mutagenesis for high level of phytase production by *Rhizopus oligosporus* MTCC 556 under solid state fermentation. Journal of Environmental Biology, **37:** 253-260.

Thakur, N., kumar, P. & Chand, D. (2017) Enhanced production of phytase from thermotolerant *Aspergillus fumigatus* isolated from rhizospheric zone of maize fields. Journal of Innovations in Pharmaceutical and Biological Sciences, **4**(3): 114-120.

Vasudevan, U.M., Shyam, K., Vidya, J. & Pandey, A. (2017) Microbial phytase: impact of advances in genetic engineering in revolutionizing its properties and applications. Bioresource Technology, **245:** 1790-1799.

Yao, M.Z., Zhang, Y.H. & Lu, W.L. (2011) Phytases: crystal structures, protein engineering and potential biotechnological applications. Journal of Applied Microbiology, **112:** 1-14.

Zaheer, A., Malik, A., Sher. A., Qaisrani, M.M., Mehmood, A., *et al.* (2019) Isolation, characterization and effect of phosphate-zinc solubilizing bacterial strains on chickpea (*Cicer arietinum* L.) growth. Saudi Journal of Biological Science, **26:** 1061-1067.

Submitted: 31/08/2021
Revised: 13/11/2021
Accepted: 27/11/2021
DOI: 10.48129/kjs.15995

Eradication of *Klebsiella pneumoniae* biofilms and persister cells using silver nitrate

Sarah Naji Aziz[1,*], Mohammed F. Al Marjani[1]

[1] *Dept. of Biology, College of Science, Mustansiriyah University, Baghdad, Iraq*

[*] *Corresponding author: sarahnaji@uomustansiriyah.edu.iq*

Abstract

To perceive the relationship between the emergences of antibiotics persistence, biofilm formation, and to study the role of silver nitrate in fighting these microbes, a total 50 clinical *Klebsiella pneumonae* isolates were collected from clinical sources and identified using genotypic identification by using specific primer (*rpoB* gene) from housekeeping genes. Detection of their biofilm-forming abilities were carried out. The eradication effect of silver nitrate to control bacterial persistence and reducing the biofilm-forming abilities were studied. We found that 40 isolate (80%) were biofilm-formers. From bacterial persisters, (75%) were biofilm-formers. Silver nitrate showed a great role to eradicate persister cells and inhibition of bacterial biofilm formation of clinical isolates of *K. pneumoniae.*

Keywords: Biofilms; *Klebsiella pneumonia*; persister cells; *rpoB*; silver nitrate.

1. Introduction

Klebsiella pneumoniae (*K. pneumoniae*), is a gram-negative, opportunistic pathogen, which belong to the "ESKAPE" group bacteria These bacteria are often inhabiting the skin, mouth, respiratory and gastrointestinal tracts (Li, *et al.,* 2014). Many infections and diseases caused by *K. pneumoniae* for examples, pneumonia, urinary tract infection, pyogenic liver abscesses, endogenous endophthalmitis and septicemia (Navon-Venezia *et al.,* 2017). Recently, *K. pneumoniae* being a universal concern in health threat due to prevailing capacity of acquiring antibiotic resistance. (Qin, *et al.,* 2020). Furthermore, persistence of bacteria due to antibiotic or other stress-response phenomenon, is also one of the most reasons for antibiotic therapy failure (Jung, *et.al.* 2019).

Persister cells formation is a phenomenon in which subpopulation inside a susceptible bacterial population can survive treatment of lethal doses of antibiotics. The persister cells show some characteristics such as being about only 0.0001% to a maximum 10% (Spoering & Lewis, 2001; Lewis, 2005), unlike resistance, persister cells cannot grow within antibiotic presence, and they barely survive (Lewis, 2010). Persister cells are not dependent on MIC and in contradiction to the resistance in which result in variations (a rise) in antibiotic MIC levels based on the bacterial capabilities to counterbalance the antibiotic's efficiency. Furthermore, they inheritable and cannot pass their factures to their new generations when stresses are removed.

Bacterial persistence is the main reason of the recalcitrance of chronic bacterial infections (Abokhalil, *et al.,* 2020). Antibiotic therapy failure is known as a serious threat which is typically related with the antibiotic resistance. But it is not the only issue. In fact, bacterial persister cells

which is antibiotic stress-response phenomenon, is also one of the most reasons for antibiotic therapy failure (Jung, *et.al.* 2019).

The ability of *K. pneumoniae* to produce biofilm encourages its survival and persistence in the hospital environments (Donlan & Costerton, 2002), which in turn participates in the *K. pneumoniae* extreme prevalence across many environments. Silver nitrate has typically been applied to newborn infants' eyes to combat their eye infections. Silver nitrate are is frequently employed in the clinic and for public health management as potent antimicrobial agents (Milionis *et al*., 2018). Besides being a strong topical broad-spectrum antimicrobial used in wound burns, as coatings for catheters and endotracheal tubes, and as disinfectant (Phan, *et al*., 2019). However, this compound has a toxic effect (especially if administered with high concentrations. This minimizes the use of silver nitrate in clinical practice and gave the light for the combination usage of silver compounds and antibiotics to promise the path for both of antibiotics activates restoring and the chemicals' toxicity precluding (Mohamed, 2019). A recent study by (Abokhalil, *et al*., 2020) have reported the complete eradication of persisters by using both of silver nitrate and ciprofloxacin antibiotic. In Iraq, there are few studies on silver nitrate role to control bacterial persistence. Therefore, the current study amid to investigate the activity of silver nitrate in eradicating bacterial persistence and biofilm formation of clinical isolates of *K. pneumoniae.*

2. Materials and methods

2.1 Bacterial isolation, identification, growth conditions and chemicals

A total of 50 *Klebsiella* species were collected from Teaching Laboratories in Medical city/ Baghdad from September 2020 to November 2020. These isolates were identified as *K. pneumonae* by Conventional PCR assay using a primer of *rpoB* gene from housekeeping genes with the following sequence (F - GGC GAA ATG GCW GAG AAC) (R- GAG TCT TCG AAG TTG TAA). The PCR reaction mixture consisted of 12.5 µl of 2X GoTaq®Green Master Mix (KAPA, 166 South Afriqa), 2 µl template DNA, 1.5 µl primers for each forward and reverse primers with final concentration (0.6 pmol/ µl), and nuclease free water up to 25 µl (6.5 µl). The amplified PCR product was run in agarose gel electrophoresis, the amplification size 1056 bp as compared with 1000 bp DNA ladder (KAPA, south Afriqa). The *rpoB* gene was visualized under UV trans-illuminator.

The bacterial isolates were routinely cultured in LB broth or agar at 37 °C. Silver nitrate powder ($AgNO_3$) was purchased from (Sigma/Aldrich/U.S) and 0.5 gm were dissolved in 50 ml dimethyl sulfoxide (DMSO), mixed and filtered by using sterile filtration (0.22 µm) membrane filter to produce 10 µg/ml of stock solution then stored at room temperature.

2.2. Detection of persister cells.

Persister cells assay was determined by measuring the ability of persister cells to survive the bactericidal doses of ciprofloxacin. An overnight culture was exposed to centrifugation at 12,000 rpm for a few minutes at 37°C and washed twice with normal saline then re-suspended and exposed to different ciprofloxacin concentrations (100–1000 ug/ml) and shacked overnight at 37 °C and 200 rpm. In the next day, the cells were washed twice with normal saline to remove ciprofloxacin.

Finally, 10 µl of the culture spread onto LB agar plates for measuring the frequencies of persister cells.

2.3. Antibacterial activity and MIC of silver nitrate

Antibacterial activity of silver nitrate toward persistence *K. pneumoniae* isolates was tested using the agar well diffusion method (Yaseen, *et al.,* 2019). The minimum inhibitory concentration (MIC) was carried out using the 96-well microtiter plate. Briefly, 100 µl of LB broth was added to flat well-microtiter plate wells, then wells of the first vertical row were filled with 100 µl of silver nitrate (10 mg/ml) followed by mixing 1:2 serial dilutions. 100µl from the last well was discarded. Then all wells of the microtiter plate were filled with 2 µl of bacterial suspension (1.5×10^8 CFU/ml) from fresh growth of an overnight (except negative control wells were filled with LB broth only) and incubated overnight at 37 °C. The next day, the MIC of silver nitrate was registered by using the optical density (OD) of ELISA reader. The test was carried out in triplicate.

2.4. Biofilm formation assay

For evaluating the biofilm-form capacity, the total 50 *K. pneumoniae* isolate were cultured in brain heart broth (BHB) overnight at 37 °C. Then, bacterial cultures were diluted to make a bacterial suspension equivalent to 0.5 McFarland solution. 20 µl of bacterial suspension were pipetted inside wells of flat microtiter plates with 180 µl of BHB added up to 2% sucrose and incubated overnight at 37 °C. After the incubation period, the plates were washed three times with sterile normal saline for removing unattached bacterial cells. After drying at room temperature, wells were stained with 200 µl of crystal violet solution for 15 min. Therefore, the unstained dye was discarded by washing with normal saline. Finally, 200 µl of 95% ethanol was added to each well. The OD was determined at 630 nm using ELISA reader (BioTek). Each isolate was tested in triplicate. The adherence capacities of the assay isolates were classified into four categories; the mean optical density of the negative control was counted as:

$OD \leq ODc$, the bacteria were non-adherent;
If $ODc < OD \leq 2 \times ODc$, the bacteria were weakly adherent;
If $2 \times ODc < OD \leq 4 \times ODc$, the bacteria were moderately adherent;
If $4 \times ODc < OD$, the bacteria were strongly adherent

2.5. Inhibition of biofilm-forming assay

The activity of silver nitrate on biofilm formation of persistence *K. pneumoniae* isolates was achieved according to the previous study (Theodora, *et al.,* 2019). Briefly, *K. pneumonia* isolates were inoculated in BHI broth overnight at 37 ˚C. The growing cultures were suspended to the (1.5×10^8 CFU/ml).Then, 20 µl of bacterial suspension was inoculated in 96 well flat microtiter plate containing 80 µl of BHI broth with 2% sucrose, and 100 µl from sub-MIC of silver nitrate (2.5mg/ ml) were added and mixed by pipette sucking up and down then incubated for 24 h at 37 ˚C. After two washes with normal saline (pH: 7.2). For draining the wells, the microtiter plate allowed to be dried at room temperature. Unattached bacterial cells were removed. 200 µl of crystal violet solution was used for biofilm staining. The stain was eluted with 200 µl of 95% ethanol, and

the optical density was measured at 630 nm using an ELISA reader. The negative control was filled with BHI broth only, while the biofilm production with bacterial suspension without silver nitrate were positive controls. The assay was carried out in triplicate. To calculate the rate of inhibition caused by silver nitrate, the following formula was applied:

Inhibition rate (%) = (Control OD − Treated OD) / (Control OD) × 100

2.6. Statistical analysis

The data results of this study were analyzed by using Graph Pad Prism 8 software and Microsoft Excel 2013 for each biological replicate. The level of probability at P values below of ≤ 0.05 that used to identify a significant difference.

3. Results and discussion

3.1 Bacterial isolates, identification and growth conditions

The isolates were collected from different clinical sources and the identification of *K. pneumoniae* isolates were carried out by gene sequence analysis of *rpoB gene*. Figure (1), shows the amplification of *rpoB* gene in the gel electrophoresis for detecting *K. pneumoniae* isolates. The advancement of *rpoB* gene analysis has given rise to rapid diagnostic techniques for the identification of *K. pneumoniae* (Kareem *et al.,* 2021).

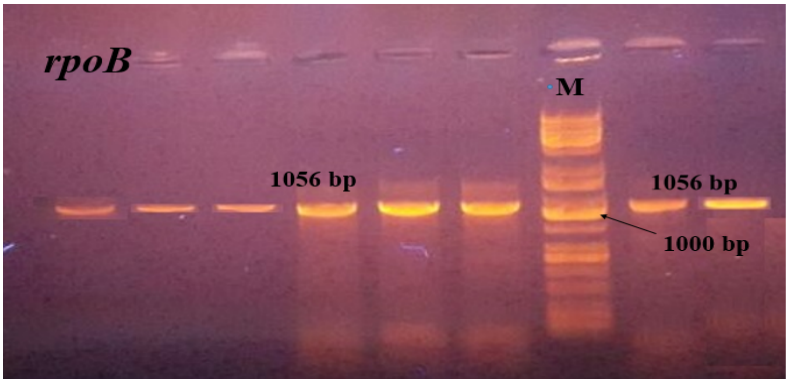

Fig. 1. Gel electrophoresis (1% agarose, 70 volt for 50 min) of 16S *rpoB* gene amplification for detecting *K. pneumoniae* isolates. Line M 1000 bp is the ladder, other lines are the positive results of *rpoB* gene of Isolates.

3.2 Detection of persister cells formation

Persister cells of *K. pneumoniae* were generated by phenotypic detection using different doses of sub-MIC for the ciprofloxacin (up to 1000 µg/ ml). Results exposed that eight isolates had persistence ability which were formed during the stationary growth phase (Song & Wood, 2021). Bactericidal antibiotics such as ciprofloxacin killed the normal growing cells, while the dormant cells during antibiotic stress, remained survived. Clinically, these persister cells are the start of the chronic infections, which results in the overuse of antibiotics and reduced antibiotic activity. *S. aurous* for an example, engages in persistent, relapsing infections that are often difficult to eliminate with antibiotics, such as osteomyelitis (Bakkeren *et al*., 2020; Ali *et al*., 2021).

3.3 Detection of persister cell inhibition by silver nitrate

To study the silver nitrate antibacterial activity against eight persistent *K. pneumoniae* isolates, agar-well diffusion assay were carried out. Results showed a potential bactericidal activity of silver nitrate toward persister cells of the *K. pneumoniae* isolates with inhibition zones between (24 mm) and (35 mm) Moreover, the MIC of silver nitrate realized the 0.31 µg/ml in the eight isolates, while the potential anti-persistence forming ability of the sub-MIC was about 0.5mg/ml. Our results confirmed the resent result of (Öztürk, *et al.,* 2020) when they reported both of the anti-biofilm and anti-microbial activities of green synthesized silver nanoparticles. Therefore, our results represent the ability of silver nitrate to eradicate the persister cells of a very urgent pathogen such as of *K. pneumoniae* which emerged as one of the most antibiotic resistant microbes responsible for outbreaks in both community and healthcare settings (Narimisa, *et al.,* 2020). Furthermore, to investigate the elimination of persister cells by silver nitrate, the method used by Aziz *et al*,2022. were done by treating of persister cells with silver nitrate for (6 h, 12h, and to 234h) and results showed that there is any observing for the persister cells in the media, which confirmed the total eradication of persister cells by silver nitrate at the concentration of 1024 mg/ml (Aziz *et al*, 2022).

3.4 Detection of biofilm and Its inhibition assay

Forty *K. pneumoniae* isoltes were biofilm producers, while only ten isolates were non producers. Fourthermore, all persistence isolates (8/50) were with biofilm forming ability. The biofilm may serve to induce resistance, persistence, and also act as a shield of persister cells from elimination by bactericidal agents. This supported by (Baek *et al.,* 2020; RAY *et al.,* 2021). Many publications have indicated that persister cells of various pathogenic bacteria were generated by lowering metabolic activity in biofilm after triggering some severe stringent responses such as the toxin-antitoxin system (Amato *et al.,* 2014; Harms *et al.,* 2016; Carvalho *et al.,* 2018; Soares *et al.,* 2019; Karimaei *et al.,* 2021; Uruén *et al.,* 2021). The biofilm inhibitory effect of silver nitrate against persister cells of *K. pneumoniae* isolates were significant due to the converting of the strong and moderate forming isolates to weak and non-biofilm producers after exposed to 2.5mg/ ml concentration dose of silver nitrate. Silver ions known as antimicrobial and so can change the biofilm profile of persister cells by many mechanisms as disrupting the multiple bacterial cellular networks and processes, resulting in the destabilization of the cellular envelope and the production of ROS in Gram-negative bacteria (Morones-Ramirez *et al*., 2013).

The frequency of persistence *K. pneumoniae* prevalence in Iraqi hospitals and laboratories has been increased, to control bacterial persistence, our study showed the effectiveness of silver nitrate in eradicating *K. pneumoniae* persister cells , and their derived biofilm formation. To our knowledge, this is the first study from Iraq to show the activity of silver nitrate compounds in inhibiting persister cells and biofilm formation of *K. pneumonia* isolates in vitro. Importantly, our findings suggest silver nitrate compounds may facilitate eradicating bacterial persistence which ssociated with chronic and periodic infections, and antibiotic therapy failure. We recommend further studies to investigate the relationship between the presences of some persisters genes and silver nitrate role of silver nitrate in persistence.

ACKNOWLEDGEMENTS

The authors would like to thank Mustansiriyah University (https://uomustansiriyah.edu.iq/)/ Baghdad, Iraq, for its support to complete this work.

References

Abokhalil, R.N., Elkhatib, W.F., Aboulwafa, M.M. and Hassouna, N.A., 2020. Persisters of *Klebsiella pneumoniae* and Proteus mirabilis: a common phenomenon and different behavior Profiles. *Current microbiology*, *77*(7), pp.1233-1244.

Ali, F., Kamal, S., Shakeela, Q. and Ahmed, S., 2021. Extended-spectrum and Metallo-beta lactamase enzymes mediated resistance in Pseudomonas aeruginosa in clinically isolated specimens. *Kuwait Journal of Science*, *48*(2).

Amato, S.M., Fazen, C.H., Henry, T.C., Mok, W.W., Orman, M.A., Sandvik, E.L., Volzing, K.G. and Brynildsen, M.P., 2014. The role of metabolism in bacterial persistence. *Frontiers in microbiology*, *5*, p.70.

Aziz, S.N., Al Marjani, M.F., Rheima, A.M. and Al Kadmy, I.M., 2022. Antibacterial, antibiofilm, and antipersister cells formation of green synthesis silver nanoparticles and graphene nanosheets against Klebsiella pneumoniae. *Reviews in Medical Microbiology*, *33*(1), pp.56-63.

Baek, M.S., Chung, E.S., Jung, D.S. and Ko, K.S., 2020. Effect of colistin-based antibiotic combinations on the eradication of persister cells in *Pseudomonas aeruginosa*. *Journal of Antimicrobial Chemotherapy*, *75*(4), pp.917-924.

Bakkeren, E., Diard, M. and Hardt, W.D., 2020. Evolutionary causes and consequences of bacterial antibiotic persistence. *Nature Reviews Microbiology*, *18*(9), pp.479-490.

Carvalho, G., Balestrino, D., Forestier, C. and Mathias, J.D., 2018. How do environment-dependent switching rates between susceptible and persister cells affect the dynamics of biofilms faced with antibiotics?. *npj Biofilms and Microbiomes*, *4*(1), pp.1-8.

Donlan, R.M. and Costerton, J.W., 2002. Biofilms: survival mechanisms of clinically relevant microorganisms. *Clinical microbiology reviews*, *15*(2), pp.167-193.

Harms, A., Maisonneuve, E. and Gerdes, K., 2016. Mechanisms of bacterial persistence during stress and antibiotic exposure. *Science*, *354*(6318).

Jung, S.H., Ryu, C.M. and Kim, J.S., 2019. Bacterial persistence: Fundamentals and clinical importance. *Journal of Microbiology*, *57*(10), pp.829-835.

Kareem, S.M., Al-Kadmy, I.M., Kazaal, S.S., Ali, A.N.M., Aziz, S.N., Makharita, R.R., Algammal, A.M., Al-Rejaie, S., Behl, T., Batiha, G.E.S., El-Mokhtar, M.A., Hetta, H. F. , M.A., 2021. Detection of gyra and parc mutations and prevalence of plasmid-mediated quinolone resistance genes in *Klebsiella pneumoniae*. *Infection and Drug Resistance*, *14*, p.555.

Karimaei, S., Aghamir, S.M.K., Foroushani, A.R. and Pourmand, M.R., 2021. Antibiotic tolerance in biofilm persister cells of Staphylococcus aureus and expression of toxin-antitoxin system genes. *Microbial Pathogenesis*, *159*, p.105126.

Lewis, K., 2005. Persister cells and the riddle of biofilm survival. *Biochemistry (Moscow)*, *70*(2), pp.267-274.

Lewis, K., 2010. Persister cells. *Annual review of microbiology*, *64*, pp.357-372.

Li, B., Zhao, Y., Liu, C., Chen, Z. and Zhou, D., 2014. Molecular pathogenesis of *Klebsiella pneumoniae. Future microbiology*, *9*(9), pp.1071-1081.

Milionis, I., Banti, C.N., Sainis, I., Raptopoulou, C.P., Psycharis, V., Kourkoumelis, N. and Hadjikakou, S.K., 2018. Silver ciprofloxacin (CIPAG): a successful combination of chemically modified antibiotic in inorganic–organic hybrid. *JBIC Journal of Biological Inorganic Chemistry*, *23*(5), pp.705-723.

Mohamed, G., 2019. COMBINATION OF CIPROFLOXACIN AND SILVER NANOPARTICLES FOR TREATMENT OF MULTI-DRUG RESISTANT PSEUDOMONAS AERUGINOSA IN EGYPT. *Al-Azhar Journal of Pharmaceutical Sciences*, *59*(1), pp.107-122.

Morones-Ramirez, J.R., Winkler, J.A., Spina, C.S. and Collins, J.J., 2013. Silver enhances antibiotic activity against gram-negative bacteria. *Science translational medicine*, *5*(190), pp.190ra81-190ra81.

Narimisa, N., Amraei, F., Kalani, B.S., Azarnezhad, A. and Jazi, F.M., 2020. Biofilm establishment, biofilm persister cell formation, and relative gene expression analysis of type II toxin-antitoxin system in *Klebsiella pneumoniae*. *Gene Reports*, *21*, p.100846

Navon-Venezia, S., Kondratyeva, K. and Carattoli, A., 2017. *Klebsiella pneumoniae*: a major worldwide source and shuttle for antibiotic resistance. *FEMS microbiology reviews*, *41*(3), pp.252-275.

Öztürk, B.Y., Gürsu, B.Y. and Dağ, İ., 2020. Antibiofilm and antimicrobial activities of green synthesized silver nanoparticles using marine red algae *Gelidium corneum*. *Process Biochemistry,* 89, pp.208-219.

Phan, D.N., Dorjjugder, N., Saito, Y., Taguchi, G., Lee, H., Lee, J.S. and Kim, I.S., 2019. The mechanistic actions of different silver species at the surfaces of polyacrylonitrile nanofibers regarding antibacterial activities. *Materials Today Communications*, *21*, p.100622.

Qin, X., Wu, S., Hao, M., Zhu, J., Ding, B., Yang, Y., Xu, X., Wang, M., Yang, F. and Hu, F., 2020. The Colonization of Carbapenem-Resistant *Klebsiella pneumoniae*: Epidemiology, Resistance Mechanisms, and Risk Factors in Patients Admitted to Intensive Care Units in China. *The Journal of infectious diseases*, *221*(Supplement_2), pp.S206-S214.

RAY, R.R., Lahiri, D., Nag, M., Dey, S. and Dutta, B., 2021. Phytocompounds of Curcuma longa extract are more effective against bacterial biofilm than pure curcumin only-an in-vitro and in-silico analysis. *Kuwait Journal of Science*, *48*(2).

Soares, A., Roussel, V., Pestel-Caron, M., Barreau, M., Caron, F., Bouffartigues, E., Chevalier, S. and Etienne, M., 2019. Understanding ciprofloxacin failure in Pseudomonas aeruginosa biofilm: persister cells survive matrix disruption. *Frontiers in microbiology*, *10*, p.2603.

Song, S. and Wood, T.K., 2021. Are we really studying persister cells?. *Environmental microbiology reports*, *13*(1), pp.3-7.

Spoering, A.L. and Lewis, K.I.M., 2001. Biofilms and planktonic cells of *Pseudomonas aeruginosa* have similar resistance to killing by antimicrobials. *Journal of bacteriology*, 183(23), pp.6746-6751.

Theodora, N.A., Dominika, V. and Waturangi, D.E., 2019. Screening and quantification of anti-quorum sensing and antibiofilm activities of phyllosphere bacteria against biofilm forming bacteria. *BMC Research Notes*, *12*(1), p.732.

Uruén, C., Chopo-Escuin, G., Tommassen, J., Mainar-Jaime, R.C. and Arenas, J., 2021. Biofilms as promoters of bacterial antibiotic resistance and tolerance. *Antibiotics*, *10*(1), p.3.

Yaseen, S.M., Abid, H.A., Kadhim, A.A. and Aboglida, E.E., 2019. Antibacterial activity of palm heart extracts collected from Iraqi *Phoenix dactylifera L*. *Journal of Techniques*, *1*(1), pp.52-59.

Submitted: 13/07/2021
Revised: 06/01/2022
Accepted: 19/04/2022
DOI: 10.48129/kjs.15153

Kuwait J.Sci., Vol.50, No.(1A),January.2023,pp(88-112

Faunistic analysis of insects of Deva Vatala National Park and agroecosystem of Gujrat Pakistan

Muhammad Umar, Mubashar Hussain *

Dept. of Zoology, University of Gujrat, Punjab, Pakistan

**Corresponding author: dr.mubashar@uog.edu.pk*

Abstract

Protected areas provide diverse resources with the least disturbance in a habitat that favours insect species belonging to different guilds to coexist and contribute to the ecosystem processes. Whereas agricultural landscapes are expected to affect the distribution patterns of insect fauna. To understand the species composition and abundance of the agricultural landscape, we explored insect fauna in Deva Vatala National Park (DVNP), Bhimber (Azad Kashmir), and associated croplands of Gujrat, Punjab, Pakistan. We explored the diversity of insect orders, families, and species. Fortnightly surveys were conducted during 2017-2019. We sampled insects by handpicking, using sweep nets, light traps, and pitfall traps. The specimens were identified by using taxonomic keys. We recorded a total of 239 insect species representing 10 orders and 69 families from both habitat types. Data showed significant differences in community composition at species, family, and order levels. Overall insect orders and families demonstrated significant differences ($p< 0.05$) in either abundance or richness or both between the two types of habitats. Coleoptera was the dominant insect order with 15 families and 71 species with a relative abundance of 14.20 %. Among families, Scarabaeidae (dung beetles), Carabidae (ground beetles), and Coccinellidae (ladybird beetles) showed greater species richness in DVNP. Similarly, we also noted 12 families and 54 species of Coleoptera with a relative abundance of 14.20 % in the croplands of Gujrat. The overall greater abundance of insect orders was observed in DVNP. The study concludes that both habitats share insect diversity though variations in species richness of different groups differ significantly. Protected areas adjacent to croplands have the potential to contribute immensely to biodiversity conservation and the provision of ecosystem services.

Keywords: Acrididae; agricultural landscapes; beetles; insect fauna; scarabaeidae.

1. Introduction

Insects constitute about three-fourths of the total organisms (Sankarganesh, 2017), and out of 5.57-9.8 million estimated animals, 4-8 million species are insects (Lokeshwari & Shantibala, 2010). Insects are one of the most diverse and successful groups of animals on this planet that make the major fauna of the terrestrial ecosystem (Samways & Samways, 2005; Collins & Thomas, 2012). Insect trophic interactions contribute to the stability of microhabitats as they regulate many ecological processes in terrestrial ecosystems (Abdala-Roberts *et al.*, 2019). They disperse seeds, pollinate plants, cycle nutrients, act as a food source for other animals, and maintain the fertility and structure of the soil (Foottit & Adler, 2018). The dynamics of insect population depend on the

nutrient quality of plants and this association between plants and insects has attracted the interest of many ecologists (Arshad, 2020).

Insect fauna has an established role in all terrestrial landscapes including agroecosystems and protected areas. Many crops, ornamental plants, and tree plantations are dependent on insects for pollination in these landscapes (Cock *et al.*, 2012; Hodgson, 2012). Agricultural sustainability, environmental quality, and food security are threatened by declining trends in biodiversity loss (Udawatta *et al.*, 2019) mainly due to habitat modification, habitat fragmentation, and ultimately habitat loss (Rogan & Lacher Jr, 2018). Agricultural expansion, one of the most dominant and impactful anthropogenic disturbances, has caused global habitat loss and fragmentation (Haddad *et al.*, 2015; Pardini *et al.*, 2017). Agroecosystems are critical in determining the biodiversity in the adjacent natural landscapes (Muñoz-Sáez *et al.*, 2017). This threatens biological diversity and ultimately poses a menace to human populations (Wilkinson *et al.*, 2018). Protected areas in the form of National Parks have been found effective at limiting deforestation and protecting biodiversity within their boundaries (Naughton-Treves *et al.*, 2005; Dosso *et al.*, 2012; Suratman, 2018).

The present study was conducted to explore the insect fauna of Gujrat and Deva Vatala National Park (DVNP), Azad Jammu & Kashmir. This study aimed to provide the first assessment of the insect fauna in the protected area (DVNP) and the associated agricultural landscape of Gujrat. We documented the insect community composition within DVNP, providing a quantified basis for insect monitoring and conservation. This provided a template for similar studies in the region for assessing characteristic species including both beneficial and pest species in croplands and protected areas. This would contribute to understanding how best to manage these landscapes for the conservation of biodiversity and local communities. Thus, the study aims to provide an up-to-date checklist of insects and their general patterns of spatio-temporal distribution in Gujrat and DVNP. We envisage this would assist in planning for the conservation of insect fauna in these agricultural landscapes.

2. Materials and Methods

2.1 Study Area

The study was conducted in Deva Vatala National Park (DVNP), Bhimber (AJ&K), and Gujrat, Punjab, Pakistan (Fig. 1). DVNP is situated to the west of the line of control between Pakistan and India at 32°51-32°55N, 74°16-74°24E, representing sub-tropical semi-evergreen forests (Grimmett *et al.*, 2008) and cultivated areas dominated by wheat crops (Anwar *et al.*, 2015; Umar *et al.*, 2021) over an undulating terrain of the Deva and Vatala ranges (GOAJ&K, 1985). DVNP was declared as a National Park in 2007, which covers an area of 2,993 ha in the Western Himalayan foothills at an elevation of 267 to 536m above sea level.

Deva Vatala National Park is located in Azad Jammu and Kashmir, area is flat and hilly with different types of trees species i.e., *Dalbergia sissoo*, *Zanthoxylum armatum*, *Launea coromendaliana*, *Butea monosperma*, *Acacia nilotica*, *Calotropis procera*, *Cassia occidentalis*, and *Mangifera indica* (Subhani *et al.*, 2010). The common names of these trees are *Dalbergia sissoo*, *Zanthoxy lumarmatum*, *Launea coromendaliana*, *Butea monosperma*, *Acacia nilotica*, *Calotropis procera*, *Cassia occidentalis,* and *Mangifera indica* (Umar *et al.*, 2021).

Whereas Gujrat is an industrial city in Punjab, Pakistan, located between the Chenab and Jhelum Rivers (32°34'26" N, 74°4'44" E). By population, it is the 20th largest city, covering an area of 65 km^2, representing a large-scale variation in topography. This region falls in the temperate zone with temperatures ranging from 2°C-45°C.

This area is mainly comprised of three habitat types: agroforestry, urban cropland area, and rural croplands. Main crops include *Triticum aestivum*, *Oryza sativa*, *Pennisetum glaucum*, *Zea mays*, and *Saccharum officinarum* are major field crops grown in Gujrat. Important trees include *Acacia nilotica*, *Azadirachta indica*, *Bauhinia purpurea*, *Bombax ceiba*, *Dalbergia sissoo*, *Ficus benghalensis*, *Melia azedarach*, and *Pongamia glabra* (Parvaiz, 2014; Umar *et al.*, 2021).

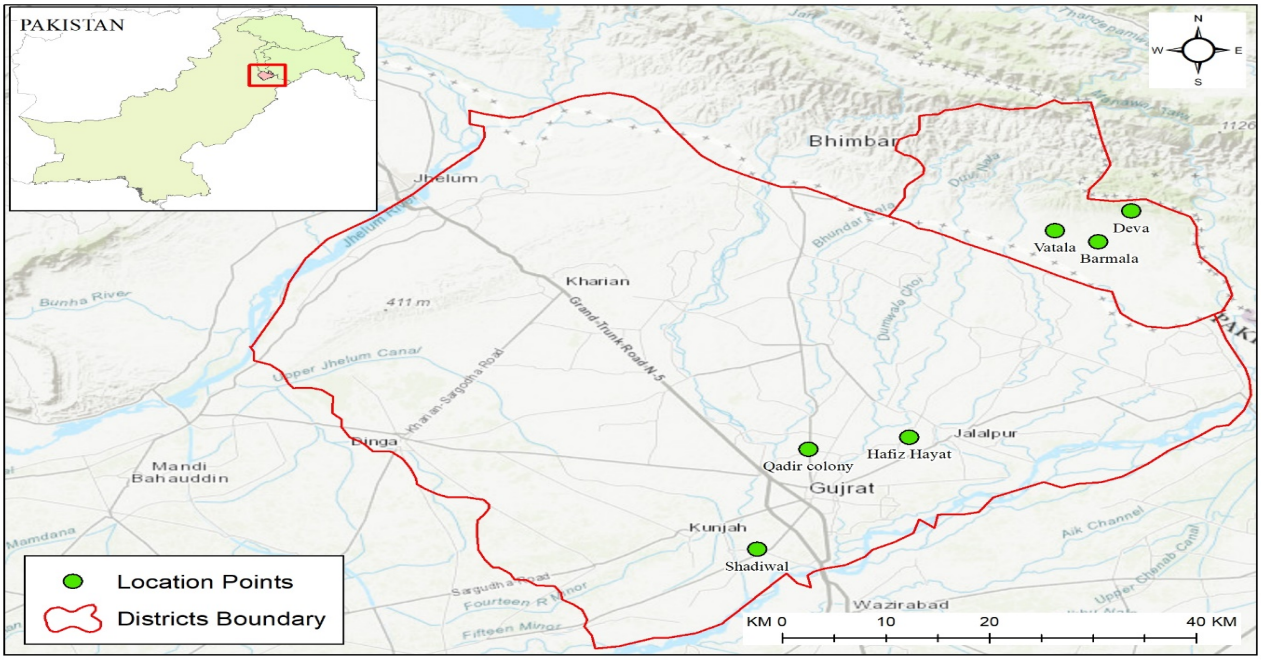

Fig. 1. Study area showing major sampling sites

2.2 Sampling sites

Barmala (32°52'58.7" N, 74°20'18.97" E) is situated at an elevation of 350-411m asl and the topography represents hilly forests. This area has seasonal streams and is dominated by tree species like *Butea monosperma*, *D. sissoo*, *D. viscosa*, *Lannea coromandelica*, *S. spontaneum*, *V. nilotica, Salvia* spp., *Senna occidentalis*, and *Zanthoxylum armatum* (Goursi *et al.*, 2012). While comparatively undisturbed, livestock grazing, cutting wood for fuel, and grass collection and burning are the factors that have an impact in this part of the study area.

2.3 Sampling procedure

At Gujrat, we categorized sampling sites into agroforestry, urban cropland area, and rural croplands in each of the selected study sites i.e., Hafiz Hayat, Qadir colony, and Shadiwal. Whereas at DVNP, we sampled all three locations (Deva, Vatala, and Barmala) at twenty-four points i.e., eight points at each habitat type (agroforestry, urban cropland area, and rural croplands). We collected data from

each of these points (separated by ~1 km) of selected locations twice a month for two consecutive years (Table 1).

Table 1. Description of sampling sites

Study area	Study sites	Coordinates / height from sea level	Topography, vegetation, and land cover characteristics
Gujrat	Hafiz Hayat	32°38′29.55″ N, 74°9′55.58″ E/ 244 m asl	The study area consists of plains with a mix of canal irrigated, rainfed, and tube well-irrigated lands. the visual estimations of land cover which were mainly based on non-agricultural vegetation or the percentage of the crop subdivided into three habitat types each represented about 40 % land cover (Muñoz-Sáez *et al.*, 2017) with a specific type of vegetation cover i.e. agroforestry (trees interspersed with cropped with cereals and fodder crops), urban cropland area (houses, sheds, cropped fragments, roads, and greenhouses), and rural croplands (cereals, pulses, and vegetables, plowed soil or soil with stubble of previous crops and weeds (Umar *et al.*, 2021).
	Qadir colony	32° 37' 50" N, 74°4' 55" E/ 239 m asl	
	Shadiwal	32° 22' 20" N, 73° 10' 50" E/ 252 m asl	
DVNP	Barmala	32°52'58.7" N, 74°20'18.97" E/ 350-411m asl	This study site is dominated by tree species like *Butea monosperma*, *D. sissoo*, *D. viscosa*, *Lannea coromandelica*, *S. spontaneum*, *V. nilotica, Salvia* spp., *Senna occidentalis*, and *Zanthoxylum armatum* and has seasonal streams and, across vegetation layers, are dominated (Goursi *et al.*, 2012). While comparatively undisturbed, livestock grazing, cutting wood for fuel, and grass collection and burning all impact upon the area (Umar *et al.*, 2021).
	Vatala	32°52'38.7" N, 74°17'44.7" E/ 350-396m asl	Vatala shares a similar plant community composition to the other sites but is particularly dense with *D. sissoo*, *M. indica*, and *D. viscosa.* Human disturbance is the highest in this area, due to a higher population density, summer visitors, and the army, with most areas impacted by stone quarrying and livestock grazing. This has left only a few undistributed areas, mainly comprising open and cultivated areas (Umar *et al.*, 2021).
	Deva	32°54'8.6" N, 74°21'29.7" E/ 306-381m asl	The forests of Deva include species characteristic of Barmala along with *Aesculus indica*, *Ziziphus mauritiana, M. indica* and *Senegalia modesta* (Subhani *et al*., 2010). Shrubs include *Calotropis procera*, *D. viscosa*, *S. spontaneum*, and *Trichodesma indicum* (Goursi *et al.*, 2012). This area of the DVNP has plains and seasonal streams. Human population density is lower than in Vatala but is impacted by the daily movement of livestock to the forest areas, and vehicles transporting quarried stones. Situated closest to the line of control, the army's presence may also disturb this area of the park (Umar *et al.*, 2021).

2.4 Insect collection methods

We selected a variety of insect collection methods described and used in different studies conducted for reporting insect fauna from different landscapes. We employed both active sampling and passive sampling for the insect collection. Active sampling included handpicking, sweep netting, foliage beating, searching the ground, and peeling tree bark for insect collection. Passive sampling approaches included pitfall traps, light traps, and yellow pans were also employed (Schauff, 2001; Upton & Mantle, 2010).

2.4.1 Pitfall traps

We placed a total of ten traps in a grid arrangement at each point separated by a 15m distance. At each location, one line transect was established with pitfall traps being allocated within the transect line by systematic random sampling technique (Leather, 2008; Ojija *et al.*, 2016). The traps were placed in the soil while their rims were at the level with the soil surface. Pitfall traps consisted of transparent plastic containers with a top diameter of 8 cm and a height of 10 cm with uncovered openings containing an aqueous solution of 10% formalin (Larsen & Forsyth, 2005; Ojija *et al.*, 2016). The traps were kept in the fields for 48 hours (Inayat *et al.*, 2010).

2.4.2 Sweeping nets

Muslin nets with a diameter of 32cm were used to sweep through the vegetation forming a figure of eight. A sweep net was used to sweep all types of insect fauna present above the canopy (Borror & White, 1970; Arya & Joshi, 2011; Kannagi *et al.*, 2013; Rajkumari *et al.*, 2014). Sweep sampling was done from herb and shrub layers of the vegetation to trap flying insects (Bhosale *et al.*, 2012; Akhtar *et al.*, 2014; Ojija *et al.*, 2016). The sampling was carried out for three hours along a line transects while walking from 10.00 am to 1.00 pm fortnightly (Inayat *et al.*, 2010; Thorp & Rogers, 2010; Belamkar & Jadesh, 2014; Capinera, 2020; Gibb & Oseto, 2020). We performed 50 sweeps at each sampling point within the location while moving in the sampling sites (Ghani & Maalik, 2020).

2.4.3 Beating sheets

We used Beating sheets for the collection of arboreal insects by selecting ten bushes, trees, and other plants randomly (Ojija *et al.*, 2016).

2.4.4 Hand collection

Manual collection of insects was accomplished by actively searching on the ground, in leaf litters and grasses, under logs, tree barks, and other substrates during the daytime for 3hrs twice a month (Oman & Cushman, 1946; Thakare & Zade, 2012; Marsh *et al.*, 2013; Ojija *et al.*, 2016).

2.4.5 Light traps

Nocturnal flying insects were collected by installing bucket-type light traps with 24-watt incandescent electric bulbs hanged were adjusted according to the height of trees at selected 1.5 m above the ground. The bottom of the bucket was filled with the ethyl acetate-based killing agent

(Mathew & Rahmathulla, 1995; McGavin, 1997; Tyagi *et al.*, 2011; Bhosale *et al.*, 2012; Gaikwad *et al.*, 2012; Singh, 2013; Ashfaq *et al.*, 2014; Nair *et al.*, 2014; Borah *et al.*, 2015; Abbas *et al.*, 2019).

2.4.6 Pan traps

The pans used to collect insects were each painted in one of the following colours, blue, white, and yellow with UV-reflecting color. The pans had a diameter of 8.5cm with a volume of 0.5 L and were filled with propylene glycol (40% concentration), to conserve the pollinators and to decrease the surface tension. One set of pan-trap consists of three pans, one in each colour placed at the same height (Berglund, 2016). Data collected from traps after 15 days constituting a single sample (Paiva *et al.*, 2020).

2.5 Identification and preservation

Principal morphological characteristics (including thoracic pattern, wing venation, abdominal appendages and features, legs, genitalia, antennae, color patterns, etc.) of each taxon (order level, family, genera, and species) were used to identify the specimens (Mouhoubi *et al.*, 2019). The insects were preserved in 70% alcohol and the specimens were separated into different orders and families and identified as morphospecies (Paiva *et al.*, 2020).

2.6 Data analysis

Diversity analysis was made using Shannon-Wiener and Simpson diversity indices and density, relative abundance, and species richness were calculated (Magurran, 1988, 2004). We tested for differences between insect communities by using a one-way Analysis of Similarities (ANOSIM). We calculated the abundance of each species abundance and the richness that were compared between two habitats using Wilcoxon's matched pairs (signed rank) test using Statistix software at a significance of 0.05. We used a paired analysis, where our samples were paired by month between two sites. We did not consider the samples for the analysis when the corresponding pair was not observed at any of the sites in order not to unbalance the analysis for insect species (Paiva *et al.*, 2020). We also performed the similarity of percentages analysis (SIMPER) to identify the species contributing most to differences in communities across space and time. Differences in the abundance of key species (those that contributed >5% to dissimilarities between insect communities) were tested non-parametrically since species abundances were not normally distributed.

Species richness measures biodiversity in its simplest form by providing number of species in a given area, however, it depends greatly on sampling size and effort. Margalef's diversity index (value varies with the variation in the number of species) and Menhinick's diversity (varies with the sampling effort) indices address species richness. Richness-Evenness indices include Shannon-Wiener diversity index (ranges from1.5 to 4.5), Brillouin index, fisher's alpha (always > 0.9 and never > 1.0), Pielou index (0 to 1; where zero represent no evenness and 1 represent complete evenness), and Simpson's index (ranges from 0 to 1; with 0 representing infinite diversity and 1 representing no diversity). Species abundance, dominance, richness, and evenness were measured

by using different indices i.e. Simpson's index $\left(\mathbf{D} = \sum_{\mathbf{i=1}}^{\mathbf{s}} \frac{\mathbf{ni(ni-1)}}{\mathbf{N(N-1)}}\right)$, Shannon-Wiener ($\mathbf{H'} = -\sum_{\mathbf{i=1}}^{\mathbf{s}} \frac{\mathbf{ni}}{\mathbf{N}} \times \mathbf{ln}\frac{\mathbf{ni}}{\mathbf{N}}$), Berger–Parker$\left(\frac{\mathbf{1}}{\mathbf{D}} = \frac{\mathbf{1}}{\frac{\mathbf{N\,max}}{\mathbf{N}}}\right)$, Margalef index for species richness$\left(\mathbf{DMg} = \frac{\mathbf{s-1}}{\mathbf{ln\ N}}\right)$, Menhinick's diversity index, fisher's alpha (S = *N(1-X)/X*), and Pielou index ($\mathbf{J'} = \frac{\mathbf{H'}}{\mathbf{ln(S)}}$) (Fisher *et al.*, 1943; Shannon & Weaver, 1949; Simpon, 1949; Berger & Parker, 1970; Whittaker, 1977; Gaines, 1999; Magurran, 2004).

3. Results

3.1 Overall taxonomic composition

We collected 11829 individuals from both DVNP and Gujrat belonging to 10 orders. We recorded, 6279 individuals representing 68 families and 213 morphospecies were recorded from DVNP whereas 5550 individuals belonging to 66 families and 222 morphospecies from Gujrat croplands (Table 1). We also observed relatively greater relative abundance of individuals at DVNP (53.08 %) as compared to Gujrat (46.92 %). Coleoptera (14.20 % DVNP; 9.77 % Gujrat) was the most abundant order followed by Orthoptera (7.57 % DVNP; 10.31 % Gujrat). Coleoptera, Orthoptera, Lepidoptera, Diptera and Hemiptera collectively contributed 80.55 % of the sampled individuals (Table 2).

Table 2. Relative abundance of insects in different orders collected from Gujrat and Deva Vatala National Park during 2017-2019. Data presented includes relative abundance (%) of insect orders (at a given location all month-wise samples were pooled, and relative abundance was calculated by using total number of individuals from both sites)

	DVNP			Gujrat		
Insect orders	Families (No.)	Species (No.)	Relative abundance (%)	Families (No.)	Species (No.)	Relative abundance (%)
Coleoptera	15	71	14.20	12	54	9.77
Lepidoptera	11	29	7.77	11	35	7.29
Hemiptera	10	15	5.70	11	18	4.40
Orthoptera	07	39	7.57	07	50	10.31
Diptera	07	19	7.14	07	23	6.40
Hymenoptera	07	17	3.53	07	19	3.59
Odonata	05	13	3.31	05	13	2.65
Neuroptera	03	03	1.25	03	03	0.73
Isoptera	02	05	1.78	02	05	1.28
Mantodea	01	02	0.83	01	02	0.49
Total	68	213	53.08	66	222	46.91

3.2 Wilcoxon's matched pairs (signed rank) test for insect orders

We also calculated diversity and richness of insect orders and species for both sites using Wilcoxon's matched pairs (signed rank) test which indicated significant differences for both diversity and abundance in the abundance and richness of species, families, and orders in either abundance or richness or both between the two types of habitats (Table 2). Several families of Coleoptera, which contained mainly scarabaeid, carabid, coccinellid beetles showed greater richness in DVNP. However, we also detected that several insect orders showed greater richness in the croplands of Gujrat. But we observed the pattern of the greater abundance (number of individuals in each order) of insect orders in DVNP. The abundance, richness and diversity within each order showed that Hymenoptera, Mantodea, Neuroptera, and Odonata had a similar abundance, and richness in both types of habitats (Table 2). Coleoptera had significantly greater abundance and Shannon's Diversity (H′) in croplands. However, richness was significantly greater in DVNP. Diptera were significantly more abundant in DVNP with no significant difference in richness and Shannon's H′ index was similar in both types of habitats. Orthoptera showed non-significant differences in the abundance, richness, and Shannon's Diversity (H′) almost similar at two types of habitats (Table 3).

Table 3. Abundance, richness, and Shannon's H′ diversity of the insects collected in the protected area (DVNP) and Gujrat.

Order	Abundance				Richness				Shannon's Diversity (H′)	
	No. of individuals		V-statistic	p value	No. of species		V-statistic	p value		
	DVNP	Gujrat			DVNP	Gujrat			DVNP	Gujrat
Coleoptera	1118	1139	928.50	0.110	71	54	2006.0	0.0003*	3.931	3.948
Diptera	844	628	162	<0.002*	19	23	176.00	0.4660	2.914	2.907
Hemiptera	674	453	117	0.0002*	15	18	141.50	0.0023*	2.694	2.702
Hymenoptera	418	387	84	0.2845	17	19	78.50	0.6384	2.791	2.778
Isoptera	211	152	15	0.0312*	05	05	15.00	0.2187	1.603	1.607
Lepidoptera	919	728	339.5	0.0003*	29	35	358.50	0.1661	3.339	3.358
Mantodea	98	58	-	-	02	02	03.00	0.7893	0.688	0.644
Neuroptera	148	86	6	0.125	03	03	07.00	0.3125	1.087	1.084
Odonata	392	313	65	0.1001	13	13	66.00	0.8160	2.519	2.549
Orthoptera	895	966	318.5	0.3218	39	50	263.0	0.0114*	3.590	3.625
Overall	5717	4910	17445	0.001*	213	222	17203	0.0014*	5.190	5.237

1. Comparison of abundance and richness is based on the non-parametric Wilcoxon matched-pairs test (exact *p* values).
2. *indicates significant differences in abundance and richness between two sites
3. ⁻Analysis was not performed due to the low number of individuals or species.

3.3 The difference in species at Gujrat and DVNP

We also detected seventeen species unique to DVNP and twenty-six species recorded only in croplands of Gujrat. At DVNP, 8 species of Acrididae and 4 species of Tephritidae were not detected. Similarly, twelve species of Scarabaeidae, 4 species of Chrysomelidae, and 3 species of Meloidae were not recorded at Gujrat (Table 4).

Table 4. Species unique at one location (not recorded both types of habitats)

Order	Family	Species	DVNP	Gujrat
Coleoptera	Buprestidae	*Sternocera sp.*	✓	X
	Carabidae	*Acinopus laevigatus*	✓	X
	Cerambycidae	*Acanthophorus serraticornis*	✓	X
	Chrysomelidae	*Chrysolina hyperici*	✓	X
		Pyrophorus sp.	✓	X
	Coccinellidae	*Adalia bipunctata*	✓	X
	Elateridae	*Aeolus mellillus*	✓	X
	Lucanidae	*Lucanus sp.*	✓	X
	Meloidae	*Zonitoschema gibdoana*	✓	X
	Oedemeridae	*Ananca sp.*	✓	X
	Scarabaeidae	*Onthophagus falsus*	✓	X
		Onthophagus dama	✓	X
		Metacatharcius inermis	✓	X
		Drepanocerus kirby	✓	X
		Coprisrepertus sp.	✓	X
		Tiniocellus modestus	✓	X
	Tenebrionidae	*Stenochinus sp.*	✓	X
Diptera	Tephritidae	*Bactrocera nigrofemoralis*	x	✓
		Bactrocera scutellaris	x	✓
		Bactrocera tau	x	✓
		Bactrocera zonata	x	✓
Hemiptera	Aphididae	*Macrosiphum euphorbiae*	x	✓
		Macrosiphum rosae	x	✓
	Lygaeidae	*Spilostethus sp.*	x	✓
Hymenoptera	Vespidae	*Delta dimidiatipenne*	x	✓

		Poekilocerus pictus	x	✓
Lepidoptera	Nymphalidae	*Danaus genuttia*	x	✓
		Ergolis merione	x	✓
		Junonia almanac	x	✓
		Vanessa cardui	x	✓
	Pieridae	*Catopsilia florella*	x	✓
		Catopsilia pyranthe	x	✓
Orthoptera	Acrididae	*Acrida ungarica*	x	✓
		Chortophaga viridifasciata	x	✓
		Dittopternis venusta	x	✓
		Hieroglyphus banian	x	✓
		Mermiria bivittata	x	✓
		Oxya japonica	x	✓
		Shistocera alutacea	x	✓
		Trilophidia annulata	x	✓
	Pyrgomorphidae	*Atractomorpha crenulata*	x	✓
	Tettigoniidae	*Ducetia japonica*	x	✓
		Neoconocephalus triops	x	✓

3.4 Species contributing to dissimilarities among site communities

Similarity Percentage Analysis (SIMPER) indicating the average percent dissimilarity in the insect community composition between DVNP and Gujrat. Presented here are the top ten species contributing to the community dissimilarity at each site and the percent contribution of each species to community dissimilarity in pair-wise comparisons. The biological dissimilarity was assessed based on insect taxonomy showed that *Aedes albopictus, Eristalis arbustorum, Eristalis tenax, Halyomorpha halys, Mantis religiosa* and *Chrysoperla carnea* were the main contributing species in the community dissimilarity (Table 5). The compositional dissimilarity between DVNP and Gujrat, based on counts at each site, indicated *Aedes albopictus* (0.34), followed by *Eristalis arbustorum* (0.33), *Eristalis tenax* (0.33), and *Halyomorpha halys* (0.33). The results showed that the compositional dissimilarity is lesser between the two sites as the Bray–Curtis dissimilarity ranges between 0 and 1, where 0 means the two sites have the same composition and 1 means the two sites do not share any species). The composition of insect communities was significantly different between locations (ANOSIM; R = 0.890, P = 0.001). Insect families showed average dissimilarity of 50.73 % between DVNP and Gujrat (ANOSIM; R = 0.078, P= 0.127). The top five species, represented by 10 species across all locations (districts), contributed 90.03% to 98.32% of community composition dissimilarities, while three species contributed to dissimilarities between all three sites' insect communities. Whereas five species contributed to dissimilarities in insect communities between at least two locations (Table 5).

Similarly, Scarabaeidae and Acrididae were two top equally contributing families in the dissimilarity between sites. We also detected that top contributing families in dissimilarities (about 28 %) in the composition belonged to Coleoptera, Orthoptera, Diptera and Hemiptera (Table 6).

Table 5. Main Species contributing to dissimilarities among site communities. Only the top ten contributing species are listed. The analysis is based on pre-treated square-root transformed abundance (Clarke & Warwick, 2001) of the samples pooled for each species at a given site.

Species	Mean abundance	Mean abundance	Mean dissimilarity	Contribution (%)	Cumulative (%)
	DVNP	**Gujrat**			
Aedes albopictus	1.64	1.85	0.3431	0.6142	0.614
Eristalis arbustorum	1.80	1.52	0.3333	0.5967	1.211
Eristalis tenax	1.86	1.22	0.3311	0.5928	1.804
Halyomorpha halys	1.80	1.30	0.3277	0.5867	2.390
Mantis religiosa	1.69	1.41	0.3159	0.5656	2.956
Chrysoperla carnea	1.67	1.3	0.3151	0.5642	3.520
Episyrphus viridaureus	1.77	1.32	0.3131	0.5605	4.081
Phenococcus solenopsis	1.64	1.26	0.3101	0.5552	4.636
Bactrocera correcta	1.74	1.23	0.3101	0.5551	5.191
Musca domestica	1.67	1.47	0.3049	0.5459	5.737

Table 6. Main families contributing to dissimilarities among site communities.
Only the top ten contributing families are listed.
The analysis is based on pre-treated square-root transformed abundance (Clarke and Warwick, 2001) of the samples pooled for each family at a given site.

*Family	Order	Mean abundance	Mean abundance	Mean dissimilarity	Contribution (%)	Cumulative (%)
		DVNP	**Gujrat**			
Scarabaeidae	Coleoptera	6.76	5.7	2.377	4.686	4.686
Acrididae	Orthoptera	4.78	6.49	2.316	4.566	9.252
Erebidae	Lepidoptera	3.80	3.42	1.372	2.704	11.96
Syrphidae	Diptera	3.73	3.08	1.316	2.594	14.55
Tephritidae	Diptera	2.98	3.5	1.241	2.447	17.00
Pieridae	Lepidoptera	3.00	3.09	1.141	2.249	19.25
Nymphalidae	Lepidoptera	2.51	3.14	1.121	2.21	21.46
Pentatomidae	Hemiptera	3.14	2.56	1.114	2.195	23.65
Gryllidae	Orthoptera	3.03	2.99	1.101	2.17	25.82
Chrysomelidae	Coleoptera	3.09	2.70	1.093	2.155	27.98

3.5 Diversity indices calculated for families and species

For families, the values Simpson diversity index for DVNP (1-D: 0.963) and croplands (1-D: 0.954) showed similarity in the species dominance. Similarly, Shannon- Wiener index for species diversity and evenness for DVNP (H= 3.74; e^= 0.640) and Croplands (H= 3.610; e^= 0.588) indicated that DVNP showed greater diversity than Gujrat croplands (Table 6). For the species, the values Simpson diversity index for DVNP (1-D: 0.994) and Gujrat (1-D: 0.995) showed similarity in the species dominance. Similarly, Shannon- Wiener index for species diversity and evenness for Gujrat (H= 5.36; e^= 0.9632) and DVNP (H= 5.277; e^= 0.919) indicated that Gujrat showed greater species diversity than DVNP. Similar trends of index values were observed in Brillouin, Menhinick, Berger-Parker and Fisher-alpha where the maximum value was calculated for Gujrat. However, Margalef index showed maximum value for DVNP (Table 7).

Table 7. Diversity indices calculated for different families and species for both habitat types

	Families		Species	
	DVNP	Gujrat	DVNP	Gujrat
Taxa_S	66	63	213	222
Individuals	6279	5550	6279	5550
Dominance_D	0.0375	0.0459	0.0059	0.0049
Simpson_1-D	0.9625	0.9541	0.9945	0.9952
Shannon_H	3.7450	3.6130	5.277	5.365
Evenness_e^H/S	0.6409	0.5883	0.9192	0.9632
Brillouin	3.7140	3.5800	5.191	5.266
Menhinick	0.8329	0.8457	2.688	2.980
Margalef	7.4330	7.1910	24.24	25.63
Equitability_J	0.8938	0.8720	0.9843	0.9931
Fisher_alpha	10.2900	9.9610	42.60	46.30
Berger-Parker	0.1317	0.1395	0.01051	0.01171
Chao-1	66	63	213	222

We plotted the Whittaker rank abundance plot for families and species of DVNP and Gujrat. The results indicated that families were more evenly distributed at DVNP than Gujrat (Fig. 2).

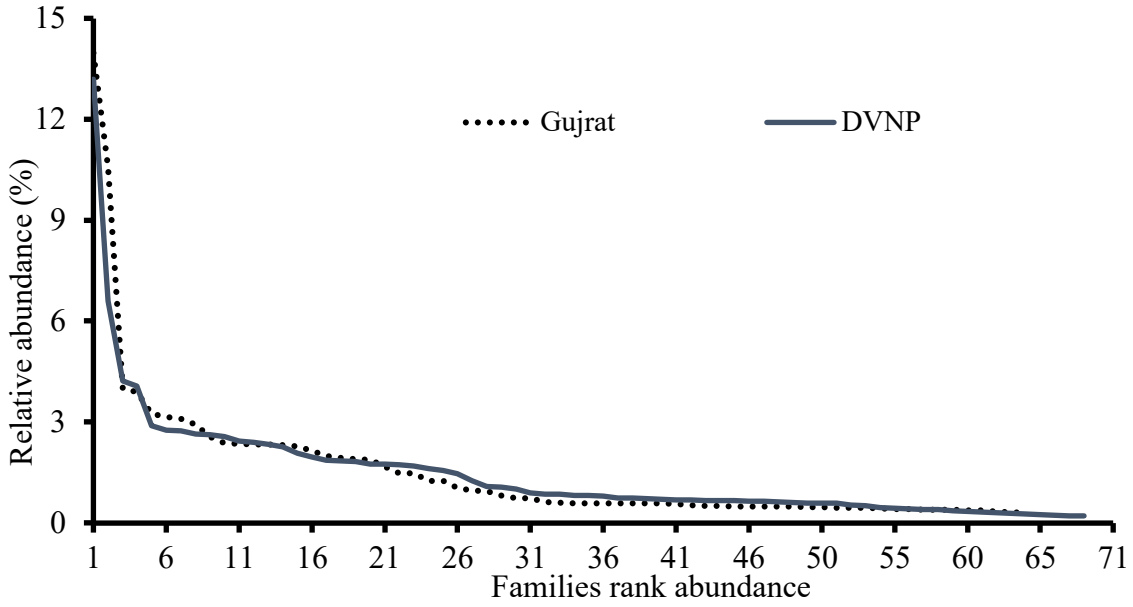

Fig. 2. Whittaker plot (rank abundance) of families was plotted for both sites using relative abundance (%) of specimens in each family

Similarly, we plotted rank abundance curve for the species which showed variation in the assemblages in two habitats. About 66 species showed greater relative abundance at DVNP and then a declining trend in the relative abundance was observed (Fig. 3).

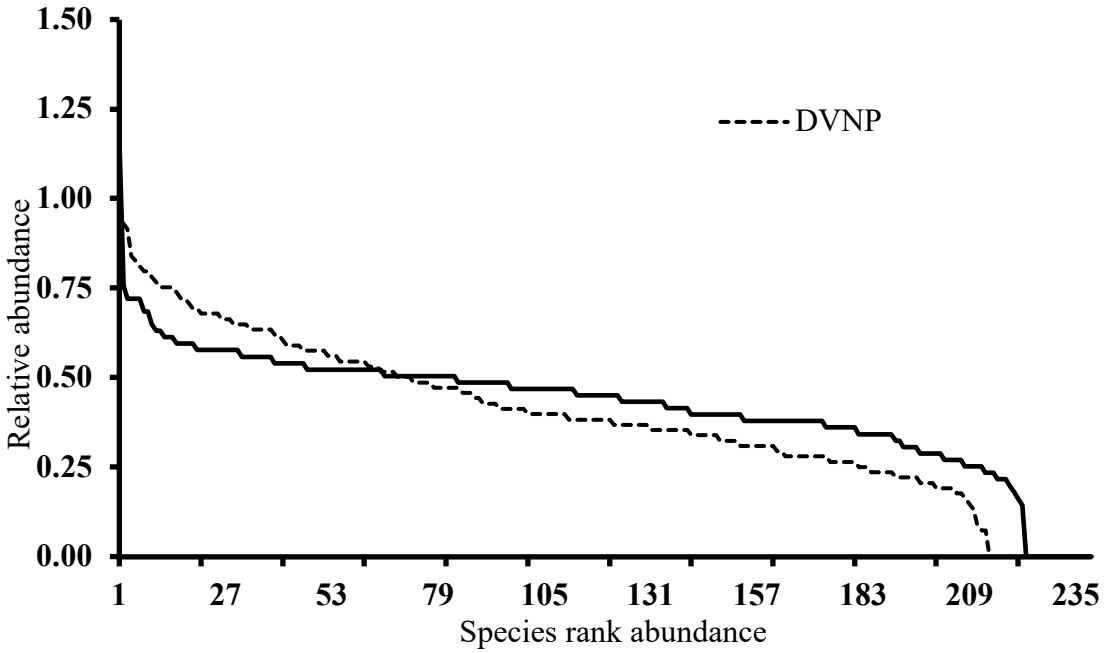

Fig. 3. Whittaker plot (rank abundance) of species was plotted for both sites using relative abundance (%) of specimens for each location

Individual rarefaction curves for species were also plotted which showed similar accumulation in both habitat types until 700 individuals, and the continued accumulating morphospecies with stabilizing trend (Fig. 4).

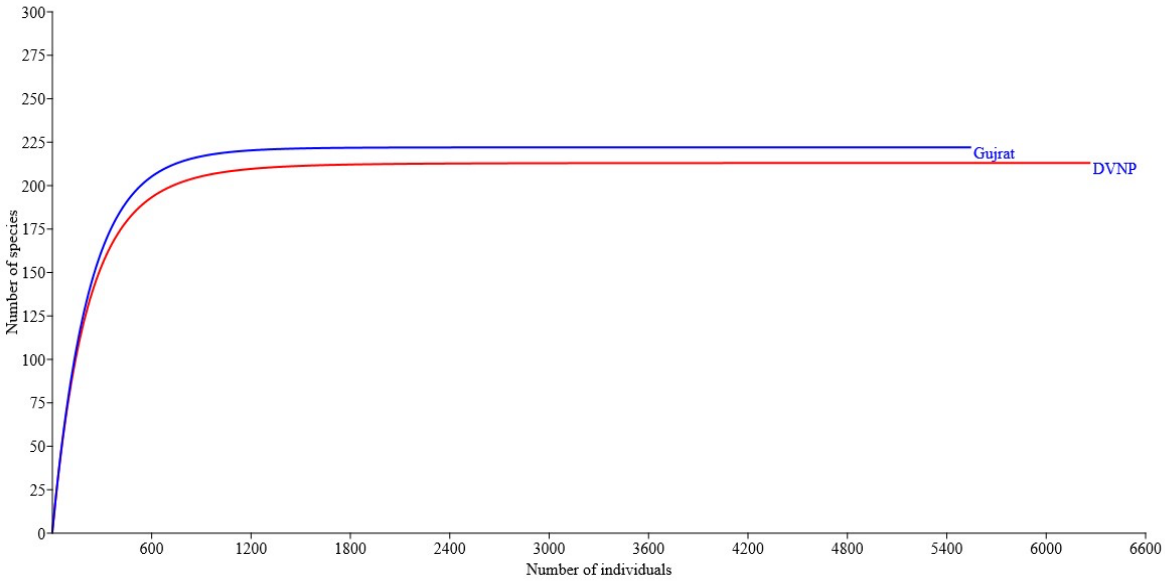

Fig. 4. Rarefaction curves from the DVNP and croplands of species collected

4. Discussion

We explored the patterns of insect communities in protected area and agroecosystem at order, family, and species level. We recorded changes in the abundance and species richness of insect orders, as well as changes in the community composition of insect families under two different habitat types i.e., protected area and agroecosystem. Our results present an overall comparison of insect diversity in protected area adjacent to croplands which highlighted the significance of both type of habitats.

We detected that both habitats support greater diversity at species and family levels. For instance, we recorded insect species belonging to 68 families in DVNP and 66 families in Gujrat. Similarly, greater number of species 222 were noted in Gujrat whereas 213 in DVNP. However, we also observed certain insect groups were more dominant in one type of habitat as compared to other. For example, the species richness and abundance of Coleoptera was greater at DVNP. However, the number of species belonging to other insect orders was nearly similar at both habitat types i.e., Hymenoptera, Odonata, Neuroptera, Isoptera and Mantodea. Earlier studies reported that species diversity under different landscapes vary significantly. Greater number of species were reported from croplands of Faisalabad (Inayat *et al.*, 2010). In the brinjal-based agroecosystem, 27 species of insects were reported (Chang *et al.*, 2019). These patterns of species composition could be attributed to the variations in the abiotic conditions in different environments of the habitats. For instance, this happens when the shift of more generalist species in the simpler environment towards more

specialists in the more complex environment without a disturbance in their richness or abundance occurs (Kruess & Tscharntke, 2002; Nemec & Bragg, 2008; Paiva *et al.*, 2020).

We found Coleoptera, Orthoptera and Lepidoptera among top three insect orders contributing 62.61 % of the species at Gujrat whereas 65.25 % at DVNP. An earlier study reported that the most abundant species belonged to Lepidoptera, Coleoptera, and Orthoptera (Wahyuni *et al.*, 2011). Though in our study, Orthoptera showed relatively greater species richness and abundance in Gujrat as compared to DVNP. Acrididae was the most diverse family represented by six subfamilies followed by Pyrgomorphidae and Tetrigidae (Kwon & Byun, 1996; Waghmare *et al.*, 2013; Hussain *et al.*, 2017; Zergoun *et al.*, 2019). We identified that in both study areas; however, some insect groups have almost similar community patterns, suggesting that habitat type is not the most important factor determining the species composition. Such community patterns where several factors contribute in the composition of communities were reported earlier (Di Giulio *et al.*, 2001). The dominance exhibited by Coleoptera, Lepidoptera and Orthoptera in both habitats indicated the greater abundance of some insect species. This may be attributed to the availability of preferred habitats to the species i.e., moist soil, litter and rotting wood (Wilson, 1990; Ross *et al.*, 2002; Sawada & Hirowatari, 2002; Sörensson, 2003; Bhusnar, 2015; Rana *et al.*, 2019).

Coleoptera exhibited species dominance in both study areas indicating that the distribution patterns in different landscapes may be due to composition of communities, and their ecological role in the ecosystems (Rykken *et al.*, 1997; Méndez-Rojas *et al.*, 2021). Coleoptera accounts for 40% of entire insects represented by 400,000 species that are known to exist in the world (Crowson, 2013; Bouchard *et al.*, 2017; Hong *et al.*, 2017). Scarabaeid species showed different patterns of assemblages in DVNP and Gujrat which may be attributed to variations in vegetation, animal type, and habitat stability. Scarabaeid beetles have been reported as an important visitor of shrubs and tree species with some role as pollinators (Rodger *et al.*, 2004; Nasir *et al.*, 2016; Ghazanfar *et al.*, 2017; Hussain *et al.*, 2020). However, the larger landscape fragments comprise of higher species abundance of Scarabaeid beetles and distinct species (Magagula, 2006; Whipple, 2011; Labidi *et al.*, 2012; Campos & Hernández, 2013; Salomão & Iannuzzi, 2015). In our study, DVNP and Gujrat offer a gradient of variations from mountainous landscapes (dominated by woody trees and shrubs) to agricultural plains (dominated by cropping monocultures). This would have facilitated the distribution of species along the altitudinal gradient with a uniform trend allowing some species to have increased abundance or vice versa. It has been synthesized that conservation of agricultural landscapes through compensation schemes to lower agriculture intensification may help to protect taxonomic groups especially Orthoptera (Kwon & Byun, 1996; Marini *et al.*, 2008). Moderate temperature ranges in both agricultural landscapes of Pakistan contribute to the distribution, diversity, and abundance of syrphid flies (Saleem *et al.*, 2001; Sajjad *et al.*, 2010; Khan & Hanif, 2016). Ecological studies, habitat management, and conservation require the estimation of community composition patterns at local, regional and global levels (Nahmani *et al.*, 2005; Ramzan *et al.*, 2021). Species diversity has been under perils due to anthropogenic changes in the landscapes which results in habitat modifications (Turner, 1989; Gibbs & Stanton, 2001; Wagner & Edwards, 2001). To understand species distributional patterns in different landscapes, insect fauna has been studied at local and regional levels (Cho *et al.*, 2008; Ahn & Park, 2012; Lim *et al.*, 2013; Rafi *et al.*, 2017). Exploring higher taxonomic categories (orders and families) allows understanding of

large changes in the biodiversity associated with different landscapes (Paiva *et al.*, 2020). Species richness and abundance vary with the suitability of habitat and mobility of the species which suggests that the density of orthopterans may be a more sensitive measure for habitat quality.

5. Conclusion

Insect diversity in the protected area and agroecosystems has demonstrated the importance of both type of habitats. Agricultural landscapes of Gujrat despite the use of farm inputs like fertilizers, herbicides, and insecticides in different crops at different stages may change the population dynamics of insect species but species thrive to exist. Whereas in protected area (DVNP), on the other hand offered uniform microenvironment to the insect fauna which helped them to maintain their population dynamics and diversity consistent throughout the study duration. We conclude variations in the species diversity at both habitat types though certain insect orders were dominant in both study areas i.e., Coleoptera, Lepidoptera, Hemiptera and Hymenoptera. We documented thirty-seven species unique in DVNP which indicates protected area has favourable conditions for these species.

ACKNOWLEDGMENTS

The authors thank the MPhil Scholars (Waqas Asghar, Aleena Naeem, Maryam Khalid, Areeba Mashaal, Amina Zafar and Somia Liaqat) of the Department of Zoology, the University of Gujrat for assisting in the data collection and identification of specimens.

Conflict of interest

The authors declare no conflict of interest for this study.

References

Abbas M., Ramzan M., Hussain N., Ghaffar A., Hussain K., Abbas S. & Raza A. (2019). Role of Light Traps in Attracting, Killing and Biodiversity Studies of Insect Pests in Thal. Pakistan Journal of Agricultural Research **32**, 562-709.

Abdala-Roberts L., Puentes A., Finke D.L., Marquis R.J., Montserrat M., Poelman E.H., Rasmann S., Sentis A., van Dam N.M. & Wimp G. (2019). Tri-trophic interactions: bridging species, communities and ecosystems. Ecology letters **22**, 2151-67.

Ahn S.-J. & Park C.-G. (2012). Terrestrial insect fauna of the Junam wetlands area in Korea. Korean journal of applied entomology **51**, 111-29.

Akhtar M., Nayeem M. & Usmani M. (2014). Abundance, distribution and taxonomic studies on Hemiacridinae (Acrididae: Acridoidea: Orthoptera) in Uttar Pradesh, India. Journal of global biosciences **3**, 910-8.

Anwar M., Mahmood A., Rais M., Hussain I., Ashraf N. & Khalil S. (2015). Population density and habitat preference of Indian peafowl (Pavo cristatus) in Deva Vatala National park, Azad Jammu and Kashmir, Pakistan. Pakistan Journal of Zoology **47**, 1381-6.

Arshad M. (2020). Consequences of leaf biochemical characters for citrus leafminer, Phyllocnistis citrella Stainton (Lepidoptera: Gracillariidae) along the microclimatic gradient of citrus plants. Kuwait Journal of Science **47**, 50-6.

Arya M. & Joshi P. (2011). Species composition, abundance and density of Hymenopteran insects in Nanda Devi Biosphere Reserve, Western Himalayas, India. Journal of Environment & Bio-Sciences **25**, 175-9.

Ashfaq M., Hebert P.D., Mirza J.H., Khan A.M., Zafar Y. & Mirza M.S. (2014). Analyzing mosquito (Diptera: Culicidae) diversity in Pakistan by DNA barcoding. PLoS One **9**, e97268.

Belamkar N.V. & Jadesh M. (2014). A preliminary study on abundance and diversity of insect fauna in Gulbarga District, Karnataka, India. International Journal of Science and Research **3**, 1670-5.

Berger W.H. & Parker F.L. (1970). Diversity of planktonic foraminifera in deep-sea sediments. Science **168**, 1345-7.

Berglund H.-L. (2016). Effects of flower abundance and colour on pan-trap catches. In: Department of Physics, Chemistry and Biology. Linköping University.

Bhosale P., Chavan R. & Gaikwad A. (2012). Studies on distribution and diversity of chironomidae larvae (Insecta: Diptera), with respect to water quality in Salim Ali lake, Aurangabad India. The Bioscan **7**, 233-5.

Bhusnar A. (2015). Acridid (Orthoptera) diversity of agriculture ecosystem from Solapur District of Maharashtra, India. International quarterly journal of biology and life sciences **3**, 461-8.

Borah N., Hazarika M., Rehman A. & Patgiri P. (2015). Diversity of Dipteran insects in Jorhat district of Assam, North East India. Insect Environment **20**, 109-10.

Borror D.J. & White R.E. (1970). A field guide to insects: America north of Mexico. Houghton Mifflin Harcourt.

Bouchard P., Smith A.B., Douglas H., Gimmel M.L., Brunke A.J. & Kanda K. (2017). Biodiversity of coleoptera. Insect Biodiversity: Science and Society. John Wiley & Sons Ltd, 337-417.

Campos R.C. & Hernández M.I.M. (2013). Dung beetle assemblages (Coleoptera, Scarabaeinae) in Atlantic forest fragments in southern Brazil. Revista Brasileira de Entomologia **57**, 47-54.

Capinera J.L. (2020). Handbook of vegetable pests. Academic press, California, USA.

Chang B.H., Chang A.H., Lanjar A.G., Bukero A., Nizamani I.A., Rajput A., Magsi F.H., Khan M., Asghar F. & Zhang Z. (2019). Insect Biodiversity in Brinjal Agro-Ecosystem. pakistan Journal of Scientific and Industrial Research (Biological Sciences) **62**, 199-205.

Cho Y.-B., Yoon S.-J., Yoon S.-M., Ryu J.-W., Min H.-K. & Oh K.-S. (2008). Insect Fauna of Gyeongju National Park, Korea. Journal of Korean Nature **1**, 11-20.

Clarke K. & Warwick R. (2001). A further biodiversity index applicable to species lists: variation in taxonomic distinctness. Marine ecology Progress series **216**, 265-78.

Cock M.J., Biesmeijer J.C., Cannon R.J., Gerard P.J., Gillespie D., Jimenez J.J., Lavelle P. & Raina S.K. (2012). The positive contribution of invertebrates to sustainable agriculture and food security. CAB Reviews **43**, 1-27.

Collins N.M. & Thomas J.A. (2012). The conservation of insects and their habitats. Academic Press. The Royal Entomological Society of London.

Crowson R.A. (2013). The biology of the Coleoptera. Academic press.

Di Giulio M., Edwards P.J. & Meister E. (2001). Enhancing insect diversity in agricultural grasslands: the roles of management and landscape structure. Journal of applied Ecology, 310-9.

Dosso K., Yéo K., Konaté S. & Linsenmair K.E. (2012). Importance of protected areas for biodiversity conservation in central Côte d'Ivoire: Comparison of termite assemblages between two neighboring areas under differing levels of disturbance. Journal of Insect Science **12**, 131.

Fisher R.A., Corbet A.S. & Williams C.B. (1943). The relation between the number of species and the number of individuals in a random sample of an animal population. The Journal of Animal Ecology, 42-58.

Foottit R.G. & Adler P.H. (2018). Insect biodiversity: science and society. John Wiley & Sons, USA.

Gaikwad S., Ghate H., Ghaskadbi S., Patole M. & Shouche Y. (2012). DNA barcoding of nymphalid butterflies (Nymphalidae: Lepidoptera) from Western Ghats of India. Molecular biology reports **39**, 2375-83.

Gaines W.L. (1999). Monitoring biodiversity: quantification and interpretation. US Department of Agriculture, Forest Service, Pacific Northwest Research Station.

Ghani A. & Maalik S. (2020). Assessment of diversity and relative abundance of insect fauna associated with Triticum aestivum from district Sialkot, Pakistan. Journal of King Saud University-Science **32**, 986-95.

Ghazanfar M., Hussain M., Abbas Z. & Batool M. (2017). Diversity, composition and distribution of dung beetle fauna in croplands and pastures of Jhelum, Punjab, Pakistan. Pakistan Journal of Science **69**, 369-74.

Gibb T.J. & Oseto C. (2020). Insect Collection and Identification: Techniques for the Field and Laboratory. Academic Press.

Gibbs J.P. & Stanton E.J. (2001). Habitat fragmentation and arthropod community change: carrion beetles, phoretic mites, and flies. Ecological Applications **11**, 79-85.

GOAJ&K (1985). Wildlife in Azad Jammu and Kashmir. p. 53 Wildlife Wing, Forest Department, Azad Government of the State of Jammu and Kashmir, Muzaffarabad.

Goursi U.H., Awan M.S., Minhas R.A., Usman A., Kabir M. & Dar N.I. (2012). Status and Conservation of Indian Rock Python (Python molurus molurus) in Deva Vatala National Park, Azad Jammu and Kashmir, Pakistan. Pakistan Journal of Zoology **44**, 1507-14.

Grimmett R., Roberts T.J. & Inskipp T. (2008). Birds of Pakistan. A&C Black, Yale University Press- New Haven, Christopher Helm. London.

Haddad N.M., Brudvig L.A., Clobert J., Davies K.F., Gonzalez A., Holt R.D., Lovejoy T.E., Sexton J.O., Austin M.P. & Collins C.D. (2015). Habitat fragmentation and its lasting impact on Earth's ecosystems. Science advances **1**, e1500052.

Hodgson E. (2012). Toxicology and human environments. Academic Press.

Hong E., Kim Y., Jeong J.-C., Kang S.-H., Jung J.-K. & Suk S.-W. (2017). Community structure and distribution of ground beetles (Coleoptera: Carabidae) in Sobaeksan National Park, Korea. Journal of Ecology and Environment **41**, 17.

Hussain M., Akbar R., Malik M.F., Kazam S.N. & Zainab T. (2017). Diversity, distribution and seasonal variations of grasshopper populations in Sialkot, Punjab, Pakistan. Pure and Applied Biology (PAB) **6**, 1372-81.

Hussain M., Younas M., Malik M.F., Umar M., Kanwal M. & Batool M. (2020). Spatio-temporal Diversity of Dung Beetles in Selected Locales of Sialkot, Punjab, Pakistan. Punjab University Journal of Zoology **35**, 35-42.

Inayat T.P., Rana S.A. & Khan H.A. (2010). Diversity of insect fauna in croplands of District Faisalabad. Pakistan Journal of Agricultural Sciences **47**, 245-50.

Kannagi A., Sivakumar V., Santhi V. & Borgia J.F. (2013). Hymenopteran diversity in a deciduous forest from South India. International Journal of Biodiversity and Conservation **5**, 666-70.

Khan S. & Hanif H. (2016). Diversity and fauna of hoverflies (Syrphidae) in Chakwal, Pakistan. Int. J of Zool. Stud **1**, 22-3.

Kruess A. & Tscharntke T. (2002). Grazing intensity and the diversity of grasshoppers, butterflies, and trap-nesting bees and wasps. Conservation Biology **16**, 1570-80.

Kwon T.-S. & Byun B.-K. (1996). Insect fauna (Hemiptera, Coleoptera, Lepidoptera) in Odaesan National Park. Korean. J. Environ. Ecol **9**, 99-114.

Labidi I., Errouissi F. & Nouira S. (2012). Spatial and temporal variation in species composition, diversity, and structure of Mediterranean dung beetle assemblages (Coleoptera: Scarabaeidae) across a bioclimatic gradient. Environmental entomology **41**, 785-801.

Larsen T.H. & Forsyth A. (2005). Trap spacing and transect design for dung beetle biodiversity studies 1. Biotropica: The Journal of Biology and Conservation **37**, 322-5.

Leather S.R. (2008). Insect sampling in forest ecosystems. John Wiley & Sons.

Lim J.-S., Park S.-Y. & Lee B.-W. (2013). A Study on the Insect Fauna in and Around Goseong-gun, Gangwon-do, South Korea. Journal of Asia-Pacific Biodiversity **6**, 221-37.

Lokeshwari R. & Shantibala T. (2010). A review on the fascinating world of insect resources: reason for thoughts. Psyche **2010**.

Magagula C. (2006). Habitat specificity and variation of coleopteran assemblages between habitats in a Southern African (Swaziland) agricultural landscape. Biodiversity & Conservation **15**, 453-63.

Magurran A.E. (1988). Diversity indices and species abundance models. In: *Ecological diversity and its measurement* (pp. 7-45. Springer.

Magurran A.E. (2004). Measuring biological diversity. John Wiley & Sons, UK.

Marini L., Fontana P., Scotton M. & Klimek S. (2008). Vascular plant and Orthoptera diversity in relation to grassland management and landscape composition in the European Alps. Journal of Applied Ecology **45**, 361-70.

Marsh C.J., Louzada J., Beiroz W. & Ewers R.M. (2013). Optimising bait for pitfall trapping of Amazonian dung beetles (Coleoptera: Scarabaeinae). PLoS One **8**, e73147.

Mathew G. & Rahmathulla V. (1995). Biodiversity in the Western Ghats-A study with reference to moths (Lepidoptera: Heterocera) in the silent valley National Park, India. Entomon **20**, 25-34.

McGavin G. (1997). Expedition Field Techniques: Insects and other terrestrial arthropods. Royal Geographical Society, London.

Méndez-Rojas D.M., Cultid-Medina C. & Escobar F. (2021). Influence of land use change on rove beetle diversity: A systematic review and global meta-analysis of a mega-diverse insect group. Ecological Indicators **122**, 107239.

Mouhoubi D., Djenidi R. & Bounechada M. (2019). Contribution to the study of diversity, distribution, and abundance of insect fauna in salt wetlands of Setif region, Algeria. International Journal of Zoology **2019**.

Muñoz-Sáez A., Perez-Quezada J.F. & Estades C.F. (2017). Agricultural landscapes as habitat for birds in central Chile. Revista chilena de historia natural **90**, 3.

Nahmani J., Capowiez Y. & Lavelle P. (2005). Effects of metal pollution on soil macroinvertebrate burrow systems. Biology and fertility of soils **42**, 31-9.

Nair A.V., Mitra P. & Bandyopadhyay S. (2014). Studies on the diversity and abundance of butterfly (Lepidoptera: Rhopalocera) fauna in and around Sarojini Naidu college campus, Kolkata, West Bengal, India. Journal of Entomology and Zoology Studies **2**, 129-34.

Nasir A., Hussain M., Fatima S., Noureen N. & Ghazanfar M. (2016). New faunal records of dung beetles from district Sialkot, Punjab, Pakistan. Journal of Biodiversity and Environmental Sciences **9**, 122-8.

Naughton-Treves L., Holland M.B. & Brandon K. (2005). The role of protected areas in conserving biodiversity and sustaining local livelihoods. Annu. Rev. Environ. Resour. **30**, 219-52.

Nemec K.T. & Bragg T.B. (2008). Plant-feeding Hemiptera and Orthoptera communities in native and restored mesic tallgrass prairies. Restoration Ecology **16**, 324-35.

Ojija F., Sapeck E. & Mnyalape T. (2016). Diversity analysis of insect fauna in grassland and woodland community at Mbeya University of sciences and Technology. Tanzania. J. Sci. Eng. Res **3**, 187-97.

Oman P. & Cushman A.D. (1946). Collection and preservation of insects. US Dept. of Agriculture.

Paiva I.G., Auad A.M., Veríssimo B.A. & Silveira L.C.P. (2020). Differences in the insect fauna associated to a monocultural pasture and a silvopasture in Southeastern Brazil. Scientific Reports **10**, 1-16.

Pardini R., Nichols E. & Püttker T. (2017). Biodiversity response to habitat loss and fragmentation. Reference Module In Earth Systems And Environmental Sciences. Encyclopedia of the Anthropocene **3**, 229-39.

Parvaiz M. (2014). Ethnobotanical studies on plant resources of mangowal, district Gujrat, Punjab, Pakistan. Avicenna Journal of phytomedicine **4**, 364.

Rafi M.A., Carpenter J.M., Qasim M., Shehzad A., Zia A., Khan M.R., Mastoi M.I., Naz F., Ilyas M. & Shah M. (2017). The vespid fauna of Pakistan. Zootaxa **4362**, 1-28.

Rajkumari P., Sharmah D., Rahman A. & Patgiri P. (2014). Diversity and distribution pattern of hymenopteran insects in Jorhat District, Assam, India. International Journal of Science and Research **3**, 1938-41.

Ramzan U., Majeed W., Rana N. & Nargis S. (2021). Occurrence of different insect species with emphasis on their abundance and diversity in different habitats of Faisalabad, Pakistan. International Journal of Tropical Insect Science **41**, 1237-44.

Rana N., Saleem M., Majeed W., Jalal F., Ehsan N. & Nargis S. (2019). Diversity of arthropods regarding habitat specialty in agro-ecosystem of Faisalabad, Pakistan. GSC Biological and Pharmaceutical Sciences **6**, 01-8.

Rodger J.G., Balkwill K. & Gemmill B. (2004). African pollination studies: where are the gaps? International journal of tropical insect science **24**, 5-28.

Rogan J.E. & Lacher Jr T.E. (2018). Impacts of habitat loss and fragmentation on terrestrial biodiversity. Reference Module in Earth Systems and Environmental Sciences. Elsevier.

Ross A.H., Thomas M.C., Skelley P.E. & Frank J.H. (2002). American Beetles, Volume II: Polyphaga: Scarabaeoidea through Curculionoidea. CRC press.

Rykken J.J., Capen D.E. & Mahabir S.P. (1997). Ground Beetles as Indicators of Land Type Diversity in the Green Mountains of Vermont: Escarabajos Terrestres como Indicadores del Tipo de Diversidad del Suelo en Green Mountains, Vermont. Conservation Biology **11**, 522-30.

Sajjad A., Saeed S. & Ashfaq M. (2010). Seasonal variation in abundance and composition of hoverfly (Diptera: Syrphidae) communities in Multan, Pakistan. Pakistan J. Zool **42**, 105-15.

Saleem M., Arif M. & Suhail A. (2001). Taxonomic studies of syrphidae of Peshawar-Pakistan. International Journal of Agriculture and Biology **3**, 533-4.

Salomão R.P. & Iannuzzi L. (2015). Dung beetle (Coleoptera, Scarabaeidae) assemblage of a highly fragmented landscape of Atlantic forest: from small to the largest fragments of northeastern Brazilian region. Revista Brasileira de Entomologia **59**, 126-31.

Samways M.J. & Samways M.J. (2005). Insect diversity conservation. Cambridge University Press.

Sankarganesh E. (2017). Insect Biodiversity: The Teeming Millions-A review. Bull Environ Pharmacol Life Sci **6**, 101-5.

Sawada Y. & Hirowatari T. (2002). A revision of the genus Acrotrichis Motschulsky (Coleoptera: Ptiliidae) in Japan. Entomological Science **5**, 77-101.

Schauff M.E. (2001). Collecting and preserving insects and mites: techniques and tools. Systematic Entomology Laboratory, USDA.

Shannon C.E. & Weaver W. (1949). The mathematical theory of communication. Urbana: University of Illinois Press **96**, 1-35.

Simpon E. (1949). Measurement of diversity. Nature **688**, 163.

Singh V. (2013). Insect Fauna of Khajjiar Lake of Chamba District, Himachal Pradesh, India. Pakistan Journal of Zoology **45**, 1053-61.

Sörensson M. (2003). New records of featherwing beetles (Coleoptera: Ptiliidae) in North America. The Coleopterists Bulletin **57**, 369-81.

Subhani A., Awan M.S. & Anwar M. (2010). Population status and distribution pattern of red jungle fowl (Gallus gallus murghi) in Deva Vatala National Park, Azad Jammu and Kashmir, Pakistan: a pioneer study. Pakistan Journal of Zoology **42**, 701-6.

Suratman M.N. (2018). Introductory Chapter: Conserving Biodiversity in Protected Areas. IntechOpen, London, UK.

Thakare V. & Zade V. (2012). Diversity of beetles (Insecta: Coleoptera) from the vicinity of Semadoh-Makhala road, Sipnarange, Melghat Tiger Reserve,(MS) India. Bioscience discovery **3**, 112-5.

Thorp J.H. & Rogers D.C. (2010). Field guide to freshwater invertebrates of North America. Academic Press, California, USA.

Turner M.G. (1989). Landscape ecology: the effect of pattern on process. Annual review of ecology and systematics **20**, 171-97.

Tyagi R., Joshi P. & Joshi N.C. (2011). Butterfly diversity of district Nainital, Uttarakhand, India. Journal of Environment and Bio-Sciences **25**, 273-8.

Udawatta P.R., Rankoth L. & Jose S. (2019). Agroforestry and biodiversity. Sustainability **11**, 2879.

Umar M., Hussain M., Malik M.F., Awan M.N. & Lee D.C. (2021). Avian Community Composition and Spatio-Temporal Patterns at Deva Vatala National Park, Azad Jammu and Kashmir, Pakistan. Pakistan Journal of Zoology **53**, 921-9.

Upton M. & Mantle B. (2010). Methods for collecting, preserving and studying insects and other terrestrial arthropods. Australian Entomological Society, Canberra, Australia.

Waghmare S., Waghmare D. & Bhatnagar P. (2013). Species diversity of short horned grasshopper (Orthoptera: Acrididae) in selected grasslands of solapur district, Maharashtra, India. Journal of Biodiversity and Endangered Species **1**, 1-2.

Wagner H.H. & Edwards P.J. (2001). Quantifying habitat specificity to assess the contribution of a patch to species richness at a landscape scale. Landscape Ecology **16**, 121-31.

Wahyuni S., Pu'u Y. & Supartha I. (2011). Diversity of insect fauna in Kelimutu National Park area, Flores [Indonesia]. In: Journal of ISSAAS [International Society for Southeast Asian Agricultural Sciences], p. 89, Philippines.

Whipple S.D. (2011). Dung beetle ecology: Habitat and food preference, hypoxia tolerance, and genetic variation. In: Graduate College, Department of Entomology p. 104. The University of Nebraska-Lincoln, USA.

Whittaker R.H. (1977). Evolution of species diversity in land communities. Evolutionary Biology **10**, 1-67

Wilkinson D.A., Marshall J.C., French N.P. & Hayman D.T. (2018). Habitat fragmentation, biodiversity loss and the risk of novel infectious disease emergence. Journal of the Royal Society Interface **15**, 20180403.

Wilson E.O. (1990). Success and dominance in ecosystems: the case of the social insects. Ecology Institute Oldendorf/Luhe, Germany.

Zergoun Y., Guezoul O., Sekour M., Bouras N. & Holtz M.D. (2019). Acridid (Orthoptera: Caelifera) diversity in agriculture ecosystems at three locations in the Mzab valley, Septentrional Sahara, Algeria. Journal of Insect Biodiversity **9**, 18-27.

Submitted: 21/08/2021
Revised: 04/11/2021
Accepted: 07/11/2021
DOI: 10.48129/kjs.15801

Kuwait J.Sci., Vol.50, No.(1A),January.2023,pp(113-124)

Insights into the role of dopamine in olfactory learning behavior of honeybee

Muhammad Fahad Raza[1, 2], Zhiguo Li[1], Hongyi Nie[1], Songkun Su [1,*]

[1] *College of Animal Sciences (College of Bee Science)*
Fujian Agriculture and Forestry University, Fuzhou, China.

[2] *College of Life Sciences, Fujian Agriculture and Forestry University,*
Fuzhou, China

Corossponding author: susongkun@zju.edu.cn

Abstract

One of the brain's primary functions is remembering and learning information related to food and odour. Since biogenic amines were discovered in invertebrates and vertebrate, dopamine is considered a key modulator and neurotransmitter in honeybees' olfactory learning. Dopamine (DA) is significant in rewarding prediction, learning, invigorating social behavior, and motivation. Here we examined the effect of dopamine in the olfactory learning behavior of honeybees. We used the same age (14-days old) honeybees, *Apis mellifera* and *Apis cerana* to evaluate the proboscis extension response and characterized brain dopamine's effect on olfactory learning behavior. Both species were individually trained by performing three learning trials with sucrose solution and odor 1-Hexanol. High-performance liquid chromatography (HPLC) determined the brain dopamine level using electrochemical detection. Our findings showed that *Apis mellifera* learned better and had higher brain dopamine levels than *Apis cerana*. Thus, we show that dopamine acts as an essential neurotransmitter and modulator of motivation and influences honeybee cognition.

Keywords: Biogenic amine; dopamine; olfactory conditioning; proboscis extension response; social insect.

1. Introduction

In animals' central nervous system, associative learning is essential for predicting the ecosystem process rules(Benca *et al*., 2009). Several types of learning behaviour have been studied, but classical learning has been acknowledged due to its basic principles in different species. In associative learning behavior, insects learn by associating conditioned stimulus (Odor) with the unconditioned stimulus (Sucrose solution). Initially, the odor (a neutral stimulus) does not exhibit the conditioned response, while the latter exhibits the instinctive response due to a biologically relevant stimulus(Webb, 2012). The pairing of odor (CS) with the sucrose solution(US) develops an associative relationship between the conditioned stimulus (CS) and the unconditioned stimulus (US), thus exhibiting the prominent response to the odor that predicts the sugar solution(Chabaud *et al*., 2006). Insects are important model organisms for the Pavlovian conditioning study(Menzel

& Müller, 1996). Numerous studies on the *Apis mellifera* have been carried out using Pavlovian conditioning protocol to describe the behavioral, molecular and neural studies (Giurfa 2007, Palottini *et al*., 2018, Schleyer *et al*., 2018). In proboscis extension response protocol, odorant (CS) was presented to retrained bees with a paired association of sucrose solution (US), which is touched with both antenna and next to the proboscis. The sugar solution is offered to the antenna for eliciting the (PER) (proboscis extension response), which is established by odor following the successful conditioning(Smith & Burden, 2014, Van Nest, 2018).

The most important principle is that behavioral plasticity and odorant stimuli association have been shown in the brain of numerous species of insects. Odorant receptors detect different odors by the antenna and the sensory information is processed in sequential steps to sensory pathways, including mushroom bodies' antennal lobes and the lateral horns (Fiala 2007, Sandoz 2011, Rössler & Brill, 2013). Changes in neural plasticity activity have been identified at these different levels due to classical or Pavlovian conditioning(Gerber *et al*., 2009, Busto *et al*., 2010, Rössler & Brill, 2013). However, neural differences exist concerning unconditioned stimulus activity in insects' brains; even conditioned stimulus (sugar solution) is rewarded with appetitive learning. While biogenic amines have a crucial effect on sucrose reward learning, the unique biogenic amine needed for this function varies between species of insects. In this instance, dopamine (DA) plays an essential signaling role in fruit flies (*Drosophila melanogaster*) trained with the pairing of odor and sucrose solution as a reward. In mammals, dopamine has been associated with motivation, reward and pleasure. Also mediate in aversion learning (Van Swinderen & Andretic 2011, Ichinose *et al*., 2017); several studies reported that dopamine neurons are also directly involved in appetitive reinforcement (reward stimuli) and aversive learning (aversive stimuli)(Roussel *et al*., 2010).

Our findings are directed at both species' appetitive olfactory learning and analysing the relationship between learning success and dopamine (DA) levels. We hypothesised that dopamine levels might be linked with the predisposition to learn the olfactory learning association between odor and sucrose and vary between learners and non-learners. This study aims to investigate olfaction learning success and evaluate the role of dopamine in the learning performance of *Apis mellifera* and *Apis cerana*. We used high-performance liquid chromatography (HPLC) with an electrochemical detection (ECD) system to quantify dopamine levels in both species' brains following appetitive olfactory learning. We revealed that olfactory learning's success was directly related to dopamine (DA) levels. The DA could act as a motivational neurotransmitter and improve olfactory learning success.

2. Materials and methods

2.1 Experimental Bees

The bees of *A. mellifera* and *A cerana* were obtained from the experimental apiary of the College of Animal Sciences, Fujian Agriculture and Forestry University. Capped combs of both species were obtained from six different healthy colonies (Three colonies of *A. mellifera* and three colonies of *A.cerana*) and placed in an incubator. The newly emerged bees were collected every day and

kept in cages. Plastic cages were kept in an incubator temperature of 30ºC (±1, 30ºC), and relative humidity 70% (±1 70%) to get new emerging bees. More or less 50 newly emerged bees were in s plastic cages. The total number of *A. cerana* (n=350) and *A. mellifera* (n=250) were used to evaluate the learning behavior. Every day, mortality was recorded and dead bees were removed from cages. The food and sugar solution was replaced after about three days. The honeybees were maintained following the standard procedure(Williams *et al*., 2013). When the bees were 14 days old, they were brought to the laboratory for olfactory PER conditioning.

2.2 Sucrose Sensitivity

Honeybees were brought for a sucrose sensitivity test and transferred to a glass vial. The glass vials were kept in the icebox for 3-4 minutes to immobilize the bees and harnessed following a standard procedure(Matsumoto *et al*., 2012) and kept in an incubator at 30ºC and relative humidity of 70% (±1, 70%) for one hour. Before conditioning, a drop of 30% (w/v) sucrose solution was delivered to the antennae to check for intact PER. Bees not responding with PER to this stimulation were discarded from the experiment. Bees were trained using odorant 1- hexanol (Sigma Aldrich, France) was always paired with 30% sucrose solution. Each CS+ trial lasted 39 sec. First, the harnessed bee was placed in front of the olfactometer and clean air was delivered to the antennae for 15 s. Then an odorant was then delivered during 4 s. Two seconds after odor onset, Sucrose sucrose solution was delivered for 2 sec, 2 sec after odor onset. Therefore, the interstimulus interval was 2 sec and the CS and US finished ended simultaneously. Finally, clean air was delivered without other stimulations for 20 sec to complete the 39-sec trial. The intertrial interval was 10 min. The PER (proboscis extension response) to each odorant (conditioned response) was recorded during training. Responses were noted as "1" or "0" (no PER).

2.3 Quantification of dopamine level

At the end of conditioning, bees were transferred to death in nitrogen liquid and stored at -80°C for subsequent brain dissection and dopamine quantifications. Brains dissection was performed into the frozen dish in dry ice under a cold-light source and kept frozen throughout all dissection. Compound eyes, hypopharyngeal glands, celli, trachea, and glandular tissues were removed during dissection. Brains in which pieces of tissue were lost and discarded so that only intact brains were used for HPLC analyses. Each brain was kept at -80° C in a 1.5 mL centrifuge tube until it was analyzed. To compare dopamine levels, we randomly chose twenty brains of ‘learners’ and twenty brains of ‘non-learners’ to detect accentuated differences, if any. We used high-performance liquid chromatography (HPLC) with electrochemical detection to measure the concentration of the biogenic amine dopamine, according to (Harris & Woodring 1992, Li *et al*., 2009). Details of the HPLC procedure are provided in the Supplementary Information.

3. Results

The in vitro rearing of emerging honeybees (*A. cerana*, *A. mellifera)* has become a gradually essential honeybee research method to get the same-age bees for our experiment specifically. In this experiment, I compared the survival percentage of *A. cerana* versus *A. mellifera* based on 14 days' intervals. Survival percentage is expressed in survival bees during the monitoring period of 14 days (Figure 1). Using Kaplan-Meier survival analysis, the Log-Rank test was used to determine the survival percentage. Both species, *A. cerana* (survivorship, 81.42%) and *A. mellifera* (survivorship, 67.6%), showed a significant difference in survival percentage during 14 days. (***p ≤ 0.001, IBM SPSS Statistics 21,) (Figure 1)**.** During the development, the bees of *A. cerana* showed a significantly higher survival range than bees of *A. mellifera*. Survival percentage is expressed of survival bees during the monitoring period of 14 days (Figure 1)**.**

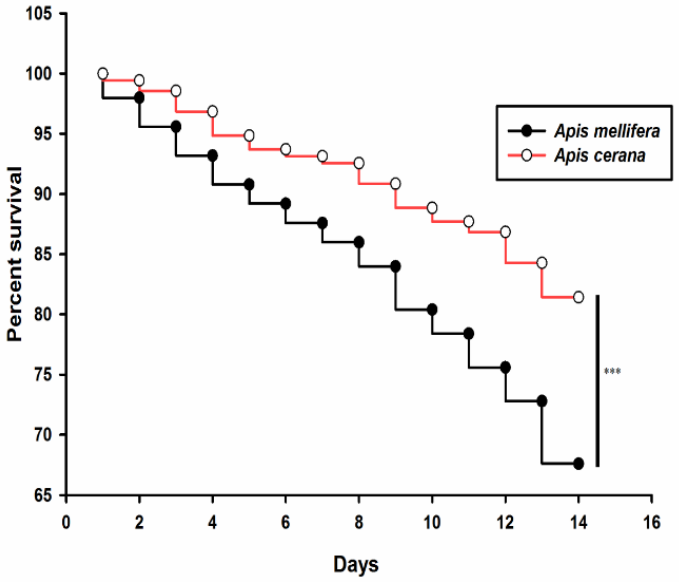

Fig. 1. Kaplan–Meier survival analysis curves showing the percentage survival among *Apis cerana* (n=350) and *Apis mellifera* (n=250) at different day's intervals. Both species *A. cerana* (survivorship, 81.42%) and *A. mellifera* (survivorship, 67.6%) showed significant differences during 14 day's intervals (Figure 1) (***p ≤ 0.001, IBM SPSS Statistics 21, ANOVA).

After 14 days, population responses of bees *A. mellifera* (n=150) versus *A. cerana* (n-=115) were trained to discriminate between the learner and non-learner during three conditioning trials (T1, T2, T3). Both species showed PER to an odor in each of the three conditioning trials; one-way ANOVA was used to analyse the learning trials (Figure 2). *A.mellifera* exhibited significance difference among three condition trials represented with small letters a,b,c ($F(2, 6) = 501.1$, p-value $P<0.0001$) and *A. cerana* showed significant difference with capital letters A,B, C ($F(2, 6) = 468.9$, p-value $P<0.0001$) (Figure 2).

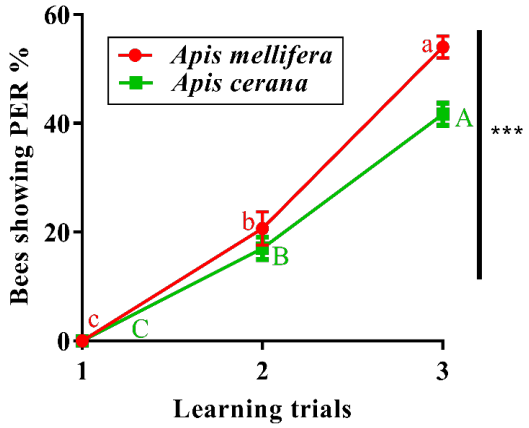

Fig. 2. Learning trials comparison in the same age bees of *A. cerana* and *A. mellifera*.

Our results indicated that *A. mellifera* has a significantly higher proboscis extension response than *A. cerana*. The bees learning ability of *A. mellifera* learner versus *A. cerana* learner was significant. Bees showing Proboscis extension reflex (Mean ± SE) of 14 days' adult honeybees from both species. The percentage proboscis extension response of *A. mellifera* was significantly higher than *A. cerana* using t-test. Proboscis extension response of leaner bees was the significant difference (Assigned letter a, b) found in *A. mellifera* and *A. cerana* (t=9.175, df=4, p-value .001***p ≤ 0.001). No significant difference (A, A) was observed between non-learner in *A. cerana* and *A. mellifera* (t=-1.091, df=4, p-value .336). The of *A. mellifera* (t=12 df=4, p-value 0.0003, ***p ≤ 0.001) and *A. cerana* (t=2.885 df=4, p-value 0.0448, *p ≤ 0.05) showed significant differences (Figure 3).

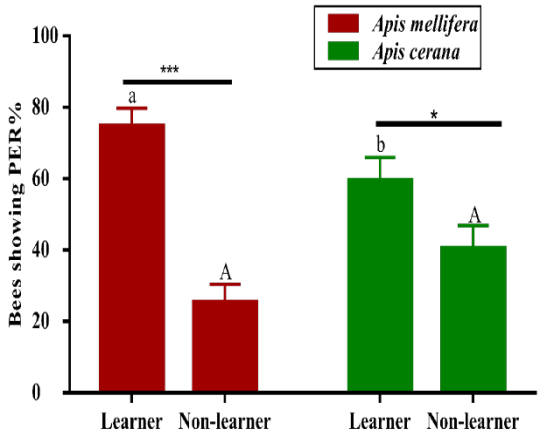

Fig. 3. Olfactory learning performance in the same age bees of *A. cerana* and *A. mellifera*. The learning trials of *A. mellifera* versus *A. cerana*. Bees showing Proboscis extension reflex (Mean ± SE) of 14 days' adult honeybees from *A. mellifera* (n=150) versus *A. cerana* (n-=115). The PER percentage of *A. mellifera* was significantly higher than *A. cerana* by t-test.

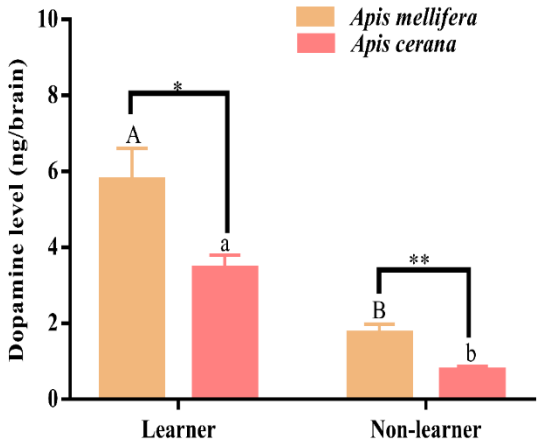

Fig. 4. Dopamine (DA) levels (ng/brain; mean ± S.E.) measured in individual brains of learners (n=40) and non-learner (n=40) of both species. DA level was higher in the learner of *A. mellifera* than *A. cerana*.

The experiment was performed to measure the dopamine level of learner and non-learner groups of both species *A. mellifera* versus *A. cerana* (Figure 4). The data of brain dopamine levels in 14 days old bees are expressed as Mean ± SE. Comparison of brain dopamine level between learner and non-learner in *A. mellifera* and *A. cerana* analysed by t-test. Dopamine levels of the learner and non-learner bees were significantly found in both species. *A. cerana (*a, b) (t=7.243 df=18, p-value 0.0001, ***p ≤ 0.001) and *A. mellifera (*A, B) (t=4.574, df=18, p-value 0.0002, ***p ≤ 0.001) showed significant difference between learners and non-learners bees. Statistically, learner bees of *A. cerana* versus *A. mellifera* showed significant results (t=2.53 df=18, p-value 0.0209, (*p ≤ 0.05). The dopamine level varies significantly in the non-learner group of *A. mellifera* versus *A. cerana* (t=3.573 df=18, p-value 0.0022 **p ≤ 0.01).

4. Discussion

For crops' pollination, Olfactory learning behavior was beneficial for ecological survival (Wright & Schiestl 2009, Iqbal *et al*., 2019). Due to honeybee's impressive learning ability, the olfactory foraging behavior is closely related to memorizing and learning the routes and local features, directly associated with the nectar source's reliability and quality (Dyer *et al*., 2008). The learning and memory mechanisms in honeybees are highly conserved. Nevertheless, several species of honeybees' learning performance variation cannot be ignored due to several factors such as geographical area, diversified foraging behavior, genetic variation, local climate, bee size, and evolutionary lability(Al-Ghamdi *et al*., 2017).

Several experiments have been conducted with free-flying honeybee visiting differently scented feeders(Reinhard *et al*., 2004). These studies have provided significant advantages in the ecosystem's context, but several experiment variables, such as bee or inter-trial intervals' physiological status, cannot be precisely controlled. Moreover, investigating olfactory learning for the neural basis needs neurophysiological measures to monitor the bees' brain. Simultaneously, it

learns odor and learning processes (Laska *et al*., 1999, Giurfa 2007). For these considerations, the experimental conditional protocol was developed to study the olfactory learning behavior of individual restrained bees (Hammer 1997). Three conditioning trials were conducted to evaluate the learning performance of both species. Our results revealed that learner bees of *A. mellifera* showed increased PER than *A,cerana*. The learning performance of A.mellifera is better than A.cerana bees revealed in our previous study(Raza *et al*., 2019). (Zhengwei WANG and Ken TAN., 2013) also reported that *A.cerana* is a slow learner and bees of *A.cerana* showed more PER than *A. mellifera* after three learning trials (Wang & Tan, 2014). Our results suggested that bees of *A. cerana* can be used as a remarkable organism for olfactory learning, neurobiological and physiological research. Here we cannot conclude that some unspecific parameters may affect olfactory learning behavior. For example, both species need different amounts of food, the difference in harnessing reactions in the metal tube before olfactory learn, and sucrose concentration level as a reward during learning trials. We predicted that *A. mellifera* bees showed more response and learned better with less concentrated sucrose solution compared to that of *A. cerana*. We've come to the conclusion that bees of *A. cerana* have a distinctive pattern in olfactory learning behavior in response to odor and sucrose solution from *A. mellifera* bees.

Our results showed that the level of biogenic amine DA is significantly elevated in learners' brains after appetitive olfactory learning trials involving an odor and sucrose solution reward. These results are innovative as the traditional view of honey bee learning has related learning success to DA signaling, which facilitates the reinforcing efficacy of sucrose solution in appetitive odor conditioning (Mizunami *et al*., 2009). On the contrary, DA is also associated with aversive learning reinforcement signalling in the bee brain (Liu *et al*., 2012). So that the higher levels found in our work after successful appetitive learning was unexpected. Yet, the question remains of why DA levels were also elevated compared to non-learners. To reconcile the opposite views referred to the role of DA in the bee brain provided by prior works (Vergoz *et al*., 2007, Guiraud *et al*., 2018, Marchal *et al*., 2019) and the present one, we suggest that besides dopaminergic neurons conveying aversive signaling in the bee brain, an additional class of such neurons exist that mediate attentional processes, and thus facilitate learning (Tedjakumala *et al*., 2014). This would explain why learners consistently have higher DA levels with greater attention to the discrimination problem. This hypothesis is reinforced by the demonstration of the mechanism of attention, similar to those described in vertebrates (Dyer & Chittka, 2004, Giurfa 2004, Miller *et al*., 2011, van Swinderen 2011, Van Swinderen & Andretic, 2011). In the fruit fly, a neural correlate of such processes is a transient increase in a 20-30 Hz local field potential recorded in a brain region called the medial protocerebrum (van Swinderen & Greenspan, 2003). Transient attenuation of DA release in fly mutants attenuates the 20-30 Hz responsiveness to the object to be attended, and oral delivery of methamphetamine, which increases DA release, rescues this responsiveness (Andretic *et al*., 2005). Thus, the higher levels of DA in learners' brains may reveal that their attentional processes were more efficient, thus leading to better discrimination learning.

The scenario emerging from our study indicates that depressing DA levels before conditioning should lead to deficits in learning performance, particularly for differential appetitive

conditioning, which requires higher levels of attention to achieve the discrimination between a rewarded stimulus (Giurfa 2004).

5. Conclusion

This study determined dopamine's effect on olfactory learning behaviour on both species' learners and non-learner bees. Both species, *A. cerana* (survivorship, 81.42%) and *A. mellifera* (survivorship, 67.6%) showed a significant difference in survival percentage during 14-days. *A. mellifera* has a significantly higher proboscis extension response than *A. cerana* . The learning ability of *A. mellifera* learner versus *A. cerana* learner bees was significant. Dopamine levels of the learner and non-learner bees were significant that found in *A. mellifera*. *A. cerana* and *A. mellifera* showed significant differences between learner and non-learner bees.

ACKNOWLEDGEMENTS

The authors are thankful to “Modern Agro-industry Technology Research System (No. CARS-44-KXJ4), the National Natural Science Foundation of China (31772684; 31702192).

Conflict of interest

The authors declare that there is no conflict of interest.

References

Al-Ghamdi, A., N. Adgaba, Y. Tadesse, A. Getachew and A. Al-Maktary (2017). Comparative study on the dynamics and performances of *Apis mellifera jemenitica* and imported hybrid honeybee colonies in southwestern Saudi Arabia. Saudi Journal of Biological Sciences. **24**(5): 1086-1093.

Andretic, R., B. van Swinderen and R. J. Greenspan(2005). Dopaminergic modulation of arousal in *Drosophila*. Current Biology, **15**(13): 1165-1175.

Benca, R., M. J. Duncan, E. Frank, C. McClung, R. J. Nelson and A. J. Vicentic (2009). Biological rhythms, higher brain function, and behavior: Gaps, opportunities, and challenges.Brain research reviews, **62**(1): 57-70.

Busto, U., I. Cervantes-Sandoval and R. L. J. P. Davis. (2010). Olfactory learning in Drosophila. Physiology, **25**(6): 338-346.

Chabaud, A., J.M. Devaud, M.Pham-Delègue, T. Preat and L.A. Kaiser (2006). Olfactory conditioning of proboscis activity in *Drosophila melanogaster*. Journal of Comparative Physiology A. **192**(12): 1335-1348.

Dyer, A. G. and L. Chittka (2004). Fine colour discrimination requires differential conditioninginbumblebees.Naturwissenschaften. **91**: 224-227.

Dyer, A. G., M. G. Rosa and D.B. Reser. (2008). Honeybees can recognise images of complex natural scenes for use as potential landmarks.Journal of experimental biology. **211**(8): 1180-1186.

Fiala, A. J. Coin. (2007). Olfaction and olfactory learning in Drosophila: recent progress. Current opinion in neurobiology. **17**(6): 720-726.

Gerber, B., R. F. Stocker, T. Tanimura and A. S. Thum (2009). Smelling, tasting, learning: Drosophila as a study case. Chemosensory systems in mammals, fishes, and insects, Springer**:** 187-202.

Giurfa, M. (2004). "Conditioning procedure and color discrimination in the honeybee *Apis mellifera*." Naturwissenschaften **91**(5): 228-231.

Giurfa, M. (2007). "Behavioral and neural analysis of associative learning in the honeybee: a taste from the magic well." Journal of Comparative Physiology A **193**(8): 801-824.

Guiraud, M., L. Hotier, M. Giurfa and M. G. de Brito Sanchez (2018). Aversive gustatory learning and perception in honey bees.Science Report. **8**(1): 1343.

Hammer, M. J. T. i. n. (1997). The neural basis of associative reward learning in honeybees. **20**(6): 245-252.

Harris, J. W. and J. Woodring (1992). "Effects of stress, age, season, and source colony on levels of octopamine, dopamine and serotonin in the honey bee (*Apis mellifera* L.) brain.Journal of Insect Physiol **38**: 29-35.

Ichinose, T., H. Tanimoto and N. J. Yamagata (2017). Behavioral modulation by spontaneous activity of dopamine neurons. Frontiers in systems neuroscience. **11**: 88.

Iqbal, J., H. Ali, A. A. Owayss, H. S. Raweh, M. S. Engel, A. S. Alqarni and B. H.Smith (2019).Olfactory associative behavioral differences in three honey bee *Apis mellifera* L. races under the arid zone ecosystem of central Saudi Arabia.**26** (3): 563-568.

Laska, M., C. G. Galizia, M. Giurfa and R. Menzel (1999).Olfactory discrimination ability and odor structure–activity relationships in honeybees. Chem senses **24**(4): 429-438.

Li, N., J. Guo, B. Liu, Y. Yu, H. Cui, L. Mao and Y. Lin (2009). Determination of monoamine neurotransmitters and their metabolites in a mouse brain microdialysate by coupling high-performance liquid chromatography with gold nanoparticle-initiated chemiluminescence. Anal Chim Acta. **645**(1-2): 48-55.

Liu, C., P. Plaçais, N. Yamagata, B. Pfeiffer, Y. Aso, A. B. Friedrich, I. Siwanowicz, G. M. Rubin, T. Preat and H. J. N. Tanimoto (2012). A subset of dopamine neurons signals reward for odour memory in Drosophila.Nature. **488**(7412): 512-516.

Marchal, P., M. E. Villar, H. Geng, P. Arrufat, M. Combe, H. Viola, I. Massou and M. Giurfa. (2019). Inhibitory learning of phototaxis by honeybees in a passive-avoidance task.Learn Memory. **26**(10): 412-423.

Matsumoto, Y., R. Menzel, J.-C. Sandoz and M. Giurfa. (2012). Revisiting olfactory classical conditioning of the proboscis extension response in honey bees: a step toward standardized procedures. **211**(1): 159-167.

Menzel, R. and U. Müller (1996). Learning and memory in honeybees: from behavior to neural substrates. Annual review of neuroscience **19**(1): 379-404.

Miller, S. M., T. Ngo and B. van Swinderen (2011). "Attentional switching in humans and flies: rivalry in large and miniature brains." Frontier Human Neuroscience. **5**: 188.

Mizunami, M., S. Unoki, Y. Mori, D. Hirashima, A. Hatano and Y. Matsumoto(2009).Roles of octopaminergic and dopaminergic neurons in appetitive and aversive memory recall in an insect. **7**(1): 46.

Palottini, F., M. C. Estravis Barcala and W. M. J. F. i. p. Farina (2018). "Odor Learning and Its Experience-Dependent Modulation in the South American Native Bumblebee Bombus atratus (Hymenoptera: Apidae)." Frontiers in psychology. **9**: 603.

Raza, M., Z. Li, M. Rizwan, H. A. Kalan and S.Su., (2019). Comparison of learning and memory of eastern (*Apis cerana cerana*) and western honeybees (*Apis mellifera* L.). Applied ecology and environemntal research. **17**(2): 4971-4984.

Reinhard, J., M. V. Srinivasan, D. Guez and S. Zhang (2004). "Floral scents induce recall of navigational and visual memories in honeybees." **207**(25): 4371-4381.

Rössler, W. and M. F. J. J. o. C. P. A. Brill (2013). Parallel processing in the honeybee olfactory pathway: structure, function, and evolution. Journal of Comparative Physiology A**. 199**(11): 981-996.

Roussel, E., J.-C. Sandoz and M. J. F. i. b. n. Giurfa (2010). Searching for learning-dependent changes in the antennal lobe: simultaneous recording of neural activity and aversive olfactory learning in honeybees." Frontiers in behavioral neuroscience. **4**: 155.

Sandoz, J.C. (2011). "Behavioral and neurophysiological study of olfactory perception and learning in honeybees." Frontiers in systems neuroscience **5**: 98.

Schleyer, M., M. Fendt, S. Schuller and B. J. Gerber (2018). "Associative learning of stimuli paired and unpaired with reinforcement: evaluating evidence from maggots, flies, bees, and rats." Frontiers in psychology **9**: 1494.

Smith, B. H. and C. M. J. J. Burden (2014). A proboscis extension response protocol for investigating behavioral plasticity in insects: application to basic, biomedical, and agricultural research. JoVE.(91): e51057.

Tedjakumala, S. R., M. Aimable and M. Giurfa (2014). "Pharmacological modulation of aversive responsiveness in honey bees." Frontiers Behavior Neuroscience. **7**.

Van Nest, B., (2018). The olfactory proboscis extension response in the honey bee: a laboratory exercise in classical conditioning.Journal of Undergraduate Neuroscience Education. **16**(2): A168.

Van Swinderen, B. and Andretic, R., (2011). Dpamine in Drosophila: setting arousal thresholds in a miniature brain. Proceedings of the Royal Society B: Biological Sciences, 278(1707): 906-913.

Van Swinderen, B. and Greenspan, R.J. (2003). Salience modulates 20-30 Hz brain activity in Drosophila. Nature Neuroscience, 6(6): 579-586.

Vergoz, V., E. Roussel, J. C. Sandoz and M. Giurfa (2007). Aversive learning in honeybees revealed by the olfactory conditioning of the sting extension reflex. PLoS One. **2**(3): e288.

Wang, Z. and K. Tan (2014). Comparative analysis of olfactory learning of *Apis cerana* and *Apis mellifera*. **45**(1): 45-52.

Webb, B., (2012). Cognition in insects." Philosophical Transactions of the Royal Society B: Biological Sciences. **367**(1603): 2715-2722.

Williams, G., C. Alaux, C. Costa, T. Csáki, V. Doublet, D. Eisenhardt, I. Fries, R. Kuhn, D. McMahon and P. Medrzycki (2013).Standard methods for maintaining adult Apis mellifera in cages under in vitro laboratory condition." **52**(1): 52-04.

Wright, G. A. and F. Schiestl (2009). The evolution of floral scent: the influence of olfactory learning by insect pollinators on the honest signalling of floral rewards. **23**(5): 841-851.

Submitted: 08/07/2021
Revised: 23/05/2022
Accepted: 24/05/2022
DOI: 10.48129/kjs.15071

Kuwait J.Sci., Vol.50, No.(1B),January.2023,pp(125-139)

Insilico analysis on the complex relationship among antibiotic resistance, virulence genes and insertion sequences in *Pseudomonas aeruginosa*

Santhiya Kalimuthu[1, *]

[1]*Dept. of Biotechnology (FoE), Karpagam Academy of Higher Education, Coimbatore, 641021, Tamilnadu*

***** *Corresponding author: santhiya.k@kahedu.edu.in*

Abstract

Pseudomonas aeruginosa is the most frequent nosocomial pathogen, causing many infections in people and posing significant health risks worldwide. The current work attempts to understand the connection between antibiotic resistance genes (ARG), virulence factors (VF), and insertion sequences (IS) in *P. aeruginosa*. Fifty-six *P. aeruginosa* complete plasmids were retrieved from the NCBI database for this investigation. The CARD and Resfinder tools are used to discover ARG in *P. aeruginosa*. The VF analyzer and ISsaga tools are used to identify virulence genes and insertion sequences in the sorted plasmids. Using the tool PHASTER, the participation of prophage and integrase genes was discovered. Resistance to sulfonamide and beta-lactam was the most common ARG among the plasmids. Fil, pil, and XCP secretion systems are prevalent virulence genes. The prophage, integrase, and transposons were also identified. The correlation analysis of ARG, VF, and IS revealed that ISs, rather than virulence factors, had the most significant effect on the *P. aeruginosa* genome studied. As a result, an understanding of infectious bacterial profiles regarding pathogenicity islands and mobile elements is required to gain knowledge of their distribution and limit their spread throughout the world.

Keywords: Antibiotic resistance; health care; insertion sequence; mobile elements; virulence genes.

1. Introduction

Antibiotic resistance is a significant global burden due to increased infection caused by MDR gram-negative bacteria in recent years. It is estimated that nearly 0.7 million people die due to antibiotic-resistant infections (Dixit *et al.*, 2019). ESKAPE (*Enterococcus faecium, Staphylococcus aureus, Klebsiella pneumonia, Acinetobacter baumannii, Pseudomonas aeruginosa,* and *Enterobacter species*) encompasses six primary nosocomial-causing pathogens and its virulence increases day by day.

Pseudomonas aeruginosa, a gram-negative bacillus commonly found in the environment, especially in water resources, was first isolated from green pus in 1882 by Gossard. It has a massive set of regulatory genes in its genome (Ali *et al*., 2021). It has the unique feature of being able to survive under various environmental conditions, making it sustainable in the clinical environment (Jose *et al.*, 2017). The microorganism's pathogenicity depends on its strong affinity

for the host system. This interaction is mediated by a set of specialized factors called the Virulence Factor (VF); it is a significant measure of pathogenicity causing infection in the host system. *P. aeruginosa* strains have been found resistant to most current antibiotics present on the market, including beta-lactams, aminoglycosides, fluoroquinolones, and tetracyclines. A mobile element such as a transposon or insertion sequence plays a prominent role in transferring resistance genes among different bacterial species. The contribution of mobile elements in promoting bacterial resistance and genome evolution is very significant (Ho *et al*., 2009).

In this study, complete plasmid sequences of *P. aeruginosa* deposited in the National Centre for Biotechnology Information (NCBI) were utilized to detect the presence of antibiotic resistance genes and virulence factors. Additionally, insertion sequence analysis was also performed to decode the correlation between resistant genes and mobile elements in the pathogenicity of *P. aeruginosa*.

2. Material and Methods

2.1 Retrieval of complete plasmid sequence

The 56 complete plasmid sequences of *P. aeruginosa* (https://www.ncbi.nlm.nih.gov/genome/browse/#!/plasmids/Pseudomonas%20aeruginosa) were used for this in silico analysis. The sequences of *P. aeruginosa* were retrieved from the NCBI public database in February 2020.

2.2 Detection of antibiotic resistant genes

A Comprehensive Antibiotic Resistance Database (CARD; https://card.mcmaster.ca) and Resfinder (https://cge.cbs.dtu.dk/services/ResFinder/) are bioinformatics curated online resource tools providing a molecular basis for bacterial antimicrobial resistance (AMR) for nucleotide and protein sequences (Alcock *et al.*, 2020). The plasmids which harbor antibiotic-resistant genes were only taken for further analysis.

2.3 Detection of virulence gene

The presence of virulence genes for the sorted plasmids was found using the tool, Virulence Factor Database (VFanalyzer, http://www.mgc.ac.cn/VFs/); it is a comparative pathogenomics pipeline. It constructs conserved regions within the query genome and conducts iterative sequence similarity searches to avoid false positives (Liu *et al.*, 2019).

2.4 Insertion sequence analysis

The mobile elements like Insertion Sequence and Transposons in the sorted plasmids were analyzed using the ISsaga database (http,//issaga.biotoul.fr/issaga_index.php), which works under the platform of the ISfinder (Varani *et al.*, 2011).

2.5 Detection of prophage, integrase, and transposons

The presence of the prophage and integrase gene in the chosen plasmid was analyzed using the tool PHASTER (https://phaster.ca/) followed by BLAST. The transposons were found using the tool ISsaga database. The analysis was done only for the plasmids which have a correlation profile (ARG, IS and VF).

2.6 Phylogenetic analysis

The evolutionary relationship of plasmids was determined using MAFFT software (https://mafft.cbrc.jp/alignment/server/) for the chosen plasmids. MAFFT is based on the Fourier transform theory. It provides multiple sequence analysis and a phylogenetic interface to the user under one platform (Katoh *et al.*, 2019).

3. Result and Discussion

The genome analysis was conducted by analyzing 56 complete plasmid sequences (Table 1) of *P. aeruginosa* (1 kb to 500 kb) retrieved from the NCBI database. This study is exclusively based on the in silico approach. Out of 56 plasmids, 26 plasmid sequences were found to have various antibiotic resistance genes based on the annotation using the CARD and ResFinder tools, whereas 22 plasmids were identified to have 100% perfect resistance gene sequences in their genome.

Table 1. Fifty-six plasmids taken for the analysis

Accession Number	Strain	Size(Mb)	GC%	CDS	Release Date
CP011370.1	S04 90	0.159187	57.7321	175	2015-05-08T
CM003767.1	BH6	0.003652	55.8598	2	2016-02-08T
CP016215.1	PA121617	0.423017	56.4067	460	2016-07-07T
AJ877225.1	Nil	0.057121	59.4702	51	2005-06-01T
AM261760.1	Nil	0.089147	59.0059	97	2006-09-16T
AM778842.1	Nil	0.024179	63.8116	29	2007-08-21T
EU410482.1	Nil	0.00214	45.7944	1	2008-05-21T
HM560971.1	Nil	0.123322	60.5829	137	2014-10-15T
AY257538.1	Nil	0.103532	60.928	105	2012-11-04T
KC189475.1	Nil	0.02188	62.8108	23	2013-03-07T
KC609322.1	Nil	0.007995	55.5222	8	2013-09-12T
KC609323.1	Nil	0.031529	60.189	26	2013-09-14T
CM007350.1	PA3448	0.049094	58.8972	58	2016-10-27T
CP015000.1	PA7790	0.049021	58.8972	57	2016-11-08T
CP018048.1	DN1	0.317349	56.9376	384	2016-12-20T
CP020602.1	E6130952	0.036454	61.3348	40	2017-04-13T

CP017294.1	PA83	0.398087	59.3712	425	2017-07-08T
CP025052.1	PB353	0.059923	57.3386	75	2017-12-08T
CP025054.1	PB354	0.059923	57.3386	75	2017-12-08T
LT969519.1	RW109	0.555265	58.0933	588	2017-12-20T
LT969521.1	RW109	0.151612	57.2778	162	2017-12-20T
CP027173.1	AR_0353	0.041559	60.7979	46	2018-03-13T
CP027175.1	AR_0230	0.071782	59.6877	82	2018-03-13T
CP027176.1	AR_0230	0.00135	48	2	2018-03-13T
CP027167.1	AR_0356	0.165365	55.7857	200	2018-03-13T
CP027168.1	AR_0356	0.057053	60.8592	68	2018-03-13T
CP027170.1	AR_0356	0.438531	57.1435	509	2018-03-13T
CP029091.1	AR441	0.165365	55.7857	190	2018-05-02T
CP029092.1	AR441	0.057052	60.8585	67	2018-05-02T
CP029094.1	AR441	0.438529	57.1426	490	2018-05-02T
CP029095.1	AR439	0.001129	54.3844	2	2018-05-02T
CP029096.1	AR439	0.437392	56.8778	474	2018-05-02T
CP020561.2	CR1	0.046804	59.1894	56	2018-04-03T
CP029708.1	K34-7	0.00444	30.0676	3	2018-06-16T
CP030914.1	Y89	0.085842	60.0953	95	2018-08-14T
CP032256.1	AR_0111	0.129422	57.515	150	2018-09-19T
CP029714.1	BH9	0.041024	63.4945	26	2018-11-19T
CP033772.1	FDAARGOS_532	0.001249	51.7214	1	2018-11-26T
CP033773.1	FDAARGOS_532	0.001089	46.3728	1	2018-11-26T
CP033834.1	FDAARGOS_570	0.036032	61.2816	42	2018-11-26T
CP034355.1	IMP-13	0.130306	57.652	147	2018-12-19T
LS998784.1	1	0.024853	57.0635	31	2019-01-29T
CP039294.1	PABL048	0.414954	56.5819	483	2019-04-22T
CP040126.1	PA298	0.395774	56.8643	454	2019-05-20T
CP041355.1	AZPAE15042	0.185168	59.3385	205	2019-07-18T
CP041355.1	C79	0.04018	58.0762	37	2019-08-06T
CM017760.1	TC4411	0.419683	56.9659	478	2019-08-23T
CP042268.1	HOU1	0.167069	64.9259	165	2019-09-15T
CP043482.1	GIMC5001:PAT-23	0.049805	59.3796	61	2019-09-15T
CP043548.1	GIMC5002:PAT-169	0.049805	59.3896	59	2019-09-15T
CP024631.1	PA59	0.046627	59.1331	54	2019-11-05T
CP039989.1	T2436	0.422811	56.8755	472	2019-12-01T
CP039991.1	T2101	0.439744	56.9816	492	2019-12-01T
CM019124.1	4068	0.051059	59.5683	62	2019-12-05T
CP049162.1	MS14403	0.05013	59.601	67	2020-03-02T
KC543497.1	PA96	0.500839	57.598	545	2013-09-12T

The antibiotic-resistant gene analysis of twenty-two *P. aeruginosa* plasmids (Table 2) indicates that the strains harbored genes mediating resistance to antimicrobial-resistant groups, namely aminoglycosides, beta-lactams, fluoroquinolone, macrolide-lincosamide-streptogramin B (MLS), phenicol, sulfonamide and tetracycline. The AMR genes against sul were found to be prominent (n=12), followed by those against OXA (n=7) and KPC (n=4 each). Most of the plasmids encode sulfonamide and beta-lactam resistance (Figure. 1).

Table 2. Resistance genes detected in the 22 plasmids of *P. aeruginosa*

Accession No	ARO Term	AMR Family	Drug Class	Resistance Mechanism
CP011370.1	VIM-2	VIM	carbapenem, cephalosporin, cephamycin, penam	antibiotic inactivation
	aac(6')-29b	AAC(6')	aminoglycoside antibiotic	antibiotic inactivation
	sul1	sul	sulfonamide antibiotic	antibiotic target replacement
CM003767.1	KPC-2	KPC	monobactam, carbapenem, cephalosporin, penam	antibiotic inactivation
	Arma	16S rRNAmethyltransferase	aminoglycoside antibiotic	antibiotic target alteration
CP016215.1	IMP-45	IMP	carbapenem, cephalosporin, cephamycin, penam	antibiotic inactivation
	OXA-1	OXA	cephalosporin, penam	antibiotic inactivation
	catB3	chloramphenicol acetyltransferase (CAT)	phenicol antibiotic	antibiotic inactivation
	sul1	sul	sulfonamide antibiotic	antibiotic target replacement
	QnrVC6	quinolone resistance protein	fluoroquinolone antibiotic	antibiotic target protection
	mph	macrolide phosphotransferase (MPH)	macrolide antibiotic	antibiotic inactivation
AJ877225.1	APH(3')-Ia	APH(3')	aminoglycoside antibiotic	antibiotic inactivation
	aac(3)-I	AAC(3)	aminoglycoside antibiotic	antibiotic inactivation
	aadA5	ANT(3")	aminoglycoside antibiotic	antibiotic inactivation
	sul1	sul	sulfonamide antibiotic	antibiotic target replacement
AM261760.1	TEM-2	TEM	monobactam, cephalosporin, penam,	antibiotic inactivation
	aadA1	ANT(3")	aminoglycoside antibiotic	antibiotic inactivation

	tet(A)	major facilitator superfamily (MFS)	tetracycline antibiotic	antibiotic efflux
	dfrA1	trimethoprim resistant dihydrofolatereductase	diaminopyrimidine antibiotic	antibiotic target replacement
	SAT-2	streptothricinacetyltransferase (SAT)	nucleoside antibiotic	antibiotic inactivation
KC189475.1	sul1	sul	sulfonamide antibiotic	antibiotic target replacement
	VIM-2	VIM	carbapenem, cephalosporin, cephamycin, penam, monobactam,	antibiotic inactivation
KC609323.1	KPC-2	KPC	carbapenem, cephalosporin, penam	antibiotic inactivation
	sul1	sul	sulfonamide antibiotic	antibiotic target replacement
	aac(6')-Ib	AAC(6')	aminoglycoside antibiotic	antibiotic inactivation
CP025052.1	OXA-101	OXA	cephalosporin, penam	antibiotic inactivation
	TEM-1B	TEM	monobactam, cephalosporin, penam	antibiotic inactivation
	CTX-M-30	CTX-M	cephalosporin	antibiotic inactivation
	sul1	sul	sulfonamide antibiotic	antibiotic target replacement
CP025054.1	aac(6')-Ib	AAC(6')	aminoglycoside antibiotic	antibiotic inactivation
	TEM-1B	TEM	monobactam, cephalosporin, penam	antibiotic inactivation
	CTX-M-30	CTX-M	cephalosporin	antibiotic inactivation
CP027173.1	GE'S-1	GES	carbapenem, cephalosporin, penam	antibiotic inactivation
CP027168.1	KPC-2	KPC	monobactam, carbapenem, cephalosporin	antibiotic inactivation
CP029092.1	KPC-2	KPC	monobactam, carbapenem, cephalosporin,	antibiotic inactivation
	sul1	sul	sulfonamide antibiotic	antibiotic target replacement
CP029096.1	IMP-18	IMP	carbapenem, cephalosporin, cephamycin, penam	antibiotic inactivation
	each	small multidrug resistance (SMR) antibiotic efflux pump	fluoroquinolone antibiotic	antibiotic efflux
	AAC(6')-Il	AAC(6')	aminoglycoside antibiotic	antibiotic inactivation
CP02970	tet(K)	major facilitator	tetracycline antibiotic	antibiotic efflux

8.1		superfamily (MFS) antibiotic efflux pump		
	VIM-6	VIM	carbapenem, cephalosporin, cephamycin, penam	antibiotic inactivation
	OXA 10	OXA	cephalosporin, penam	antibiotic inactivation
CP03383 4.1	aac(6')-Ib3	AAC(6')	aminoglycoside antibiotic	antibiotic inactivation
	aph(6)-Id	APH(6)	aminoglycoside antibiotic	antibiotic inactivation
	cmx	major facilitator superfamily (MFS) antibiotic efflux pump	phenicol antibiotic	antibiotic efflux
	sul1	sul	sulfonamide antibiotic	antibiotic target replacement
CP03929 4.1	aadA10	ANT(3")	aminoglycoside antibiotic	antibiotic inactivation
	OXA-10	OXA	cephalosporin, penam	antibiotic inactivation
	ANT(2")-Ia	ANT(2")	aminoglycoside antibiotic	antibiotic inactivation
	IMP-45	IMP	carbapenem, cephalosporin, cephamycin, penam	antibiotic inactivation
CP04012 6.1	catB3	chloramphenicol acetyltransferase (CAT)	phenicol antibiotic	antibiotic inactivation
	sul1	sul	sulfonamide antibiotic	antibiotic target replacement
	VIM-1	VIM	carbapenem, cephalosporin, cephamycin, penam	antibiotic inactivation
CP04135 5.1	sul1	sul	sulfonamide antibiotic	antibiotic target replacement
CP04226 8.1	CpxR	resistance-nodulation-cell division (RND) antibiotic efflux pump	a macrolide antibiotic	antibiotic efflux
	APH(3")-Ib	APH(3")	aminoglycoside antibiotic	antibiotic inactivation
	sul1	sul	sulfonamide antibiotic	antibiotic target replacement
	OXA-10	OXA	cephalosporin, penam	antibiotic inactivation
CP03998 9.1	cmlA5	major facilitator superfamily (MFS) antibiotic efflux pump	phenicol antibiotic	antibiotic efflux
	arr-2	rifampin ADP-ribosyltransferase (Arr)	rifamycin antibiotic	antibiotic inactivation
	ANT(2")-Ia	ANT(2")	aminoglycoside antibiotic	antibiotic inactivation
	VEB-2	VEB	monobactam,	antibiotic

			cephalosporin	inactivation
	OXA-10	OXA	cephalosporin, penam	antibiotic inactivation
	FEB-1	VEB	monobactam, cephalosporin	antibiotic inactivation
	tet(G)	major facilitator superfamily (MFS)	tetracycline antibiotic	antibiotic efflux
CP039991.1	ANT(2")-Ia	ANT(2")	aminoglycoside antibiotic	antibiotic inactivation
	CARB-2	CARB	Penam	antibiotic inactivation
	FEB-1	VEB	monobactam, cephalosporin	antibiotic inactivation
	sul1	sul	cephalosporin, penam	antibiotic inactivation
	OXA-10	OXA	cephalosporin, penam	antibiotic inactivation
	sul1	sul	sulfonamide antibiotic	antibiotic target replacement
KC543497.1	AAC(6')-Ib4	AAC(6')	aminoglycoside antibiotic	antibiotic inactivation
	IMP-9	IMP	carbapenem, cephalosporin, cephamycin, penam, penem	antibiotic inactivation

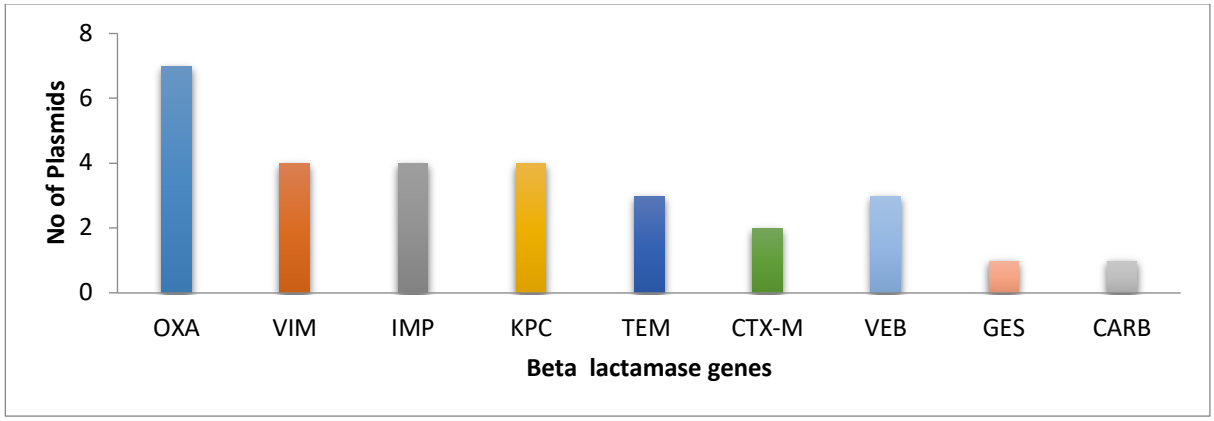

Fig. 1. Frequency of Beta-lactam resistant genes in the plasmids studied

Sulfonamide resistance is frequently associated with florfenicol and oxytetracycline resistance, and it will be transferred to-resistant genes through selection (Dominguez *et al*., 2019). However, in this study, sul genes coexisted with beta-lactam resistant genes like OXA10, CTX-M-30, and TEM in most of the plasmids. The beta-lactam resistant genes like OXA, VIM, IMP, TEM, CTX, and KPC have been detected in the plasmids taken for the analysis. Beta-lactam antibiotics are commonly used for the treatment of *P. aeruginosa* infections. Antibiotic resistance is caused by lactamase enzymes cleaving antibiotics (Zilberberg *et al*., 2010). In *P. aeruginosa*, there is a significant association between toxin secretion and beta-lactamase

producers. In clinical isolates of *P. aeruginosa*, pigment production was more strongly linked to beta-lactam antibiotic resistance than the development of virulence components such as elastases and proteases (Finlayson *et al*., 2011).

3.1 Involvement of Virulence Factors

Among 22 plasmids analyzed in the VFDB database, only 11 plasmids were found to have virulence genes in their genome (Table 3). The virulence factors for adherence and secretion systems were prominent in the *P.aeruginosa* plasmid taken for the study.

Table 3. Virulence gene profile for plasmids

S. No	Accession No	Virulence genes
1	CP039294.1	xcpU
2	CP016215.1	mtrD, xcpU, xcpA
3	AJ877225.1	cyaB, cyaA
4	CP029096.1	bplL, xcpU, xcpA
5	CP039989.1	xcpU, xcpA
6	CP011370.1	pilB, pilQ
7	CP039991.1	xcpU, xcpA
8	CP040126.1	xcpU, xcpA
9	CP027173.1	fliD
10	KC543497.1	xcpU, xcpA
11	CP042268.1	fimV, xcpQ, xcpR, xcpS, xcpY, xcpW, xcpP, xcpU, xcpT, xcpV, pilB, pilT, pilQ, pilB, gspE, bplL, tagT, ybtP, eccCa1, cyaB, fha1, pchl, fleR, popN

P.aeruginosa has various cell surface pili and flagella related to genes responsible for the twitching motility of the bacteria and involved in its biogenesis, expression, and functionality of pilus. It attaches to the host cell and guides the bacteria to accelerate along the cell surface. It also helps biofilm formation, avoids the host immune system, and creates resistance against antibiotics (Sriramulu *et al.*, 2005).The secretory system plays a significant role in bacterial pathogenicity. There were about eight types of secretory systems (Tseng *et al.*, 2009). Xcp factor comes under T2SS and has been identified in *P. aeruginosa*. Xcp needs the proper localization of PilB and PilC and secretes toxins in the extracellular fluid. Xcp secretes the quorum sensing regulated virulence factors elastaseA, elastase B and exotoxin A.

3.2 Existence of Insertion sequence in plasmids

A mobile genetic element such as transposons, insertion sequence, and integrons plays a crucial role in *P. aeruginosa* to become multidrug-resistant bacteria. The sorted plasmids are predicted to have 12 different transposon families and various insertion sequences like ISKpn6, ISKpn7,

ISPa16, ISPa17, IS6100, ISPt3, ISPen2, TnAs3 and IS222. Among the 12 types, IS21 and IS6 are the most prominent families (Figure. 2).

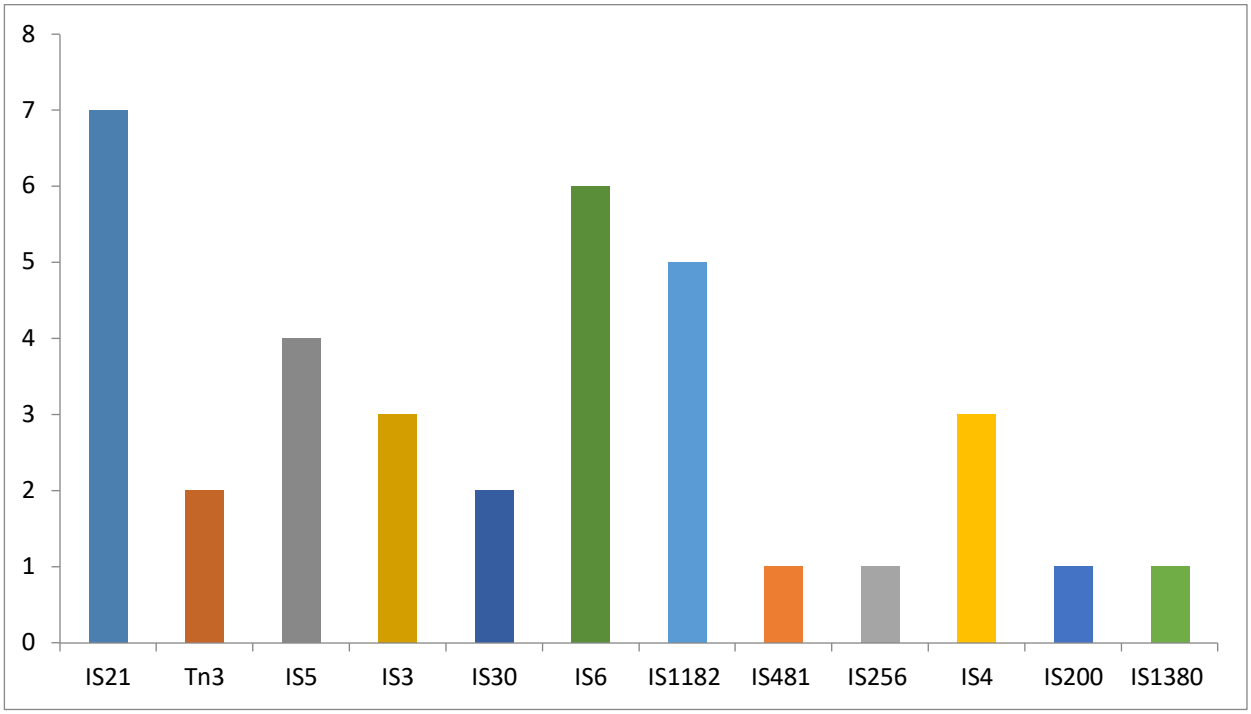

Fig. 2. ISs profile for plasmids taken for study

The study by Bouteille *et al., 2004* suggested that IS mediated efflux pump depression has been detected in the IS21 family due to more repressors, especially in *P. aeruginosa*, that tend to increase the occurrence of beta-lactam resistant genes in the genome. According to the study, the majority of the beta-lactam resistance identified has an IS21 family of ISs.

The resistant gene KPC belongs to the beta-lactam resistance and has been chiefly carried along with the Tn3 like transposon family. This genome arrangement plays a role in disseminating the blaKPC gene among varied species, especially in *P. aeruginosa*. The current study shows the presence of the blaKPC gene along with ISKpn6 and ISKpn7 belonging to the IS1182 and IS21 families, respectively. The study by Johnson TA *et al*., 2016 revealed that IS6100 type transposon has an abundance of genes conferring resistance to about six antibiotic classes and class 1 integrase. In relevance to this study, IS6100 is likely to have a resistance gene profile (APH(3")-Ib, sul1, cmlA5, arr-2, ANT (2")-Ia, VEB-2) in two plasmids and another resistance pattern (OXA-10, sul1, AAC(6')-Ib4, IMP-9) found in three plasmids.

The correlation profile among ARG, IS, and VG for 7 out of 22 *P.aeruginosa* plasmids taken for analysis is listed in Table 4. The correlation analysis shows that five plasmids had similar kinds of ARGs and are profiled in their genomes, and it is interesting that VF was not found in those five plasmids. The remaining two plasmids found virulence genes for adherence with similar ARG patterns.

Table 4. Correlation profile on ARG, IS and VF

S. No	Accession No	Sample source	Location	ARG	IS	VF
1	KC609323.1	Bronchial secretion	France	KPC-2	ISApu1,ISKpn6	No
2	CP025052.1	Urine	USA	sul1 TEM-1 CTX-M-30	IS6100,ISEcp1	No
3	CP025054.1	Urine	USA	sul1 TEM-1 CTX-M-30	IS6100	No
4	CP027168.1	-	USA	KPC-2	ISKpn6, ISKpn7	No
5	CP029092.1	-	USA	KPC-2	ISKpn6, ISKpn7	No
6	CP039989.1	Adult male sputum	UK	APH(3")-Ib sul1 OXA - 10 arr-2 ANT(2")-Ia	IS10A, IS6100	xcpU, xcpA
7	CP039991.1	Adult male sputum	UK	VEB-2 OXA-10 FEB-1 ANT(2")-Ia FEB-1 sul1	IS6100	xcpU, xcpA

3.3 Detection of Prophage, Integrase and Transposons

Prophages are bacteriophages that have been identified to contribute to interstrain genetic diversity by integrating into bacterial chromosomes via an integrase gene. A transposase is indeed an attributed recombinase that facilitates transposition or an integrase in the case of a retrovirus with RNA intermediate in its life cycle. The transposons Tn3, ISEc9, IS600, IS3, IS6100, Tn5041, and IS1479 were identified in the plasmids taken for the study using the ISsaga database. The same resistance gene appears to be linked to many mobile elements; a closer look shows a more complicated picture.

The prophage and integrase genes were found using the PHASTER tool. The intI1 integrase was present in three plasmids taken for the study. Integrons can significantly improve the host bacterium's fitness in clinical settings. Several outbreaks of bacteria generating beta-lactamases have been linked to integron-associated antibiotic resistance genes. The presence of intI1 in recycled water is strongly linked with sul1 and tet antibiotic-resistant genes (Gillings *et al*., 2015).

Table 5. Plasmids bearing Integrase, Prophage and Transposon

S. No	A. No	Integrase	Prophage	Transposon
1	CP029096.1	intI1	exonuclease, Hef nuclease, methyltransferase	Transposase IS3/IS911family
2	CP025054.1	intI1	No	ISEc9 and IS6100
3	CP025052.1	intI1	No	ISEc9 and IS6100
4	CP039989.1	No	exonuclease, Hef nuclease	Tn3
5	CP039991.1	No	exonuclease, Hef nuclease, methyltransferase,	Tn3 and IS600
6	KC609323.1	No	No	Tn5041 and Tn5044
7	CP027168.1	No	No	Tn5041 and Tn5044

Prophages detected in this study are exonuclease, Hefnuclease and methyltransferase (Table 5). Many bacteriophages carry methyltransferase genes. Methylation seems to be required for pathogen survival in certain strains. Hef includes a domain linked to a wide range of endonucleases. However, it has no sequence homology with the other Hef families. The survival of a hef in a population depends on repeated transposition to various destinations followed by subsequent dissemination among phages via homing (Zund *et al*., 2021).

3.4 Phylogenetic analysis

Phylogenetic analysis was performed using MAFFT software. The analysis was done for seven plasmids with a correlation profile (ARG, IS, and VF) as per the above results. The result shows that the plasmids encoding the similar pattern of ARG and IS was presented under a single clade compared to other plasmids. The influence of prophage and integrase genes was not as prominent as per this phylogeny analysis. It indicates that plasmids play an essential role in promoting the transmission of ARG and mobile elements amongst varied plasmid categories and distant evolutionary lineages.

The sequences CP039989 and CP039991 have the same prophage and antibiotic resistance genes. However, the sequence KC609323 from France lacks any prophage genes, although all three plasmids belong to the same clade (Figure. 3). A similar situation happened in the sequences, CP027168 and CP029092.

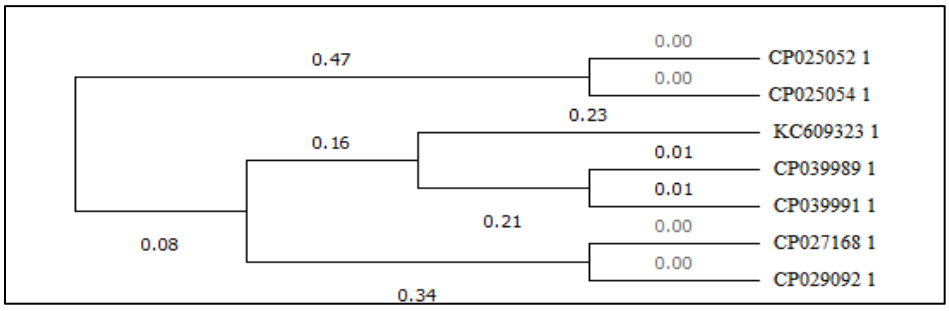

Fig. 3. Phylogeny relation of plasmids

Zhang *et al.* 2019 illustrated that the bacteria have different ARG profiles in different time intervals. However, selective pressure has little effect on most virulence genes. In this study, the absence of virulence factors was seen in some plasmids even though they tended to have ARG and ISs in their genome. This may be due to the genome reduction in the infectious bacteria, which tends to the absence of virulence factors (Beceiro *et al.*, 2013). Hence, the results suggest that the possible spread of *P. aeruginosa* among various microbial communities is due to the influence of some virulence genes. The abundance of insertion sequences in their genome plays a notable role in pathogenicity.

4. Conclusion

In this study, 22 out of 56 complete plasmids of *P. aeruginosa* were found to have known antibiotic resistance genes. The most prominent resistant genes are sulfonamide and beta-lactam and mainly related to adherence and xcp secretion system. IS21 and IS6 are the prominent IS families observed in plasmids taken for the analysis. The plasmids were identified as the intI1 gene and prophages like exonuclease, Hef nuclease, and methyltransferase. The correlation among ARG, VF, and IS indicates that IS elements occurring within the plasmids significantly influence the antibiotic resistance profile in the analysed *P. aeruginosa* plasmids. In contrast, the proportion of VF was lower and predicted to have less influence on the genome. It could be that environmental factors might have some influence on the genome features of ARGs and VFs in the plasmids taken for the study. However, the coexistence of antibiotic resistance genes and mobile elements needs to be considered to understand the dissemination and influence on each other in multidrug-resistant bacteria like *P. aeruginosa* to identify more specific and accurate drug treatments to overcome the infections in the future.

References

Alcock, B.P., Raphenya, A.R., Lau, T.T.Y., Tsang, K.K., Bouchard, M., Edalatmand, A., *et al*. (2020) CARD 2020: antibiotic resistome surveillance with the comprehensive antibiotic resistance database. Nucleic Acids Research, 48(**D1**): D517-D525.

Ali, F., Kamal, S., Shakeela, Q. & Ahmed, S. (2021) Extended-spectrum and Metallo-beta lactamase enzymes mediated resistance in Pseudomonas aeruginosa in clinically isolated specimens. Kuwait Journal of Science, 48(**2**): 1-9.

Beceiro, A., Tomás, M. & Bou, G. (2013) Antimicrobial resistance and virulence: a successful or deleterious association in the bacterial world? Clinical Microbiology Reviews, 26(**2**):185-230.

Boutoille, D., Corvec, S., Caroff, N., Giraudeau, C., Espaze, E., Caillon, J., Plésiat, P., & Reynaud, A. (2004) Detection of an IS21 insertion sequence in the mexR gene of Pseudomonas aeruginosa increasing beta-lactam resistance. FEMS microbiology letters, 230(**1**), 143–146.

Dixit, A., Kumar, N., Kumar, S. &Trigun, V. (2019) Antimicrobial Resistance: Progress in the Decade since Emergence of New Delhi Metallo-β-Lactamase in India. Indian Journal of Community Medicine, 44(**1**):4-8.

Domínguez, M., Miranda, C. D., Fuentes, O., de la Fuente, M., Godoy, F. A., Bello-Toledo, H., & González-Rocha, G. (2019) Occurrence of Transferable Integrons and *sul* and *dfr* Genes Among Sulfonamide-and/or Trimethoprim-Resistant Bacteria Isolated From Chilean Salmonid Farms. Frontiers in microbiology, 10, 748.

Finlayson, E.A. & Brown, P.D, (2011) Comparison of antibiotic resistance and virulence factors in pigmented and non-pigmented *Pseudomonas aeruginosa*. The West Indian medical journal, 60 (**1**), 24–32.

Gillings, M.R., Gaze, W.H., Pruden, A., Smalla, K., Tiedje, J.M, & Zhu, Y.G. (2015). Using the class 1 integron-integrase gene as a proxy for anthropogenic pollution. ISME J, 9(**6**):1269-1279.

Ho Sui, S.J., Fedynak, A., Hsiao, W.W., Langille, M.G., & Brinkman, F.S. (2009) The association of virulence factors with genomic islands. PloS one, *4*(**12**), e8094.

Johnson, T. A., Stedtfeld, R. D., Wang, Q., Cole, J. R., Hashsham, S. A., Looft, T., Zhu, Y. G., &Tiedje, J. M. (2016) Clusters of Antibiotic Resistance Genes Enriched Together Stay Together in Swine Agriculture. mBio, 7(**2**), e02214–e2215.

Jose, J., Santhiya, K., Jayanthi, S. &Ananthasubramanian, M. (2017) Insertion sequence-based analysis of clinical isolates with NDM *(bla*NDM-1) resistance, Indian Journal of Biotechnology; 16(**2**): 182-188.

Katoh, K., Rozewicki, J. & Yamada, K.D. (2019) MAFFT online service: multiple sequence alignment, interactive sequence choice and visualization. Briefings in Bioinformatics 20:1160-1166

Liu, B., Zheng, D.D., Jin, Q., Chen, L.H. & Yang, J. (2019) VFDB 2019: a comparative pathogenomic platform with an interactive web interface. Nucleic Acids Res; 47(D1): D687-D692.

Sriramulu, D.D., Lunsdorf, H., Lam, J.S. & Romling, U. (2005) Microcolony formation: a novel biofilm model of Pseudomonas aeruginosa for the cystic fibrosis lung. Journal of Medical Microbiol;54:667-676.

Tseng, T.T., Tyler, B.M. & Setubal, J.C. (2009) Protein secretion systems in bacterial-host associations, and their description in the Gene Ontology. BMC Microbiology, 9, S2.

Varani, A.M., Siguier, P., Gourbeyre, E., Charneau, V. & Chandler, M. (2011)ISsaga is an ensemble of web-based methods for high throughput identification and semi-automatic annotation of insertion sequences in prokaryotic genomes. Genome Biology, 12(**3**): R30.

Zilberberg, M.D., Chen, J., Mody, S.H., Ramsey, A.M. &Shorr, A.F. (2010) Imipenem resistance of Pseudomonas in pneumonia: a systematic literature review. BMC Pulmonary Medicine, 10:45.

Zünd, M., Ruscheweyh, H.J., Field, C.M., Natalie, M., Miguelangel, C., Daniel, H. et al. (2021) High throughput sequencing provides exact genomic locations of inducible prophages and accurate phage-to-host ratios in gut microbial strains. Microbiome, 9, 77.

Submitted: 06/06/2021
Revised: 17/05/2022
Accepted: 01/06/2022
DOI: 10.48129/kjs.14591

Instability of alloxan-induced diabetes and its impact on sex and thyroid hormones in male wistar rats-a pilot study

Martin Osibemhe*, Blessing O. Orji, Gloria O. Omaji, Elizabeth Amune, John Ezekiel

Dept. of Biochemistry and Molecular Biology, Faculty of Life Science, Federal University Dutsin-Ma, Katsina State, Nigeria.

**Corresponding author: mosibemhe@fudutsinma.edu.ng*

Abstract

The relationship between diabetes mellitus and sex and/or thyroid hormones has been well documented in both human and animal studies ditto auto-reversibility of alloxan. However, the correlation between unstable diabetes and these hormones has little or no information in the literature; hence, the focus of this study. Diabetes was induced with a single intraperitoneal injection of 150 mg/kg of freshly prepared alloxan. Twenty-five adult male Wistar rats (weight 120-150 g) were used in this study. Alloxan was administered to 20 rats and 5 rats served as control. Alloxan-administered rats were further divided into two groups. One group (diabetic rats) was used as diabetic control and the other group served as reversed diabetic, which contained rats whose fasting blood glucose was confirmed to be normoglycemic post-diabetic. All rats were maintained on normal rat feed and water *ad libitum* and were monitored for 14 days. Blood glucose was monitored at intervals of 7 days after basal (before diabetes induction) and day 1(diabetes confirmation) values had been noted. Sex hormones: Luteinizing hormone (LH), follicle stimulating hormone (FSH), and estrogen (E) as well as thyroid hormones: Triiodothyronine (T3), tetraiodothyronine (T4) and thyroid stimulating hormone (TSH) were assayed after 14 days. Alloxan caused alteration in blood glucose levels of both diabetic and reversed diabetic groups. T4 level was lowered significantly in both diabetic (11.32 ± 0.26 μg/ml) and reversed diabetic (11.00 ± 0.16 μg/ml) groups in relation to the control. Other assayed hormones were not different significantly from the control. These findings indicate that influence of diabetes on these hormones may not be dependent on glucose gradation.

Keywords: Alloxan; Diabetes; Glucose; Hormones; Normoglycemic

1. Introduction

Alloxan and streptozotocin are the two most widely used chemicals to induce experimental diabetes. They both work by selectively destroying the beta cells of the pancreas. While streptozotocin destroys the beta cells by its alkylating potency, alloxan exerts its toxic effects on the beta cells via reactive oxygen species (ROS) generation and inhibition of glucokinase (Lenze, 2008). Nevertheless, the auto reversibility of the toxic effects of alloxan has been widely reported (Soni*et al.,* 2019). According to Soudamani *et al*. (2005); lowering of the epithelial diameter, luminal volume, stromal density of seminiferous tubules and plasma testosterone are

some ways by which alloxan causes reproductive dysfunctions in rats. Most of these changes are attributed to the ability of alloxan to inhibit the activities of some antioxidants such as superoxide dismutase and glutathione reductase in the testis in addition to its ability to increase testicular lipid peroxidation (El-Missiry, 1999).

Evidence abounds in the literature that thyroid hormones have profound effects on blood glucose levels. On the other hand, abnormal thyroid hormone levels have also been reported in diabetic patients with poor glucose control (Gursoy & Tuncel, 1999). Thyroid hormones have an opposite action to insulin in hepatic tissues. While insulin inhibits glucose production in the liver by inhibiting gluconeogenesis and glycogenolysis, thyroid hormones promote both pathways in the liver (Weinstein *et al.,* 1994). Reports have shown that thyroid hormones act synergistically with insulin by promoting glucose removal and utilization by peripheral tissues. They increase the expressions of Glut-4 and phosphoglycerate kinase genes that respectively participate in glucose transportation and glycolysis (Clement *et al.,* 2002; Viguerie, 2002).

Whereas several reports have shown the association between diabetes, sex, and thyroid hormones- there is little or no information in the literature about the impact of unstable alloxan-induced diabetes on sex and thyroid hormones. Hence, considering these relationships deserve to be given attention.

2. Methods

2.1 Animals

Twenty-five adults male Wistar rats weighing between 120-150 g were purchased from the National Institute for Trypanosomiasis Research (NITR), Kaduna, Nigeria. These rats were kept in laboratory cages (made of metal wire on all sides with wooden stand) and housed for two weeks to be acclimatized to the new environment. They were maintained under standard laboratory conditions (at 26±2°C temperature and 35±5% relative humidity) and exposed to equal amount of light/dark cycle (12 h/each). All animals had access to drinking water and food (produced by vital feeds, Bukuru, Jos, Nigeria) *ad libitum*. They were properly catered for following internationally accepted practices for use and care of laboratory animals, per US guidelines (NIH, 1992). At the end of the experiment, rats were fasted overnight and euthanized under moderate chloroform anesthesia.Registration and approval for this research was granted by the Departmental Ethics and Animal Welfare Committee of our institution in a letter with reference number: BCHEAWC-05/06/2019.

2.2 Chemical and Reagents

Alloxan was purchased from Zigma Aldrich, Jos Nigeria branch office. Normal saline was purchased from a Pharmacy shop, DutsinMa, Nigeria.

2.3 Induction of Diabetes

Fasted animals (overnight but with free access to water) were induced diabetes by intraperitoneal injection (by a single dose of 150 mg/kg body weight) of freshly prepared alloxan reconstituted with 0.9% normal saline (in a ratio of 10 mg/1 ml). Confirmation of diabetes (using a glucometer) was carried out on the 7^{th} day post alloxan injection. Animals with fasting blood glucose (mmol/L) more than double of the basal values were considered diabetic (Osibemhe *et al.*, 2017).

2.4 Experimental Design

In this study, twenty-five adult male Wistar rats (weight 120-150 g) were used. Alloxan was administered to 20 rats and 5 rats served as control. Rats administered with alloxan were further divided into two groups. One group (diabetic rats) consisted of 5 rats was used as diabetic control and another group (5 rats) served as reversed diabetic which contained rats that had confirmed fasting blood glucose as normoglycemic (within the range of basal glucose values) post-diabetic. This group was included in anticipation of reversal of the diabetic action of alloxan. Extra rats of the alloxan-injected that showed impaired glucose values (10 rats) were excluded from this study. All animals were monitored for 14 days. Blood glucose was monitored at intervals of 7 days after basal (before diabetes induction) and day 1 (day diabetes was confirmed) values had been noted. Sex hormones: Luteinizing hormone (LH), follicle stimulating hormone (FSH), and estrogen (E) and thyroid hormones: Triiodothyronine (T3), tetraiodothyronine (T4) and thyroid stimulating hormone (TSH) were assayed after 14 days. All analyses on each rat in each group were based on a single determination.

2.5 Collection and Preparation of Blood Sample for Analyses

At the end of the observation period, the rats were fasted overnight and euthanized under moderate chloroform anesthesia. Before death, blood was collected through the abdominal aorta using 5 ml syringe and kept in plain sample bottles. Samples were subsequently centrifuge at 3500 rpm for 15 min after proper clotting had been obtained and the serum was aspirated into plain sample containers (appropriately labeled with codes) for hormonal analysis.

2.6 Biochemical Analysis

Fasting blood glucose was monitored using a glucometer (accu-check). In this procedure, the tail of rats kept in a restrainer was cleaned with cotton wool that contains disinfectant (methylated spirit). And after massaging the tail, a syringe was used to prink the tip of the tail and a drop of blood was placed on the test strip already inserted in the glucometer (Osibemhe *et al.,* 2017). The result (mmol/L) displayed on the screen of the meter was recorded. Sex hormones: LH, FSH, and E and thyroid hormones: T3, T4, and TSH were assayed using fully automatic Finecare 3 Plus Immunoassay Analyzer (WondFo).

2.7 Sex Hormones and Thyroid Hormones Analysis

These hormones were assayed by using the fully automatic Finecare 3 Plus Immunoassay Analyzer (WondFo). The Finecare sex/thyroid hormones rapid qualitative test is based on fluorescence immunoassay (FIA) technique. The assay procedure involves five basic steps: preparation, sampling, mixing, loading and testing. In this analysis, the machine was prepared by activating it for "use" mode. This was followed by inserting into the machine an ID chip corresponding to the test Cartridge. Subsequently, 75 µL of each of the serum sample was transferred with the aid of a pipette into a Detection Buffer tube, the lid of the detection buffer was closed, and the sample was thoroughly mixed by shaking for about 10 mins. This was followed by pipetting 75 µL of each of the sample mixture and loading it into the sample well of the test Cartridge. By using the standard test mode, the test command was executed, and the results displayed on machine screen were printed.

2.8 Statistical Analysis

Data analyzed were presented as means ± SEM (n=5). One-way ANOVA followed by Duncan post hoc test to compare the means using the Statistical Package for the Social Sciences (SPSS) version 16. Statistically significant difference was set at $P<0.05$.

3. Results

3.1 Fasting Blood Glucose Level

Result of the fasting blood glucose levels is as shown in Figure 1. Data show no significant change in fasting blood glucose levels of the normal control rats from day 1-14 when compared with the basal values. The diabetic control had significant increase in fasting blood glucose level from day 1-14. However, the reversed diabetic rats exhibited increase in fasting blood glucose concentration on day 1 that normalized from day 7-14.

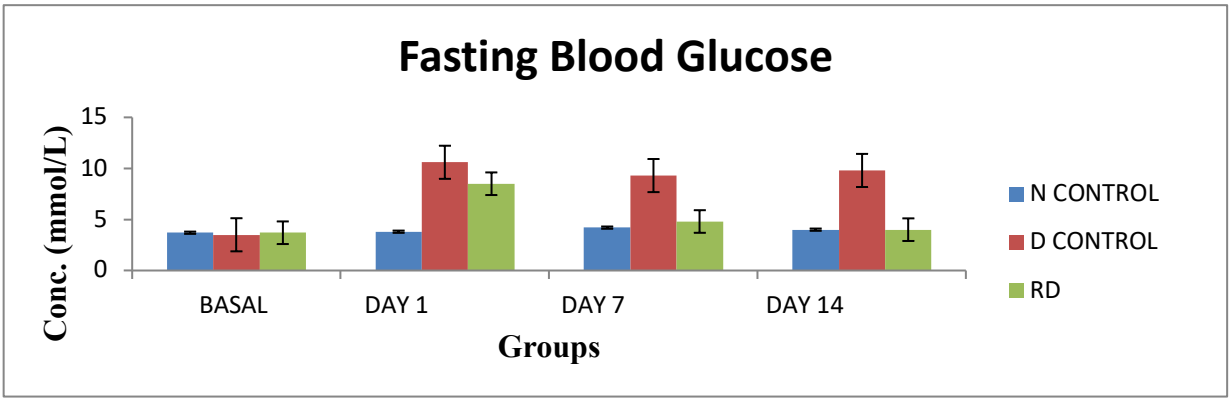

Fig. 1. Mean Fasting blood glucose concentration of diabetic and reversed diabetic rats fed with normal rat feed and monitored for 14 days. Values are expressed as concentration of glucose in mmol/L and are means ± SEM of n = 5. Significant difference was considered at $P \leq 0.05$ compared with basal (before diabetes induction). N CONTROL= normal control; D CONTROL = diabetic control; RD = reversed diabetic.

3.2 Sex Hormone

Data of the assayed sex hormones are as shown in Table 1. The results show no significant difference in the sex hormones (FSH, LH and E) analyzed in all the groups.

Table 1 Levels of sex hormones of male rats monitored for 14 days

Parameters Groups	FSH(MIu/ml)	LH(MIu/ml)	E(pg/ml)
Normal Control	95.00 ± 3.28	41.20 ±1.98	54.80±2.55
Diabetic Control	102.40 ±4.01	43.60 ±2.73	56.80 ±1.52
Reverse diabetic	100.40 ±6.24	42.40 ±4.61	60.40±1.69

Values are Means ± SEM (n=5).

3.3 Thyroid Hormone Levels

Table 2 shows the levels of the analyzed thyroid hormones: triiodothyronine (T3), tetraiodothyronine (T4) and thyroid stimulating hormone (TSH). T4 was significantly ($P \leq 0.05$) lowered in both the diabetic and reversed diabetic animals when compared with the normal control.

Table 2. Levels of thyroid hormone in male rats monitored for 14 days

PARAMETERS (serum)	**T3(ng/ml)**	**T4(µg/ml)**	**TSH(µU/ml)**
Normal Control	1.79 ± 0.03^{a}	12.02 ± 0.05^{b}	6.11 ± 0.36^{a}
Diabetic Control	1.66 ± 0.10^{a}	11.32 ± 0.26^{a}	6.50 ± 0.17^{a}
Reverse diabetic	1.81 ± 0.18^{a}	11.00 ± 0.16^{a}	6.79 ± 0.18^{a}

Values are Means ± SEM (n=5). Values with different superscript letters within each column represent significant difference ($P \leq 0.05$). While values with same letter "a" within each column represent no significant difference ($P \geq 0.05$).

4. Discussion

The relationships between diabetes, sex and thyroid hormones have been well documented. Diabetes has been reported to affect both hormones and the hormones can equally affect diabetes (Matsushita *et al.,* 2005; Hage *et al.,* 2011). Thyroid hormones are insulin antagonists in their response to glucose metabolism in the liver, and also work in synergy with insulin to effectively utilize glucose in peripheral tissues. The opposite and synergetic actions of insulin and thyroid hormones help to maintain glucose homeostasis under physiological conditions. Occurrence of hypothyroidism has been reported in type 1 diabetes mellitus; whereas hyperthyroidism tends to

constitute peripheral insulin resistance which progresses to diabetes (Pearce & Merriman, 2009; Kordonouri *et al.,* 2009). On the other hand, hyperthyroidism has been linked with normal, increased or reduced beta cell functions (Ortega *et al.,* 2008). Additionally, hypothyroidism has been reported to detonate a reduced rate of glucose production in the liver (Sol´a *et al.,* 2002).
On the correlation between sex hormones and diabetes, type 1 diabetes mellitus has been associated with testicular tissue and cell damage in experimental animals (Navarro-Casado *et al.,* 2010; Pavlinkova *et al.,* 2017). Whereas some existing literature have shown the association between diabetes, sex and thyroid hormones, there is a dearth of information about the impact of unstable alloxan- induced diabetes on sex and thyroid hormones levels.

In this study, the alterations in fasting blood glucose and the instability of alloxan observed, as presented in Figure 1 are not unusual as reports have demonstrated increased fasting blood glucose from alloxan injection (El-khamisy & Rezq, 2013; Amanda *et al.,* 2015); an action that is attributed to the capacity of alloxan to:1)-inhibit glucokinase enzyme and/or 2)-generate reactive oxygen species that in turn damages the β-cells of the pancreas leading to insulin deficiency and ultimately diabetes. These two mechanisms underlie the diabetogenicity of alloxan (Dunn & McLetchie, 1943; Jorns *et al.,* 1997; Osasenaga *et al.,* 2017). On the other hand, instability and auto-reversibility of alloxan as a diabetogenic drug has also been widely reported (Jain & Arya, 2011; Monika & Umme, 2012). The observed reversal of diabetes in this study may be attributed to the capacity of the pancreatic β-cells of the animals to regenerate (Dor *et al.,* 2004). Other possible reason for the observed reversal could be attributed to genetic polymorphism in drug metabolism within and between species (Pierre-Louis, 2010) or it may be as a result of differences in the expression of antioxidant enzymes. Glutathione has been reported to confer natural protection against the action of alloxan (Zhao *et al.,* 1987). Kubisch *et al.* (1997) and Tiedge *et al.* (1998) have also noted protection against alloxan action in transgenic mice with over expression of antioxidant enzymes. These possibilities may not be unconnected to the mechanism of action of alloxan. Diabetogenicity of alloxan has been attributed to the formation of reactive oxygen species (Dunn & McLetchie, 1943; Jorns *et al.,* 1997; Osasenaga *et al.,* 2017; Gisela, *et al.,* 2000). Other documented literature has also demonstrated the possibility of the toxicity and diabetogenicity of alloxan to vary widely among animals of the same species (Zhao *et al*., 1987; Monika & Umme, 2012).

Furthermore, the non-significant ($P \geq 0.05$) effects observed in the levels of the analyzed sex hormones in this study contradicts the findings of Ballester *et al.* (2004), who reported lowered levels of LH and FSH in diabetic rats. However, this result partly agrees with the findings of Hylmarova *et al.* (2020) who reported normal levels of FSH and estrogen in diabetic human males. Nevertheless, the normal levels of FSH and LH observed in this study may be attributed to uninterrupted level of estrogen balance. Hayes *et al.* (2001) have noted the regulation of gonadotropins secretion to be an association between the stimulation of gonadotropin releasing hormone (GnRH) from the hypothalamus and its inhibition by sex steroids (testosterone and estradiol) from the gonads. Other researchers have further narrowed the regulation of gonadotropins secretion predominantly to estrogen effect in both *in vitro* and *in*

vivo studies (Emons *et al.,* 1986; Fisher *et al.,* 1998; Hylmarova *et al.*, 2020).The distinctions in the findings of this research with other similar studies support the postulation by Ballester *et al.* (2004) who noted the regulation of testicular function in Wistar rats to be a result of multiple mechanisms involving the association between insulin/glucose with LH and FSH. We surmise that estrogen may also be a factor in these multiple regulatory mechanisms. However, the specific correlation between insulin/glucose and estrogen was not evaluated in this study and constitutes one of the study's setbacks.

The regulatory role of thyroid hormones on glucose homeostasis has earlier been noted. The results of the effect of diabetes/reversed diabetes on thyroid hormones in this study (Table 2) partly agree with the findings of Udiong *et al.* (2007), who noted normal levels of T3 and TSH in diabetic patients. The results also partly agree with the findings of Bharat *et al*. (2013), who reported lowered T4 levels in diabetic patients against non-diabetics. Abnormal thyroid hormone levels have also been reported in diabetic patients by Gursoy & Tuncel (1999). Abdul Azeem *et al.* (2021) have similarly reported decreases in thyroid hormone levels in alloxan induced diabetic male Wistar rats which were restored to normal upon stabilization of the blood glucose with γ-irradiated pumpkin seeds dried powder administration. The lowered T4 level observed in both reversed diabetic and diabetic animals' groups may reflect the selective effect of diabetes on thyroid hormone that may not be dependent on glucose gradation. This postulation is premised on the fact that, if hyperglycemia was the causation of decreases in the levels of thyroid hormones; it would be logical to have normal levels when the blood glucose stabilizes and/or abnormal levels when blood glucose is high. However, inconsistent findings have been reported in the levels of these hormones under diabetic conditions (Gursoy & Tuncel, 1999; Udiong *et al.*, 2007; Bharat *et al*., 2013) in both human and animal studies. Our postulation is further supported by the findings of Coiro *et al.* (1997) who recorded abnormality in the normal nocturnal TSH peak in type 1 diabetic patients even after amelioration in glycemic control.

5. Conclusions

This study, to our knowledge, has reported for the first time the influence of reversed diabetes on sex and thyroid hormones levels. Based on the findings, we surmise that diabetes exerts a selective effect on thyroid hormones that are not dependent on glucose gradation. In order to validate the postulations noted herein, we recommend that a prolonged study on the influence of diabetes/reversed diabetes on sex and thyroid hormones be carried out to make confirmed decisions. Also, the specific correlation between insulin/glucose and estrogen in the stimulation/inhibition of gonadotropins secretion needs to be investigated.

Abbreviations

GnRH: gonadotropin releasing hormone; ROS: reactive oxygen species; SEM: Standard error of mean.

References

Abdul Azeem, A.M., Mounir, A.M. & El-Shahat, A.N. (2021) Studying the Anti-Diabetic Effect of Gamma-Irradiated Pumpkin Seeds. Pakistan J. Zool., 2021:1-7.

Amanda, N.L., Lucas, L.C., & César, T.S. (2015) Alloxan-Induced Diabetes Causes Morphological and Ultrastructural Changes in Rat Liver that Resemble the Natural History of Chronic Fatty Liver Disease in Humans. Journal of Diabetes Research, 2015:1-11

Ballester, J., Munoz, M.C., Dominguez, J., Rigau, T., Guinovart, J.J. & Rodríguez-Gil, J.E. (2004) Insulin-dependent diabetes affects testicular function by FSH- and LH-linked mechanisms. J Androl, 25: 706–719.

Bharat, Hijam, D., Gangte, D., Lalnunpui, Premchand, Devi, I. & Singh, G.W. (2013). Thyroid Status in Diabetes Mellitus. JGL, 3(**1**):1-4.

Clement, K., Viguerie, N., Diehn, M.A.A., Barbe, P., Thalamas, C., Storey, J.D., Brown, P.O., Barsh, G.S. & Langin, D. (2002) In vivo regulation of human skeletal muscle gene expression by thyroid hormone. Genome Res, 12: 281-291.

Coiro, V., Volpi, R., Marchesi, C., Capretti, L., Speroni, G., Caffarri, G. & Chiodera, P. (1997) "Influence of residual C-peptide secretion on nocturnal serum TSH peak in well controlled diabetic patients," Clin Endocrinol, 47(**3**): 305–310.

Dor, Y., Brown, J., Martinez, O.I. & Melton, D.A. (2004) Adult pancreatic β cells are formed by self-duplication rather than stem cell differentiation. Nature, 429: 41–46.

Dunn, J.S. & McLetchie, N.G. (1943) Experimental alloxan diabetes in the rat. Lancet, 242:384–387.

El-Missiry, M.A. (1999). "Enhanced testicular antioxidant system by ascorbic acid in alloxan diabetic rats," Comp BiochemPhysiol C Pharmacol Toxicol Endocrinol, 124(**3**): 233–237.

El-Khamisy, A.E & Rezq, A.A. (2013) Hypoglycemic effect of Hazelnut and its effect on some sex hormones in alloxan induced diabetic in female rats. Pakistan Journal of Nutrition, 12(**3**): 229-238.

Emons, G., Ortmann, O., Thiessen, S. & Knuppen, R. (1986) Effects of estradiol and some antiestrogens (clomiphene, tamoxifen, and hydroxytamoxifen) on luteinizing hormone secretion by rat pituitary cells in culture. Arch Gynecol, 237:199–211.

Fisher, C.R., Graves, K.H., Parlow, A.F. & Simpson, E.R. (1998) Characterization of mice deficient in aromatase (ArKO) because of targeted disruption of the *cyp*19 gene. Proc Natl Acad Sci, 95:6965– 6970.

Gisela, D., Claudia, K., Martina, D. & Peter, K. (2000) Contrasting effects of alloxan on islets and single mouse pancreatic **b**-cells.Biochem J, 352:389-397.

Gursoy, N.T. & Tuncel, E. (1999) "The relationship between the glycemic control and the hypothalamus-pituitary-thyroid axis in diabetic patients," Turkish J. Endocrinol Meta, 4:163–168.

Hage, M., Zantout, M.S. & Azar, S.T. (2011) Thyroid Disorders and Diabetes Mellitus. J Thyroid Res, 2011:1-7.

Hayes, F.J., Decruz, S., Seminara, S.B., Boepple, P.A. & Crowley, W.F. (2001) Differential Regulation of Gonadotropin Secretion by Testosterone in the Human Male: Absence of a Negative Feedback Effect of Testosterone on Follicle-Stimulating Hormone Secretion. *J Clin* Endocrinol Metab, 86:53–58.

Hylmarova, S., Stechova, K., Pavlinkova, G., Peknicova, J., Macek, M.&Kvapil, M. (2020) The impact of type 1 diabetes mellitus on male sexual functions and sex hormone levels. Endocr. J, 67(**1**): 59–71.

Jain, D.K. & Arya, R.K. (2011) Anomalies in alloxan-induced diabetic model: It is better to standardize it first. Indian J Pharmacol, 43(**1**):91.

Jorns, A., Munday, R., Tiedge, M. &Lenzen, S. (1997) Comparative toxicity of alloxan, N-alkylalloxans and ninhydrin to isolated pancreatic islets in vitro. J Endocrinol, 155: 283–293.

Kordonouri, O., Maguire, A.M. &Knip, M. (2009). Other complications and associated conditions with diabetes in children and adolescents. Pediatr Diabetes, 10:204-210.

Kubisch, H.-M., Wang, J., Bray, T. M. & Phillips, J. P. (1997) Targeted overexpression of Cu/Zn superoxide dismutase protects pancreatic b-cells against oxidative stress. Diabetes, 46: 1563-1566.

Lenzen, S. (2008) The mechanisms of alloxan- and streptozotocin-induced diabetes. Diabetologia**,** 51: 216–226.

Matsushita, M., Tamura, K., Osada, S., & Kogo, H. (2005) Effect of troglitazone on the excess testosterone and leutinizing hormone secretion in thyroidectomized insulin-resistance, type 2 diabetic Goto-Kakizaki rats. Endocrine, 27:301-305.

Monika, M. & Umme, A. (2012) Alloxan: An unpredictable drug for diabetes induction? Indian J Pharmacol, 44(**4**): 538–539.

National Institute of Health (1992) Institutional Animal Care and use Committee Guidebook. NIH Publication. Washington, D. C: U.S. Government Printing Office 92-345.

Navarro-Casado, L., Juncos-Tobarra, M.A., Cháfer-Rudilla, M., Íñiguez de Onzoño, L., Blázquez-Cabrera, J.A., & Miralles-García, J.M., (2010) Effect of experimental diabetes and STZ on male fertility capacity. Study in rats. J. Androl., 31: 584-592.

Osasenaga, M.I., Abiola, M.A. & Oluseyi, A.A. (2017) Alloxan-induced diabetes, a common model for evaluating the glycemic-control potential of therapeutic compounds and plants extracts in experimental studies. Medicina, 53:365-374.

Osibemhe, M., Lawal, N., Umar, D., Omaji, G.O. &Jibiya, S.A. (2017) Effect of aqueous extract of *Anisopus manni* in alloxan-induced diabetic rats. Sc Word J., 12(**3**):1597-6343.

Pavlinkova, G., Margaryan, H., Zatecka, E., Valaskova, E., Elzeinova, F., Kubatova, A., Bohuslavova, R., & Peknicova, J. (2017) Transgenerational inheritance of susceptibility to diabetes-induced male subfertility. *Sci Rep*, 7:4940

Pierre-Louis, T., Aude, F., & Alain, B. (2010). Species differences in pharmacokinetics and pharmacodynamics. Handb Exp. Pharmacol, 199:19-48.

Sol´a, E., Morillas, C., Garz, S., Omez-Balaguer, M.G. &Hern´andez-Mijares, A. (2002) "Association between diabetic ketoacidosis and thyrotoxicosis," Acta Diabetologica, 39(**4**):235–237.

Soni, Mishra, A.N. & Upendrakumar, (2019) "Alloxan Not an Ideal Drug for Diabetes Induction."IOSR-JDMS, 18(**6**):14-17.

Soudamani, S., Malini,T.&Balasubramanian, K. (2005) "Effects of streptozotocin-diabetes and insulin replacement on the epididymis of prepubertal rats: histological and histomorphometric studies," Endocrine Res, 31**(2**): 81–98.

Tiedge, M., Lortz, S., Munday, R. &Lenzen, S. (1998) Complementary action of antioxidant enzymes in the protection of bioengineered insulin-producing RINm5F cells against the toxicity of reactive oxygen species. Diabetes, 47: 1578-1585.

Udiong, C.E.J., Udoh, A.E. &Etukudoh, M.E. (2007) Evaluation of thyroid function in diabetes mellitus in Calabar, Nigeria. Indian J Clin Biochem, 22(**2**): 74-78.

Viguerie, N., Millet, L., Avizou, S., Vidal, H., Larrouy, D.&Langin, D. (2002) Regulation of human adipocyte gene expression by thyroid hormone. J Clin Endocrinol Metab, 87:630-634.

Weinstein, S.P., O'Boyle, E., Fisher, M. & Haber, R.S. (1994) Regulation of GLUT2 glucose transporter expression in liver by thyroid hormone: evidence for hormonal regulation of the hepatic glucose transport system. Endocrinol, 135: 649-654.

Zhao, Z.H., Watschinger, B., Brown, C.D., Monica M. Beyer & Friedman, E.A. (1987) Variations of Susceptibility to Alloxan Induced Diabetes in the Rabbit. Hormmetabol Res, 19: 534-537.

Submitted: 18/09/2021
Revised: 19/12/2021
Accepted: 26/12/2021
DOI: 10.48129/kjs.15291

Investigation of *Terminalia arjuna* as potential IL-4 and IL-13 modulator for the prevention of autoimmune diabetes: A Pharmacoinformatics-based study

Aziz Unnisa[1,*], Saheem Ahmad[2], Suresh Babu Jandrajupalli[3], Kareem M. Younes[1,4], Sally Hassan Abobaker[5], Swarnalatha Chandolu[2], Mohammad Khalid[6], Lakshmi Sudeepthi N[7]

[1]*Dept. of Pharmaceutical Chemistry, College of Pharmacy, University of Hail, KSA.*
[2]*Dept. of Medical Laboratory Sciences, College of Applied Medical Sciences, University of Hail, KSA.*
[3]*Dept. of Preventive Dental Sciences, College of Dentistry, University of Hail, KSA.*
[4]*Dept. of Analytical Chemistry, Faculty of Pharmacy, Cairo University, Cairo, Egypt.*
[5]*Dept. of Basic Dental and Medical Sciences, College of Dentistry, University of Hail, KSA.*
[6]*Dept. of Pharmacognosy, College of Pharmacy, Prince Sattam Bin Abdulaziz University, Al-Kharj, KSA*
[7]*Dept. of Pharmacology, KVSR Siddhartha College of Pharmaceutical Sciences, Vijayawada, A.P, India.*

**Corresponding author: khushiazeez@yahoo.co.in*

Abstract

Cytokines are proteins that play a critical role in immune cells' development, maturation, and functional activities. For the first time, we have investigated the potential role of *Terminalia arjuna* as IL-4 and IL-13 modulators for preventing T1DM, i.e., autoimmune diabetes. It has been well documented that the stimulation of IL-4 and IL-13 can regulate the level of type 2 cytokines which can be maintained with the level of type 1 cytokines. The present study investigated gallic acid, arjunolic acid, luteolin, ellagic acid, and arjunone for their potential modulating activity of IL-4 and IL-13. The active amino acid residues identified for IL-4 are VAL51, HIS58, ASP87, THR30, GLN54, THR63, ARG64, LYS84, and GLU60. The active amino acid residues identified for IL-13 are H: GLU46, H: TRP47, H: GLN61, L: PHE98, L: VAL97, L: GLU162, L: THR163, H: ARG105, L: GLN38, L: ASP85, H: GLY42, L: GLY41, H: PRO41, H: TRP47, and L: PHE98. The phytoconstituents demonstrated better modulating activity towards IL-13 than IL-4. Luteolin displayed better potential for both IL-4 and IL-13, and therefore we concluded that it could be used to modulate the activity of IL-4 and IL-13 for the prevention of autoimmune diabetes.

Keywords: IL-4, IL-13, T1DM, *Terminalia arjuna*, luteolin, autoimmune diabetes

1. Introduction

Cytokines are proteins that are vital in immune cell development, maturation, and function (Hill & Artis, 2010). The type 1 and type 2 cytokines are frequently antagonistic to one another in their activities (Zaccone *et al.,* 1999). Type 2 anti-inflammatory cytokines such as

interleukin-13, interleukin-10, interleukin-6, interleukin-5, and interleukin-4, which are not cytotoxic, promote humoral immune responses, aid in the formation of IgE, IgG1, and IgG2b (Swain, 1995), and induce a functional state of T cells and macrophages. The balance of the two types of cytokines is tightly regulated. Type 1 proinflammatory cytokine dysregulation may play a role in the clinical course, and possibly even the emergence, of organ-specific autoimmune diseases such as thyroiditis, multiple sclerosis, and type 1 diabetes mellitus (T1DM) (Mandrup-Poulsen *et al*., 1996), (Rabinovitch, 1994), (Zaccone *et al*., 1999).

T1DM is an autoimmune disorder characterised by the gradual and insidious depletion of insulin-producing beta cells. Current T1DM treatment is mainly based on exogenous insulin replacement, emphasising the need for immunotherapies to both restrict the progression of the illness and enhance clinical results in the long term (Bach, 1994). Growing data indicates that in humans and rodents with type 1 diabetes, an elevated type 1 cytokine response is encouraged by a deficient generation of type 2 cytokines. On the other hand, non-obese diabetic (NOD) mice generate less IL-4 and more IFN-γ in vitro due to reduced CD1-restricted T-cells. Furthermore, in humans and BioBreeding (BB) rats with type 1 diabetes, blood levels of type 1 cytokines, but not type 2 cytokines, increase during the disease's beginning (Zaccone *et al.,* 1999).

A type 2 cytokine profile defined by elevated levels of IL-4 and decreased levels of IFN-g is seen in the insulitis lesions of both male and female NOD mice with low T1DM incidence (Fox & Danska, 1997), (Rabinovitch *et al.,* 1995). It could be concluded that IL-4 (Cameron *et al.,* 1997), (Rapoport *et al.,* 1993), pancreatically generated IL-4, and IL-10 (Pennline et al., 1994) all prevent T1DM in female NOD mice, and the effects of IL-4 are linked to a shift in cytokine production toward a type 2 phenotype. IL-13 is an essential anti-inflammatory cytokine produced primarily by Th-2 lymphocytes. It is produced in significant quantities by lymphocytes of the Th-2 subset (Zaccone *et al.,* 1999). The effect of IL-13 treatment on the development of T1DM in diabetic NOD mice was studied. Long-term therapy of recombinant human IL-13 significantly reduced the incidence of spontaneous T1DM in mice (De Vries, 1998).

Terminalia arjuna has been used as a cardiotonic in treating ischemic heart disease, heart failure, myocardium necrosis, cardiomyopathy, atherosclerosis, and a variety of human diseases such as anaemia, viral disease, and venereal disease, as well as for general health maintenance. It has antibacterial, hypocholesterolemic, antitumoral, antimicrobial, antiallergic, antioxidant, and antifeedant properties, as well as antifertility and anti-HIV properties (Amalraj & Gopi, 2017), (Bachaya *et al.,* 2009), (Ram *et al.,* 1997). Terminalia arjuna has been proven to have significant hypolipidemic properties and is used to treat ulcers, fractures, and hepatic disease. *Terminalia arjuna's* saponin glycosides are believed responsible for its inotropic effects. At the same time, flavonoids/phenolics may provide antioxidant potential in addition to vasodilation action, validating the plant's multiple activities for its cardioprotective function (Dwivedi, 2007). In animal models, *Terminaliashown*hown has anti-diabetic activity (Kapoor *et al.,* 2014).

It has been well documented that the stimulation of IL-4 and IL-13 can regulate the level of type 2 cytokines which can be maintained with the level of type 1 cytokines. For the first time, we have investigated the potential role of *Terminalia arjuna* as IL-4 and IL-13 modulators for preventing T1DM, i.e., autoimmune diabetes. We have screened the major

phytoconstituents using the Lipinski rule of five, ADMET properties, toxicity prediction, and binding affinity towards IL-4 and IL-13.

2. Material and Methods

2.1 Pharmacokinetics and toxicity prediction of phytoconstituents

The Lipinski rule and the pharmacokinetic characteristics of phytoconstituents were investigated using PubChem (Kim *et al.,* 2021), molinspiration ("Molinspiration cheminformatics," 2006), (Unnisa *et al.,* 2020), and SwissADME (Daina *et al.,* 2017), (Unnisa *et al.,* 2020) servers. The major phytoconstituents have been selected from each class of chemicals in *Terminalia arjuna*. The toxicity of the phytoconstituents has been predicted using ProTox-II, an accessible webserver for *in silico* toxicity predictions of new derivatives (http://tox.charite.de/protox_II).

2.2 Molecular docking studies

To perform molecular docking, the Autodock vina 1.1.2 with PyRx Virtual Screening Tool 0.8 software of the Chimera version 1.10.2 (Dallakyan & Olson, 2015), (Dian *et al.*, 2021) and the Biovia Discovery studio were used (Miyata, 2015). The structure of selected phytoconstituents (SDF File) was obtained from the US National Library of Medicine PubChem database (https://pubchem.ncbi.nlm.nih.gov/). Figure 1 depicts the structures of all of the selected phytoconstituents. Universal Force Field (UFF) (Rappé *et al.,* 1992), performed the energy minimisation. The RCSB-PDB (https://www.rcsb.org/) was used to obtain the crystal structures of IL-4 and IL-13. Figure 2 depicts the 3D structures of the enzymes along with their PDB IDs. The three-dimensional grid box of known size (IL-4, size x = 52.3300A^o, size y = 64.5243A^o, size z = 57.4915A^o; IL-13, size x = 48.9548A^0, size y = 44.6697A^o, size z = 64.2511A^o) was adjusted with an exhaustiveness value of 8 for MD simulation. The entire molecular docking procedure was performed exactly as described by S. L. Khan *et al.* . (S. Khan *et al.,* 2020), (Khan *et al*., 2021), (S. L. Khan *et al*., 2021).

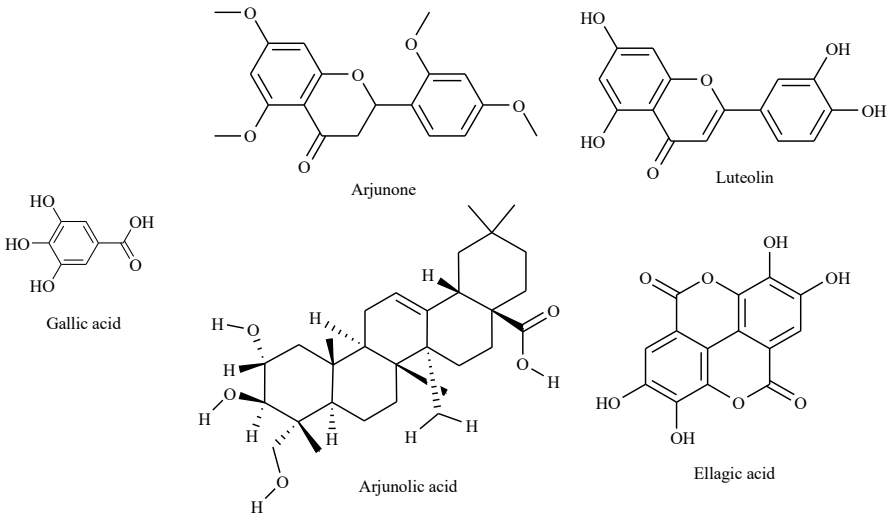

Fig. 1. The structures of selected major phytoconstituents from *Terminalia arjuna*

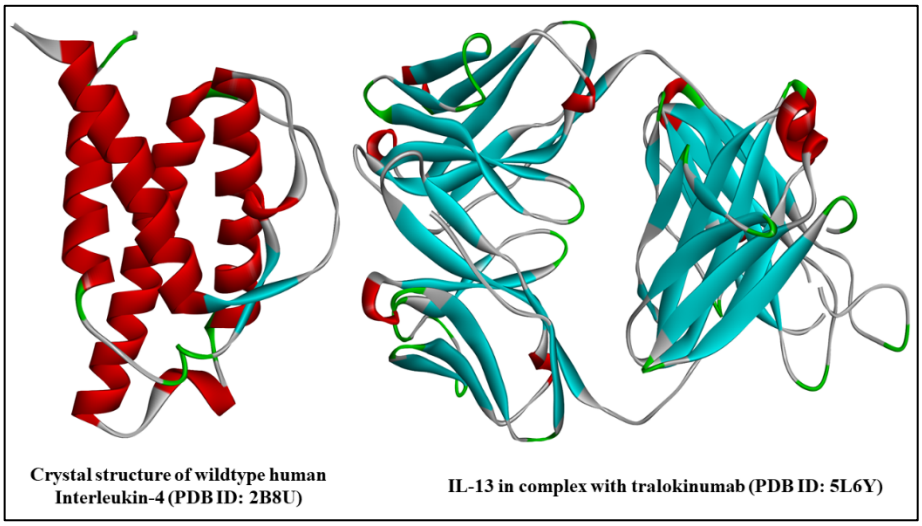

Fig. 2. 3D ribbon view with PDB IDs of the enzymes obtained from the RCSB Protein Data Bank

3. Results

3.1 Pharmacokinetics and toxicity prediction of phytoconstituents

Pharmacokinetic characteristics are a critical component of drug development because they allow researchers to determine the biological features of drug candidates. To determine whether or not the substance was drug-like, Lipinski's rule of five and Veber's rules were used (Table 1). To understand their pharmacokinetics profile, phytoconstituents were investigated for their ADMET properties better (Table 2). Oral acute toxicity has been predicted along with LD_{50} (mg/kg), toxicity class, hepatotoxicity, carcinogenicity, immunotoxicity, mutagenicity, and cytotoxicity (Table 3).

Table 1. Physicochemical Properties of the Major Chemical Constituents of *Terminalia arjuna*

Name of Compound	Lipinski's Rule of 5					Veber's Rule	
	Log P	Mol. Wt.	Hydrogen Donor	Hydrogen Acceptor	No. of Violations	Total polar surface area (Å^2)	No. of rotatable bonds
Gallic acid	0.59	170.12	4	5	0	97.99	1
Arjunolic Acid	4.63	488.70	4	5	0	97.99	2
Luteolin	1.97	286.24	4	6	0	111.13	1
Ellagic Acid	0.94	302.19	4	8	0	141.34	0
Arjunone	3.24	344.36	0	6	0	63.22	5

Table 2. The ADMET properties of the Major Chemical Constituents of *Terminalia arjuna*

Name of Compound	Absorption			Distribution			Toxicity	
	Solubility Log S (log mol/L)	Caco-2 perm. (nm/sec)	Intestinal. Absorption (% Abs)	Skin perm. (logKp, cm/hour)	BBB pen. (C.brain/C.blood)	PPB (%)	Metabolism	Carcinogenicity (Mouse)	Ames Toxicity
Gallic acid	-2.34	13.8492	53.69685	-3.62686	0.348084	65.38	CYP3A4 inhibitor	Negative	Mutagenic
Arjunolic Acid	-7.67	20.9815	91.23332	-3.57106	0.588608	97.04	---	Positive	Non-mutagenic
Luteolin	-4.51	4.53973	79.42723	-4.28017	0.367582	99.71	CYP1A2, CYP2D6, CYP3A4 inhibitor	Positive	Mutagenic
Ellagic Acid	-3.66	20.5635	50.89231	-5.09432	0.299777	43.82	CYP1A2 inhibitor	Positive	Non-mutagenic
Arjunone	-3.91	57.0533	98.54008	-3.50358	1.5995	88.41	CYP1A2, CYP2C19, CYP2C9, CYP2D6, CYP3A4 inhibitor	Negative	Mutagenic

BBB: Blood-brain barrier, CYP: Cytochrome, PPB: Plasma-protein binding, perm: permeability.

Table 3. The predicted acute toxicity of phytoconstituents

Parameters	Molecule Name				
	Gallic acid	Arjunolic Acid	Luteolin	Ellagic Acid	Arjunone
LD50 (mg/kg)	2000	2000	3919	2991	2000
Toxicity class	4	4	5	5	4
Prediction accuracy (%)	70.97	70.97	70.97	70.97	69.26
Hepatotoxicity (Probability)	I (0.61)	I (0.92)	I (0.69)	I (0.83)	I (0.66)
Carcinogenicity (Probability)	A (0.56)	I (0.63)	A (0.68)	A (0.59)	I (0.54)
Immunotoxicity (Probability)	I (0.99)	I (0.70)	I (0.97)	I (0.81)	A (0.85)
Mutagenicity (Probability)	I (0.94)	I (0.84)	A (0.51)	I (0.84)	I (0.71)
Cytotoxicity (Probability)	I (0.91)	I (0.96)	I (0.99)	I (0.90)	I (0.83)

Where: I, Inactive; A, Active

3.2 Molecular docking

The 2D- and 3D-docking poses of phytoconstituents with IL-4 are depicted in Figure 3, whereas IL-13 are illustrated in Figure 4. The active amino residues, atoms responsible for interactions from ligand molecules, bond type, bond category, and bond length (A^0) involved in the interactions are tabulated in Table 4. The ligand energies (kcal/mol), PubChem CID, and binding affinities (kcal/mol) of ligands with IL-4 and IL-13 are tabulated in Table 5.

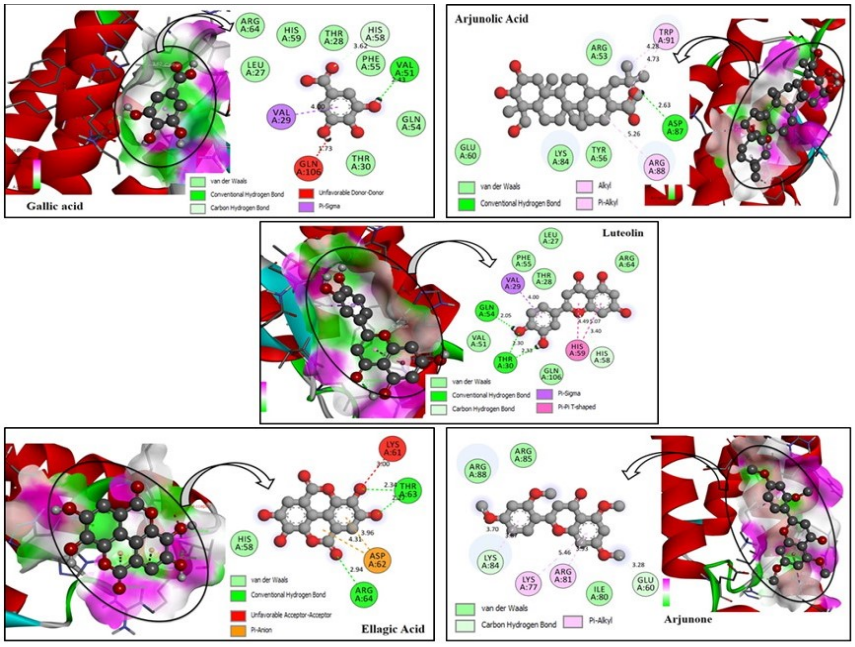

Fig. 3. 2D-and -3D molecular interactions of Gallic acid, Arjunolic acid, Luteolin, Ellagic acid and Arjunone with IL-4

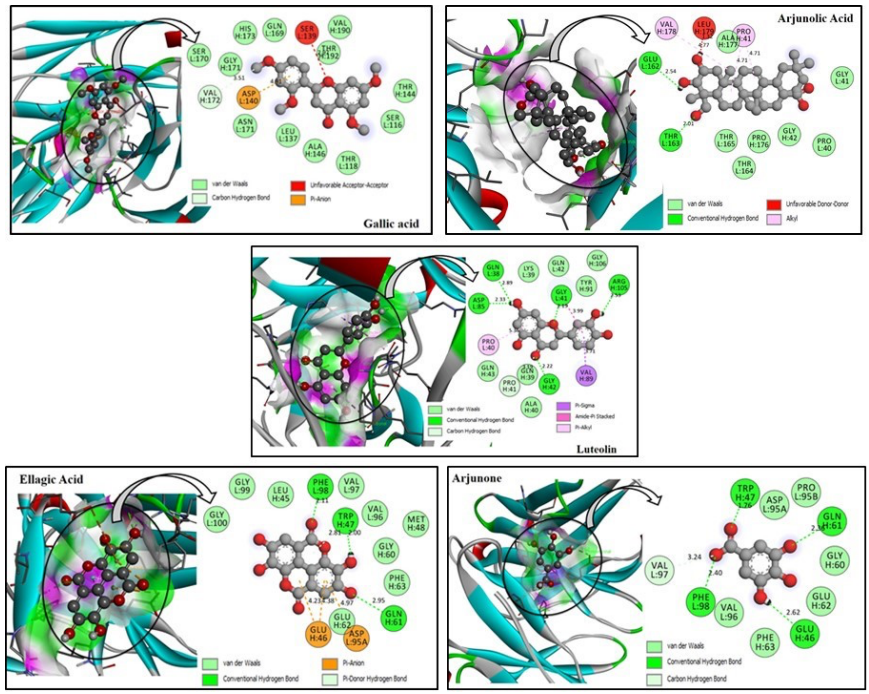

Fig. 4. 2D-and -3D molecular interactions of Gallic acid, Arjunolic acid, Luteolin, Ellagic acid and Arjunone with IL-13

Table 4. The interactions of ligands with IL-4 and IL-13

Active amino acid residue	Atom from ligand	Bond length (A^0)	Bond type	Bond category
		IL-4		
		Gallic acid		
VAL51	H	2.43261	Hydrogen Bond	Conventional Hydrogen Bond
HIS58	O	3.61654		Carbon Hydrogen Bond
VAL29	Pi-orbitals	3.99997	Hydrophobic	Pi-Sigma
		Arjunolic acid		
ASP87	H	2.6309	Hydrogen Bond	Conventional Hydrogen Bond
ARG88	Alkyl	5.25841		Alkyl
TRP91	Alkyl C C	4.73276 4.06776 5.17395	Hydrophobic	Pi-Alkyl
		Luteolin		
THR30	H	2.32649	Hydrogen Bond	Conventional Hydrogen Bond
GLN54	H	2.04949		
THR30	O	2.30473		
HIS58	O	3.4019		Carbon Hydrogen Bond
VAL29	Pi-orbitals	3.99582	Hydrophobic	Pi-Sigma
HIS59	Pi-orbitals Pi-orbitals	4.49401 5.06782		Pi-Pi T-shaped
		Ellagic acid		
THR63	O	2.33726	Hydrogen Bond	Conventional Hydrogen Bond
	O	2.27405		
ARG64	O	2.93604		
ASP62	Pi-orbitals Pi-orbitals	3.96054 4.31447	Electrostatic	Pi-Anion
		Arjunone		
LYS84	C	3.69721	Hydrogen Bond	Carbon Hydrogen Bond
GLU60	C	3.27655		
LYS77	Pi-orbitals	5.46366	Hydrophobic	Pi-Alkyl
ARG81	Pi-orbitals	3.92705		
LYS84	Pi-orbitals	3.87081		
		IL-13		
		Gallic acid		
H: GLU46	H	2.61626	Hydrogen Bond	Conventional Hydrogen Bond
H: TRP47	O	1.75911		
H: GLN61	O	2.35868		
L: PHE98	O	2.40313		
L: VAL97	O	3.24093		Carbon Hydrogen Bond

		Arjunolic acid		
L: GLU162	H	2.54362	Hydrogen Bond	Conventional Hydrogen Bond
L: THR163	O	2.01198		
H: VAL178	C	4.77331		
H: PRO41	Alkyl	4.71425	Hydrophobic	Alkyl
	Alkyl	4.71373		
		Luteolin		
H: ARG105	H	2.53011		
L: GLN38	H	2.88796		
L: ASP85	H	2.32687	Hydrogen Bond	Conventional Hydrogen Bond
H: GLY42	O	2.22481		
L: GLY41	O	2.18872		
H: PRO41	O	3.18868		Carbon Hydrogen Bond
H: VAL89	Pi-orbital	3.70973		Pi-Sigma
L: GLY41; GLN42	Pi-orbital	3.99091	Hydrophobic	Amide-Pi Stacked
L:PRO40	Alkyl	5.36427		Pi-Alkyl
		Ellagic acid		
H: TRP47	H	2.00407		
H: GLN61	O	2.95449	Hydrogen Bond	Conventional Hydrogen Bond
L: PHE98	O	2.10703		
H: GLU46	Pi-orbital	4.22682		
	Pi-orbital	4.38107	Electrostatic	Pi-Anion
L:ASP95	Pi-orbital	4.97265		
H: TRP47	Pi-orbital	2.81399	Hydrogen Bond	Pi-Donor Hydrogen Bond
		Arjunone		
H: VAL172	C	3.50648	Hydrogen Bond	Carbon Hydrogen Bond
L: ASP140	Pi-orbital	4.91005	Electrostatic	Pi-Anion

Table 5. The ligand energies (kcal/mol), PubChem CID, and binding affinities (kcal/mol) of ligands with IL-4 and IL-13

Name of Compound	PubChem CID	Ligand energy (kcal/mol)	Binding affinity (kcal/mol)	
			IL-4	IL-13
Gallic acid	370	76.79	-5.6	-6.2
Arjunolic Acid	73641	1250.56	-6.2	-8.1
Luteolin	5280445	195.94	-7.2	-8.1
Ellagic Acid	5281855	215.78	-5.8	-7.9
Arjunone	14034821	313.16	-5.9	-7.3

4. Discussion

4.1 Pharmacokinetics and toxicity prediction of phytoconstituents

Following Lipinski's(Barret, 2018) and Veber's criteria(Veber *et al.,* 2002) (Table 1), all of the chosen phytoconstituents presented in Figure 1 demonstrate drug-likeness characteristics without violating any of the requirements. The Log P values of all the selected phytoconstituents fall between 0.59 and 4.63, which is within an acceptable range. The phytoconstituents have a molecular weight of less than 500, a number of H-donors less than 5, and a number of H-acceptors less than 10, which are within the range of acceptable values. Veber's rules are followed by selected phytoconstituents, with total polar surface area (TPSA, should be less than 140) values and the number of rotatable bonds (should be less than 10) falling within the acceptable range for oral availability.

The Caco-2 cell line, derived from a human colon epithelial cancer cell line, is used to study medication absorption in the human digestive tract. This model may be used to determine if a molecule is appropriate for oral administration, predict intestinal permeability, and study drug efflux. The criteria for assessing drug absorption were solubility and Caco-2 permeability, given in Table 2 for reference. The solubility of gallic acid, luteolin, ellagic acid, and arjunone varies from -2 to -4 log mol/L, showing that chosen phytoconstituents have acceptable solubility. However, arjunolic acid displayed -7.67 log mol/L solubility showing poor solubility. It might be due to its steroidal structure. The Caco-2 permeability of selected phytoconstituents was high except for luteolin which displayed low permeability. The gastrointestinal absorption of arjunolic acid, luteolin, and arjunone was more than 75%, whereas gallic acid and ellagic acid showed 53.69 and 50.89%, respectively. The skin permeation values of selected phytoconstituents are optimum. The distribution of drug candidates considers the permeability of the blood-brain barrier (BBB) and the plasma proteins binding (PPB). The selected phytoconstituents did not show BBB permeability. However, arjunone displayed BBB permeability. The % PPB of the phytoconstituents was significantly high. The metabolism and toxicity assessment of phytoconstituents was performed. Arjunolic acid, luteolin, and ellagic acid showed carcinogenicity. Galli acid, luteolin, and arjunone were found to be mutagenic.

In acute toxicity predictions, gallic acid, arjunolic acid, and arjunone fall under toxicity class IV, indicating that the molecules are harmful after swallowing ($300< LD_{50}\leq2000$). Luteolin and ellagic acid fall under the class V, which indicate may be detrimental after consuming ($2000< LD_{50}\leq5000$)(Drwal *et al*., 2014). The prediction accuracy was 70.97% for all the molecules except for arjunone was 69.26%. Medication-induced hepatotoxicity is a leading cause of abrupt liver failure, and one of the most common reasons for drug recalls. In the present investigation, none of the phytoconstituent displayed hepatotoxicity. Carcinogens are chemicals that can cause cancer or raise the risk of cancer. Mutagens are chemicals that produce aberrant genetic mutations, such as alterations in a cell's DNA. Immunotoxicity is the detrimental impact of xenobiotics on the immune system. The ability to predict cytotoxicity is critical for screening chemicals that might induce both unwanted and desired cell harm, the latter being particularly relevant in the case of tumour cells (Drwal *et al*., 2014). Many molecules did not exhibit hepatotoxicity, carcinogenicity, immunotoxicity, mutagenicity, and

cytotoxicity but displayed the activity with a much lower probability score (Table 3). The ADMET profile and toxicity prediction of a chosen phytoconstituent are acceptable, making it appropriate for *in silico* investigations with IL-4 and IL-13.

4.2 Investigation of phytoconstituents as IL-4 modulators

There was no native ligand present in the PDB structure (PDB id: 2B8U) selected for docking studies. There was only one chain present in the structure. Gallic acid exhibited -5.6 kcal/mol binding free energy and formed one conventional and one carbon-hydrogen bond with VAL51 (2.43261A^0) and HIS58 (3.61654A^0), respectively. It has formed one Pi-sigma bond with VAL29 (3.99997A^0). The binding poses of gallic acid with IL-4 are illustrated in Figure 3. Arjunolic acid demonstrated -6.2 kcal/mol binding affinity and formed one conventional hydrogen bond with ASP87 (2.6309A^0). It has developed an alkyl bond with ARG88 (5.25841A^0) and a Pi-alkyl bond with TRP91 (4.73276A^0, 4.06776A^0, 5.17395A^0). The binding poses of arjunolic acid with IL-4 are depicted in Figure 4. Luteolin showed the most potent -7.2 kcal/mol binding free energy and formed three conventional hydrogen bonds with THR30 (2.32649A^0, 2.30473A^0) and GLN54 (2.04949A^0). It has formed one carbon-hydrogen bond with HIS58 (3.4019A^0). It has developed a Pi-sigma bond with VAL29 (3.99582A^0) and Pi-Pi T-shaped bonds with HIS59 (4.49401A^0, 5.06782A^0). The binding poses of luteolin with IL-4 are depicted in Figure 5. Ellagic acid displayed -5.8 kcal/mol binding affinity and formed three conventional hydrogen bonds with THR63 (2.33726A^0, 2.27405A^0) and ARG64 (2.93604A^0). It has developed electrostatic Pi-anion bonds with ASP62 (3.96054A^0, 4.31447A^0). The binding poses of luteolin with IL-4 are illustrated in Figure 6. Arjunone demonstrated -5.9 kcal/mol binding affinity and two carbon-hydrogen bonds with LYS84 (3.69721A^0) and GLU60 (3.27655A^0). It has developed three Pi-alkyl bonds with LYS77 (5.46366A^0), ARG81 (3.92705A^0), and LYS84 (3.87081A^0). The binding poses of arjunone with IL-4 are illustrated in Figure 7. From the above results, it was observed that luteolin has enough potential to modulate the activity of IL-4. It is a lead molecule for further development some IL-4 agonists or modulator.

4.3 Investigation of phytoconstituents as IL-13 modulators

The PDB structure selected for the docking studies of IL-13 was 5L6Y. There were two chains present in the target structure, i.e., chain L and chain H. Gallic acid displayed -6.2 kcal/mol binding affinity and formed four conventional hydrogen bonds with H: GLU46 (2.61626A^0), H: TRP47 (1.75911A^0), H: GLN61 (2.35868A^0), and L: PHE98 (2.40313A^0). It has formed one carbon-hydrogen bond with L: VAL97 (3.24093A^0). The binding poses of gallic acid with IL-13 are illustrated in Figure 8. Arjunolic acid exhibited -8.1 kcal/mol binding free energy and formed two conventional hydrogen bonds with L: GLU162 (2.54362A^0) and L: THR163 (2.01198A^0). It has developed hydrophobic bonds with H: VAL178 (4.77331A^0) and H: PRO41 (4.71425A^0, 4.71373A^0). The binding poses of arjunolic acid with IL-13 are depicted in Figure 9. Luteolin also displayed -8.1 kcal/mol binding free energy and formed five conventional hydrogen bonds with H: ARG105 (2.53011A^0), L: GLN38 (2.88796A^0), L: ASP85 (2.32687A^0), H: GLY42 (2.22481A^0), and L: GLY41 (2.18872A^0). It has formed one carbon-hydrogen bond with H: PRO41 (3.18868A^0). It has developed a Pi-sigma bond with H:

VAL89 (3.70973A^0), amide-Pi stacked bonds with L: GLY41; GLN42 (3.99091A^0), and Pi-alkyl bond with L: PRO40 (5.36427A^0). The binding poses of luteolin with IL-13 are demonstrated in Figure 10. Ellagic acid exhibited -7.9 kcal/mol binding free energy and formed three conventional hydrogen bonds with H: TRP47 (2.00407A^0), H: GLN61 (2.95449A^0), and L: PHE98 (2.10703A^0). It has developed an electrostatic bond with H: GLU46 (4.22682A^0, 4.38107A^0) and L: ASP95 (4.97265A^0). It has formed one Pi-donor hydrogen bond with H: TRP47 (2.81399A^0). The binding poses of ellagic acid with IL-13 are demonstrated in Fig. 11. Arjunone displayed -7.3 kcal/mol binding free energy but did not form any conventional hydrogen bond with the target. It has formed one carbon-hydrogen bond with H: VAL172 (3.50648A^0) and one Pi-anion bond with L: ASP140 (4.91005A^0). The binding poses of arjunone with IL-13 are demonstrated in Figure 12. From the above results, it was observed that luteolin has the potential to modulate the activity of IL-13. The selected phytoconstituents have displayed better modulating activity towards IL-13 than IL-4.

4.4 Structural Activity Relationship (SAR)

Among selected phytoconstituents, luteolin has been chosen as the most potent molecule that exhibited good binding affinity towards IL-4 and IL-13 with hydrogen and hydrophobic interactions. Arjunone and luteolin have a similar nucleus (4H-chromen-4-one), but both have different binding affinities and a number of hydrogen bonds. Even arjunone exhibited the least potent interaction with IL-13. This might be due to arjunone having methoxy substituents while lueolin has hydroxyl (polar) groups. Ellagic and gallic acid both have hydroxyl substituents but do not possess a 4H-chromen-4-one nucleus, which might be the reason behind their poor potency. In the case of arjunolic acid, it has a steroidal nucleus and exhibited equal binding affinity as luteolin with IL-13, but with IL-4, it displayed less potency than luteolin. It indicates polar substituents with benzo fused-4H-chromen-4-one nucleus and at least one free phenyl ring can exhibit the better modulatory activity of IL-4 and IL-13. The predicted SAR is demonstrated in Figure 5.

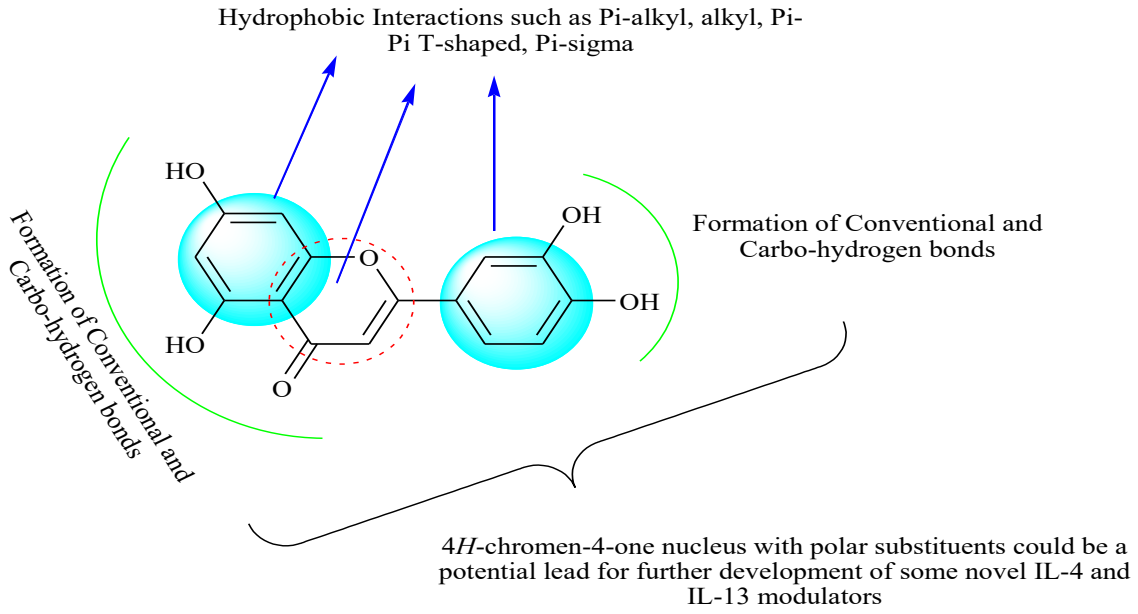

Fig. 5. Predicted SAR for the further development of some novel IL-4 and IL-13 modulators

5. Conclusion

The main phytoconstituents of *Terminalia arjuna* were evaluated *in silico* for their pharmacokinetic characteristics and were found to be druglike, indicating that they are potentially therapeutic. It is mandatory to balance cytokine type 1 and type 2; moreover, it has been observed that cytokine type 1 level was increased in autoimmune disorders. It has been well documented that the stimulation of IL-4 and IL-13 can regulate the level of type 2 cytokines which can be maintained with the level of type 1 cytokines. The present study investigated gallic acid, arjunolic acid, luteolin, ellagic acid, and arjunone for their potential modulating activity of IL-4 and IL-13. The active amino acid residues identified for IL-4 are VAL51, HIS58, ASP87, THR30, GLN54, THR63, ARG64, LYS84, and GLU60. The active amino acid residues identified for IL-13 are H:GLU46, H:TRP47, H:GLN61, L:PHE98, L:VAL97, L:GLU162, L:THR163, H:ARG105, L:GLN38, L:ASP85, H:GLY42, L:GLY41, H:PRO41, H:TRP47, and L:PHE98. The phytoconstituents demonstrated better modulating activity towards IL-13 than IL-4. Luteolin displayed better potential for both IL-4 and IL-13; therefore, we concluded that it could be used to modulate the activity of IL-4 and IL-13 for the prevention of autoimmune diabetes.

ACKNOWLEDGMENTS

This research has been funded by the scientific research deanship at the University of Hail-Saudi Arabia through project number RG 20165.

References

Amalraj, A. & Gopi, S. (2017) Medicinal properties of Terminalia arjuna (Roxb.) Wight & Arn.: A review. J. Tradit. Complement. Med, **7**:65–78.

Bach, J.F. (1994) Insulin-Dependent Diabetes Mellitus as an Autoimmune Disease. Endocr. Rev, 15:516–542

Bachaya, H.A., Iqbal, Z., Khan, M.N., Jabbar, A. & Gilani, A.H. & **Islam, U. (2009)** In vitro and In vivo Anthelmintic activity of Terminalia arjuna bark. Int. J. Agric. Biol, 11:273–278

Barret, R. (2018). Lipinski's Rule of Five. Therapeutical Chemistry, 97–100

Cameron, M.J., Arreaza, G.A., Zucker, P., Chensue, S.W., Strieter, R.M., Chakrabarti, S. & Delovitch, T.L. (1997) IL-4 prevents insulitis and insulin-dependent diabetes mellitus in nonobese diabetic mice by potentiation of regulatory T helper-2 cell function. J. Immunol, 159:4686–92

Daina, A., Michielin, O. & Zoete, V., (2017) SwissADME: a free web tool to evaluate pharmacokinetics, drug-likeness and medicinal chemistry friendliness of small molecules. Sci. Rep, 7:42717

Dallakyan, S. & Olson, A.J. (2015) Small-molecule library screening by docking with PyRx. Chemical Biology, 1263:243–250

De Vries, J.E. (1998) The role of IL-13 and its receptor in allergy and inflammatory responses. J. Allergy Clin. Immunol, 102:165–169

Dian, L. P., Sholihatul, M., Muhaimin, R. & Widodo (2021) Exploring the mechanism of the anti-hypertension properties of Morindacitrifoliathrough a bioinformatics approach, Kuwait J.Sci, 48(**3**):1-10

Drwal, M.N., Banerjee, P., Dunkel, M., Wettig, M.R. & Preissner, R. (2014) ProTox: A web server for the in silico prediction of rodent oral toxicity. Nucleic Acids Res. 42(**W1**): W53–W58

Dwivedi, S. (2007). Terminalia arjuna Wight & Arn.-A useful drug for cardiovascular disorders. J. Ethnopharmacol, 114:114–129

Fox, C.J. & Danska, J.S. (1997) IL-4 Expression at the Onset of Islet Inflammation Predicts Nondestructive Insulitis in Nonobese Diabetic Mice. J. Immunol, 158:2414–2424

Hill, D.A. & Artis, D. (2010) Intestinal bacteria and the regulation of immune cell homeostasis. Annu. Rev. Immunol, 28**:**623–667

Kapoor, D., Vijayvergiya, R. & Dhawan, V. (2014) Terminalia arjuna in coronary artery disease: Ethnopharmacology, pre-clinical, clinical & safety evaluation. J. Ethnopharmacol, 155:1029–1045

Khan, S., Kale, M., Siddiqui, F. & Nema, N. (2021) Novel pyrimidine-benzimidazole hybrids with antibacterial and antifungal properties and potential inhibition of SARS-CoV-2 main protease and spike glycoprotein. Digit. Chinese Med, 4:102–119

Khan, S.L., Siddiqui, F.A., Shaikh, M.S., Nema, N. V. & Shaikh, A.A. (2021) Discovery of potential inhibitors of the receptor-binding domain (RBD) of pandemic disease-causing SARS-CoV-2 Spike Glycoprotein from Triphala through molecular docking. Curr. Chinese Chem, 01

Khan, S.L., Sonwane, G.M., Siddiqui, F.A., Jain, S.P., Kale, M.A. & Borkar, V.S. (2020) Discovery of Naturally Occurring Flavonoids as Human Cytochrome P450 (CYP3A4) Inhibitors with the Aid of Computational Chemistry. Indo Glob. J. Pharm. Sci, 10:58–69

Kim, S., Chen, J., Cheng, T., Gindulyte, A. & He, J. (2021) PubChem in 2021: New data content and improved web interfaces. Nucleic Acids Res, 49**:**D1388–D1395

Mandrup-Poulsen, T., Nerup, J., Reimers, J.I., Pociot, F. & Andersen, H.U. (1996) Cytokines and the endocrine system. II. Roles in substrate metabolism, modulation of thyroidal and pancreatic endocrine cell functions and autoimmune endocrine diseases. Eur. J. Endocrinol, 134:21–30.

Miyata, T. (2015) Discovery studio modeling environment. Ensemble, 17: 98–104

Molinspiration cheminformatics, 2006. Choice Rev. Online 43:6538-6538

Pennline, K.J., Roque-Gaffney, E. & Monahan, M. (1994) Recombinant human IL-10 prevents the onset of diabetes in the nonobese diabetic mouse. Clin. Immunol. Immunopathol, 71:169–175

Rabinovitch, A. (1994). Immunoregulatory and cytokine imbalances in the pathogenesis of IDDM. Therapeutic intervention by immunostimulation? Diabetes, 43:613–621

Rabinovitch, A., Suarez-Pinzon, W.L., Sorensen, O., Bleackley, R.C. & Power, R.F. (1995) IFN-gamma gene expression in pancreatic islet-infiltrating mononuclear cells correlates with autoimmune diabetes in nonobese diabetic mice. J. Immunol, 154**:**4874–82

Ram, A., Lauria, P., Gupta, R., Kumar, P. & Sharma, V.N. (1997) Hypocholesterolaemic effects of Terminalia arjuna tree bark. J. Ethnopharmacol, 55**:**165–169.

Rapoport, M.J., Jaramillo, A., Zipris, D., Lazarus, A.H., Serreze, D. V., Leiter, E.H., Cyopick, P., Danska, Jane S. & Delovitch, T.L. (1993) Interleukln 4 reverses T cell proliferative unresponsiveness and prevents the onset of diabetes in nonobese diabetic mice. J. Exp. Med, 178**:**87–99

Rappé, A.K., Casewit, C.J., Colwell, K.S., Goddard, W.A. & Skiff, W.M. (1992) UFF, a Full Periodic Table Force Field for Molecular Mechanics and Molecular Dynamics Simulations. J. Am. Chem. Soc, 114:10024–10035

Swain, S.L. (1995) CD4 T cell development and cytokine polarization: An overview, in: Journal of Leukocyte Biology, 57(**5**):795–798

Unnisa, A., Abouzied, A.S., Anupama, B., Chenchu, L.K.N.V., Hussain, T., Kunduru, R.D., Banu, H., Bushra Fatima, S. Hussian, A. & Selvarajan, K.K. (2020) Design, synthesis, characterization, computational study and in-vitro antioxidant and anti-inflammatory activities of few novel 6-aryl substituted pyrimidine azo dyes. Arab. J. Chem, 13(**12**):8638-8649

Unnisa, A., Abouzied, A.S., Anupama, B., Chenchu, L.K.N.V., Kunduru, R. & Kesavanarayan, K. (2020) Design, synthesis, computational study, and biological evaluation of 6-aryl substituted pyrimidine schiff bases. Pharmacophore, 11(**6**):74-103

Veber, D.F., Johnson, S.R., Cheng, H.Y., Smith, B.R., Ward, K.W. & Kopple, K.D. (2002) Molecular properties that influence the oral bioavailability of drug candidates. J. Med. Chem, 45(**12**):2615-2623

Zaccone, P., Phillips, J., Conget, I., Gomis, R., Haskins, K., Minty, A., Bendtzen, K., Cooke, A. & Nicoletti, F. (1999) Interleukin-13 prevents autoimmune diabetes in NOD mice. Diabetes, 48:1522–1528

Submitted: 23/11/2021
Revised: 09/01/2022
Accepted: 01/02/2022
DOI: 10.48129/kjs.17337

Investigation of the value-added potential of some selected freshwater cyanobacteria

Tharangika K. Bowange[1], Md. Fuad Hossain[1, 2, 3], Kavinda A. Wijesekera[1], K.L. Wasantha Kumara[2], R.R. Ratnayake[1, *]

[1] *National Institute of Fundamental Studies, Hantana Road, Kandy, Sri Lanka*

[2] *Dept. of Agricultural Biology, Faculty of Agriculture, University of Ruhuna, Mapalana, Kamburupitiya, 81100, Sri Lanka*

[3] *Dept. of Biochemistry and Molecular Biology, Gono Bishwabidyalay, Savar, Dhaka, Bangladesh*

[*] *Corresponding Author: renuka.ra@nifs.ac.lk*

Abstract

Ever growing population and environmental degradation lead to a rapid deterioration of global health, causing malnutrition and Ultra Violet radiation-induced skin damages to be more prevalent. It is critical to address these health issues quickly and sustainably. Compared to natural botanicals, cyanobacteria could be more promising due to their superior photosynthetic capabilities, rapid growth, low space and simple nutrients requirements, low capital investment, and zero environmental pollution. Therefore, this study explores the value-added potential of freshwater cyanobacteria in addressing the above health issues sustainably. Eight cyanobacteria strains, isolated from freshwater reservoirs in the dry zone of Sri Lanka were analyzed for total carbohydrate, protein, macro and micro minerals using Dubois' method, Lowry method, and Inductively Coupled Plasma Optical Emission Spectrometry. Mansur equation was applied to determine the Sun Protection Factor (SPF). Total carbohydrate and protein contents were in the range of 7.08 ± 0.32% - 53.08 ± 0.32% and 15.27 ± 0.90% - 49.77 ± 9.62%, respectively. Oscillatoriales had the highest total carbohydrate content (53.08 ± 0.32%), higher than the carbohydrate content of other previously reported *Oscillatoria* species. Calcium and iron were the most abundant macro and micro minerals, respectively. Oscillatoriales recorded the highest SPF (1.57 ± 0.002), whereas all the other strains had considerably greater or similar SPFs compared to other previously reported herbal extracts. Cyanobacteria with rich nutrition profiles and high SPF values may thus represent interesting alternatives for offering sustainable and ecofriendly solutions to significant health challenges associated with population growth.

Keywords: Cyanobacteria; food insecurity; global health; macronutrients; sun protection factor

1. Introduction

Uncontrollable population growth has caused the rapid reduction of arable lands thus limiting the crop-based food production (Elmi *et al*., 2019). Insufficient food production and uneven

distribution of nutritious food create nutritional inequality among communities. Malnutrition has become a more prevalent, serious health issue especially among children and adolescents from the poorest and developing countries, causing frequent deaths, severe deficiencies and infections (UNICEF, 2019). For instance, micronutrient deficiencies of Iron, Iodine and Zinc are the most prevalent, causing major public health issues in a considerable portion of the world population. However, this issue is comparatively unnoticed (Müller & Krawinkel, 2005).

Due to the rapid deteriorating pattern of global health and nutrition status (UNICEF, 2019), introducing dietary diversification through easily available, accessible, natural, low cost and nutritionally rich alternatives would be an important and immediate requirement. Most importantly their utilization should be sustainable, since, the unsustainable utilization would create many other irreversible environmental problems such as deforestation, water scarcity and ecological imbalance. Productivity limit reached by traditional crops due to seasonal limitations, specific growth requirements, climatic changes and unsustainable utilization of resources has made cyanobacteria more attractive as a natural alternative food source. This is evident by the usage of few certain cyanobacteria such as *Spirulina* spp., *Nostoc* sp. and *Anabaena* sp. as food and feed additives in countries such as Chile, Mexico, Peru, and Phillipines (Hoseini *et al*., 2013; Singh *et al*., 2016).

Rapid environmental degradation has also led to poor health status of global population. In the event of UV radiation, a rapid increase in undesirable skin problems, such as mutagenicity, accelerated skin aging, and photodermatoses, occurs (Dubey and Venkatesh, 2021; Mishra *et al*., 2011; Nohynek and Schaefer, 2001). Therefore, people are more conscious of skin protecting agents and sunscreens which are natural or synthetic chemicals with a variety of immunosuppressive effects of sunlight by absorbing and blocking UV rays (Nohynek & Schaefer, 2001). However, applications of synthetic sunscreens in cosmetic industry are limited, due to the known potential toxicity of certain synthetic sunscreens to humans (Chanchal & Saraf, 2009).

In contrast, natural sun protecting agents discourage skin carcinogenesis and are known to have higher level of safety over synthetic sunscreens. Among them, natural botanicals, including many plant extracts (Wagemaker *et al*., 2011) and lichens had been studied for photo protection (Radice *et al*., 2016). Active compounds extracted from microalgae also show a significant effect in preventing blemishes, repairing skin damages, inhibiting inflammation, accelerating healing process and maintaining skin moisture (Mourelle *et al*., 2017). *Chlorella*, *Spirulina*, *Nostoc* and *Nannochloropsis* are among the most studied species in cosmetics production (Mourelle *et al*., 2017). Therefore, identifying and introducing natural botanicals with efficient sun protecting properties together with beneficial mineral profiles, would be important in finding solutions for UV induced skin damages.

Higher photosynthetic ability, simple, rapid and ubiquitous growth, equal or better nutritional quality compared to some traditional crops, the ability to utilize the same space for regrowth and continuous production of quality harvest throughout the year with less capital investment and zero environmental pollution, make cyanobacteria more promising and

sustainable to be used in food and cosmetics industry to ensure good health status in global population.

Diversity of cyanobacteria in tropics is remarkably high and tropical islands such as Sri Lanka provide habitats for a diverse collection of cyanobacteria (Hossain *et al*., 2020; Senanayake & Yatigammana, 2017; Wanigatunge *et al*., 2014) with an unexplored industrial potential, specifically in food and cosmetic industries. Therefore, the major objective of the study was to evaluate the value-added potential of some selected Sri Lankan freshwater cyanobacteria in providing sustainable solutions for malnutrition and UV induced skin damage. We hypothesized that cyanobacteria could provide a sustainable and environmentally friendly solution to some of the most prevalent health issues such as malnutrition and UV radiation induced complications on skin in the global population.

2. Materials and Methods

2.1 Research Materials

Hydrochloric Acid (37%; Germany), Sulfuric Acid (95%-97%; 30743; Germany), Nitric Acid (69%; extra pure AR grade; 30702; Germany), Phenol (GC; 16017; UK), Ammonium Ferrous Sulphate (99%; 215406; Japan), Ammonium Molybdate Tetrahydrate (A7302; USA), Folin–Ciocalteu reagent (F9552), Bovine Serum Albumin (A9056), Sodium Dodecyl Sulfate salt (L4509, GC; ≥ 98.5%) and Copper II Sulfate Pentahydrate (209198; ACS reagent; ≥ 98.0%) were purchased from Sigma Aldrich for media preparation and nutrient analysis. Sodium Carbonate (7541-4405), Potassium Sodium Tartrate Tetrahydrate (6618-4405), Citric Acid monohydrate (2562-4405), and Sodium Nitrate (7599-4405) were of extra pure quality and purchased from Daejung, Korea. D-Glucose (101174Y), Sodium Hydroxide (ACS reagent; 28244.262) used for standard preparation, media preparation and nutrient analysis were purchased from VWR BDH PROLABO, Belgium. Absolute ethanol (ACS reagent, 20821.321, France) was used for DNA extraction and SPF analysis. Magnesium Sulphate heptahydrate (A546586; Merck, Germany) was used for media preparation. The following reagents were prepared in distilled water for total protein analysis. Lysis buffer: (5 mLL^{-1} of TritonX-100 (437002A; EC), 0.3722 gL^{-1} of Ethylenediaminetetraacetic Acid Disodium salt (AR grade; 20301.186), and 0.0348 gL^{-1} of Phenyl Methyl Sulfonyl Fluoride (P-470-10, US)), 5% SDS solution: (0.05 gL^{-1} of Sodium Dodecyl Sulfate salt), Reagent A: (4.0 gL^{-1} of Sodium Hydroxide and 20.0 gL^{-1} of Sodium Carbonate), Reagent B1: (0.001 gL^{-1} of Copper II Sulfate pentahydrate), Reagent B2: (0.002 gL^{-1} of Potassium Sodium Tartrate tetrahydrate (6618-4405, Korea) and Reagent C: (100 mL of reagent A, 1 mL of reagent B1 and 1 mL of reagent B2 prepared just prior to use). Folin–Ciocalteu reagent (1:1 v/v Folin reagent/distilled water) prepared just prior to use. CTAB buffer: (100 mM of Tris.HCl [pH 8]; Promega Corporation, USA), 20 mM of Ethylenediaminetetraacetic Acid, 1.4 M Sodium Chloride (ACS reagent, 152575, MP Biomedicals, France) and 2% Cetyl Trimethyl Ammonium Bromide (Janssen Chimica, Belgium)) and TE buffer: (10 mM of Tris.HCl [pH 8] and 1 mM of Ethylenediaminetetraacetic

Acid) were prepared for DNA extraction. Whatman No: 42 (ashless, 90 mm, 1442090) and syringe filters (cellulose acetate, hydrophilic, 0.45 µm and 25 mm diameter) were used for sample filtration in ICP-OES analysis. Risheng- RS-2800 ultra-quiet air oxygen pump (50 Hz; 2.5w; China) was used for aeration of cultures. Compound light microscope (Euromex BioBlue.Lab BB. 1153-PLi, Euromex Microscopen BV, Netherlands, equipped with Euromex DC.5000C CMEX microscope USB Camera) was used for microscopic imaging. Microcentrifuge (Ortoalresa Bioprocen 22R, Spain) was used for DNA extraction. Thermal cycler (Techne TC 3000 Thermal Cycler, USA) was used for PCR amplification and PCR clean up system PCR purification kit (Promega Corporation, USA) was used for PCR product purification. Water bath (YCW-010E, Germany) was used in DNA extraction and nutrient analysis. Agilent UV-Vis Cary 60 spectrophotometer (G68 60A; USA) was used to obtain absorbance of colorimetric analyses. Inductively Coupled Plasma Optical Emission Spectrometry (ICPA 7000, Thermo Fisher Scientific) was used for macro and micro mineral analysis.

2.2 Isolation, purification and culturing of cyanobacteria isolates

Water samples were collected from the photic zone of freshwater reservoirs in the Dry zone of Sri Lanka (5° 54′ N - 9° 52′ N latitude and 79° 39′ E - 81° 53′ E longitude) (Hossain *et al*., 2020) using a Ruttner sampler. Ten mL of the sample which was filtered through 20 µm mesh size planktonic net was transferred into 100 mL conical flasks with 40 mL of BG11 medium with 7.5 pH (Table 1). The cultures were incubated at room temperature, under 2000 lux, on a shaker at 200 rpm. Once the initial bluish green color growth was observed, 100 µL of the sample was sub cultured into agar plates containing BG11 medium solidified with 1.5% (w/v) bacteriological agar. To establish pure monocultures, isolated cyanobacteria in streak or spread plates were repeatedly sub cultured, and numerous microscopic examinations were performed. After isolation, monocultures were maintained in 250 mL Erlenmeyer flasks filled with 200 mL of BG11 medium (Hossain *et al*., 2020).

Table 1. BG11 media components, their concentrations to prepare stock solutions, and the volume required to prepare 1 L of the medium (Stanier *et al*., 1971).

Component	Stock solution concentration (g/L)	Volume required to prepare 1L of BG11 (mL)
$NaNO_3$	150 g/L	10 mL
K_2HPO_4	40 g/L	1 mL
$MgSO_4.7H_2O$	75 g/L	1 mL
$CaCl_2.2H_2O$	36 g/L	1 mL
Citric Acid	6 g/L	0.5 mL
Ferric Ammonium Citrate	6 g/L	0.5 mL
EDTA	1 g/L	1 mL
Na_2CO_3	20 g/L	1 mL

A5 Trace Metal Solution		
H_3BO_3	2.86 g/L	1 mL
$MnCl_2.4H_2O$	1.81 g/L	
$ZnSO_4.7H_2O$	0.222 g/L	
$Na_2MoO_4.2H_2O$	0.390 g/L	
$CuSO_4.5H_2O$	0.079 g/L	
$Co(NO_3)_2.6H_2O$	0.049 g/L	

2.3 Morphological characterization of the isolates

Microscopic images observed under the compound light microscope (Euromex BioBlue.Lab BB. 1153-PLi equipped with Euromex DC.5000C CMEX microscope USB Camera, Euromex Microscopen BV, Netherlands) were photographed using Image Focus 04 software. Morphological characterization was done based on the morphological characteristics described by Desikachery (1959) and Mcgregor (2013 and 2018).

2.4 DNA extraction, 16S rRNA region amplification and DNA sequencing

DNA extraction of the selected cyanobacteria isolates was carried out using the method by Smoker & Barnum (1988) with slight modifications.

One milliliter aliquot of cyanobacteria culture was centrifuged at 2000 rpm for 5 min and the BG11 medium was decanted. The pellet was suspended in a 2 mL microcentrifuge tube with 700 µL of CTAB extraction buffer and incubated in a water bath at 60°C for 1 hour. The contents were mixed by inverting the tubes at regular intervals. Then 700 µL of chloroform/isoamylalcohol (24:1) solution was added to the tube and mixed for 2 min by repeatedly inverting the tube. The tube was centrifuged at a speed of 10000 rpm for 15 min. Next 300 µL of the aqueous supernatant was carefully transferred to a fresh 2 mL microcentrifuge tube. Total genomic DNA was precipitated by adding 600 µL of absolute ethanol followed by centrifugation at 10000 rpm for 15 min. Then the supernatant was decanted and the DNA pellet was washed with 70% ice cold ethanol. The tubes were centrifuged briefly in between washes to prevent the DNA pellet getting disturbed. Then the pellet was dried in the laminar flow chamber for 10 min, allowing any residual ethanol to evaporate. Finally, the DNA pellet was suspended in 50 µL of TE buffer and was stored at -20°C for further analysis (Figure 1).

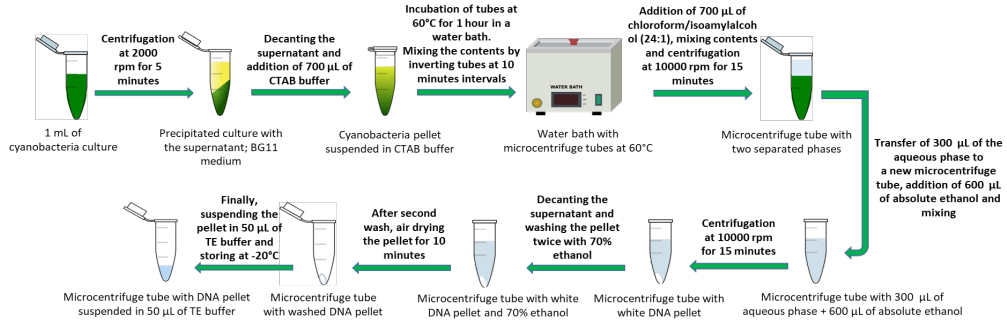

Fig. 1. Steps in DNA extraction of cyanobacteria isolates using the method described by Smoker & Barnum (1988) with slight modifications.

PCR amplification of the 16S rRNA gene region was carried out using two primer sets; CYA106F and CYA359F as forward primers and CYA781Ra and CYA781Rb as reverse primers (Hossain *et al*., 2020) (Table 2).

Table 2. Primers used in the PCR amplification and their information

Primer name	Primer sequence	Number of bases
CYA106F	5′-CGG ACG GGT GAG TAA CGC GTG A-3′	22
CYA781Ra	5′-GAC TAC TGG GGT ATC TAA TCC CAT T-3′	25
CYA359F	5′-GGG GAA TYT TCC GCA ATG GG-3′	20
CYA781Rb	5′-GAC TAC AGG GGT ATC TAA TCC CTT T-3′	25

The PCR amplification cycle of 16S rRNA region including an initial denaturation step of template DNA at 94°C for 5 min, 40 cycles of 94°C for 1 min, annealing step at 60°C for 1 min, elongation at 72°C for 1 min and the final elongation at 72°C for 15 min, was carried out in the Thermal Cycler (Techne TC 3000 Thermal Cycler, USA) (Hossain *et al*., 2020). Then PCR product purification was carried out using a Wizard SV gel and PCR clean up system PCR purification kit (Promega Corporation, USA) and DNA sequencing of the amplified PCR products for forward and reverse primers was carried out at Macrogen, South Korea using ABI 3730XL DNA sequencer (Hossain *et al*., 2020). The strains were identified at the molecular level using BLAST software and the partial DNA sequences obtained were compared and multiple-aligned with the reference sequences from GenBank using Clustal Omega and the phylogenetic tree was constructed (Figure 4). The information of the identified strains was then deposited in the GenBank through BankIt submission tool under the accession numbers: KX962076, KX962083, KX96208, KX962090, KX962091, KX962093, KX962095 and KX962098 (Table 3) (Hossain *et al*., 2020.)

2.5 Evaluation of value-added potential of cyanobacteria strains

Mass culturing of cyanobacteria was carried out in 1/5th strength of BG11 (Table 1) at a pH of 7.5, in 100 L large fish tanks, under natural greenhouse light and temperature conditions and the system was agitated using aerators (Risheng- RS-2800 ultra-quiet air oxygen pump; 50 Hz; 2.5w; China) (Figure 2).

Fig. 2. Mass culturing of cyanobacteria strains under greenhouse conditions.

The fresh biomass was harvested in the 5th week after initial culturing and the biomass of filamentous strains was harvested using continuous filtration while unicellular strains were harvested through centrifugation at 2000 rpm for 5 min at 27°C. The harvested fresh biomass was then oven dried at 50°C to obtain 10-15 g of dry biomass and the powdered dry biomass was stored in the freezer for further analysis.

2.5.1 Total carbohydrate content analysis

Twenty-five mg of dry biomass powder was hydrolyzed with 2.5 N HCl at 100°C for one hour. Then the samples were neutralized with sufficient amounts of Na_2CO_3 (7541-4405), filtered with Whatman No 42 (ashless, 90 mm, 1442090) filter papers and diluted in 25 mL volumetric flasks. One mL of the extract was analyzed by Dubois' method (Dubois *et al*., 1956). In brief, 5% Phenol (GC grade, Sigma Aldrich, UK) was added to each tube with 1 mL of the extract. Then 5 mL of Conc. H_2SO_4 (95-97%, ACS reagent, Sigma Aldrich, Germany) was added and the tubes with the content were vortex-mixed and kept for color development in a water bath (YCW-010E, Germany) at 25°C for 30 min. After 30 min, the absorbance of each sample was measured at 490 nm using UV spectrophotometer (Agilent UV-Vis Cary 60 spectrophotometer, G68 60A, USA). Total carbohydrate concentration (in mg/mL) was calculated based on the standard curve of D-Glucose (101174Y).

2.5.2. Total protein content analysis

Twenty mg of the dry biomass powder was lysed with 10 mL of lysis buffer and the lysate was centrifuged at 4800 rpm for 5 min. Then 0.5 mL of the supernatant was analyzed using Lowry method (Lowry *et al*., 1951). In brief, 0.5 mL of 5% SDS (L4509, GC; ≥ 98.5%) solution was added to 0.5 mL of the extract and the contents were mixed using a vortex. Then 5 mL of the Reagent C was added and the contents were mixed again. After 10 min, 0.5 mL of Folin reagent was added to each tube and the tubes were vortex-mixed again. The tubes were then kept for 30 min for color development and the absorbance was measured at 750 nm, using UV spectrophotometer (Agilent UV-Vis Cary 60 spectrophotometer, G68 60A, USA). Total protein concentration in mg/mL was calculated based on the standard curve of Bovine Serum Albumin (A9056).

2.5.3 Analysis of macro and micro minerals

Hundred mg of dried biomass powder was digested with 3 mL of 69% HNO_3 (extra pure AR grade; 30702; Germany) for 25 min. The digested volume was filtered using Whatman No 42 filter papers (ashless, 90 mm, 1442090) and diluted in 10 mL volumetric flask. The filtrate was filtered twice using 0.45 μm syringe filters (cellulose acetate, hydrophilic, and 25 mm diameter). Final filtrate was analyzed by Inductively Coupled Plasma Optical Emission Spectrometry (ICPA 7000, Thermo Fisher Scientific).

2.5.4 Determination of Sun Protection Factor (SPF)

Sun Protection Factor of the ethanol extracts of dry biomass was determined by the method described by Dutra *et al*. (2004). Cyanobacteria dry biomass powder (1000 mg) was transferred into a 100 mL volumetric flask, diluted with absolute ethanol (ACS reagent, 20821.321, France) followed by ultra-sonication for 5 min. The content was then filtered using Whatman No 42 filter papers (ashless, 90 mm, 1442090). Five mL aliquot from the filtrate was diluted fifty times with absolute ethanol (ACS reagent, 20821.321, France) and the absorbance of the samples were obtained at 5 nm intervals in the range of 290-320 nm using a UV spectrophotometer (Agilent UV-Vis Cary 60 spectrophotometer, G68 60A, USA). Mansur equation (Kaur & Saraf, 2010; Mishra *et al.*, 2012) was applied to calculate the SPF value of the product as per Equation (1).

$$SPF = CF \times \sum_{290}^{320} EE(\lambda) \times I(\lambda) \times Abs(\lambda) \quad (1)$$

Where;
CF = Correction Factor (10), EE (λ) = Erythmogenic Effect of radiation with wavelength λ, Abs (λ) = spectrophotometric absorbance values at wavelength λ. The values of EE x λ are constants.

2.6 Statistical Analysis

Three replicates were carried out per sample in each analysis. Results were statistically analyzed using One-way ANOVA in Minitab 17 (Hossain *et al*., 2016).

3. Results and Discussion

3.1 Morphological characterization of the isolates

As a basic step towards value addition of the isolates, their characterization was confirmed through a polyphasic approach. Observable morphological features of each isolate are described below.

Limnothrix sp. (Figure 3a.) was green, having non-branching, thin, straight or slightly curved filaments without sheath or with very fine, colorless, facultative sheath. The filaments were solitary, free floating or arranged in separate bundles (Desikachery, 1959; Mcgregor, 2013 and 2018).

Croococcidiopsis sp. (Figure 3b.) was unicellular; spherical cells, sometimes gathered in free-living irregular agglomerations or forming somewhat spherical or irregular colonies. Cells or small groups of cells are enveloped by thin, firm, colorless, sometimes slightly layered sheaths (Desikachery, 1959; Mcgregor, 2013 and Mcgregor ,2018).

Calothrix sp. (Figure 3c.) was simple, green heteropolar filaments and found as solitary or in small groups, separated from one another. Filaments were rarely with single, lateral, false branches. Cells were cylindrical or barrel-shaped. Basal cells were funnel shaped and wide,

while the filaments were tapering. Sheaths were always present, usually firm, sometimes lamellated and yellow-brownish colored (Desikachery, 1959; Mcgregor, 2013 and 2018).

Limnothrix sp. (Figure 3d.) showed similar morphological features as shown in Figure 3a. However, these filaments were slightly curved, smaller and thin.

Geitlerinema sp. (Figure 3e.) was observed as simple, bluish green, thin, straight or slightly wavy filaments with rounded or conical apical cells, while the filaments were arranged in bundles and showed slight gliding movements. Cells were longer than wide and sheaths were absent (Desikachery, 1959; Mcgregor, 2013 and 2018).

Oscillatoriales (Figure 3f. and 3h.) were observed as green, simple, unbranched filaments (trichomes) with cylindrical cells. Heterocyst formation or false branching was not observed. Filaments were solitary or arranged in bundles.

Synechocystis sp. (Figure 3g.) was green to yellowish green, unicellular, solitary, spherical or widely oval cells containing narrow, fine colorless mucilaginous envelopes (Mcgregor, 2013 and 2018).

However, identification of isolates based solely on classical morphological features would be impossible as some cyanobacteria can be detectable with unclear morphological features which are not distinguishable in microscopic observations (Komárek, 2016). Therefore, for the strains which cannot be identified with distinguishable morphological features, molecular characterization is essential. On the other hand, there are some strains which are detectable with clearly distinguishable morphological markers. Morphological characterization of these strains would be useful in more reliable identification (Komárek, 2016). Hence, a polyphasic approach where both morphological and molecular characterizations can be used together would be useful in more accurate identification of any strain.

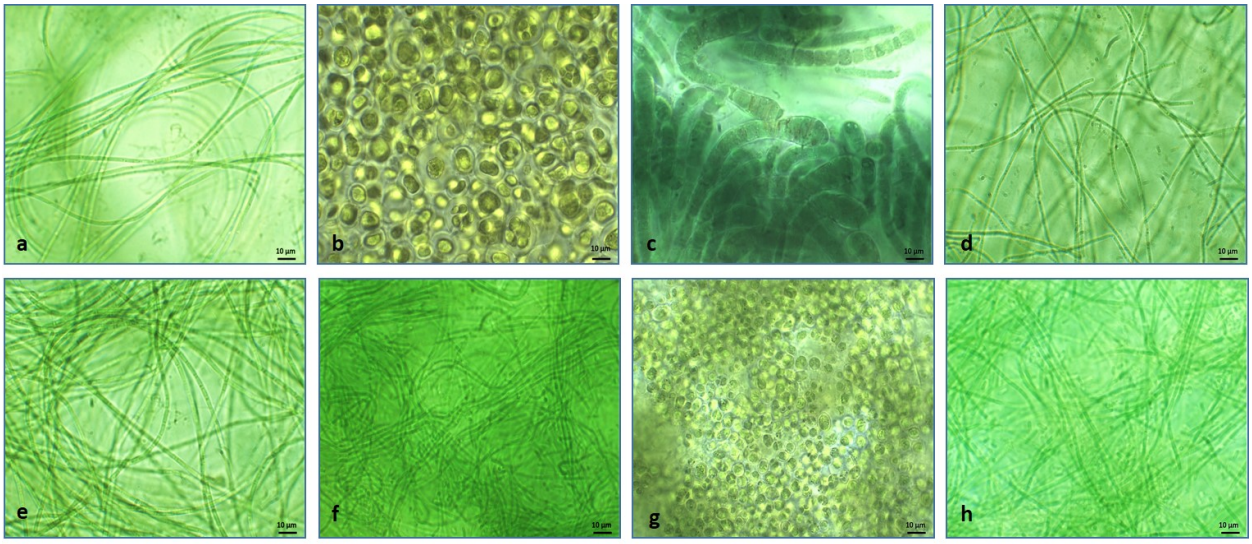

Fig. 3. Microscopic images of some purified strains obtained under oil immersion (1000x) a: *Limnothrix* sp. (U03), b: *Croococcidiopsis* sp. (U13), c: *Calothrix* sp. (U15), d: *Limnothrix* sp. (U33), e: *Geitlerinema* sp. (U36), f: Oscillatoriales (U40), g: *Synechocystis* sp. (U42) and h: Oscillatoriales (U55).

3.2 DNA extraction, 16S rRNA region amplification and DNA sequencing

All isolates were identified up to the genus or order level, based on the molecular characterization (Table 3).

Table 3. Molecular identification of the strains

Strain ID	Molecular identification	Query cover	Identity	Genbank accession no
U03	*Limnothrix* sp.KW3	100%	100%	KX962076
U13	*Chroococcidiopsis*	100%	91%	KX962083
U15	*Calothrix* sp.KK15	97%	94%	KX962084
U33	*Limnothrix* sp.UW33	100%	96%	KX962090
U36	*Geitlerinema* sp.KK36	100%	100%	KX962091
U40	Oscillatoriales.PK40	99%	92%	KX962093
U42	*Synechocystis* sp.MW42	99%	98%	KX962095
U55	Oscillatoriales.DL55	99%	92%	KX962098

Obtained partial DNA sequences were compared and multiple-aligned with the reference sequences from GenBank using Clustal Omega and the phylogenetic tree was constructed (Figure 4).

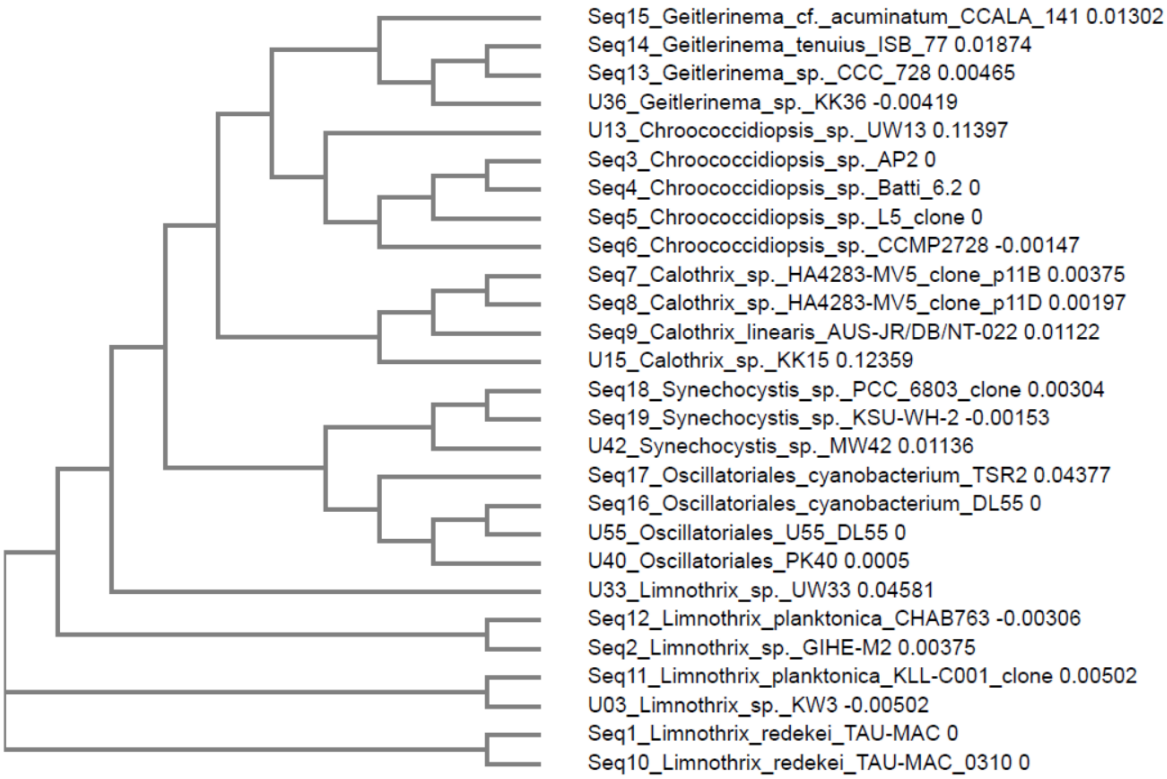

Fig. 4. Phylogenetic tree constructed using Clustal Omega, showing the relationship between the of 16S rRNA gene sequences of the isolates obtained from this study (denoted by 'U') and the closely related reference sequences (denoted by 'Seq') obtained from the National Center for Biotechnology Information (NCBI) database.

Morphological characteristics (Figure3), together with molecular characterization (Hossain *et al*., 2020) (Figure 4 and Table 3) confirmed the identity of the isolates. Based on the molecular characterization, four strains (U03, U33, U36 and U42) showed ≥ 95% similarity with both query cover and identity, while other four strains (U13, U15, U40 and U55) showed ≥ 95% similarity with either query cover or identity (Hossain *et al*., 2020). The identity of the morphologically characterized strains was confirmed with the closest matching data through molecular characterization (Table 3).

3.3 Total carbohydrate content

In this study, the highest total carbohydrate content was recorded in Oscillatoriales (53.08 ± 0.32%) while the lowest content was in *Limnothrix* sp. (7.08 ± 0.32%) (Figure 5).

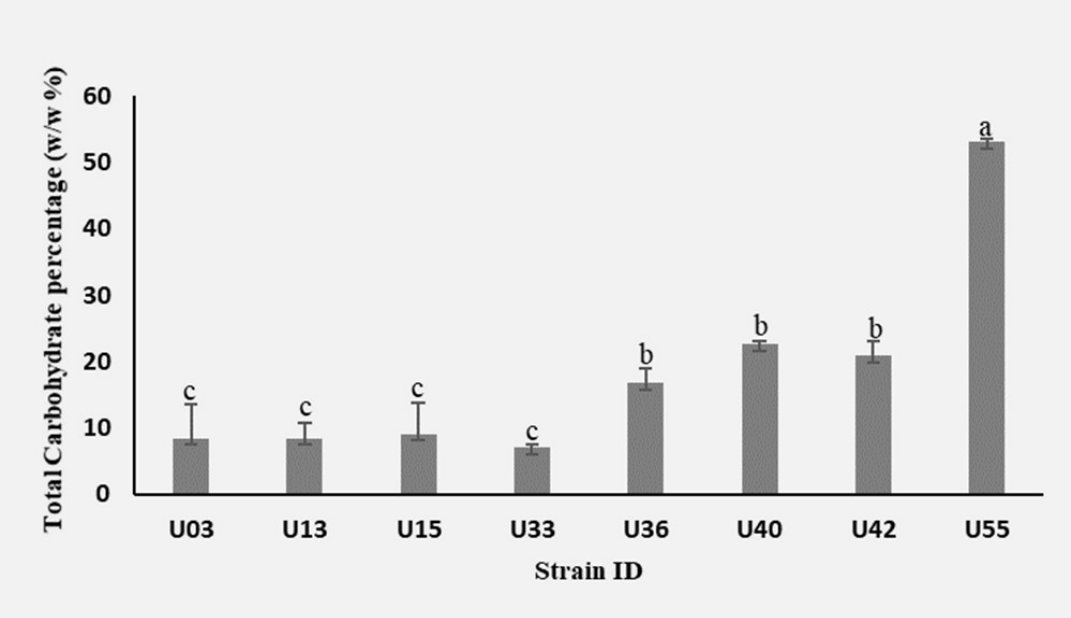

Fig. 5. Total carbohydrate content (% w/w) of eight selected strains namely; *Limnothrix* sp. (U03), *Croococcidiopsis* sp. (U13), *Calothrix* sp. (U15), *Limnothrix* sp. (U33*), Geitlerinema* sp. (U36), Oscillatoriales (U40), *Synechocystis* sp. (U42) and Oscillatoriales (U55). (a, b and c show the significant difference among mean values; One Way Analysis of Variance: Tukey pairwise comparison at $P< 0.05$ and 95% confidence level).

Results were comparable with some previous studies. Total carbohydrate content of two Oscillatoriales (U40 - 22.62 ± 0.32% and U55 - 53.08 ± 0.32%) were higher, compared to previously reported values of 12.05% in *O. formosa* and 16.23% in *O. salina* from Vethalai coastal regions, India (Kanimozhi *et al*., 2017). They were also significantly higher than *O. accuminata* (14%), *O. foreaui* (8%) and *O. calcuttensis* (9.6%) isolated from effluent waters (Rajeshwari & Rajashekhar, 2011). Carbohydrate contents reported for some cyanobacteria

including *Anabaena cylindrica*, *Spirulina platensis*, *Spirulina maxima* and *Synechococcus* sp. were also within the range of 8% - 30% (Koyande *et al*., 2019) which were comparable for many recorded carbohydrate contents in this study. *Synechocystis* sp. (20.92 ± 1.2%) recorded in this study was higher than previously recorded *Synechocystis* sp. (9.8%) (Patel *et al*., 2018). The total carbohydrate content recorded in Oscillatoriales (53.08 ± 0.32%) in this study was significantly higher compared to all the previously reported species mentioned above.

Compared to eukaryotic algae, cyanobacteria are easily digestible and more acceptable for human consumption as cyanobacteria cell wall lacks polysaccharides such as cellulose, and other monosaccharaides such as xylose, and mannose (Richmond & Preiss 1980). Therefore, easily digestible cyanobacteria strains with higher carbohydrate contents would be one of the best, easily available food alternatives to fulfill the energy requirement of the malnourished communities.

3.4 Total protein content

The highest and the lowest total protein contents were recorded in *Limnothrix* sp. (49.77 ± 9.62%) and Oscillatoriales (15.27 ± 0.90%) respectively. Total protein contents of other strains were in the range of 19.3 ± 2.69% to 44.33 ± 1%. Out of 8 strains, five contained more than 30% of total protein contents (Figure 6).

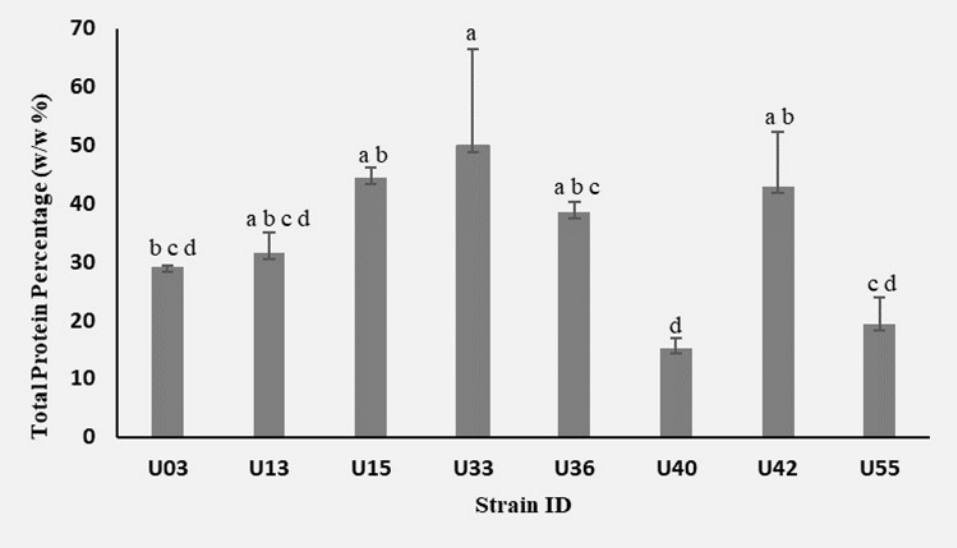

Fig. 6. Total protein content (% w/w) of eight selected strains namely; *Limnothrix* sp. (U03), *Croococcidiopsis* sp. (U13), *Calothrix* sp. (U15), *Limnothrix* sp. (U33), *Geitlerinema* sp. (U36), Oscillatoriales (U40), *Synechocystis* sp. (U42) and Oscillatoriales (U55). (a, b and c show the significant difference among mean values; One Way Analysis of Variance: Tukey pairwise comparison at $P < 0.05$ and 95% confidence level).

Five strains showed more than 30% of total protein content similar to the previously reported protein contents (30% - 55%) of the microalgae and cyanobacteria including *Synechocystis aquatilis* and *Arthrospira platensis* (López *et al*., 2010). However, the highest total protein content recorded for *Limnothrix* sp. (49.77 ± 9.62%) in the study was lower than that of *Spirulina platensis* (63%) previously recorded by Tokus¸oglu & Ünal (2006). The protein contents of the two studied *Limnothrix* sp.; (U03 - 29.23 ± 0.08% and U33 - 49.77 ± 9.62%) were significantly different. Though both of them were from freshwater reservoirs in the dry zone of Sri Lanka, they were isolated from two distant locations where the environmental conditions were considerably different. Thus, their physiology could be differently adapted to survive under the environmental conditions of their natural habitats. Variations of the environmental conditions of the two natural habitats of these *Limnothrix* sp. therefore could be a major reason for the significant difference of their total protein contents (Billi & Potts, 2000; Muhetaer *et al*., 2020).

Strains reported in this study with considerable amounts of total protein contents, highlight the potential for eradication of protein related malnutrition by introducing diverse dietary options.

There is an inverse relationship between the total carbohydrate content and the total protein content of the tested strains. Strains with higher total protein contents were recorded with lower total carbohydrate contents. This inverse relationship of higher total protein contents and low carbohydrate contents can be commonly observed in majority of microalgal species (Markou *et al*., 2012). However, the total protein and carbohydrate contents can be dependent on several factors such as the nutrient availability in the growth medium, light intensity and temperature (Markou *et al*., 2012).

In this study, many tested strains with comparatively and significantly higher total protein and carbohydrate contents would be promising food alternatives to promote dietary diversification among poor communities. It would provide a sustainable, low cost and natural solution to global protein-energy malnutrition, ensuring nutrition equity. Therefore, crop-based agriculture should be transformed by introducing modern agricultural practices where these nutrient alternatives are incorporated.

3.5 Macro and micro minerals contents

Cyanobacteria are rich sources of macro and micro minerals as they contribute to the formation of cyanobacterial internal cellular structures (Rajeshwari & Rajashekhar, 2011). Significantly high amounts of Ca in all strains highlight their suitability as a supplement of Ca. Ca of the tested strains ranged between 1145.33 ± 58.25 – 10456.00 ± 32.35 ppm and these contents were closely comparable with the recorded Ca contents in *Spirulina* (1300-14000 ppm), considered to be comparable to the amounts found in milk (Falquet & Hurni, 1997). Thus, tested cyanobacteria could be promising in fulfilling Ca mineral requirements with a similar potential of Ca sources such as milk.

Table 4. Macro and micro mineral profiles of the cyanobacteria strains

Strain ID	Cd [ppb]	Ni [ppb]	Zn [ppb]	Mn [ppb]	Cr [ppb]	Pb [ppb]	Co [ppb]	Cu [ppb]	As [ppb]	Fe [ppm]	Mg [ppm]	Ca [ppm]	K [ppm]	Sr [ppb]
U03	0.89± 0.09	167.61± 2.20	1587.06± 22.17	28529.31 ± 57.95	184.73± 3.49	31.24± 0.68	174.19± 4.84	894.45 ± 43.11	ND	104.82± 2.01	910.12± 7.54	4026.52± 2.91	474.23± 7.91	215.33± 8.84
U13	1.16± 0.01	18.24± 0.62	1481.67± 8.27	5580.98± 87.55	28.87± 2.74	10.52± 0.85	125.55± 2.96	104.78± 3.62	5.47± 0.70	10.56± 0.03	526.86± 4.64	4421.78± 28.34	57.11± 1.52	420.94± 9.32
U15	1.48± 0.02	23.87± 1.34	1106.03± 9.01	7995.11± 42.93	35.09± 11.94	10.41± 1.93	105.86± 0.31	110.77± 0.62	ND	5.93± 0.04	474.74± 1.15	3253.21± 51.57	53.44± 0.64	97.00± 0.22
U33	1.14± 0.05	81.13± 2.60	990.22± 3.22	674089 ± 474.59	503.13± 8.11	23.57 ± 2.46	97.97± 6.44	400.43± 51.93	ND	20.05± 0.98	559.43± 5.69	4080.83 ± 78.48	273.02± 18.71	57.38± 2.73
U36	0.74± 0.13	540.75± 16.16	1309.01± 11.42	4281.91± 94.59	34.89± 2.31	12.42± 2.07	69.81± 1.56	115.11± 0.75	ND	9.53± 0.83	313.57± 2.41	2758.40± 6.10	67.29± 0.93	58.54± 3.35
U40	1.55± 0.27	106.95± 5.30	1775.08± 27.06	16325.27 ± 343.03	239.54± 17.67	24.42± 0.86	114.57 ± 0.36	352.12± 1.91	ND	45.25± 0.88	807.87± 5.90	5066.67± 45.32	246.56± 10.15	156.03± 5.83
U42	1.18± 0.08	30.04± 1.03	1645.97± 67.34	6578.31± 150.18	76.20± 0.88	23.01± 1.03	89.61± 1.26	159.45± 1.98	11.62± 0.73	20.93± 0.61	412.27± 1.91	1145.33± 58.25	62.92± 1.44	611.65± 6.83
U55	1.58± 0.01	31.51± 0.26	1442.17± 101.64	4464.89± 27.13	59.38± 1.30	17.59± 0.59	102.09± 1.00	114.52± 1.31	18.18± 0.14	19.31± 0.12	348.65± 1.55	10456.00 ± 32.35	44.11± 0.19	461.14± 10.53

(Concentration (mean concentration ± standard error of mean); Concentrations are given in ppb and ppm; ND: Not Detectable)

Iron deficiencies are common and widely spread in all communities, particularly among children and pregnant women (Müller & Krawinkel, 2005). However, iron rich food sources are rare. Average iron content in cereals and grains is within the range of 25 - 80 ppm (Moreira *et al*., 2013). However, the bioavailability of iron in some cereals could be limited while iron supplements may sometimes cause toxic effects (Johnson & Shubert, 1986). In this study, iron showed the highest amounts, followed by Mn, Zn, Cu, Co and Ni, respectively, among all micro minerals (Table 4). Comparatively, the highest iron content recorded was 104.82 ± 2.01 ppm in *Limnothrix* sp. and the iron content of five more cyanobacteria strains was within the range of 10.56 ± 0.03 – 45.25 ± 0.88 ppm range. Thus, tested cyanobacteria strains could be far more promising representative sources of iron (Table 4).

Sufficient amount of Zinc is essential for the activity of many enzymes and its deficiency can cause major health issues including pneumonia. Zinc content of tested strains ranged between 0.990 ± 3.22 ppm - 1.775 ± 27.06 ppm (Table 4) and these results were comparable with the recorded zinc contents in commercialized *Spirulina* products (0.533-6.255 ppm), considered as safe food (Al- Dhabi, 2013). Out of 25 *Spirulina* products, 24 showed >1.200 ppm Zn contents which was comparable to this study where 6 out of 8 strains showed >1.200 ppm of Zn contents (Table 4). Furthermore, these amounts are below the recommended daily intake of heavy metal elements for Zn (13 mg/daily) (Iyengar, 1985) suggesting higher potential of improving these strains into alternative sources of Zn for safe consumption. According to Table 4, *Limnothrix* sp. had the highest Mg (910.12 ± 7.54 ppm), K (474.23 ± 7.91 ppm), Fe (104.82 ± 2.01 ppm), Cu (894.45 ± 43.11 ppb) and Mn (28529.31 ± 57.95 ppb) contents, whereas Ni (540.75 ± 16.16 ppb) was the highest in *Geitlerinema* sp. The presence of greater amounts of many minerals in *Limnothrix* sp. nominates itself as the most promising alternative source of essential macro and micro elements. Thus, few grams of these mineral rich cyanobacteria biomass could be easily sufficient to meet the recommended daily intakes of major macro and

micro minerals for both adults and children. Cd, Cr, Pb, As, Co and Sr quantities were below the accepted maximum level recommended by the World Health Organization, eliminating all risk levels of their utilization (Table 4). These recommendations for developing cyanobacteria as a commercial product will improve global public health and economy.

3.6 Sun Protection Factor

The mean SPF values of the strains are shown in Figure 7.

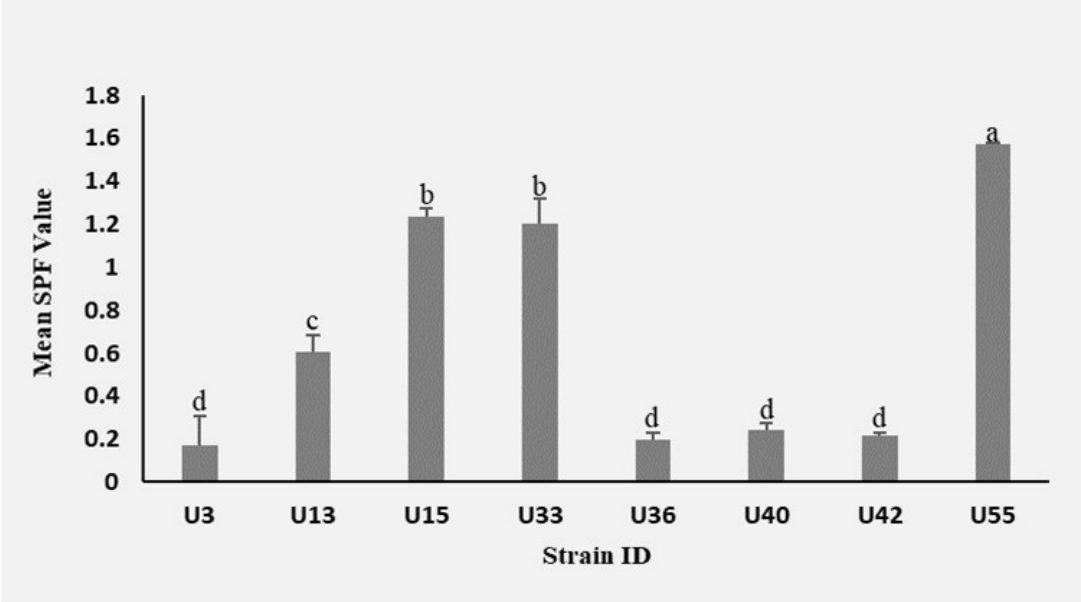

Fig. 7. Mean Sun Protection Factor (SPF) of eight selected strains namely; *Limnothrix* sp. (U03), *Croococcidiopsis* sp. (U13), *Calothrix* sp. (U15), *Limnothrix* sp. (U33), *Geitlerinema* sp. (U36), Oscillatoriales (U40), *Synechocystis* sp. (U42) and Oscillatoriales (U55). (a, b and c show the significant difference among mean values; One Way Analysis of Variance: Tukey pairwise comparison at $P < 0.05$ and 95% confidence level).

The mean SPF of the cyanobacteria biomass ranged between 0.17 ± 0.091 in *Limnothrix* sp. (U03) and 1.57 ± 0.002 in Oscillatoriales (U55). There was no significant difference among the mean SPF of *Limnothrix* sp. (U03), *Geitlerinema* sp. (U36), Oscillatoriales (U40), and *Synechocystis* sp. (U42) all of which showed comparatively very low mean SPF. SPF of *Calothrix* sp. (U15) and *Limnothrix* sp. (U33) were comparatively higher with no significant difference between them.

Compared to previous studies, results of this study suggest that cyanobacteria could be more effective over many plant extracts (Table 5).

Table 5. Comparison of Sun Protection Factor of different plant extracts and tested cyanobacteria strains

Cyanobacteria strain/ Plant species	Sun Protection Factor	Reference
Limnothrix sp. (U03)	0.17 ± 0.091	
Chroococcidiopsis sp. (U13)	0.61 ± 0.057	
Calothrix sp. (U15)	1.24 ± 0.026	
Limnothrix sp. (U33)	1.21 ± 0.078	The present study
Geitlerinema sp. (U36)	0.20 ± 0.024	
Oscillatoriales (U40)	0.24 ± 0.021	
Synechocystis sp. (U42)	0.22 ± 0.007	
Oscillatoriales (U55)	1.57 ± 0.002	
Oil extracts of coffee beans of;		
C. canephora	0.35	
C. congensis	1.08	Wagemaker *et al*., 2011
C. kapakata	0.06	
C. arabica	1.50	
C. racemosa	1.59	
C. liberica var. dewevrei 'Abeokutae'	0.42	
C. liberica var. dewevrei 'Excelsa'	0.88	
C. liberica var. liberica	0.48	
C. liberica var. liberica 'Passipagore'	0.29	
Aqueous herbal extracts of;		
Aloe vera	1.28	Malsawmtluangi *et al*., 2013
Carrot	1.34	
Coconut	7.38	
Cucumber	1.45	
Watermelon	0.97	

The highest SPF reported in Oscillatoriales (U55) was comparatively higher than many previously reported coffee species namely, *C. canephora* (0.35), *C. congensis* (1.08), *C. kapakata* (0.06) and four varieties of *C. liberica* (Wagemaker *et al*., 2011). However, the most cultivated coffee species around the world, *C. arabica* (1.50) bearing many important cosmetic properties, and C. *racemosa* (1.59) (Wagemaker *et al*., 2011) (Table 5) showed similar SPF values as Oscillatoriales (1.57 ± 0.002).

The SPF reported for seven herbal extracts from aloe vera, carrot, coconut, cucumber, papaya, strawberry, and watermelon by Malsawmtluangi *et al*. (2013) ranged between 0.97 and 7.38. Oscillatoriales (U55) showed a higher SPF (1.57 ± 0.002) than aloe vera (1.28), carrot (1.34), cucumber (1.45) and watermelon (0.97) (Malsawmtluangi *et al*., 2013), highlighting its effectiveness in sun protection over many previously reported herbal extracts. As seen in Table 5, *Calothrix* sp. (1.24 ± 0.026) and *Limnothrix* sp. (1.21 ± 0.078) had similar SPF values as aloe vera (1.28) (Malsawmtluangi *et al*., 2013). In the cosmetics industry, the use of natural botanical ingredients is well-known to be safe and has gained widespread customer acceptability. Many studies have proved that different extracts, vitamins (Schaeffer & Krylov, 2000) and secondary

metabolites (Priyadarshani and Rath, 2012) isolated from cyanobacteria have effective sun screening properties. This study further reports many freshwater cyanobacteria strains with higher or similar UV filtering properties compared to many other plant extracts. Thus, cyanobacteria could be more promising as better natural botanical alternatives with effective UV screening properties to provide effective solutions to health issues emerged with environmental destructions such as UV induced skin damages.

4. Conclusion

Rapid deterioration of global health with increased malnutrition and UV induced skin mutagenesis needs to be addressed immediately with natural, sustainable alternatives such as cyanobacteria, for which everyone has easy access. With the aim of evaluating the potential of cyanobacteria in providing sustainable solutions, especially for malnutrition and UV induced skin mutations, selected freshwater cyanobacteria strains from freshwater reservoirs in the tropical Asian region, Sri Lanka, were analyzed for macro nutrients, mineral profiles and sun screening properties. Nutrient profiles and SPF values reported for the selected cyanobacteria were higher compared to nutrient profiles and SPF values of many previously reported strains and herbal/plant extracts, emphasizing potential applicability in food and cosmetic industries. Thus, they can be used as potential protective resources for UV induced skin problems and can be improved to be used as nutrient supplements to address the malnutrition developed through macro and micro nutrient deficiencies. Their commercially beneficial characteristics over plant material, such as higher photosynthetic ability, rapid growth, requirement of lesser area and simple nutrients for the growth and higher production with less capital investment and zero environmental pollution, make cyanobacteria more promising in providing sustainable and ecofriendly solutions to major health issues arisen with population growth.

5. ACKNOWLEDGEMENTS

The authors wish to acknowledge Mr. L. Mahadeva and Mrs. R.K.C. Karunaratne (Staff, National Institute of Fundamental Studies, Sri Lanka) for their support during laboratory analyses.

References

Al-Dhabi, N.A. (2013) Heavy metal analysis in commercial Spirulina products for human consumption. Saudi journal of biological sciences**, 20**(4):383-388.

Billi, D., & Potts, M. (2000) Life without water: responses of prokaryotes to desiccation. Environmental stressors and gene responses, **1**:181-192.

Chanchal, D. & Swarnlata, S. (2009) Herbal photoprotective formulations and their evaluation. The Open Natural Products Journal, **2**:71-76.

Desikachary, T. (1959) Cyanophyta. Indian Council of Agricultural Research, New Delhi. Pp. 686.

Dubey, R.S., & Venkatesh, Y. (2021) Engineering of Ultra-Violet Reflectors by varying Alternate Layers of Titania/Silica for Harmful UV-Protection. Kuwait Journal of Science.

Dubois, M., Gilles, K.A., Hamilton, J.K., Rebers, P.T. & Smith, F. (1956) Colorimetric method for determination of sugars and related substances. Analytical chemistry, **28**(3):350-356.

Dutra, E.A., Oliveira, D.A.G.D.C., Kedor-Hackmann, E.R.M. & Santoro, M.I.R.M. (2004) Determination of sun protection factor (spf) of sunscreens by ultraviolet spectrophotometry. Revista Brasileira de Ciências Farmacêuticas, **40**(3):381-85.

Elmi, A., Anderson, A.K., & Albinali, A.S. (2019) Comparative study of conventional and organic vegetable produce quality and public perception in Kuwait. Kuwait Journal of Science, **46**(4):120-127.

Falquet, J., & Hurni, J.P. (1997) The nutritional aspects of Spirulina. Antenna Foundation. Available online at: https://www. antenna. ch/wp-content/uploads/2017/03/AspectNut_UK. pdf (Accessed on 20th February, 2022).

Hoseini, S.M., Khosravi-Darani, K. & Mozafari, M.R. (2013) Nutritional and medical applications of spirulina microalgae. Mini reviews in medicinal chemistry, **13**(8):1231-1237.

Hossain, M.F., Ratnayake, R.R., Meerajini, K. & Wasantha Kumara, K.L. (2016) Antioxidant properties in some selected cyanobacteria isolated from fresh water bodies of Sri Lanka. Food science & nutrition, **4**(5):753-758.

Hossain, Md.F., Bowange, R.W.T.M.R.T.K., Kumara, K.L.W., Magana-Arachchi, D.N. & Ratnayake, R.R. (2020) First record of cyanobacteria species: Cephalothrix komarekiana, from tropical Asia. Environmental Engineering Research, **26**(2):1-11.

Johnson P. & Shubert E. (1986) Availability of iron to rats from spirulina, a blue green algae. Nutrition Research, **6**:85-94.

Kanimozhi R., Arvind P.D. & Subramanian G. (2017) Total carbohydrate, lipid and protein content of some species of marine cyanobacteria from vethalai coastal region, gulf of mannar, India. World Journal of Pharmaceutical Research, **6**(10):954-961.

Kaur, C.D. & Saraf, S. (2010) In vitro sun protection factor determination of herbal oils used in cosmetics. Pharmacognosy research, **2**(1):22.

Komárek, J. (2016) A polyphasic approach for the taxonomy of cyanobacteria: principles and applications. European Journal of Phycology, **51**(3): 346-353.

Koyande, A.K., Chew, K.W., Rambabu, K., Tao, Y., Chu, D.T. & Show, P.L. (2019) Microalgae: A potential alternative to health supplementation for humans. Food Science and Human Wellness, **8**(1):16-24.

López, C.V.G., García, M.D.C.C., Fernández, F.G.A., Bustos, C.S., Chisti, Y. & Sevilla, J.M.F. (2010) Protein measurements of microalgal and cyanobacterial biomass. Bioresource technology, **101**(19):7587-7591.

Lowry, O.H., Rosebrough, N.J., Farr, A.L. & Randall, R.J. (1951) Protein measurement with the folin phenol reagent. J biol Chem, **193**(1):265-275.

Markou, G., Angelidaki, I., & Georgakakis, D. (2012) Microalgal carbohydrates: an overview of the factors influencing carbohydrates production, and of main bioconversion technologies for production of biofuels. Applied microbiology and biotechnology, **96**(3):631-645.

Malsawmtluangi, C., Nath, D.K., Jamatia, I., Zarzoliana, E. & Pachuau, L. (2013) Determination of Sun Protection Factor (SPF) number of some aqueous herbal extracts. Journal of Applied Pharmaceutical Science, **3**(9):150-151.

Mcgregor, G.B. (2013) Freshwater cyanobacteria of north-eastern Australia: 2. Chroococcales. Phytotaxa, **133**(1):1-130.

Mcgregor, G.B. (2018) Freshwater Cyanobacteria of North-Eastern Australia: 3. Nostocales. Phytotaxa, **359**(1):1-166.

Mishra, A.K.., Mishra, A. & Chattopadhyay, P. (2011) Herbal cosmeceuticals for photoprotection from ultraviolet B radiation: a review. Tropical Journal of Pharmaceutical Research, **10**(3).

Mishra, A.K., Mishra, A. & Chattopadhyay, P. (2012) Assessment of in vitro sun protection factor of Calendula officinalis L.(asteraceae) essential oil formulation. Journal of Young Pharmacists, **4**(1):17-21.

Moreira, L.M., Ribeiro, A.C., de Morais, M.G., & de Souza Soares, L.A. (2013) Spirulina platensis biomass cultivated in Southern Brazil as a source of essential minerals and other nutrients. African Journal of Food Science, **7**(12): 451-455.

Mourelle, M.L., Gómez, C.P. & Legido, J.L. (2017) The potential use of marine microalgae and cyanobacteria in cosmetics and thalassotherapy. Cosmetics, **4**(4):46.

Muhetaer, G., Asaeda, T., Jayasanka, S.M., Baniya, M.B., Abeynayaka, H.D., Rashid, M.H., & Yan, H. (2020) Effects of light intensity and exposure period on the growth and stress responses of two cyanobacteria species: Pseudanabaena galeata and Microcystis aeruginosa. Water, **12**(2): 407.

Müller, O. & Krawinkel, M. (2005) Malnutrition and health in developing countries. Canadian Medical Association Journal, **173**(3):279-286.

Nohynek, G.J. & Schaefer, H. (2001) Benefit and risk of organic ultraviolet filters. Regulatory Toxicology and Pharmacology, **33**(3):285-299.

Patel, V.K., Sundaram, S., Patel, A.K. & Kalra, A. (2018) Characterization of seven species of cyanobacteria for high-quality biomass production. Arabian Journal for Science and Engineering, **43**(1): 109-121.

Priyadarshani, I., & Rath, B. (2012) Commercial and industrial applications of micro algae–A review. Journal of Algal Biomass Utilization, **3**(4): 89-100.

Radice, M., Manfredini, S., Ziosi, P., Dissette, V., Buso, P., Fallacara, A. & Vertuani, S. (2016) Herbal extracts, lichens and biomolecules as natural photo-protection alternatives to synthetic UV filters. A systematic review. Fitoterapia, **114**:144-162.

Rajeshwari, K.R. & Rajashekhar, M. (2011) Biochemical composition of seven species of cyanobacteria isolated from different aquatic habitats of Western Ghats, Southern India. Brazilian archives of biology and technology, **54**(5):849-857.

Richmond, A. & Preiss, K. (1980) The biotechnology of algaculture. Interdisciplinary Science Reviews, **5**(1):60-70.

Schaeffer, D.J., & Krylov, V.S. (2000) Anti-HIV activity of extracts and compounds from algae and cyanobacteria. Ecotoxicology and environmental safety, **45**(3):208-227.

Senanayake, P.A.A.P.K. & Yatigammana, S.K. (2017) Quantitative observations of Cyanobacteria and Dinoflagellata in reservoirs of Sri Lanka. Ceylon Journal of Science, **46**(4):55-68.

Singh, J.S., Kumar, A., Rai, A.N. & Singh, D.P. (2016) Cyanobacteria: a precious bio-resource in agriculture, ecosystem, and environmental sustainability. Frontiers in microbiology, **7**:529.UNICEF (2019). The state of the world's children 2019: Children, food and nutrition.

Smoker, J.A. & Barnum, S.R., (1988) Rapid small-scale DNA isolation from filamentous cyanobacteria. FEMS Microbiology letters, **56**(1):119-22.

Stanier, R., Kunisawa, R., Mandel, M. **&** Cohen-Bazire, G., (1971) Purification and properties of unicellular blue-green algae (order chroococcales). Bacteriological reviews, **35**(2):171

Tokuşoglu, Ö & üUnal, M.K. (2006) Biomass Nutrient Profiles of Three Microalgae: Spirulina platensis, Chlorella vulgaris, and Isochrisis galbana. Journal of Food Science, **68**:1144-1148.

Wagemaker, T.A.L., Carvalho, C.R.L., Maia, N.B., Baggio, S.R. & Guerreiro Filho, O. (2011) Sun protection factor, content and composition of lipid fraction of green coffee beans. Industrial Crops and Products, **33**(2):469-473.

Wanigatunge, R.P., Magana-Arachchi, D.N., Chandrasekharan, N.V. & Kulasooriya, S.A. (2014) Genetic diversity and molecular phylogeny of cyanobacteria from Sri Lanka based on 16S rRNA gene. Environmental Engineering Research, **19**(4):317-329.

Submitted: 21/07/2021
Revised: 20/05/2022
Accepted: 30/05/2022
DOI: 10.48129/kjs.15295

Involvement of *miR-3648* mediated *APC2* dysregulation in early onset and breast cancer progression

Mehwish Batool[1], Javeria Qadir[1,2,3],
Misbah Shan[1], Feiya Li[2,3], Faraz A. Malik[1], Hassaan M. Awan[1,]*

[1]Dept. of Biosciences, COMSATS University Islamabad, Park Road, Tarlai Kalan, 45550, Islamabad, Pakistan.
[2]Dept. of Laboratory Medicine and Pathobiology, University of Toronto, ON- Canada.
[3]Sunnybrook Research Institute, Sunnybrook Hospital, ON- Canada

**Corresponding email: hassaan.awan@comsats.edu.pk*

Abstract

Multiple cancers arise due to aberrations in the wingless integrated (Wnt) signaling pathway. Several miRNAs modulate the integral components of the Wnt signaling pathway. *miR-3648* is a human-specific miRNA that is of particular interest due to its minimal off-targeting effect. In this study, we investigated the expression of *miR-3648* and *APC2* in breast cancer patients of Pakistan. Correlations of *miR-3648* and *APC2* expression with clinico-pathological features and breast cancer subtypes were observed in tissue samples by means of quantitative real time PCR. Our results showed that *miR-3648* was relatively downregulated in Luminal A subtype, with corresponding upregulation of *APC2* in these patients. Moreover, the transcript levels of both *miR-3648* and *APC2* were found to be inversely regulated in breast cancer women presented with early disease onset, pre-menopause, low tumor grade, early clinical stage, absence of nodal invasion and metastasis, further suggesting the molecular interplay of these molecules in breast cancer development and progression.

Keywords: *APC2*; breast cancer; luminal A; miR-3648; Wnt signaling

1. Introduction

Breast cancer is one of the most commonly diagnosed cancer worldwide (Sung *et al*, 2021). Various genetic and environmental factors contribute towards breast cancer leading to the accumulation of mutations in essential genes that regulate maintenance, cell growth and tumor microenvironment (Rich *et al*, 2015).

MicroRNAs (miRNAs) are 22-25nt long, single stranded, small non-coding RNAs (Yang *et al*, 2015). They modulate gene expression by targeting 3'UTR of mRNAs, resulting in translation repression or mRNA destabilization, thus, playing an essential role in cellular and biological processes such as differentiation, stress response, apoptosis and cell cycle (Mittal *et al,* 2017; López-Knowles *et al,* 2010). While a specific mRNA could be targeted by multiple miRNAs, a single miRNA can have several mRNA targets as well (Di Vizio *et al*, 2012). miRNAs are virtually

involved in almost every disease including cancers. The regulatory actions of miRNAs on normal expression of oncogenes or tumor suppressor genes lead a cell transit toward cancerous state (Vannini *et al*, 2018). They have great potential to be used as therapeutic target for disease treatment such as in breast cancer (Davey *et al*, 2021; Petrovic *et al*, 2021)

Many cancers arise due to irregularities in the Wnt signaling pathway (Anastas *et al,* 2013). The tumor suppressor Adenomatous polyposis coli (*APC*) plays a role in Wnt signaling pathway, a pathway whose irregularities have been shown to be related with many cancers, and its association has been observed with multiple cancers. Several studies have described alterations in Wnt/APC2 signaling pathway, thus, discerning its role in the process of carcinogenesis (Jafarzadeh & Soltani, 2021; Koni *et al*, 2020; Castagnoli *et al*., 2020). In this regard, there have been quite a number of miRNAs reported to modulate integral components of the Wnt signaling pathway, therefore, contributing to the pathogenesis of various cancers. *miR-3648* is one of the many human specific miRNAs identified, and is of particular interest due to its minimum off-targeting (Hu *et al,* 2012). Previously, a highly sensitive luciferase assay was employed to show that *miR-3648* directly targets APC2 mRNA, harboring three *miR-3648* binding sites (Rashid *et al*, 2017). Following endoplasmic reticulum stress, downregulation of APC2 expression due to elevated *miR-3648* expression results in enhanced cell proliferation (Rashid *et al,* 2017). Its correlation with other cancer types is also reported (Xing, 2019; Emmadi *et al,* 2015). However, its role in breast cancer remains elusive.

Therefore, the aim of this study was to investigate and compare the expression of *miR-3648* and *APC2* in fresh tissue samples of breast cancer patients as well as in the healthy controls in Pakistani cohort. Furthermore, the study also aimed at exploring the potential associations of *miR-3648* and *APC2* with clinico-pathological features and breast cancer subtypes.

2. Materials & Methods

2.1. Tissue Specimen and Data Collection

This research was conducted in agreement with prior approvals from the Ethical Review Board (ERB) of CUI (CUI/Bio/ERB/12-19/03). The study cohort comprised of 80 breast cancer affected women with ages ranging from 27-97 years collected from Holy family Hospital, Rawalpindi in agreement with the ethical guidelines set forth by the collaborating institutes. The mean age was calculated to be 50 years. Freshly excised tumor tissues along with their adjacent healthy tissues (2cm away from tumor area) were collected and stored in RNA*later*® (Invitrogen, California, USA) and maintained at 4^{o}C in an ice bucket during transportation to the laboratory. Demographic data and clinico-pathological characteristics including tumor grade, nodal involvement, stage, and age were obtained from the patients who underwent Modified Radical Mastectomy (MRM).

2.2. RNA isolation and quantification

RNA extraction from tissue samples was carried out using standard TRIzol™ reagent method using an already established protocol (Qadir *et al.,* 2021). Extracted RNA was quantified on a nanodrop (IMPLEN GmbH, Germany). For each sample, 1µl of RNA was loaded onto nanodrop

and absorbance was recorded at 260 and 280nm. A ratio of 260/280 was measured to assess the quality of extracted RNA and samples with a ratio > 1.9 were used for further analysis.

2.3. cDNA Synthesis

To examine the expression of miRNA-*3648* and APC*2*, RNA isolated from each sample was subjected to cDNA synthesis. A cDNA synthesis kit from Thermo Scientific (Cat#K1622) was used to transcribe RNA into cDNA in accordance with the manufacturer's instructions. Oligo dT primers and *miR-3648* stem loop (SL) primer was added to each reaction mixture. The cDNA, thus formed, was confirmed using 2% agarose gel electrophoresis. The sequence of *miR-3648* stem loop primer is given in the (Table 1).

2.4. Quantitative Real Time Polymerase Chain Reaction

Relative expression of *miR-3648* and *APC2* was analyzed using gene specific primers and qPCR SYBR Green Master Mix on quantitative PCR machine (Applied Biosystems). Transcript levels of *miR-3648* and *APC2* were determined based on the threshold cycle (C_t) values. Livak's method was used to analyze the data. GAPDH was used as an internal control for *miR-3648* and *APC2* gene data normalization (Rashid *et al*, 2017). Primers used in this study are given in (Table 1).

2.5. Statistical analysis

Statistical analysis for the results, thus acquired, was performed using nonparametric tests. Mainly Wilcoxon Signed Ranked Test for paired variables while Mann-Whitney and Kruskal Wallis tests were used for unpaired variables. GraphPad Version 5.0 was employed as a tool for statistical analysis.

Table 1. Oligo sequences used in this study.

S. No	Oligo	Sequence
1	miR-3648 (SL)	GTCGTATCCAGTGCAGGGTCCGAGGTATTCGCACTGGATACGACCCC
2.	miR-3648 (F)	CACAGCCGCGGGGAT
3.	miR-3648 (R)	CCAGTGCAGGGTCCGAGGTA
4.	APC2 (F)	CGCTGCAGGAGCTGAAGAT
5.	APC2 (R)	GGCTGGAGTTGTCCCTTAGC
6.	GAPDH (F)	CAAGGTCATCCATGACAACTTT
7.	GAPDH (R)	GTCCACCACCCTGTTGACAACTTG
8.	β-catenin (F)	TGCAGCTTCTGGGTTCCGATGATA
9.	β-catenin (R)	AGATGGCAGGCTCAGTGATGTCTT

3. Results

The obtained patient data was distributed according to clinico-pathological parameters including age, menopausal status, tumor size, tumor grade, tumor stage (I-IV), nodal involvement and metastasis. To establish the clinical relevance of *miR-3648* and *APC2* in breast cancer patients, their change in expression levels was shown as depicted (Table 2).

Table 2. Expressional Association of *miR-3648* and *APC2* with Clinico-pathological Parameters and Intrinsic Molecular Subtypes in Breast Cancer

Variable(s)	Categories	Relative Expression of *miR-3648* (Mean±SEM)	Relative Expression of *APC2* (Mean±SEM)	*p*-Value
Tumor Tissues	80 Samples	1.095± 0.3759	0.3325± 0.1461	**0.0002*** **
Age	<50 Yrs	1.190± 0.4357	0.2389± 0.1259	0.0002***
	>50 Yrs	0.5850± 0.2519	170.9± 167.1	0.1993
Grade	I	0.5169± 0.5131	0.02738± 0.02695	**0.0234***
	II	0.8850± 0.3773	29.56± 29.13	**0.0406***
	III	1.226±0.4782	0.4335±0.2248	0.111
Stage	I	0.8568±0.5737	0.03199±0.02661	**0.0234***
	II	1.350±0.7832	0.4172±0.2494	0.3564
	III	0.9887±0.5012	14.45±14.05	0.0503
	IV	1.071±0.9495	1.070±1.001	0.8960
Menopausal Status	Pre-Menopause	0.6632±0.3308	0.1056±0.05867	**0.009** **
	Post-Menopause	1.996±0.9377	21.59±20.43	0.0572
Tumor Size	<2cm	0.8620± 0.6105	2.043± 1.453	0.1099
	2-5cm	2.095± 1.192	0.3092± 0.1645	**0.0028** **
	>5cm	0.6952± 0.2859	10.71± 10.38	0.0754
Nodal Involvement	Positive (N1)	1.157± 0.4279	8.998± 8.482	0.0877
	Negative (N0)	0.7187± 0.3745	0.1332± 0.09612	**0.0017** **
Metastasis	M0	1.100±0.4097	5.305±5.065	**0.0009*** **
	M1	1.071±0.9495	1.070±1.001	0.896
Intrinsic Molecular Subtypes	Luminal A	0.02584± 0.01604	1.167± 1.061	**0.0245***
	Luminal B	2.350± 1.177	0.8384± 0.4512	0.1276
	HER2 Positive	0.04797± 0.04303	0.006327± 0.003353	0.0510
	TNBC	7.258± 7.219	3.631± 1.726	0.4688

3.1. Expression profile of *miR-3648* and *APC2* in tumor tissue samples

Expression profiling of *miR-3648* and *APC2* in breast cancer patients revealed that transcript levels of both molecules were negatively correlated, i.e., *miR-3648* showed slight upregulation in tumor samples whereas *APC2* was found to be downregulated, suggesting that the loss of *APC2* function in breast cancer patients of Pakistan may partially be due to the presence of *miR-3648* (Figure 1A). Interestingly, the difference in expression levels of these two entities was statistically significant with $p<0.001$.

3.2. Association of *miR-3648* and *APC2* expression with Clinico-pathological Parameters

APC2 mRNA expression was observed to be significantly upregulated in patients with moderately differentiated tumors, whereby, *miR-3648* was relatively downregulated in these patients. This expressional variation between the *miR-3648* and *APC2* was found to be statistically significant (Figure 1B). In pre-menopausal breast cancer patients, there was a slight upregulation of *miR-3648* but downregulation of *APC2* (Figure 1C). This implied the potential role of *APC2* being a tumor suppressor with regulatory roles in premenopausal patients. Regarding different age groups, *APC2* mRNA expression was observed to be downregulated in younger patients with ages <50 years whereas *miR-3648* was relatively upregulated in these patients. This variation between these two molecular entities was found to be statistically significant (Figure 1D).

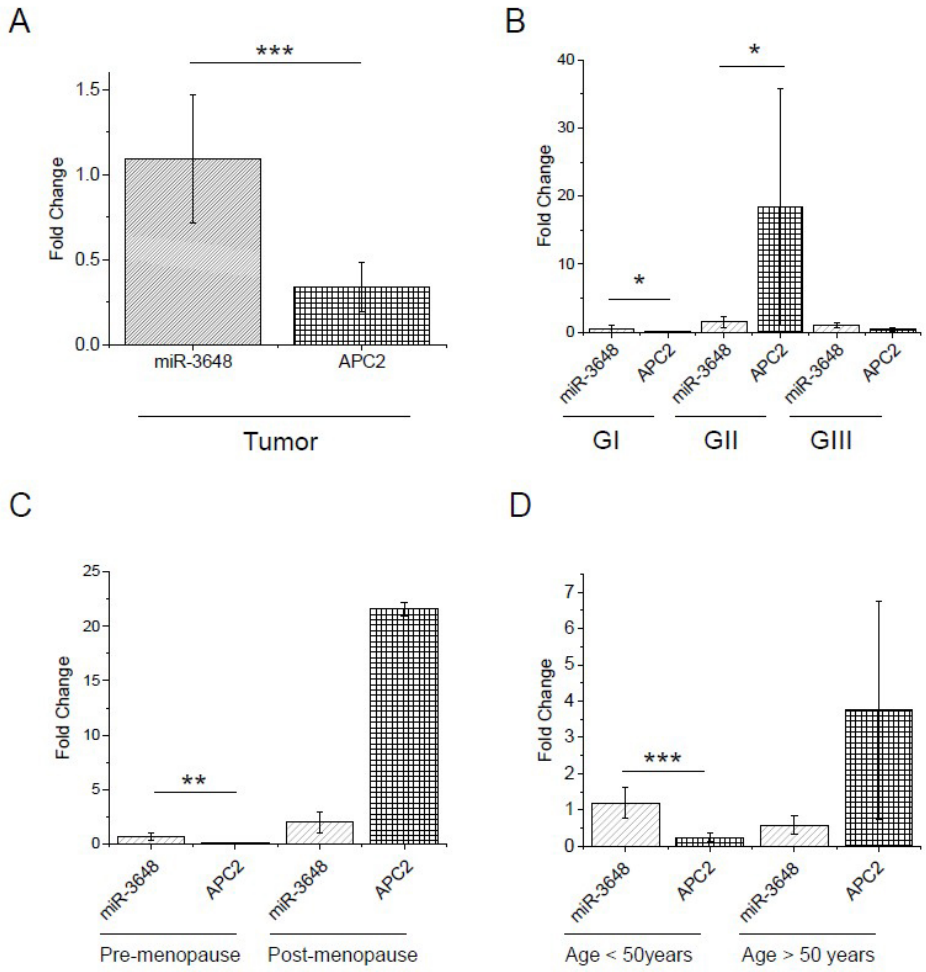

Fig. 1. Expression of *miR-3648* and *APC2* in breast tumor samples and its association with clinico-pathological parameters. (A) Significant downregulation of *APC2* expression was observed in breast tumors with miR-3848 upregulation. (B) In moderately differentiated tumors, *APC2* gene expression was significantly upregulated with *miR-3648* downregulation unlike well differentiated and poorly differentiated tumors. Similarly (C, D) shows significant downregulation of *APC2* in early disease onset and pre-menopausal women. $p<0.05$ was considered as statistically significant.

3.3. Association of *miR-3648* and *APC2* expression with TNM and Molecular Breast Cancer Subtypes

As shown in (Figure 2A), breast tumor samples with size between 2-5cm showed increased transcript levels of *miR-3648* while *APC2* was relatively decreased in these patients. Similar pattern of expression for these two was observed in patients who exhibited no lymph node involvement (Figure 2B). Moreover, an upregulation of *APC2* gene accompanied with a downregulation of *miR-3648* in breast cancer patients with no distant metastasis was observed, and was statistically significant, as shown in (Figure 2C).

Interestingly, both *miR-3648* and *APC2* were observed to be significantly associated at molecular level, explicitly in Luminal B breast cancer subtype in Pakistani women. Similar pattern of *miR-3648* and *APC2* expression was also observed in triple negative breast cancer (TNBC) breast tumors subtype, however, the findings were not statistically significant. It may be inferred that *miR-3648* and *APC2* may have role in estrogen-receptor (ER) and progesterone-receptor (PR) regulation in breast cancer patients (Figure 2D).

APC2 interacts with *β-catenin* and negatively regulates the *β-catenin* signaling pathway (Pai *et al.,* 2017). Downregulation of *APC2* should influence the downstream expression of *β-catenin*, therefore, the expression of *β-catenin* was measured and as expected, the overall expression of *β-catenin* mRNA was significantly upregulated (Figure 2E). Furthermore, its expression showed inverse relationship with the expression of *APC2* in pre-metastatic tumors of patients having pre-menopausal status with age < 50 (Figure 2F). These findings further corroborated with our findings that *miR-3648* mediated repression of *APC2* influence the early onset of breast cancer.

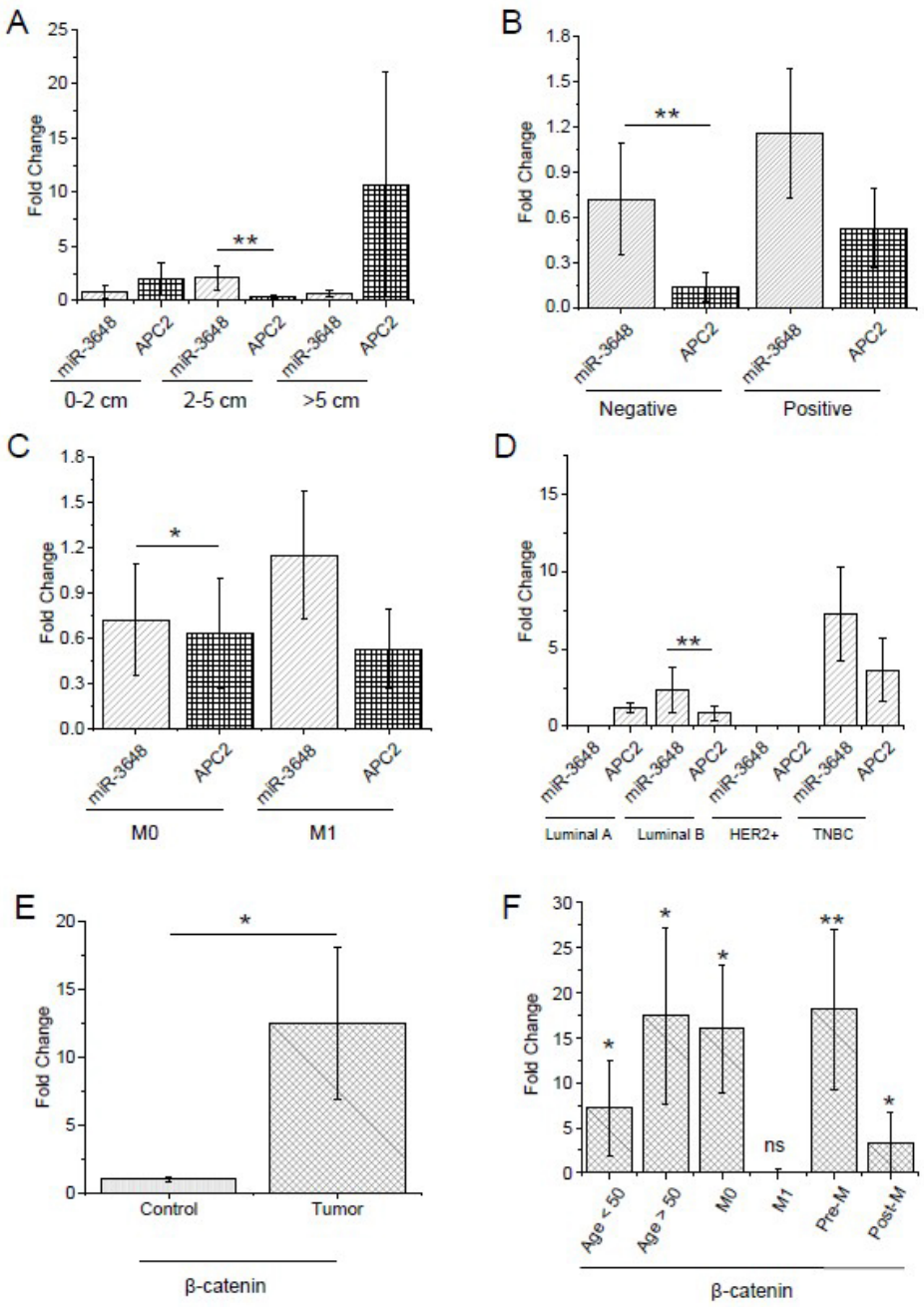

Fig. 2. Expressional association of *miR-3648* and *APC2* with TNM and molecular subtypes in breast cancer. (A) Increased expression of *miR-3648* and corresponding downregulation of *APC2* was observed in moderate sized tumors. (B) Decreased expression of *APC2* in tumors devoid of lymph node involvement and in (C) non-metastatic tumors. (D) Strong association of *miR-3648* higher expression and corresponding low expression of *APC2* in Luminal B subtype hints at ER & PR regulation in breast cancer. (E) Higher *β-catenin* expression in breast tumors and in (F) pre-metastatic tumors of patients of age <50 and pre-menopausal status. M0, no metastasis. M1, metastasis. TNBC, triple negative breast cancer. ER, Estrogen receptor. PR, progesterone receptor. $p<0.05$ was considered as statistically significant.

4. Discussion

Aberrations in the Wnt signaling pathway have been shown to be associated with multiple cancers (Anastas & Moon, 2013). Several studies have described that the alterations in Wnt/APC2 signaling pathway play roles in the process of carcinogenesis (Wen *et al.,* 2020). There have been quite a number of miRNAs reported to modulate integral components of the Wnt signaling pathway, therefore, contributing to the pathogenesis of various cancers (Tabnak *et al.,* 2021). Of these, *miR-3648* is one of the many human specific miRNAs identified and is of particular interest due to its minimum off-targeting (Hu *et al*, 2012). Previously, the dysregulation of *miR-3648* and *APC2* genes have been reported in different cancers, with *miR-3648* to be upregulated in bladder cancer, neuroblastoma, and prostate cancer (Xing, 2019; Saeki *et al*, 2018; Sun *et al,*2019). However, there is limited or no data regarding *miR-3648* and *APC2* altered gene expression in breast cancer. Hence, the current study was the first to explore the expression levels of *miR-3648* and *APC2* and their correlation and clinical relevance in breast cancer patients.

Expression profiling of *miR-3648* and *APC2* in breast cancer patients revealed the roles of these molecules in the process of carcinogenesis. Specifically, the transcript levels of both molecules were inversely regulated i.e., *miR-3648* showed slight downregulation in luminal type A whereas *APC2* was found to be upregulated, exhibiting enhanced tumor suppressor activity of *APC2* in the absence of *miR-3648* in patients with this intrinsic breast cancer subtype.

According to an already published report, almost 10% from total reported breast cancer cases are categorized as luminal B subtype (Parise & Caggiano, 2014). Interestingly, another more recent study reported higher prevalence of luminal B subtype in Pakistani population (Qadir *et al,* 2020). TNBC, being the most aggressive cancer is not easy to treat. In the current study cohort, however, no significant association of altered *miR-3648* and *APC2* expression could be established in TNBC subtype. According to previous studies, the change observed specifically in triple negative and luminal breast cancer subtypes may be due to imbalance of estrogen and progesterone hormones (Radojicic *et al,* 2011). It may possibly be attributed to the cross-talk between *APC2*, *miR-3648* and estrogen receptor alpha (ERα), progesterone receptor (*PR)* and growth factor receptor (*HER2)* in breast cancer (Daly *et al,* 2017). Consistent to these studies, *miR-3648* may be playing a very important role in regulating the expression of these receptors by regulating *APC2* activity but this aspect needs to be explored further.

APC2 gene is reported as a tumor suppressor gene. Literature review suggests the involvement of *APC2* gene in the *Wnt* Signaling, a pathway whose dysregulation leads to breast cancer (Daly *et al,* 2017). In ovarian homeostasis, *APC2* regulates the *Wnt* signaling control and acts as a tumor suppressor gene (Mohamed *et al,* 2019). Although, *APC2* gene dysregulation is well studied in breast cancer but using mouse mammary epithelium (Daly *et al,* 2017). Particularly, the expression profile of *APC2* gene in human breast cancer has yet to be examined in the context of its regulation by miRNA-3648. Hence, this study was the first to report the regulatory interplay between these two entities in breast cancer patients of Pakistan.

To examine the clinical relevance of *miR-3648* and *APC2* in breast cancer patients, parameters including age, tumor size, grade, stage, metastasis, nodal involvement and menopausal status were observed and compared. Among different age groups, *APC2* mRNA expression was significantly downregulated in younger patients with ages <50 years but accompanied with a slightly upregulated level of *miR-3648*. These findings endorsed the loss of *APC2* function in patients exhibiting early disease onset i.e., breast cancer, in a *miR-3648* dependent manner. Comparably, patients with age older than 50 years, showed no significant association between *APC2* and *miR-3648*. Furthermore, relatively higher expression of *β-catenin* due to downregulation of *APC2* was also observed in samples corresponding to early disease onset (Figure 2E and 2F). While 3'UTR of *β-catenin* mRNA is devoid of *miR-3648* binding sites, the observed dysregulation of *APC2* expression may in part be due to dysregulation of *miR-3648* and higher expression of *β-catenin* that was *APC2* dependent. These findings explain the role of *APC2* dysregulation mediated by *miR-3648* levels in breast cancer initiation, development and progression in Pakistani women.

5. Conclusion and Perspective

The current study concluded that *miR-3648* is relatively downregulated in Luminal A breast cancer subtype, with corresponding upregulation of *APC2* in these patients. Moreover, the transcript levels of both *miR-3648* and *APC2* are inversely regulated in breast cancer affected women who presented with early disease onset, pre-menopause, low tumor grade, early clinical stage, absence of nodal invasion and metastasis. This study affirmed the molecular interplay of these molecules in breast cancer development and progression.

Knowing that miRNAs follow an exclusive mechanism of directly targeting the transcripts and the proteins, thus, modulating their functions, an in-depth analysis of miRNA function is still required. The present study will add to the existing pool of information published for miRNAs that specifically regulate Wnt signaling pathway in cancer. Pertinently, extensive *in vitro* and *in vivo* research studies are required to establish the translational significance of *miR-3648* in conjunction with WNT signaling pathway in breast tumorigenesis. Such findings, if adequately furnished, can elucidate the usability of miRNAs as tools for prognosis as well as therapy for cancer patients in the future.

ACKNOWLEDGEMENTS

The authors of the study want to acknowledge all those breast cancer patients who participated in the study. This work was supported by Start-up Research Grant Program of Higher Education Commission of Pakistan (Grant #2069).

Conflict of Interest

The authors of the study have no conflict of interest to declare.

References

Anastas, J.N., & Moon, R.T. (2013) WNT signalling pathways as therapeutic targets in cancer. Nature Reviews Cancer, 13(**1**):11-26.

Castagnoli, L., Tagliabue, E., & Pupa, S.M. (2020) Inhibition of the Wnt signalling pathway: An avenue to control breast cancer aggressiveness. International Journal of Molecular Sciences, 21(**23**): 9069.

Daly, C.S., Shaw, P., Ordonez, L.D., Williams, G.T., Quist, J., Grigoriadis, A., Van Es, J.H., Clevers, H., Clarke, A.R., & Reed, K.R. (2017) Functional redundancy between Apc and Apc2 regulates tissue homeostasis and prevents tumorigenesis in murine mammary epithelium. Oncogene, 36(**13**):1793-1803.

Davey, M.G., Davies, M., Lowery, A.J., Miller, N., & Kerin, M.J. (2021) The role of microNRA as clinical biomarkers for breast cancer surgery and treatment. International Journal of Molecular Sciences, 22(**15**): 8290.

Di Vizio, D., Morello, M., Dudley, A.C., Schow, P.W., Adam, R.M., Morley, S., Mulholland, D., Rotinen, M., Hager, M.H., Insabato, L., Moses, M.A., Demichelis, F., Lisanti, M.P., Wu, H., Klagsbrun, M., Bhowmick, N.A., Rubin, M.A., D'Souza-Schorey, C., & Freeman, M.R. (2012) Large oncosomes in human prostate cancer tissues and in the circulation of mice with metastatic disease. The American Journal of Pathology, 181(**5**):1573-1584.

Emmadi, R., Canestrari, E., Arbieva, Z.H., Mu, W., Dai, Y., Frasor, J., & Wiley, E. (2015) Correlative Analysis of miRNA Expression and Oncotype Dx Recurrence Score in Estrogen Receptor Positive Breast Carcinomas. PloS One, 10(**12**): e0145346.

Hu, H.Y., He, L., Fominykh, K., Yan, Z., Guo, S., Zhang, X., Taylor, M.S., Tang, L., Li, J., Liu, J., Wang, W., Yu, H., & Khaitovich, P. (2012) Evolution of the human-specific microRNA miR-941. Nature Communication, 3: 1145.

Jafarzadeh, M., & Soltani, B.M. (2021) miRNA-Wnt signalling regulatory network in colorectal cancer. Journal of Biochemical and Molecular Toxicology, 35(**10**): e22883

Koni, M., Pinnarò, V., & Brizzi, M.F. (2020) The Wnt signalling pathway: A tailored target in cancer. International Journal of Molecular Sciences, 21(**20**): 7697.

López-Knowles, E., Zardawi, S.J., McNeil, C.M., Millar, E.K.A., Crea, P., Musgrove, E.A., Sutherland, R.L., & O'Toole, S.A. (2010) Cytoplasmic localization of beta-catenin is a marker of poor outcome in breast cancer patients. Cancer Epidemiology, Biomarkers & Prevention, 19(**1**):301-309.

Mittal, S., Kaur, H., Gautam, N., & Mantha, A.K. (2017) Biosensors for breast cancer diagnosis: A review of bioreceptors, biotransducers and signal amplification strategies. Biosensors and Bioelectronics, 88:217-231.

Mohamed, N.E., Hay, T., Reed, K.R., Smalley, M.J., & Clarke, A.R. (2019) APC2 is critical for ovarian WNT signalling control, fertility and tumour suppression. BMC Cancer, 19(**1**): 677.

Pai, S. G., Carneiro, B. A., Mota, J. M., Costa, R., Leite, C. A., Barroso-Sousa, R., Kaplan, J.B., Chae, Y.K., & Giles, F. J. (2017). Wnt/beta-catenin pathway: modulating anticancer immune response. *Journal of Hematology & Oncology*, 10(**1**): 101.

Parise, C.A., & Caggiano, V. (2014) Breast cancer survival defined by the ER/PR/HER2 subtypes and a surrogate classification according to tumor grade and immunohistochemical biomarkers. Journal of Cancer Epidemiology, 2014: 469251.

Petrovic, N., Nakashidz, I., & Nedeljovic, M. (2021) Breast cancer response to therapy: can microRNAs lead the way? Journal of Mammary Gland Biology and Neoplasia, 26(**2**):157-178.

Qadir, J., Riaz, S.K., Taj, K., Sattar, N., Sahar, N.E., Khan, J.S., Kayani, M.A., Haq, F., & Malik, M.F.A. (2021). Increased YAP1 expression is significantly associated with breast cancer progression, metastasis and poor survival. *Future Oncology*, 17**(21):**2725-2734.

Qadir, J., Riaz, S.K., Sahar, N., Aman, D., Khan, M.J., & Malik, M.F.A. (2020) Transcriptional elucidation of tumor necrosis factor-α-mediated nuclear factor- ϰB1 activation in breast cancer cohort of Pakistan. *Journal of Cancer Research and Therapeutics*, 16(**6**):1443-1448.

Radojicic, J., Zaravinos, A., Vrekoussis, T., Kafousi, M., Spandidos, D.A., & Stathopoulos, E.N. (2011) MicroRNA expression analysis in triple-negative (ER, PR and Her2/neu) breast cancer. Cell Cycle, 10(**3**):507-517.

Rashid, F., Awan, H.M., Shah, A., Chen, L., & Shan, G. (2017) Induction of miR-3648 upon ER stress and its regulatory role in cell proliferation. International Journal of Molecular Sciences, 18(**7**): 1375.

Rich, T.A., Woodson, A.H., Litton, J., & Arun, B. (2015) Hereditary breast cancer syndromes and genetic testing. Journal of Surgical Oncology, 111(**1**):66-80.

Saeki, N., Saito, A., Sugaya, Y., Anemia, M., & Sasaki, H. (2018) Indirect Down-regulation of Tumor-suppressive let-7 Family MicroRNAs by LMO1 in Neuroblastoma. Cancer Genomics & Proteomics, 15(**5**):413-420.

Sun, W., Li, S., Yu, Y., Jin, H., Xie, Q., Hua, H., Wang, S., Tian, Z., Zhang, H., Jiang, G., Huang, C., & Huang, H. (2019) MicroRNA-3648 is upregulated to suppress TCF21, resulting in promotion of invasion and metastasis of human bladder cancer. Molecular Therapy Nucleic Acids, 16:519-530.

Sung, H., Ferlay, J., Siegel, R.L., Laversanne, M., Soerjomataram, I., Jemal, A., & Bray, F. (2021) Global cancer statistics 2020: GLOBOCAN estimates of incidence and Mortality worldwide for 36 cancers in 185 countries. CA: A Cancer Journal for Clinicians, 71(**3**):209-249.

Tabnak, P., Mafakheri, A., Emsailpoor, Z. H., Kazemi, T., & Shekari, N. (2021). Regulatory interplay between microRNAs and WNT pathway in glioma. *Biomedicine & Pharmacotherapy*, 143: 112187.

Vannini, I., Fanini, F., & Fabbri, M. (2018) Emerging roles of microRNAs in cancer. Current Opinion in Genetics & Development, 48:128-133.

Wen, X., Wu, Y., Awadasseid, A., Tanaka, Y., & Zhang, W. (2020). New advances in canonical Wnt/β-catenin signaling in cancer. *Cancer Management and Research*, 12:6987-6998.

Xing, R. (2019) mir-3648 promotes prostate cancer cell proliferation by inhibiting adenomatous polyposis coli 2. Journal of Nanoscience and Nanotechnology, 19(**12**):7526-7531.

Yang, L., Tang, H., Kong, Y., Xie, X., Chen, J., Song, C., Liu, X., Ye, F., Li, N., Wang, N., & Xie, X. (2015) LGR5 Promotes Breast Cancer Progression and Maintains Stem-Like Cells Through Activation of Wnt/β-Catenin Signaling. Stem cells, 33(**10**):2913-2924.

Submitted: 25/08/2021
Revised: 20/11/2021
Accepted: 25/12/2021
DOI: 10.48129/kjs.15891

Kuwait J.Sci., Vol.50, No.(1A),January.2023,pp(198-211)

Lower feed and water consumptions and body weight in rats consuming aqueous extracts or ground *leptadenia pyrotechnica*

Bushra S. Alsahafi, Sawsan H. Mahassni*

Department of Biochemistry, Faculty of Science, King Abdualziz University, Jeddah, Saudi Arabia

**Corresponding author: sawsanmahassni@hotmail.com*

Abstract

Leptadenia pyrotechnica (Forssk.) Decne. (LP) is used in folk medicine for the treatment of different ailments. No published studies exist on the effects of ground LP while only one study exists on the effects of aqueous LP extract. Thus, this study is the first to investigate the difference between using ground or aqueous extract of LP on body weight parameters and consumptions of feed and water in young adult Wistar albino rats. Four groups (one rat of either sex per each group) were administered with 25%, 50% and 75% ground LP mixed with the regular feed for 7 days, while the control rats were given the regular diet. Five groups (two rats of either sex per each group) were orally gavage with 3, 9, 15 and 20 g LP extract/kg body weight, while the control group was gavage with water, daily for 14 days. Findings were compared with the control groups. The mean body weight loss and feed inefficiency ratio s for the ground LP groups were higher, leading to lower feed and water intakes. Rats that consumed 15 and 20 g LP extract/kg had higher mean body weight loss and feed inefficiency ratio and lower water and feed intakes for the first but not for the second week. Therefore, both forms of LP affect weights and consumptions of water and feed during the first week. Thus, while using LP for any medicinal or therapeutic uses in humans, any effects on weight or feed and water consumptions may last only for a week.

Keywords: Body weight; feed intake; *Leptadenia pyrotechnica*; rats; water intake.

1. Introduction

Worldwide, between 1980 and 2013, the prevalence of overweight and obesity increased with 2.1 billion individuals being overweight or obese (Ng *et al.,* 2014). According to the World Obesity Federation (2018), by the year 2025 around 3 billion people around the world will be overweight or obese. Obesity is associated with heightened inflammation, which leads to an increased risk for inflammatory and other types of diseases, such as cardiovascular diseases, atherosclerosis, type 2 diabetes, and some types of cancer.

Many plants and seeds have been used in folk and traditional medicinal systems as natural methods for the reduction of weight and lipid levels. There are several published studies on the effectiveness and safety of certain medicinal plants, seeds, and herbs for weight reduction, such as ginger (Nguyen, 2012), nigella sativa (Hasani-Ranjbar *et al.,* 2013), rhubarb, coptis, cassiae semen, and *citrus aurantium* (Zhou *et al.,* 2014), and for

reducing levels of lipids like *eurycoma longifolia* (Lim *et al.,* 2019).

Leptadenia pyrotechnica (Forssk.) Decne. (LP) belongs to the family of Asclepiadaceae, which is a desert plant that grows in the sandy regions in countries of the Arabian Gulf and equatorial regions of Asia and Africa. LP is a shrub that has many green branches with a height of 0.5 to 2.6 meters (Khasawneh *et al.,* 2015). All parts of the plant contain five major active components, which are alkaloids, flavonoids, tannins, saponins (Munazir *et al.,* 2015) and cardiac glycosides (Youssef *et al.,* 2009). The stem contains polyphenolic compounds (Preet & Chand 2018) along with some other chemical components, such as fatty acids, steroids and terpenes (Youssef *et al.,* 2007).

The decoction extract of the young stems of LP is used in Saudi Arabian local traditional medicine for the treatment of flu and as a tussive (Randa & Youssef, 2013), in India it is used to treat tuberculosis (Patel *et al.,* 2014), rheumatism and gout and in Pakistan it is used as an antihistaminic and expectorant (Bhabootra, 2016). In Sudan, the decoction extract of LP roots is used to treat constipation (Bhabootra, 2016), while in Yamen the stem paste is used for the treatment of wounds (Upadhyay *et al.,* 2007) and the sap of young steams is used for diabetes, eczema and other skin diseases (Katewa & Galav, 2006). None of these effects has been proven scientifically.

Only one previous study, done by us (Alsahafi & Mahassni, 2021), used the aqueous LP extract and it determined its effects on the immune system, daily body weights, and feed and water consumptions. After an extensive search in the internet, no other research studies using aqueously extracted or ground LP in animals or humans were found. In addition, there is only one study on the effect of the alcoholic extract of LP on weights. This study used LP alcoholic extracts on rats for two months finding no effects on weights (Soliman *et al.,* 2012). Since there are no published studies on the effectiveness of aqueous extracts or ground LP for weight reduction in humans and animals, this study aimed to determine the suitability of using LP (aqueously extracted or ground) to suppress appetite and/or to reduce body weight (BW) in rats.

2. Materials and methods

2.1 Rats and diet

Female and male Wistar albino rats used for this study were all provided with the regular rats feed ad libitum. The diet (Grain Silos and Flour Mills Organization, Jeddah, KSA) contained 20.0 % protein, 4.0 % fat, 5.0 % fiber, 6% ash, 1.0% vitamin mix (vitamin A, D and E), 3.50% mineral mix (calcium, phosphorus, cobalt, copper, iodine, iron, manganese, selenium and zinc), 0.25% choline chloride, and 60.25% cornstarch to complete the 100%. One kilogram of this diet provides 2850 kcal.

2.2 Preparation of the ground LP diets

Freshly collected young LP stems were washed with water and allowed to air dry. Then the stems were coarsely ground and mixed with the ground rat feed at three different

concentrations, as described below. Subsequently, these diets were repelleted, with the aid of a small amount of water, and allowed to air dry.

2.3 Collection of LP stems and preparation of the aqueous extract

Young LP stems were harvested from the Khulais governorate, Makkah, KSA, and then washed with distilled water. Subsequently 500 g of stems were boiled in 1 L of water for 5 minutes (Patel *et al.,* 2014). The hot water extract was filtered using cotton balls and it was allowed to air dry for two days. The extract resulted in a greenish brown colored semisolid precipitate. The evaporation of 30 ml of extract resulted in 18 g of semisolid precipitate.

The LP dose used for the rats was calculated (Reagan-Shaw *et al.,* 2008; Pandy, 2020) based on the previously used human dose (30 ml/day) (Patel *et al.,* 2014).

2.4 Study design

Fourteen female and fourteen males healthy Wistar albino rats, weighing between 170-250 g, were allowed to adapt to the laboratory for one week, after which, they were divided into two groups, with one administered ground LP while the other administered the aqueous LP extracts. For each group, the overall mean BW loss, percent relative overall BW loss, feed and water consumptions and feed inefficiency ratio (FIR) were calculated daily and weekly.

Three ground LP groups (LPG) and a control group (one female and one male per group) were administered, daily for one week, with ground LP at different concentrations (LPG 1: 25%, LPG 2: 50% and LPG 3: 75% ground LP mixed with the regular ground rat feed) while the control rats were administered with the regular feed.

Four LP aqueous extract groups (LPE) and a control group (two females and two males per group) were used. Based on the results of a previous unpublished acute toxicity study (Mahassni & Alsahafi, 2022), four different doses of dried LP extract, dissolved in 3 ml water, were orally gavaged (LPE 1: 3, LPE 2: 9, LPE 3: 15, and LPE 4: 20 g LP/kg rat BW) while the control was gavaged with 3 ml of water, daily for two weeks.

2.5 Statistical analysis

The Mega Stat statistical program (Version 9.4, Butler University, and Indianapolis, Indiana, USA) was used for the statistical analysis. The pairwise *t*-test was used for the significance testing between groups for all parameters. The statistical difference was considered significant for $P < 0.05$, highly significant for $P < 0.01$ and non-significant for $P \geq 0.05$.

3. Results and discussion

There are no previous research studies in humans or laboratory animals on the effects of ground LP and only one published study (Alsahafi & Mahassni, 2021), done in rats, on the effects of the aqueous LP extracts on BW gain/loss, feed and water consumptions, and FIR

in humans or laboratory animals. Therefore, this is the first study to determine these effects for different concentrations of ground LP, mixed with the regular diet of rats, and aqueous LP extract gavage to rats. In addition, this study is the first to investigate the differences in the effects of ground and aqueous LP extracts on weights and weight related parameters, and feed and water consumptions. Thus, we were unable to compare any of our evaluations and findings with previous studies.

The amounts of ground LP used were not based on any previous studies since it was never used before. This is also the case for the amount used for the extract, although a toxicity study using the extract was done previously by us (Mahassni & Alsahafi, 2022). In this unpublished study, the extract was found to be safe up to a dose of 40 g/kg body weight. Therefore, the highest dose used in the present study (20 g/kg) is well below the highest safe dose.

3.1 Daily physiological evaluation

The mean overall BW loss (Table 1) for the rats in the LPG 2 and 3 groups were significantly higher compared with the control. In addition, the mean percent relative overall BW loss was significantly higher for the LPG 1, 2 and 3 rats. The mean daily feed and water consumptions for the LPG 1, 2 and 3 groups were significantly lower compared with the respective control. Mean daily FIRs were significantly higher for the LPG 1, 2 and 3 groups compared with the control.

It is noteworthy that as the percent of LP mixed with the diet increases so does the BW loss, while the feed and water consumptions decrease and the feed inefficiency increases. Thus, the increased BW loss for the ground LP groups may be due to the reduced feed consumption resulting from the possibility that the diets with the higher amounts of LP were non-palatable. In fact, the rats showed signs of dislike for the diet since they scattered it in the cage instead of eating it. In addition, this was more apparent for the higher percent of LP. This reduced feed consumption may have subsequently resulted in a reduced need for water consumption as evidenced by the results.

The mean overall BW loss (Table 2) for the rats of the LPE 3 and 4 groups were significantly higher compared with the control. In addition, compared to the control, the mean percent relative overall BW loss was significantly higher for all LPE rats. Compared with the control, the mean daily feed consumptions for the LPE 2, 3, and 4 groups were significantly lower. The LPE 3 and 4 groups showed significantly lower mean water consumptions and significantly higher mean FIR compared with the respective controls.

Table 1. Physiological evaluation for the ground LP groups.

Parameter	Group	Mean±SD	P-value
Daily BW (g)	Control	198.00±19.80	
	LPG 1	174.50±20.51	0.285
	LPG 2	168.50±23.33	0.196
	LPG 3	171.00±9.90	0.229
Overall BW loss (g)	Control	2.00±2.83	
	LPG 1	20.00±22.63	0.330
	LPG 2	51.00±18.38	0.039*
	LPG 3	72.00 ±14.14	0.012*
Percent relative overall	Control	1.00±1.41	
BW loss (%)	LPG 1	19.50±0.71	0.010*
	LPG 2	25.00±5.66	0.004**
	LPG 3	34.00±5.66	0.001**
Daily feed consumption (g)	Control	22.00±0.71	
	LPG 1	19.50±1.41	0.001**
	LPG 2	10.00±2.83	0.000**
	LPG 3	11.10±1.41	0.000**
Daily water consumption	Control	20.50±3.54	
(ml)	LPG 1	13.50±0.71	0.026*
	LPG 2	12.00±2.83	0.021*
	LPG 3	8.50±0.71	0.005**
	Control	0.10±0.00	
Daily FIR	LPG 1	0.30±0.00	0.017*
	LPG 2	0.50±0.28	0.034*
	LPG 3	1.50±0.42	0.009**

LPG: ground LP group; *Significant; **highly significant

Table 2. Daily and weekly physiological evaluation for the extract groups.

Parameter	Group	Daily		Weekly			
				First week		Second week	
		Mean±SD	P-value	Mean±SD	P-value	Mean±SD	P-value
BW (g)	Control	208.50±21.21		207.00±23.23		209.75±19.72	
	LPE 1	200.00±18.79	0.626	200.00±20.51	0.620	200.50±18.72	0.592
	LPE 2	197.50± 26.89	0.518	190.75±14.57	0.276	194.75±25.12	0.388
	LPE 3	196.25±13.00	0.472	191.30±11.62	0.290	179.00±13.14	0.088
	LPE 4	195.00±32.69	0.429	207.50±29.86	1.000	199.30±36.14	0.543
BW loss (g)	Control	2.25±2.63		2.75±2.63		0.50±0.58	
	LPE 1	7.50±5.69	0.238	6.75±7.89	0.311	0.00±0.00	0.308
	LPE 2	8.25±4.79	0.103	10.50±1.73	0.060	0.00±0.00	0.308
	LPE 3	17.25±3.86	0.000**	15.25±7.41	0.005**	0.70±0.96	0.605
	LPE 4	15.57±6.55	0.000**	17.00±4.32	0.002**	0.50±1.00	1.000
Percent relative BW loss (%)	Control	1.00±1.15		1.25±1.19		0.24±0.28	
	LPE 1	4.50±3.70	0.029*	3.12±3.61	0.331	0.00±0.00	0.371
	LPE 2	4.80±1.71	0.021*	5.20±1.24	0.051	0.00±0.00	0.371
	LPE 3	8.25±1.71	0.000**	7.43±3.17	0.005**	0.41±0.53	0.542
	LPE 4	9.50±0.58	0.000**	7.97±2.96	0.002**	0.29±0.59	0.854
Feed consumption (g)	Control	23.50±2.31		26.00±5.77		28.50±8.66	
	LPE 1	22.00±1.15	0.323	26.00±1.15	1.000	25.00±2.31	0. 384
	LPE 2	20.00± 0.00	0.030*	26.50±1.73	0.849	26.00±3.46	0. 531
	LPE 3	19.50± 2.31	0.015*	22.50±2.89	0.197	23.00±5.77	0.220
	LPE 4	19.25±2.87	0.011*	24.00±4.62	0.452	23.50±5.20	0.179
Water consumption (ml)	Control	30.00± 2.31		29.00±1.15		25.50±2.89	
	LPE 1	28.50±0.58	0.582	26.00±2.31	0.179	26.00±1.73	0.876
	LPE 2	28.50±5.20	0.582	25.00±3.46	0.079	26.50±0.00	0.755
	LPE 3	20.00±2.31	0.002**	19.00±2.31	0.000**	22.00±6.93	0.285
	LPE 4	24.00±5.77	0.040*	24.00±4.62	0.033*	23.50±6.35	0.535
FIR	Control	0.06±0.04		0.10±0.10		0.02±0.02	
	LPE 1	0.08±0.03	0.514	0.25±0.29	0.464	0.00±0.00	0.262
	LPE 2	0.08±0.02	0.464	0.39±0.07	0.173	0.00±0.00	0.262
	LPE 3	0.15±0.05	0.012*	0.58±0.47	0.032*	0.03±0.03	0.818
	LPE 4	0.17±0.05	0.002**	0.74±0.28	0.006**	0.03±0.05	1.000

LPE: LP extract group; *Significant; **highly significant

3.2 Weekly physiological evaluation for the extract groups

As shown in (Figure 1), the weight loss for the first week for the LP groups increased with the increase of the extract dose, while for the second week the differences between the groups, compared to the control, were much smaller. The mean for all groups (including the control) for the first week was nearly the same as the mean for the LPE 2 group, while for the second week the mean for all groups was the same as for the control group. Therefore, the weight loss for the LP groups for the first week were higher than for the control, meaning the extract led to a reduction in the BWs of the rats. On the other hand,

the weight losses for the LP groups for the second week were negligible and nearly the same as for the control rats.

In the first week, the mean weekly BW loss and its mean percent and FIR (Table 2) were significantly higher for the LPE 3 and 4 groups compared with the respective controls. The mean water consumptions for the LPE 3 and 4 groups were significantly lower for the first week compared with the respective control.

When comparing the mean weekly BW loss and it's percent between the two weeks for all LP aqueous extract groups, shown in (Tables 3 and 4), it was revealed that there were significant decreases for the second week compared to the first week for LPE 2, 3 and **4.** As for the feed and water consumptions (Tables 5 and 6), there were no significant differences between the weeks for all groups. Comparing the mean weekly FIR between the two weeks for all extract groups (Table 7), there were a significant decrease for the LPE 2, 3 and 4 groups for the second week.

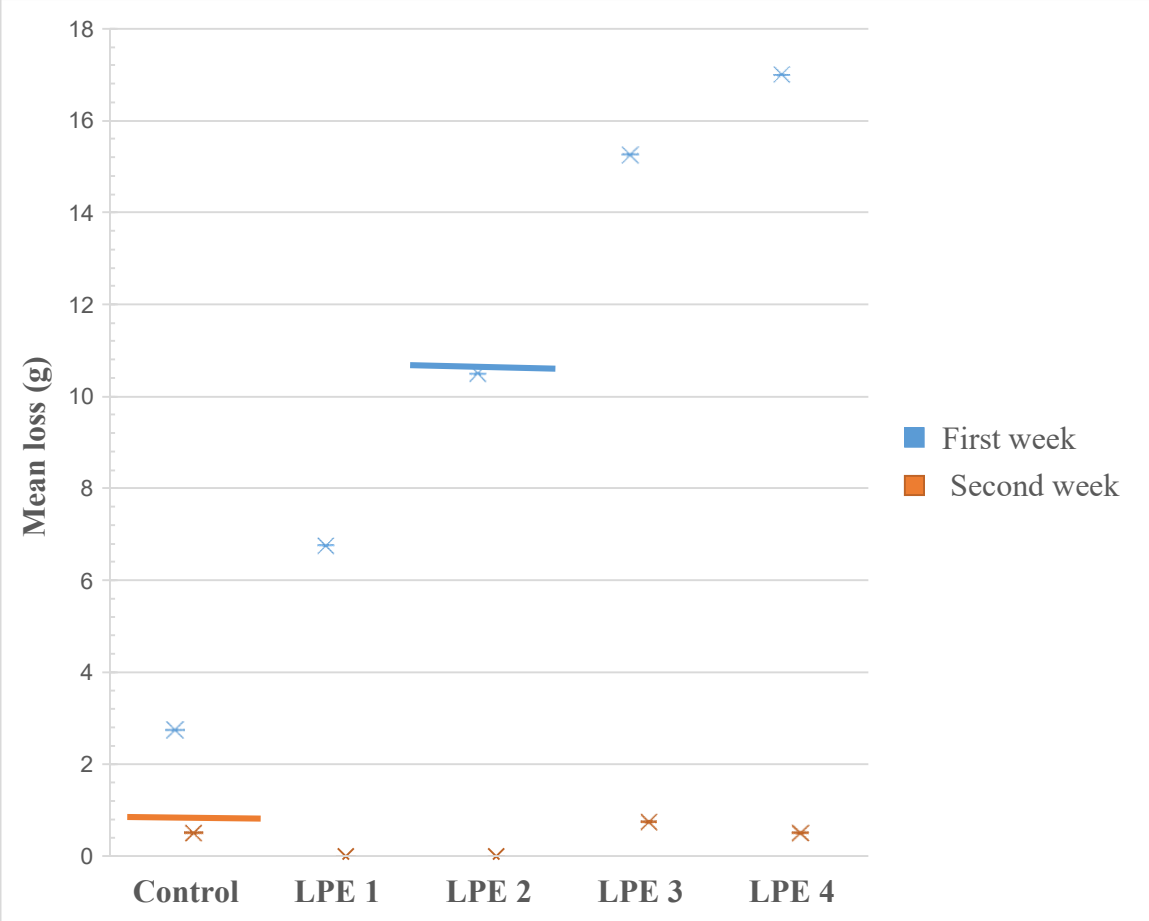

Fig. 1. Mean weekly BW loss (g) for each group for the first and second weeks (stars) and the overall mean for all groups for each week (lines).

Table 3. Comparing the weekly BW loss for the extract groups between the two weeks.

Group	Week	Weekly BW loss (g)		
		Mean±SD	Mean difference±SD	P-value
Control	First	2.75±2.63	2.25±2.75	0.200
	Second	0.50±0.58		
LPE 1	First	6.75±7.89	6.75±7.89	0.185
	Second	0.00±0.00		
LPE 2	First	10.50±1.73	10.50±1.73	0.001**
	Second	0.00±0.00		
LPE 3	First	15.25±7.41	14.50±8.34	0.040*
	Second	0.75±0.96		
LPE 4	First	17.00±4.32	16.50±4.12	0.004**
	Second	0.50±1.00		

LPE: LP extract group; *Significant; ** highly significant

Table 4. Comparing the percent relative weekly BW loss for the extract groups between the two weeks.

Group	Week	Percent relative weekly BW loss (%)		
		Mean±SD	Mean difference±SD	P-value
Control	First	1.25±1.19	1.00±1.47	0.266
	Second	0.24±0.28		
LPE 1	First	3.12±3.61	3.12±3.61	0.181
	Second	0.00±0.00		
LPE 2	First	5.20±1.24	5.20±1.24	0.003**
	Second	0.00±0.00		
LPE 3	First	7.43±3.17	6.95±3.69	0.032*
	Second	0.41±0.53		
LPE 4	First	7.97±2.96	7.67±2.518	0.008**
	Second	0.29±0.59		

LPE: LP extract group; *Significant; **highlysignificant

Table 5. Comparing the weekly feed consumption for the extract groups between the two weeks.

Group	Week	Weekly feed consumption (g)		
		Mean±SD	Mean difference±SD	P-value
Control	First	26.00±5.77	-2.50±2.88	0.181
	Second	28.50±8.66		
LPE 1	First	26.00±1.15	1.00±3.46	0.604
	Second	25.00±2.31		
LPE 2	First	26.50±1.73	0.50±1.73	0.604
	Second	26.00±3.46		
LPE 3	First	22.50±2.89	-0.50±8.66	0.915
	Second	23.00±5.77		
LPE 4	First	24.00±4.62	0.50±9.81	0.925
	Second	23.50±5.20		

LPE: LP extract group

Table 6. Comparing the weekly water consumption for the extract groups between the two weeks.

Group	Week	Weekly water consumption (g)		
		Mean±SD	Mean difference±SD	P-value
Control	First	29.00±1.15	3.50±3.10	0.109
	Second	25.50±2.89		
LPE 1	First	26.00±2.31	0.00±2.30	1.000
	Second	26.00±1.73		
LPE 2	First	25.00±3.46	-1.50±3.87	0.495
	Second	26.50±0.00		
LPE 3	First	19.00±2.31	-3.00±9.23	0.562
	Second	22.00±6.93		
LPE 4	First	24.00±4.62	0.50±7.85	0.906
	Second	23.50±6.35		

LPE: LP extract group

Table 7. Comparing the weekly FIR for the extract groups between the two weeks.

Group	Week	Weekly FIR		
		Mean±SD	Mean difference±SD	P-value
Control	First	0.10±0.10	0.08±0.10	0.239
	Second	0.02±0.02		
LPE 1	First	0.25±0.29	0.25±0.29	0.183
	Second	0.00±0.00		
LPE 2	First	0.39±0.07	0.39 ±0.07	0.001**
	Second	0.00±0.00		
LPE 3	First	0.58±0.47	0.53±0.32	0.044*
	Second	0.03±0.03		
LPE 4	First	0.74±0.28	0.71±0.29	0.016*
	Second	0.03±0.05		

LPE: LP extract group; *Significant; **highly significant

Results of the present study showed that both the ground and extract LP diets resulted in higher overall and percent relative body weight losses for the groups, which was linked to lower feed and water consumptions and higher feed inefficiency ratios. These effects increased as the amount of ground or LP extract administered increased. In addition, these effects for the LP extract were apparent for the first week only, but not for the second week. Therefore, any effects of LP on weight might only be during the first week.

The significant decrease in BW, feed intake and significant increase in weight loss in the rats may be due to the phenolic compounds, such as tannin, that are naturally present in vegetables and plants (Manzoor *et al.,* 2021) including LP (Munazir *et al.,* 2015) and has been shown to reduce weight and feed intakes in rats (Chung *et al.,* 1998; Nakamura *et al.,* 2001; Manzoor *et al.,* 2021). This is in addition to the previously mentioned undesirability of the feed mixed with the LP.

As stated above, there are no previous studies that can be compared with the current results with the exception for the previously mentioned study on BW using the alcoholic extract and on BW gain/loss, feed and water consumptions and FIR using aqueous LP extracts. Thus, studies on medicinal plants, other than LP, and seeds are compared here. The current results disagree with a previous study in rats consuming ground *lepidium sativum* seeds mixed with the regular diet for 39 days that showed higher overall BW gain percent and lower consumed feed and water compared to the control (Mahassni & Nabulsi, 2020). Moreover, a previous study (Gauthaman *et al.,* 2003) using different concentrations of the puncturevine plant extract on male rats for two months showed an increase in BW. A previous study (Mahassni & Khudauardi, 2017) also using an aqueous extract of *lepidium sativum* seeds on mice for 19-21 days showed an increase in BW. An increase in

the body weights of Wistar rats following oral administration of methanol extract of *ganoderma lucidum* for 21 days was found in a previously study (Shamaki *et al.,* 2017).

On the other hand, the present findings agree with our previous study (Alsahafi & Mahassni, 2021) on the aqueous LP extract gavaged to rats for three weeks that resulted in a significantly lower BW and feed and water intakes and significantly higher BW loss and FIR. Another study in agreement with the current findings is a study (Eddouks *et al.,* 2005) on aqueouse *lepidium sativum* extract administered for two weeks to healthy rats, which showed lower BW and feed intake. Additionally, findings of a previous study (Alsoodeeri, *et al.,* 2020) in rats administered with *cinnamomum cassia* for 30 days showed a reduction in BW gain, feed intake and feed efficiency ratio. A previous study (Manal *et al.,* 2016) using ethanol and ethyl acetate extracts of *maerua psuedopetalosa* administered to Wistar rats for a week also showed a reduction in BW.

4. Conclusions

The ground and LP extracts resulted in higher overall and percent relative BW losses for the groups, which was linked to lower feed and water consumptions and higher FIRs. These effects increased as the amount of ground or LP extract administered increased. In addition, the effects for the LP extract were apparent for the first week only, but not for the second week. Therefore, any effects of LP on weight might only be during the first week. The same may be expected to happen in humans. Thus, while using LP for any medicinal or therapeutic uses, any effects on weight or feed and water consumptions may last only for the first week of usage.

References

Alsahafi, B. S. & Mahassni, S. H. (2021) *Leptadenia Pyrotechnica* Aqueous Extract Suppresses Innate Immunity and Enhances Adaptive Immunity in Rats. International Journal of Pharmaceutical and Phytopharmacological Research*,* 11(5): 25-33.

Alsoodeeri, F. N., Alqabbani, H. M. & Aldossari, N. M. (2020). Effects of Cinnamon (*Cinnamomum cassia*) Consumption on Serum Lipid Profiles in Albino Rats. Journal of lipids, 2020: 8469830.

Bhabootra, R. (2016). Important uses of *Leptadenia pyrotechnica* of Bikaner. International Journal of Advances in Science Engineering and Technology*,* 4 (4): 26-28.

Chung, K.T., T. Y. Wong, I.W. Cheng, Y. W. Huang & Y. Lin (1998). Tannins and Human Health: A Review. Critical reviews in food science and nutrition. 38(6): 421-464.

Eddouks, M., Maghrani, M., Zeggwagh, N. A. & Michel, J. B. (2005). Study of the hypoglycaemic activity of *Lepidium sativum* L. aqueous extract in normal and diabetic rats. Journal of Ethnopharmacology, 97(2): 391-395.

Gauthaman, K., Ganesan, A. P. & Prasad, R. N. V. (2003). Sexual effects of puncturevine (*Tribulus terrestris*) extract (protodioscin): an evaluation using a rat model. The Journal of Alternative and Complementary Medicine, 9 (2): 257-265.

Hasani-Ranjbar, S., Jouyandeh, Z. & Abdollahi, M. (2013). A systematic review of anti-obesity medicinal plants-an update. Journal of Diabetes and Metabolic Disorders, 12 (1): 1-10.

Katewa, S. S. & Galav, P. K. (2006). Additions to the traditional folk herbal medicines from Shekhawati region of Rajasthan. Indian Journal of Traditional Knowledge, 5 (4): 494-500.

Khasawneh, M. A., Koch, A., Elwy, H. M., Hamza, A. A. & Schneider-Stock, R. (2015). *Leptadenia pyrotechnica* induces p53-dependent apoptosis in colon cancer cells. Natural Products Chemistry and Research, 3 (3): 1-8.

Lim, P. J., Gan, C. S. & Yusof, A. (2019). Lipid lowering effect of *Eurycoma longifolia* Jack aqueous root extract in hepatocytes. Kuwait Journal of Science, 46 (2): 52:58.

Mahassni, S. H. & Alsahafi, B. S. (2021). A pilot study: ground and aqueous Extract of *leptadenia Pyrotechnica* modulate the immune system affecting white blood cell counts and increasing red blood cell counts. Jordan Journal of Biology Sciences, 15(3): 413-421.

Mahassni, S. H. & Khudauardi, E. R. (2017). A pilot study: The effects of an aqueous extract of Lepidium sativum seeds on levels of immune cells and body and organs weights in Mice. Journal of Ayurvedic and Herbal Medicine, 3(1), 27-32.

Mahassni, S. H. & Nabulsi, K. K. (2020). Ground *Lepidium sativum* Seeds Affect Immune System Cells, IgM Levels, BWs, and Hematology in Rats. Journal of Pharmaceutical Negative Results, 11(1):35-41.

Manal, A. I., El Bushra, E. & Ahmed, A. G. (2016). Changes in body weight and serum biochemical parameters of wistar rats orally dosed with *Maerua pseudopetalosa* (gilg and bened.) De wolf tuber extracts. European Journal of Research in Medical Sciences, 4(1): 52-59.

Manzoor, F., Nisa, M. N., Hussain, H. A., Ahmad, N. & Umbreen, H. (2021). Effect of chestnut hydrolysable tannin on weight management and ovarian histopathology of healthy female rats. Journal of Animal & Plant Sciences, 31 (3): 831-840.

Munazir, M., Qureshi, R. & Munir, M. (2015). Preliminary phytochemical screening of roots and aerial parts of *Leptadenia pyrotechnica*. Pakistan Journal of Botany, 47 (2): 659-664.

Ng, Marie, Fleming, T., Robinson M., Thomson B., Graetz N., Margono, C., *et al.* (2014). Global, regional, and national prevalence of overweight and obesity in children and adults during 1980–2013: a systematic analysis for the Global Burden of Disease Study 2013. The lancet, 384 (9945): 766-781.

Nguyen, L. H. (2012). Does the use of ginger extract effectively help patient with obesity loses weight? M.D Thesis, Philadelphia College of Osteopathic Medicine, Philadelphia.

Nakamura, Y., A. Kaihara, K. Yoshii, Y. Tsumura, S. Ishimitsu & Y. Tonogai (2001). Effects of the Oral Administration of Green Tea Polyphenol and Tannic Acid on Serum and Hepatic Lipid Contents and Fecal Steroid Excretion in Rats. Journal Health of Sciences, 47(2):107-117.

Pandy, V. (2020). A Simple Method for Animal Dose Calculation in Preclinical Research. Pharmacology and Toxicology, 8 (3): 1-2

Patel, S. K., Desai, P. R. & Pandey, V. B. (2014). Ethnomedicinal plants used by the tribal in Bhiloda taluka of Saba kantha district, Gujarat. Indian Journal of Advances in Plant Research, 1(6): 33-36.

Preet, R. & Chand Gupta, R. (2018). Simultaneous Determination of Phenolic Compounds in *Leptadenia pyrotechnica* (Forssk.) Decne. by Using High-Performance Liquid Chromatography (HPLC-DAD-UV). Advances in Pharmacological Sciences, 3: 1-4.

Randa, S. & Youssef, A. (2013). Medicinal and non-medicinal uses of some plants found in the middle region of Saudi Arabia. Journal of Medicinal Plants Research, 7(34): 2501-2517.

Reagan-Shaw, S., Nihal, M. & Ahmad, N. (2008). Dose translation from animal to human studies revisited. Federation of American Societies for Experimental Biology, 22 (3): 659-661

Shamaki, B. U., Sandabe, U. K., Abdulrahaman, F. I., Ogbe, A. O. & Hassan, Z. I. (2017). Toxicity studies and body weights changes in Wistar rats following oral administration of methanol extract from indigenous ganoderma sp. Nigeria. Med Crave Online Journal of Biology and Medicine, 1(5): 138-141.

Soliman, G. A., Donia, A. M., Awaad, A. S., Alqasoumi, S.I. & Yusufoglu, H. (2012). Effect of *Emex spinosa*, *Leptadenia pyrotechnica*, *Haloxylon salicornicum* and *Ochradenus baccatus* extracts on the reproductive organs of adult male rats. Pharmaceutical Biology, 50 (1):105-112.

Upadhyay, B., Roy, S. & Kumar, A. (2007). Traditional uses of medicinal plants among the rural communities of Churu district in the Thar Desert, India. Journal of Ethnopharmacology, 113(3): 387-399.

World Obesity Federation (2018). Obesity and Non-Communicable Diseases report. https://www.who.int/ncds/governance/high-levelcommission/Bangkok-Association-of-Regenerative-and-theStudy-of-Obesity.pdf

Youssef Moustafa, A. M, Khodair, A. I & Mahmoud, A. S. (2007). Phytochemical Investigation and Toxicological studies of lipid constituents isolated from *Leptadenia Pyrotechnic.* Journal of Pharmacology and Toxicology, 2 (6): 681-697.

Youssef Moustafa, A. M., Khodair, A. I. & Saleh, M. A. (2009). Structural elucidation and evaluation of toxicity and antitumor activity of cardiac glycosides isolated from *Leptadenia pyrotechnica*. Pharmaceutical Biology, 47 (9): 826-834.

Zhou, Q., Chang, B., Chen, X. Y., Zhou, S. P., Zhen, Z., Zhang, L. L. & Tong, X. L. (2014). Chinese herbal medicine for obesity: a randomized, double-blinded, multicenter, prospective trial. The American journal of Chinese medicine, 42 (2): 1345-1356.

Submitted: 21/08/2021
Revised: 03/02/2022
Accepted: 07/02/2022
DOI: 10.48129/kjs.14617

Mass attenuation coefficient, stopping power, and penetrating distance calculations via Monte Carlo simulations for cell membranes

Yiğit Ali Üncü[1], Gençay Sevim[2], Osman Ağar[3], Hasan Özdoğan[4,*]

[1]*Dept. of Biomedical Equipment Technology, Akdeniz University, Vocational School of Technical Sciences, 07070, Antalya, Turkey*

[2]*Dept. of Medical Imaging Techniques, Ufuk University, Vocational School of Health Services, 06805, Ankara, Turkey*

[3]*Dept. of Medical Imaging Techniques, Karamanoğlu Mehmetbey University, Vocational School of Health Services, 70100, Karaman, Turkey*

[4]*Dept. of Medical Imaging Techniques, Antalya Bilim University, Vocational School of Health Services, 07190, Antalya, Turkey*

[*]*Corresponding author: hasan.ozdogan@antalya.edu.tr*

Abstract

The Monte Carlo (MC) method is a computer simulation that is widely used in different disciplines including physics, biology, biophysics, medical imaging, biomedical engineering, etc. In addition, MC method is often used to simulate the interaction of radiation with cells, tissues, and the environment. In the present study, mass attenuation coefficient, stopping power, and penetrating distance calculations were performed for cell membranes having an approximately 60-100Å thickness. These calculations have been done for lipid bilayer structure of cell membrane via MC techniques employing two of the most known computer-aided calculation and simulation software which are MC methods such as SRIM-2013 (The Stopping and Range of Ions in Matter) and MCNPv6 (Monte Carlo N-Particle) with XCOM software. Stopping power and penetrating distance calculations were obtained using SRIM-2013. Also, both XCOM software and MCNPv6 simulation code were used to obtain photon interaction parameters within the energy range of 0.01 – 10000keV. Obtained all results from different codes have been visualized by graphing for evaluation.

Keywords: Cell membrane; mass attenuation coefficient; penetrating distance; stopping power; simulation software

1. Introduction

The cell has a plasma membrane on the surface of its cytoplasm. The cell membrane (plasma membrane) is a structure that surrounds the cell and is located between the cytosol and the extracellular environment (Korn, 1968; Stryer, 1995). The main function of cell membrane is to

set the boundaries of cell and to separate the parts of cell. While separating the inner and outer environments of the cells, membranes also control the entry and exit of certain substances for the cell. Various nutrients, gases, water, and other substances enter and exit the cell. Since membranes have different permeability to different substances, each substance enters and leaves the cell in different ways. The cells generally receive electrical and chemical signals from the environment. The cell membrane is responsible for receiving signals and responding to them. The molecules or structures required for these functions are located in the structures of membrane (Brady *et al.,* 2005; Félix, 2014; Grecco *et al*., 2011; Korn, 1968).

Using an electron microscope, it was seen that they consist of 3 layers in their chemical structure. The upper and lower layers consist of hydrophilic groups, whereas the middle layer consists of hydrophobic groups. This structure is also the same in the plasma membrane that limits the cell and in other organelle membranes. For this reason, the term "unit membrane" is used as a general term (Félix, 2014; Korn, 1968; Stryer, 1995).

The cell membrane consists of molecules having lipid content such as phospholipids, glycolipids, cholesterol, proteins (Membrane proteins), and carbohydrates (Glycocalyx). Phospholipids made of glycerol are called phosphoglycerides. A phosphoglyceride contains glycerol, two fatty acid chains, and phosphorylated alcohol (Félix, 2014).

Membrane proteins forming the basic structure of biological membranes such as lipid bi-membranes fulfill the most specific functions in membranes. Therefore, proteins are molecules that give the membrane its characteristic structure. Membrane properties vary depending on the amount and type of proteins. Most plasma membranes are 50% lipid and 50% protein by weight, with the carbohydrate portions of glycolipids and glycoproteins constituting 5 to 10% of the membrane mass. Since proteins are much larger than lipids, this ratio is equivalent to approximately one protein molecule for every 50 to 100 lipid molecules (Lodish *et al.,* 2000). In addition, proteins participating in the structure of the cell membrane play a role as integral proteins embedded in phospholipid layers or as peripheral proteins attached to the inner or outer surface of these layers (Brady *et al.,* 2005; Hung & Link, 2011; Korn, 1968).

In the present study, the mass attenuation coefficients and stopping power of cell membrane were calculated by using Monte Carlo Simulation methods. In the calculations, SRIM-2013 (The Stopping and Range of Ions in Matter) (Ziegler *et al,.* 2010) and MCNPv6 (Monte Carlo N-Particle) (Goorley *et al.,* 2013) codes were used. The calculation results have been compared and the results have been graphed for better visual understanding.

2. Material and Methods

In the present study, stopping power, penetrating distance, and mass attenuation coefficients were calculated for cell membranes by using MC simulation methods. SRIM-2013 was used for the stopping power and penetrating distance, whereas MCNPv6 and XCOM were used for the mass attenuation coefficient. MC method is a useful analysis tool and is widely used in different disciplines including physics, biology, biophysics, medical imaging, biomedical engineering, etc. The application of MC method to a problem is based on the idea that the problem is simulated by

using random numbers and the parameter to be calculated is approximated by making use of the results obtained from these simulations.

It is well-known that cell membranes consist of 50% lipid and 50% protein by weight and these rates vary at different points of the plasma membrane (density = 1.12 g/cm^3) (Lodish *et al.,* 2000). The elemental components of the cell membrane, which are quite complex and different in every cell, make exact modeling difficult. Considering this difficulty and the 50% lipid concentration of the membrane, the elemental component of the phospholipid bilayer was used in modeling the phospholipid bilayer structure of the cell membrane (Table 1). For this purpose, the average element amount of modeled phospholipid was calculated by using different phospholipid derivatives (Mashaghi *et al.,* 2012; Ulmschneider *et al*., 2005; Yang, 2014). This average amount of elements was determined separately for both the hydrophilic head and hydrophobic tail of the phospholipid. The average chemical structure was used in determining the amount of elements in each structure (Ulmschneider *et al.i* 2005).

Table 1. Average elemental component of modelled phospholipid bilayer cell membrane

Lipid Structure	Element	Number of Element per unit
Hydrophilic Head (0.7 – 1 nm)	Hydrogen	18
	Oxygen	8
	Carbon	10
	Nitrogen	1
	Phosphor	1
Hydrophobic Tail (1.5 – 2 nm)	Hydrogen	66
	Carbon	36
	Oxygen	2
Sum of Phospholipid Bilayer	Hydrogen	168
	Oxygen	20
	Carbon	92
	Nitrogen	2
	Phosphor	2

SRIM-2013 code was used in order to calculate the penetrating distance and stopping power using the Equations (1-10). Lambert-Beer law equation is presented in Equation (1),

$$I = I_0 e^{-\mu x} \quad (1)$$

μ (cm^{-1}) is the linear attenuation coefficient for a material, where I is the attenuated photon intensity, I_o is non-attenuated photon intensity, and x (cm) is the thickness. The following equation for the linear attenuation coefficient is obtained by mathematically rearranging the Equation (2);

$$\mu = \frac{1}{x} \ln(I_0/I) \quad (2)$$

Using the density of target materials (ρ), the mass attenuation coefficients are calculated using Equation (3).

$$\mu/\rho = \frac{1}{\rho x} \ln(I_0/I) \quad (3)$$

As charged particles move through the material, they perform many interactions before consuming all their kinetic energy. During these interactions, the charged particle' trajectory of motion may vary such as elastic and inelastic collisions. It can lose some of its energy by transferring it to the collision loss or radiative loss as photons. The loss of energy of a charged particle trying to move through a material depends on the characteristic properties of the material as the particle.

The linear stopping power (*-dE/dx*) is the rate of energy loss per unit length of motion of a charged particle through matter. Stopping power is a characteristic feature peculiar to the material. Average energy loss per unit motion length of charged particles is $dE/d\ell$. For a certain energy loss, the cross-section expression σ_{ni} and the energy loss ΔE_{ni} are expressed as shown in Equation (4) and the sum of all possible *i* states (Podgorsak, 2016).

$$-\frac{\mathrm{d}E}{\mathrm{d}\ell} = \sum_i N_i \sum_n \Delta E_{ni} \sigma_{ni} \quad (4)$$

Where, N_i refers to the atomic density and can be valued in two different ways due to the possible sizes of i. First, it is the number of atoms per unit volume that allows the $-dE/d\ell$ expression to be defined as the energy loss per unit movement length in the material, in other words, linear stopping power *-dE/dx.* The typical unit of linear stopping power expression is MeV/cm, although *keV/μm* is also used in some cases. Then, it is the number of atoms per unit mass that allows the expression dE/dl to be defined as the energy loss per unit g/cm^2 in the material, the mass stopping power $S = -(1/\rho)\mathrm{dE/dx}$. The typical unit of mass stopping power expression is *MeV.cm2/g* (Podgorsak, 2016).

Regarding the charged particle interaction, there are two types of stopping forces known as radiative (nuclear) stopping power and collision (electronic or ionized) stopping power. Radiation stopping power is the stopping power arising from the Coulomb interactions between atomic nuclei of matter and charged particles. In addition, the charged particles such as electrons and positrons experience significant energy loss through these interactions, commonly referred as Bremsstrahlung interactions. For heavily charged particles such as protons and alpha, the radiative stopping power loss is negligible when compared to the collision stopping power. The power to stop the collision is the stopping power created by the Coulomb interactions between the orbital electrons of matter and the charged particle. Both lightly and heavily charged particles experience

this interaction that causes ionization or excitation in matter atoms as a result of the energy transfer between charged particles and orbital electrons.

The total stopping power for a charged particle having kinetic energy E_K moving through a material with the atomic number Z, which is S_{total}, is generally the sum of radiative stopping power $S_{radiative}$ and collision stopping power $S_{collision}$, as expressed in Equation (5).

$$S_{total} = S_{radiative} + S_{collision} \tag{5}$$

The collision stopping power can be expressed as in Equation (6), divided into two subcomponents as $S_{collision}^{soft}$ and $S_{\text{collision}}^{\text{hard}}$.

$$S_{collision} = S_{collision}^{soft} + S_{collision}^{hard} \tag{6}$$

By combining Equations (5-6), the total stopping power can be expressed as in Equation (7).

$$S_{total} = S_{radiative} + S_{collision} = S_{radiative} + S_{collision}^{soft} + S_{collision}^{hard} \tag{7}$$

Energy transfer from energetic heavily charged particles to matter occurs mainly through Coulomb interactions (collision or electronic loss) between the nucleus and orbital electrons of charged particles. Inelastic Coulomb interactions (radiation loss) between heavily charged particles and nuclei of matter atoms are negligible and, therefore, they are ignored (Podgorsak, 2016).

The total collision stopping power is expressed as the sum of soft and hard collisions in Equation (8),

$$\begin{aligned} S_{collision} &= S_{collision}^{soft} + S_{collision}^{hard} \\ &= 2\pi \frac{ZN_A}{A}\left(\frac{e^2}{4\pi\varepsilon_0}\right)^2 \frac{z^2}{m_e c^2 \beta^2} \times \left\{ ln\frac{2m_e c^2 \beta^2 \eta}{(1-\beta^2)I^2} + ln\frac{2m_e c^2 \beta^2}{(1-\beta^2)\eta} - 2\beta^2 \right\} \\ &= 4\pi \frac{ZN_A}{A}\left(\frac{c^2}{4\pi\varepsilon_0}\right)^2 \frac{z^2}{m_e e^2 \beta^2}\left\{ ln\frac{2m_e c^2}{I} + ln\frac{\beta^2}{1-\beta^2} - \beta^2 \right\} \\ &= C_0 \frac{z^2}{A\beta^2} Z\left\{ ln\frac{2m_e c^2}{I} + ln\frac{\beta^2}{1-\beta^2} - \beta^2 \right\} \end{aligned} \tag{8}$$

where, η refers to the energy separating the soft and hard collisions that would disappear in the final state of the equation; C_0, r_e refers to the collision stopping power constant shown by Equation (9), where r_e is the classical electron radius $(r_e = e^2/(4\pi\varepsilon_0 m_e c^2) = 2.818\, fm)$ (Podgorsak, 2016).

$$C_0 = 4\pi N_A \left(\frac{e^2}{4\pi\varepsilon_0}\right)^2 \frac{1}{m_e c^2} = 4\pi N_A r_e^2 m_e c^2 = 0{,}3071 \text{ MeV.cm}^2/\text{mol} \quad (9)$$

The average atomic stopping power of a mixture will be expressed by Equation (10) (Evans, 1955).

$$(\mathrm{S_n})_{\mathrm{av}} = \frac{(ds)_0}{(ds)_{\mathrm{av}}}\frac{N_0}{N} = \frac{B_{\mathrm{av}}}{B_0} = n_1\mathrm{S}_1 + n_2\mathrm{S}_2 + n_3\mathrm{S}_3 + \cdots \quad (10)$$

where, N refers to the number of atoms in one cm^3 of the mixture or compound selected as the stopping; values of n_1, n_2, n_3,… ; S_1, S_2, S_3,… express the atomic ratios of atoms having stopping power values in the material.

SRIM-2013 provides many calculations including range, collision, penetration, stopping powers, and straggling distributions for any ion. In the present study, using Ion Stopping and Range Tables application in the SRIM-2013 package for each ion, stopping powers of a cell membrane and ions' penetration distances were theoretically calculated. Lipid membrane structure was modelled as an elemental target and 5 different ions were used at 0.01 – 10000 keV. The reason for modelling such a wide range of energy is to be able to derive a wide scale of the stopping power for the cell membrane and to be able to determine the minimum energies of ions that can penetrate the phospholipid membrane.

MCNPv6, which uses the Monte Carlo technique, is a program that can simulate cases such as particle-matter interaction and nuclear reactions, in which it is not possible to get exact and accurate results by using analytical algorithms. It is a general Monte Carlo transport code that solves the time-dependent continuous energy transfer of radiation such as neutron, photon, electrons in three-dimensional geometry. In MCNPv6, the input file contains the information of geometry description, description of materials and selection of cross-section evaluations, location, and properties of a radiation source, type of desired response or tasks, and variance reduction techniques.

The geometry used in MCNPv6 calculations is presented in Figure 1. In this study, the simulations include a point photon source placed in a cylinder (r=0.5 cm; h=1cm) which emits mono-energetic photons directed in a parallel manner toward a cylindrical sample 100 cm away from isotropic point source to calculate the counts of photons entering the detector per $MeVcm^2s^{-1}$. All the components of the problem geometry were surrounded by a vacuum sphere to avoid interactions in materials other than the sample. The "F4" tally gives the average photon flux in the detection field. In, the number of histories (NPS variable) used in the MCNPv6 simulations is 5.10^6. The test of the recent MCNPX simulation has been implemented by using the D00205ALLCP03 MCNPXDATA package is included of DLC-200/MCNPDATA cross-section lib.s. Also, Population Control Methods have been employed as variance reduction in MCNP simulations. These methods artificially increase/decrease the number of particles in spatial or energy regions that are important/unimportant to the tally score. The weight cutoff has been used

for variance reduction. In this study, photons with energies below 1 keV are neglected. All the calculations were performed using computer hardware (Intel Core I7 CPU 2.6 GHz). First, calculations were performed in the absence of a cell membrane, which gives us I_0. Then, the cell membrane was placed between the source and the detector and the flux through the membrane was calculated (I). After the calculations, the Beer-Lambert formula was used in order to obtain the mass attenuation coefficients.

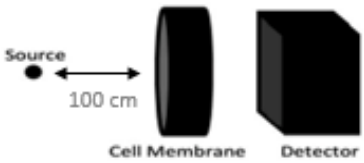

Fig. 1. The geometry which is used in MCNPv6 simulations

3. Results

Using Monte Carlo Simulation methods, the stopping power, penetrating distance, and mass attenuation coefficients of cell membrane were calculated in this paper. Stopping power and penetrating distance calculations, which were obtained using SRIM-2013, are illustrated in Figures 2 and 3. Moreover, the minimum projectile energy required to pass through the membrane is presented in Tables 2 and 3. Mass attenuation coefficients of the cell membrane are shown in Figure 4. Stopping power calculations versus projectile energy is shown in Figure 2. Alpha and helium-3 have the highest stopping power results, followed by tritium, deuterium, and proton, respectively. The charge of the projectile particle is directly proportional to the stopping power.

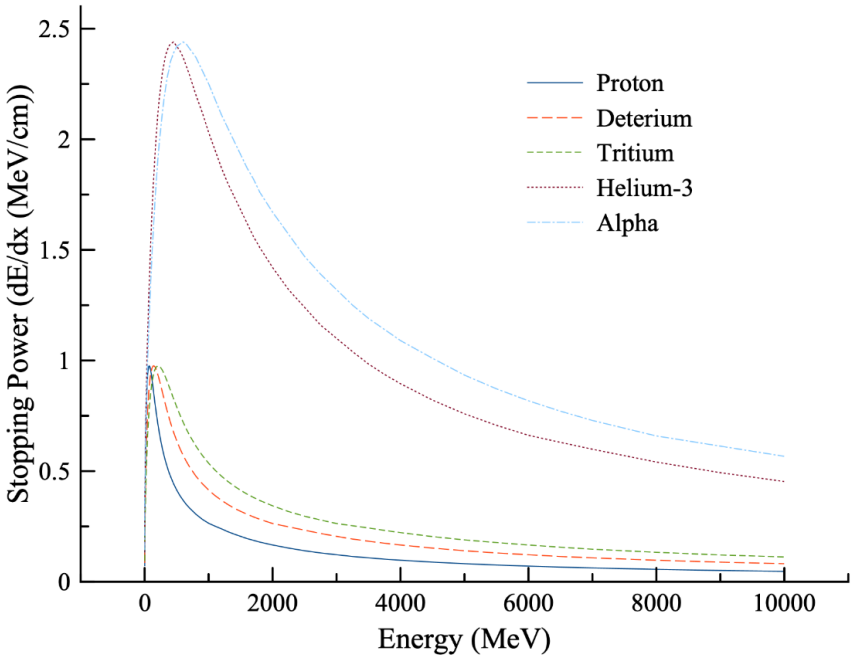

Fig. 2. Stopping power calculations of cell membrane

Penetrating distance calculations of charged particles within the cell membrane are illustrated in Figure 3. As expected, alpha has the smallest range, which is in parallel with tritium, deuterium, and proton stopping power results. On the contrary with the stopping power results, penetrating distance decreased as the charge of projectiles increased. It is well known that the cell membrane thickness is approximately 60-100 Å (Greenberg *et al.,* 2002). The minimum energy levels for the charged particles to pass through the membrane are given in Tables 2 and 3.

Table 2. Minimum energy range that can pass through the membrane for proton, deuterium, and tritium

Ion Energy (eV)	Proton Projected Range (Å)	Deuterium Projected Range(Å)	Tritium Projected Range(Å)
140	58	58	58
150	61	62	62
160	65	66	66
170	68	69	69
180	72	73	73
200	79	80	80
225	88	89	89
250	97	99	98
275	106	108	107

Table 3. Minimum energy range that can pass through the membrane for helium-3 and alpha

Ion Energy (eV)	Projected Range 3He (Å)	Projected Range ∝ (Å)
275	61	61
300	65	66
325	70	70
350	75	75
375	79	79
400	84	84
450	93	93
500	103	102

According to these calculations, the ion energy interval of 140-275 eV is enough for proton, deuterium, and tritium to pass through the cell membrane, whereas a higher ion energy interval (275-500 eV) is required for helium-3 and alpha to pass through the membrane.

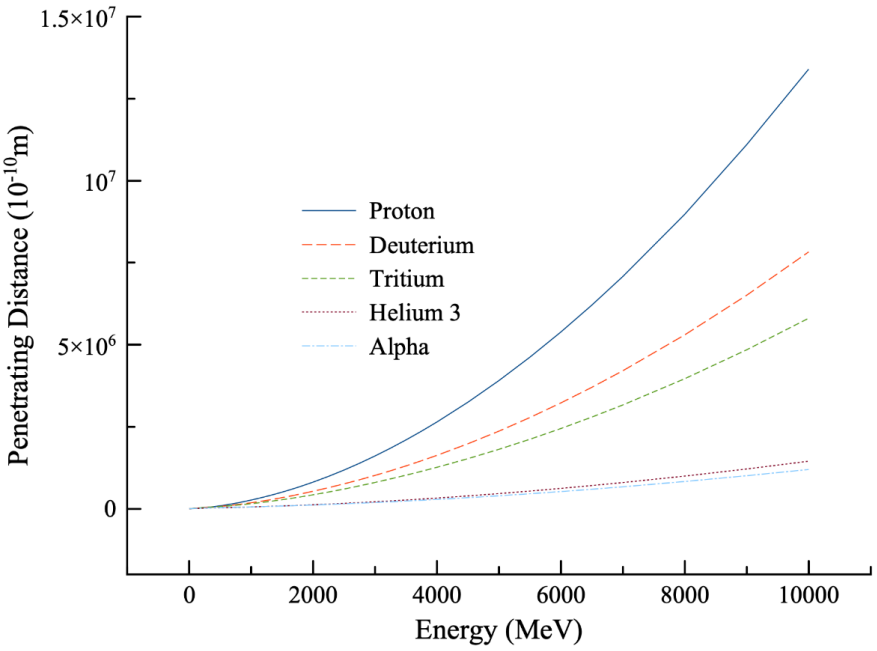

Fig. 3. Penetrating distance calculations of charged particles within the cell membrane

The mass attenuation coefficients of the cell at 0.05, 0.1, 0.2, 0.3, 0.4, 0.5, 0.6, 0.7, 0.8, 0.9, 1.0, 2.0, 4.0, 6.0, 8.0, and 10.0 MeV photon energies were calculated by using MCNPv6 and XCOM programs and the following graphs were obtained (Table 4). The comparison of MCNPv6 and XCOM results show the mass attenuation coefficients of the cell membrane in Figure 4. In addition, relative deviations (RD) of MCNP6 and WinXCOM μ/ρ values were calculated by using following equation;

$$RD = |\,(\mu/\rho WinXCom - \mu/\rho MCNP6)/\mu/\rho WinXCom * 100| \qquad (11)$$

As seen in Table 2, the RDs of the results of two methods at all energies is generally < 2%. Therefore, it is clear that XCOM, which is web-based computational tool (Berger *et al.,* 2010), results and MCNPv6 results are in harmony with each other. Additionally, mass attenuation coefficients of the cell membrane sharply decrease throughout the low energy region for less than 400 keV while tending to be almost constant for the photon energy region of 400 <E < 3000 keV. The basic reason of this trend can be attributed to principal radiation physics concepts. One of three, the photoelectric absorption is the most dominant interaction mechanism over 50 keV < E < 400 keV as compared to Compton scattering mechanism, where is more effective for E > 400 keV. Both processes are related to the energy as E−3.5 and E−1, respectively. Also, the above-mentioned rapid and linear declines are resulting from the dependence of these processes with the atomic number as Z4−5 and Z, respectively. These mass attenuation coefficients are close to zero in the high energy region where pair production which has cross-section depending on Z2 are dominant.

Table 4. Mass attenuation coefficient results of cell membrane

Energy (MeV)	μ/ρ (cm²/g)		RD
	MCNP6	XCOM	
0.05	0.2175	0.2183	0.36
0.1	0.1692	0.1678	0.82
0.2	0.1363	0.1352	0.78
0.3	0.1172	0.1172	0.04
0.4	0.1050	0.1049	0.05
0.5	0.0965	0.0957	0.77
0.6	0.0890	0.0885	0.60
0.7	0.0832	0.0827	0.67
0.8	0.0784	0.0777	0.92
0.9	0.0737	0.0735	0.22
1.0	0.0705	0.0699	0.86
2.0	0.0493	0.0488	1.01
4.0	0.0328	0.0334	1.66
6.0	0.0270	0.0270	0.06
8.0	0.0233	0.0235	0.86
10.0	0.0212	0.0213	0.66

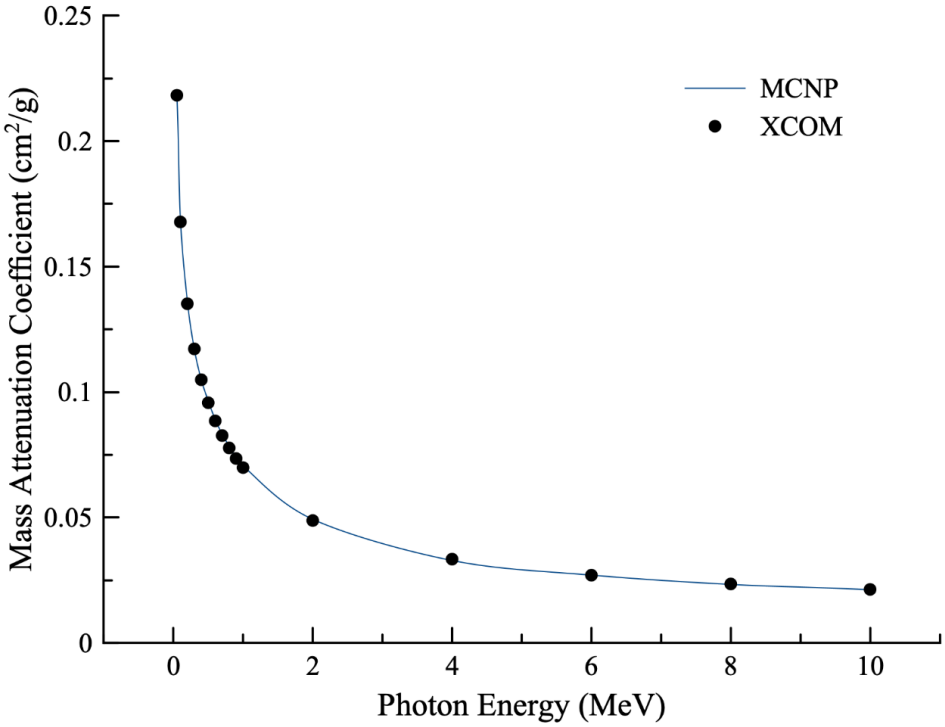

Fig. 4. Mass attenuation coefficient calculations for cell membrane

4. Conclusions

In this study, we focused on how the radiation affects the cell membrane. The radiation can damage the cell membrane and the effect of radiation on the cells will be investigated as a major topic in future clinical studies. Stopping power is the retarding force acting on charged particles (typically helium-3, tritium, deuterium, and proton particles) causing loss of particle energy due to interaction with cell membrane. It is known that the cell membrane thickness is approximately 60-100 Å. The range of a particle moving through the cell thickness depends on the excess energy of the particle. The stopping power increases with the excess energy of the particle in Figure 2.

The present study revealed the minimum energy range that can pass through the membrane for proton, deuterium, and tritium for 58-108 Å cell thickness (Table 2) and can pass through the membrane for helium-3 and alpha for 61-103 Å (Table 3). As seen in Figure 3, the penetrating distance of charged particles impinging in the cell membrane was calculated using SRIM-2013. This fit is important for the validation of the MCNPv6 and the result is corroborated by the result that the Monte Carlo method is a powerful tool in such studies. There is no experimental or theoretical study on the mass attenuation coefficient and stopping powers of the cell membrane in the literature. It is thought that the findings achieved in the present study can be used with researchers studying in radiobiology.

References

Brady, S., Siegel, G., Albers, R. W. & Price, D. L. (2005) Basic neurochemistry: molecular, cellular and medical aspects. Elsevier. Pp. 26.

Berger, M.J., Hubbell, J.H., Seltzer, S.M., Chang, J., Coursey, J.S., Sukumar, R., Zucker, D.S. & Olsen, K. (2010) XCOM: Photon Cross Section Database, National Institute of Standards and Technology, Gaithersburg, MD.

Evans, R.D. (1955) The Atomic Nucleus. McGraw Hill, New York. Pp. 972.

Félix, M.D. (2014) The basic structure and dynamics of cell membranes: An update of the Singer–Nicolson model. Biochimica et Biophysica Acta (BBA) – Biomembranes, 1838(6):1467-1476.

Goorley, J.T., James, M.R., Booth, T.E., Brown, F.B., Bull, J.S., Cox, L.J., Durkee, Jr., Joe W., Elson, J.S., Fensin, M.L., Forster, III, Robert A., Hendricks, J.S., Hughes, III.H. G., Johns, R.C., Kiedrowski, B.C., Martz, R.L., Mashnik, S.G., McKinney, G.W., Pelowitz, D.B., Prael, R.E., Sweezy, J. Ed., Waters, L.S., Wilcox, T., & Zukaitis, A.J. (2013) Initial MCNP6 Release Overview - MCNP6 version 1.0. United States.

Grecco, H.E., Schmick, M. & Bastiaens, P.I. (2011) Signaling from the living plasma membrane. Cell, 144: 897–909.

Greenberg, A., Breneman, C. M. & Liebman, J. F. (2002) The amide linkage: Structural significance in chemistry, biochemistry, and materials science. Wiley, New York. Pp. 599.

Hung, M.C. & Link, W. (2011) Protein localization in disease and therapy. Journal of Cell Science, 124(Pt 20):3381–3392.

Korn, E.D. (1968) Structure and Function of the Plasma Membrane: A biochemical perspective. Journal of General Physiology, 52(1):257-278.

Lodish, H., Berk, A., Zipursky, S.L., Matsudaira, P., Baltimore, D. & Darnell, J. (2000) Photosynthetic Stages and Light-Absorbing Pigments. Molecular Cell Biology. W. H. Freeman and Company, New York. Pp. 152.

Mashaghi, A., Partovi-Azar, P., Jadidi, T., Nafari, N., Maass, P., Tabar, M.R.R., Bonn, M. & Bakker, H.J. (2012) Hydration strongly affects the molecular and electronic structure of membrane phospholipids. The Journal of chemical physics, 136(11): 114709-5.

Podgorsak, E.B. (2016) Radiation Physics for Medical Physicists. Springer, Switzerland. Pp. 906.

Sharma, A., Sayyed, M.I., Ağar, O. & Tekin, H.O. (2019) Simulation of shielding parameters for TeO2 WO3 GeO2 glasses using FLUKA code. Results in Physics, 13:102199.

Stryer, L. (1995) Biochemistry.W. H. Freeman and Company, New York. Pp. 263.

Ulmschneider, M. B., Sansom, M. S., & Di Nola, A. (2005) Properties of integral membrane protein structures: derivation of an implicit membrane potential. Proteins: Structure, Function, and Bioinformatics, 59(2): 252-265.

Yang, Y., & Hu, B. (2014) Bio-based chemicals from biorefining : Lipid and wax conversion and utilization. Advances in Biorefineries: Biomass and Waste Supply Chain Exploitation, Pp. 693-720. Elsevier Ltd.

Ziegler, J.F., Ziegler, M.D. & Biersack, J.P. (2010) SRIM - The Stopping and Range of Ions in Matter. Nuclear Instruments and Methods in Physics Research, Section B: Beam Interactions with Materials and Atoms, 268(11–12):1818–23.

Submitted: 18/09/2021
Revised: 19/12/2021
Accepted: 2612/2021
DOI: 10.48129/kjs.15657

Molecular docking and molecular dynamic study of multiple medicinal plants' bioactive compounds as human papillomavirus type 16 E5 protein inhibitor

Arief Hidayatullah[1], Wira Eka Putra[2,*], Muhaimin Rifa'i[3], Sustiprijatno[4], Muhammad Fikri Heikal[5], Diana Widiastuti[6], Galuh Wening Permatasari[7], Hendra Susanto[1], Adawiyah Suriza Shuib[8]

[1]*Dept. of Biology, Faculty of Mathematics and Natural Sciences, Universitas Negeri Malang, East Java, Indonesia*

[2]*Biotechnology Study Program, Department of Applied Science, Faculty of Mathematics and Natural Sciences, Universitas Negeri Malang, East Java, Indonesia.*

[3]*Dept. of Biology, Faculty of Mathematics and Natural Sciences, Brawijaya University, East Java, Indonesia*

[4]*Indonesian Center for Agricultural Biotechnology and Genetic Resources Research and Development, West Java, Indonesia*

[5]*Tropical Medicine International Program, Faculty of Medicine, Khon Kaen University, Khon Kaen, Thailand.*

[6]*Dept. of Chemistry, Faculty of Mathematics and Natural Science, Universitas Pakuan, West Java, Indonesia*

[7]*Indonesian Research Institute for Biotechnology and Bioindustry, Bogor, West Java, Indonesia*

[8]*Institute of Biological Sciences, Faculty of Science, Universiti Malaya, Kuala Lumpur, Malaysia*

**Corresponding author: wira.putra.fmipa@um.ac.id*

Abstract

Cervical cancer is the second most prevalent form of cancer in Indonesia. HPV16 and HPV 18 are the leading causes of cervical cancer, accounting for 70-90% of cases. The E5 protein may play a critical role in the disease's development. Although the high-risk (HR) version of this protein may have some benefits in evading the immune system through MHC I and influencing the cell cycle via p21/p27, very few studies have been performed owing to its tiny size and high hydrophobicity. The purpose of this research is to predict the anti-viral activity of asarinin and thiazolo[3,2-a]benzimidazole-3(2H)-one,2-(2-fluorobenzylideno)-7,8-dimethyl (thiazolo) using molecular docking and molecular dynamics. The docking results showed that the two candidate drugs had a lower docking affinity than rimantadine but comparable stability. Both potent compounds are predicted to disrupt MHC I localization in the ER, the ability of infected cells to proliferate, and the virion assembly process. In contrast, rimantadine is predicted to disrupt infected cells' proliferation ability via the epidermal growth factor receptor (EGFR) regulation and inhibit the activation process of mitogenic signalling in keratinocytes.

Keywords: Cervical Cancer, dynamic simulation, E5 protein, HPV16, molecular docking.

1. Introduction

Cervical cancer is the second most prevalent form of cancer in Indonesia and the second most common type of cancer in females aged 15 to 44 years (Domingo *et al.*, 2008; Nurcahyanti, 2016). Cervical cancer accounted for approximately 9-10% of all cancer cases reported in 2018 (Arbyn *et al.*, 2020). Every year, its incidence and prevalence rates tend to increase by around 17 and 20%, respectively (Wahidin *et al.*, 2020). Primarily, cervical cancer is caused by Human Papillomavirus (HPV), a collection of non-enveloped DNA viruses that primarily infect the keratinocytes' basal layer. It is known to be spread by skin-to-skin contact, most notably through sexual intercourse (Tao *et al.*, 2003). There are now over 200 different kinds of HPV, which are usually classified into five genotype groups and two risk categories, high-risk (HR) and low-risk (LR) HPV (Bzhalava *et al.*, 2013; Venuti *et al.*, 2011). HPV16 and 18 are the leading causes of anogenital malignancies, most commonly cervical cancer, and are the leading causes of concern for HPVs. Around 70–90% of cervical cancer cases are caused by HPV16 and HPV 18, respectively, with HPV16 alone accounting for 55% of all instances (Graham, 2017; Venuti *et al.*, 2011; Wang *et al.*, 2018). Around 4% of women in the general population are thought to be exposed to HPV16 or 18 at any particular time (ICO/IARC HPV Information Centre, 2019). Additionally, high-risk HPV might have a crucial role in the pathogenesis of various forms of cancer, such as the respiratory tract, eyes, esophagus, non-small-cell lung, colorectal, breast, prostatic, and urinary bladder cancers (Venuti *et al.*, 2011).

The majority of research on HPV-related cancer has concentrated on two oncoproteins, the E6 and E7 proteins (Doorbar *et al.*, 2012; Pal & Kundu, 2020; Yeo-Teh *et al.*, 2018). These proteins are essential oncoproteins that distinguish high-risk from low-risk variants, owing to their well-characterized actions and pathways (Graham, 2017). For example, E6 interacts with and degrades the cellular tumor suppressor p53, while E7 interacts with and inactivates the retinoblastoma (Rb) proteins, resulting in tumor development. (Doorbar *et al.*, 2012; Egawa & Doorbar, 2017; Tao *et al.*, 2003; Underbrink *et al.*, 2016). Also, both proteins interact with various proteins that leads mainly to immune evasion and genomic instability (Yeo-Teh *et al.*, 2018). Some research suggests another significant oncoprotein in the HR type of HPV is the E5 protein, an 83 amino acid long hydrophobic transmembrane protein that interacts with various cellular proteins and required for the protein's biological activity during cell transformation (Campo *et al.*, 2010; DiMaio & Petti, 2013; Krawczyk *et al.*, 2010; Suprynowicz *et al.*, 2008). Some effects caused by E5 protein activity are relocalization of calpactin I to the perinuclear region, enhancement of growth factor signaling patterns by activation of EGF-R, suppressing three key proteins of the ER stress pathway such as cyclooxygenase-2 (COX-2), XBP-1, and IRE1a, and downregulation of the Major Histocompatibility Complex class (MHC I) (DiMaio & Petti, 2013; Gruener *et al.*, 2007; Venuti *et al.*, 2011). In addition, E5 also alters endosomal pH by interacting with the vacuolar H+-ATPase, acidifying cellular organelles. However, due to their tiny size and hydrophobicity, the E5 proteins lack the substantial soluble, globular domains required for specialized protein-protein interactions (DiMaio & Petti, 2013; Disbrow *et al.*, 2005; Marshansky & Futai, 2008; Venuti *et al.*, 2011). Additionally, HR HPV E5 is engaged in the early stages of carcinogenesis by extending the survival of infected cells and increasing their pool. However, the E5 ORF is almost exclusively found in the HR-HPV genome since it is missing from the genomes of many other HPVs, including beta-, gamma-,

and mu-HPVs, suggesting that the protein is not required for the virus's life cycle but may provide some advantage on infection and transformation (Doorbar *et al.*, 2012; Longworth & Laimins, 2004; Wang *et al.*, 2018).

As one of the largest tropical countries, Indonesia is home to about 7000 medicinal plants. However, less than 10% of these taxa are classified as phytopharmaca (Salim & Munadi, 2017). For hundreds of years, the Indonesian culture has depended on a range of medicinal plants to treat or alleviate mild to severe diseases, backed up by empirical evidence from the community, even though scientific data is often sparse. Around 55% of Indonesians regularly use alternative treatments, and over 95% think they benefit from them (Jennifer & Saptutyningsih, 2015; Sumayyah & Salsabila, 2017). These results lay the groundwork for future research into treatment options for various diseases, including HR-HPV infection. Research into drug creation would be a lengthy endeavor, much more so if the components are natural. Chemical screening, as well as screening and testing *in silico*, is one of the first stages, as shown in this study (Kitchen *et al.*, 2004; Lionta *et al.*, 2014). Our previous study in HPV16 E6 protein showed that the two most potent compounds against E6 protein are asarinin and thiazolo, found in *Zanthoxylum spp* and *Myristica fragrans,* respectively. This study aimed to target the HPV16 E5 protein directly with those specific compounds, hoping for potent inhibition activity in the protein target activities.

2. Materials and Methods

The objective of this research was to target the HPV16 E5 oncoprotein specifically. The amino acid sequence for the target protein was acquired from UniProt (https://www.uniprot.org/uniprot) under the accession number P06927. The 3D structure was then modeled using I-TASSER webserver (https://zhanglab.dcmb.med.umich.edu/I-TASSER/). The modeled was chosen based on the C-score value and RMSD score, representing suitable position of each atom to be modelled.

Asarinin (CID: 11869417) and thiazolo (CID: 1823738) are used as particularly potent natural compounds, whereas Rimantadine (CID: 5071) is used as a control (Wetherill *et al.*, 2012). All of these possible chemicals were obtained in SDF format from PubChem (https://pubchem.ncbi.nlm.nih.gov/).

2.1. Pathway Analysis

The HPV infection pathway analysis in the host cells is based on KEGG's database (https://www.genome.jp/kegg/) to identify which protein and biological process disrupted by HPV16 E5 protein inducing the cancer development. Through the KEGG map, then we analyzed the potential target protein related to the HPV infection.

2.2. Molecular Docking Process

AutoDock Vina is used for docking, which is integrated with PyRx (https://pyrx.sourceforge.io/) (Trott & Olson, 2009). First, we examine the target protein's complete structure. The molecular coverage area (in Angstroms) is 39.3567; 40.9481; 35.1306, whereas the center coordinates are 56.3238; 40.9481; 35.1306, respectively. The primary docking findings are the compound's

affinity in kcal/mol, the location of the binding site, and the subsequent visualization of the protein-ligand interaction.

2.3. Visualization Process

The visualization method is divided into two stages: the 3D visualization of possible chemical binding sites on the E5 protein and the 2D visualization of interaction in each protein-ligand combination. PyMOL (https://pymol.org/2/) is used for 3D visualization, whereas LigPlot+ 2.1 (https://www.ebi.ac.uk/thornton-srv/software/LigPlus/) is used for 2D visualization.

2.4. Molecular Dynamics Simulations

Ligands with the lowest binding affinity scores were selected for molecular dynamic simulation against E5 protein. The parameters were set up according to the normal physiological conditions (37°C, 1 atm, pH 7.4, 0.9% salt content) for 1000 picoseconds simulation time. Molecular dynamics simulation was run through md_run macro program, and the analysis followed by using md_analyze and md_analyeres on yasara program.

3. Results

3.1. Pathway Analysis Results

The infection pathway in KEGG (hsa05165) revealed that E5 protein activity was associated with three distinct biological processes: immune evasion via inhibition of MHC I in the endoplasmic reticulum (ER), activation of a growth factor such as platelet-derived growth factor receptor beta (PDGFRB) that directly stimulates cell proliferation, and immortalization mechanisms via MAPK and calcium signaling pathways.

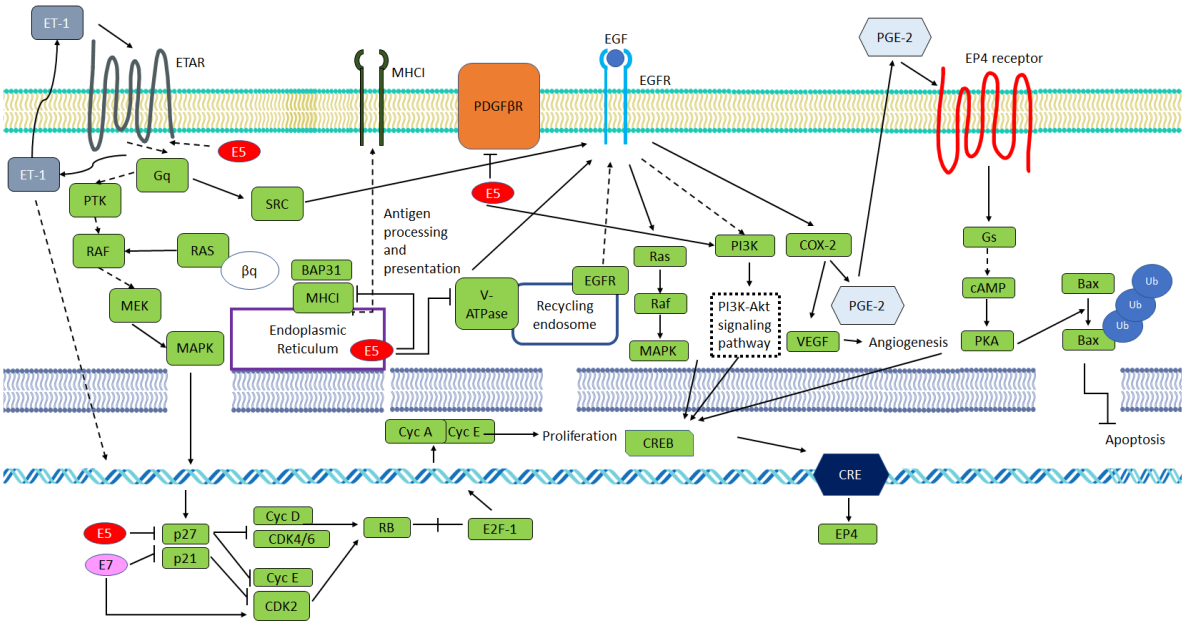

Fig. 1. The infection pathway of HPV in KEGG (hsa05165). A showed E5 protein promotes PDGFRB activation and immune evasion mechanism by downregulating the MHC I. B showed E5 protein bypassing infected cell straight to S-phase by inhibiting p21 and p27.

In figure 1A, it appears as though the HPV16 E5 protein localized to the ER membrane is intending to suppress adaptive immune responses by downregulating MHC class I, thereby presenting ER-derived peptides on the cell surface for exposure to cytotoxic T- cells that cannot accumulate on the surface of infected cells. Additionally, it appears as though E5 protein interacts with B-cell receptor-associated protein 31 (BAP31). BAP31 is a ubiquitously expressed transmembrane protein found primarily in the ER that acts as a chaperone protein for MHCI, forcing it to localize to the ER and Golgi and maintain an infected host cell proliferation-competent state (Dang *et al.*, 2018; Quistgaard, 2021; Regan & Laimins, 2008).

Additionally, the KEGG pathway showed that the E5 protein suppresses tumor suppressors p21 and p27 (figure 1B), which are cell cycle inhibitors that induce cells to enter the S-phase by inhibiting G1-phase markers such as CDK2/4/6 and Cys D/E, thus disrupting cell cycle checkpoint mechanisms. In addition, it causes infected cells aggressively synthesize DNA during the S phase, resulting in the formation of koilocytes, which are often employed as a morphological marker of HR-HPV infection. The KEGG viral carcinogenesis pathway (not shown here) also reveals that the HPV16 E5 protein downregulates the V-ATPase protein, particularly the 16 kDa subunit of V-ATPase disrupts endosomal acidification, resulting in increased EFGR recycling and active cell proliferation. Because all biological processes affected by the E5 protein contribute to cancer development, the HPV16 E5 protein was classified as an oncoprotein in this research.

3.2. Molecular Docking Results

The docking results (Table 1) show that the two potential natural compounds exhibited 50% and 31% lower affinity values than the control drug (rimantadine; -4.8 kcal/mol). As a result, these compounds should have a higher propensity for initiating interactions with the target protein than drug controls (Murcko & Ajay, 1995). The negative value in the results represents the spontaneous interaction between the ligand and target protein when the ligand-protein complex reaches equilibrium under constant pressure and temperature conditions simulated throughout the docking process (Bronowska, 2011; Du *et al.*, 2016; Murcko & Ajay, 1995).

Table 1. Docking and 2D visualization two potent compounds against HPV16 E5 protein

Compounds	ΔG	Amino Acid Residue	Interactions (Å)
Asarinin (CID: 11869417) *Zanthoxylum spp* (bark)	-7.2 (Kcal/mol)	Thr76; Leu71; Ser37; Tyr39; Ser35; Leu23; Ala78; Pro31	Hydrophobic contact
		Arg79	Hydrophobic contact
			Hydrogen bond (2.92)
Thiazolo[3,2-a]benzimidazol-3(2H)-one,2-(2-fluorobenzylideno)-7,8-dimethyl (CID: 1823738) *Myristica fragrans* (seeds)	-6.3 (Kcal/mol)	Tyr39; Leu23; Thr76; Ser35; Ala78; Leu71	Hydrophobic contact
Rimantadine (CID: 5071) *Drug controls*	-4.8 (Kcal/mol)	Pro70; Thr38; Leu71; Ile64; Ser41; Ile43	Hydrophobic contact
		Tyr39	Hydrophobic contact
			Hydrogen bond (2.97)

3.3. Post-docking Visualization Results

The results of the post-docking visualization results demonstrate that asarinin and thiazolo did not intersect at the same binding site as the control. However, when verified using two-dimensional visualization, two residues, Tyr39 and Leu71, were shown to be shared by the control and potent compounds (figure 2).

Additionally, 2D visualization demonstrates that asarinin and thiazolo are colocalized at the same binding site, flanking the first hydrophobic domain (first α-helix; red), the third hydrophobic domain (third α-helix; yellow), and the C-terminal region (cyan). Thus, Asarinin interacts with the first hydrophobic domains located at Leu23 and Pro31, the third hydrophobic domain located at Leu71, and the C-terminal at Thr76, Ala78, and Arg79. Thiazolo binds to the first hydrophobic domain at Leu23, the third hydrophobic domain at Leu71, and the C-terminal area at Thr76, Ala78. These findings show that the two natural chemicals (Leu23, Thr76, and Leu71) share conserved residues, indicating that the two possible compounds bind to the same binding site. Simultaneously, it was anticipated that rimantadine, as a control, would interact with the second and third hydrophobic domains at Phe43, Ile64, Pro70, and Leu71.

3.4. Molecular Dynamic Simulation Results

To assess docked complexes' flexibility and overall stability, we performed a time-dependent MD simulation at 1000 picoseconds. The energy potential graph reveals that all E5 complexes have near identical values and a horizontal trend throughout the simulation period, about -4.96e5 kJ/mol, indicating that all complexes were energetically stable during the simulation (figure 3).

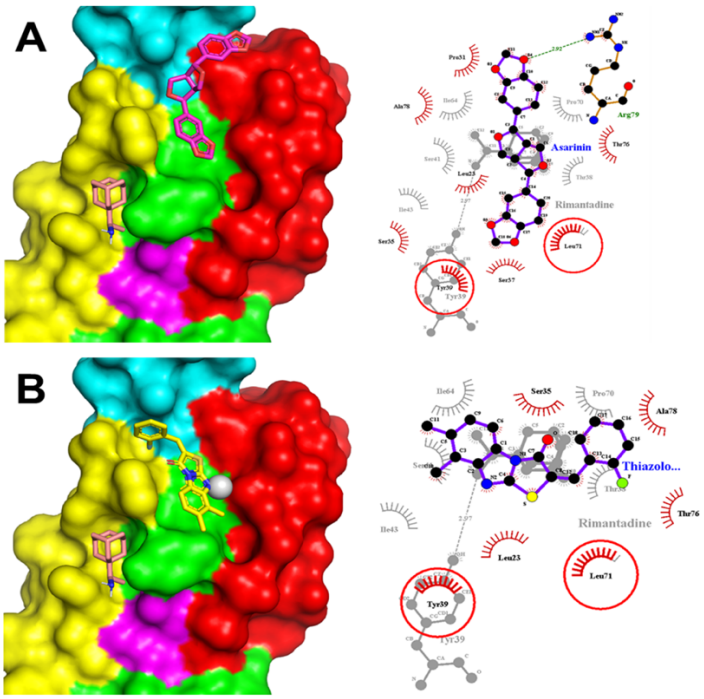

Fig. 2. An overview of the binding sites based on 3D visualization results with HPV16 E5 protein. The interaction between the two potent compounds with HPV16 E5 protein is based on the 2D visualization results. (A) asarinin, (B) thiazolo[3,2-a]benzimidazol-3(2H)-one. First hydrophobic domain (first α-helix; red), the third hydrophobic domain (third α-helix; yellow), and the C-terminal region (cyan).

The root mean square deviation was determined throughout the course of 1000 picoseconds of simulation (figure 4). The RMSD results of E5-asarinin showed a mean value of 5.915±1.099Å with a minimum value of 1.166Å and a maximum value of 7.316Å. The E5-thiazolo complex showed a mean value of 5.067±0.733Å with a minimum value of 1.231Å and a maximum value of 6.062. The E5-rimantadine showed a mean value of 5.396±1.176Å with a minimum value of 1.181Å and a maximum value of 7.113Å.

The RMSD values indicated that the E5-thiazolo complex exhibited minor variations at 100, 350, and 950 ps, but stabilized in about 5Å after 150 ps. Meanwhile, the E5-asarinin complex stabilized after 150 ps but deviated to approximately 7Å at 550 ps and subsequently exhibited a decreasing trend in the RMSD value after 600 ps until the conclusion of the test period. Before 550 ps, the E5-rimantadine complex exhibited a constant RMSD value less than 6Å, but indicating an increasing trend in value from that point until the simulation period ended. Stable RMSD values suggest that the interactions established in the complex are stable, implying that the target protein will tend to retain its structure, while variations in the RMSD value are due to changes in the conformation of the chemical tested at its binding site.

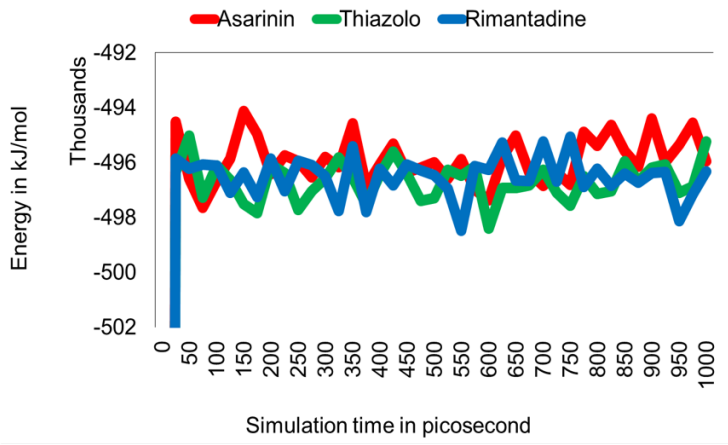

Fig. 3. Total potential energy of the system among HPV16 E5 and ligands interaction over a 1000 picosecond simulation

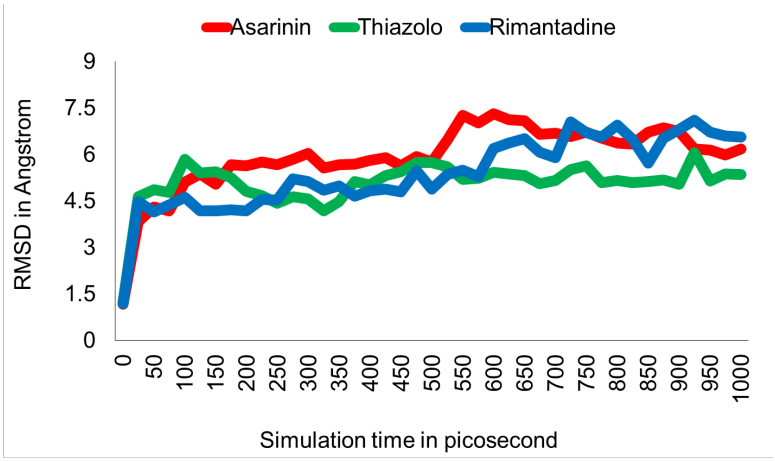

Fig. 4. RMSD plot showed the stability of protein-ligand complex interaction among HPV16 E5 and ligands over a 1000 picosecond simulation

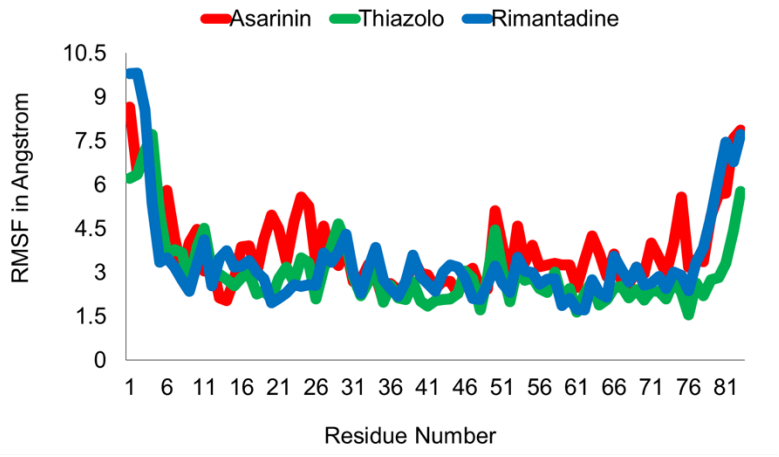

Fig. 5. RMSF plot showed the stability of amino acid residues among HPV16 E5 and ligands over a 1000 picosecond simulation

The RMSF plot (figure 5) demonstrates that no major differences occurred between the three tested substances throughout the simulation period. The E5-thiazolo, and E5-rimantadine complexes, on the other hand, consistently demonstrated lower RMSF values than the E5-asarinin complex. Because the RMSF value did not fluctuate much in any of the three complexes examined, it was believed that the three protein-ligand complexes produced were in a stable conformation. However, the data reveals that asarinin had the greatest variability, even more than the other two chemicals examined. The RMSF figure reveals that the least flexible amino acid residues are clustered around the second hydrophobic domain (AA 36-50). Except at the extreme C-terminus, the RMSF value of the residue that interacted with each compound was often lower than that of the other residues in each complex examined.

4. Discussion

The HPV16 E5 protein is a critical component of the HPV infection mechanism. Along with the E6 and E7 proteins, the much smaller E5 protein is believed to be a critical oncoprotein, particularly during cancer development (DiMaio & Petti, 2013; Venuti *et al.*, 2011; Wetherill *et al.*, 2018). Due to the protein's small size and highly hydrophobic structure, few studies have examined it in detail (Wetherill *et al.*, 2012; Nath *et al.*, 2006). According to the KEGG pathway, the HPV16 E5 protein plays several critical roles, including immune evasion by downregulating MHC I and BAP31 in the ER and promoting infected cells to S-phase by inhibiting the tumor suppressors' p21 and p27. Due to the breadth of its functions, despite its small size and relatively simple structure, HPV16 E5 contains a large number of active domains, including the first hydrophobic domain/first helix (AA 11-34) that interacts with a heavy chain of MHC I via leucine pairs, resulting in the downregulation of MHC I, the five final AA in the C-terminus that are thought to interact with the epidermal growth factor receptor (EGFR), and the third hydrophobic domain/first α-helix (Ashrafi *et al.*, 2006; Wetherill *et al.*, 2012; Nath *et al.*, 2006; Regan & Laimins, 2008; Rodríguez *et al.*, 2000; Venuti *et al.*, 2011).

The docking findings indicated that the two potential compounds previously evaluated on the HPV16 E5 protein had a lower docking affinity value than rimantadine, implying a greater and more stable probability of contact between the two potent compounds and the E5

protein (Murcko & Ajay, 1995). However, when the RMSD and RMSF values were compared, only thiazolo had a lower mean value than rimantadine. The potential energy of the three complexes was investigated, and it was observed that they remained constant during the simulation duration. It suggests that the electrostatic and van der Waals interactions of the three complexes remained constant during simulation, implying that no abnormalities occurred during the process (Albaugh *et al.*, 2016). The RMSD plot revealed that thiazolo exhibited the most stable interaction of the three compounds complex examined, but its docking affinity was lower than asarinin. Meanwhile, asarinin, which has the highest docking affinity, exhibits similar stability to rimantadine, if not slightly worse, as it exhibits a slightly higher flexibility pattern than control, indicating that the E5-asarinin complex is relatively less stable when compared to control and thiazolo (Aier *et al.*, 2016; Schneider *et al.*, 2011; Sivaramakrishnan *et al.*, 2020).

The two possible compounds are expected to interact with three key regions of the E5 protein, particularly the first hydrophobic domain, the third hydrophobic domain, and the C-terminus, based on the findings of the 2D visualization and the RMSF plot. Stabilized interaction with the first hydrophobic domain, particularly with Leu23 and Pro31, which are located in the middle of the α-helix structure, is thought to disrupt the E5 protein's interaction with the heavy chain of MHC I, resulting in delocalization of MHC I in the ER, thereby destroying the virus's immune evasion mechanism (Abe *et al.*, 2009; Campo *et al.*, 2010; Gruener *et al.*, 2007; Nath *et al.*, 2006; Venuti *et al.*, 2011). Both compounds are also believed to disrupt the endosomal acidification process mediated by v-ATPase, thus decreasing the rate of EFG-receptor recycling to the plasma membrane. Consequently, these infected cells lack the number of EFGR receptors seen in other infected cells and do not achieve the EFGR ratio found in normal cells (Ilahi & Bhatti, 2020; Müller *et al.*, 2015; Venuti *et al.*, 2011). Although a decreased EFGR ratio is anticipated to delay the proliferation and angiogenesis of infected cells, the percentage of reduction cannot be predicted. Potent drugs interacting with extreme C-terminus residues such as Thr76 and Ala78 would inhibit future EGFR pathway hyperactivation, eventually reducing the cell's proliferative capacity. Additionally, it is believed that potent compounds interacting with the extreme C-terminus inhibit the interaction of E5 protein with BAP31, which is involved in the export of MHC I to the cell surface, the maintenance of infected cells' proliferation ability, and the virion assembly process, resulting in decreased expression in infected cells' MHC I is in its membrane, its proliferation is less aggressive than other infected cells, and the rate of HPV virion assembly is also lower (Abe *et al.*, 2009; DiMaio & Petti, 2013; Ilahi & Bhatti, 2020; Kotnik Halavaty *et al.*, 2014; Müller *et al.*, 2015; Regan & Laimins, 2008).

Rimantadine demonstrated a distinct inhibition pattern of the E5 protein compared to the other two natural drugs examined, based on docking and visualization results. Rimantadine is expected to interact with only third hydrophobic domains through Pro70, Leu71, and Ile64, resulting in a decrease in endosomal acidification and the rate of EGFR recycling. Iso64 and Pro70 are also suspected of functioning as voltage gating motifs, with interactions between these residues potentially inhibiting the diffusion of certain critical ions, although the intricacies of the voltage gating motif's function on the HPV16 E5 protein remain mostly unclear (Nath *et al.*, 2006; Scott & Griffin, 2015). More often referred to as an anti-viroporin, rimantadine is believed to bind with one of the residues that comprise the viroporin's lumen in its oligomer

state structure, such as Ser41 and therefore block the activation process of mitogenic signaling in keratinocytes. A comparable direct blockage of the viroporin channel is believed to be caused by the interaction between Ser37, which constitutes the viroporin lumen, and asarinin (Wetherill *et al.*, 2012; Scott & Griffin, 2015; Wetherill *et al.*, 2018).

5. Conclusion

The HPV16 E5 protein plays a vital role in the HPV infection process. By suppressing the tumor suppressors p21 and p27, it downregulates MHC I and BAP31 in the ER and promotes the entry of infected cells into the S-phase. The docking results indicated that asarinin and thiazolo had a lower docking affinity value than rimantadine, implying a greater and more stable probability of contact between the two compounds and the protein, but comparable stability as measured by the RMSD and RMSF plots. Both potent compounds are predicted to disrupt MHC I localization in the ER, infected cells' ability to proliferate, and the virion assembly process. In contrast, rimantadine is expected to impair infected cells' proliferation ability via EGFR regulation and inhibit the activation process of mitogenic signaling in keratinocytes. Additional *in vivo* or *in vitro* investigations are required to verify the *in silico* prediction findings from this study.

ACKNOWLEDGEMENTS

This study was funded by PNBP Universitas Negeri Malang with contract number 5.3.619/UN32.14.1/LT/2021 and 5.3.517/UN32.14.1/LT/2021 (Wira Eka Putra). Authors thank Universitas Negeri Malang for support this study.

Conflict of Interest

Authors declare there is no conflict of interest in this study.

References

Abe, F., Van Prooyen, N., Ladasky, J. J., & Edidin, M. (**2009**) Interaction of Bap31 and MHC class I molecules and their traffic out of the endoplasmic reticulum. Journal of Immunology, 182(**8**), 4776–4783.

Aier, I., Varadwaj, P. K., & Raj, U. (**2016**) Structural insights into conformational stability of both wild-type and mutant EZH2 receptor. Scientific Reports, 6(**1**), 1-10.

Albaugh, A., Boateng, H. A., Bradshaw, R. T., Demerdash, O. N., Dziedzic, J., Mao, Y., Margul, D. T., Swails, J., Zeng, Q., Case, D. A., Eastman, P., Wang, L.-P., Essex, J. W., Head-Gordon, M., Pande, V. S., Ponder, J. W., Shao, Y., Skylaris, C.-K., Todorov, I. T., Head-Gordon, T. (**2016**) Advanced potential energy surfaces for molecular simulation. The Journal of Physical Chemistry B, 120(**37**), 9811–9832.

Arbyn, M., Weiderpass, E., Bruni, L., Sanjosé, S. de, Saraiya, M., Ferlay, J., & Bray, F. (**2020**) Estimates of incidence and mortality of cervical cancer in 2018: A worldwide analysis. The Lancet Global Health, 8(**2**), 191–203.

Ashrafi, G. H., Haghshenas, M., Marchetti, B., & Campo, M. S. (**2006**) E5 protein of human papillomavirus 16 downregulates HLA class I and interacts with the heavy chain via its first hydrophobic domain. International Journal of Cancer, 119(**9**), 2105–2112.

Bronowska, A. K. (2011) Thermodynamics of ligand-protein interactions: Implications for molecular design. in (Ed.), thermodynamics - interaction studies - solids, liquids and gases. IntechOpen. https://doi.org/10.5772/19447.

Bzhalava, D., Guan, P., Franceschi, S., Dillner, J., & Clifford, G. (**2013**) A systematic review of the prevalence of mucosal and cutaneous human papillomavirus types. Virology, 445(**1**), 224–231.

Campo, M. S., Graham, S. V., Cortese, M. S., Ashrafi, G. H., Araibi, E. H., Dornan, E. S., Miners, K., Nunes, C., & Man, S. (**2010**) HPV-16 E5 down-regulates expression of surface HLA class I and reduces recognition by CD8 T cells. Virology, 407(**1**), 137–142.

Dang, E., Yang, S., Song, C., Jiang, D., Li, Z., Fan, W., Sun, Y., Tao, L., Wang, J., Liu, T., Zhang, C., Jin, B., Wang, J., & Yang, K. (**2018**) BAP31, a newly defined cancer/testis antigen, regulates proliferation, migration, and invasion to promote cervical cancer progression. Cell Death & Disease, 9(**8**), 1–15.

DiMaio, D., & Petti, L. (**2013**) The E5 Proteins. Virology, 445(**0**), 99–114.

Disbrow, G. L., Hanover, J. A., & Schlegel, R. (**2005**) Endoplasmic reticulum-localized human papillomavirus type 16 E5 protein alters endosomal pH but not trans-Golgi pH. Journal of Virology, 79(**9**), 5839–5846.

Domingo, E., Noviani, R., Noor, M., Ngelangel, C., Limpaphayom, K., Thuan, T., Louie, K., & Quinn, M. (**2008**) Epidemiology and prevention of cervical cancer in Indonesia, Malaysia, the Philippines, Thailand and Vietnam. Vaccine, 26(**12**), 71-79.

Doorbar, J., Quint, W., Banks, L., Bravo, I. G., Stoler, M., Broker, T. R., & Stanley, M. A. (**2012**) The biology and life-cycle of human papillomaviruses. Vaccine, 30(**5**), 55–70.

Du, X., Li, Y., Xia, Y.-L., Ai, S.-M., Liang, J., Sang, P., Ji, X.-L., & Liu, S.-Q. (**2016**) Insights into protein–ligand interactions: mechanisms, models, and methods. International Journal of Molecular Sciences, 17(**2**). 1-34.

Egawa, N., & Doorbar, J. (**2017**) The low-risk papillomaviruses. Virus Research, 231, 119–127.

Graham, S. V. (**2017**). The human papillomavirus replication cycle, and its links to cancer progression: a comprehensive review. Clinical Science, 131(**17**), 2201–2221.

Gruener, M., Bravo, I. G., Momburg, F., Alonso, A., & Tomakidi, P. (**2007**) The E5 protein of the human papillomavirus type 16 down-regulates HLA-I surface expression in calnexin-expressing but not in calnexin-deficient cells. Virology Journal, 4(**1**), 1-15.

ICO/IARC HPV Information Centre. (**2019**) Indonesia: Human Papillomavirus and related cancers, Fact Sheet 2019. ICO/IARC HPV Information Centre.

Ilahi, N. E., & Bhatti, A. (**2020**) Impact of HPV E5 on viral life cycle via EGFR signaling. Microbial Pathogenesis, 139, 103923.

Jennifer, H., & Saptutyningsih, E. (**2015**) Preferensi individu terhadap pengobatan tradisional di Indonesia. Jurnal Ekonomi dan Studi Pembangunan, 16(**1**), 26-41.

Kitchen, D. B., Decornez, H., Furr, J. R., & Bajorath, J. (**2004**) Docking and scoring in virtual screening for drug discovery: methods and applications. Nature Reviews Drug Discovery, 3(**11**), 935–949.

Kotnik Halavaty, K., Regan, J., Mehta, K., & Laimins, L. (**2014**) Human papillomavirus E5 oncoproteins bind the A4 endoplasmic reticulum protein to regulate proliferative ability upon differentiation. Virology, 0, 223–230.

Krawczyk, E., Suprynowicz, F. A., Sudarshan, S. R., & Schlegel, R. (**2010**) Membrane orientation of the human papillomavirus type 16 E5 oncoprotein. Journal of Virology, 84(**4**), 1696–1703.

Lionta, E., Spyrou, G., K. Vassilatis, D., & Cournia, Z. (**2014**) Structure-based virtual screening for drug discovery: Principles, applications and recent advances. Current Topics in Medicinal Chemistry, 14(**16**), 1923–1938.

Longworth, M. S., & Laimins, L. A. (**2004**) Pathogenesis of human papillomaviruses in differentiating epithelia. Microbiology and Molecular Biology Reviews, 68(**2**), 362–372.

Marshansky, V., & Futai, M. (**2008**) The V-type H+-ATPase in vesicular trafficking: targeting, regulation and function. Current Opinion in Cell Biology, 20(**4**), 415–426.

Müller, M., Prescott, E. L., Wasson, C. W., & Macdonald, A. (**2015**) Human papillomavirus E5 oncoprotein: function and potential target for antiviral therapeutics. Future Virology, 10(**1**), 27–39.

Murcko, M. A., & Ajay. (**1995**) Computational methods to predict binding free energy in ligand-receptor complexes. Journal of Medicinal Chemistry, 38(**26**), 4953–4967.

Nath, R., Mant, C. A., Kell, B., Cason, J., & Bible, J. M. (**2006**) Analyses of variant human papillomavirus type-16 E5 proteins for their ability to induce mitogenesis of murine fibroblasts. Cancer Cell International, 6(**19**), 1-9.

Nurcahyanti, A. D. R. (**2016**) Cervical cancer: The case in Indonesia and natural product based therapy. Journal of Cancer Biology & Research, 4(**1**). 1078.

Pal, A., & Kundu, R. (**2020**) Human papillomavirus E6 and E7: The cervical cancer hallmarks and targets for therapy. Frontiers in Microbiology, 10(**3116**). 1-15.

Quistgaard, E. M. (**2021**) BAP31: Physiological functions and roles in disease. Biochimie, 186, 105–129.

Regan, J. A., & Laimins, L. A. (**2008**) Bap31 is a novel target of the human papillomavirus E5 protein. Journal of Virology, 82(**20**), 10042–10051.

Rodríguez, M. I., Finbow, M. E., & Alonso, A. (**2000**) Binding of human papillomavirus 16 E5 to the 16 kDa subunit c (proteolipid) of the vacuolar H + -ATPase can be dissociated from the E5-mediated epidermal growth factor receptor overactivation. Oncogene, 19(**33**), 3727–3732.

Salim, Z., & Munadi, E. (**2017**) Info komoditi tanaman obat. Badan Pengkajian dan Pengembangan Perdagangan Kementerian Perdagangan Republik Indonesia.

Schneider, M. A., Spoden, G. A., Florin, L., & Lambert, C. (**2011**) Identification of the dynein light chains required for human papillomavirus infection. Cellular Microbiology, 13(**1**), 32–46.

Scott, C., & Griffin, S. (**2015**) Viroporins: structure, function and potential as antiviral targets. Journal of General Virology, 96(**8**), 2000–2027.

Sivaramakrishnan, M., Kandaswamy, K., Natesan, S., Devarajan, R. D., Ramakrishnan, S. G., & Kothandan, R. (**2020**) Molecular docking and dynamics studies on plasmepsin V of malarial parasite *Plasmodium vivax*. Informatics in Medicine Unlocked, 19(**100331**). 1-7.

Sumayyah, S., & Salsabila, N. (**2017**) Obat tradisional : Antara khasiat dan efek sampingnya. Majalah Farmasetika, 2(**5**), 1–4.

Suprynowicz, F. A., Disbrow, G. L., Krawczyk, E., Simic, V., Lantzky, K., & Schlegel, R. (**2008**) HPV-16 E5 oncoprotein upregulates lipid raft components caveolin-1 and ganglioside GM1 at the plasma membrane of cervical cells. Oncogene, 27(**8**), 1071–1078.

Tao, M., Kruhlak, M., Xia, S., Androphy, E., & Zheng, Z.-M. (**2003**) Signals that dictate nuclear localization of human papillomavirus type 16 oncoprotein E6 in living cells. Journal of Virology, 77(**24**), 13232–13247.

Trott, O., & Olson, A. J. (**2009**) AutoDock Vina: Improving the speed and accuracy of docking with a new scoring function, efficient optimization, and multithreading. Journal of Computational Chemistry, 31(**2**), 455-461.

Underbrink, M. P., Dupuis, C., Wang, J., & Tyring, S. K. (**2016**) E6 proteins from low-risk human papillomavirus types 6 and 11 are able to protect keratinocytes from apoptosis via Bak degradation. The Journal of General Virology, 97(**3**), 715–724.

Venuti, A., Paolini, F., Nasir, L., Corteggio, A., Roperto, S., Campo, M. S., & Borzacchiello, G. (**2011**) Papillomavirus E5: The smallest oncoprotein with many functions. Molecular Cancer, 10(**1**), 1-18.

Wahidin, M., Febrianti, R., & Susanty, F. (**2020**) Burden of cervical cancer in Indonesia: findings from the global burden of disease study 1990–2017. Advances in Health Sciences Research, 22, 213–217.

Wang, X., Huang, X., & Zhang, Y. (**2018**). Involvement of human papillomaviruses in cervical cancer. Frontiers in Microbiology, 9(**2896**). 1-14.

Wetherill, L. F., Holmes, K. K., Verow, M., Müller, M., Howell, G., Harris, M., Fishwick, C., Stonehouse, N., Foster, R., Blair, G. E., Griffin, S., & Macdonald, A. (**2012**) High-risk human papillomavirus E5 oncoprotein displays channel-forming activity sensitive to small-molecule inhibitors. Journal of Virology, 86(**9**), 5341–5351.

Wetherill, L. F., Wasson, C. W., Swinscoe, G., Kealy, D., Foster, R., Griffin, S., & Macdonald, A. (**2018**) Alkyl-imino sugars inhibit the pro-oncogenic ion channel function of human papillomavirus (HPV) E5. Antiviral Research, 158, 113–121.

Yeo-Teh, N. S. L., Ito, Y., & Jha, S. (**2018**) High-risk human papillomaviral oncogenes E6 and E7 target key cellular pathways to achieve oncogenesis. International Journal of Molecular Sciences, 19(**6**), 1-27.

Submitted: 10/10/2021
Revised: 23/04/2022
Accepted: 08/05/2022
DOI: 10.48129/kjs.16169

New fossils of *Miotragocerus gluten* from the Lower Siwaliks, Pakistan

Kiran Aftab[1, *], Muhammad Shadab[1], Muhammad A. Khan[2], Mubashar Hussain[1], Muhammad A. Babar[3], Syed G. Abbas[4], Muhammad F. Malik[1], Riffat Iqbal[5], Areej Arif[1]

[1]*Dept. of Zoology, University of Gujrat, Gujrat, Pakistan*
[2]*Dr. Abu Bakr Fossil Display & Research Centre, Institute of Zoology, University of the Punjab, Lahore, Pakistan*
[3]*Dept. of Zoology, University of Okara, Okara, Pakistan,*
[4]*Department of Zoology, University of Sialkot, Sialkot, Pakistan*
[5]*Dept of Zoology, Government College University, Lahore, Pakistan.*

[*] *Corresponding author: dr.kiran@uog.edu.pk*

Abstract

The five specimens of *Miotragocerus gluten* were collected from the Lower Siwalik outcrops nearby the villages Chabbar Sayadan and Phadial in Punjab, Pakistan. The newly discovered specimens include the two horn cores and isolated teeth. *Miotragocerus gluten* is the medium-sized bovids, having brachydont to the sub-hypsodont type of dentition. The cusps are elevated, and the crown is surrounded by a rugose enamel layer. The present study reveals the abundance of bovids in the middle Miocene deposits which indicates a grassland ecosystem in this area.

Keywords: Artiodactyla; Chinji; Mammalia; middle Miocene; Siwaliks.

1. Introduction

Siwalik Group is one of the important geological regions of Pakistan which imparts a great contribution to science especially in the field of paleontology. The fossil remains from Lower Siwalik of Pakistan give out much useful evidence and a better understanding of mammalian evolution and biogeography (Asim *et al*., 2020; Khan *et al*., 2017, 2021; Colbert, 1935; Pilgrim, 1913).

The geographical distribution and diversity of *Miotragocerus* have been studied from Indo-Pakistani Siwaliks (Khan *et al*., 2009), Sub-Saharan Africa (Bibi, 2011), China (Zhang, 2005), Asia minor (Kostopoulos, 2005; Kohler, 1987), and Europe (Hartung *et al*., 2020; Fuss *et al*., 2015; Gentry & Kaiser, 2009; Spassov & Geraads, 2004; Morales *et al*., 1999; Stromer, 1928,). Many well-known species are belonging to *Miotragocerus* including *M. cyrenaicus, M. monacensis, M. gluten, M. pannoniae, and M. valenciennesi.* From all these *M. pannoniae* and *M. monacensis* were closely related to each other but *Miotragocerus valenciennesi* is considered as the youngest species (Kirscher *et al*., 2016). This genus also has junior synonyms which include *Dystychoceras, Pikermicerus, Tragocerus, Sivaceros,* and *Graecoryx* (Kostopoulos, 2005).

Miotragocerus also has been recovered from Georgia, Moldova, Ukraine (Korotkevich, 1988; Pevzneret *et al*., 1987; Lungu, 1984), Spain (Moya-Sola, 1983), Iran and Turkey (Kohler, 1987), Germany (Fuss *et al*., 2015; Romaggi, 1987; Tobien, 1953), Austria (Vislobokova, 2007; Thenius, 1948), Bulgaria, Central and Western Europe (Spassov & Geraads, 2004), Pikemi and Samos (Greek), Platania and Nikiti (Greece, Drama Basin) (Vasileiadis *et al*., 2019 Gentry & Kaiser, 2009; Kostopoulos, 2005). *Miotragocerus* were found in the geological time scale of Astaracian and continued to the end of Vallesian and extended to the Turolian time (Gentry & Kaiser, 2009).

The remains of *Miotragocerus* are found in Chinji and Nagri Formations of Pakistani Siwaliks. They feed on shrubs, soft stems, or leaves which indicates that these animals adapt to a special kind of herbivory and are called browsers (Kostopoulos, 2016). The first appearance of *Miotragocerus* was in the middle Miocene and it extend to the late Miocene in Siwaliks. Some remains of *Miotragocerus* large sp. were recovered from the Dhok Pathan localities (Khan *et al*., 2010).

1.1 Geography and Geology

Chabbar Sayadan village (Late. 33° 00′ N; Long. 73° 22′ E) is in District Jhelum (Figure 1), Punjab Pakistan. The outcrops consist of 70% crimson red clay and 30% gray to brown sandstones. (Willis & Behrensmeyer, 1994). The sandstones are tough and cross-bedded. The stratigraphic range of the assemblage area is between 14.2 and 11.2 million years (Barry *et al.,* 2002). Most fossils are observed in claystone.

Phadial village (Late. 32° 83′ N; Long. 73° 16′ E) located in Jhelum valley (Figure 1). The outcrops are red with gray sandstones. It has yielded several mammalian groups such as early tragulids, giraffids, and suids (Sarwar, 1973).

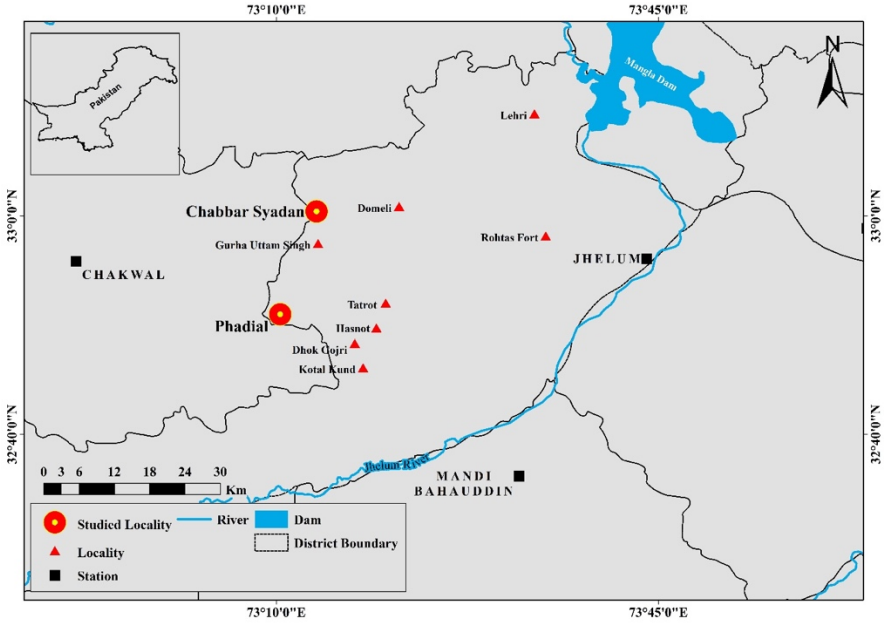

Fig. 1. Location of the middle Miocene sites of Chabbar Sayadan and Phadial in Lower Siwalik of Pakistan. Boundary dates are from Barry *et al.* (2002).

Abbreviations. Ma, million years ago; UOGPC, University of Gujrat Paleontological Collection, Gujrat Pakistan; PC-GCUF, Paleontological collection of Government College University, Faisalabad, Pakistan; AMNH, American Museum of Natural History, New York, USA; MTLA, Mytilini, Greece; PUPC, Punjab University Paleontological Collection, Lahore, Pakistan; M, upper molar; p, lower premolar; m, lower molar; W/L, Width/Length ratio; r, right; l, left; mm, millimeters.

2. Materials and methods

The collections were recovered from Chabbar Sayadan and Phadial outcrops of Lower Siwalik (Figure 1). The isolated upper and lower dentitions were collected in addition to the horn cores for study. Some samples were embedded in the rocks and were collected with the use of a chisel and hammer. Needles were used to remove the tough impurities like claystone and sandstone from the specimens before preparing them for further study.

Metric Vernier Caliper was used to measure the samples, and measurements were taken in millimeters. The numbering on the specimens represents the serial number (denominator) and collection year (numerator) e.g., UOGPC 19/71 in which 19 is the collection year and 71 is the serial number. The studied material was compared to the samples which have been placed in the Paleontological collection of Government College University, Faisalabad, Pakistan (PC-GCUF), American Museum of Natural History New York (AMNH), Mytilini Greece (MTLA), and Punjab University Paleontological Collection stored in Zoology Department, University of the Punjab, Lahore, Punjab, Pakistan (PUPC). The terminology follows Khan *et al*. (2021), Gentry & Hooker (1988).

3. Results

Systematic Palaeontology

Order**:** Cetartiodactyla Montgelard, Catzeflis and Douzery, 1997
Infraorder**:** Pecora Linnaeus, 1758 Sensu Webb, and Taylor, 1980
Family**:** Bovidae Gray, 1821
Subfamily**:** Bovinae Gray, 1821
Tribe**:** Boselaphini Knottnerus-Meyer, 1907
Genus**:** *Miotragocerus* Stromer, 1928

Miotragocerus gluten (Pilgrim, 1937)

New material (in parentheses, the inventory numbers are given). Right horn core (UOGPC 20/79, Chabbar Sayadan); basal fragment of right horn core (UOGPC 20/78, Phadial); rM3 (UOGPC 19/73, Phadial); lp3 (UOGPC 20/76, Chabbar Sayadan); rm3 (UOGPC 20/77, Chabbar Sayadan).

3.1 Description

Horn cores: At the base of the right horn core, a small portion of the frontal and right orbit is preserved (Figures 2a-2d). A prominent infra-orbital foramen is present in the orbit. The pedicel is complete. The horn core is recovered in two pieces with a broken apex. The anterior keel is prominent, and a small step is present at its base. It is slightly compressed laterally at the base, while towards the apex, both sides become rounded. The cross-section at the base is semi-oval but oval at the apex. The total preserved length is 80.19 mm, DAP is 26.20 mm and DT is 14.33 mm.

The basil fragment of the right horn core (Figures 2e-2h) is partially broken at the base anteriorly resulting in the partial loss of the anterior keel. The pedicel is well preserved. At the base of the pedicel, the cross-section is triangular while at the pressurized apex of the horn core, the cross-section is oval. The total preserved length is 35.21 mm, DAP is 25.47 mm and DT is 20.09 mm.

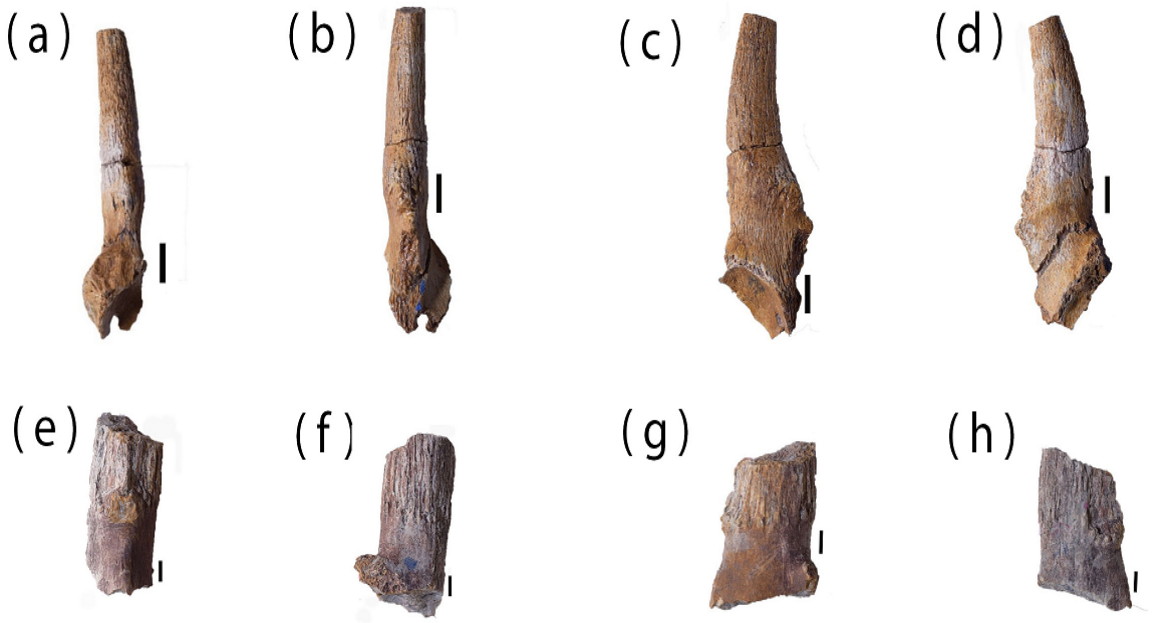

Fig. 2. ***Miotragocerus gluten.*** UOGPC 20/79, Right horn core (a–d); UOGPC 20/78, basal fragment of right horn core (e-h). Views, anterior (a, e); posterior (b, f); medial (c, g) lateral (d, h). Scale bar 30 mm.

Upper dentition: The specimen UOGPC No. 19/73 is an isolated upper third molar of the right side. It is finally preserved, largely worn and the dentine is mostly exposed. A thick cingulum is present at the anterior and lingual side of the crown while it is quite thin at the labial side. The enamel layer is thick shiny and corrugated (Figures 3i-3k). The protocone and paracone are well preserved, but the tooth is partially broken from the posterior side resulting in loss of the apex of the metacone. Both the anterior and posterior fossettes are preserved but

the posterior fossette is narrow anteriorly and broader posteriorly. All the styles are well developed and strong. A thick and strong entostyle covers the medium valleys completely. A weak but prominent cingulum is present at the base of preprotocrista. The paracone rib is well developed and strong. Longitudinal valleys are wavy and deep while transverse valleys are linear and open labially.

Lower dentition: An isolated left p3 (UOGPC 20/76) is well preserved and moderately worn. All the cusps are well developed and prominent (Figure 3l-3m). The protoconid is extensively worn out and form dentinal Island with metaconid and hypoconid. The hypoconid is supported by cingulum and cingular ridges posteriorly. The entoconid is extensively worn out and is contiguous with the metaconid anteriorly. The anterior valley is open and broad while the posterior valleys are closed by a large metastylid that joins the entoconid at the posterior border of the premolar.

The specimen UOGPC 20/77 is an isolated lower third molar of the right side. It is in the late stage of wear. All four types of conids are well preserved. The enamel layer is thick, shiny, smooth, and corrugated. In general contour, it is quadrangular in outline. The anterior fossette is well preserved and C-shaped while the posterior fossette is narrow. The postprotocristid is contiguous with prehypocristid. The mesostylid is well preserved and it is divergent posteriorly. The entoconid is supported by a strong entostylid posteriorly. At its posterior end, a fold is produced in m3 known as hypoconulid (Figures 3n-3p).

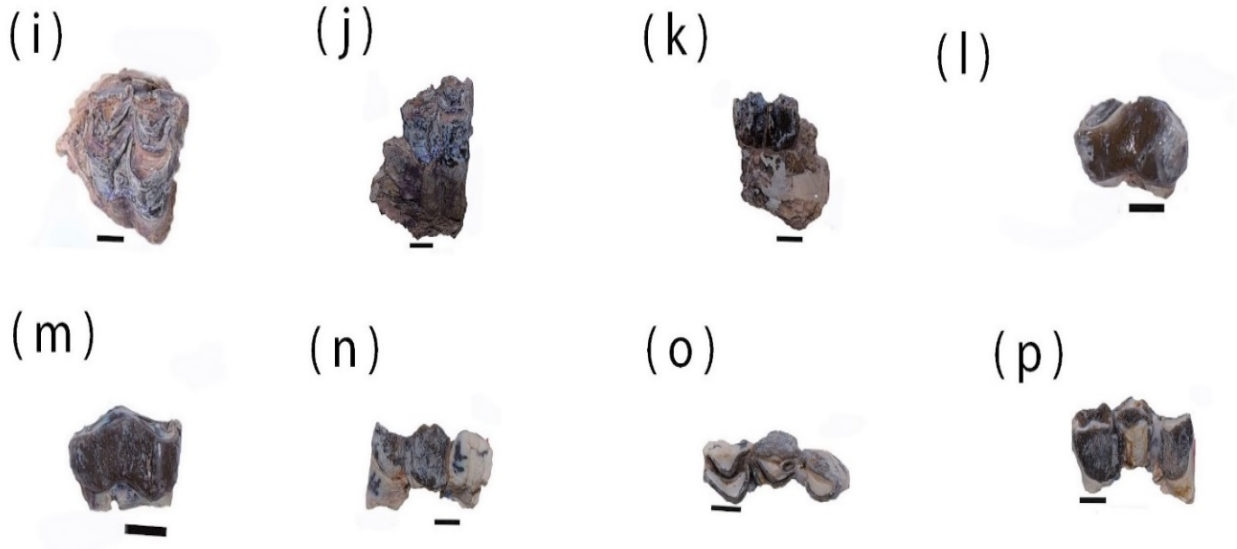

Fig. 3. ***Miotragocerus gluten.*** UOGPC 19/73, rM3(i-k); UOGPC 20/76, lp3(l-m); UOGPC 20/77, rm3 (n-p). views, occlusal (i,o), lingual (j,l,n); labial (k,m,p);. Scale bar 10 mm.

Table 1. Comparative measurements (in mm) of the teeth of ***Miotragocerus gluten*****.** *The studied specimens. Referred data are taken from Iqbal, (2010), Khan *et al*. (2010, 2012, and 2013).

Taxa	Inventory No.	Position	Length	Width	W/L
Miotragocerus gluten	UOGPC 19/73*	rM3	15.07	15.21	1.00
	UOGPC 20/76*	rp3	11.51	8.07	0.70
	UOGPC 20/77*	rm3	26.78	10.06	0.37
	PC-GCUF 11/57	lM3	16.00	16.50	1.03
	PC-GCUF 10/12	p3	12.00	6.20	0.52
	PC-GCUF 11/14	rp3	9.00	5.00	0.55
		rm3	17.00	8.50	0.50
	PC-GCUF 11/13	rm3	17.00	8.00	0.47
	AMNH 29862	M3	16.00	16.0	1.00
Miotragocerus valenciennesi	MTLB 161	M3	19.6	19.0	0.97
	MTLA 190	M3	17.20	15.00	0.87
	MTLA 492	M3	7.40	16.80	0.97
	MTLA 324	M3	19.0	18.50	0.97
	MTLC 25	p3	16.1	8.60	0.53
		m3	24.5	11.8	0.48
	MTLA 299	p3	14.0	8.00	0.57
		m3	21.7	11.8	0.54
	MTLA 284	m3	21.5	11.4	0.53
	MTLA 184	m3	21.1	10.0	0.47
***Miotragocerus* large sp.**	PUPC 83/708	rp3	15.2	6.30	0.41
	PUPC 83/709	lp3	14.0	8.00	0.57
	PUPC 09/86	lm3	25.4	11.4	0.44
***Miotragocerus* sp.**	PUPC 08/20	M3	21.01	9.20	0.43

4. Discussion and comparison

The bovids were in abundance in the Lower Siwalik of Pakistan. The discovered specimen depicts the characters of a medium-sized Bovidae and exhibit the morphology of Miocene boselaphines. *Miotragocerus* and *Tragoportax* are medium-sized boselaphines but *Eotragus, Helicoportax* and *Elachistoceras* are comparatively small size boselaphines (Pilgrim, 1937; Khan *et al*., 2009).

These boselaphines from the Chinji Formation vary in certain characteristics (Khan *et al*., 2009; Thomas, 1984; Pilgrim, 1939, 1937). *Miotragocerus* teeth have a divergent style which is the reason for their inclusion in boselaphine. The upper molars are sub-hypsodont and quadrate in *Miotragocerus gluten* (Table1, Figure 4). In M3 entostyle are smaller than *Tragoportax* (Solounias, 1981). The parastyle and endostyle are very well developed in M3. In the lower premolar, the metaconid is weak and the cavity between the paraconid and metaconid is open and shallow. In the lower 3rd molar, the hypoconulid is compressed transversely. There are certain features of *Miotragocerus* lower molar which include taloned, an anterior flange which is transverse in shape, shiny enamel, convex shape, and a strong mesostylid. The morphological studies and measurements (Table1, Figure 4) show that these newly discovered specimens are similar to the already described remains of *Miotragocerus gluten* (Khan *et al*., 2010; Spassov & Geraads, 2004).

Tangential compression of horn cores is a distinctive feature of *Miotragocerus*. Distinguishing by tangentially constricting horn cores, weak posterolateral keel, little size, clear delineation, and clockwise rotation present the individual characters of *Miotragocerus* (Kostopoulos & Koufos, 1996). It has been found that the horn core of *Miotrgocerus gluten* recovered from central Europe is denser and has a more vertical shape as compared to the *Miotragocerus* (Stromer, 1928). The horn core of *Miotrgocerus gluten* is larger from *Miotrgocerus* cf. *pannoniae* (Kostopoulos & Koufos, 1996). The medial and lateral surfaces of the horn core are flattened, and it is mediolaterally compressed. The anterior keel is sharp, but the posterior keel is absent or poorly developed. A divergent tip and a convergent basal portion are found due to the little torsion at the base of the horn core, in the front view. (Abbas *et al,* 2021). The characteristic features of recovered horn cores are similar to the already described *Miotragocerus gluten*.

The Artiodactyls are in abundance in Lower Siwalik of Pakistan during the middle Miocene age. *Miotragocerus* are medium-sized bovids that prefer wood mean forested areas (Spassov & Geraads, 2004). The bovids together with tragulid indicate a wet and forested landscape. Chinji Formation exbibit half-closed and half-opened woodland ecosystem (Barry *et al*., 2002: Ameen *et al*., 2020).

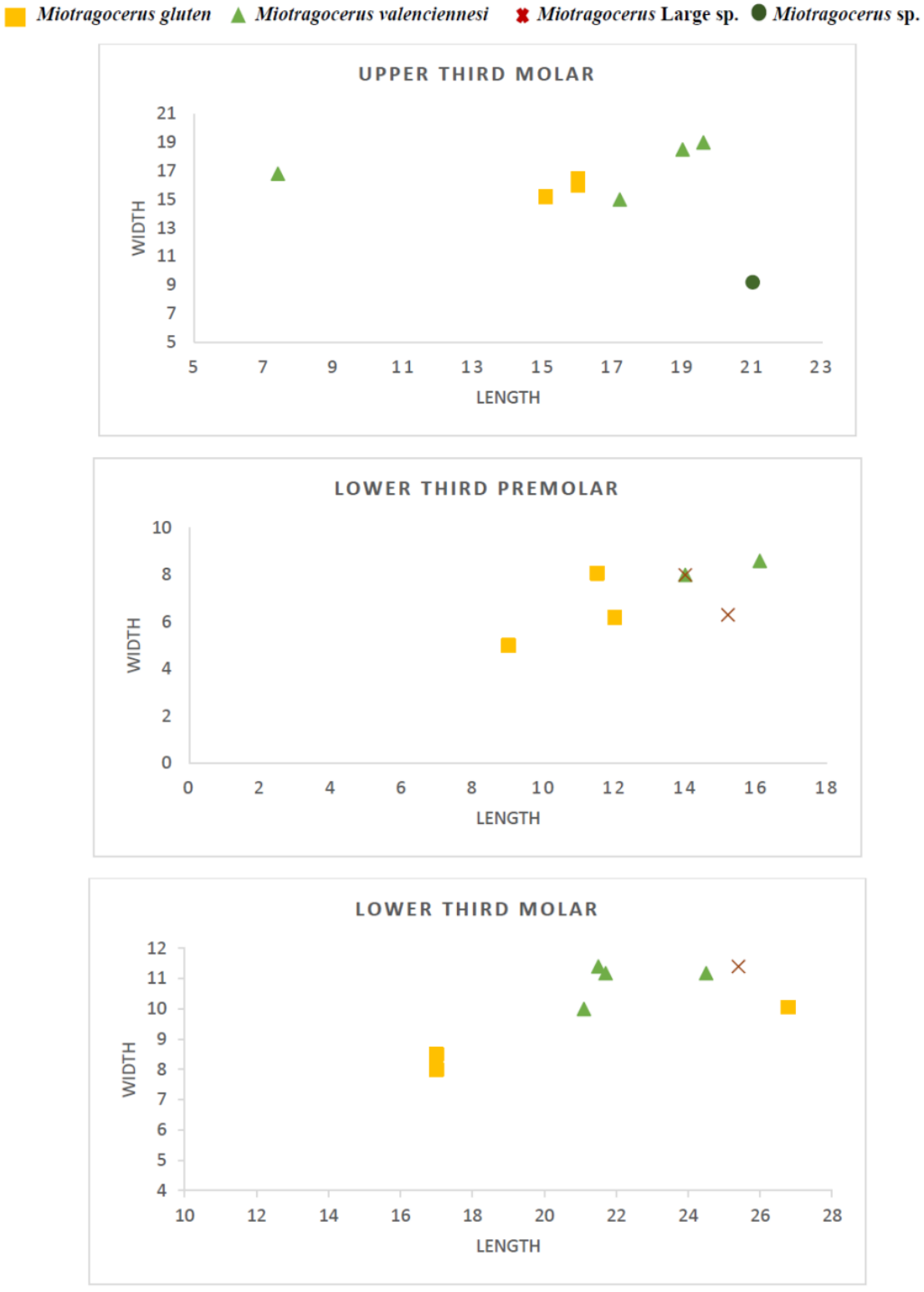

Fig. 4. Scatter diagram showing dental proportions of the *Miotragocerus gluten*. Referred data are taken from Iqbal (2010), Khan *et al*. (2010, 2012, and 2013).

5. Conclusions

Miotragocerus gluten have been recorded from the Chinji Formation of Lower Siwaliks (Pakistan), which is dated to 14.2–11.2 Ma. The cheek teeth are sub-hypsodont with moderately thick and rugose enamel. The middle Miocene boselaphine represents a mixture of habitats, ranging from wetlands with densely forested pockets to woodlands. The early Siwalik bovids with giraffids and tragulids indicate humid, forested habitats.

References

Abbas, S.G., Babar, M.A., Khan, M.A., Hussain, I., Akhtar, M., Yasin, A. & Khalid, M. (2021). *Tragoportax* and *Miotragocerus* from Nagri Formation type locality, Siwalik Group, Pakistan (early Late Miocene): Taxonomic problems and hypotheses regarding their resolution. Annales de Paléontologie, **107** (3): 1-9.

Ameen, F.A., Fattah, A.I. & Qader, B.O. 2020. Microfacies and depositional environment of the Upper Oligocene and Lower Miocene successions from Iraqi Kurdistan Region. Kuwait Journal of Science, **47**(4): 127-136.

Asim, M., Aftab, K., Nawaz, M.K., Khan, M.A., Babar, M.A. *et al.* (2020). New Specimens of *Merycopotamus* (Artiodactyla: Anthracotheriidae) from middle Miocene of Potwar Plateau, Pakistan, **30**(6): 1435-1441.

Barry, J.C., Morgan, M., Flynn, L., Pilbeam, D., Behrensmeyer, A.K., *et al.* (2002). Faunal and environmental change in the Late Miocene Siwaliks of northern Pakistan. Paleobiology, **28**: 1-72.

Bibi, F. (2011). Mio-Pliocene faunal exchanges and African biogeography. The record of fossil bovids. Plos one, **6** (2): e16688.

Colbert, E.H. (1935). Siwalik mammals in the American Museum of Natural History. American Philosophical Society.

Fuss, J., Prieto, J. & Böhme, M. (2015). Revision of the boselaphin bovid *Miotragocerus monacensis* Stromer, 1928 (Mammalia, Bovidae) at the Middle to Late Miocene transition in Central Europe. Neues Jahrbuch für Geologie und Paläontologie Abhandlungen, **276**: 229-265.

Gentry, A.W. & Hooker, J.J. (1988). The phylogeny of Artiodactyla. In: Benton M.J. (Ed.). The phylogeny and classification of the tetrapods, Vol. 2: Mammals, Systematics Association Special Volume No. 35B Clarendon, Oxford, Pp. 235-272.

Gentry, A.W. & Kaiser, T.M. (2009). The Bovidae of Dorn-Dürkheim 1, Germany (Turolian age). Paläontologische Zeitschrift, **83**: 373-392.

Iqbal, M. (2010). Taxonomy and dental morphological studies of fossil Artiodactyls from type locality of Dhok Pathan, Punjab, Pakistan. Ph.D. thesis, University of the Punjab Lahore, Pakistan.

Hartung, J., Lechner, T. & Böhme, M. (2020). New cranial material of *Miotragocerus monacensis* (Mammalia: Bovidae) from the late Miocene hominid locality Hammerschmiede (Germany). Neues Jahrbuch Fur Geologie Und Palaontologie-Abhandlungen, **298** (3): 269-284.

Khan, M.A., Akhtar, M. & Ikram, T. (2012). True ungulates from the Nagri type locality (Late Miocene), northern Pakistan. Journal of Animal and Plant Sciences, **22** (1 Supplement), 1-59.

Khan, M.A., Akhtar, M. & Iqbal, M. (2010). The late Miocene artiodactyls in the Dhok Pathan type locality of the Dhok Pathan formation, the Middle Siwaliks, Pakistan. Pakistan Journal of Zoology, **10**: 1-90.

Khan, M.A., Akhtar, M., Babar, M.A., Abbas, S.G., Siddiq, M.K. *et al.* (2013). Some new remains of middle Miocene mammals from the Chinji Formation, northern Pakistan. Pakistan Journal of Zoology, **13**: 1-55.

Khan, M.A., Iqbal, M., Ghaffar, A. & Akhtar, M. (2009). Proamphibos (Bovini, Bovidae, Mammalia) from the Tatrot Formation in the Upper Siwaliks of Pakistan. Journal of Animals and Plants Sciences, **19**(2): 104-107.

Khan, M.A., Abbas, S.G., Babar, M.A., Kiran, S., Riaz, A. *et al.* (2017). *Dorcatherium* (Mammalia: Tragulidae) from lower Siwaliks of Dhok Bun Amir Khatoon, Punjab, Pakistan. Pakistan Journal of Zoology, **49**: 883-888.

Khan, M.A., Asim, M., Babar, M.A., Abbas, S.G., Nawaz, M.K. *et al.* (2021). New remains of Gazella (Bovidae) from Middle Miocene, Pakistan. Arabian Journal of Geosciences, **14**(17): 1-8.

Khan, M.A., Malik, M., Khan, A.M., Iqbal, M. & Akhtar, M. (2009). Mammalian remains in the Chinji type locality of the Chinji Formation: A new collection. The Journal of Animal & Plant Science, **19** (4): 224-229.

Kirscher, U., Prieto, J., Bachtadse, V., Aziz, H.A., Doppler, G. *et al.* (2016). A biochronologic tie point for the base of the tortonian stage in European terrestrial settings: Magnetostratigraphy of the topmost Upper freshwater molasses sediments of the north alpine foreland basin in Bavaria (Germany). Newsletters on Stratigraphy, **49**: 445-467.

Kohler, M. (1987). Boviden des türkischen Miozäns (Käno- zoikum und Braunkohlen der Türkei). Paleontologia iEvolutió, **21**: 133-246.

Korotkevich, E.L. (1988). History of the Formation of the Hipparion Fauna in Eastern Europe. Naukova Dumka [in Russian].

Kostopoulos, D.S. (2016). Artiodactyla - Palaeontology of the upper Miocene vertebrate localities of Nikiti (Chalkidiki Peninsula, Macedonia, Greece). Geobios **49**:119-234.

Kostopoulos, D.S. & Koufos, G.D. (1996). Late Miocene bovids (Mammalia, Artiodactyla) from the locality "Nikiti-1" (NKT), Macedonia, Greece. In Annales Paleontologie, **81**: 251–300.

Kostopoulos, D.S. (2005). The Bovidae (Mammalia, Ar-tiodactyla) from the late Miocene of Akkaşdağı, Turkey. In: Sen, S. (Ed.). Geology, mammals, and environments at Akkaşdağı, late Miocene of Central Anatolia. Geodiversitas, **27**(4): 747-791.

Lungu, A.N. (1984). Hipparion Fauna of the Middle Sarmatian of Moldova. Stiinca: Kisinev, 1-144 [In Russia].

Morales, J., Nieto, M., Kohler, M. & Moya-Sola, S. (1999). Large mammals from the Vallesien of Spain. In: Agustí, J., Rook, L. & Andrews, P. (Eds.). Hominoid evolution of Neogene terrestrial ecosystems in Europe, Pp113-126. Press, Cambridge University.

Moya-Sola, S. (1983) Los Boselaphini (Bovidae Mammalia) of the Neogeno de la Península Ibérica (Doctoral dissertation, Universitat Autònoma de Barcelona, **18**: 1–236.

Pevzneret, M.A., Lungu, A.N., Vangengeim, E.A. & Basilyan, A.E. (1987). Position of Vallesian localities of the Hipparion fauna of Moldova on the magnetochrono- logical scale. – Izvestiya Akademii Nauk SSSR, Seriya Geologicheskaya, **4**: 50–59.

Pilgrim, G. E. (1913). The correlation of the Siwalik with mammal horizons of Europe. Record of Geological. Survey of India, **43**: 264-325.

Pilgrim, G.E. (1937). Siwalik antelopes and oxen in the American Museum of Natural History. Bulletin of the American museum of Natural History, **72**: 729–874.

Romaggi, J.P. (1987). Les antilopes du Miocène supérieur du Coiron (Ardèche, France). Thèse de doctorat, Cen- tre des Sciences de le Terre, Université Claude Bernard Lyon: Pp.395

Sarwar, M. (1973). A new genus of the family Hyracodontidae Cope from the Lower Siwalik beds of the Punjab. Pakistan Journal of Zoology, **5** (2): 197–201.

Solounias, N. (1981). The Turolian fauna from the Island of Samos, Greece. Karger Publishers.

Spassov, N. & Geraads, D. (2004). *Tragoportax* Pilgrim, 1937 and *Miotragocerus* Stromer, 1928 (Mammalia, Bo- vidae) from the Turolian of Hadjidimovo, Bulgaria, and a revision of the late Miocene Mediterranean Boselaphini. Geodiversitas, **26**(2): 339–370.

Stromer, E. (1928). Wirbeltiere im obermiocänen Flinz Münchens. – Abhandlungen der Bayerischen Akademie der Wissenschaften, mathematisch-naturwissenschaftliche Abteilung, **32** (1): 1-74.

Thenius, E. (1948). Über die Entwicklung des Hornzapfens von Miotragocerus. Springer-Verlag.

Thomas, H. (1984). Les bovides ante-hipparions des Siwaliks inferieurs (Plateau du Potwar), Pakistan. Memoirs of the Geological Society of France, **145**: 1–68.

Tobien, H. (1953). Miotragocerus Stromer (Bovidae, Mamm.) aus den unterpliocänen Dinotheriensanden Rheinhessens. – Notizblatt des Hessischen Landesamtes für Bodenforschung, **81**: 52–58.

Vasileiadis, N., Tsoukala, E., & Kostopoulos, D. S. (2019). The late Miocene bovids from Platania (Drama Basin, Greece), with description of a new species of Palaeoryx. Geobios, **55**: 57-76.

Vislobokova, I.A. (2007). New data on late Miocene mammals of Kohfidisch, Austria. – Paleontological Journal, **41**: 451–460. doi: 10.1134/S0031030107040119.

Willis, B.I. & Behrensmeyer, A.K. (1994). Architecture of Miocene over bank deposits in northern Pakistan. Journal of Sedimentary Research, **64:** 60–67.

Willis, B.J. & Behrensmeyer A.K. (1995). Fluvial systems in the Siwalik Neogene and Wyoming Paleogene. Palaeogeography, Palaeoclimatology, Palaeoecology, **114**: 13-35.

Zhang, Z.Q. (2005). Late Miocene Boselaphini (Bovidae, Artiodactyla) from Fugu, Shaanxi Province, China. Vertebrata Palasiatica, **43** (3): 208-218.

Submitted: 20/08/2021
Revised: 11/11/2021
Accepted: 21/11/2021
DOI: 10.48129/kjs.15777

Nutritional composition and biochemical characteristics of five date palm fruit (*Phoenix dactylifera* L.) varieties at the Khalal stage grown in Kuwait.

Maryam Al-Hilal[1,] *, Zeinab Moussa[2] & Alfred Anderson[2]

[1] *Dept. Medical Research, Primary Healthcare, Ministry of Health, Kuwait*
[2]*Dept. of Food Science and Nutrition, Kuwait University, P.O. Box 5969, Safat 13060, Kuwait*

**Corresponding author: maryam.alhilal@gmail.com*

Abstract

Palm dates are among the most highly cultivated and consumed fruits in Kuwait and other Arabian Gulf countries. However, data on the nutritional content of Kuwaiti date fruits remain scarce. The purpose of the current study was to determine the nutritional composition and biochemical characteristics of five date palm fruit varieties at the Khalal stage grown in Kuwait. Samples of five different cultivars (Berhi (samples from 2 different locations), Ikhlas, Saamaran, and Khanizi) grown in Kuwait were analyzed for energy, protein, carbohydrates, sugars, antioxidants, and micro-minerals. Varieties studied had high energy values ranging between 351.63 kcal/100g and 368.35 kcal/100g. They were rich in potassium (4450-7128mg/100g), with significant amounts of calcium (287.8-469.1mg/100g), magnesium (130.3 -294.5 mg/100g), sodium (70.7-123.3 mg/100g), iron (2.45-3.2 mg/100g) and manganese (0.7-1.55 mg/100g). Gallic (19.97-5.47 mg/100g), chlorogenic (0-0.712mg/100 g), and ascorbic (0.624-0.875 μg/1mg) acids were the main antioxidants. The data indicate that the Kuwaiti date fruit is a rich source of essential nutrients making it an important local product that requires further investigations for its nutritional properties and industrial utilization prospects.

Keywords: Date fruits; nutrition content; antioxidant, khalal stage, Kuwait

1. Introduction

Date palm (*Phoenix dactylifera L.)* is a monocotyledon from the *Palmaceae* family. The date palm fruit is mainly cultivated in the Middle Eastern countries mostly Egypt, Iran, Saudi Arabia, Algeria, Iraq, Pakistan, Oman, United Arab Emirates, Tunisia and Libya (Eid *et al*., 2014). The fruit maturation can be divided into five stages: hababouk, kimri, khalal (or besser), rutab, and tamar, respectively, with different characteristics at each stage (Abdul-Afiq *et al*., 2013).

The date fruit contains naturally occurring compounds that exhibit antibacterial and antioxidant activities (Samad *et al*., 2016), mainly due to the presence of significant amounts of polyphenolics, anthocyanin and other bioactive compounds. Samad *et al*., (2016) reported that the methanolic extract of Ajwa demonstrated an antibacterial activity against four different types of bacteria, indicating that dates can be utilized as a natural antibacterial compound.

Date palm fruit has received special attention from the nutritional and therapeutic perspective. They are known as rich sources of sugars and thus considered a high energy food source (Al-Shahib *et al*., 2003). Furthermore, dates are a rich source of dietary fiber.

Date palm has been a major agricultural crop in Kuwait for over 90 years. Approximately 601,563 trees are planted in 4,181 registered farms located in three main regions of Kuwait: Abdhally, Wafra and Sulaibia. Cultivation area has increased progressively from 870 ha in 1998 to 5,099 ha in 2011 with an increase in annual fruit production from 6,662 mt in 1998 to 33,562 mt (FAO, 2013). However, data on nutritive as well as bioactive compounds of the date palm varieties grown in Kuwait are scarce.

The purpose of the current study, therefore, was to determine the nutritional composition and biochemical characteristics of five date palm fruit varieties at the Khalal stage grown in Kuwait.

2. Material and Methods

2.1. Sample

Fresh date fruits grown in Kuwait were donated by farms located in Wafra, Sabhan, Sabah area and Abdali, which are the main date plantation areas in Kuwait. Five samples were obtained from the varieties Berhi (samples from 2 different locations), Ikhlas, Saamaran, and Khanizi. Samples were freeze-dried and stored under -40^{O}C until analysis.

2.2. Ash content

Ash was determined using the standard laboratory method for ash determination by ashing in a furnace at 550°C for 6 hr.

2.3. Energy content

Samples were ground into powder and analyzed in Parr Bomb 6400 Calorimeter (Parr Instrument, IL. USA) in which the energy values were determined automatically.

2.4. Macronutrient analysis

2.4.1. Total protein

Nitrogen content was determined using 0.1 g of powdered sample from each cultivar in Elemental Analyzer (Leco Truespec, St. Joseph, MI. USA). Total protein was calculated from nitrogen content using the equation %N x 6.25 (Habib and Ibrahim, 2011).

2.4.2. Total carbohydrates and sugars

A 1.5 g ground sample of each cultivar was mixed with 7.5 ml of HPLC grade water. Reaction mixtures were sonicated for 30 min at 40°C and centrifuged at 8000 rpm for 15 min at 10°C. The supernatant was filtered through 0.45 µM membrane filter, and a 20 µl sample of filtrate was injected into Agilent 1260 Infinity II HPLC (Agilent, Santa Clara, CA, USA), equipped with a RI detector, and connected with Thermo Scientific™ HyperREZ™ XP Carbohydrate column Pb++ (7.7 id x 300 mm, particle size: 8 microns). The mobile phase was DI water at a flow rate of 0.600 ml/min at 80°C.

2.5. Micronutrient Analysis

A one g sample of each cultivar was cold-digested with HNO_3 overnight, followed by further digestion with HNO_3, HCl, and 30% H_2O_2 at 95°C. Prepared samples were then analyzed with Inductively Coupled Plasma – Optical Emission Spectrometer (ICP-OES) Optima 7300 (Perkin Elmer, Waltham, MA, US).

2.5.1. Ascorbic Acid

A 0.5 g of powdered sample was mixed with 30 ml of 70:30 v/v methanol-water extraction solvent. The mixture was sonicated for 20 min at 27±3°C, diluted up to mark, filtered through a 0.45 µm membrane, and injected into Nexera X2 UFLC HPLC (Shimadzu, Japan). The column was Zorbax SB-C18 (4.6 x 250 mm, 5 microns), with flow rate of 1 ml/min, UV detector at 254nm, mobile phase A – 25mM NaH_2PO_4 pH 2.5 and Mobile phase B – Methanol.

2.5.2. Phenolics

A five-gram sample of each cultivar was mixed with 25 g of methanol. The reaction mixture was stirred for 24 hours. The supernatant was filtered using Whatman No. 1 filter paper and stored at 4°C until analysis. A sample of 20 microliters were injected into Nexera X2 UFLC HPLC system (Shimadzu, Japan) equipped with a UV at 254 nm detector and connected with Waters Nova-pak C18 column (4.6 x 150 mm, 5 microns). The mobile phase was 0.4% phosphoric acid: acetonitrile: methanol (80:10:10), flow rate: 0.7 ml/min, ambient temperature, and isocratic elution.

2.6. Statistical analysis

Statistical analysis was performed using IBM SPSS (version 25.0). Multivariate Analysis of variance (MANOVA) and Post Hoc LSD tests ($p \leq 0.05$) were performed to evaluate the influence of cultivar on nutritional composition of the date samples and to determine significant differences between means.

3. Results

3.1 Energy, protein, and ash

Table 1 shows the data for calories, protein, and ash in the date samples. Energy values ranged from 351.63 to 368.35 kcal/100 g. Berhi from Wafra farm had the highest energy (368.3 kcal/100 g), followed by Khanizi from Wafra (367.9 kcal/100 g), Berhi from Sabah Area (365.2 kcal/100 g), Ikhlas from Wafra (364.29 kcal/100 g), and Saamran from Sabhan (351.6 kcal/100 g). The difference between the first two varieties was not statistically significant while Saamaran from Sabhan was significantly ($p \leq 0.05$) different from the rest.

The highest protein content was in cultivars from Wafra farms: Berhi (4.77% ± 0.01), Khanizi (4.23% ± 0.01), and Ikhlas (4.11% ± 0.04). Berhi from Sabah Area has 3.56% ± 0.05 protein, with the least being in Saamaran from Sabhan farms (2.82% ± 0.21). All differences were significant ($p \leq 0.05$) across all samples. This result could possibly indicate that cultivation location, and/or related factors such as soil, weather, and farming techniques may have a significant effect on protein content, possibly even more than cultivar.

Saamran contained the least value of ash (2.08% ± 0.12), with the highest being that of Ikhlas from Wafra farms (6.84% ± 0.06). All the differences were statistically significant ($p \leq 0.05$) between cultivars.

Table 1. Energy, Protein, and Ash contents of five varieties of dates at Khalal stage

Cultivar (Area)	Kcal/100 g[1]	% Protein	% Ash
Berhi (Sabah Area)	$365.2 \pm 1.86^{b,c}$	3.56 ± 0.05^{b}	4.56 ± 0.17^{b}
Berhi (Wafra)	368.4 ± 0.85^{d}	4.77 ± 0.01^{d}	4.88 ± 0.54^{b}
Ikhlas (Wafra)	364.3 ± 0.17^{b}	4.11 ± 0.04^{c}	6.84 ± 0.06^{c}
Khanizi (Wafra)	$367.9 \pm 0.17^{c,d}$	4.23 ± 0.01^{c}	4.28 ± 0.16^{b}
Saamaran (Sabhan)	351.6 ± 0.17^{a}	2.82 ± 0.21^{a}	2.08 ± 0.12^{a}

[1]Weight of edible portion of dried Khalal.
Values are shown as mean ± standard deviation of two replicates.
Means within a column with different letters differ significantly ($p \leq 0.05$).

3.2. Sugars

Table 2 shows the data for the different sugars in the date samples analyzed. All cultivars were high in fructose and glucose, in equal proportions, and had non-detectable sucrose. The variations in sugar content across cultivars in this study was high and significant ($p \leq 0.05$). The highest cultivar in glucose, fructose, and total sugars was Berhi from Wafra (34.4 g/100 g, 33.6 g/100 g, 68.0 g/100 g, respectively), followed by Khanizi from Wafra (29.6 g/100 g, 30.35 g/100 g, 60.1 g/100 g, respectively), Saamaran from Sabhan (25.2 g/100 g, 25.7 g/100 g, 50.9 g/100 g, respectively), Berhi from Sabah area (22.5 g/100 g, 20.9 g/100 g; 43.4 g/100 g, respectively). The glucose/fructose ratios across all samples were close to 1, indicating almost equal amounts of glucose and fructose were present.

Table 2. Sugar contents of five varieties of dates at Khalal stage

Cultivar (Area)	Sucrose (g/100 g)[1]	Glucose (g/100 g)[1]	Fructose (g/100 g)[1]	Glu/Fru	Total Sugars (g/100 g)[1]
Berhi (Sabah Area)	0000^{a}	22.5 ± 0.3^{b}	20.9 ± 0.2^{b}	1.07	43.4 ± 0.5^{b}
Berhi (Wafra)	0000^{a}	34.4 ± 0.5^{e}	33.6 ± 0.4^{e}	1.02	68.0 ± 0.9^{e}
Ikhlas (Wafra)	0000^{a}	19.7 ± 0.05^{a}	18.9 ± 0.09^{a}	1.04	38.6 ± 0.06^{a}
Khanizi (Wafra)	0.22 ± 0.4^{a}	29.5 ± 0.6^{d}	30.4 ± 0.3^{d}	0.97	60.1 ± 1.3^{d}
Saamaran (Sabhan)	0000^{a}	25.2 ± 0.1^{c}	25.7 ± 0.1^{c}	0.98	50.9 ± 0.2^{c}

[1]Weight of edible portion of dried Khalal.
Values are shown as mean ± standard deviation of four replicates.
Means within a column with different letters differ significantly ($p \leq 0.05$).

3.3. Minerals

Table 3 shows the data for mineral content of the dates varieties studied. The highest mineral in all cultivars was potassium, followed by calcium, magnesium, and sodium, with trace amounts of iron and manganese. All other minerals tested were below detection limits. Minerals commonly found in other cultivars, such as copper, zinc, phosphorous and selenium, were not detectable in the samples of this study. This can be attributed to either the nature of the cultivars, the maturation stage, the nature of Kuwaiti soil and farming conditions, or the detection limits of the methods employed.

Potassium was found in high amounts, ranging from 7128 ± 103 mg/100g (Khanizi, Wafra) to 2786 ± 76.4 mg/100g (Saamaran, Sabhan). The second most abundant mineral was calcium, ranging from 469.10 ± 4.38 mg/100 g (Khanizi, Wafra) to 287.8 ± 7.92 mg/100g (Berhi, Wafra).

Table 3. Mineral content of five varieties of dates at Khalal stage

Cultivar (Area)	K (mg/100 g)[1]	Ca (mg/100 g)[1]	Mg (mg/100 g)[1]	Na (mg/100 g)[1]	Fe (mg/100 g)[1]	Mn (mg/100 g)[1]	% of fruit weight
Berhi (Sabah Area)	4485±3.54 [b]	331.0±1.98[c]	229.2± 1.06[b]	103.2±0.28[b]	2.85±0.071[a,b]	1.2±0.00[c]	5.2
Berhi (Wafra)	4450±48.1 [b]	287.8±7.92[a]	217.2±3.47[b]	70.7± 2.62[a]	2.80±0.141[a,b]	1.55±0.071[d]	5
Ikhlas (Wafra)	5506±77.1[c]	292.55±3.46[a]	130.3± 2.33[a]	123.3±1.56[c]	2.45±0.071[a]	0.90±0.00[b]	6
Khanizi (Wafra)	7128±103.2[d]	469.10± 4.38[b]	294.5±4.67[c]	100.9±2.26[b]	3.2±0.28[b]	1.20±0.00[c]	8
Saamaran (Sabhan)	2786±76.4 [a]	299.0±0.00[a]	137.2±5.8[a]	76.4±0.92[a]	3.1±0.14[b]	0.70±0.00[a]	3.3

[1]Weight of edible portion of dried Khalal.
Values are shown as mean±standard deviation of two replicates.
Means within a column with different letters differ significantly ($p \leq 0.05$).

Magnesium values decreased from 294.5±4.67 mg/100g (Khanizi, Wafra) to 229.2±1.06 mg/100g (Berhi, Sabah Area) to 217.2±3.47 mg/100g (Berhi Wafra) to 137.2±5.8 mg/100g Saamaran Sabhan and finally to 130.3±2.33 mg/100g (Ikhlas, Wafra). Ikhlas, Wafra, had the highest sodium content (123.3±1.56 mg/100g), followed by Berhi from Sabah Area (103.2±0.28 mg/100g), Khanizi from Wafra (100.9±2.26 mg/100g), Saamran from Sabhan (76.4± 0.92 mg/100g), and finally Berhi from Wafra (70.7±2.62 mg/100g).

Macro-mineral differences between the samples were significant. Iron ranged from 3.2 ±0.283 mg/100g (Khanizi, Wafra) to 2.45±0.071 mg/100g (Ikhlas, Wafra), but the differences between cultivars was mostly insignificant. Manganese ranged between 1.55±0.07 mg/100g (Berhi, Wafra) and 0.70±0.00 mg/100g (Saamaran, Sabhan), with cultivars varying significantly, except for Khanizi (Wafra) and Berhi (Sabah Area). Khanizi (Wafra) was the richest cultivar in minerals, except in sodium and manganese. The difference between it and other Wafra-based cultivars was significant, possibly indicating that cultivar had a larger effect on mineral composition than soil content and farming conditions.

3.4. Antioxidants

3.4.1 Phenolics

Table 4 shows the data for phenolic content of the date samples. Among the phenolic acids, gallic acid was the highest in the samples, followed by chlorogenic acid, while caffeic acid and coumaric acid were below detection limits. The highest amount of gallic acid was 19.97±3.52 mg/100g (Khanizi, Wafra), followed by 11.9±3.2 mg/100g (Berhi, Sabah Area), 9.59±0.83

mg/100g (Ikhlas, Wafra), 8.98±0.62 mg/100g (Berhi, Wafra) and 5.47±0.151 mg/100g (Saamaran, Sabhan). Only Khanizi was significantly different from the rest.

Table 4. Values of phenolic content of the five varieties of dates at Khalal stage

Cultivar (Area)	Gallic Acid (mg/100 g)	Chlorogenic acid (mg/100 g)	Caffeic acid (mg/100 g)	Coumaric Acid (mg/100 g)
Berhi (Sabah Area)	11.9±3.20^{b}	0.71±0.006^{b}	0.0±0.0	0.0±0.0
Berhi (Wafra)	8.98±0.62^{a,b}	0.12±0.01^{c}	0.0 ± 0.0	0.0 ± 0.0
Ikhlas (Wafra)	9.59± 0.83^{a,b}	0.064± 0.01^{b}	0.0 ± 0.0	0.0 ± 0.0
Khanizi (Wafra)	19.97± 3.52^{c}	0.17± 0.002^{d}	0.0 ± 0.0	0.0 ± 0.0
Saamaran (Sabhan)	5.47± 0.15^{a}	0.0± 0.0^{a}	0.0 ± 0.0	0.0 ± 0.0

Weight of edible portion of dried Khalal.
Values are shown as mean ± standard deviation of three replicates.
Means within a column with different letters differ significantly ($p \leq 0.05$).

Berhi (Sabah Area) was significantly the highest in chlorogenic acid (0.71 ± 0.006 mg/100g), followed by Khanizi (Wafra) (0.17 ± 0.00263 mg/100g), Berhi (Wafra) (0.12± 0.01 mg/100g), Ikhlas (Wafra) (0.064± 0.01 mg/100g), and the lowest was Saamaran, which was below detection limits. Caffeic acid and coumaric acid were also below detection limits.

3.4.2. Ascorbic acid

Table 5 shows the values for ascorbic acid. Ascorbic acid ranged from 0.88±0.03 µg/mg (Khanizi, Wafra) to 0.62±0.008 µg/mg (Berhi, Sabah Area). Ikhlas (Wafra) had 0.75± 0.02 µg/mg, Saamaran (Sabhan) had 0.72 ± 0.1 µg/mg, and Berhi (Wafra) had 0.71± 0.03 µg/mg. All difference between cultivars were significant. ($p \leq 0.05$).

Table 5. Ascorbic acid content of five date varieties at Khalal stage

Cultivar (Area)	µg/mg	mg/100 g[1]
Berhi (Sabah Area)	0.62 ± 0.008^{a}	6.2E-6 ± 8.1E-8^{a}
Berhi (Wafra)	0.71 ± 0.03^{b}	7.1E-6 ± 2.6 E-7^{b}
Ikhlas (Wafra)	0.75 ±0.02^{b}	7.4E-6 ± 2.3 E-7^{b}
Khanizi (Wafra)	0.88 ± 0.03^{c}	8.7E-6 ± 2.7 E-7^{c}
Saamaran (Sabhan)	0.72 ± 0.1^{a}	7.1E-6 ± 9.7 E-7^{a}

[1]Weight of edible portion of dried Khalal.
Values are shown as mean ± standard deviation of four replicates. Means within a column with different letters differ significantly ($p \leq 0.05$).

4. Discussion

4.1. Energy, Protein, and Ash

Date fruits are a rich source of energy, with values varying according to cultivar (Ghnimi *et al*. 2017). A review by Nasir *et al*. (2015) indicated that the average calorie from fresh dates is 314 kcal/100g and 213 kcal/100g for dried dates. The averages in the current study are slightly higher than the reported averages. The energy value of the Berhi cultivar from Sabah area was significantly lower than that from Wafra farm, suggesting that cultivar may not be the only determinant of nutritional composition. Differences in farming location and factors related to that may have significant impact.

Dates have limited amounts of ash and protein (Assirey, 2015). Proteins make 1-3% of the date fruit and have a good amino acid profile (Sidhu, 2012). However, protein, amino acid, and ash concentrations decrease across developmental stages (Al-Hooti *et al*. 1997; Sidhu, 2012). The current study indicated that dates were not high in protein. The dates with the highest protein - Berhi, Khanizi, and Ikhlas - were from Wafra farms, a possible indication that location, soil, weather, farming techniques etc., may have a significant impact on protein content, possibly even more than cultivar.

The ash concentrations of dates in this study were similar to previous studies on Kuwaiti dates at Tamr stage, where the ash content constituted 5% of the total weight of all varieties. However, these averages are higher than the reported average of 1.67g/100g for dates (Nasir *et al*. 2015).

4.2.Sugars

All cultivars were high in fructose and glucose, in equal proportions, and had non-detectable amounts of sucrose, similar to previous reports that major sugars in dates are glucose and fructose in equal proportions with negligible sucrose (Sidhu, 2012; Vayalil, 2012). The variation in sugar content across cultivars in the current study is high and significant ($p \leq 0.05$). A study on Berhi grown in Iran was found to have fructose and glucose as the most abundant sugars, with a Glu/Fru ratio of 1.03, and with negligible sucrose (Mortazavi *et al*., 2010). The Glu/Fru ratios across all samples in the current study are close to 1, indicating the presence of equal amounts of glucose and fructose.

4.3. Minerals

Palm dates are among the richest fruits in minerals, with the most abundant being potassium, in addition to micro-minerals (Vayalil, 2012; Ghnimi, *et al*., 2017; Al-Alawi *et al*., 2017). The total amount of minerals for most samples in the current study were significantly higher than the averages reported. Minerals constituted a relatively high percentage of the total fruit weight, with an average of 6.5%. This is higher than previously reported data which do not exceed 0.916% (Nasir *et al*. 2015). The highest mineral in all the cultivars studied was potassium, followed by calcium, magnesium, and sodium, with trace amounts of iron and manganese. Calcium and Magnesium values were higher than the averages previously reported (Mohamed *et al*., 2014). The values in these studies, however, were reported for dates at the tamr stage.

Minerals commonly found in other cultivars, such as copper, zinc, phosphorous and selenium, were not detectable. This may be due to either the nature of the cultivars, the maturation stage, the nature of Kuwaiti soil and farming conditions, or the detection limits of the methods employed.

Minerals are reported to decrease across maturation stages (Al-Alawi *et al*., 2017). In the current study, values for calcium, sodium, potassium and magnesium for Behri and Khalas cultivars were all higher than those found in U.A.E. Berhi and Khalas in the Tamr stage (Habib and Ibrahim, 2011).

4.4. Antioxidants

Among the phenolic acids, gallic acid was the highest in the varieties studied, followed by chlorogenic acid. Caffeic acid and coumaric acid were below detection limits. Gallic acid was previously reported to be the most abundant phenolic compound in Omani and Saudi dates at the Tamr stage (Al-Harthi *et al*., 2015; Hamad *et al*., 2014; Hamad *et al*., 2015).

The highest and lowest amount of gallic acid in the current samples were similar to that of gallic acid in Saudi and Omani date cultivars (Hamad *et al*., 2015; Al-Harthi *et al*., 2015). This means that Kuwaiti dates are an important source of gallic acid, which is a powerful antioxidant. Gallic acid is well absorbed by the body and has anticarcinogenic effects.

Berhi (Sabah Area) was significantly the highest in chlorogenic acid and the lowest is Saamaran, which was below detection limits. This range is also similar to the results for chlorogenic acid concentrations reported by Hamad *et al*., (2015).

Ascorbic acid is an antioxidant that contributes to date fruits' health-enhancing effects (Tang *et al*., 2013), although its concentration is relatively low. Ascorbic acid in the cultivars of the current study ranged from 0.624±0.00806 μg/mg (Berhi, Sabah Area) to 0.875±0.0266 μg/mg (Khanizi, Wafra). A report by Al-Gboori and Krepl (2010) on Iraqi dates at the Tamr stage showed dates to be insignificant source for ascorbic acid at this stage. Other studies had shown that antioxidant activity sharply decreases across maturation stages (Allaith, 2007).

5. Conclusion

The aim of the present study was to determine the nutritional composition and biochemical characteristics of five date palm fruit varieties at the Khalal stage grown in Kuwait. The date fruits studied in the current research had higher than average energy values, most of which came from sugars. The most abundant sugars in the date cultivars examined were glucose and fructose. The cultivars were high in potassium. Calcium was also present in considerable amounts, followed by magnesium and sodium, with trace amounts of iron and manganese. The cultivars also contained antioxidants such as gallic acid, chlorogenic acid, and ascorbic acid. Ash and protein were low in amount compared to other components.

This study may serve as the starting point for future research on the nutritional properties of Kuwaiti date fruits, and their potential effects on health. The nutritional compositions of the different cultivars at various stages need to be studied further, in addition to the effect of various confounding factors such as farming conditions and locations on the nutritional components.

ACKNOWLEDGEMENTS

The authors would like to acknowledge the Research Sector Projects Unit, Kuwait University (RSPU - Project No. GS 01/03) and the National Unit for Environmental Research and Services (NUERS - Project No. SRUL01/13), Kuwait University, for granting access to their research laboratories to conduct this study. The authors are also grateful to the Palm Tree Friends Society of Kuwait for arranging for the donation of fruit samples for the research.

References

Abdul-Afiq MJ, Abdul Rahman R, Che Man YB, AL-Kahtani HA, Mansor TS (2013). Date seed and date seed oil. Int Food Res J 20:2035-2043.

Al-Alawi RA, Al-Mashiqri JH, Al-Nadabi JM, Al-Shihi BI, Baqi Y (2017). Date Palm Tree (Phoenix dactylifera L.): Natural Products and Therapeutic Options. Front. Plant Sci 8:1–12. doi.org/10.3389/fpls.2017.00845

Al-Gboori B, Krepl V (2010). Importance of Date Palms as A Source Of Nutrition, Institute of Tropics and Subtropics, 43(4): 341–347.

Al Harthi S, Mavazhe A, Al Mahroqi H, Khan S (2015). Quantification of phenolic compounds, evaluation of physicochemical properties and antioxidant activity of four date (Phoenix dactylifera L.) varieties of Oman. J. Taibah Univ. Med. Sci. 10(3): 346-352. doi:10.1016/j.jtumed.2014.12.006

Al-Hooti S, Sidhu JS, Qabazard H (1997). Physicochemical characteristics of five date fruit cultivars grown in the United Arab Emirates. Plant Foods Hum. Nutr. 50(2):101-113. doi:10.1007/bf02436030

Allaith AA (2008). Antioxidant activity of Bahraini date palm (Phoenix dactyliferaL.) fruit of various cultivars. Int J Food Sci Tech 43(6):1033-1040. doi:10.1111/j.13652621.2007.01558.x

Al-Shahib W & Marshall RJ (2003). The fruit of the date palm: its possible use as the best food for the future? Int J Food Sci Nutr. 54:4,247-259. doi: 10.1080/09637480120091982

Assirey EA (2015). Nutritional composition of fruit of 10 date palm (Phoenix dactylifera L.) cultivars grown in Saudi Arabia. J. Taibah Univ. Sci. 9(1):75-79 doi:10.1016/j.jtusci.2014.07.002

Eid N, Enani S, Walton G, Corona G, Costabile A, Gibson G *et al*. (2014). The impact of date palm fruits and their component polyphenols, on gut microbial ecology, bacterial metabolites and colon cancer cell proliferation. J. Nutr. Sci, 3(46). doi:10.1017/jns.2014.16

FAO (2013). The state of food and agriculture 2013: food systems for better nutrition. http://www.fao.org/3/i3300e/i3300e00.htm. Accessed 6 August 2020

Ghnimi S, Umer S, Karim A, Kamal-Eldin A (2017). Date fruit (Phoenix dactylifera L.): An underutilized food seeking industrial valorization. NFS Journal, 6:1-10. doi:10.1016/j.nfs.2016.12.001

Habib HM, & Ibrahim WH (2011). Nutritional quality of 18 date fruit varieties. Int J Food Sci Nutr. 62(5): 544–551. doi.org/10.3109/09637486.2011.558073

Hamad I, AbdElgawad H, Al Jaouni S, Zinta G, Asard H, Hassan S, Selim S *et al*. (2015). Metabolic Analysis of Various Date Palm Fruit (Phoenix dactylifera L.) Cultivars from Saudi Arabia to Assess Their Nutritional Quality. Molecules, 20(12):13620-13641. doi:10.3390/molecules200813620

Hamad I (2014). Phenolic profile and antioxidant activity of Saudi date palm (Phoenix dactylifera L.) fruit of various cultivars. Life Sci J. 11(10): 1268-1271. doi:10.7537/marslsj111014.188

Mohamed RA, Fageer AM, Eltayeb MM, Ahmed IM (2014). Chemical composition, antioxidant capacity, and mineral extractability of Sudanese date palm (Phoenix dactylifera L.) fruits. Food Sci. Nutr. 2:478–489.

Mortazavi SA, Arzani K, Barzegar M (2010). Analysis of sugars and organic acids contents of date palm (phoenix dactylifera l.) 'Barhee' during fruit development. Acta Horticulturae (882):793-801. doi:10.17660/actahortic.2010.882.90

Nasir MU, Hussain S, Jabbar S, Rashid F, Khalid N, Mehmood A (2015). A review on the nutritional content, functional properties and medicinal potential of dates. Science. Letters 3(1):17–22.

Samad MA, Hashim SH, Simarani K, Yaacob JS (2016). Antibacterial Properties and Effects of Fruit Chilling and Extract Storage on Antioxidant Activity, Total Phenolic and Anthocyanin Content of Four Date Palm (Phoenix dactylifera) Cultivars. Molecules 21(4):419. doi:10.3390/molecules21040419

Sidhu JS (2012). Production and Processing of Date Fruits. In: Sinha NK, Sidhu JS, Barta J, Wu JS and Cano MP (eds) Handbook of Fruits and Fruit Processing, end edn. Wiley, New York. doi:10.1002/9781118352533.ch34

Vayalil PK. (2012). Date fruits (phoenix dactylifera Linn): An emerging medicinal food. Crit Rev Food Sci Nutr 52(3):249–271. doi.org/10.1080/10408398.2010.499824

Submitted: 18/09/2021
Revised: 19/12/2021
Accepted: 26/12/2021
DOI: 10.48129/kjs.17169

QadirVax-19: A multi epitope-based vaccine against COVID-19

Misha Mukhtar , Muhammad I. Qadir*

Institute of Molecular Biology & Biotechnology, Bahauddin Zakariya University, Multan, Pakistan

**Corresponding author: mrimranqadir@hotmail.com*

Abstract

An outbreak of COVID-19, caused by a novel virus named SARS-corona virus 2 (SARS-CoV-2), has become a global challenge which needs to be addressed immediately. It has high rate of transmission and severity of the disease varying from person to person. Researchers are trying to find effective vaccines and therapeutic targets to control this novel type of coronavirus. In the present study, surface glycoprotein was used to identify B cell and T cell epitopes that have strong immunogenic potential. Highly conserved region of the surface glycoprotein was identified from seven related human coronaviruses. Epitopes and their prominent features were predicted by using immunoinformatics tools. Epitopes which have high binding energy were joined together through linker to form an epitope-based subunit vaccine construct. Molecular docking was performed by MOE to predict the binding energies of construct with B cell receptor, MHC Class I and MHC Class II receptors. The sequence of the multi-epitope construct finally came out as LQYGSFCTQLNRGPGPGTFGAGAALQGPGPGNFTTAPAICGPGPGHWFVTQRNFAA YQYIKWPWYI. It was named as QadirVax-19. Multi-epitope construct was highly antigenic along with proteasomal cleavage sites and full population coverage. The highest binding energies were obtained which shows that the construct has the ability to produce stronger humoral and immune response against structural glycoproteins of SARS-CoV-2. *In-silico* cloning of the construct revealed its stable expression in *E. coli*. Our study suggests that reverse vaccinology approaches give the immunogenic profile of the epitopes which helped us in designing the subunit vaccine against the SARS-corona virus 2.

Keywords: B cell receptors; molecular docking; SARS-CoV-2; surface glycoprotein; T cell receptors.

1. Introduction

The first outbreak of COVID-19 started in Wuhan, Hubei, China in November 2019. On 13 January 2020, it was reported outside of China and then up to March 2, 2020, the virus spread to 67 territories. COVID-19 was declared as “global pandemic” when the virus significantly affected more than 118 countries by March 11, 2020 (Di Gennaro *et al.,* 2020). The actual impact of this outbreak is difficult to measure accurately because it is important to calculate both mild and serious cases (Lipsitch *et al.,* 2020). Age seems to be an important risk factor for the progression of disease. Different geographical regions show variation in the mortality rate. Immune profile of people plays an essential role in susceptibility to the virus (Albitar *et al.,* 2020).

Coronaviruses was first described by Tyrell and Bynoe in 1966. The formal name of the SARS-CoV-2 is given by the International Committee on Taxonomy of Viruses. Corona is a Latin word meaning “Crown”. Coronavirus is called so due to the crown like appearance on its surface. Coronaviruses are of four types, alpha, beta, delta, and gamma coronaviruses. Human coronaviruses include two alpha coronaviruses (hCoV-NL63 and hCoV-229E) and five beta coronaviruses (hCoV-OC43, HKU1, MERS-CoV, SARS-CoV and SARS-CoV-2). SARS-CoV-2 is the human beta coronavirus and has sequence similarity with other human coronaviruses. Researchers are trying to find the main host and carriers of coronavirus-2. COVID-19 is likely to have a zoonotic origin (Rothan & Byrareddy, 2020). Homology studies show that genome of SARS-CoV and Bat coronaviruses are 79.5% and 96% similar to SARS-CoV-2 respectively (Wang *et al.,* 2020).

The modes of transmission of coronavirus are respiratory droplets, aerosols, and contaminated areas (Bassetti *et al.,* 2020). Mostly asymptomatic individuals and patients with mild symptoms are unnoticeable due to low sickness of these patients. Mildly symptomatic patients also contain the viral load and spread the same amount of virus. Computed Tomography scan’s detail and virologic order of mildly symptomatic patients and asymptomatic patients is not completely described (Li *et al.,* 2020). Symptoms include breathing difficulty, dry coughing, fever, fatigue, nausea and myalgia. Severe complications are pneumonia, severe acute respiratory syndrome, acute liver, cardiac and kidney injury. The onset of disease from time of exposure to symptom is 2-7 days (Wiersinga *et al.,* 2020).

SARS-CoV-2 consists of single positive strand RNA with genome length of 29,881 nucleotides encoding 9860 amino acids. They are spherical enveloped viruses with a diameter of 60-140 nm. Surface (S protein), Enveloped (E protein), Matrix (M protein) and Nucleocapsid (N protein) are the structural proteins (Sarma *et al.* 2020). Envelope glycoprotein of SARS-CoV-2 is made up of 75 amino acids. Virus particles which lack the E protein are not able to infect the host and produce very low titers (Tilocca *et al.,* 2020). Membrane glycoprotein is 230 amino acids long. It maintains the shape and size of virions. All the other structural proteins of virus are assembled through M protein (Mahtarin *et al.,* 2020). The length of nucleocapsid protein is 419 amino acids. N protein is essential for replication and it moves into the host cell along with the RNA (Zeng *et al.,* 2020).

Surface glycoproteins bind with the angiotensin converting enzyme 2 (ACE-2) receptors of the host cells. Serine protease enzyme of host cell facilitates the entry of the virus by activating the S protein. After entry into cell, RNA genome of the virus is replicated and transcribed by the replicase-transcriptase complex. Structural proteins package the virus and release the mature viral particles (Ling *et al.* 2020). Surface proteins are responsible for virus attachment and recognition of receptors. They are the most highly conserved proteins among all other proteins and are considered as the main therapeutic target for producing vaccine. S proteins are 1273 aa long with the size of 180-200 kDa. Structure of S protein consists of N terminus domain, S1 subunit and S2 subunit. S1 subunit has receptor binding domain which cleaves off by furin protein. S2 subunit consists of Fusion peptide (FP), Heptad repeat 1 (HR1), Heptad repeat 2 (HR2), Transmembrane domain (TD) and cytoplasmic domain (CD). RBD region of S1 subunit is highly mutable and is not ideally used. Epitopes derived from the S2 subunit and fusion peptide are used to elicit a strong immune response (Huang *et al.,* 2020). Coronaviruses have the high potential of gene

modifications and possess extra plasticity (Woo *et al.,* 2009). Complete understanding of the SARS-CoV-2 is currently in progress.

Neutralizing antibodies and immune cells combat the viruses. T cells do not recognize the antigen directly. Major histocompatibility complex (MHC) molecules are responsible for presenting the antigens and protein fragments to T cells. T cells also activate B cells for producing antibodies which will target the Surface glycoprotein (Fast & Chen, 2020).

For the control of SARS-CoV-2 infection, vaccination is the most appropriate strategy. Studies reported that recombinant vectors, mRNA containing lipid nanoparticles and subunits of antigenic proteins were main strategies used in the formation of vaccines against COVID-19 (Hu *et al.,* 2020). Some vaccines are based on using the whole attenuated or killed form of the viruses. Due to the contagious nature of the virus and high transmission rate, such types of vaccines demand high biosafety levels. Therefore, it is not feasible for the researchers to develop it for the large-scale population. Virus-based vaccines are extremely immunogenic and have the probability of reversion to more virulent pathogen (Rahman MS *et al.,* 2020). Vaccines were produced using the replicating or non-replicating viral vectors such as adenoviruses. These viral vectors contain the protein part of SARS-CoV-2, mainly spike protein, for expressing into the cell. However, it can cause adverse reactions and mixed immunogenicity. In other cases, pre-existing immunity may present in the body against the carrier viral vectors. In nucleic acid (DNA or RNA) based vaccines, the major concerning issues are the genetic integration of nucleic acid and the stability of RNA. All the mentioned type of vaccines are more time consuming and require high cost (Rahman N *et al.,* 2020). Epitope based vaccines are relatively safe, more stable as compared to these vaccines. They allow to deliver the desired antigenic peptides of specified length (Purcell *et al.,* 2007).

With the revolution of Whole Genome Sequencing, it has become possible to find out the potential antigens as vaccine candidates. Classical vaccinology has certain limitations in term of selecting the protective antigens. The main advantage of reverse vaccinology is that it does not require the maintenance of growth conditions. Reverse vaccinology relies on *In-silico* analysis of genome and proteome. Moreover, the detection of gene expression is not needed. Molecular simulations and dockings are the main *In-silico* tools which give promising results (Mustafa *et al.,* 2020). Many web-based tools are designed on the basis of MHC binding affinity for the prediction of B and T cell epitopes and their population coverage. *In-silico* methods are used as an essential tool in modern era for drug discovery (Qadir *et al.,* 2018). Programs of molecular docking evaluate the binding of ligand with the receptor through the quantification of interactions (Pagadala *et al.,* 2017).

In terms of significance, our novel multi-epitope construct was designed only from the highly conserved and non-mutagenic residues of Surface glycoprotein. Moreover, each epitope in the construct has the ability to interact with both B cells and T cells. The construct is shorter in length which makes it more stable and easier to synthesize. The construct gave high binding energies equivalent to that of long length peptides.

The study focused on the molecular docking of the B cell and T cell epitopes which targeted the structural glycoproteins of SARS-CoV-2 by producing antibodies against it. The present study was based on the hypothesis that conserved region of the surface glycoprotein of SARS-CoV-2 was used to make a novel multi-epitope vaccine construct which will also be effective against new emerging strains of virus.

2. Materials and Methods

2.1 Identification of conserved region

The conserved region of the surface glycoprotein present among all the seven human coronaviruses was obtained through multiple sequence alignment on Clustal Omega. Surface glycoprotein sequences of seven coronaviruses 229E, NL63, OC43, HKU1, MERS-CoV, SARS-CoV and SARS-CoV-2 was retrieved in FASTA format from NCBI database with the accession numbers >AWH62679.1, >APF29063.1, >AWW13575.1, >BBA20983.1, >AMO03401.1, >ARO76382.1, >YP_009724390.1 respectively. Sequence similarity of surface glycoprotein and homology of all the seven coronaviruses was found by BLASTp and phylogenetic tree construction.

2.2 Prediction of B cell and T cell epitopes

B cell and T cell epitopes were predicted from the conserved region of the surface glycoprotein by using online epitope designing servers. Linear epitopes of B cell were determined through ABCpred on the basis of their percentile rank. All the epitopes of length ranging from 10 to 16 were predicted.

T cell epitopes of length 9mer for all the HLA alleles were obtained by using the NetMHC server (Jensen *et al.,* 2018). NetMHC 4.0 designed the cytotoxic T cell epitopes while NetMHC 2.3 was used for predicting helper T cell epitopes. Threshold value of percentile rank for the strong binders was set as less than 0.5.

2.3 Analysis of predicted epitopes

Antigenicity and Immunogenicity of the predicted epitopes was determined through VaxiJen 2.0 and Immune Epitope Database (IEDB) respectively (Doytchinova & Flower 2007) (Dhanda *et al.* 2018). Toxicity of each epitope was obtained by ToxinPred server (Gupta *et al.,* 2013). Epitopes having high antigenic value and immunogenicity score were further selected for molecular docking. Binding energies of the best predicted epitopes were calculated by docking on MOE. PDB structures of the epitopes were obtained from PEPFOLD server. Population coverage analysis of the epitopes of construct was performed for both MHC Class I and MHC Class II alleles by Population Coverage IEDB tool (Bui *et al.,* 2006).

2.4 Designing and Analysis of Multi-epitope construct

Best B cell and T cell epitopes having high binding energies were joined together through linkers to form a Multi-epitope construct. The purpose of the linker is to provide the flexibility and stability in the overall conformation of construct. Linkers are used to join the epitopes, thereby, distinguish their functional domains (Dong *et al.,* 2020). All the physicochemical properties, molecular weight, isoelectric point, instability index and extinction coefficient of the construct were measured by Expasy Protparam tool. Antigenicity and allergenicity was obtained by VaxiJen and AllerTop v. 2.0 respectively. NetChop IEDB tool was used for determining the proteasomal cleavage sites present within the construct (Nielsen *et al.,* 2005). Expasy Peptide cutter found out the positions of enzymatic cleavage sites of the construct as well as the enzymes which do not cut (Maillet 2020).

2.5 Structure predictions for Molecular docking

Secondary structure of the construct was predicted by SOPMA server. RaptorX structure prediction server was used for designing the PDB structure of the construct. Any error present in the 3D structure of the construct was further detected and validated by ProSA-web tool. Molecular docking of the construct with the B cell receptors and MHC molecules was performed by MOE (Vilar *et al.,* 2008). Interaction of the construct with the receptors was visualized on Pymol. Java Codon Adaption tool (JCat) carried out the reverse translation and codon optimization of the construct.

2.6 Physicochemical Properties of construct

All the physicochemical properties of multi-epitope construct were computed by ProtParam tool-Expasy and PepCalc tool. Amino acid sequence of the peptide was entered in both tools. These tools provided the results for different properties which included pI, molecular weight, amino acid and atomic composition, half-life, extinction coefficient, instability index, aliphatic index, GRAVY, and water solubility. ProtParam tool performed all the calculations on the basis of amino acid composition

2.7 *In-Silico* Cloning

Reverse translation of the multi-epitope based vaccine was carried out by Java Codon Adaption tool (JCat). Protein sequence of the construct was entered for codon optimization. SnapGene was used for restriction mapping of the construct and *In-silico* cloning.

3. Results

3.1 Conserved region of surface glycoprotein

From the position of amino acid 714 to 1240 in the surface glycoprotein, the region was shown as conserved among the human coronaviruses. This region encodes for the HR1, HR2 and fusion peptide of the S protein. Phylogenetic relationship analysis shpwed that S2 subunit of SARS-CoV-2 is 99% similar to bat SARS-like coronaviruses (ZXC21 and ZC45) and human SARS-CoV. pBLAST of S glycoproteins of human coronaviruses revealed that SARS-CoV-2 is 74.28% and 35.19% similar to SARS-CoV and MERS-CoV respectively. Human coronaviruses OC43 and HKU1 have percent identity of 37.63% and 35.29% with SARS-CoV-2. While the percent identity of S protein of human coronaviruses 229E and NL63 with SARS-CoV-2 is 31.32% and 30.57% respectively.

3.2 B cell and T cell epitopes

Epitopes having antigenic value greater than 0.5 and toxicity value less than 0.0 were selected. Best predicted epitopes were shown as antigenic, highly immunogenic and non-toxin. Among many predicted epitopes ten B cell epitopes, five helper T cell epitopes and five cytotoxic T cell epitopes were subjected to molecular docking. All the epitopes showed high binding energies with the receptors ranging from 8 to 10.

3.3 Multi-epitope Construct

One B cell epitope (LQYGSFCTQLNR) having the highest binding affinity among all the epitopes joined with two helper T cell epitopes (TFGAGAALQ, NFTTAPAIC) and two cytotoxic T cell epitopes (HWFVTQRNF, QYIKWPWYI) through linkers. The multi-epitope construct is the pentavalent molecules with the molecular weight of 7061.98 Daltons. GPGPG linker used to join the B cell epitope with the helper T cell epitopes. It also combined two helper T cell epitopes with each other and with cytotoxic T cell epitopes. AAY linker was present among the two cytotoxic T cell epitopes for joining them (Tahir ul Qamar *et al.,* 2020). The sequence of the multi-epitope construct finally came out as LQYGSFCTQLNR**GPGPG**TFGAGAALQ**GPGPG**NFTTAPAIC**GPGPG**HWFVTQRNF**A AY**QYIKWPWYI. It was named as QadirVax-19.

Each epitope in the construct has the cleavage sites for proteasome. Amino acid which has the value greater than threshold value of 0.5 represented the cleavage site. All the epitopes of multi-epitope construct showed the world population coverage of 100% in case of both MHC class I and MHC class II receptors. Protein structure validation tool calculated the ProSA-Z score as -4.8. It showed that the structure of multi-epitope vaccine was similar to the native protein structure.

3.4 Molecular docking

Molecular docking structures of the construct with their targets are given in Figure 1. The ligand was effectively in bonded form with the receptor. Predicted binding energies values given by MOE upon docking were shown to be greater with all the three receptors (Table 1). Multi-epitope construct gave higher binding energy with MHC class II receptor as compared to others. The binding energy with MHC class I receptor is more than that of B cell receptor. Overall, all the binding energies were considered high with the receptors. The higher binding energy and the interaction with all the receptor made the multi-epitope construct a good subunit vaccine candidate for eliciting a stronger immune response.

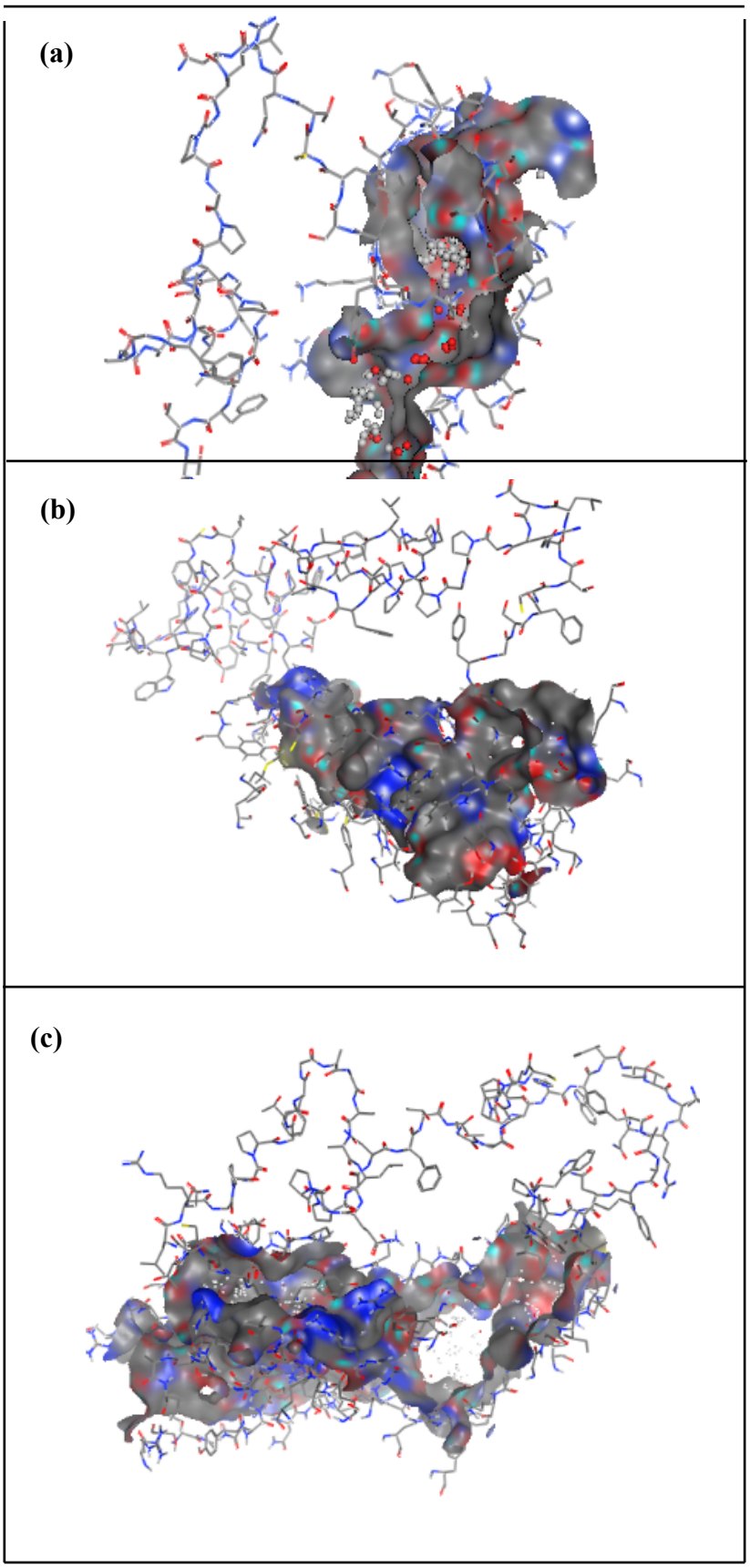

Fig. 1. Docking of the multi-epitope construct with **(a)** B cell receptor **(b)** MHC Class I receptor **(c)** MHC Class II receptor

Table 1. Binding energies of the construct by MOE

	B cell receptor	MHC Class I	MHC Class II
RSEQ	1	1	1
MSEQ	1	1	1
S	-11.8771	-15.2431	-22.275
RMSD_REFINE	5.553171	4.686814	5.042731
E_CONF	-406.839	-367.689	-366.265
E_PLACE	647.1857	467.0003	426.3775
E_SCORE1	49.96589	54.59181	55.68112
E_REFINE	-50.9681	-64.9148	-95.1125
E_SCORE2	-11.8771	-15.2431	-22.275

3.5 Physicochemical Properties

Physicochemical properties and other parameters for the construct were analysed. Multi-epitope construct in the present study was predicted as the probable antigen and non-allergen. Molecular weight, pI, net charge, solubility, and other properties predicted through bioinformatics tools are shown in Table 2. The extinction coefficient of the construct is the light absorbed by it at a specific wavelength. The half-life is the time taken by the construct after its synthesis to degrade in the cell. The prediction for half-life estimation is not applicable to such proteins which have modified N-terminal ends. The lower value of instability index indicated the construct as stable. Aliphatic index is the measure of the relative volume taken by the aliphatic amino acids present in the construct. This characteristic is useful for globular proteins in terms of increasing their thermostability. Hydropathicity of all the amino acids is added and then divided by the total number of residues in the construct. The value that obtained is referred as GRAVY. It represented the hydrophilic and hydrophobic properties of construct. Isoleucine and valine have the high hydrophobicity of 4.5 and 4.2 respectively. The antigenicity score of the construct was 0.5045. The theoretical isoelectric point of the construct was 9.24 with the net charge of +3 at pH 7. The extinction coefficient was predicted as 22585 M^{-1} cm^{-1}. The lower value of instability index 13.95 showed the construct as stable. The construct has the poor water solubility as predicted by the Protparam tool.

Table 2. Physicochemical properties of construct

Sr. No.	Properties of construct	Predicted Values
1	Antigenicity	0.5045
2	Allergenicity	Non-Allergen
3	Total number of amino acids	66
4	Molecular Weight (Da)	7061.98
5	Theoretical isoelectric point	9.24
6	Net Charge at pH 7	3
7	Total Atoms	969
8	Total number of negatively charged residues (Asp + Glu)	0
9	Total number of positively charged residues (Arg + Lys)	3
10	Extinction Coefficient (M^{-1} cm^{-1})	22585
11	Abs 0.1% (280 nm)	3.198
12	Half-life (mammalian reticulocytes, in vitro)	5.5 hours
13	Half-life (yeast)	3 min
14	Half-life (*E. coli*)	2 min
15	Instability Index	13.95
16	Aliphatic Index	50.45
17	Grand average of hydropathicity (GRAVY)	-0.200
18	Water Solubility	Poor

Different types of enzymes and proteases cleaved the construct at the predicted positions of cleavage sites (Table 3). These enzymes which do not cut the sequence are given in table also. The table shows that the construct will be destroyed by given orally and it will be stable when given directly to the blood circulation.

Table 3. Cleavage of the construct by enzymes and their cleavage sites by Expasy Peptide Cutter

Name of enzymes	Number of cleavages	Positions of cleavage sites in construct
Chymotrypsin -high specificity	11	3 6 19 33 47 48 54 57 59 64 65
Chymotrypsin-low specificity	14	1 3 6 10 19 25 33 47 48 54 57 59 64 65
Clostripain	2	12 52
Iodosobenzoic acid	3	47 62 64
LysC	1	61
LysN	1	60
NTCB (2-nitro-thiocyanobenzoic acid)	2	6 39
Pepsin (pH 1.3)	13	1 5 6 9 10 18 19 24 25 32 33 47 53
Pepsin (pH>2)	22	1 2 3 5 6 9 10 18 1924 25 32 33 46 47 53 56 57 58 59 62 65
Proteinase K	31	1 3 6 8 10 18 19 21 23 24 25 33 34 35 36 38 39 47 48 49 50 54 55 56 57 59 60 62 64 65 66
Thermolysin	17	5 9 18 20 22 23 24 32 37 38 47 48 53 54 55 59 65
Trypsin	3	12 52 61
Enzymes which do not cut		
Asp-N endopeptidase, Asp-N endopeptidase + N-terminal Glu, CNBr, Caspases 1-10, Enterokinase, Factor Xa, Formic acid, Glutamyl endopeptidase, Granzyme B, Hydroxylamine, Prolineendopeptidase, Staphylococcal peptidase I, Thrombin		

All the epitopes of multi-epitope construct showed the world population coverage of 100% in case of both MHC class I and MHC class II receptors (Figure 2).

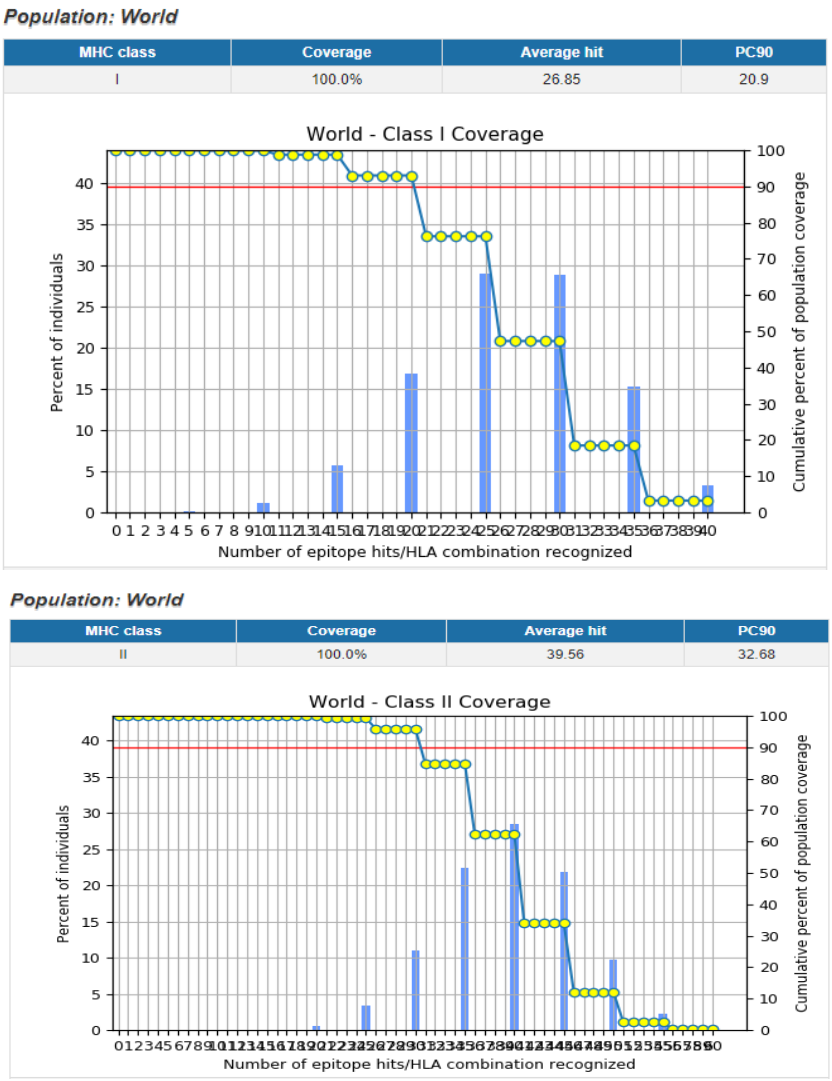

Fig. 2. Population coverage analysis of construct epitopes for MHC Class I and MHC Class II in the World population

3.6 *In-Silico* Cloning

In-Silico Cloning results are given in Figure 3. The length of the multi-epitope construct is 198 nucleotides after codon optimization. The optimum value of Codon Adaption Index (CAI) is 0.8 to 1.0 while optimum GC content value must be 30-70%. The CAI value and GC content for our multi-epitope construct was 1.0 and 61.1% respectively. The values in this range show the good expression of the construct in the *E. coli*.

The aim of the *In-Silico* cloning is to determine that whether the construct is suitable for expression into prokaryotes. pUC19 vector was selected from the SnapGene database because of its easy blue-white screening method of selection for the recombinants. Restriction site for Xba1 and BamH1 were placed at the first and last position at the construct by keeping in view the position and direction of these sites on vector. The orientation of our construct was in accordance with the direction of vector. Our construct was inserted into the lacZ gene of

the vector so that the recombinants will be selected due to the disruption of lacZ gene. Recombinants will produce white colonies on media plate containing X-Gal and IPTG inducer. Our construct will express under the lacZ promoter and terminator. The level of expression will be checked by designing the primers on SnapGene for PCR.

The length of the multi-epitope construct was 198 nucleotides after codon optimization. The optimum value of Codon Adaption Index (CAI) should be 0.8 to 1.0 while optimum GC content value must be 30-70%. The CAI value and GC content for our multi-epitope construct was 1.0 and 61.1% respectively. The values in this range show the good expression of the construct in the *E. coli* by *in-silico* cloning. The higher binding energies values predicted by MOE made the multi-epitope construct a good subunit epitope-based vaccine candidate.

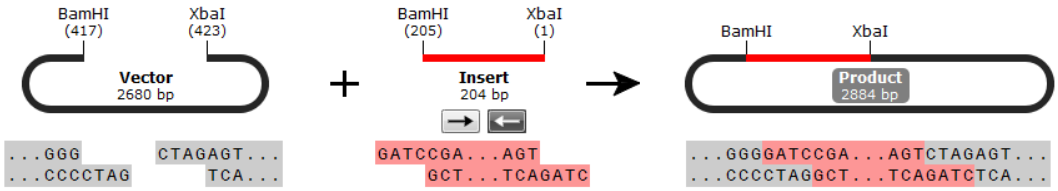

(a)

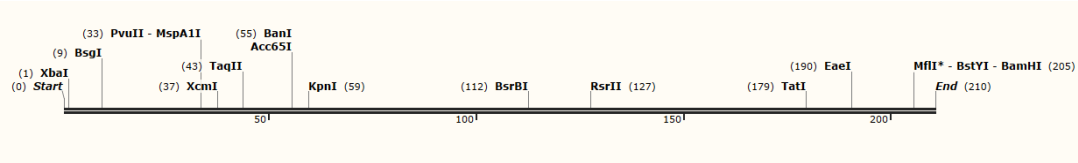

(b)

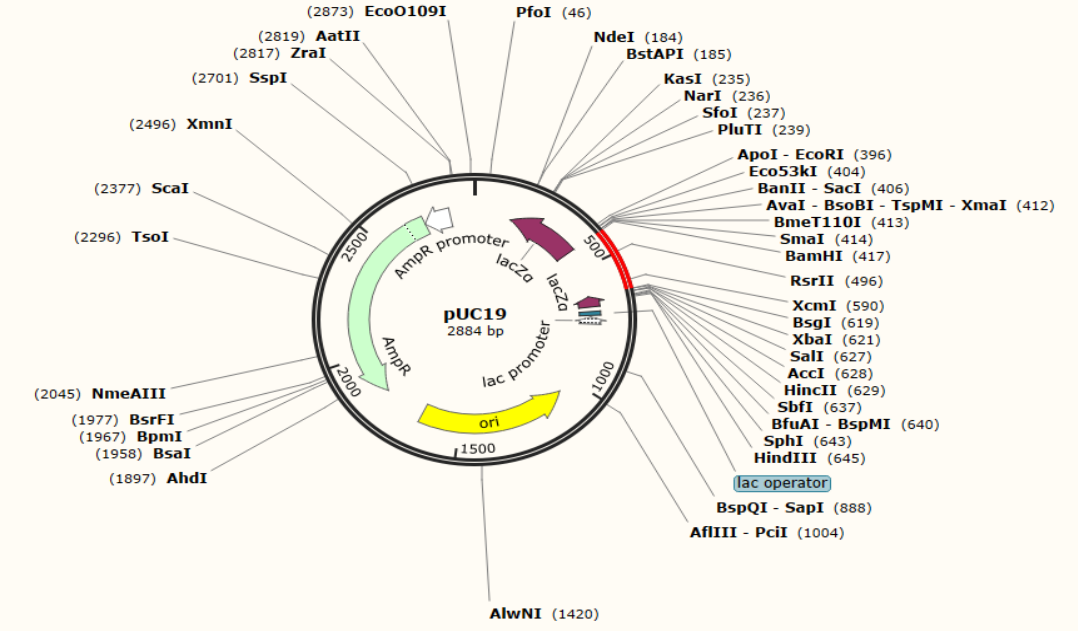

(c)

Fig. 3. *In-Silico* Cloning of multi-epitope vaccine construct into *E.coli* vector by SnapGene (a) Restriction map of multi-epitope construct (b) Insertion of vaccine construct into vector (c) Cloned product of pUC19 vector and multi-epitope insert

4. Discussion

Researchers are trying at their full potential to combat the deadly infectious virus, the Novel Coronavirus-2019 (Qadir, 2020). In order to understand the pathophysiology and transmission of virus, data is gathering by the researchers. The whole genome of the virus was sequenced and reported on January 29, 2020. Different types of vaccines with various mechanisms are currently in their trial stages. The work is being done for the construction of peptide-based subunit type of vaccines by many research groups (Sarkar *et al.,* 2021). Epitope-based subunit vaccines are preferred over the traditional vaccines in terms of better immunogenic control, experimental handling, and reproducibility. Peptides are used because of their chemical stability and ease of production (Patronov & Doytchinova, 2013). Different groups of workers are struggling to produce SARS-CoV-2 vaccines on the basis of epitope-based vaccine strategy taking the benefit from the genome sequence of the virus. However, none of these epitope-based vaccines are available on commercial level due to its low immunogenicity. Another reason is the immediate need of vaccine by massive population on large scale.

One of the major impediments of the COVID-19 vaccine is the emergence of new variants, not fully susceptible to the antibodies. Our study designed a highly antigenic epitope-based subunit vaccine against SARS-CoV-2 and its strains by using immunoinformatic tools and software. The conserved amino acids that present among all the seven human coronaviruses were retrieved for finding the best antigenic epitopes. S2 subunit of surface glycoprotein is less likely to undergo mutations as compared to S1 subunit. The present study identified and selected the epitopes from S2 subunit encoding HR1 and HR2 domains. Epitopes were sorted on the basis of their percentile rank comparing to threshold value. Antigenic epitopes have the value greater than 0.5. Toxicity and immunogenicity of all the epitopes were also predicted. Binding energies of ten B cell epitopes and ten T cell epitopes were *in-silico* predicted by using MOE 2014. Multi-epitope vaccine construct was designed by combining the five epitopes using GPGPG and AAY linkers. Physicochemical properties, proteasomal and enzymatic cleavage, allergenicity, antigenicity and population coverage of the vaccine construct were interpreted. The current study clarified the binding capability of the construct with the receptors by predicting its binding energies. The binding energy of the construct come out as -11.8771, -15.2431 and -22.275 with B cell receptor, MHC class I receptor and MHC class II receptor respectively.

Many different epitope-based vaccines were forecasted and determined by taking other structural proteins (nucleocapsid, membrane and envelope) of SARS-CoV-2. Chen at al identified the T cell epitopes from the nucleocapsid protein of SARS-CoV-2 (Chen *et al.,* 2020). Different studies were also performed on immunodominant epitopes and discontinuous B cell epitopes. TLR receptors are also utilizing for epitope-based vaccines in molecular simulation and docking in the literature (Banerjee *et al.,* 2020).

5. Conclusion

Different computational methods have paved the way and made it easier to design epitope-based subunit vaccines which are safe, cheap and less time consuming. These vaccines are

helpful in eliciting the stronger humoral and cellular immune responses which in turn fight with the deadly virus through producing antibodies against it. To conclude, Multi Epitope-Based Subunit vaccine against COVID-19 was designed through reverse vaccinology approaches and bioinformatics tools.

List of abbreviations

COVID-19: Coronavirus disease-2019; SARS: Severe Acute Respiratory Syndrome; CoV-2: Coronavirus-2; MERS: Middle East Respiratory Syndrome; ACE2: Angiotensin Converting Enzyme 2; S: Surface Glycoprotein; MHC: Major Histocompatibility Complex; HLA: Human Leukocyte Antigen; MOE: Molecular Operating Environment; IEDB: Immune Epitope Database; PDB: Protein Data Bank

ACKNOWLEDGEMENTS

Authors are thankful to Dr. Syed Aun Muhammad for his contribution in completion of this work.

References

Albitar O, Ballouze R, Ooi JP, Ghadzi SMS (2020). Risk factors for mortality among COVID-19 patients. Diabetes Res Clin Pract 166:108293. doi: 10.1016/j.diabres.2020.108293

Banerjee S, Majumder K, Gutierrez GJ, Gupta D, Mittal B (2020). Immuno-informatics approach for multi-epitope vaccine designing against SARS-CoV-2. BioRxiv 39:1087-1095. doi: 10.1016/j.vaccine.2021.01.011

Bassetti M, Vena A, Giacobbe DR (2020). The novel Chinese coronavirus (2019-nCoV) infections: Challenges for fighting the storm. Eur J Clin Invest 50:e13209. doi: 10.1111/eci.13209

Bui H-H, Sidney J, Dinh K, Southwood S, Newman MJ, Sette A (2006). Predicting population coverage of T-cell epitope-based diagnostics and vaccines. BMC Bioinform 7:1-5. doi : 10.1186/1471-2105-7-153

Chen H-Z, Tang L-L, Yu X-L, Zhou J, Chang Y-F, Wu X (2020). Bioinformatics analysis of epitope-based vaccine design against the novel SARS-CoV-2. Infect Dis Poverty 9:1-10. doi: 10.1186/s40249-020-00713-3

Di Gennaro F, Pizzol D, Marotta C, Antunes M, Racalbuto V, Veronese N, Smith L (2020). Coronavirus diseases (COVID-19) current status and future perspectives: a narrative review. Int J Environ Res Public Health 17:2690. doi: 10.3390/ijerph17082690

Dong R, Chu Z, Yu F, Zha Y (2020). Contriving multi-epitope subunit of vaccine for COVID-19: immunoinformatics approaches. Front Immunol 1784. doi: 10.3389/fimmu.2020.01784

Doytchinova IA, Flower DR (2007). VaxiJen: a server for prediction of protective antigens, tumour antigens and subunit vaccines. BMC Bioinform 8:1-7. doi : 10.1186/1471-2105-8-4

Fast E, Chen B (2020) Potential T-cell and B-cell Epitopes of 2019-nCoV. J BioRxiv 10.1101/2020.02.19.955484

Gupta S, Kapoor P, Chaudhary K, Gautam A, Kumar R, Raghava GP, Consortium OSDD (2013). In silico approach for predicting toxicity of peptides and proteins. PloS One 8:e73957. doi : 10.1371/journal.pone.0073957

Hu B, Guo H, Zhou P, Shi Z-L (2020). Characteristics of SARS-CoV-2 and COVID-19. Nat Rev Microbiol 1-14. doi: 10.1038/s41579-020-00459-7

Huang Y, Yang C, Xu X-f, Xu W, Liu S-w (2020). Structural and functional properties of SARS-CoV-2 spike protein: potential antivirus drug development for COVID-19. J Acta Pharmacologica Sinica 41:1-9. 10.1038/s41401-020-0485-4

Jensen KK, Andreatta M, Marcatili P, Buus S, Greenbaum JA, Yan Z, Sette A, Peters B, Nielsen M (2018). Improved methods for predicting peptide binding affinity to MHC class II molecules. J Immunol 154:394-406. doi : 10.1111/imm.12889

Li Y, Shi J, Xia J, Duan J, Chen L, Yu X, Lan W, Ma Q, Wu X, Yuan Y (2020). Asymptomatic and symptomatic patients with non-severe coronavirus disease (COVID-19) have similar clinical features and virological courses: a retrospective single center study. Front Microbiol 11:1570. doi: 10.3389/fmicb.2020.01570

Ling Y, Xu SB, Lin YX, Tian D, Zhu ZQ, Dai FH, Wu F, Song ZG, Huang W, Chen J, Hu BJ (2020). Persistence and clearance of viral RNA in 2019 novel coronavirus disease rehabilitation patients. Chinese M J. 133(09):1039-43.

Lipsitch M, Swerdlow DL, Finelli L (2020). Defining the epidemiology of Covid-19—studies needed. N Engl J Med 382:1194-1196. doi: 10.1056/NEJMp2002125

Mahtarin R, Islam S, Islam MJ, Ullah MO, Ali MA, Halim MA (2020). Structure and dynamics of membrane protein in SARS-CoV-2. J Biomol Struct Dyn 1-14. doi : 10.1080/07391102.2020.1861983

Maillet N (2020). Rapid Peptides Generator: fast and efficient in silico protein digestion. NAR genom bioinform 2:lqz004. doi : 10.1093/nargab/lqz004

Mustafa MI, Abdelmoneim AH, Makhawi AM (2020). Immunoinformatics Patterns and Characteristic of Epitope-Based Peptide Vaccine candidates against COVID-19. AIJR Preprints doi: 10.21467/preprints.164

Nielsen M, Lundegaard C, Lund O, Keşmir C (2005). The role of the proteasome in generating cytotoxic T-cell epitopes: insights obtained from improved predictions of proteasomal cleavage. Immunogenetics 57:33-41. doi : 10.1007/s00251-005-0781-7

Pagadala NS, Syed K, Tuszynski J (2017). Software for molecular docking: a review. Biophys Rev 9:91-102. doi : 10.1007/s12551-016-0247-1

Patronov A, Doytchinova I (2013). T-cell epitope vaccine design by immunoinformatics. Open Biol 3:120139. doi: 10.1098/rsob.120139

Purcell AW, McCluskey J, Rossjohn J (2007). More than one reason to rethink the use of peptides in vaccine design. Nat Rev Drug Discov 6:404-414. doi: 10.1038/nrd2224

Qadir MI, Mushtaq H, Mobeen T (2018). *In-silico* study of potential carboxylic acid derivatives as D-glutamate ligase inhibitors in *Salmonella typhi*. Kuwait Journal of Science 45:100-107.

Qadir MI (2020). QadirVID-19: A fusion inhibitor against Novel Coronavirus-2019 for specific management of COVID-19. Pak J Pharm Sci 33(5): 2187-2191.

Rahman MS, Hoque MN, Islam MR, Akter S, Alam ARU, Siddique MA, Saha O, Rahaman MM, Sultana M, Crandall KA (2020). Epitope-based chimeric peptide vaccine design against S, M and E proteins of SARS-CoV-2, the etiologic agent of COVID-19 pandemic: an in silico approach. PeerJ 8:e9572. doi: 10.1101/2020.03.30.015164

Rahman N, Ali F, Basharat Z, Shehroz M, Khan MK, Jeandet P, Nepovimova E, Kuca K, Khan H (2020). Vaccine design from the ensemble of surface glycoprotein epitopes of SARS-CoV-2: An immunoinformatics approach. Vaccines 8:423. doi: 10.3390/vaccines8030423

Rothan HA, Byrareddy SN (2020). The epidemiology and pathogenesis of coronavirus disease (COVID-19) outbreak. J Autoimmun 109:102433. doi: 10.1016/j.jaut.2020.102433

Sarkar B, Ullah A, Araf Y, Islam NN, Zohora US (2021). Immunoinformatics-guided Designing and In Silico Analysis of Epitope-based Polyvalent Vaccines against Multiple Strains of Human Coronavirus (HCoVs). Expert Rev Vaccines doi: 10.1080/14760584.2021.1874925

Sarma P, Shekhar N, Prajapat M, Avti P, Kaur H, Kumar S, Singh S, Kumar H, Prakash A, Dhibar DP, Medhi B (2021). *In-silico* homology assisted identification of

inhibitor of RNA binding against 2019-nCoV N-protein (N terminal domain). J Biomolecular Structure & Dynamics. 20;39(8):2724-32.

Tahir ul Qamar M, Rehman A, Tusleem K, Ashfaq UA, Qasim M, Zhu X, Fatima I, Shahid F, Chen L-L (2020). Designing of a next generation multiepitope based vaccine (MEV) against SARS-COV-2: Immunoinformatics and in silico approaches. PloS One 15:e0244176. doi: 10.1101/2020.02.28.970343

Tilocca B, Soggiu A, Sanguinetti M, Babini G, De Maio F, Britti D, Zecconi A, Bonizzi L, Urbani A, Roncada P (2020). Immunoinformatic analysis of the SARS-CoV-2 envelope protein as a strategy to assess cross-protection against COVID-19. Microbes Infect 22:182-187. doi : 10.1016/j.micinf.2020.05.013

Vilar S, Cozza G, Moro S (2008). Medicinal chemistry and the molecular operating environment (MOE): application of QSAR and molecular docking to drug discovery. Curr Top Med Chem 8:1555-1572. doi : 10.2174/156802608786786624

Wang L-s, Wang Y-r, Ye D-w, Liu Q-q (2020). A review of the 2019 Novel Coronavirus (COVID-19) based on current evidence. J International Journal of Antimicrobial Agents 55:105948. 10.1016/j.ijantimicag.2020.105948

Wiersinga WJ, Rhodes A, Cheng AC, Peacock SJ, Prescott HC (2020). Pathophysiology, transmission, diagnosis, and treatment of coronavirus disease 2019 (COVID-19): a review. JAMA 324:782-793. 10.1001/jama.2020.12839

Woo PC, Lau SK, Huang Y, Yuen K-Y (2009). Coronavirus diversity, phylogeny and interspecies jumping. Exp Biol Med 234:1117-1127. doi : 10.3181/0903-MR-94

Zeng W, Liu G, Ma H, Zhao D, Yang Y, Liu M, Mohammed A, Zhao C, Yang Y, Xie J (2020). Biochemical characterization of SARS-CoV-2 nucleocapsid protein. Biochem Biophys Res Commun 527:618-623. doi : 10.1016%2Fj.bbrc.2020.04.136

Submitted: 27/12/2021
Revised: 22/04/2022
Accepted: 25/05/2022
DOI: 10.48129/kjs.17575

Kuwait J.Sci., Vol.50, No.(1A),January.2023,pp(278-295)

Sequence analysis of tumor necrosis factor-α (TNF-α) promoter, 5'UTR and exon1 and association of rs361525 (-238 G>A) with BMI

Sahar A. Barhoush, Maryam H. Alrashid, Rubina F. Hussain,
Suzanne A. Al-Bustan*

Department of Biological Sciences, Faculty of Science,
Kuwait University, Kuwait

**Corresponding author: s.albustan@ku.edu.kw*

Abstract

Obesity is among the most common complex diseases with a high rate of morbidity and mortality globally and locally in Kuwait. Tumor Necrosis Factor-α(TNF-α) is a pro-inflammatory cytokine that is primarily secreted by monocytes/macrophage. Increased expression of TNF-α has been observed in the adipodse tissue of obese subjects that could disrupt lipid metabolism and lead to and lead to sustained obese state and obesity-related diseases. The human *TNF-α* promoter exhibits a high number of genetic variants, mainly single nucleotide polymorphisms (SNPs) that have been shown to influence the level of transcription in association with diseases. The human *TNF-α* genetic variants have never been fully reported in Arabs, therefore, we aimed to identify these variants by sequencing the *TNF-α* promoter, 5' UTR, and exon 1 in 290 Kuwaiti Arabs. As a result, we identified 14 genetic variants, including one novel SNP. Two promoter SNPs; rs1800750 (-376G>A) and rs361525 (-238G>A) were found to be in strong linkage disequilibrium ($r^2 = 0.73$) and ($D' = 1$, LOD = 32). To investigate the association of rs361525 (-238G>A) with obesity, we genotyped an additional 573 samples of the general Kuwaiti population by Real-time PCR (total n=863). Linear and logistic regression analysis have not shown any significant association in carriers of the A allele of rs361525 with continuous and categorical BMI, respectively. This is the first study in the Middle East and Kuwait that has sequenced and identified the common, rare and novel genetic variants of *TNF-α* promoter, 5'UTR and exon 1 in Arabs.

Keywords: BMI; Kuwait; obesity; sequencing; TNF-α.

1. Introduction

Obesity is a chronic metabolic disease that is characterized by the storage of excessive amounts of triglycerides in the adipose tissue (Herrera & Lindgren, 2010). Obesity is commonly defined with body mass index (BMI) of 30.0 kg/m² or greater according to WHO Expert Committee (1995). According to Global Burden of Diseases (GBD) report in 2015, obesity pandemic affected over 700 million individuals with estimate of 4 million deaths globally (Afshin *et al.,* 2017). Kuwait has the second highest obesity prevalence of 41% in men and 49% in women in

2015 within the Eastern Mediterranean Region (EMR), thus marking obesity as significant risk factors in Kuwait (Mokdad *et al.,* 2018).

Tumor necrosis factor-alpha (TNF-α) is a pro-inflammatory cytokine that is primarily secreted by monocytes/macrophages, including those that are found in adipose tissue, making adipose tissue a major source of TNF-α (de Ferranti & Mozaffarian, 2008; Russo & Polosa, 2005; Skibola *et al.,* 2005). The pleiotropic biological responses of TNF-α such as regulation of inflammation, cytokine production and energy metabolism are mediated through two types of TNF-α membrane receptors (TNFR1 and TNFR2) that trigger different signal transduction pathways, thus activating the expression of different genes (Parameswaran & Patial, 2010). It has been suggested that TNF-α regulates obesity through TNFR2, that was found to be overexpressed in obese individuals in comparison to lean subjects (Hotamisligil *et al.,* 1997). Transcriptional profiling studies have revealed that inflammatory and stress-response genes are among the most abundantly regulated gene sets in adipose tissue of obese animals (Wellen & Hotamisligil, 2005). Elevated levels of *TNF-α* mRNA was found in the adipose tissue of obese rodents, and was associated with obesity-induced insulin resistance (Alcalá *et al.*, 2017; Hotamisligil *et al.*, 1993). In obese vs lean humans, the expression level of adipose tissue TNF-α (Hotamisligil et al., 1995), and the level of systemic serum TNF-α (Berberoğlu, 2001; Moon *et al.*, 2004) were positively correlated with body fat percentage and BMI.

The human *TNF*-α gene locus is located on chromosome 6p21.31 spanning 3 kb and consisting of 4 exons that encode a 233 amino acid protein (Feldman et al., 2000; Laddha *et al.,* 2012). *TNF-α* promoter is about 1.3 kb upstream from the transcription start site (TSS) (Baena *et al.,* 2002). Some SNPs within the promoter region have been constantly reported such as rs1800630 (-863C>A,) rs1799724 (-857C>T), rs1800750 (-376G>A), rs1800629 (-308G>A), rs673 (-244G>A), and rs361525 (-238G>A), whereas others were less reported such as rs4645838 (C insertion that can be located at +68 - +71) at 5'UTR (Bayley *et al.,* 2004; Hajeer & Hutchinson, 2001; Posch *et al.,* 2003). This high density of promoter SNPs have been shown to influence the rate of transcription and protein production of TNF-α in association with diseases by affecting the binding of transcription factors (Elahi *et al.,* 2009). The genetic variants of the promoter at positions: −238, −308, −857, and −1031 (relative to TSS) may upregulate *TNF*-α gene transcription whereas, −863 downregulates the transcription (Laddha *et al.,* 2012).

In many cases, it is difficult to study the effect of a single SNP in isolation especially that in some populations, such as Caucasians, some SNPs are in linkage disequilibrium, i.e. the -376 A, -308 G and -238 A alleles (Hajeer & Hutchinson, 2001). Thus, functional genetic variants may act in a cooperative manner and interact together to determine the overall activity of the *TNF-α* promoter. That is an important reason to justify our approach in choosing to re-sequence the promoter, 5'UTR and exon 1 region in our study cohort. In our study we aimed to sequence *TNF-α* promoter in 290 Kuwaiti Arabs whose both parents are settlers from the Arabian Peninsula (Al-Bustan *et al*., 2005). This is the first sequencing of this region that has been performed on Arabs and Kuwaitis in particular. Furthermore, we investigated the

association of rs361525 (-238G>A) in 863 samples of the general Kuwaiti population which is an admixture between settlers from the Arabian Peninsula and other populations (Al-Bustan *et al*., 2005).

2. Materials and methods

2.1. Studied Samples

This study was conducted within the guidelines of the Declaration of Helsinki, and the protocol was approved by the Local Ethical Committee at Kuwait University. The samples recruited for sequencing were 290 Kuwaiti Arabs, while for validation, 573 Kuwaitis of the general population. All samples were recruited from volunteers who attend the regional polyclinics or the major hospitals in Kuwait. A written informed consent was obtained from all 863 participants of the Kuwaiti general population. BMI, medical and family medical history of hypertension, hypercholesterolemia, hypertension, type 2 diabetes mellitus (T2DM) and coronary heart disease (CHD) were documented. Ethnicity was verified by tracing both maternal and paternal lineages at least four generations using pedigree analysis. The cohort consisted of 425 females and 279 males with age range 18-80 years old. Subjects were divided into two groups according to their BMI. Non-obese group (n=558) with BMI < 30 kg/m^2 and obese group (n=305) with BMI ≥ 30 kg/m^2. Phenotypic variables including BMI and medical history in the studied cohort (n=863) are summarized in Table 1.

Table 1. Demographic and clinical features of study cohort (n = 863).

Variable	Descriptive Statistic
Age (years)	35 ± 17
Sex	
Male	43% (n=370)
Female	57% (n=493)
BMI (kg/m^2)	28.94 ± 7.61
<30	65% (n=558)
≥30	35% (n=305)
Medical History of:	
T2DM	11.8% (n=102)
Hypercholesterolemia	7.4% (n=64)
Hypertension	10.2% (n=88)
CHD	14.3% (n=123)

2.2. DNA Analysis

Total genomic DNA was extracted from whole blood using the salting-out procedure described by Miller *et al.* (1988). Three sets of primers were custom designed to cover 1394 bp target region at nucleotide position 31574504 to 31575900 spanning the *TNF-α* promoter, 5'UTR and

exon 1 based on the reference sequence NG_007462.1 (NCBI Genbank). Primer 3 Input software version 0.4.0 (//Frodo.wi.mit.edu/) was used in primer design (Supplementary Table S1). Amplification reactions were performed by PCR in an Applied Biosystems Fast thermal cycler (Version 1.01, Life Technologies, USA) (Supplementary Table S2 and Table S3). PCR products were purified using Nucleospin® extract II column Kit (Clontech Laboratories, Inc., Version No. PR48598) following the suggested protocol (Macherey-Nagel, Germany). Cycle sequencing was then performed according to the manufacturer's instructions using the BigDye Terminator v.3.1 in Fast Thermal Cycler (Life Technologies, Applied Biosystems, USA) (Supplementary Table S4). The extension products were purified using BigDye® XTerminator™ Kit (Life Technologies, Applied Biosystems, USA). Capillary electrophoresis was then performed in ABI-3130xl Genetic Analyser (GS01/02) (Life Technologies, Applied Biosystems, USA).

2.3. Sequence Analysis and Variants Identification

The obtained DNA sequences for each sample were analysed using the AB DNA Sequencing Analysis Software version 5.3.1 (Life Technologies, Applied Biosystems, USA). Genetic variants were detected by scanning the resulting chromatograms and aligning the obtained sequence from two reactions for quality assurance with the reference sequence (NG_007462.1) using ClustalW software (Multiple Alignment Tool). The common, rare and novel variants in each sample were reported and compared with NCBI and Ensembl databases (NG_007462.1, ENSG00000232810).

2.4. Association of the identified Genetic Variants

One SNP; rs361525, was selected for validation in 573 randomly selected samples of the Kuwaiti general population and were genotyped by real-time PCR [ABI 7800HT (GS01/02)] (Life Technologies, Applied Biosystems, USA) with commercially available pre-designed primer and probe sets (Applied Biosystems, Assay # C__2215707_10 # 4351379); [VIC/FAM]:GGCCCAGAAGACCCCCCTCGGAATC[A/G]GAGCAGGGAGGATGGGGA GTGTGAG. The genotyping assay and protocol were followed based on the manufacturer's recommendations for Taqman™ Genotyping Master Mix (Applied Biosystems # 4371355).

2.5. Linkage Disequilibrium and Haplotype Analysis

Linkage disequilibrium (LD) between the selected SNPs with minor allele frequency (MAF) ≥ 0.05 was analysed using Haploview (Barrett *et al.,* 2005) (version 4.2.)**.** Squared coefficient of correlation (r^2) and the standard color scheme of D'/LOD were calculated for each pair of SNPs. In this study, r^2 above 0.7 and (D′=1; LOD ≥2) with bright red color indicate strong linkage disequilibrium. Haplotype block was created according to Gabriel *et al.,* (2002) criteria that require 95% of informative comparisons to be in strong LD defined by the confidence bounds of D'.

2.6. Statistical Analysis

Genotype and allele frequencies were estimated using a simple gene counting method in which MAF was determined for each genetic variant in the total cohort and studied groups. Hardy-Weinberg equilibrium (HWE) was tested using online calculator and confirmed using the GENEPOP software (Version 4.2) (Rousset, 2008). One-way analysis of variance (ANOVA) was used to test the statistical difference in BMI (mean ± standard deviation) between the genotype groups of selected variants that showed MAF ≥ 0.05. Genetic modeling of rs361525 was performed in multiple linear regression and logistic regression adjusting for age, sex and ethnicity in the studied cohort (n=863). The statistical significance level for all tests was set at $p < 0.05$ using SPSS software (version 25; SPSS Inc., Chicago, IL, USA). The power of study in 863 samples was analysed using the Power and Sample Calculation Program (version 3.1.6) (Dupont & Plummer, 1990) assuming an odd ratio (OR) of 2.5.

3. Results

3.1. Identification of Genetic Variants

Sequenicng of the *TNF-α* promoter, 5'UTR and exon 1 regions (1394 bp) at nucleotide position 31574504 to 31575900 in 290 samples of Kuwaiti Arabs allowed the identification of 14 genetic variants among all the samples sequenced. Across the sequenced region, ten variants were found in the promoter, two in the 5'UTR and two, including a novel SNP, in exon 1 **(Figure 1)**. A new reference for *TNF-α* promoter, 5'UTR and exon 1 for Kuwaiti Arabs was defined and deposited in GenBank with an accession number: MH287061.

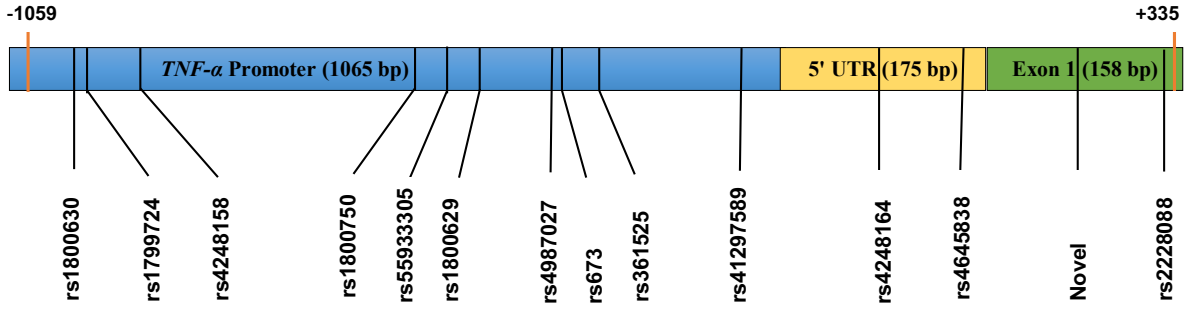

Fig. 1. The fourteen identified genetic variants in TNF-α target region on chromosome 6p21.31 form nucleotide (nt) -1059 to +335 (ch6: 31574504:31575900).

Among the detected genetic variants (Table 2), one SNP in exon 1, rs2228088 (c.87G>T), was defined as a synonymous mutation causing a G to T transversion at nucleotide position 267. Another identified variant rs4645838 (c.-108_-107 InsC); C nucleotide insertion in the 5' UTR that apparently does not cause a frame shift mutation due to its position in a non-coding region. The novel SNP in exon1 (c.39C>T) at position 6:31575780 is a synonymous mutation that causes a C to T transition at nucleotide position 219 that does not change the Alanine (Ala) at

residue 13. The sample with the novel SNP belongs to a 21 years old female whose ancestry was traced to the Arabian Peninsula (AP). The case is overweight (BMI=29.6 kg/m^2) and had been diagnosed with T2DM, hypertension and hypercholesterolemia, but had no history for Cardiovascular diseases (CVD) while her family medical history is positive for T2DM and CVD. A heterozygote C insertion of rs4645838 was also identified in an upstream position (6:31575634) in the same sample, thus making the novel SNP only detectable in the reverse sequence of primer 3 as G>A transition (Supplementary Figure S1).

Table 2. Characterization of the identified genetic variants at *TNF-α* promoter and exon 1 region among Kuwait Arabs.

Genetic Variants Ref. No.	Global MAF	Position at Ref. Seq.	*Chromosomal Position	mRNA Position**	Type	Amino Acid Change
rs1800630	C	-863C>A	g.31574699C>A	NR	Upstream	NR
rs1799724	C	-857C>T	g.31574705C>T	NR	Upstream	NR
rs4248158	C	-806C>T	g.31574756C>T	NR	Upstream	NR
rs1800750	G	-376G>A	g.31575186G>A	NR	Upstream	NR
rs55933305	C	-347C>T	g.31575215C>T	NR	Upstream	NR
rs1800629	G	-308G>A	g.31575254G>A	NR	Upstream	NR
rs4987027	C	-245C>T	g.31575317C>T	NR	Upstream	NR
rs673	G	-244G>A	g.31575318G>A	NR	Upstream	NR
rs361525	G	-238G>A	g.31575324G>A	NR	Upstream	NR
rs41297589	T	-76T>A	g.31575485T>A	NR	Upstream	NR
rs4248164	C	+4C>T	g.31575571C>T	c.-171C>T	5' UTR	NR
rs4645838	-	+68Ins -/C	g.31575634dupC	c.-108_-107insC	5' UTR	NR
Novel	UR	+213C>T	g.31575780C>T	c.39C>T	Synonymous	p.Ala13=***
rs2228088	G	+261G>T	g.31575828G>T	c.87G>T	Synonymous	p.Arg29=

*Chromosomal position is based on chromosome 6 published reference sequence using GRCh38.p7 primary assembly (NC_000006.12) in the NCBI GenBank database.
**mRNA position is based on the TNF-α mRNA sequence (NM_000594.3) in GenBank database.
***change in amino acid was predicted using TNF-α protein sequence (CCDS4702.1) in CCDS database.
NR: Not-Reported.

3.2. Genotype and Allele Frequencies

The population homogeneity was tested for HWE in the studied cohort for sequencing (n = 290) and in the two divided groups based on BMI; non-obese (n = 211; BMI<30) and obese (n = 79; BMI ≥ 30) (Table 3). Ten genetic variants in the studied population were in HWE (*p*-value > 0.05) except for four SNPs. A significant deviation was found with rs1800630 in the total population ($p = 0.002$) and non-obese group ($p = 0.010$). Similarly, rs4248158 was deviated in the total population ($p = 0.006$) and non-obese ($p = 0.001$). Whereas rs1800750 and rs361525 were deviated from HWE in the total population at $p = 0.002$ and 0.004, respectively, and in obese group at $p < 0.001$ for both (Table 3).

In the studied population (n=290), six genetic variants were found to be common with MAF ≥ 5%, four variants were considered less frequent with MAF 1-5%, whereas the remaining 4 SNPs were rare (MAF < 1%) (Table 3). The most common genetic variant was rs1800630C>A with MAF of 0.17 in the total samples followed by rs1800629G>A with MAF of 0.157. Within the common variants, the most common genotype was the homozygous wild type GG of rs361525 and TT of rs41297589 with a frequency of 0.890 for both followed by the homozygous CC of rs1799724 (0.852).

Table 3. Genotypic and allelic frequencies of the identified genetic variants of *TNF-α* in the studied Kuwaiti Arabs population (n=290) and in two groups divided based on BMI. The MAF in our study and the global MAF were reported.

Genetic Variants	Genotypes and Alleles	Non-obese (n=211)	Obese (n=79)	Total Sample (n=290)	Global MAF
	CC	0.740 (156)	0.650 (51)	0.714 (207)	
rs1800630	CA	0.210 (45)	0.280 (22)	0.231 (67)	
	AA	0.050 (10)	0.070 (6)	0.055 (16)	
MAF	A=	0.150	0.215	0.170	0.1542/772
HWE *p*-value		**0.010***	0.120	**0.002***	
	CC	0.830 (175)	0.911 (72)	0.852 (247)	
rs1799724	CT	0.170 (36)	0.089 (7)	0.148 (43)	
	TT	0	0	0	
MAF	T=	0.085	0.044	0.074	0.0990/496
HWE *p*-value		0.175	0.680	0.173	
	CC	0.934 (197)	0.937 (74)	0.934 (271)	
rs4248158	CT	0.057 (12)	0.063 (5)	0.059 (17)	
	TT	0.009 (2)	0	0.007 (2)	
MAF	T=	0.038	0.032	0.036	0.0258/129
HWE *p*-value		**0.001***	0.771	**0.006***	
	GG	0.910 (192)	0.937 (74)	0.917 (266)	
rs1800750	GA	0.085 (18)	0.038 (3)	0.072 (21)	
	AA	0.005 (1)	0.025 (2)	0.013 (3)	
MAF	A=	0.047	0.044	0.047	0.0112/56
HWE *p*-value		0.422	**<0.001***	**0.002***	

	CC	0.995 (210)	1 (79)	0.997 (289)	
rs55933305	CT	0.005 (1)	0	0.003 (1)	
	TT	0	0	0	
MAF	T=	0.002	-	0.002	0.0004/2
HWE *p*-value		0.972	-	0.977	
	GG	0.711 (150)	0.722 (57)	0.713 (207)	
rs1800629	GA	0.251 (53)	0.278 (22)	0.259 (75)	
	AA	0.038 (8)	0	0.028 (8)	
MAF	A=	0.164	0.139	0.157	0.0903/452
HWE *p*-value		0.235	0.150	0.702	
	CC	0.991 (209)	0.987(78)	0.990 (287)	
rs4987027	CT	0.009 (2)	0.013 (1)	0.010 (3)	
	TT	0	0	0	
MAF	T=	0.005	0.006	0.005	0.0002/1
HWE *p*-value		0.944	0.955	0.929	
	GG	0.962 (203)	0.937 (74)	0.955 (277)	
rs673	GA	0.038 (8)	0.063 (5)	0.045 (13)	
	AA	0	0	0	
MAF	A=	0.019	0.032	0.022	0.0192/96
HWE *p*-value		0.778	0.771	0.696	
	GG	0.872 (184)	0.937 (74)	0.890 (258)	
rs361525	GA	0.118 (25)	0.038 (3)	0.100 (28)	
	AA	0.010 (2)	0.025 (2)	0.010 (4)	
MAF	A=	0.069	0.044	0.062	0.0609/305
HWE *p*-value		0.280	**<0.001***	**0.004***	
	TT	0.886 (187)	0.899 (71)	0.890 (258)	
rs41297589	TA	0.104 (22)	0.101 (8)	0.103 (30)	
	AA	0.010 (2)	0	0.007 (2)	
MAF	A=	0.062	0.051	0.060	0.0106/53
HWE *p*-value		0.153	0.635	0.286	
	CC	1 (211)	0.987(78)	0.997 (289)	
rs4248164	CT	0	0.013 (1)	0.003 (1)	
	TT	0	0	0	
MAF	T=	-	0.006	0.002	0.0012/6
HWE *p*-value		-	0.955	0.999	
	-/-	(165)	(63)	0.787 (228)	
rs4645838	-/Ins C	(43)	(16)	0.203 (59)	
	Ins C/Ins C	(3)	0	0.010 (3)	
MAF	Ins C=	0.116	0.082	0.112	0.009/44
HWE *p*-value		0.917	0.316	0.931	
	CC	0.995 (210)	1 (79)	0.997 (289)	
Novel	CT	0.005 (1)	0	0.003 (1)	
	TT	0	0	0	
MAF	T=	0.002	-	0.002	-
HWE *p*-value		0.972	-	0.999	
	GG	0.967 (204)	0.962 (76)	0.966 (280)	
rs2228088	GT	0.033 (7)	0.038 (3)	0.034 (10)	
	TT	0	0	0	
MAF	T=	0.017	0.019	0.017	0.0176/88
HWE *p*-value		0.806	0.863	0.956	

*Significant at $p<0.05$

3.3. Linkage Disequilibrium and Haplotype

A total of 182 pairs were analysed and one SNP pair was found in strong LD with D' = 1, LOD = 32 and r^2 value of 0.73 between rs1800750 (-376G>A) and rs361525 (-238G>A) that indicate their co-segregation **(Figure 2)**. These two SNPs are located within 138 bp where four SNPs are found in between; rs55933305 (-347C>T), rs1800629 (-308G>A), rs4987027 (-245C>T) and rs673 (-244G>A). No haplotype block could be created applying Gabriel *et al*., 2002 criteria, since the majority of the pairs were non-informative.

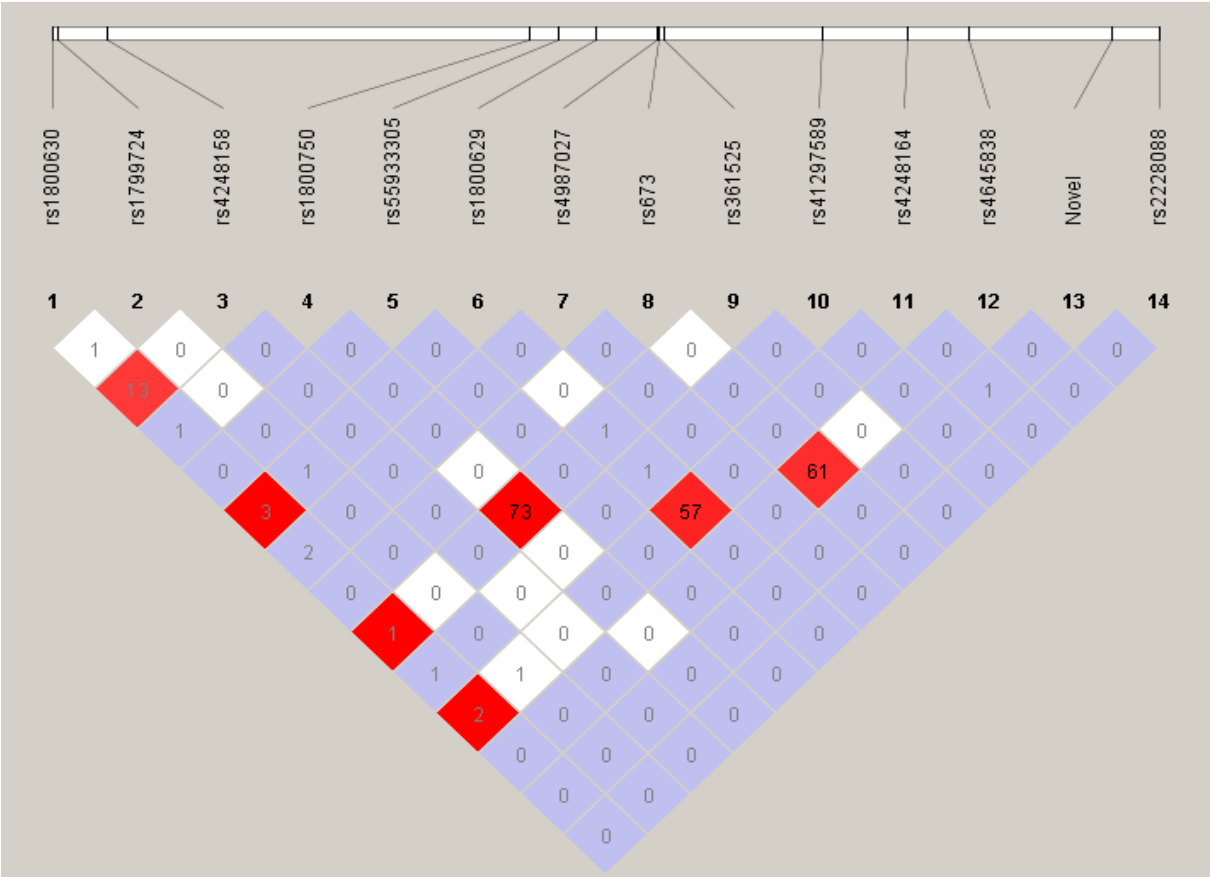

Fig. 2. Schematic representation of linkage disequilibrium (LD) between the fourteen genetic variants of TNF-α in 290 Kuwaiti Arabs. LD was defined by r^2 value expressed as percentile inside each pair and the standard D'/LOD color scheme with bright red indicates strong LD (D'=1; LOD ≥2), shades of pink/red indicate intermediate LD, and white color means no LD.

3.4. Association of Common Variants with BMI and obesity

Six genetics variants with MAF ≥ 0.05 were selected for analysing the distribution of mean BMI between genotype groups in 290 samples using one way-ANOVA **(Table 4)**. A significant (p = 0.003) increase in BMI has been found in carriers of the minor homozygous genotype of rs361525 -238 AA (39.60 kg/m^2 ± 17.14) in comparison to carriers of the heterozygous genotype GA (27.03 kg/m^2 ± 7.34), and the major homozygous genotype GG (28.87 kg/m^2 ± 6.57).

Table 4. Distribution of the mean BMI in the three genotype groups of the six selected genetic variants of *TNF-α* in 290 Kuwaiti Arabs.

Genetic variants	Genotype	Mean BMI ± S.D	*p*-value
rs1800630	CC (n=207)	28.47 ± 6.73	
	CA (n=67)	29.51 ± 7.45	0.284
	AA (n=16)	30.84 ± 7.59	
rs1799724	CC (n=247)	29.09 ± 7.15	
	CT (n=43)	27.40 ± 5.58	0.142
	TT (n=0)	-	
rs1800629	GG (n=207)	29.01 ± 7.23	
	GA (n=75)	28.64 ± 6.48	0.549
	AA (n=8)	26.35 ± 2.49	
rs361525	GG (n=258)	28.87 ± 6.57	
	GA (n=28)	27.03 ± 7.34	**0.003***
	AA (n=4)	39.60 ± 17.14	
rs41297589	TT (n=258)	28.94 ± 6.85	
	TA (n=30)	28.23 ± 8.07	0.669
	AA (n=2)	25.30 ± 2.63	
rs4645838	-/- (n=228)	28.87 ± 7.10	
	-/Ins C (n=59)	25.64 ± 3.72	0.726
	InsC/Ins C (n=3)	28.91 ± 6.56	

*Significant result at *p*-value<0.05

Analysis of rs361525 correlation with continuous BMI in 290 samples in linear regression recessive model had shown a significant positive association with carriers of the minor homozygous genotype -238 AA (β = 12.57; 95% CI = 5.98-19.16; $p < 0.001$) adjusting for age and sex (Supplementary Table S5). All samples with the minor homozygous genotype (n = 4) were Kuwaiti Arab male with BMI (28.30 - 64.80 kg/m^2) (Supplementary Figure S2).

Additional 573 Kuwaiti samples were added to the final cohort to increases statistical power and validate our preliminary results. The genotyping of rs361525 by real time PCR resulted in 506 samples with the major allele homozygous genotype GG (0.883), 66 with heterozygous genotype GA (0.115) and 1 with the minor homozygous genotype AA (0.002). The carrier the -238 AA was a Kuwaiti Arab female with a BMI of 23.80 kg/m^2.

The association of *TNF-α* rs361525 (-238G>A) with BMI was further investigated in the extended studied cohort (n = 863) and the allele frequencies were found in HWE ($p = 0.262$) with MAF of 0.060. Analysis of variance (ANOVA) revealed no significant difference in BMI distribution between the three genotype groups of rs361525 at $p = 0.060$ (Table 5). In multiple linear regression, a significant positive correlation with BMI was found in carriers of the minor homozygous genotype AA (β = 7.21; 95% CI = 0.53-13.88; $p = 0.034$) but not with carriers of the A allele (Table 5). However, the low number of samples in the recessive model is not

sufficient to solely accept these results. Logistic regression between obese (n = 305) vs non-obese (n = 558) groups showed no significant association of rs361525 with obesity in any models after adjusting for age, sex and ethnicity (Table 6).

Table 5. Multiple linear regression of *TNF-α* rs361525 (-238G>A) with BMI in 863 Kuwaiti samples adjusting for age, sex and ethnicity.

Genetic Model	Allele/Genotype	BMI	ANOVA p-value	β-coefficient	95% CI	*p*-value
G vs A (n=1748)	G (n=1622)	28.94 ± 7.50		1		
	A (n=104)	29.03 ± 9.59	0.902	0.08	-1.42-1.59	0.913
Recessive	GG+GA (n=858)	28.99 ± 7.56	**0.030***	1		
	AA (n=5)	39.44 ± 16.44		7.21	0.53-13.88	**0.034***
Dominant	GG (n=764)	29.08 ± 7.44	0.604	1		
	GA+AA (n=99)	28.66 ± 9.09		-0.38	-1.98-1.21	0.637
Additive (0,1,2)	GG (n=764)	29.98 ± 7.44	0.060	0.02	-1.47-1.50	0.982
	GA (n=94)	28.24 ± 8.49				
	AA (n=5)	36.44 ± 16.44				

-BMI is reported as the mean value ± S.D
-ANOVA stands for analysis of variance
**p*-value<0.05 is significant

Table 6. Logistic regression of *TNF-α* rs361525 (-238G>A) with obesity in 863 Kuwaiti samples adjusting for age, sex and ethnicity.

Genetic Model	Obese (n=305)	Non-obese (n=558)	OR (95% CI)	*p*-value
Codominant				
GG	90.8% (277)	87.3% (487)	1	
GA	8.5% (26)	12.2% (68)	0.68 (0.42-1.09)	0.106
AA	0.7% (2)	0.5% (3)	1.18 (0.19-7.11)	0.860
Dominant				
GG	90.8% (277)	87.3% (487)	1	
GA+AA	9.2% (28)	12.7% (71)	0.70 (0.44-1.10)	0.125
Recessive				
GG+GA	99.3% (303)	99.5% (555)	1	
AA	0.7% (2)	0.5% (3)	1.22 (0.20-7.40)	0.825
Additive Model (0,1,2)	-	-	0.74 (0.48-1.14)	0.168

**p*-value<0.05 is significant

4. Discussion

This is the first study on an Arab population in the Middle East and Kuwait to sequence the *TNF-α* promoter, 5'UTR and exon 1 regions and report fourteen genetic variants; ten in the promoter region (1065 bp), two in the 5'UTR (175 bp) and two, including a novel SNP, in exon 1 (158 bp). Genetic variants at the *TNF*-α promoter were never fully reported in any Middle Eastern population prior to this study, thus identifying and selecting essential common variants for our association study was limited to data from other ethnic groups that may be different from Arabs. The MAF for most of the identified genetic variants in our study were consistent with the global MAF reported in the 1000 genomes project. The MAF of rs41297589 was found to be closer to the South Asian (SAS) population while MAF of rs1800629 was similar to the European (EUR) and African (AFR) population. In our study, the MAF of rs4645838 Ins C was identified as a common variant in Arabs but rare in other populations. Interestingly, our number of detected SNPs in *TNF-α* promoter was also consistent to the reported level of variation in the human genome where 10 SNPs were estimated to be found per 1 Kb in this region (Baena *et al.,* 2002).

One interesting finding from this study was the unlikely separation by genetic recombination of the rare allele of rs1800750 (-376A) indicating it probably arose as a mutation within the haplotype carrying the rare allele of rs361525 (-238A) which is supported by their close proximity (Knight *et al.,* 1999). Our study further supports the strong LD between rs1800750 (-376G>A) and rs361525 (-238G>A) with r^2 value of 0.73 and D' of 1. The relationship between these SNPs has been preserved in East African, West African and European populations (Bănescu *et al*., 2019; Georgescu *et al*., 2020; Knight *et al.,* 1999), and apparently in the Arab population as reported in this study.

Hotamisligil *et al.* (1993) provided the first evidence of functional link between obesity and TNF-α that was elevated in models of obese rodents. The increased expression of TNF-α level associated with obesity could affect the metabolic status of adipose tissue, disrupt lipid metabolism, regulation of fatty acid uptake, lipogenesis and lipolysis that can lead to the development of obesity-related complications such as, insulin resistance and atherosclerosis (Jung & Choi, 2014; Sethi & Hotamisligil, 1999; Zietek & Rath, 2016). TNF-α as a powerful pro-inflammatory cytokine has never been sequenced in Kuwaiti and Arab population. Therefore, it was found to be a suitable candidate gene to investigate metabolic and cardiovascular diseases in Arabs focusing on obesity in this study. Two genetic variants of *TNF-α* promoter; rs1800750 and rs361525 were found to be significantly deviated in the obese group compared to other variants, thus could indicate an association with obesity. The *TNF-α*-238G>A has been annotated within a 25 bp region known as the *TNF-α* repressor site (TRS) which is localized between base pairs -254 and -230 in the promoter (Fong *et al*., 1994). The functional significance of rs361525 at TRS remains controversial between increasing the repression activity or blunt it or having no effect at all. Previous studies showed that the A allele of -238G>A was found to be associated with either an increase in TNF-alpha transcript levels (Baylel *et al*., 2001; Laddah *et al*., 2012), a decrease in the transcriptional activity (Huizinga *et*

al., 1997; Kaluza *et al*., 2000), or has no effect (Kaijzel *et al*., 1998). Furthermore, a construct mutant (-376A) was found to induce the expression level of TNF-α by 35% in comparison with the wild type -376G through altering the general topology of the region and creation of a binding site for the transcription factor organic cation transporter 1 (OCT-1) (Knight *et al*., 1999).

Five out of the six common genetic variants showed no significant association with BMI including; rs1800629 (-308G>A), this is consistent with what was previously reported in a sample of Kuwaiti individuals (Alrashid *et al*., 2021), which supports our findings. Our preliminary analysis showed significant association between carriers of the minor homozygous genotype of rs361525 (-238 AA, n=4) and BMI in Kuwaiti Arabs. However, considering the low number of carriers and to validate our results, the size of the cohort was increased to 863 samples from the Kuwaiti general population; which is an admixture between settlers from the Arabian Peninsula and other populations (Al-Bustan *et al.,* 2005). Although, linear regression confirmed the significant association between rs361525 and BMI in the recessive model, it was disregarded because of the persisting low number of carriers that could be misleading. Moreover, adjusting the significance level using Bonferroni correction has resulted in non-significant association. To confirm our finding, logistic regression between rs361525 and obesity had revealed no significant association in any of the genetic models after adjusting for age, sex and ethnicity. The sample size has been a critical factor in this study as the power has significantly increased from 74% to 96% with larger cohort (assuming OR of 2.5 and MAF of 0.66) supporting our results. Few studies had investigated the genetic association between obesity and rs361525 (-238G>A). Consistent with our results, studies in an Iranian population and a population from Johns Hopkins Weight management center reported no significant association between rs361525 (-238G>A) and obesity *(Hedayati et al.,* 2012; Walston *et al.,*1999). Contradictory to these findings, one study had reported a significant association between carriers of the -238 A allele (GA+AA) and higher body fat percentage in black South African woman (p<0.001) and in the combined group of black and white South African women (p=0.004) revealing an increased risk of obesity (Joffe *et al.,* 2012). On the other hand, the G Allele of -238G>A had presented a significant association in a Korean population with overweight/obesity as the frequency of the G/G genotype in the overweight/obese group was 9.3% higher than that in the control group (p= 0.0046) (Yu *et al.,* 2011).

5. Conclusion

This is the first study in the Middle East and Kuwait that sequenced and identified the common, rare and novel variants of *TNF-α* promoter, 5'UTR and exon 1 in Arabs. The common variants showed no significant association with BMI. Similarly, the selected rs361525 (-238G>A) has shown no significant genetic association with either continuous or categorical BMI in 863 Kuwaitis of the general population. The findings in this study do not rule out the association of *TNF-α* with obesity and may suggest a potential for *TNF-α* variants to interact with other genes

variants to predispose to obesity under epigenetic control. Moreover, the findings merit the importance of sample size in establishing a genetic association.

Data Availability

The authors declare that all data supporting the findings of this study are available within the article or from the corresponding author upon reasonable request.

Conflict of interest

The authors declare that there are no known conflicts of interest associated with this publication and the institutions where the work has been carried out.

Acknowledgment

This Study was supported and funded by Kuwait University Research Administration and College of Graduate Studies, Project Grant (YS01/16). The authors would also like to acknowledge the General Facility Project (GS01/02) for the use of the ABI 3130xl Gene Analyser with deep gratitude to Mrs. Sheela Thankakkon for her technical assistance. An extended sincere gratitude to Mrs. Babitha Annice for her guidance, designing the primers and technical support.

References

Afshin, A., Forouzanfar, M. H., Reitsma, M. B., Sur, P., Estep, K., *et al.* (2017). Health effects of overweight and obesity in 195 countries over 25 years. *New England Journal of Medicine*, *377*(1), 13–27. https://doi.org/10.1056/NEJMoa1614362

Al-Bustan, S. A., Alnaqeeb, M. A., Annice, B. G., Ibrhim, G., Al-Rubaian, J., *et al*. (2005). Apolipoprotein E genotyping among the healthy Kuwaiti population. *Human biology*, 487-498.

Alcalá, M., Calderon-Dominguez, M., Bustos, E., Ramos, P., Casals, N., *et al*. (2017). Increased inflammation, oxidative stress and mitochondrial respiration in brown adipose tissue from obese mice. *Scientific reports*, *7*(1), 1-12.

Alrashid, M. H., Al-Serri, A., Alshemmari, S. H., Geo, J. A., & Al-Bustan, S. A. (2021). Association analysis of genetic variants in the ghrelin and tumor necrosis factor α genes and the risk for non-Hodgkin's lymphoma in Kuwaitis. *Cancer Biomarkers*, (Preprint), 1-8.

Baena, A., Leung, J. Y., Sullivan, A. D., Landires, I., Vasquez-Luna, N., *et al.* (2002). TNF-α promoter single nucleotide polymorphisms are markers of human ancestry. *Genes and Immunity*, *3*(8), 482–487. https://doi.org/10.1038/sj.gene.6363898

Bănescu, C., Tripon, F., Trifa, A. P., Crauciuc, A. G., Moldovan, V. G., e*t al.* (2019). Cytokine rs361525, rs1800750, rs1800629, rs1800896, rs1800872, rs1800795, rs1800470, and rs2430561 SNPs in relation with prognostic factors in acute myeloid leukemia. *Cancer Medicine*, *8*(12), 5492-5506. https://doi.org/10.1002/CAM4.2424

Barrett, J. C., Fry, B., Maller, J., & Daly, M. J. (2005). Haploview: Analysis and visualization of LD and haplotype maps. *Bioinformatics*, *21*(2), 263–265. https://doi.org/10.1093/bioinformatics/bth457

Bayley, J. P., de Rooij, H., van Den Elsen, P. J., Huizinga, T. W., & Verweij, C. L. (2001). Functional analysis of linker-scan mutants spanning the− 376,− 308,− 244, and− 238 polymorphic sites of the TNF-α promoter. *Cytokine*, *14*(6), 316-323.

Bayley, J. P., Ottenhoff, T. H. M., & Verweij, C. L. (2004). Is there a future for TNF promoter polymorphisms? In *Genes and Immunity* (Vol. 5, Issue 5, pp. 315–329). https://doi.org/10.1038/sj.gene.6364055

Berberoğlu, M. (2001). Evaluation of the correlation between serum tumor necrosis factor-α and relative body mass index (RBMI) in childhood. *Journal of Pediatric Endocrinology and Metabolism*, *14*(5), 543–547. https://doi.org/10.1515/jpem.2001.14.5.543

de Ferranti, S., & Mozaffarian, D. (2008). The perfect storm: Obesity, adipocyte dysfunction, and metabolic consequences. In *Clinical Chemistry* (Vol. 54, Issue 6, pp. 945–955). https://doi.org/10.1373/clinchem.2007.100156

Dupont, W. D., & Plummer, W. D. (1990). Power and sample size calculations. A review and computer program. *Controlled Clinical Trials*, *11*(2), 116–128. https://doi.org/10.1016/0197-2456(90)90005-M

Elahi, M. M., Asotra, K., Matata, B. M., & Mastana, S. S. (2009). Tumor necrosis factor alpha - 308 gene locus promoter polymorphism: An analysis of association with health and disease. *Biochimica et Biophysica Acta - Molecular Basis of Disease*, *1792*(3), 163–172. https://doi.org/10.1016/j.bbadis.2009.01.007

Feldman, A. M., Combes, A., Wagner, D., Kadakomi, T., Kubota, T., *et al.* (2000). The role of tumor necrosis factor in the pathophysiology of heart failure. *Journal of the American College of Cardiology*, *35*(3), 537–544. https://doi.org/10.1016/S0735-1097(99)00600-2

Fong, C. L., Siddiqui, A. H., Mark, D. F. (1994). Identification and characterization of a novel repressor site in the human tumor necrosis factor alpha gene. *Nucleic Acids Research*, *22*(6), 1108-1114.

Gabriel, S. B., Schaffner, S. F., Nguyen, H., Moore, J. M., Roy, J., *et al.* (2002). The structure of haplotype blocks in the human genome. *Science*, *296*(5576), 2225–2229. https://doi.org/10.1126/science.1069424

Georgescu, A. M., Banescu, C., Azamfirei, R., Hutanu, A., Moldovan, V., *et al.* (2020). Evaluation of TNF-α genetic polymorphisms as predictors for sepsis susceptibility and progression. *BMC infectious diseases*, *20*(1), 1-11.

Hajeer, A. H., & Hutchinson, I. V. (2001). Influence of TNFα gene polymorphisms on TNFα production and disease. *Human Immunology*, *62*(11), 1191–1199. https://doi.org/10.1016/S0198-8859(01)00322-6

Hedayati, M., Sharifi, K., Rostami, F., Daneshpour, M. S., Zarif Yeganeh, M., *et al.* (2012). Association between TNF-α promoter G-308A and G-238A polymorphisms and obesity. *Molecular Biology Reports*, *39*(2), 825–829. https://doi.org/10.1007/s11033-011-0804-4

Herrera, B. M., & Lindgren, C. M. (2010). The genetics of obesity. In *Current Diabetes Reports* (Vol. 10, Issue 6, pp. 498–505). https://doi.org/10.1007/s11892-010-0153-z

Hotamisligil, G. S., Arner, P., Atkinson, R. L., & Spiegelman, B. M. (1997). Differential regulation of the p80 tumor necrosis factor receptor in human obesity and insulin resistance. *Diabetes*, *46*(3), 451–455. https://doi.org/10.2337/diabetes.46.3.451

Hotamisligil, Gökhan S., Arner, P., Caro, J. F., Atkinson, R. L., & Spiegelman, B. M. (1995). Increased adipose tissue expression of tumor necrosis factor-α in human obesity and insulin resistance. *Journal of Clinical Investigation*, *95*(5), 2409–2415. https://doi.org/10.1172/JCI117936

Hotamisligil, Gökhan S., Shargill, N. S., & Spiegelman, B. M. (1993). Adipose expression of tumor necrosis factor-α: Direct role in obesity-linked insulin resistance. *Science*, *259*(5091), 87–91. https://doi.org/10.1126/science.7678183

Huizinga, T. W., Westendorp, R. G., Bollen, E. L., Keijsers, V., Brinkman, B. M., *et al.* (1997). TNF-α promoter polymorphisms, production and susceptibility to multiple sclerosis in different groups of patients. *Journal of Neuroimmunology*, *72*(2), 149-153.

Joffe, Y. T., Van Der Merwe, L., Evans, J., Collins, M., Lambert, E. V., *et al.* (2012). The tumor necrosis factor-α gene-238 G>A polymorphism, dietary fat intake, obesity risk and serum lipid concentrations in black and white South African women. *European Journal of Clinical Nutrition*, *66*(12), 1295–1302. https://doi.org/10.1038/ejcn.2012.156

Jung, U. J., & Choi, M. S. (2014). Obesity and its metabolic complications: the role of adipokines and the relationship between obesity, inflammation, insulin resistance, dyslipidemia and nonalcoholic fatty liver disease. *International Journal of Molecular Sciences*, *15*(4), 6184-6223.

Kaijzel, E. L., Van Krugten, M. V., Brinkman, B. M., Huizinga, T. W., Van der Straaten, T., *et al.* (1998). Functional analysis of a human tumor necrosis factor alpha (TNF-alpha) promoter polymorphism related to joint damage in rheumatoid arthritis. *Molecular Medicine*, *4*(11), 724-733.

Kaluza, W., Reuss, E., Grossmann, S., Hug, R., Schopf, R. E., *et al.* (2000). Different transcriptional activity and in vitro TNF-α production in psoriasis patients carrying the TNF-α 238A promoter polymorphism. *Journal of Investigative Dermatology*, *114*(6), 1180-1183.

Knight, J. C., Udalova, I., Hill, A. V. S., Greenwood, B. M., Peshu, N., *et al.* (1999). A polymorphism that affects OCT-1 binding to the TNF promoter region is associated with severe malaria. *Nature Genetics*, *22*(2), 145–150. https://doi.org/10.1038/9649

Laddha, N. C., Dwivedi, M., & Begum, R. (2012). Increased Tumor Necrosis Factor (TNF)-α and Its Promoter Polymorphisms Correlate with Disease Progression and Higher Susceptibility towards Vitiligo. *PLoS ONE*, *7*(12). https://doi.org/10.1371/journal.pone.0052298

Miller, S. A., Dykes, D. D., & Polesky, H. F. (1988). A simple salting out procedure for extracting DNA from human nucleated cells. *Nucleic Acids Research*, *16*(3), 1215. https://doi.org/10.1093/nar/16.3.1215

Mokdad, A. H., El Bcheraoui, C., Afshin, A., Charara, R., Khalil, I., *et al.* (2018). Burden of obesity in the Eastern Mediterranean Region: findings from the Global Burden of Disease 2015 study. *International Journal of Public Health*, *63*, 165–176. https://doi.org/10.1007/s00038-017-1002-5

Moon, Y. S., Kim, D. H., & Song, D. K. (2004). Serum tumor necrosis factor-α levels and components of the metabolic syndrome in obese adolescents. *Metabolism: Clinical and Experimental*, *53*(7), 863–867. https://doi.org/10.1016/j.metabol.2004.02.007

Parameswaran, N., & Patial, S. (2010). Tumor necrosis factor-a signaling in macrophages. In *Critical Reviews in Eukaryotic Gene Expression* (Vol. 20, Issue 2, pp. 87–103). https://doi.org/10.1615/CritRevEukarGeneExpr.v20.i2.10

Posch, P. E., Cruz, I., Bradshaw, D., & Medhekar, B. A. (2003). Novel polymorphisms and the definition of promoter "alleles" of the tumor necrosis factor and lymphotoxin α loci: Inclusion in HLA haplotypes. In *Genes and Immunity* (Vol. 4, Issue 8, pp. 547–558). https://doi.org/10.1038/sj.gene.6364023

Rousset, F. (2008). GENEPOP'007: A complete re-implementation of the GENEPOP software for Windows and Linux. *Molecular Ecology Resources*, *8*(1), 103–106. https://doi.org/10.1111/j.1471-8286.2007.01931.x

Russo, C., & Polosa, R. (2005). TNF-α as a promising therapeutic target in chronic asthma: A lesson from rheumatoid arthritis. In *Clinical Science* (Vol. 109, Issue 2, pp. 135–142). https://doi.org/10.1042/CS20050038

Sethi, J. K., & Hotamisligil, G. S. (1999). The role of TNF alpha in adipocyte metabolism. *Seminars in Cell & Developmental Biology*, 10, 19–29.

Skibola, D. R., Smith, M. T., Bracci, P. M., Hubbard, A. E., Agana, L., *et al.* (2005). Polymorphisms in ghrelin and neuropeptide Y genes are associated with non-Hodgkin lymphoma. *Cancer Epidemiology Biomarkers and Prevention*, *14*(5), 1251–1256. https://doi.org/10.1158/1055-9965.EPI-04-0895

Walston, J., Seibert, M., Yen, C., Cheskin, L. J., & Andersen, R. E. (1999). Tumor necrosis factor-alpha-238 and -308 polymorphisms do not associate with traits related to obesity and insulin resistance. *Diabetes*, *48*, 2096–2098.

Wellen, K. E., & Hotamisligil, G. S. (2005). Inflammation, stress, and diabetes. In *Journal of Clinical Investigation* (Vol. 115, Issue 5, pp. 1111–1119). https://doi.org/10.1172/JCI200525102

WHO Expert Committee. (1995). Physical status: the use and interpretation of anthropometry. *World Health Organization Technical Report Series*, *854*, 1–452. https://doi.org/10.1002/(sici)1520-6300(1996)8:6<786::aid-ajhb11>3.0.co;2-i

Yu, G. I., Ha, E., Park, S. H., Park, J. H., Jang, H. S., *et al.* (2011). Association of tumor necrosis factor-α (TNF-α) promoter polymorphisms with overweight/obesity in a Korean population. *Inflammation Research*, *60*(12), 1099–1105. https://doi.org/10.1007/s00011-011-0372-z

Zietek, T., & Rath, E. (2016). Inflammation Meets Metabolic Disease: Gut Feeling Mediated by GLP-1. *Frontiers in Immunology*, *7*, 154-170.

Submitted: 18/04/2021
Revised: 26/08/2021
Accepted: 02/11/2021
DOI: 10.48129/kjs.13771

Stimulatory effect of medium components on phytase production by *Aspergillus niger* and biotechnological application as a poultry feed additive

Shahzad Mahmood[1,2]*, Memuna G. Shahid[1], Muhammad Nadeem[2],
Muhammad S. A. Ahmad[3], Muhammad Irfan[4]

[1]*Dept. of Botany, Government College University, Katchery Road, Lahore-54000, Pakistan*
[2]*Food and Biotechnology Research Centre (FBRC),*
Pakistan Council of Scientific and Industrial Research (PCSIR) Laboratories Complex,
Ferozepur Road, Lahore-54600, Pakistan

[3]*Dept. of Botany, University of Agriculture, University Road Faisalabad-38000, Pakistan*
[4]*Dept. of Biotechnology, University of Sargodha, Sargodha-40100, Pakistan*

**Corresponding Author: shahzadbiology@gmail.com*

Abstract

The present study was conducted for the phytase production using solid-state fermentation (SSF) by *Aspergillus niger*. Optimization of various medium components was carried out for better production of phytase. Maximum enzyme activity (265.12±5.51 IU/g) was obtained, when the fungus was grown in the optimized culture medium containing glucose (1%), NH_4NO_3 (0.5%), $FeSO_4.7H_2O$ (0.1%), KCl (0.1%), and $MgSO_4.7H_2O$(0.1%) at 35 °C after 5 days of incubation time with pH 6. Then phytase was supplemented as poultry feed additive and given to broiler chickens during a feeding trial of 5 weeks. For this purpose, the birds of the control group (T0) were fed on a basal diet without external phytase, whereas, the birds of the experimental group (T3) were given basal feed + 3000 IU phytase per Kg diet. The results exhibited that there was an improvement in the body weight gain (BWG) of chicks i.e. 1903 g - 2090 g for the control group (T0) and experimental group (T3), respectively. The current study thus indicated the affectivity of phytase as a supplement in the broilers diet for better growth performance and recommended its use as an efficient additive in poultry feed formulation.

Keywords: Feed additive; medium components; optimization; phytase; solid state fermentation.

1. Introduction

Phosphorous (P) is an important mineral for growth performance and bone formation of broilers. It also supports energy conversion, egg production, and nervous system development (Li *et al*., 2020). A low amount of phosphorous is available in plant-based diets used for broilers because a large quantity of P is in the form of phytic acid, an organic P source. This phytic acid phosphorous is not usually accessible to the birds fed on plant-based diets due to insufficiency or lack of endogenous enzyme activity (Marchal *et al*., 2021), and is excreted as manure without being digested (Kumar *et al*., 2012; Lalpanmawia *et al*., 2014) and absorbed in the digestive tract

of monogastric animals. Due to the anti-nutritional effect, phytate has a negative effect on the digestion of other nutrients and thus reduces the poultry growth performance (Woyengo *et al*., 2013; Morgan *et al*., 2016).

To fulfill the requirements of phosphorous for the birds, monocalcium phosphate (MCP) or dicalcium phosphate (DCP) in the form of inorganic phosphorous may be supplemented to the poultry feed. But, in this way, the cost of feed and the amount of P released in the form of excreta will be increased causing environmental pollution (Saleh *et al*., 2021). To deal with such problems, supplementation of phytase in the bird's feed is a suitable solution (Lalpanmawia *et al*., 2014).

Phytase, a phosphatase enzyme, can hydrolyze phytic acid (Inositol hexakisphosphate) to inositol, inorganic phosphate, and potentially chelated minerals which are readily absorbed by monogastric animals e.g. poultry and fish (Ajith *et al*., 2018). The main objective of phytase supplementation in animal diet is to (i) use the inorganic P source and other important minerals already present in the plant-based feed (ii) improve the availability of myo-inositol (iii) counter the anti-nutritional effect of phytate (iv) conserve non-renewable sources of phosphorus due to decreasing requirement of its addition in the animal feed (v) minimize the environmental excretion of phosphate (Mahmood *et al*., 2021; Thorsen *et al*., 2021).

Submerged fermentation (SmF) or solid-state fermentation (SSF) can be used for the production of many biocatalysts such as phytase. However, it has been reported that SSF is the best method for the extracellular enzymes production by fungi (Cakmak & Aydogdu, 2021).

Phytase has a very profound role in the animal feed industry as an animals diet supplement, where it improves the digestion and assimilation of phosphorous and a few other inadequately available nutrients including copper, manganese, iron, and zinc in the monogastric animals digestive system (Munir & Maqsood, 2013; Vasudevan *et al*., 2017; Mahmood *et al*., 2021). Phytase plays important role in increasing the body weight gain (BWG) and growth performance of these animals. Phytases also decrease the amount of phosphorous in the animals excrement, which can otherwise cause environmental pollution. Phytases as an animal feed additive can thus be used as a substitute for expensive di-calcium phosphate and reduce the cost of animals feed (Dahiya, 2016; Jatuwong *et al*., 2020).

The present study was carried out to optimize the parameters for phytase production, and then to utilize the phytase as poultry feed additive to check its effect on the growth performance of broilers.

2. Materials and methods

2.1. Chemicals and biochemicals

In this study, the chemicals used were purchased from Sigma-Aldrich (USA), and Merck (Germany) and of analytical grade, however, the biological media were procured from Oxoid (UK).

2.2. Microorganism

A fungal strain i.e. *Aspergillus niger* was obtained from the Microbiology Laboratory, PCSIR Laboratories Complex, Lahore, Pakistan. The strain was maintained on potato dextrose agar (PDA) slants and used further for enzyme production.

2.3. Phytase production

Aspergillus niger was employed for phytase production in solid-state fermentation process. Growth medium (Rice polish, (% w/w) 0.1 $FeSO_4.7H_2O$, 0.1 KCl, 0.1 $MgSO_4.7H_2O$, 0.5 NH_4NO_3) was taken in an Erlenmeyer flask (250 ml) and an appropriate volume of distilled water (pH 5.5) was added in it. The culture medium was sterilized in an autoclave for 15 minutes at 121°C. Then, under aseptic conditions, 10% (v/w) inoculums of *Aspergillus niger* were amended in the fermentation medium after cooling at room temperature and incubation was done at 35°C for 5 days in an incubator (Mahmood *et al*., 2021).

At the end of the incubation period, 50 ml of 0.2 M citrate buffer (pH 5.5) was poured into all SSF media (including control) and shaken in a water bath for 1.5 hours. The content was firstly filtered through sterilized muslin cloth and then centrifugation was performed at 4°C for 15 min at 10,000 rpm in a centrifuge machine. The obtained filtrates were used as a crude source of enzyme for measuring the enzyme activities.

The activity of phytase was measured according to a slightly modified procedure as used by McKie & McCleary (2016) by calculating the amount of inorganic phosphorous liberated from the phytic acid solution.

2.4. Screening and optimization of different medium components for enhanced phytase production

2.4.1. Effect of different carbon and nitrogen sources on phytase production

Different carbon sources e.g. 1% (w/w) glucose, maltose, fructose, glycerol, sucrose, starch, and nitrogen sources i.e. 0.5% (w/w) urea, yeast extract, tryptone, malt extract, peptone, $(NH_4)_2SO_4$, CH_3COONH_4, NH_4NO_3, $NaNO_3$, and NH_4Cl were studied for their effect on enhanced phytase production.

2.4.2. Effect of various concentrations of medium components on phytase production

Influence of different concentrations of medium ingredients i.e. NH_4NO_3, KCl, $MgSO_4.7H_2O$, and $FeSO_4.7H_2O$ on phytase production was studied and the suitable concentration level of each ingredient was determined. The concentration of each component was used in the range of 0.025% to 0.15% (w/w), except for NH_4NO_3 with concentration varying from 0.25% to 1.5% (w/w). All experiments were conducted in triplicate by changing the concentration of one medium component at a time but keeping the concentration of others constant.

2.5. Biotechnological application of phytase as a poultry feed supplement

Basal feed containing phytase as an additive was given to experimental birds group compared to control group (without external phytase) and effect of phytase on the growth performance of broilers was investigated (a preliminary experimental work was revealed in an early published study).

2.5.1. Birds, housing, and experimental design

For this purpose, a feeding trial of 5-week for broiler chicken was performed with four dietary treatment groups i.e. T0, T1, T2, and T3, as shown in Table 1. One day old, 40 broiler chicks (Cobb) were purchased from the Punjab chicks hatchery, Lahore, Pakistan. The chicks were at random separated into four groups such as T0 (control group), T1, T2 & T3 (experimental groups) containing 10 birds each based on given feed (Table 1).

Table 1. Feed supplementation groups of experimental birds

Groups	Supplementation (Phytase @ IU/Kg basal feed)	No. of chicks
T0	0.00 (basal feed without phytase)	10
T1	1000	10
T2	2000	10
T3	3000	10

The feeding experiment of broiler chicks was conducted in a clean room at PCSIR Laboratories Complex, Lahore. A digital thermometer was used to monitor the temperature and humidity. The temperature was retained at the beginning of the experiment at 33°C and then progressively decreased to 24-25°C by lowering 3°C each week. The relative humidity of 50-60% and room temperature 24-25°C were maintained during the remaining period of the experiment. Throughout the experimental period of 35 days, the light was continuously provided. Fresh water and feed were given to the birds of each group ad libitum. Feed intake (FI), Body weight gains (BWG), and feed conversion ratio (FCR) of broilers was determined at the weekly interval. The animal experimental procedure was done according to approved protocols of the Animal Ethics Committee, Govt. College University, Lahore.

FCR was calculated by applying the following formula:

$$\text{Food conversion ratio (g/g)} = \frac{\text{Total Feed intake (g)}}{\text{Total weight gain (g)}}$$

2.5.2. Formulation of diets for the growth of broiler chickens

Different components of basal diets given to control and experimental groups of chicken birds are shown in Table 2. Phytase was mixed in liquid form to the feed and given to experimental birds.

Table 2. Composition of experimental diets (g/100 g) for chicks

Ingredient composition (%)	Starter feed (0-3 weeks)	Finisher feed (4-5 weeks)
Maize	60.2	65.65
Soybean meal	30	24
Corn gluten meal	2.5	3.0
Soybean oil	2.8	3.0
Limestone	1.2	1.2
Dicalcium phosphate (DCP)	1.7	1.6
Vitamin mineral mix	1	1
Salt	0.3	0.3
Lysine	0.15	0.15
Methionine	0.15	0.1

2.6. Statistical analysis

A completely randomized design (CRD) was set up to conduct all experiments with three replicates. Analysis of variance (ANOVA) of all parameters was computed using COSTAT computer package (CoHort Software, 2003, Monterey, California).

3. Results

During the present research work, optimization of different medium components was carried out for maximum phytase production from *Aspergillus niger*. The obtained phytase was then used as poultry feed additive.

3.1. Effect of different carbon sources on phytase production

The fermentation medium was amended separately with various carbon sources i.e. (1% w/w) fructose, maltose, glucose, sucrose, starch, and glycerol. The results indicated that different carbon sources showed a different effect on phytase production, whereas, glucose gave maximum phytase yield such as 213.29±3.92 IU/g compared to the control (without any external carbon source) i.e. 198.66±2.59 IU/g, as shown in Figure 1.

3.2. Effect of various nitrogen sources on phytase production

Different nitrogen sources i.e. 0.5% (w/w) peptone, urea, tryptone, yeast extract, malt extract, $(NH_4)_2SO_4$, NH_4NO_3, NH_4Cl, CH_3COONH_4 and $NaNO_3$ were employed in growth medium to obtain higher yield of phytase. It was exhibited by the results that enhanced production of phytase (241.79±5.84 IU/g) was obtained when NH_4NO_3 was supplemented in a culture medium (Figure 2) and $NaNO_3$ produced the second-highest phytase yield (240.28±3.59IU/g).

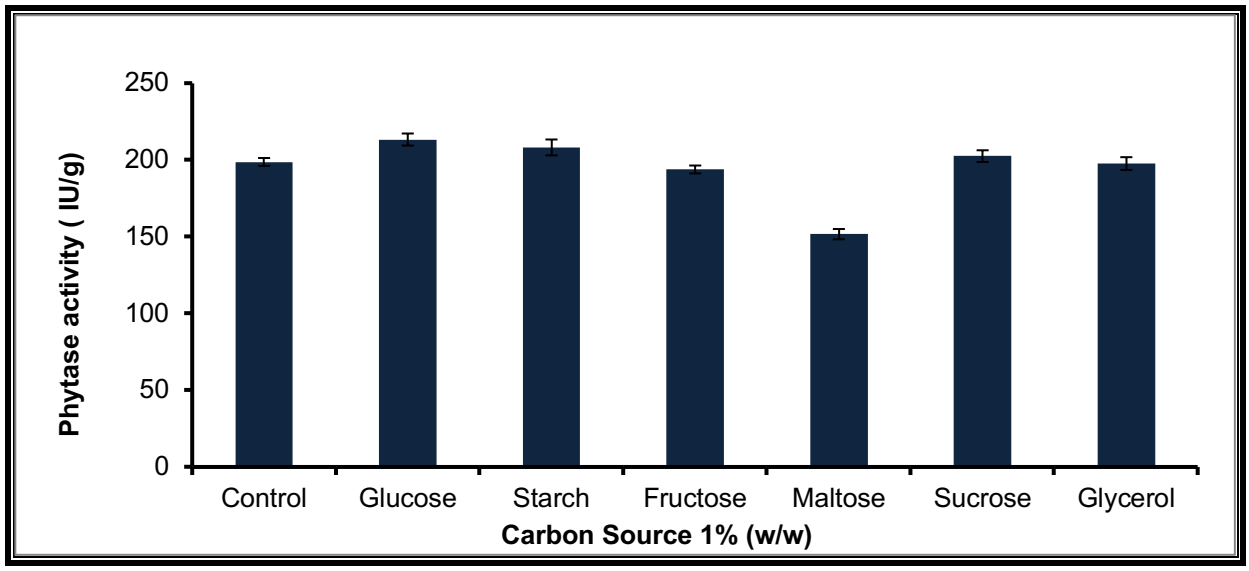

Fig. 1. Effect of different carbon sources on phytase production. Bars represent standard errors.

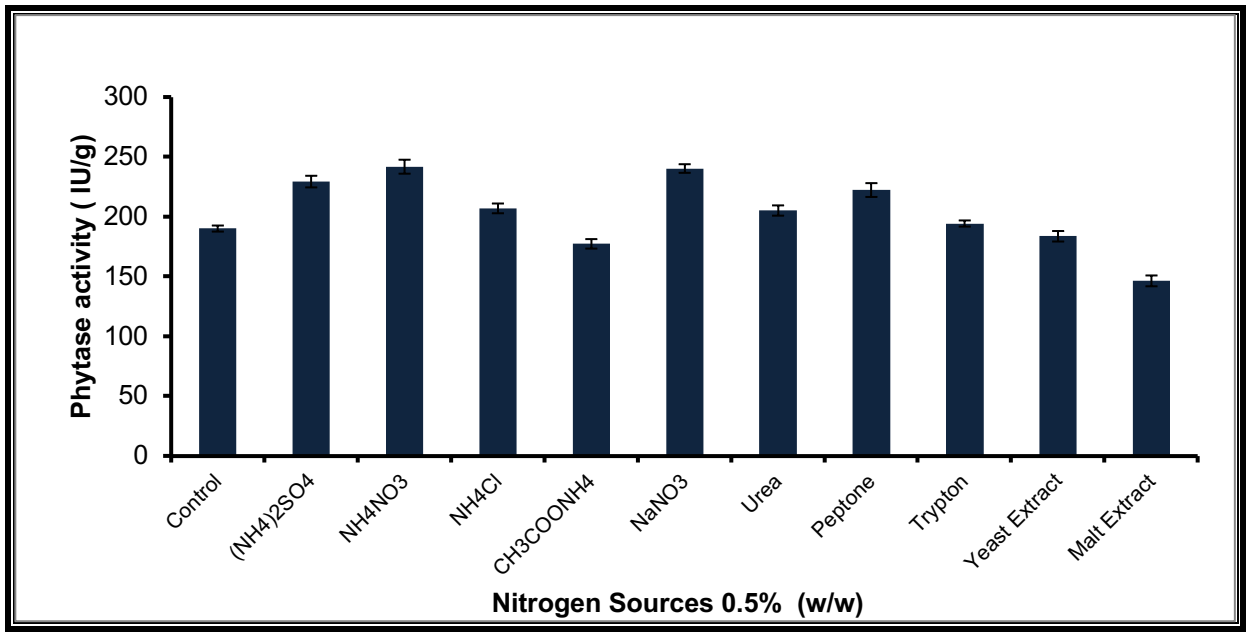

Fig. 2. Effect of various nitrogen sources on phytase production. Bars represent standard errors.

3.3. Effect of different concentrations of NH_4NO_3

Various conc. of NH_4NO_3 ranging from 0.25% to 1.5% (w/w) were applied in the culture medium over the control (without any external source of NH_4NO_3) to determine the optimum concentration for the maximum yield of phytase. The highest phytase production (252.28±5.29 IU/g) was observed at 0.5% NH_4NO_3 (Figure 3). A decrease in enzyme production was noted at lower or higher concentrations of NH_4NO_3 other than the optimum.

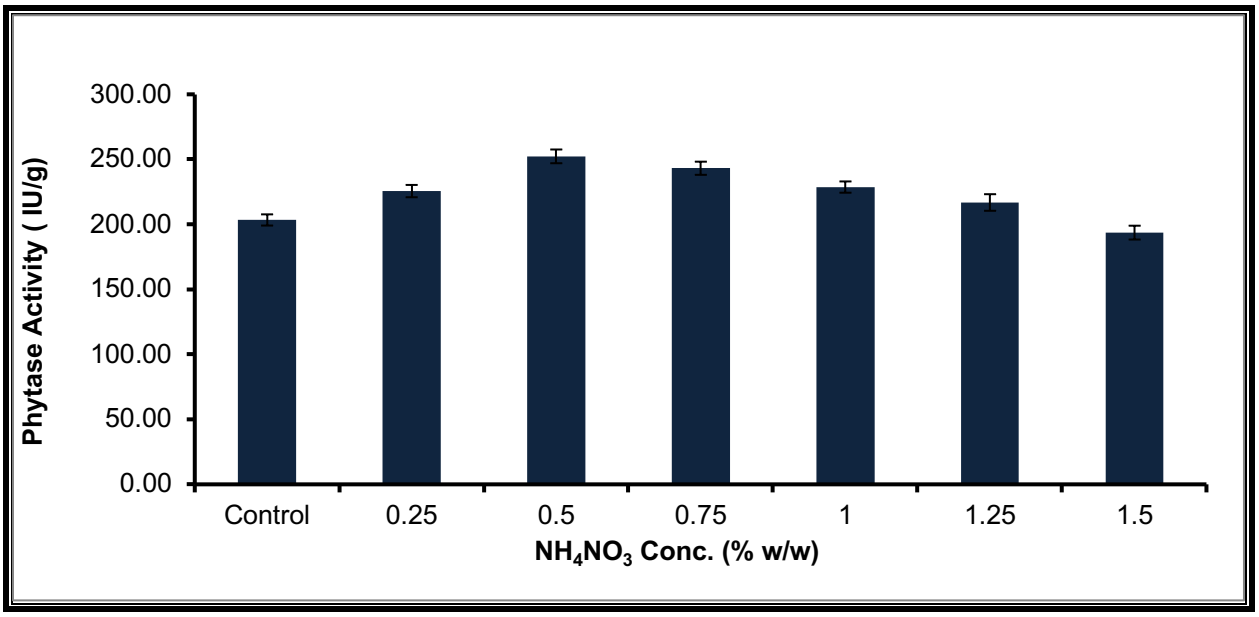

Fig. 3. Effect of various conc. of NH_4NO_3 on phytase production. Standard errors are shown.

3.4. Effect of different concentrations of KCl

The influence of various amounts i.e. 0.025% to 0.15% (w/w) of KCl in the growth medium was studied for the optimum yield of phytase. The growth of the fungus is slightly supported due to the presence of KCl in the culture medium as indicated by the increase in enzyme production. It was reported that 0.1% (w/w) KCl conc. gave the maximum production of phytase (263.23±5.12 IU/g) as shown in Figure 4.

3.5. Effect of different concentrations of $MgSO_4.7H_2O$

Various quantities of $MgSO_4.7H_2O$ such as 0.025% to 0.15% (w/w) were utilized in the growth medium for increased synthesis of phytase. The results revealed that phytase production was maximum (259.78±5.23IU/g) in the presence of 0.1% (w/w) $MgSO_4.7H_2O$, as represented in Figure 5.

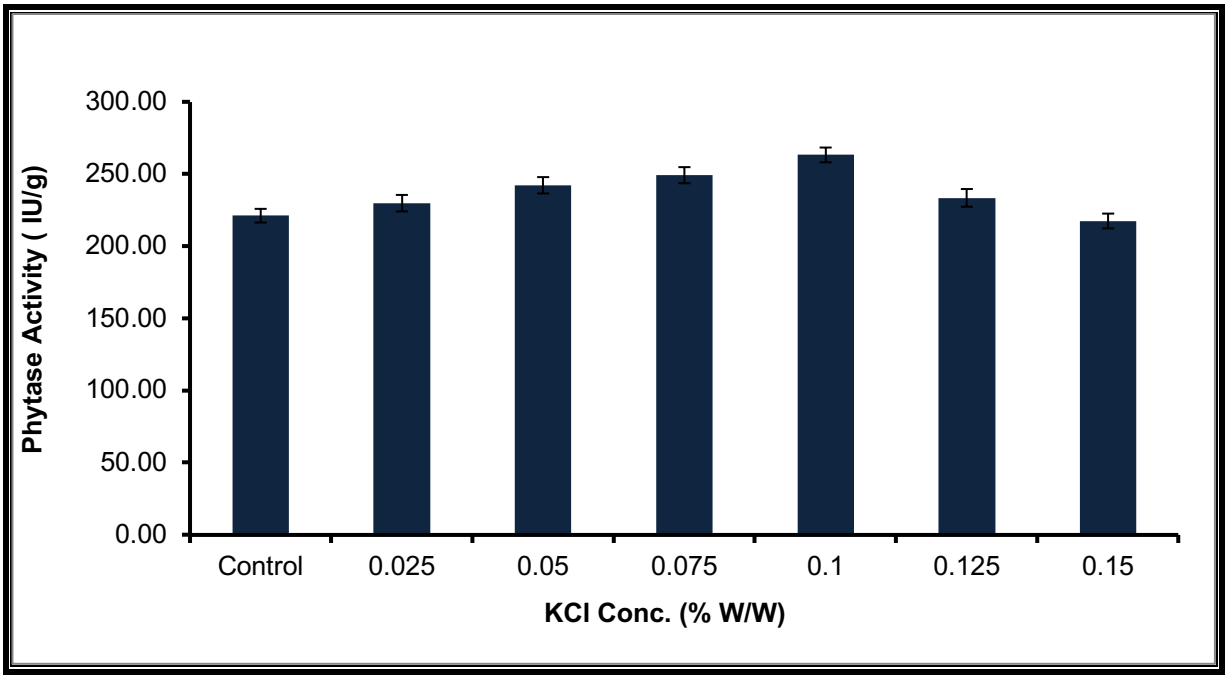

Fig. 4. Effect of various conc. of KCl on phytase production. Standard errors are exhibited.

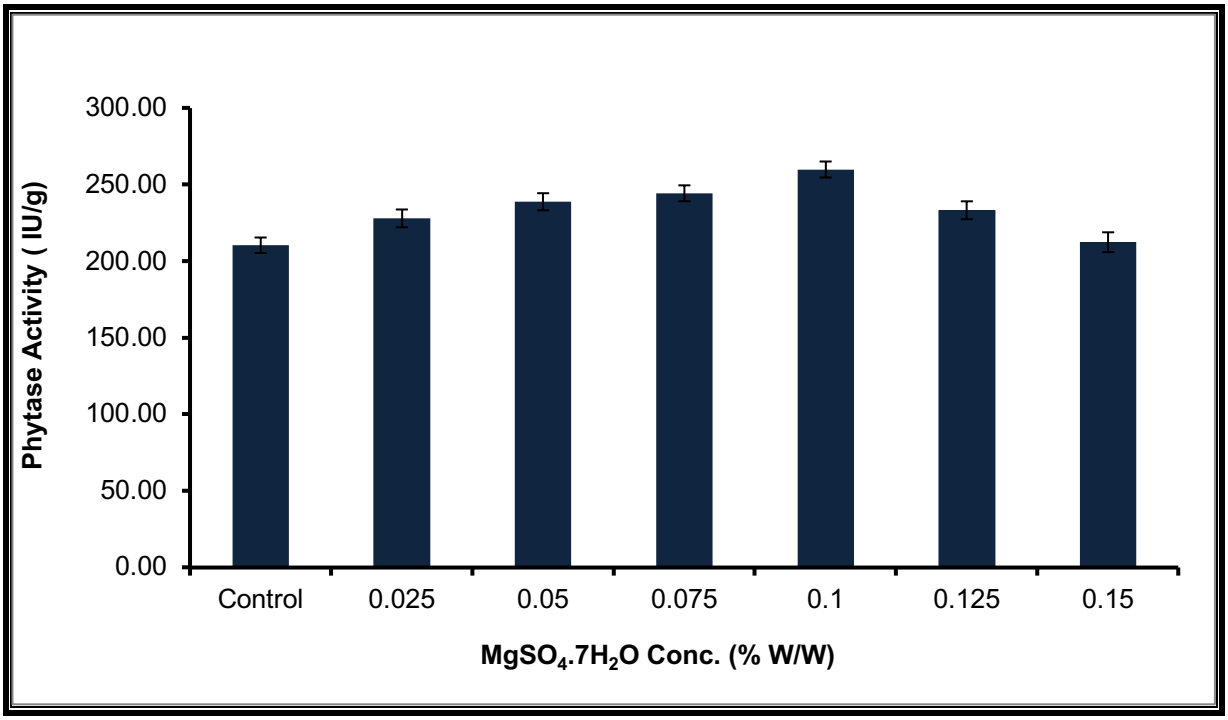

Fig. 5. Effect of various conc. of $MgSO_4.7H_2O$ on phytase production. Standard errors are given.

3.6. Effect of different $FeSO_4.7H_2O$ concentrations

The influence of Fe++ ions on phytase yield was investigated by amending the cultivation medium with different concentrations (0.025% to 0.15% w/w) of $FeSO_4.7H_2O$. Among all the concentrations tested, 0.1% (w/w) $FeSO_4.7H_2O$ gave better phytase production i.e. 265.12±5.51 IU/g (Figure 6).

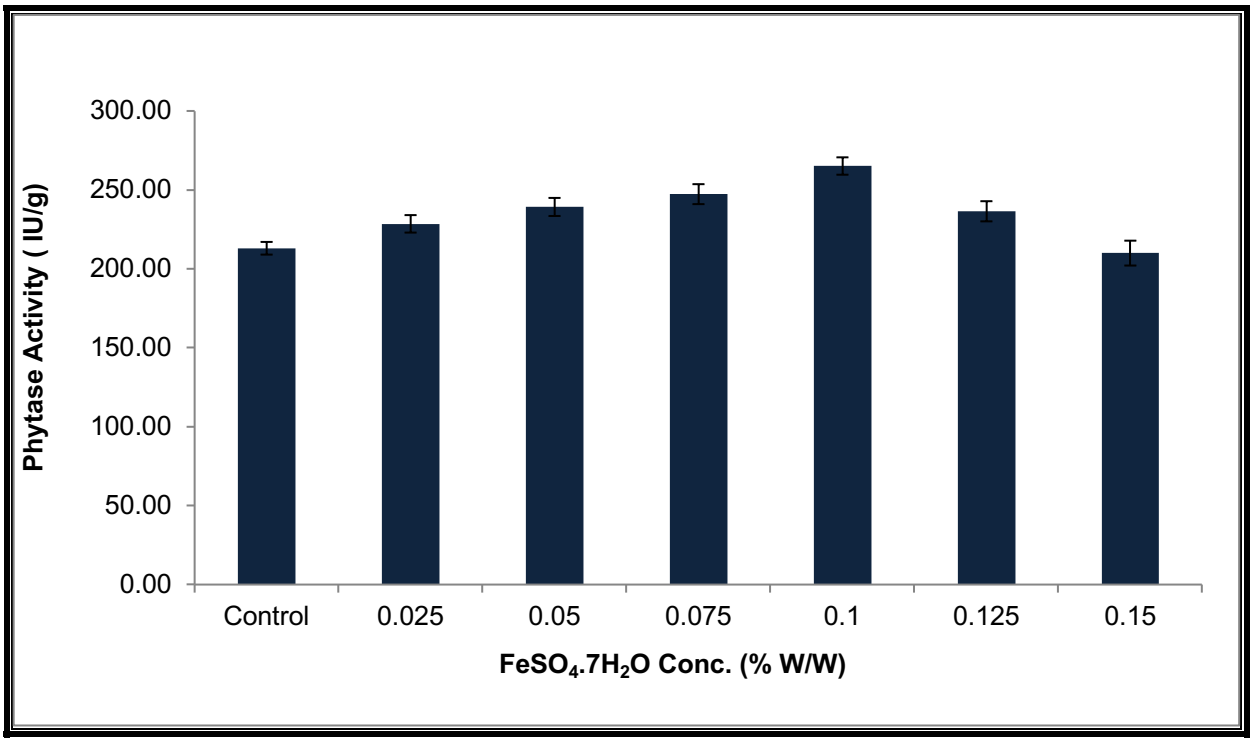

Fig. 6. Effect of various conc. of $FeSO_4.7H_2O$ on phytase production. Standard errors are indicated.

3.7. Impact of phytase on the growth performance of broiler chickens

Feed intake (FI) and BWG (Body weight gain) for broiler chicks were determined after every week. Then feed conversion ratio (FCR) was estimated as described in Table 3 & 4. The results showed that during the first three weeks of the experiment, the chicks kept in group T3 fed on starter feed exhibited the highest body weight gain (905 g) and feed intake (1240 g), whereas the highest food conversion ratio (1.40 g/g) was with group T0 in comparison to other groups (Table 3). After 3rd week, birds were grown on a finisher diet for the next two weeks. After five-week of the feeding trial, the results indicated that maximum feed intake (3240 g) and body weight gain (2090 g) was shown by the group (T3) of experimental birds compared to others (Table 4).

Table 3. Growth performance characteristics of broiler chickens after 0-3 weeks

Groups	Bodyweight gain (g/bird)	Feed intake (g/bird)	Feed conversion ratio (g/g)
T0	780±2.95	1092±3.18	1.40±0.0055
T1	840±4.51	1138±5.93	1.35±0.0046
T2	869±3.65	1190±4.89	1.37±0.0033
T3	905±5.55	1240±6.77	1.37±0.0023

Table 4. Growth performance characteristics of broiler chickens after 0-5 weeks

Groups	(Bodyweight gain) g/bird	(Feed intake) g/bird	(Feed conversion ratio) g/g
T0	1903±6.85	3114±12.81	1.64±0.0027
T1	1970±7.57	3160±12.13	1.60±0.0023
T2	2028±8.21	3200±13.03	1.58±0.0026
T3	2090±10.07	3240±15.31	1.55±0.0040

Each value in the table 3 & 4 is an average of ten replicates, ± indicates standard error T0 = Control group (Basal feed without phytase), T1, T2, T3 = Experimental groups (Basal feed with 1000 IU, 2000 IU, 3000 IU phytase per Kg diet)

4. Discussion

For the improved phytase production from *Aspergillus niger*, selection and optimization of different medium components were conducted under solid-state fermentation. The phytase enzyme produced during the present study was then applied as a supplement in the diets of broiler chickens.

The production of any cultivation is affected by medium composition and process parameters. The earlier studies indicated that the yield of phytase was affected by many physico-chemical parameters i.e. composition of culture medium, nitrogen and carbon sources, different minerals, the type of microorganism, growth of the cell, cultivation methods, size of inoculums, incubation period, temperature and pH of the medium (Suleimenova *et al*., 2016).

During the present study different carbon (1% w/w) and nitrogen (0.5% w/w) sources, were tested for higher phytase production. The results revealed that 0.5% (w/w) NH_4NO_3 produced the best phytase yield (252.28±5.29 IU/g) as shown in Figure 3. Many researchers had obtained similar results that NH_4NO_3 was proved as best nitrogen source and showed the highest production of phytase by *Rhizopus sp*. And *Aspergillus niger* (Sandhya *et al*., 2015; Suresh & Radha, 2016; Tian & Yuan, 2016). Figure 1 showed that glucose 1% (w/w), among different carbon sources, gave a maximum phytase yield (213.29±3.92IU/g). Glucose was investigated as

an appropriate carbon source for enhanced phytase production during many earlier fermentation studies (Buddhiwant *et al*., 2016; Qasim *et al*., 2017).

Different inorganic salts ($MgSO_4.7H_2O$, KCl, $FeSO_4.7H_2O$) were also added in culture medium in order to test their effect on phytase production. Figure 4, 5 & 6 showed that the production of phytase is improved due to utilization of these salts. An experiment was conducted by Mahmood *et al*. (2021), in which a better amount of phytase was produced by *Aspergillus niger*, when fermentation studies were carried out in a medium comprising rice polish, 0.5% NH_4NO_3, 1% Glucose, 0.1% each of KCl, $MgSO_4.7H_2O$ and $FeSO_4.7H_2O$ using solid-state fermentation.

Biotechnological application of phytase enzyme was performed as poultry feed additive and the effect of phytase was investigated on the growth of broilers. For this purpose, one control group (T0) without phytase in the basal feed and three experimental groups (T1, T2, T3) with varying concentrations of phytase in the basal feed were made (Table 1). It was revealed by the results that the average body weight of chicks related to experimental groups was higher compared to the control group and it was highest for experimental group T3 (with phytase @ 3000 IU/Kg diet) compared to the other three groups during the 5 weeks of chicks growth (Table 3 & 4).

Ajith *et al*. (2018) experimented with the submission of phytase as poultry feed additive and the growth characteristics of broilers were monitored. The study indicated that better growth performance for broilers was achieved by supplementing their feed with 500 FTU/kg phytase and 0.8% calcium in the diet, with decreased phosphorous excretion in the surrounding environment.

For the biotechnological application of phytase, the effect of phytase was studied on the growth performance of broilers by pre-treating corn-soya diets with microbial phytase. The results showed that there was an increase of the availability of 60% inorganic phosphorus when phytase obtained from microorganisms was provided to the broilers fed on diets containing less phosphorous. There was a decrease of 50% phosphorous in the chickens manure. The results also indicated the 5.8-13.2% increase in body weights of chickens, after 21 days of phytase supplementation in their diets (Jatuwong *et al*., 2020).

5. Conclusion

In the current study, the production of phytase by *Aspergillus niger* was investigated. The optimization of different medium ingredients was carried out using solid-state fermentation. The optimized conditions were determined as glucose (1%), KCl (0.1%), NH_4NO_3 (0.5%), $FeSO_4$.7H2O (0.1%) and $MgSO_4.7H_2O$ (0.1%). Under optimized culture conditions, the maximum production of phytase was recorded as 265.12±5.51 IU/g. It was further reported that the incorporation of phytase in poultry diets enhances the body weight gain (BWG) of broilers (2090 g) belonging to the experimental group (T3) in comparison to the control group (T0) (1903 g). The biotechnological studies of phytase as poultry feed additive indicated its beneficial effect

on the growth performance of poultry birds. Collectively, all these results may justify the possibility of the production of phytase by *Aspergillus niger* and its utilization as a supplement in poultry diet formulations.

ACKNOWLEDGEMENTS

The authors gratefully acknowledge the research assistance from the Food and Biotechnology Research Centre (FBRC), PCSIR Laboratories Complex, Lahore, to conduct this research work.

References

Ajith, S., Shet, D., Ghosh, J., Awachat, V.B., Bhat, K. *et al.*(2018). Effect of immobilized fungal phytase on growth performance and bone traits of broilers fed with low dietary calcium and phosphorus. Veterinary World, **11:** 758-764.

Buddhiwant, P., Bhavsar, K., Kumar, R. & Khire, V. (2016). Phytase production by solid state fermentation of groundnut oil cake by *Aspergillus niger*: a bioprocess optimization study for animal feed stock applications. Preparative Biochemistry and Biotechnology, **46(6):** 531-538.

Cakmak, M. & Aydogdu, H. (2021). Screening of microfungi for lipolytic activity and optimization of process parameters in lipase production by solid substrate fermentation using selected microfungi (*Penicillium aurantiogriseum*). Kuwait Journal of Science, **48 (1):** 98-105.

Dahiya, S. (2016). Industrial applications of phytases. International Journal of Applied Research, **2(2):** 95-98.

Jatuwong, K., Suwannarach, N., Kumla, J., Penkhrue, W. & Kakumyan. (2020). Bioprocess for production, characteristics and biotechnological applications of fungal phytases. Frontier Microbiology, **11(18):** 1-18.

Kumar, V., Sinha, A.K., Makkar, H.P., De Boeck, G. & Becker, K. (2012). Phytate and phytase in fish nutrition. Journal of Animal Physiology and Animal Nutrition, **96**: 335-364.

Lalpanmawia, H., Elangovan, A., Sridhar, M., Shet, D., Ajith, S. *et al.* (2014). Efficacy of phytase on growth performance, nutrient utilization and bone mineralization in broiler chicken. Animal Feed Science and Technology, **192:** 81-89.

Li, T., Xing, G., Shao, Y., Zang, L., Li, S. *et al.* (2020). Dietary calcium or phosphorous deficiency impairs the bone development by regulating related calcium or phosphorous metabolic utilization parameters of broilers. Poultry Science, **99:** 3207-3214.

Mahmood, S., Shahid, M.G., Nadeem, M. & Haq, I.U. (2021). Screening of phytate degrading fungi and optimization of culture conditions for phytase synthesis using agro-industrial by-products. Pakistan Journal of Botany, **53(2):** 763-770.

Marchal, L., Bello, A., Sobotik, E.B., Archer, G., Dersjant-Li, Y. *et al.* (2021). A novel consensus bacterial 6-phytase variant completely replaced inorganic phosphate in broiler diets, maintaining growth performance and bone quality: data from two independent trials. Poultry Science, **100:** 1-14.

McKie, V.A. & McCleary, B.V. (2016). A novel and rapid colorimetric method for measuring total phosphorus and phytic acid in foods and animal feeds. Journal of AOAC International, **99:** 738-743.

Morgan, N.K., Walk, C.L., Bedford, M.R., Scholey, D.V., Burton, E.J. *et al*. (2016). Effect of feeding broilers diets differing in susceptible phytate content. Animal Nutrition, **2:** 33-39.

Munir, K. & Maqsood, S. (2013). A review on role of exogenous enzyme supplementation in poultry production. Emirates Journal of Food and Agriculture, **25:** 66-80.

Qasim, S.S., Shakir, K.A., Al-Shaibani, A.B. & Walsh, M.K. (2017). Optimization of culture conditions to produce phytase from *Aspergillus tubingensis* SKA. Food and Nutrition Science, **8:** 733-745.

Saleh, A.A., Elsawee, M., Soliman, M.M., Elkon, R.Y.N., Alzawqari, M.H. *et al*. (2021). Effect of bacterial or fungal phytase supplementation on the performance, egg quality, plasma biochemical parameters, and reproductive morphology of laying hens. Animals, **11:** 1-11.

Sandhya, A., Sridevi, A., Devi, P.S. & Narasimha, G. (2015). Production and optimization of phytase by *Aspergillus niger*. Der Pharmacia Lettre, **7(12):** 148-153.

Suleimenova, Z., Akhmetsadykov, N., Kalieva, A., Mustafin, K., Saduyeva, Z.*et al*. (2016). Effect of different cultural conditions for phytase production by *Aspergillus niger* in submerged fermentation. Advances in Enzyme Research, **4(2):** 62-67.

Suresh, S. & Radha, K.V. (2016). Statistical optimization and mutagenesis for high level of phytase production by *Rhizopus oligosporus* MTCC 556 under solid state fermentation. Journal of Environmental Biology, **37:** 253-260.

Thorsen, M., Nielsen, L.A., Zhai, H., Zhang, Q., Wulf-Andersen, L. *et al*. (2021). Safety and efficacy profile of a phytase produced by fermentation and used as a feed additive. Heliyon, **7:** 1-12.

Tian, M. & Yuan, Q. (2016). Optimization of phytase production from potato waste using *Aspergillus ficuum*. 3 Biotech, **6(256):** 1-8.

Vasudevan, U.M., Shyam, K., Vidya, J. & Pandey, A. (2017). Microbial phytase: impact of advances in genetic engineering in revolutionizing its properties and applications. Bioresource Technology, **245:** 1790-1799.

Woyengo, T. & Nyachoti, C. (2013). Anti-nutritional effects of phytic acid in diets for pigs and poultry - current knowledge and directions for future research. Canadian Journal of Animal Science, **93:** 9-21.

Submitted: 27/12/2021
Revised: 22/04/2022
Accepted: 25/05/2022
DOI: 10.48129/kjs.17947

Stress response of the coral *Stylophora pistillata* towards possible anthropogenic impacts in the Gulf of Aqaba, Red Sea

Fuad A. Al-Horani[1*], Sewar T. Al-Talafhah[2], Maysoon Kteifan[1], Emad I. Hussein[3, 4]

[1]*School of Basic and Marine Sciences, The University of Jordan, Aqaba, Jordan*
[2]*Aya Specialist Medical Hospital, Jeddah, Saudi Arabia.*
[3]*Dept. of Food Science and Human Nutrition, College of Applied and Health Sciences, A'Sharqiyah University, Ibra, Oman.*
[4]*Dept. of Biological Sciences, Yarmouk University, Irbid, Jordan*

***** *Correspondence; f.horani@ju.edu.jo*

Abstract

Coral deterioration is often linked with coastal pollution. This aimed to study biochemical stress responses in the common coral *Stylophora pistillata* collected and/or planted in coastal sites subject to pollution and sites without pollution in the Gulf of Aqaba. DNA damage and lipid peroxidation were analyzed to measure stress in corals. High DNA damage was found in natural corals from polluted sites, while higher lipid peroxidation was found in control site compared with polluted sites. Lipid peroxidation was higher in polluted sites after one-year of deployment. Corals' incubations with copper and lead produced high levels of DNA damage and lipid peroxidation compared with control samples. The results suggested that although corals are visually looking healthy, but they are suffering at subcellular levels. The consequences of such stress might affect the fecundity and growth rates of corals. The results suggest that biomarkers used are efficient tools for early stress detection in corals, though the cost of assessing DNA damage is relatively expensive compared with lipid peroxidation.

Keywords: Biomarker**;** comet assay; **c**oral; DNA damage; Gulf of Aqaba; lipid peroxidation.

1. Introduction

Coral reefs are globally significant ecosystems due to their ecological and socioeconomic importance to mankind (Burke *et al.,* 2012). Red Sea coral reefs are significant ecosystems at global scale (Gladstone *et al.,* 1999). The Gulf of Aqaba (GoA) is the only marine access of Jordan, where all sea-related human activities are concentrated (Al-Horani & Khalaf, 2013). Coral reefs are vulnerable to impacts from overlapping human activities, of which marine pollutants are major threat to them (Al-Horani *et al.,* 2011; Binelli & Provini, 2003).

When corals are impacted by anthropogenic stressors, their colonies display signs of stress like bleaching or tissue necrosis, which may result in their final death (Ginsburg *et al.,* 2001). Proper evaluation of the impacts of pollutants on corals is essential to avoid their death since sublethal status can be missed when visual inspection is used to check on their health status, where biomarkers are useful tools for such purposes (Wells *et al.,* 2001).

The DNA damage in living cells leads to the appearance of lesions and can cause various cell dysfunctions, genome mutations and gene instabilities. Therefore, there is an essential demand for assessments that can evaluate DNA damage (Boer *et al.,* 2002). The comet assay technique (single cell gel electrophoresis) is efficient for testing DNA damage and can be used as monitoring tool for environmental pollution (Wilson *et al.,* 1998; Collins, 2004). The method is reliable and sensitive to measure DNA strand breaks induced by various agents in eukaryotic cells using florescence microscopes.

Lipid peroxidation (LPO) is a process mediated by reactive oxygen species (ROS) and might lead to degradation of polyunsaturated fatty acids and cell membrane disorganization and can be used as oxidative damage bioindicator (Valavanidis & Vlachogianni, 2010; Vijayavel *et al.,* 2012). Levels of ROS might increase as a result of stress response mechanisms related to temperature, UV exposure, oxygen levels in addition to pollutants such as heavy metals (Lesser, 2011; Banc-Prandi, & Fine, 2019). The products of LPO indicate the levels of ROS in the cell, which in turn reflects the oxidative stress by internal and external factors (Girotti, 1998). Malondialdehyde (MDA) is one of the major end products of LPO that can be used as indicator to detect oxidative stress in biological objects (Yadav, 2010).

This study aims to assess stress responses of *Stylophora pistillata* towards marine pollutants in contaminated versus uncontaminated sites in GoA. The assessment examines DNA damage and LPO as biomarkers to measure stress in corals.

2. Methods Coral Samples

Stylophora pistillata colonies were collected from shallow reef slope (<10m) at the Marine Science Station (MSS) and were housed temporarily in coral wet laboratory. The mother colonies (ca. 10 mother colonies) were fragmented into small pieces (5cm long) and were glued to plastic tubes and placed in a flow-through seawater raceway for two weeks before deployment as described by Al-Horani (2013). Coral fragments were fixed on aluminum racks (80x40x60 cm) and were placed at 8m depth in front of the MSS. Three types of samples were collected; aged fragments (one year old), newly planted fragments (one week old), and natural colonies found in the site (4 replicates were collected from each site). From each treatment group, four replicates were collected by SCUBA divers.

3. Study Sites

Study sites included the Industrial Complex (IC) site, where various industries are concentrated, the Public Beach (PB) site, which is regularly exploited by the general public and the MSS site, located within the MPA and has no direct human impacts (used as control site) (Figure 1). Pollutants at the IC and PB sites may include oil spills, antifouling paints, organic and solid wastes including metal cans and plastics. Runoff during winter bring various pollutants to the sea in the three sites when it occurs.

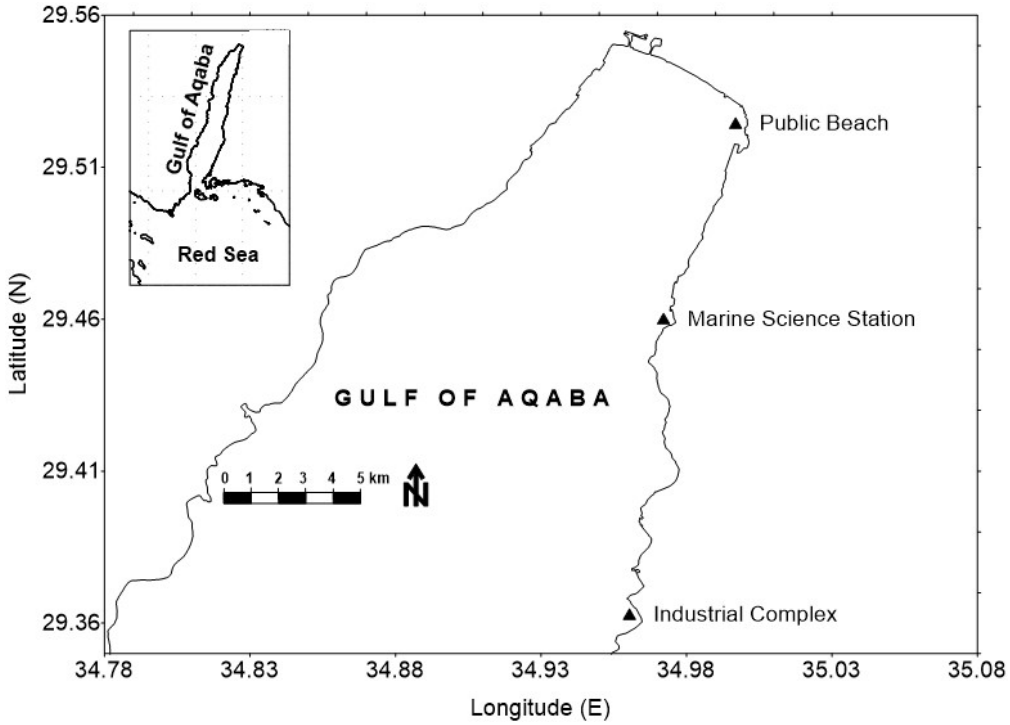

Fig. 1. GoA map with latitude (N) and longitude (E) drawn by surfer software.

4. Isolation and preparation of coral cells

Artificial seawater free of Ca^{2+} and Mg^{2+} was used to dissociate the tissue from skeleton (Rinkevich *et a*l., 2005). Samples were immersed for 10min. at room temperature, followed by gentle shaking until the tissue was fully dissociated. The isolated tissue suspension was centrifuged at 4000rpm for 5min to remove zooxanthellae and the supernatant was then centrifuged for 15min at 4000rpm. The pellet was used for LPO analysis and the cells for the comet assay were resuspended in 500µL PBS until analysis.

5. Measurement of DNA damage

Trevigen® comet assay kit was used to measure DNA damage in coral cells according as described by Szeto *et al.,* (2012). In this method, coral cells were centrifuged at 10000rpm for 5min and the cell suspension (10µL) was mixed with LMA and 50µl/well was pipetted onto the comet slide and electrophoresis was run as described. Then, slides were examined by inverted fluorescence microscope (EVOS®) on 100x magnification (GFP filter, 470nm excitation, 525nm emission) to measure the migration of damaged DNA from the nuclei.

The formation of specific structures like comets in the gel indicates DNA inside the tissue is damaged. The comet tail intensity relative to head reflects the number of DNA breaks. For scoring of the DNA damage in cells, the damage levels were graded from 0 to 4 (Figure 2), where score 0 represents no damage and score 4 represents severe damage. The score of each sample was calculated by using the following equation:

$$\text{Score} = \frac{0*\text{N0}+1*\text{N1}+2*\text{N2}+3*\text{N3}+4*\text{N4}}{\text{total number of cells}}$$

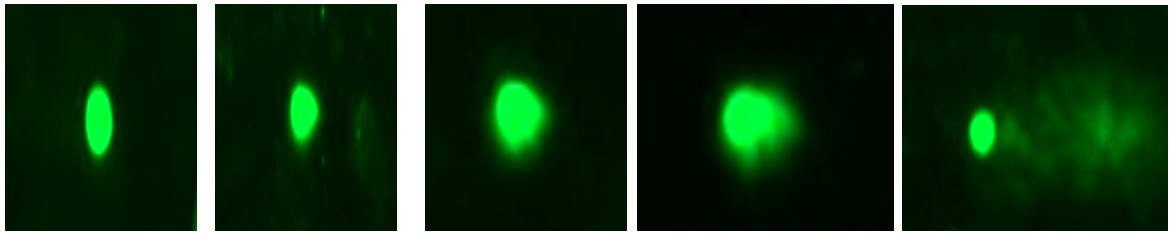

Fig. 2. Comet assay score (0-4) showing DNA damage levels in *S. pistillata* cells.

6. Measurement of lipid peroxidation

Lipid peroxide was measured by analyzing MDA, an end product of lipid peroxidation, which reacts with thiobarbituric acid (TBA) as a reactive substance, and produces a red colored complex (MDA-TBA) that has a peak absorbance at 535nm (Wahsha *et al.,* 2012; Saeed *et al.,* 2020). The coral cells were prepared as described previously and the absorbance was measured at 532nm and 600nm with TBA-TCA mixture used as blank, and the lipid peroxides quantified by using Beer's law with an extension coefficient of $155mM^{-1}$ cm^{-1}. The results were expressed as M/g wet pelleted coral tissue weight.

7. Effects of addition of heavy metals on lipid peroxidation

Fragments of *S. pistillata* were glued in an upright position to a small (5x5 cm) ceramic plates using epoxy glue. The following incubations were carried out; the first included five plastic aquaria that were filled with 5L seawater with aeration. The first aquarium was used as negative control. Copper (Copper Chloride) was added to two aquaria at two different concentrations (1 and 5ppm), while the last two aquaria were supplemented with lead (Lead Nitrate) (1 and 5ppm). In the second incubation experiment, the concentrations of Cu and Pb were adjusted to 0.1 and 0.2ppm. In the first day (0 time), coral fragments from the five aquaria were taken and prepared for LPO test as described earlier. Samples were incubated for 10 days or until they died and were taken every two days for LPO analysis, and samples from the Cu and Pb 1 and 5ppm incubations were used for comet assay analysis.

8. Statistical analysis

Statistical analysis was performed using one- and two-ways ANOVA. Statistical significance was considered at p-value of 0.05 or less. Data was analyzed by using Sigma Stat software.

9. Results Comet assay *in situ* experiments

DNA damage in coral fragments incubated *in situ* at MSS site were not significantly different in the 1wk incubated, 1yr incubated and natural colonies, though a DNA damage was recorded in MSS samples. The 1wk incubated samples from PB and IC sites had similar levels of DNA damage to the MSS site. While, after 1yr of deployment in the sea, the DNA damage increased significantly by 22% and 24% compared to 1wk in PB and IC sample, respectively. High DNA damage scores was recorded in natural corals collected from PB and IC sites (Figure 3).

10. Comet assay for ex *situ* experiments

DNA damage scores was much higher in copper- and lead-incubated corals when compared to all field incubated-corals. The lead-incubated corals had average DNA damage scores of 2.35, regardless of the metal concentration. In the copper-incubated samples, DNA damage scores was lower than those incubated with lead (Figure 4), although copper-incubated samples suffered with severe tissue necrosis and died after four days of incubation.

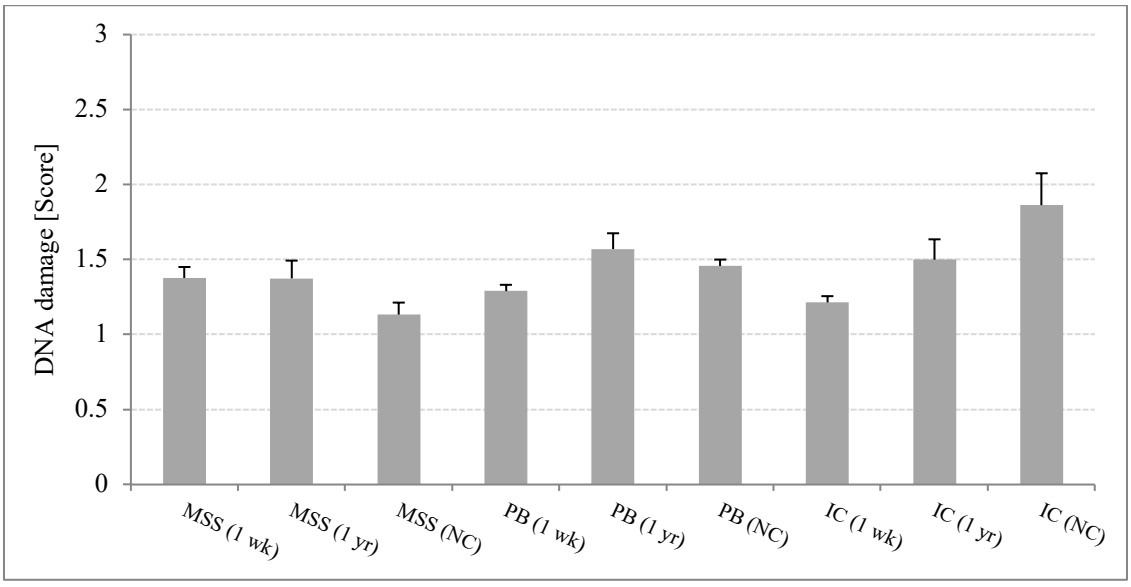

Fig. 3: Scores of DNA damage in corals at the 3 sites (wk; week, yr; year, NC; natural corals). Results presented as average±SD.

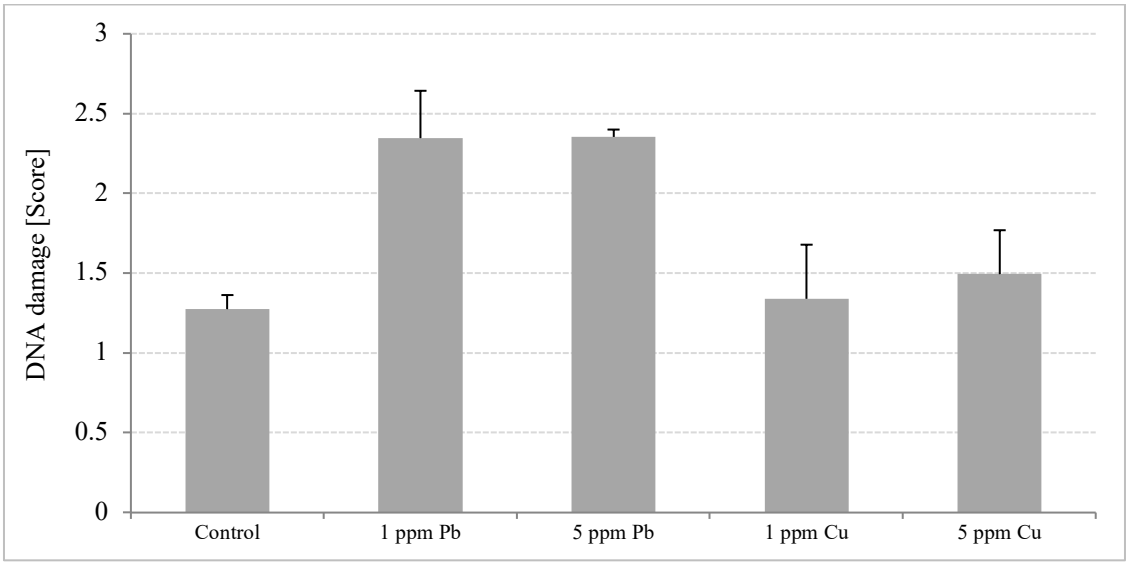

Fig. 4: Scores of DNA damage in corals incubated with Pb and Cu and control samples.

11. Lipid peroxidation *in situ* experiments

Analysis of LPO in field-incubated corals showed high levels of peroxidation in all samples except for the natural corals in IC site. There were no observed trends among the values obtained (Figure 5).

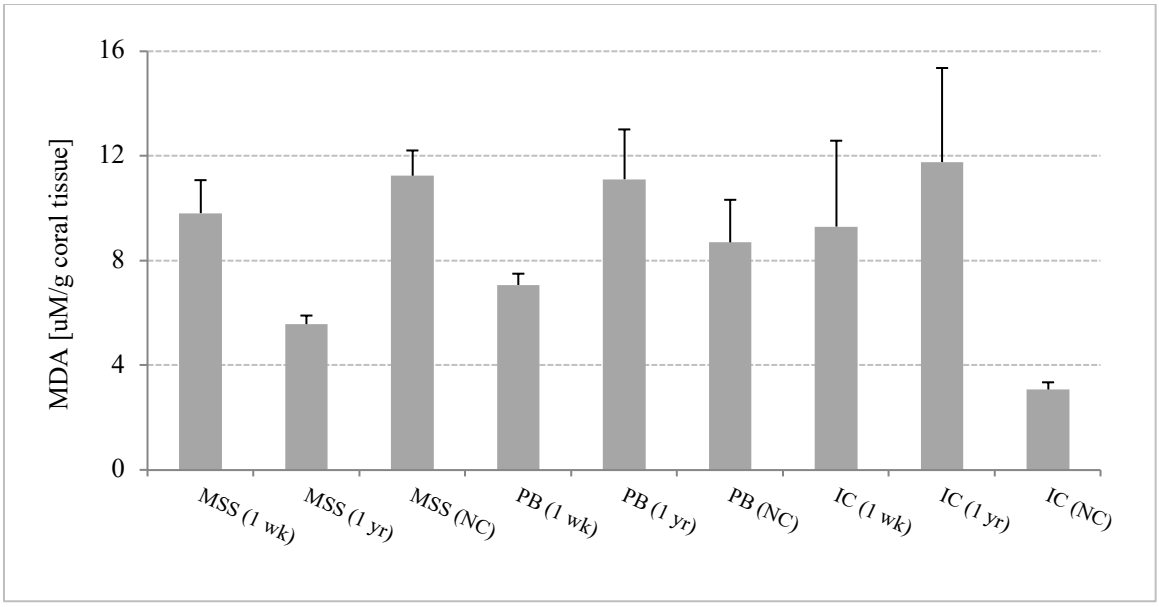

Fig. 5. MDA levels in corals incubated at MSS, IC and PB sites (wk; week, yr; year, NC; natural corals).

12. Lipid peroxidation ex *situ* experiments

The MDA concentrations in control samples showed low levels of LPO for the whole incubation period. When 0.1ppm Pb was added, the MDA concentration increased gradually to about 5µM after 10 days incubation. When 0.2ppm Pb was added, the MDA increased to about 11µM after 8 days, which then started to decrease as a result of tissue necrosis (Figure 6). Cu had more deleterious effects on corals, which showed primary increase in MDA levels, then started to suffer from tissue necrosis and died after 4 days of incubation with 0.1 and 0.2ppm concentrations (Figure 7).

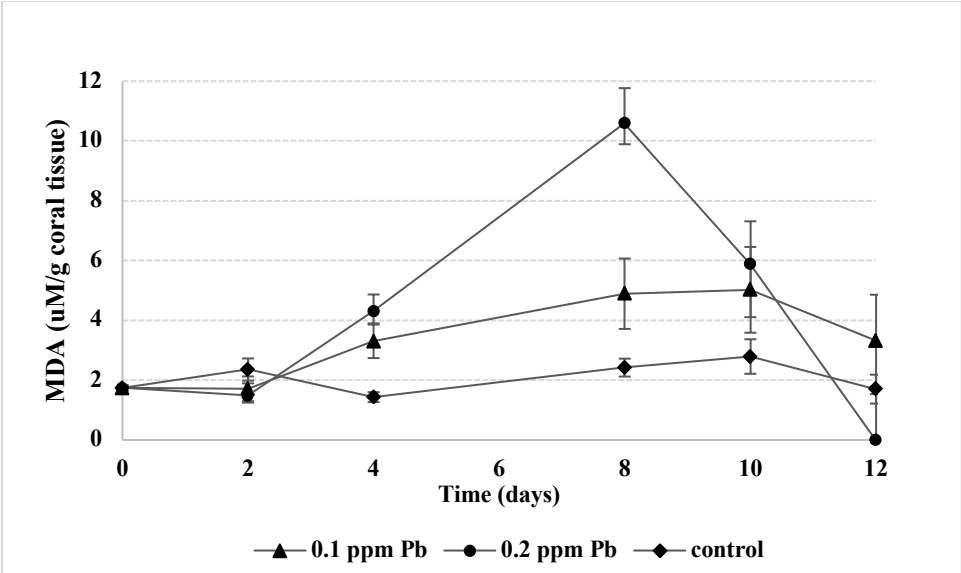

Fig. 6. MDA levels in *S. pistillata* incubated with 0.1 and 0.2ppm lead.

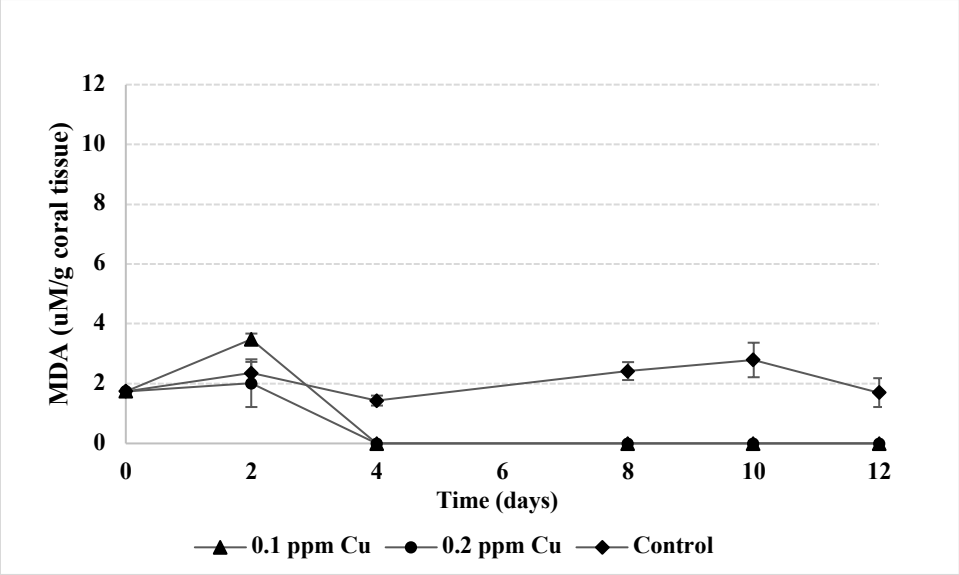

Fig. 7. MDA levels in *S. pistillata* incubated with 0.1 and 0.2ppm copper.

13. Discussion

In this study, *S. pistillata* were used as proxies for environmental pollution using DNA damage and LPO as stress indicators (regardless of the type of pollutant) and demonstrate the magnitude of response towards pollutants as prognostic tools. The sites selected (MSS, IC and PB) are distributed along the Jordanian GoA, to determine levels of sublethal responses of corals towards environmental stresses at those sites.

Heavy metals pollution is central environmental issue due to their toxicity, which influence growth and longevity of organisms, biochemical persistency and tendency to bioaccumulate in biological systems (Jia *et al.,* 2011; Al-Rousan *et al.,* 2012). Exposure to heavy metals generates ROS, which can damage DNA and cells and lead to LPO through oxidative stress (Richier *et al.,* 2005; Lesser, 2011).

The DNA damage in coral cells was measured by comet assay. After one year of planting corals *in situ*, the DNA damage score was highest in samples planted at PB site, followed by samples at IC site, while samples at MSS had the lowest DNA damage score. Those results suggest that PB and IC sites have sublethal levels of pollutants that can damage DNA in corals. Also, in PB and IC sites, both the 1yr planted samples and the natural colonies collected from the sites had no significant differences among them, however they were statistically higher than the 1wk planted samples in both sites. Those results suggest that corals introduced to the sites became biologically similar to natural coral in the site after long time of deployment.

The 1wk planted samples at MSS had the highest DNA damage, followed by samples at PB and IC sites, respectively. This suggests that there might be some environmental disturbances presented at the MSS site during this period, which caused DNA damage. Although the MSS site is protected area with restricted access, its proximity to Containers and Passengers Ports, where oil spills and antifouling paints may reach the MSS site from time to time, and have the ability to cause stress on corals. The DNA damage found in natural colonies at the MSS site was significantly lower than that in the natural colonies at the IC and PB sites, while no significant differences were found between the IC and PB samples. These findings

suggest that the MSS site can be considered as control site, despite the environmental disturbances described above. It is possible that corals at MSS site had DNA damage due to natural factors prevailing at the site. For example, it was found that anemone cells exhibit high control or background levels of DNA strand breaks (Mitchelmore & Hyatt, 2004). DNA damage in corals may result from thermal stress, exposure to UV radiation and/or from oxidative stress due to the symbiotic algae in corals exposed to sunlight (Baruch *et al.,* 2005; Nesa *et al.,* 2012). It was observed in corals that photoreactivation (a light-stimulated response) is the main repair pathway for UV-induced DNA damage in which photolyase proteins repair damaged DNA (Reef *et al.,* 2009). It is possible that the efficiency of repair systems differs among the different coral species as well as among individuals of the same species.

The *ex situ* incubations of corals with Cu and Pb produced significantly higher DNA damage than control samples, which showed some DNA damage that can be reasoned to background DNA damage or to incubation stress (Kteifan *et al.,* 2017). Heavy metals may damage DNA, cause bleaching and final death of corals (Jia *et al.,* 2011; Schwarz *et al.,* 2013). It was also suggested that cnidarians with symbiotic algae experience high levels of oxidative stress, which may result in DNA damage (Lesser, 2011).

The results suggest that IC and PB sites have pollutants that can produce stress at cellular levels of corals. It also suggests that these corals have efficient repair systems since they could survive such stress factors, though their growth, survival, and fecundity might be affected due to energy diversion during repair process when combatting adverse environmental conditions (Banaszak, 2003). Other factors that might affect coral survival include aging, which impair coral ability to counter oxidative stress, while larvae produced under stressed conditions are less sensitive to stress (Pacific & Davies, 1991; Farina *et al.,* 2008).

Lipid peroxidation through its product (MDA), was used as biomarker for subcellular structural integrity and gives indication that ROS exceeds the capacity of antioxidant defense system, which might lead to fatty acid degradation and destabilize membranes (Rikans & Hornbrook, 1998; Wahsha *et al.,* 2012). Heavy metals generate ROS and increase MDA production in corals (Kteifan *et al.,* 2017). MDA production was a direct response towards stress, which indicates health status of corals during the study.

Except for samples at IC site, there were no significant diffenrences of LPO results for field samples, which suggests higher stress levels at IC site. Also, when corals were incubated with Pb and Cu, the MDA concetrations increased before the corals died. The MDA level increased gradually for 10 days incubation with 0.1ppm Pb, which decreased afterwards, while the level was more than doubled when upon incubation with 0.2ppm Pb concentration and died by the end of the incubation period. The corals could not survive after two days of incubation with Cu, as it was also suggested earlier (Jia *et al.,* 2011). Copper is considered the most toxic metal as it affects fertilization, larval settlement, cause tissue necrosis and impair photosynthesis in corals (Reichelt-Brushett & Harrison, 1999; Schwarz *et al.,* 2013).

14. Conclusions

The bioindicators used in this study were useful tools for detecting sub-lethal effects of pollutants on corals. The comet and lipid peroxidation assays are useful tools for monitoring stressed marine environmental areas, and certainly have potential for use as early warning

applications for environmental disturbances. The results obtained suggest that the use of DNA damage as biomarker is suitable for the long-term monitoring of coral health, while LPO is only suitable for short-term purposes. The results also revealed that corals in study sites are facing environmental disturbances resulting in high levels of LPO and DNA damage, which were also shown by *ex situ* testing of Cu and Pb added to incubation tanks. The results found here are promising, though further research is still needed to verify their application with other coral reef organisms.

ACKNOWLEDGMENTS

This study was funded by MERC-USAID (Grant; TA-MOU-13-M33-001). We are grateful to MSS for providing laboratory facilities. We are thankful to M.Wahsha, T.Salman, I.Al-Zgoul, S.Basyouni, A.Jahmani for their valuable assistance and to S.Barnett for her English editing.

References

Al-Horani, F. A. (2013). Sustainable Resources of Corals for the Restoration of Damaged Coral Reefs in the Gulf of Aqaba, Red Sea. Life Science Journal, 10(3): 352-360.

Al-Horani, F. A., & Khalaf, M. A. (2013). Developing artificial reefs for the mitigation of man-made coral reef damages in the Gulf of Aqaba, Red Sea: coral recruitment after 3.5 years of deployment. Marine Biology Research, 9(8): 749-757.

Al-Horani, F. A., Hamdi, M. & Al-Rousan, S. (2011). Study of *Drupella cornus* prey selection and grazing on corals from the Jordanian coast of the Gulf of Aqaba-Red Sea. Jordan Journal of Biological Sciences, 4(4): 191-198.

Al-Rousan, S., Al-Shloul, R., Al-Horani, F. A. & Abu-Hilal, A. (2012). Heavy metals signature of human activities recorded in coral skeletons along the Jordanian coast of the Gulf of Aqaba, Red Sea. Environmental Earth Sciences, 67(7): 2003-2013.

Banaszak, A. (2003). Photoprotective physiological and biochemical responses of aquatic organisms. In: Helbling E, Zagarese H, editors. UV Effects in Aquatic Organisms and Ecosystems. Cambridge: The Royal Society of Chemistry, pp: 329-356.

Banc-Prandi, G. & Fine, M., 2019. Copper enrichment reduces thermal tolerance of the highly resistant Red Sea coral *Stylophora pistillata*. Coral Reefs, 38(2); 285-296.

Baruch, R., Avishai, N. & Rabinowitz, C. (2005). UV incites diverse levels of DNA breaks in different cellular compartments of a branching coral species. The Journal of Experimental Biology, 208(5): 843-848.

Binelli, A. & Provini, A. (2003). POPs in edible clams from different Italian and European markets and possible human health risk. Marine Pollution Bulletin, 46(7): 879-886.

Boer, J. D., Andressoo, J.O., De Wit, J., Huijmans, J., Beems, R.B., Van Steeg, H., Weeda, G., Van der Horst, G.T., Van Leeuwen, W., Themmen, A.P. & Meradji, M. (2002). Premature aging in mice deficient in DNA repair and transcription. Science, 296(5571): 1276-1279.

Burke, L. M., Reytar, K., Spalding, M. & Perry, A. (2012). World Resources I. Reefs at risk revisited in the Coral Triangle. Washington, D.C: World Resources Institute.

Collins, A.R. (2004). The comet assay for DNA damage and repair: principles, application and limitations. Molecular Biotechnology, 26: 249-261.

Farina, O., Ramos, R., Bastidas, C. & García, E. (2008). Biochemical Responses of Cnidarian Larvae to Mercury and Benzo(a) pyrene exposure. Bulletin of Environmental Contamination and Toxicology, 81(6): 553-557.

Ginsburg, R.N., Gischler, E. & Kiene, W.E. (2001). Partial mortality of massive reef-building corals: an index of patch reef condition, Florida Reef Tract. Bulletin of Marine Science, 69(3): 1149-1173.

Girotti, A. W. (1998). Lipid hydroperoxide generation, turnover, and effector action in biological systems. Journal of Lipid Research, 39(8): 1529-1542.

Gladstone, W., Tawfiq, N., Nasr, D., Andersen, I., Cheung, C., Drammeh, H., Krupp, F. Lintner, S. (1999). Sustainable use of renewable resources and conservation in the Red Sea and Gulf of Aden: issues, needs and strategic actions. Ocean and Coastal Management, 42(8): 671-697.

Jia, X., Zhang, H. & Liu, X. (2011). Low levels of cadmium exposure induce DNA damage and oxidative stress in the liver of Oujiang colored common carp Cyprinus carpio var. color. Fish Physiology and Biochemistry, 37(1): 97-103.

Kteifan, M., Wahsha, D. M. & Al-Horani, F A. (2017). Assessing stress response of Stylophora pistillata towards oil and phosphate pollution in the Gulf of Aqaba, using molecular and biochemical markers. Chemistry and Ecology, 33(4): 281-294.

Lesser, M. P. (2011). Coral bleaching: causes and mechanisms. In Coral reefs: an ecosystem in transition (pp. 405-419). Springer, Dordrecht.

Mitchelmore, C. & Hyatt, S. (2004). Assessing DNA damage in cnidarians using the Comet assay. Marine Environmental Research, 58(2-5): 707-711.

Nesa. B., Baird, A., Harii, S., Yakovleva, I. & Hidaka, M. (2012). Algal symbionts increase DNA damage in coral planulae exposed to sunlight. Zoological Studies, 51(1):12.

Pacific, R. & Davies, K. (1991). Protein, lipid and DNA repair systems in oxidative stress: the free-radical theory of aging revisited. Gerontology, 37(1-3): 166-180.

Reef, R., Dunn, S., Levy, O., Dove, S., Shemesh, E., Brickner, I., Leggat, W. & Hoegh-Guldberg, O. (2009). Photoreactivation is the main repair pathway for UV-induced DNA damage in coral planulae. The Journal of Experimental Biology, 212(17): 2760-2766.

Reichelt-Brushett, A. & Harrison, P. (1999). The Effect of Copper, Zinc and Cadmium on Fertilization Success of Gametes from Scleractinian Reef Corals. Marine Pollution Bulletin, 38(3): 182-187.

Richier, S., Furla, P., Plantivaux, A., Merle. P. & Allemand, D. (2005). Symbiosis-induced adaptation to oxidative stress. The Journal of Experimental Biology, 208(2): 277-285.

Rikans, L. & Hornbrook, K. R. (1998). Lipid peroxidation, antioxidant protection and aging. Biochimica et Biophysica Acta, 1362(2-3): 116-127.

Rinkevich, B., Avishai, N., & Rabinowitz, C. (2005). UV incites diverse levels of DNA breaks in different cellular compartments of a branching coral species. Journal of Experimental Biology, 208(5): 843-848.

Saeed, Z., Iqbal, S., Younas, U., Bukhari, S.M. & Zaidi, A. (2020). Variation in antioxidant potential of *Vigna Unguiculata* grown in pure and amended soil. Kuwait Journal of Science, 47(3): 2-14.

Schwarz, J. A., Mitchelmore, C. L., Jones, R., O'Dea, A. & Seymour, S. (2013). Exposure to copper induces oxidative and stress responses and DNA damage in the coral *Montastraea franksi*. Comparative Biochemistry and Physiology, 157(3): 272-279.

Szeto, Y. T., Lee, A., Benzie, I. & Obied H. (2012). Optimized noninvasive procedures to measure DNA damage in comet assay. Human and Experimental Toxicology. 31(11): 1144-1150.

Valavanidis, A., & Vlachogianni, T. (2010). Integrated Biomarkers in Aquatic Organisms as a Tool for Biomonitoring Environmental Pollution and Improved Ecological Risk Assessment. Science Advances on Environment, Toxicology & Ecotoxicology Issues, 10: 1-13.

Vijayavel, K., Downs, C. A., Ostrander, G. K. & Richmond, R. H. (2012). Oxidative DNA damage induced by iron chloride in the larvae of the lace coral *Pocillopora damicornis*. Comparative Biochemistry and Physiology, 155(2): 275-280.

Wahsha, M., Wahsha,A., Bini, C., Fontana, S., & Zilioli, D. (2012). Toxicity assessment of contaminated soils from a mining area in Northeast Italy by using lipid peroxidation assay. Journal of Geochemical Exploration, 113: 112-117.

Wells, P.G., Depledge, M.H., Butler, J.N., Manock, J.J. & Knap, A.H. (2001). Rapid toxicity assessment and biomonitoring of marine contaminants-exploiting the potential of rapid biomarker assays and microscale toxicity tests. Marine Pollution Bulletin, 42(10): 799-804.

Wilson, J.T., Pascoe, P.L., Parry, J.M. & Dixon, D.R. (1998). Evaluation of the comet assay as a method for the detection of DNA damage in the cells of a marine invertebrate, *Mytilus edulis* L. (Mollusca: Pelecypoda). Mutation Research/Fundamental and Molecular Mechanisms of Mutagenesis, 399(1): 87-95.

Yadav, S.K. (2010). Heavy metals toxicity in plants: An overview on the role of glutathione and phytochelatins in heavy metal stress tolerance of plants. South African Journal of Botany, 76(2): 167-179.

Submitted: 13/09/2021
Revised: 19/04/2022
Accepted: 06/07/2022
DOI: 10.48129/kjs.16207

Suppression of Fas expression in the hypertensive placental histology of rats given Nano herbal of *Rhodomyrtus tomentosa* leaves

Putri C.Situmorang[1,*], Rony A. Syahputra[2], Rostime H. Simanullang[1,3]

[1]*Dept. of Biology, Faculty of Mathematics and Natural Sciences, Universitas Sumatera Utara, Medan, Indonesia.*
[2]*Dept. of Pharmacology, Faculty of Pharmacy, Universitas Sumatera Utara, Medan, Indonesia.*
[3]*Sekolah Tinggi Ilmu Kesehatan Murni Teguh, Sumatera Utara, Medan, Indonesia*

**Corresponding author: putri.cahaya@usu.ac.id*

Abstract

High blood pressure during pregnancy can signal a high-risk pregnancy and result in difficulties. The expression of Fas is critical for maintaining hypertensive immunity. Fas is prevalent in the trophoblast and enhances maternal-derived apoptosis. Because it contains acylphloroglucinol, flavonoids, tannins, and triterpenes, *Rhodomyrtus tomentosa* (haramonting) is commonly used in traditional Indonesian medicine to treat high blood pressure. This study aimed to investigate and determine the role of haramonting in lowering Fas expression in hypertensive rats' placental histopathology. The rats were confirmed to be pregnant and divided into five groups: normal pregnant rats (control); hypertensive rats without treatment; and hypertensive rats given nanoherbal *Rhodomyrtus tomentosa (*NRT) at different doses: 100 mg/kg body weight (BW), 200 mg/kg BW, and 400 mg/kg BW. On gestation day 20, pregnant rats were euthanized under ketamine anaesthesia. Enzyme-linked immunosorbent assay (ELISA) analysis was used to examine the expression of the HSP family. Immunohistochemistry was used to assess Fas expression. In hypertensive rats, NRT lowered the systolic and diastolic blood pressure ($P < 0.01$), and NRT improved placental efficiency and restored birth weight. In hypertensive rats, higher doses of NRT were associated with higher levels of HSP27, HSP70, and HSP90. In placental histology, NRT suppresses Fas expression, acting as an anti-apoptotic agent in trophoblast cells. Because NRT is high in antioxidants and protects cells from hypoxia and dehydration, it suppresses Fas activity in the labyrinthine zone, basal zone, and yolk sac.

Keywords: Fas; herbal medicines; HSP; hypertensive; Immunohistochemistry.

1. Introduction

Hypertension, or high blood pressure, is considered a marker for the emergence of chronic inflammatory diseases and is an indicator of high-risk pregnancy. Hypertension in pregnancy can be mild, but if it is not handled properly, it can cause serious problems and threaten the lives of the mother and the foetus (McLaughlin *et al*., 2018). It is a generalized inflammatory disorder complicating gestation, with most of cases developing in the third trimester (Ali *et al*.,

2020). If chronic hypertension is not treated effectively during pregnancy, it can develop into chronic hypertension and preeclampsia. Protein in the urine is a symptom of hypertension, which can lead to complications, such as congestive heart failure, visual abnormalities, stroke, seizures, and kidney or liver disorders (McLaughlin *et al*., 2018).

Fas is a glycoprotein that causes apoptosis and is involved in the maintenance of tumour immunity as well as hypertension. Fas was shown to be a crucial molecule in the immune system's cell death signal transduction; it triggered apoptosis in Fas-positive cells through the binding of the Fas ligand to the extracellular domain of Fas (Ramezani *et al*., 2019). In the lipopolysaccharide (LPS) animal model, the activation of the Fas system and the induction of apoptosis can cause placental abnormalities (Ramezani *et al*., 2019). The extravillous trophoblast and the syncytiotrophoblast layer, the major sites of the feto-maternal interface, display consistent immunoreactivity to Fas in the placenta (Ejima *et al*., 2000). FasL's distribution pattern is nearly identical to that of Fas and Bcl-2 (Ejima *et al*., 2000). Fas is prevalent in the trophoblast, which contributes to immunity and causes apoptosis in maternally derived activated Fas-expressing cells. The Fas pathway can trigger apoptosis in placental cells during implantation (Ejima *et al*., 2000). Oxidants can regulate Fas-mediated cell death. In addition, both pharmacological antioxidants and antioxidant enzymes affect this process. Fas signalling induces ROS production, and Fas-induced activation of caspase-8 may be a target for redox regulation (Benhar, 2020). ROS generation was detected in cells sensitive to apoptosis but not in those inherently resistant to anti-Fas. Thus, the level of oxidative stress (arising from exogenous sources or endogenously generated upon receptor stimulation) was found to regulate the sensitivity of tumour cells or hypertensive cells undergoing Fas-mediated apoptosis.

This study used an antioxidant from *Rhodomyrtus tomentosa* leaves known in Indonesian as haramonting. This plant belongs to the *Myrtaceae* family and has woody stems (lignosus) with a habitus or shrub stature. The direction of stem growth is perpendicular (erectus), and the direction of branch growth is inclined upwards. The leaves are green and have a simple-leaf structure. This plant is often used in traditional Indonesian medicine to treat colic diarrhoea, dysentery, abscesses, bleeding, and high blood pressure and to improve smokers' lungs (Ilyas *et al*., 2019). Extracts from haramonting contain acylphloroglucinol, flavonoids, tannins, and triterpenes, and the plant exhibits high phenolic and antioxidant activity (Vo & Ngo, 2019). Haramonting leaves have antioxidant activity in vitro and in vivo (Jeong *et al*., 2013). Antioxidants from this plant can inhibit lipid peroxidation; improve the histology of the placenta, testes, and diabetic wounds; increase the expression of HSP70; and increase the ability to reduce free radicals (Ilyas & Situmorang, 2021; Ilyas *et al*., 2020; Situmorang *et al*., 2018a; Irianti *et al*., 2020). The high levels of phenolic compounds impart high antioxidant capacity; thus, haramonting is a potential source of health-promoting compounds (Zhang *et al*., 2018). This study aimed to determine and analyse haramonting's suppression of Fas expression in the histology of the placenta of hypertensive rats before investigating this process in human cells. Haramonting was converted to a nano-size to improve its penetration of and bioavailability in cells. It is hoped that this plant can be developed for molecular hypertension therapy in humans.

2. Materials and Methods

2.1 Materials

The leaves of haramonting (*Rhodomyrtus tomentosa*) were obtained in January 2021 from the yards of residents of Rantauprapat in the district of Labuhanbatu, North Sumatera Province, Indonesia. The plant was classified and authenticated by the Head of Botany at the Universitas Sumatera Utara and deposited into the Medanense Botanical Herbarium (registration range 6675/MEDAN/2021). Nanoherbal *R. tomentosa* (NRT) was produced at the Indonesian Research Institute (LIPI) in Jakarta, Indonesia, by high-energy milling (HEM) (Ilyas *et al*., 2020; Situmorang *et al*., 2021a). LPS was intraperitoneally administered within 3 hours using *Escherichia coli* 026:B6 (1 mg/kg BW) dissolved in 0.9% NaCl. Ketamine hydrochloride (30 mg/kg; Ketalar, Parke-Davis, Morris Plains, NJ, USA) was used as an anaesthetic before surgery. Santa Cruz Biotechnology provided anti-Fas (sc-715) antibodies (SanverTech, Heerhugowaard, the Netherlands). Cell Signaling Inc. provided mouse anti-phosphotyrosine and rabbit anti-Hsp27, anti-Hsp70, and anti-Hsp90 antibodies (Danvers, MA, USA).

2.2 Animal Handling

The experimental animals were pregnant female Wistar rats that weighed 150–200 g, were 2 months old, and were in a healthy condition (Situmorang *et al*., 2021a). This research passed the animal ethics review from the Ethics Commission of the Faculty of Mathematics and Natural Sciences, USU (ethical clearance no. 0259/KEPH-FMIPA/2021).

1. Acclimatisation: The rats were acclimatized for 2 months before being treated in the laboratory in an air-conditioned room with a 12-hour light/dark cycle. Male rats are separated from female rats (Ilyas *et al*., 2019)

2. Diet for the animals: Rats were fed conventional laboratory diets in the form of pellets and corn and given free access to water. Food was provided ad libitum (Ilyas *et al*., 2019).

3. Hypertension pregnancy: Each pair of Wistar rats was mated overnight and observed using the CCTV camera provided in the cage. Pregnancy was confirmed by a vaginal plug, and the day was defined as day 0. On gestational day 6, systemic inflammation was induced in pregnant rats by infusing *Escherichia coli* lipopolysaccharide (LPS) into the peritoneal cavity using a small osmotic pump (Irianti *et al*., 2020).

4. Surgery: The rats were sedated with ketamine on the 19th day of pregnancy. Then, surgery was performed to obtain the blood, foetus, and placenta (Situmorang *et al*., 2021a).

2.3 Design of experimental

This study used 50 pregnant rats (10 each in each group). The rats with confirmed pregnancy were divided into five treatments: (a) normal pregnant rats (C–), (b) hypertensive rats (C+), (c) hypertensive rats + NRT 100 mg/kg body weight (BW), (d) hypertensive rats + NRT 200 mg/kg BW, and (e) hypertensive rats + NRT 400 mg/kg BW. Pregnant rats were excised on gestational

day 20 under ketamine anaesthesia. The markers of hypertension were characterized by measuring blood pressure, and Heat Shock Protein (HSP) family expression was analysed by ELISA. Fas protein expression was evaluated by immunohistochemistry.

2.4 Measurement of systolic and diastolic blood pressure in pregnant rats

Blood pressure was determined before LPS injection and after LPS injection and NRT administration. Systolic and diastolic arterial blood pressure was recorded in conscious and uncontrolled animals for 1 hour, and the mean arterial blood pressure was measured using the non-invasive tail cuff method.

2.5 Enzyme-linked immunosorbent assay (ELISA)

The ELISA test from Enzo Life Sciences was used to perform quantitative HSP analysis. The HSP27 (rabbit) ELISA kit, HSP70 high-sensitivity ELISA kit, and HSP90 (rabbit) ELISA kit were utilised in this study. Following the manufacturer's recommendations, each sample was evaluated three times.

2.6 Hematoxylin-eosin (H&E) staining

The placenta in a formalin medium was removed from the storage area and placed in xylol for 15 min. Subsequently, the tissues were alternately hydrated in 96% and 70% pure alcohol, sequentially, for 5 minutes and then rinsed in distilled water. Haematoxylin dye was applied for 5 min, and then the tissues were rinsed for 3 min in distilled water. Eosin dye was added for 1 minute. The slides were dehydrated with 70%, 96%, and 100% alcohol, immersed in xylol, and placed on a cover glass. The sample was examined using a light microscope with 5 times the field of view (Irianti *et al.,* 2020).

2.6 Immunohistochemistry

To suppress endogenous peroxidase activity, 5 m thick paraffin-embedded placental slices were deparaffinized and treated with 1% H_2O_2 in methanol for 30 min before immunohistochemistry. Subsequently, the slides were rinsed in 0.01 M Tris-buffered saline (TBS pH 7.4). Tissue slices were treated with primary anti-Fas antibody (1:100 dilution in PBS containing 1% BSA) for 2 h after blocking non-specific binding to 1%skimmed milk in PBS. The Vectastain Elite ABC kit (Vector Laboratories, Burlingame, CA, USA) was used to identify immunoreactivity, which was counterstained with Mayer's haematoxylin.

2.7 Statistical analysis

Research data: Blood pressure and HSP family levels were analysed using a one-way analysis of variance with independent continuous variables and Duncan's multiple range test was used for comparison tests (Maramis *et al.,* 2015). Immunohistochemistry and tunnel assay was performed using Kruskal–Wallis and Mann Whitney Test on Sigmaplot software (Weiner & Craighead, 2010)

3. Results and discussion

3.1 Impact of nanoherbal *R. tomentosa* (NRT) on systolic and diastolic blood pressure

Table 1. The effects of hypertension on systolic and diastolic blood pressures with and without maternal NRT treatment

Groups	Systolic blood pressures (mmHg) (Mean ± SD)			Diastolic blood pressures (mmHg) (Mean ± SD)		
	Day 0	Day 6	Day 19	Day 0	Day 6	Day 19
C-	121 ± 8.02[a]	122 ± 9.12[a]	120 ± 5.99[a]	85 ± 2.34	90 ± 4.90[a]	87 ± 3.99[a]
C+	122 ± 7.71[a]	146 ± 9.23[b]	150 ± 6.76[b]	90 ± 4.01	118 ± 3.98[b]	120 ± 6.98[b]
NRT100	122 ± 4.54[a]	146 ± 3.56[b]	136 ± 7.55[ab]	89 ± 4.91	115 ± 5.88[b]	115 ± 5.87[b]
NRT200	123 ± 5.98[a]	150 ± 4.98[b]	130 ± 6.89[ab]	87 ± 4.89	116 ± 5.99[b]	100 ± 5.89[a]
NRT400	121 ± 7.78[a]	145 ±.7.22[b]	127 ± 6.22[a]	88 ± 8,21	115 ± 7.04[b]	95 ± 4.76[a]

Note: C-: Untreated, C+: Hypertension rat, NRT100: Hypertension rat given a dosage of 100mg/kgBW, NRT200: Hypertension rat given a dosage of 200mg/kgBW, NRT400: Hypertension rat given a dosage of 400mg/kgBW. NRT: Nano herbal *R.tomentosa,* Day 0: Before LPS Injection, Day 6: After LPS Injection, Day 19: After administration of NRT. Data were expressed as the mean ± standard deviation (The same letters denoting no difference).

NRT lowered blood pressure at all doses. No significant differences between treatments ($P > 0.05$) were observed on day 0; all animals had normal systolic and diastolic blood pressure. On the sixth day, all groups except the control group (C–) were given LPS injections, and a significant increase in systolic and diastolic blood pressure ($P < 0.01$) was observed compared with the control group (C–). NRT was administered to hypertensive rats for one week, from the 13th to the 19th gestational days, and lowered systolic and diastolic blood pressure ($P < 0.01$). Multiple comparisons indicated that NRT reduced hypertension, most likely because of NRT antioxidants such as glutathione, which is a potent antioxidant and can improve placental–uterine function (Wu, 2021). Glutathione is a natural antioxidant that aids in the preservation of all other antioxidants (Wu, 2021). Glutathione levels in the decidua were significantly higher than those in the placenta. Glutathione levels were higher in the decidua in patients with pre-eclampsia and patients with haemolysis, elevated liver enzymes, and low platelets (HELLP) than in patients with normotensive pregnancy, and only in the placenta of pre-eclampsia patients (Robaczewska *et al.,* 2016). Glutathione plays a role in combating oxidative stress and maintaining nitric oxide bioavailability via the formation of nitrosothiols and nitrosohemoglobin; disruptions in glutathione metabolism can cause an increase in blood pressure (Robaczewska *et al.,* 2016).

Under normal circumstances, antioxidants work to counteract ROS production by scavenging existing free radicals and promoting the repair of ROS-induced cell structure damage (Kudhur & Moustafa, 2018). At low levels, oxidative stress promotes some physiological reproductive functions; however, at high levels, it is linked to pathological processes in the reproductive tract that contribute to infertility and poor pregnancy outcomes

(Kudhur & Moustafa, 2018). Malondialdehyde levels in the plasma and placenta increased significantly, whereas glutathione and superoxide dismutase levels decreased significantly as diastolic blood pressure increased (Madazli *et al*., 2002). This Plant like *Morinda citrifolia* plays a pivotal role in controlling blood pressure (Purwaningroom *et al*., 2021). This research supports the findings of Irianti *et al*. (2020), which indicated that haramonting can lower the blood pressure in pregnant rats with preeclampsia while increasing the trophoblast count and improving placental histology.

3.2 Effects of Nano herbal *R.tomentosa* (NRT) treatment on birth weight

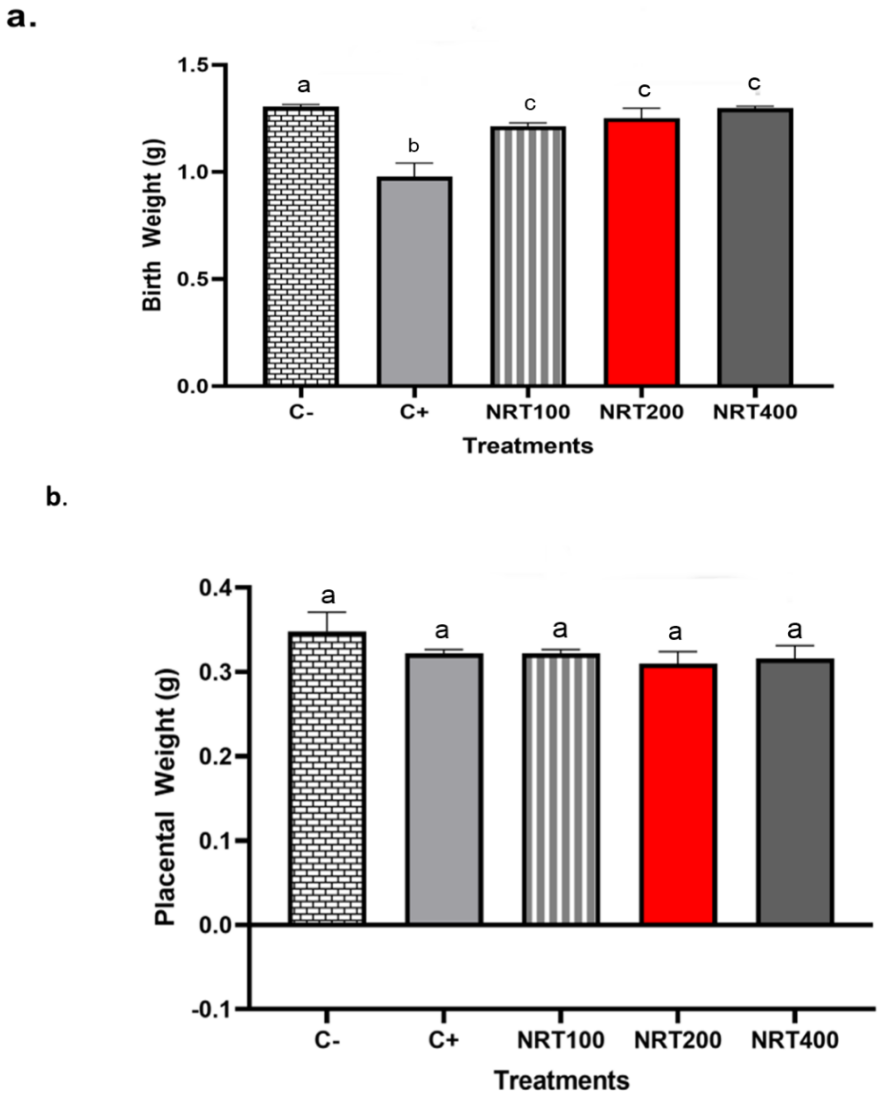

Fig. 1. Effects of Nano herbal *R.tomentosa* (NRT) treatment on fetal and placental weight, a.Birth Weight, b. Placental weight.
C-: Untreated, C+: Hypertension rat, NRT100: Hypertension rat given a dosage of 100mg/kgBW, NRT200: Hypertension rat given a dosage of 200mg/kgBW, NRT400: Hypertension rat given a dosage of 400mg/kgBW. Data were expressed as the mean ± standard deviation (The same letters denoting no difference)**.**

NTR treatment resulted in a significant difference in the birth weight of hypertensive rats ($P<0.01$). The multiple comparisons analysis revealed no significant differences at various NRT doses, but significant differences were observed when all NRT doses were compared with the C– and C+ groups. Hypertension can lead to foetal weight loss and disrupt the passage of nutrients from the mother to the foetus. However, the administration of NRT at the lowest to the highest doses demonstrated that this herb can restore foetal weight in hypertension ($P < 0.5$) (Figure 1a). It did not affect placental weight in healthy, hypertensive, or NRT-treated rats (Figure 1b). Pregnancy complications, including placental insufficiency, hypertension, and preeclampsia, slow the transport of nutrients to the foetus because of reduced placental and umbilical blood flow (Thornburg *et al.,* 2010). Therefore, intrauterine growth retardation, caused by reduced nutrition delivery to the foetus during pregnancy, is a significant health burden because of its associated perinatal morbidity and mortality (Thornburg *et al.,* 2010). One of the causes of the slowed transportation of nutrients and oxygen is the delayed growth of the foetus due to the development of cardiovascular and metabolic illnesses or hypertension (Thornburg *et al.,* 2010). Antioxidants can aid in the promotion of placental function while also lowering intrauterine growth. NRT can overcome this because it contains extremely potent antioxidants (Situmorang *et al*., 2021b). Perhaps NRT, like glutathione, plays a role in maintaining the biological value of germ cells; it has been linked to the fertilization process and early embryo development. Fortunately, glutathione can be recycled by the body if it is properly optimized, and it can also be destroyed (Aljaser *et al.,* 2021). Oxidative stress in the placenta and foetus may be exacerbated by a lack of nutrients and oxygen (Wu *et al*., 2012). The findings of this study confirm this theory, indicating that treating gestational hypertension with haramonting can increase placental efficiency and restore birth weight.

3.3 Effects of Nano herbal *R. tomentosa* (NRT) in Expression of HSP27, HSP70 and HSP90

HSP27 levels in hypertensive rats that received NTR therapy differed significantly from those of hypertensive (C+) rats ($P < 0.05$). The multiple comparisons analysis revealed that the 400 mg/kg NRT dose was associated with the highest HSP27 value, but the HSP27 levels associated with the 200 mg/kg doses was also significantly higher than those in the 100 mg/kg doses and C+ group. In hypertensive rats, higher doses of NRT were associated with higher levels of HSP27. HSP27 maintains intracellular redox homeostasis by maintaining glutathione in its reduced form and decreasing intracellular iron levels. As a result, it has anti-oxidative activity (Arrigo et *al*., 2005). NRT treatment induced high levels of HSP27 expression because it acts as a molecular chaperone, regulating the folding and renaturation of damaged proteins, which can occur after LPS and oxygen free radicals are injected. HSP27 also plays a role in physiological reactions to body fluid homeostasis, which influences blood pressure-regulating systems (Gostimirovic *et al*., 2020).

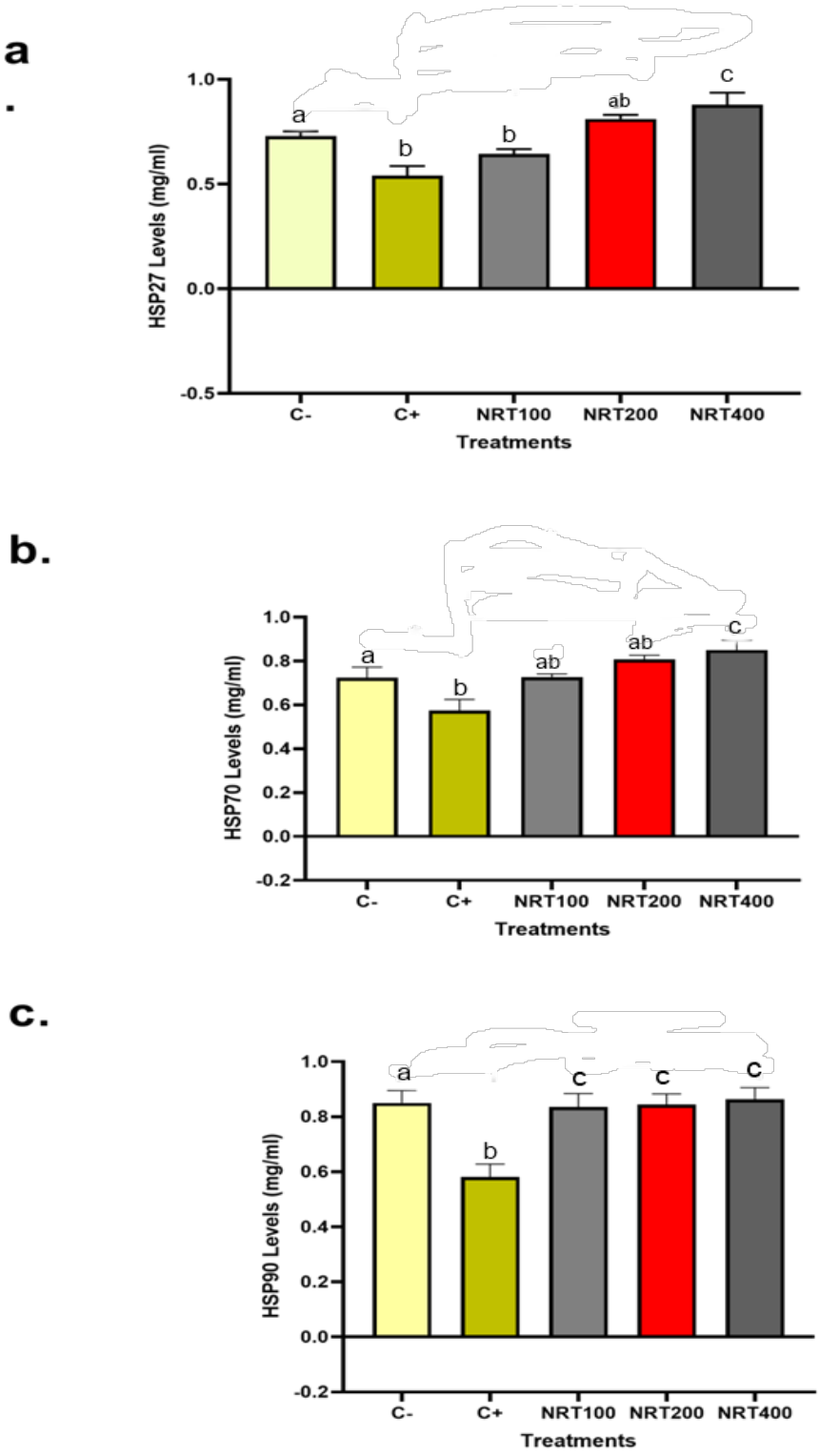

Fig 2. Effects of Nano herbal *R.tomentosa* (NRT) in Head Shock protein family, a. HSP27, b. HSP70, c.HSP90. C-: Untreated, C+: Hypertension rat, NRT100: Hypertension rat given a dosage of 100mg/kgBW, NRT200: Hypertension rat given a dosage of 200mg/kgBW, NRT400: Hypertension rat given a dosage of 400mg/kgBW. NRT: Nano herbal *Rhodomyrtus tomentosa*. Data were expressed as the mean ± standard deviation (The same letters denoting no difference).

HSP70 levels among hypertensive rats treated with NTR at dosages of 100 to 400 mg/kg BW differed significantly ($P < 0.05$). The multiple comparisons analysis revealed that the 100 NRT dose was associated with the highest HSP70 value, which was almost the same value as the 400 NRT dose group. Glutathione, which is similar to an antioxidant in NRT, regulates many cellular functions; it reduces hydrogen peroxide and peroxynitrite directly and indirectly with the help of glutathione peroxidase, detoxifies electrophiles, modulates reversible oxidation and reduction of protein thiols, and is crucially involved in the regulation of enzymes, transcription factors, and signal transduction (Oyagbemi *et al.,* 2018). HSP70 expression improves postischemic ventricular recovery, and overexpression of HSP70 in transgenic rats improves postischemic cardiac function and reduces neuronal cell death (Gostimirovic *et al*., 2020). LPS-induced protection in hypertension and inflammation is due in part to suppression of NF-kB activation and lymphocyte activation. Lipid peroxidation as well as superoxide and hydroxyl radical anion activity can be prevented and countered by the antioxidant action of haramonting (Situmorang *et al*., 2021b). Flavonoids in this plant extract can boost SOD and GSH-Px activity while also lowering MDA levels (Wu *et al*., 2015).

The multiple comparisons analysis revealed no significant differences ($P > 0.05$) between rats treated with NRT doses of 100 to 400 mg/kg BW. However, a significant difference was observed when all doses were compared with the C+ group ($P < 0.05$), as shown in Figure 2c. HSP90 is a key player in the signalling pathway that leads to eNOS activation. HSP90 regulates vasomotor activity in resistance vessels by inhibiting HSP90 signalling, which plays a role in modulating vasoactive responses in blood vessels (Jones *et al*., 2011). Increased HSP90 signalling promotes NO-dependent vascular hyporeactivity, indicating a link between protein–protein interactions in hypertension (Ai *et al*., 2003).

3.4 Fas expressions after given Nano herbal *R. tomentosa* (NRT) to placental rats

According to the findings of the histopathological examination (Figure 3), an increase in the number of syncytial nodes in all placental tissue preparations may be present in the mature placenta (Figure 3a), but syncytial nodes are also present in the hypertensive placenta (Figure 3b) because of the hypoxic state of the foetal placenta. Hypoxia causes the villi's ends or terminals to become irregularly shaped, increasing the likelihood of trophoblast accumulation and the creation of a syncytial knot. A shortage of oxygen perfusion caused an increase in the cytotrophoblast. In the placentas in the control and 400 mg/kg NRT groups, mature cytotrophoblast cells with a normal shape were formed, but the histology of rats with hypertension revealed that many new villi formed to support the lack of placental perfusion. The more trophoblast cells and new villi are formed, the more trophoblast cells and new villi are formed. Inadequate oxygen perfusion causes trophoblasts to expand and become cytotrophoblasts. The cytotrophoblast functions as the site of gas exchange, replacing the endothelial function of the arterioles (Staff *et al*., 2020). The absence or partial invasion of the spiral arteries by trophoblast cells causes vascular anomalies in hypertensive placentas. This invasion involves the replacement of musculo-elastic spiral artery walls with fibrinoid-filled walls. However, the administration of NRT at all doses (Figure 3c–e) began to improve these vascular abnormalities.

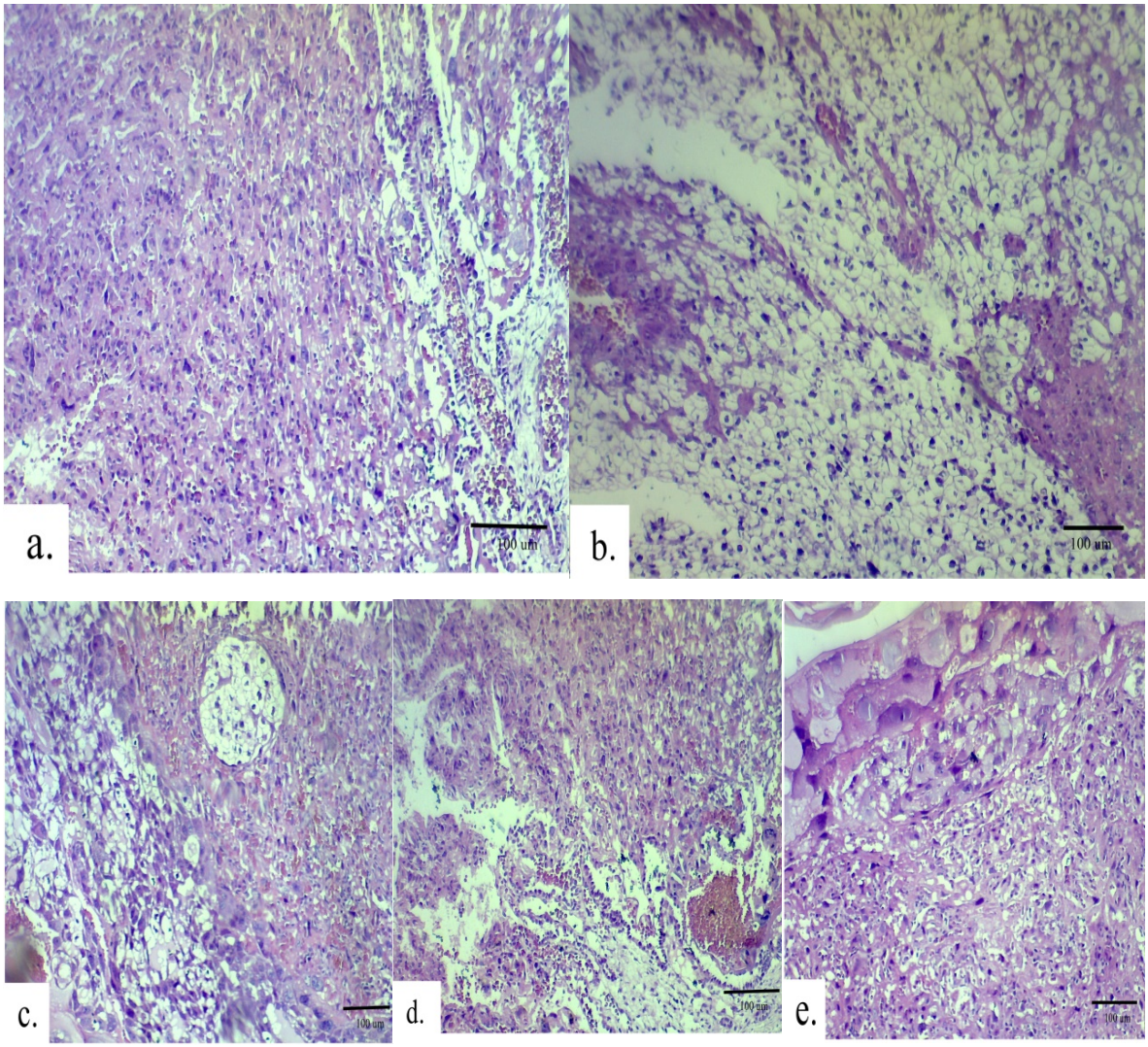

Fig. 3. Histology of placental hypertension by Nano herbal *R.tomentosa* (NRT) a. Untreated, b. Hypertension rat, c. Hypertension rat given by NRT 100mg/kgBW, d. Hypertension rat given by NRT 200mg/kgBW, e: Hypertension rat given by NRT 400mg/kgBW (10x).

NTR treatment resulted in a significant difference in Fas expression in hypertensive rats ($P < 0.05$). The highest NRT dose resulted in a greater difference ($P < 0.01$). Lower Fas activity in hypertensive rats was associated with higher NRT doses (Table 2). In trophoblast cells, NRT suppression of Fas expression in placental histopathology may be anti-apoptotic (Figure 4). In humans, trophoblast tissue is involved in the regulation of maternal–foetal gas, nutrition, and waste product exchange. In rats, maternal–foetal exchange takes place in the labyrinthine zone, whereas placental hormone production takes place in the basal zone. An increase in Fas expression was observed in the basal zone in the hypertensive state, but Fas expression decreased with increasing doses of NRT (Figure 4). Caspase-8 may not be involved

in the rise in Fas in the histology of hypertension. The intrinsic apoptotic pathway can mediate increased caspase-3 and PARP levels (Staff *et al*., 2020). However, further research into the mechanism causing apoptosis-induced cell death in the basal zone is needed. The labyrinthine zone of hypertension histology, in contrast to the basal zone, reveals elevated expression of all Fas pathway-related proteins that activate death via caspase-8 (Staff *et al*., 2020). The yolk sac had the highest Fas expression revealed by placental histopathology in our investigation. The yolk sac is a nutrient transfer system that takes nutrients from the uterine gland secretions or the mother's blood. Most eutherian yolk sacs lose contact with the peripheral chorion ontogenetically, forming free splanchnopleuric yolk sacs that transport chemicals from the exocoelomic cavity (Zhao *et al*., 2018). Embryonic deformities, miscarriages, and growth problems can all be caused by errors in the yolk sac's development and function. In the labyrinth zone, basal zone, and yolk sac, NRT could decrease Fas activity (Table 2 and Figure 4). This is due to the presence of antioxidants such as anthocyanins, acylphloroglucinol, flavonoids, tannins, and triterpenes in NRT, which protect cells from hypoxia and death (Situmorang *et al*., 2021b; Situmorang *et al*., 2018b).

Table 2. Fas expression in histology of hypertension placental

Treatment	Labyrinth zone (Mean ± SD)	Labyrinth zone (Mean ± SD)	Yolk salc (Mean ± SD)
C-	12 ± 4.21^{a}	13± 5.89^{a}	20 ± 2.44 ^{a}
C+	32 ± 5.44^{b}	30 ± 4.21^{b}	61 ± 4.43^{b}
NRT100	22± 9.61^{c}	21± 5.22^{c}	31± 4.91^{c}
NRT200	20± 9.63^{bc}	19± 8.04^{ac}	22 ± 5.70^{d}
NRT400	14± 3.28 ^{a}	13± 7.32^{a}	15± 3.53^{a}

Note: C-: Untreated, C+: Hypertension rat, NRT100: Hypertension rat given a dosage of 100mg/kgBW, NRT200: Hypertension rat given a dosage of 200mg/kgBW, NRT400: Hypertension rat given a dosage of 400mg/kgBW. NRT: Nano herbal *R. tomentosa*. Data were expressed as the mean ± standard deviation (The same letters denoting no difference).

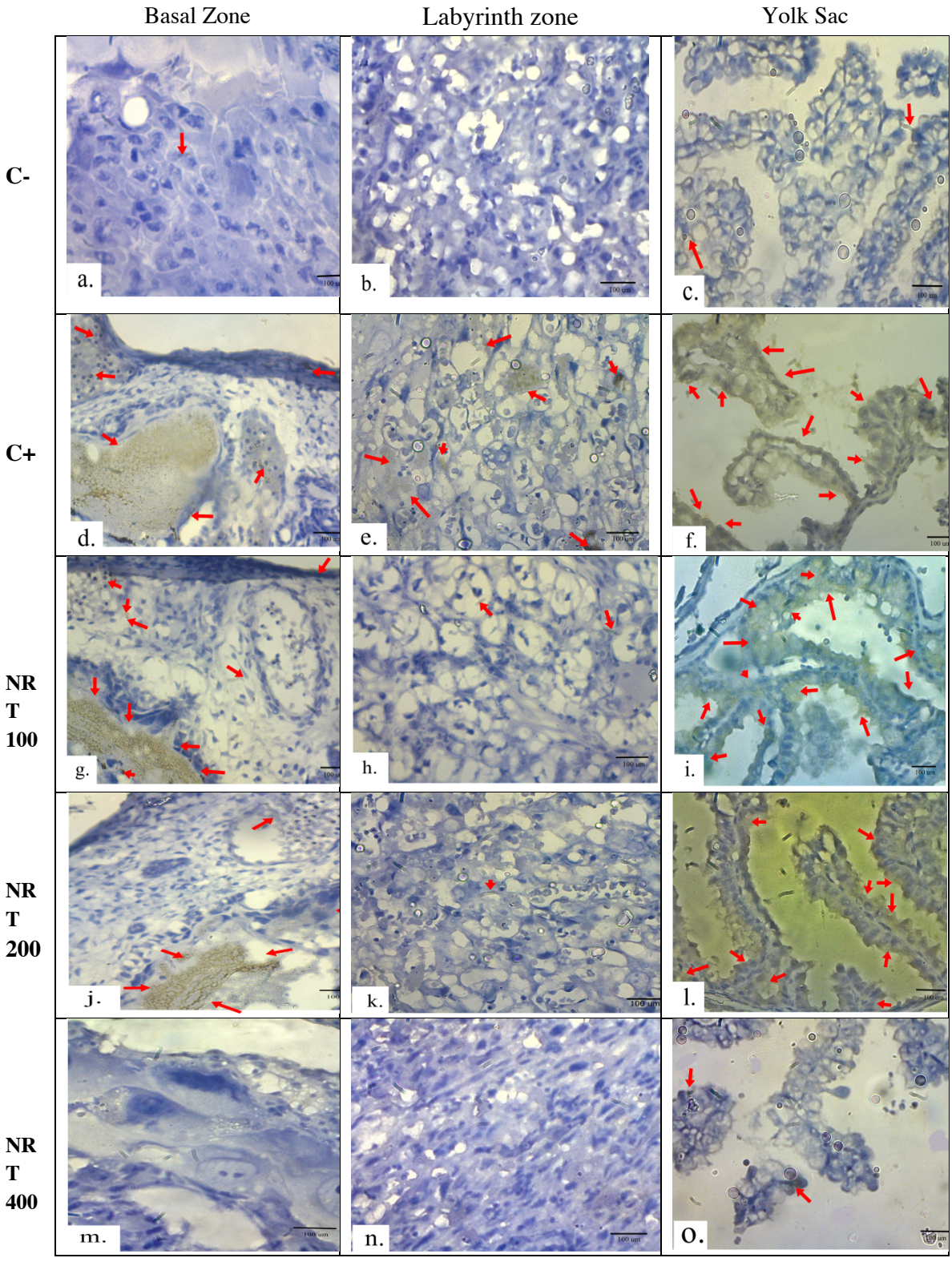

Fig. 4. Fas expression in hypertensive rat placenta histology. C-: Untreated, C+: Hypertension rat, NRT100: Hypertension rat given a dosage of 100mg/kgBW, NRT200: Hypertension rat given a dosage of 200mg/kgBW, NRT400: Hypertension rat given a dosage of 400mg/kgBW. NRT: Nano herbal *R.tomentosa* (40x).

4. Conclusion

According to the histopathological findings in this study, an increase in the number of syncytial nodes may be present in the mature placenta, but syncytial nodes are also present in the hypertensive placenta because of the placenta's hypoxic state. In contrast to the basal zone, the labyrinthine zone and yolk sac exhibit elevated expression of all Fas pathway-related proteins that activate death via caspase; the yolk sac had the highest Fas expression in our study. Embryonic deformities, miscarriages, and growth issues can all be caused by errors in the development and function of the yolk sac. Because of the presence of antioxidants, such as anthocyanins, acylphloroglucinol, flavonoids, tannins, and triterpenes, in nanoherbal *R. tomentosa* (NRT), cells in the labyrinth zone, basal zone, and yolk sack are protected from hypoxia and death. These findings demonstrated that hypertension caused a loss in placental efficiency in rats; a drop in HSP levels caused by hypoxia; and an increase in Fas expression, which thereby promoted the apoptotic pathway and resulted in a decrease in foetal birth weight. However, NRT treatment improved the placental function and birth weight in hypertensive pregnancy.

Conflict of interest

The authors declare that they have no conflict of interest

References

Ai, J.H., Yang, Z., Qiu, F. Z. & Zhu, T. (2003) Heat shock protein 90 is responsible for hyperdynamic circulation in portal hypertensive rats. World journal of gastroenterology, 9(**11**):2544–2547.

Ali, Z., Zaki, S., Zafar, U., Tauseef, A., Tariq,S. & Khalid.T. (2020) Correlation of maternal neutrophil to lymphocyte ratio with fetal birth weight in preeclampsia. Kuwait Journal of Sciences,**48**:87-92.

Aljaser, F.S., Ghneim, H.K., ALshubaily, M.M., Abudawood, M., Almajed, F. & Fatima, S. (2021) Glutathione and oxidized nicotinamide adenine dinucleotide ([NAD.sup.+]) redox status in plasma and placental tissue of Saudi patients with intrauterine growth restriction. Saudi Medical. Journal, 42(**5**): 491

Arrigo, A-P., Virot, S., Chaufour, S., Firdaus, W., Kretz-Remy, C. & Diaz-Latoud, C. (2005) Hsp27 Consolidates Intracellular Redox Homeostasis by Upholding Glutathione in Its Reduced Form and by Decreasing Iron Intracellular Levels. Antioxidants. Redox Signaling, 7(**3-4**):414-422.

Benhar, M. (2020) Oxidants, Antioxidants and Thiol Redox Switches in the Control of Regulated Cell Death Pathways. Antioxidants, 9(**4**): 309

Ejima, K., Koji, T., Tsuruta, D., Nanri, H., Kashimura M., *et al* (2000) Induction of Apoptosis in Placentas of Pregnant Mice Exposedto Lipopolysaccharides: Possible Involvement of Fas/Fas Ligand System, Biology of Reproduction, 62(**1**): 178–185.

Gostimirovic, M., Novakovic, R., Rajkovic, J., Djokic, V., Terzic, D., Putnik, S., *et al* (2020) The influence of climate change on human cardiovascular function. Archives of Environmental & Occupational Health, **1–9.**

Ilyas, S., Murdela, F., Hutahaean, S., & Situmorang, P.C. (2019) The Effect of Haramounting Leaf Ethanol Extract (Rhodomyrtus tomentosa (Aiton) Hassk.) on the Number of Leukocyte Type and Histology of Mice Pulmo (Mus Musculus L.) Exposed to Electronic Cigarette. Open Access Macedonia Journal of Medical Sciences, 7(**11**):1750-1756.

Ilyas, S., Hutahaean, S., Rosidah, R., & Situmorang, P.C. (2020) Effects of Nanoherbal Haramonting (*Rhodomyrtus tomentosa*) and Extra Virgin Olive Oil on Histology of Liver and Kidney of Preeclamptic Rats. Pakistan .Journal of Biological Sciences, 23(**12**):1629-1635.

Ilyas, S., & Situmorang, P.C. (2021) Role of Heat Shock Protein 70 (HSP-70) after Giving Nanoherbal Haramonting (*Rhodomyrtus tomentosa*) in Preeclamptic Rats. Pakistan .Journal of Biological Sciences, 24(**1**):139-145

Irianti, E., Ilyas, S., Hutahaean, S., Rosidah, Situmorang, P.C. (2020) Placental histological on preeclamptic rats (*Rattus norvegicus*) after administration of nanoherbal haramonting (*Rhodomyrtus tomentosa*). Research Journal of Pharmacy Technology, 13 (**8**):3879- 3882.

Kudhur,S.F., & Moustafa S.R. (2018) The potential role of malondialdehyde, glutathione peroxidase, and interleukin-18 in the development of essential hypertension. International Journal of Medical Sciences, 22(**2**): 227–237.

Jeong, D., Yang, W.S., Yang, Y., Nam, G., Kim, J.H., Yoon, D.H. *et al.* (2013) In vitro and in vivo anti-inflammatory effect of *Rhodomyrtus tomentosa* methanol extract. Journal of Ethnopharmacology, 46(**1**):205-13

Jones, Q. S., Voegeli, T., Li, G., Chen, Y., & William Currie, R. (2011) Heat Shock Proteins Protect Against Ischemia and Inflammation Through Multiple Mechanisms. Inflammation & Allergy . Drug Targets, 10(**4**), 247–259.

Madazli, R., Benian, A., Aydin, S., Uzun H., Tolun. N. (2002) The plasma and placental levels of malondialdehyde, glutathione and superoxide dismutase in pre-eclampsia. Journal of Obstetrics and Gynaecology, 22(**5**):477-480

Maramis, A. A., Amin, M.M., Corebima, A. D. (2015) Apoptosis in Mice Liver Cells Caused by Formalin–containing Food: Normalization of HSP70 Overexpression by Chlorophyllin. Procedia Chemistry, **14**: 27–35.

McLaughlin, K., Zhang, J., Lye, S.J., Parker, J.D., & Kingdom, J. C. (2018) Phenotypes of Pregnant Women Who Subsequently Develop Hypertension in Pregnancy. Journal of the American Heart Association, 7(**14**):e009595

Oyagbemi, A.A., Omobowale, T.O., Ola-Davies, O.E., Asenuga, E.R., Ajibade, T.O., Adejumobi, O.A. Et al. (2018) Quercetin attenuates hypertension induced by sodium fluoride via reduction in oxidative stress and modulation of HSP 70/ERK/PPARγ signaling pathways. BioFactors*,* 44 (**5**):465–479

Purwaningroom, D.L., Maghfirah,S., Rifai, M., & Widodo (2021) Exploring the mechanism of the anti-hypertension properties of Morindacitrifoliathrough a bioinformatics approach. Kuwait Journal of Sciences, 48 (**3**):1-10

Ramezani, G., Pourgheysari, B., Shirzad, H., & Sourani, Z. (2019) Pterostilbene increases Fas expression in T-lymphoblastic leukemia cell lines. Research in Pharmaceutical Sciences, 14(**1**):55–63.

Robaczewska, J., Kedziora-Kornatowska, K., Kozakiewicz, M., Pawluk, H., Pawliszak, W., & Kedziora, J. (2016) Role of glutathione metabolism and glutathione-related antioxidant defense systems in hypertension. Journal of Physiology and Pharmacology, 67(**3**):331-337.

Situmorang, P.C., & Ilyas, S. (2018a) Description of Testis Histology of Mus musculus after Giving Nano Herbal *Rhodomyrtus tomentosa* (Haramonting). Asian Journal of Pharmaceutical and Clinical Research, 11(**11**): 460.

Situmorang, P.C., & Ilyas, S. (2018b) Review: germinal cell apoptosis by herbal medicine. Asian Journal of Pharmaceutical and Clinical Research, 11(**9**):24-31.

Situmorang, P.C., Ilyas, S., Hutahaean, S., Rosidah, R. (2021a) Histological changes in placental rat apoptosis via FasL and cytochrome c by the nano-herbal *Zanthoxylum acanthopodium*. Saudi Journal Biological Sciences, 28**(5**):3060–3068.

Situmorang, P.C., & Ilyas, S., Hutahaean, S., & Rosidah, R. (2021b) Components and acute toxicity of nanoherbal haramonting (*Rhodomyrtus tomentosa*). Journal of Herbmed Pharmacology, 10(**1**): 139-148.

Staff, A. C., Fjeldstad, H. E., Fosheim, I. K., Moe, K., Turowski, G., Johnsen, G. M. *et al*. (2020) Failure of physiological transformation and spiral artery atherosis: their roles in preeclampsia. American Journal of Obstetrics & Gynecology, S0002937820311169

Thornburg, K. L., O'Tierney, P. F., & Louey, S. (2010) Review: The Placenta is a Programming Agent for Cardiovascular Disease. Placenta, **31**:S54–S59.

Vo, T., & Ngo, D. (2019) The Health Beneficial**.** Properties of *Rhodomyrtus tomentosa* as Potential Functional Food. Biomolecules, 9(**2**): 76.

Weiner, I. B., & Craighead, W. E. (2010) Kruskal-Wallis Test. The Corsini Encyclopedia of Psychology. doi:10.1002/9780470479216.corpsy0491

Wu, P., Ma, G., Li, N., Deng, Q., Yin, Y., & Huang, R. (2015) Investigation of in vitro and in vivo antioxidant activities of flavonoids rich extract from the berries of *Rhodomyrtus tomentosa*(Ait.) Hassk. Food Chemistry, **173**:194–202.

Wu,G., Imhoff-Kunsch, B., & Girard, A.W. (2012) Biological Mechanisms for Nutritional Regulation of Maternal Health and Fetal Development. Paediatric and Perinatal Epidemiology, **26**: 4–26.

Wu,G. (2021) Amino Acids: Biochemistry and Nutrition, 2nd edition. CRC Press, Boca Raton, Florida

Zhang, Y.-B., Li, W., Jiang, L., Yang, L., Chen, N.-H., Wu, Z.-N. *et al* (2018) Cytotoxic and anti-inflammatory active phloroglucinol derivatives from *Rhodomyrtus tomentosa*. Phytochemistry, **153**:111–119.

Zhao, F., Lei, F., Zhang, S., Yan, X., Wang, W., & Zheng, Y. (2018) Hydrogen sulfide alleviates placental injury induced by maternal cigarette smoke exposure during pregnancy in rats. Nitric Oxide, **74**: 102–111.

Submitted: 20/10/2021
Revised: 18/04/2022
Accepted: 30/05/2022
DOI: 10.48129/kjs.16833

Cost benefit analysis of vaccination for sheep in Kuwait farms

Hana'a Burezq [1], * , Faten Khalil [1]

[1]*Desert Agriculture and Ecosystems Program,*
Environment and Life Sciences Research Centre,
Kuwait Institute for Scientific Research, PO 24885 Safat 13109

**Corresponding Author: haborizq@kisr.edu.kw*

Abstract

Sheep mortality is a common agenda noticed in sheep farms globally. The mortality rate of newborn lambs in Kuwait ranges between 35 to 50 per cent (~43 per cent), leading to low profitability or loss to the farmer. Vaccination gives a better remedy to withstand the infections and stresses. Vaccines are available at various rates and hence the feasibility of the farmers to afford for vaccines and the subsequent profit to be earned need to be clarified for vaccinating their sheep confidently. With this objective, an investigation was conducted to cost analyze vaccinated sheep production that includes their feed, drinking water and housing values. A cost benefit analysis is an imperative activity that includes break down of total cost of each component and synthesizing to reach a value to compare with the profit gain from such activity. The total cost was calculated by vaccinating 5 groups of 30 ewes each along with the cost of feed, water and electricity for a period of 1 year to raise ewes. According to the results, a very slight difference in vaccine cost which is very nominal is recorded suggesting to vaccinate the ewes for the combined vaccine (*Pasteurella* + *Clostridia* + *Pest de Petites Ruminants (PPR)*) to protect for multiple diseases causing high mortality rate.

Keywords: Cost benefit analysis, farms; Kuwait; sheep; vaccination.

1. Introduction

Sheep farming is an important component of farming community of Kuwait for its multi-faceted utilities such as meat, milk, wool, skin and organic manure. Mortality and morbidity are the chief factors intervening in sheep production with considerable economic loss (Singaravadivelan *et al*., 2019). Steady increase in the mortality rate of new born lambs is a serious concern in sheep industry of Kuwait accounting for 35 to 50 per cent especially in the first three weeks of birth causing significant economic losses for the sheep producers (Un published data, Public Authority of Agricultural Affairs and Fish Resources (PAAFR)). Neonatal mortality of lambs is also affected by maternal nutrition (e.g., arginine provision) in ewes (Wu *et al*., 2022). Kuwait accounts for 588,618 heads of sheep and 11-12 per cent of red meat need of the country is met by sheep industry (Burezq & Khalil, 2021). Efforts to minimize lamb mortality could enhance the productivity of red meat by Kuwait Sheep industry. Mortality of lambs could be due to low level of immunity in the initial days of birth (United states Department of Agriculture, 2011). To maintain healthy ewes, vaccination is of utmost need to prevent diseases and develop immunity (Rathod *et al*. 2016). Vaccination aids to raise

Ig levels in the colostrum which ultimately transferred to the newborn lambs through colostrum that reduce the risk of mortality (Mohammed *et al*., 2009). Vaccines help the body to fight disease by giving it a "preview" of a pathogen that it might someday have to fight in earnest. Vaccines contain a *version* of a microbe, often an inactive form of a virus or bacterium, which triggers the immune system to make antibodies (Burezq *et al*., 2020). Virtually across the board, benefits of vaccines outweigh their costs, so farmers cannot afford and skip the process of vaccination. In view of the above facts, an investigation on cost benefit analysis of vaccination for Sheep in Kuwait farms was conducted.

2. Materials and Methods

A total of 150 ewes were selected and divided into 5 groups, representing five treatments. Ewes were made pregnant in the experiment by natural mating.

2.1 Breeding Program of Ewes Used in the Field Experiment

A straight breeding program of mating Naeemi rams with Naeemi ewes was done for breeding. The reproduction and mating procedures involved synchronizing the estrus induction of ewes (Gizaw, 1995) by inserting the vaginal sponge chronogest for ewes, to improve conception rates. The synchronized ewes with clear signs of estrus were allowed to mate with rams with proven libido. One ram was allowed to mate a flock of six to eight ewes by natural mating. Successful jumping and mating of ewes were marked. The marking procedure of ewes involved mounting a marking harness, which was strapped around the ram's shoulders and neck, and holding a crayon between the front legs. This arrangement was made so that when the rams mate ewes successfully, the crayon (colored chalk) would mark a color on the hip of the ewes. The marking of ewes was recorded with time/date to know the approximate date of lambing (Razzaque, 1995).

2.2 Diagnosis of Pregnancy

Diagnosis of pregnancy was carried out by ultrasound scanner after 42─50 days of breeding. Post successful mating of ewes, if any ewe found empty (not pregnant) will be rebred.

2.3 Vaccination Protocol Used in the Field Experiment.

Ewes were vaccinated on the side of the neck, using a syringe with 18 gauge needles. The injection area was cleaned with alcohol and the vaccines were administered under the skin.

The treatments of the experiment have been selected specifically to prevent 5 common diseases in Ewes, briefly described below.

T1- *Pasteurella*
T2- *Clostridia*
T3- *Foot and Mouth Disease (FMD)*
T4- *Pest de Petites Ruminants (PPR)*
T5- *Pasteurella + Clostridia + Pest de Petites Ruminants (PPR)*

Pasteurellosis is a devastating condition affecting sheep of all ages and the most common causes of mortality. *Clostridia* is not contagious but highly infectious and globally

pervasive. Bacterial spores are found in soil and enter the animal via the oral route. *Foot-and-mouth disease (FMD)* in adult sheep usually causes milder clinical signs and is often restrained to go undiagnosed. In contrast, FMD in lambs has been reported to cause high mortality during field outbreaks. *Peste des petits ruminants (PPR)* are a viral disease of both goats and sheep characterized by fever, sores in the mouth, diarrhea, pneumonia, and sometimes death. It is caused by a morbillivirus in the family of paramyxoviruses, which is related to rinderpest, measles and canine distemper. Ewes falling under different treatments were vaccinated with the respected vaccines as mentioned in Table 1. Ewes were vaccinated twice during pregnancy period, 1st vaccination was at the beginning of the pregnancy period, and 2nd booster dose was given four weeks prior to lambing.

Table 1. Experimental treatments with vaccination details

Treatments	No. of Vaccinated Ewes	Type of Vaccines
T-1	30	*Pasteurella*
T-2	30	*Clostridia*
T-3	30	*Foot and Mouth Disease (FMD)*
T-4	30	*Pest de Petites Ruminants (PPR)*
T-5	30	*Pasteurella + Clostridia + Pest de Petites Ruminants (PPR)*

Each group was submitted to a vaccination process twice during pregnancy to achieve maximum immunity according to Table 1. The ewes under treatments (1, 2, 4 and 5) were vaccinated with *Pasteurella, Clostridia, Pest de Petites Ruminants (PPR)* and *Pasteurella + Clostridia + Pest de Petites Ruminants (PPR)* were injected with 2ml twice a year, while ewes under treatment (3) vaccinated for *Foot and Mouth Disease* (*FMD*) was injected with 1 ml twice a year as its sanctioned dosage. In addition to vaccination, the ewes were submitted to a feeding process twice a day that includes special feeding ingredients which in turn assists in the immunity process. The amount of feed intake per day, was 0.800 kg and 1.250 kg for non-pregnant and pregnant ewes respectively. The final body weights of ewes were 58.75 ± 2.47 - 61.75 ± 6.01kg in an average. The pregnant ewes give birth to one lamb each; therefore, the litter size is one per ewe. The average milk consumption by lambs was 600 ml / day. The body weights of lambs at birth and the end of the study were 19.5 ± 1.41 and 44.73 ± 1.46 kg.

The total vaccination cost of group was calculated by considering cost per 200 ml and number of vaccination cycles per year. The feed cost was calculated by taking into account the feed portion and cost per kg. Some of the standard terms used in the cost analyses are material cost, which is the calculations of all the materials required for the experiment, that include the costs of vaccination, feed, drinking water and electricity, total cost which is the aggregated totals of all of the above cost groups for the required period of the experiment which is determined by costing all materials used, including the feed, drinking water, electricity and the vaccinations costs and unit cost, that is the final cost determined once all of the above groups are calculated.

3. Results and Discussion

3.1 Feed cost

The first material cost calculated was on feed material. The details of feed ingredients, their proportion and associated cost were enumerated in Table 2 and 3. The total cost of feed materials was calculated in portions and listed in Table 4. The diverse ingredients of feed materials are barley, wheat bran, corn, soybean meal, vitamins and minerals, limestone, salt, alfalfa hay and wheat straw. The average total portions were 1 kg and the corresponding cost was 1.094 KD. Accordingly, the cost per portion was 0.099 KD. The aggregated cost of feed of 30 ewes per year was listed in Table 3. The cost per portion for 30 ewes was 2.97 KD, where 2 portions per day was supplied accounting for 5.94 KD per day and consequently 2168.1 per year. All the five treatments marked the same value as the same feed was given for all treatments irrespective of their vaccination.

Table 2. Cost of Feed Per Portion

Feed materials	Portion(kg)	Cost Per kg (KD)	Cost per Portion (KD)
	G70:30		**G70:30**
Barely	0.405	0.084	0.034
Wheat bran	0.100	0.080	0.008
Corn	0.100	0.090	0.009
Soya bean meal	0.065	0.175	0.011
Vitamin and minerals	0.010	0.320	0.003
Limestone	0.010	0.030	0.000
Salt	0.010	0.100	0.001
Alfalfa hay	0.150	0.150	0.023
Wheat straw	0.150	0.065	0.010
Totals/Average	**1.000**	**1.094**	**0.099**

Table 3. Aggregated Feed Cost of the Ewes per year

Treatments	Cost of Feed per Portion (KD)	No of Ewes	Total Cost of Portion Per Group KD	No of Portions Per day	Total per day (KD)	Total per year (KD)
T-1	0.099	30	2.97	2	5.94	2168.1
T-2	0.099	30	2.97	2	5.94	2168.1
T-3	0.099	30	2.97	2	5.94	2168.1
T-4	0.099	30	2.97	2	5.94	2168.1
T-5	0.099	30	2.97	2	5.94	2168.1

3.2 Vaccination Cost

The second material cost is for the vaccinations and the total vaccination cost of the experiment is enumerated in Table 4 and 5. For treatment 1 and 2, the ewes vaccinated with *Pasteurella* and *Clostridia* respectively reported 2.100 KD as total cost, which is the minimal cost used for vaccination. Ewes vaccinated with Treatment 4, which is *Pest de Petites Ruminants (PPR)*

recorded the next lowest total cost of 3.900 KD. The total cost of the ewes vaccinated with combined vaccine of *Pasteurella, Clostridia* and *Pest de Petites Ruminants (PPR)* recorded 8.100 KD. The highest total cost of 16.500 KD was observed in ewes vaccinated with *Foot and Mouth Disease (FMD)* though it was injected with 1 ml twice a year, while the other vaccines were injected at 1 ml, twice a year. The treatment wise vaccination cost in each group of 30 ewes is enumerated in Table 6.

3.3 Total vaccination and feeding cost

The total feed and vaccine cost was enumerated in Table 7. The total vaccination and feed cost of treatments 1 and 2 (*Pasteurella* and *Clostridia* Vaccine) were 2170.200 KD, whereas treatment 4 (*Pest de Petites Ruminants (PPR)*) was 2172.000 KD and the combined vaccine (*Pasteurella* + *Clostridia* + *Pest de Petites Ruminants (PPR)*) was 2176.200 KD, while FMD vaccination was the highest showing 2184.600 KD.

Table 4. Total Vaccination cost -I (Group 1-4)

Treatments	Vaccination	Cost Per 200 ml (KD)	(1ml) Unit Cost (KD)	Unit /ml	(2 ml) Unit Cost (KD)	No of Vaccination per Cycle	Cost of Vaccination per Cycle (KD)	Ewes Per Group	Cost Per Group (KD)
T-1	*Pasteurella*	3.500	0.0175	2	0.035	2	0.070	30	2.100
T-2	*Clostridia*	3.500	0.0175	2	0.035	2	0.070	30	2.100
T-3	*Foot and Mouth Disease (FMD)*	55.000	0.275	1	0.275	2	0.550	30	16.500
T-4	*Pest de Petites Ruminants (PPR)*	6.500	0.0325	2	0.065	2	0.130	30	3.900

Table 5. Total Vaccination cost -II (Group 5)

Treatments	Vaccination	Cost Per 200 ml (KD)	(1ml) Unit Cost (KD)	Unit /ml	(2 ml) Unit Cost (KD)	No of Vaccination per Cycle	Cost of Vaccination per Cycle (KD)	Ewes Per Group	Cost Per Group (KD)
T-5	*Pasteurella*	3.500	0.0175	2	0.035	2	0.070	30	2.100
	Clostridia	3.500	0.0175	2	0.035	2	0.070	30	2.100
	Pest de Petites Ruminants (PPR)	6.500	0.0325	2	0.065	2	0.130	30	3.900
	Total	**13.500**	**0.0675**	**6**	**0.135**	**6**	**0.270**	**30**	**8.100**

Table 6. Treatment wise Vaccination Cost for 30 Ewes

Treatments	Vaccines for diseases	Sub Total (KD)
1.	*Pasteurella*	2.100
2.	*Clostridia*	2.100
3.	*Foot and Mouth Disease (FMD)*	16.500
4.	*Pest de Petites Ruminants (PPR)*	3.900
5.	*Pasteurella + Clostridia + Pest de Petites Ruminants (PPR)*	8.100

Table 7. Total Vaccination and Feed Unit Costs (30 Ewes in each group per year)

Treatments	Vaccination	Total of Vaccination per Group (KD)	Total of Feed Cost per Group/year (KD)	Total (KD)
1	*Pasteurella*	2.100	2168.100	2170.200
2	*Clostridia*	2.100	2168.100	2170.200
3	*Foot and Mouth Disease (FMD)*	16.500	2168.100	2184.600
4	*Pest de Petites Ruminants (PPR)*	3.900	2168.100	2172.000
5	*Pasteurella + Clostridia + Pest de Petites Ruminants (PPR)*	8.100	2168.100	2176.200

4. Miscellaneous cost

4.1 Electricity cost

Assuming each group of ewes (30 each) was kept separately in each pen, electricity consumption and cost was calculated for a period of one year (Table 8).

Table 8. Electricity costs for Ewes Per Year

Treatments	No of Ewes	Electricity consumption kw/year	Cost of electricity KD/kw	Cost of electricity per year KD
1	30	1666.67	0.015	25.000
2	30	1666.67	0.015	25.000
3	30	1666.67	0.015	25.000
4	30	1666.67	0.015	25.000
5	30	1666.67	0.015	25.000

4.2 Drinking Water Cost

Cost of drinking water was calculated for two seasons i.e., spring (6 months) and summer (6 months). During spring each ewe drunk 2.1 liters of water daily, whereas in summer each ewe drunk 4.6 liters. Based on the cost of water as 0.00105 KD, calculations were done and presented in tables 9 and 10.

Table 9. Cost of Water for 5 Ewes Groups (each group 30 ewes) in Spring (6 months)

Treatments	No of Ewes	Daily water consumption (L) in Spring per Ewe	Total daily water consumption per group of 30 Ewes (L)	Total water consumption per group of 30 Ewes for six months (L)	Cost of water per liter (KD)	Total cost of water for Spring (6 months) (KD)
1	30	2.100	63.000	11,498	0.00105	12.073
2	30	2.100	63.000	11,498	0.00105	12.073
3	30	2.100	63.000	11,498	0.00105	12.073
4	30	2.100	63.000	11,498	0.00105	12.073
5	30	2.100	63.000	11,498	0.00105	12.073

Table 10. Cost of Water for 5 Ewes Groups (each group 30 ewes) in Summer (6 months)

Treatments	No of Ewes	Daily water consumption (L) in Spring per Ewe	Total daily water consumption per group of 30 Ewes (L)	Total water consumption per group of 30 Ewes for six months (L)	Cost of water per liter (KD)	Total cost of water for Summer (6 months) (KD)
1	30	4.600	138.000	25,185	0.00105	26.444
2	30	4.600	138.000	25,185	0.00105	26.444
3	30	4.600	138.000	25,185	0.00105	26.444
4	30	4.600	138.000	25,185	0.00105	26.444
5	30	4.600	138.000	25,185	0.00105	26.444

whereas, Table 11 presents aggregate cost of total materials (vaccination, feed, water, electricity) and unit cost per Ewe.

Table 11. Aggregated Cost for Each Ewe Group (30) Per Year and Per Ewe (last column)

Treatments	No of Ewes	Cost of vaccination (KD)	Cost of feed (KD)	Cost of Electricity (KD)	Cost of Water (KD) Spring	Cost of Water (KD) Summer	Total cost (KD)	Cost per Ewe per year (KD)
1	30	2.100	2168.100	25.000	12.073	26.444	2233.717	74.50
2	30	2.100	2168.100	25.000	12.073	26.444	2233.717	74.50
3	30	16.500	2168.100	25.000	12.073	26.444	2248.117	74.94
4	30	3.900	2168.100	25.000	12.073	26.444	2235.517	74.52
5	30	8.100	2168.100	25.000	12.073	26.444	2239.717	74.66

4.3 Cost Analyses to Raise the Lambs for 21 Months

The ewes under each vaccination treatment were vaccinated after pregnancy to enhance the immunity system against potential diseases. No mortality rate was noticed after the birth of the lambs in all 5 groups of ewes vaccinated. The lambs took colostrum and milk from their ewes for the first three months. After the preliminary three-month period the lambs were given 2 portions of feed daily for a period of 1 year and 9 months (21 months), before they were expected to be sold. It is only after three months they start drinking water. Based on these facts, cost valuation is made as shown in Table 12.

Table 12. Aggregated cost for each group (30) of lambs for 21 months

Treatments	No of lambs	Cost of feed (KD) 639 days (21 months)	Cost of Water (KD) 639 days (21months)	*Total raising cost (KD)	Raising cost per lamb per year (KD)	Total selling price per 30 lambs @ 160 KD/lamb	Total profit (KD)
T1	30	3794.2	67.40	3861.6	128.72	4,800	938.4
T2	30	3794.2	67.40	3861.6	128.72	4,800	938.4
T3	30	3794.2	67.40	3861.6	128.72	4,800	938.4
T4	30	3794.2	67.40	3861.6	128.72	4,800	938.4
T5	30	3794.2	67.40	3861.6	128.72	4,800	938.4
Total profit from 5 treatments							3,753

*Since the lambs were living with Ewes, therefore, electricity cost is omitted.

5. Mortality Rate of Lambs after Birth and Cost Analyses

A mortality rate between 35 and 50 percent (~ 43%) is very common without vaccinating the ewes (Hinch & Brien, 2014). Accordingly, the cost of raising the lambs born to non-vaccinated ewes was calculated. The lambs usually die within 4 weeks after birth. Comparison of tables 12 and 13 clearly shows that there was a gain of 3753 KD profit due to vaccination (Table 12) and a loss of 5707.75 KD on overall 5 groups with an average of 43% mortality rate.

Table 13. Aggregated Cost of Lambs for 21 Months and Profit

Treatments	No of lambs born	No of lambs survived @ 43% mortality rate	Cost of feed (KD) 639 days (21 months)	Cost of Water (KD) 639 days (21 months)	Total cost (KD)	Cost per lamb per year (KD)	Total cost to raise 17 lambs (KD)	Total selling price per 17 lambs @ 160 KD/lamb	Total loss (KD)
T1	30	17.0	2150.05	38.19	2188.24	227.15	3861.55	2720.0	1141.55
T2	30	17.0	2150.05	38.19	2188.24	227.15	3861.55	2720.0	1141.55
T3	30	17.0	2150.05	38.19	2188.24	227.15	3861.55	2720.0	1141.55
T4	30	17.0	2150.05	38.19	2188.24	227.15	3861.55	2720.0	1141.55
T5	30	17.0	2150.05	38.19	2188.24	227.15	3861.55	2720.0	1141.55
Total							19,308	13,600	**5707.75**

6. Conclusion

The cost benefit analysis of vaccinating sheep in Kuwait and raising for 21-month period until taken to market showed that vaccination has great promise to control the mortality rate in ewes to gain maximum profits. Though the profit gained was more or less similar for all vaccinations, it was higher for FMD vaccination. The combined vaccination is suggested as it combines the effect of three vaccines together in almost similar cost per year for other sole vaccines. With

regards to the new born lambs from the vaccinated and non-vaccinated ewes to calculate the cost of raising the lambs from both vaccinated and non-vaccinated groups with the assumption of an average of 43% mortality rate to non-vaccinated group of ewes. It is concluded that the farmer will spend 227.15 KD per lamb (due to 43% mortality) to raise before he will sell at the rate of 160 KD, so there is net loss of 67 KD to the farmer per lamb and a total loss of 5707.75 KD from a group of 30 ewes. It is clearly illustrated that vaccination has great promise to control the mortality rate in ewes to gain maximum profits, as none of the lamb from all five groups (total of 150) were dead after the birth. The cost of raising 30 ewes for a year showed a slight difference due to difference in vaccine cost which is very nominal suggesting to vaccinate the ewes for the combined vaccine (*Pasteurella + Clostridia + Pest de Petites Ruminants (PPR)*) to protect for multiple diseases causing high mortality rate.

References

Burezq, HA.,; Khalil, F. 2021. Diagnosing and Mitigating the Risks of Lambs'Mortality in the Sheep Farms of Kuwait. Kuwait Journal of Science. DOI: https://doi.org/10.48129/kjs.14607.

Burezq, HA.,; Khalil, F.,; Dashti, J.,; Essawi, A.,; Al-Thefeeri, F.,; Farouq, M. 2020. Controlling lamb's mortality through ewes vaccination in the farms of Kuwait. The journal of Animal and Plant Sciences. 30(3): 595-602. ISSN (print): 1018-7081; ISSN (online): 2309-8694.

Gizaw, S. 1995. Estimation of bodyweight from linear body measurements and the influence of body condition and age on the accuracy of body weight estimation in Ethiopian Horro sheep. Small Ruminant Network Newsletter, 1995, 31, 9.

Hinch, G.N.; Brien, F. 2014. Lamb survival in Australian flocks: A review. Anim. Prod. Sci. 54: 656–666.

Mohammed, I.B.,; Nikhaila, A.,; Abdel Moneim, M. 2009. Effect of parity on the productivity of Taggar goats. International Journal of Arts and Science Research. 8: 278.

Rathod, P.K.,; Chander, M.,; Banger, Y. 2016. Livestock vaccination in India: an analysis of theory and practice among multiple stakeholders: Revue scientifique et technique (international office of Epizootics). 35(3):729-739. 3.

Razzaque, M.A.1995. Intensive lamb production using local and imported sheep. Final Research Report, KISR No. 1763, Kuwait Institute for scientific Research, 1995.

Singaravadivelan, A.,; Kumaravelu, N.,; Vijayakumar, P.,; Sivakumar, T. 2019. An economic analysis of migratory sheep production system in Tamil Nadu, India. Journal of Animal Health and Production. 7(2): 58-64. 2.

United States Department of Agriculture. **2011.** Vaccination practices on US Sheep operations, Animal and plant health Inspection service.

Wu, G.,; Bazer, F.W.,; Satterfield M.C.,; Gilbreath, K.R.,; Posey, E.A.,; Sun, YX. 2022. L-Arginine nutrition and metabolism in ruminants. Adv. Exp. Med. Biol. 1354:177-206.

Submitted: 16/10/2021
Revised: 05/04/2022
Accepted: 11/04/2022
DOI: 10.48129/kjs.16761

The Effects of Javanese turmeric (*Curcuma xanthorriza Roxb*) on fibroblasts, granulation, blood vessel density, and contraction in wound healing of STZ-induced diabetic rats

Heri Kristianto[1,*], Husnul Khotimah[2], Ryharti A. Sholeha[3], Eky W. Mardianto[3], Hasnah C. Sani[4], Hardika A. Paratiwi[5]

[1]*School of Nursing, Faculty of Health Science, Brawijaya University, Malang, Indonesia*
[2]*Laboratory of Pharmacology, Faculty of Medicine, Brawijaya University, Malang, Indonesia*
[3]*Petrokimia Gresik Hospital, Gresik, Indonesia*
[4]*Lavalete Hospital, Malang, Indonesia*
[5]*Persada Hospital, Malang, Indonesia*

**Corresponding author: heri.kristianto@ub.ac.id*

Abstract

Diabetic ulcers usually occur in the lower extremities of diabetic patients. One in 20 diabetic patients will develop an ulcer, and 10% of those cases lead to amputation. This study aimed to investigate the effects of Javanese turmeric (*Curcuma xanthorriza* Roxb.) extract on the number of fibroblasts, granulation, blood vessel, and the rate of wound contraction in a Wistar rat model of the diabetic ulcer. This was an experimental study with post-test observations only and randomized control group design. Rats were divided into five groups: (1) negative control (KN); (2) positive control (KP); (3) P1; (4) P2; and (5) P3. Every rat was assessed for fibroblast number, granulation, blood vessel density, and wound contraction percentage. Javanese turmeric extract had a significant effect on histological parameters (fibroblast, blood vessels and tissue granulation) ($p < 0.05$) and wound contraction ($p < 0.05$). The double linear test revealed a significant relationship between fibroblasts, granulation, blood vessel quantity, and wound contraction ($p < 0.05$). Correlation and regression tests showed that Javanese turmeric extract explained 91% of the effects on fibroblasts, blood vessels, and granulation. Treatment with Javanese turmeric extract increased the number of fibroblasts, tissue granulation, blood vessel density and wound contraction in male diabetic Wistar rats.

Key words: Blood vessel; contraction; *Curcuma xanthorriza;* fibroblasts; granulation.

1. Introduction

Diabetes mellitus (DM) is a chronic metabolic disease caused by the interruption of insulin production or the inability of the pancreas to utilize insulin effectively, leading to hyperglycemia or a high level of glucose in the blood (Hinkle *et al.*, 2018). The global prevalence of DM in the adult population (20-79 years old) almost reached 415 million in 2015 and is predicted to increase to 642 million in 2040. Indonesia is one of 10 countries with the highest DM prevalence, ranked 7th with 10 million patients in 2015. It will be in the 6th

place by 2040 with 16.2 million patients if curative and preventative actions are not implemented (Atlas, 2015).

Diabetic wound is defined by an ulcer or wound in a diabetic patient, usually in the lower extremities (Lazzarini *et al.*, 2018). The symptoms are neuropathy, ischemia, infection, ulceration, and/or fibrous tissue destruction in the lower limbs (Mavrogenis *et al.*, 2018). Diabetic patients commonly undergo wound treatment, infection treatment, amputation, and hospital treatment (Vibha *et al.*, 2018). Levine's model of wound treatment should be implemented to increase the quality of services in hospitals (Laksmi *et al.*, 2020).

DM complications are a severe and complex problem that affects multiple vital organs (Singh *et al.*, 2013; Harding *et al.*, 2019). It can be classified as acute or chronic. Chronic complications are divided into two groups, which are micro and macrovascular complications. Microvascular complications can involve angiopathy, neuropathy, and retinopathy. Macrovascular complications can affect the coronary arteries or involve cerebrovascular problems and peripheral vascular diseases (Huang *et al.*, 2017). Peripheral vascular disease and neuropathy occur prior to the onset of diabetic ulcers. In a study on 20 DM patients with diabetic ulcers, 10% of them had to undergo amputation (Stoekenbroek *et al.*, 2014). Amputation as a result of a diabetic ulcer often happens in the lower extremities (Kristianto *et al.*, 2013).

The normal wound healing process is marked by cellular and tissue responses in four phases: hemostasis, inflammation, proliferation, and maturation or remodeling. DM disrupts these phases. Hyperglycemia causes oxidative stress and reactive oxygen species (ROS) production that exceeds tissue antioxidant capacity. This condition also induces the production of advanced glycation end-products (AGE) that will interact with the AGE receptor (RAGE). This eventually disrupts the wound healing process via nuclear factor-κB (NF-κB) pathway activation and extracellular matrix degradation (Prompers *et al.*, 2008). Induction of diabetic wound models with streptozotocin in experimental animals is recommended by several research results (Luan & Wang, 2020; Yan *et al.*, 2020).

Javanese turmeric (*Curcuma xanthorrhiza Roxb*) contains major metabolites such as curcuminoid, terpenoid, and xanthorrhizol essential oil that affect human organs, such as the gallbladder, liver, pancreas, rheumatism, stomach disease, and skin inflammation (Musfiroh *et al.*, 2013). Xanthorrhizol from *Curcuma xanthorrhiza Roxb* has been reported as having antimicrobrial activity for S.aureus resistance (Kesumayadi *et al.*, 2021). Xanthorrhizol also has the potential to inhibit Matrix Metalloproteinase -1 (MMP-1), in which excessive MMPs induced chronic wounds (Oh *et al.*, 2009; Caley *et al.*, 2015).

Javanese turmeric has the effect of reducing oxidative stress during diabetic wound treatment. Oxidative stress occurs when free radical molecules are produced to a greater extent than the body's ability to neutralize them (Pizzino *et al.*, 2017). The antioxidant activity of Javanese turmeric is supported by its bioactive components, such as tannins, alkaloids, flavonoids, and polyphenols. A preclinical study demonstrated that Javanese turmeric functions as as an antioxidant, hepatoprotective, anti-inflammatory, anti-cancer, anti-diabetic, anti-microbial, anti-hyperlipidemic, anti-choleric, and anti-bacterial agent (Fatmawati, 2008; Rahmat *et al.*, 2021; Rukayadi *et al.*, 2013). Another study revealed that Javanese turmeric contains flavonoids with strong antioxidant properties (Labban, 2014).

The tannins in Javanese turmeric can also influence the wound healing process via multiple cellular mechanisms, such as fibroblast proliferation, angiogenesis, and increased wound contraction (Singh *et al.*, 2013).

This study aimed to investigate the effect of Javanese turmeric extract on the number of fibroblasts, granulation, blood vessel density, and wound contraction rate in a male Wistar rat model of the diabetic ulcer.

2. Material and Methods

2.1 Study Design

This was an experimental study with post-test only observations and randomized control group design. Twenty-five rats were divided into five groups: (1) negative control rats without DM (KN); (2) positive control rats with DM (KP); (3) rats with diabetic wounds treated with 15% Javanese turmeric extract (P1); (4) rats with diabetic wounds treated with 20% Javanese turmeric extract (P2); and (5) rats with diabetic wounds treated with 25% Javanese turmeric extract (P3). Ethical clearance for this study was granted by Ethic Committee for Health Research of the Faculty of Medicine, Universitas Brawijaya, Malang, Indonesia.

2.2 Animal Model

Male Wistar rats (*Rattus norvegicus*) were used in this study. Each experiment used at least five rats, 2.5-3 months of age, weighing around 180-200 g per rat.

2.3 Study Location

This study was conducted at the Pharmacology Laboratory, Medical Faculty, Universitas Brawijaya, Malang, Indonesia. Treatment was conducted for 21 days. Skin histopathology and assessments were performed at the Anatomy and Pathology Laboratory and Micro Anatomy Laboratory, Medical Faculty, Universitas Brawijaya, Malang, Indonesia.

2.4 Javanese Turmeric Extraction

The Javanese turmeric was obtained from Materia Medica, Batu, Malang East Java Indonesia. A kilogram of Javanese turmeric was washed and sliced. It was then dried at 80°C in an incubator then powdered. The powder of Javanese turmeric (100 g) was soaked and shaken in 900 mL 98% ethanol for 24 by maceration method. The supernatant was filtered and evaporated at 70 °C. The extraction obtained about one third and it was stored in dark bottle at 0°C until it dissolved and it could be used for treatment.

2.5 Javanese Turmeric Ointment Production

The standard formulation for the ointment comprised extract paste and Vaseline. Three formulations were prepared in this study: (1) 15% v/b Javanese turmeric: 0.75 mL paste + 5 g Vaseline; (2) 20% v/b Javanese turmeric: 1 mL paste + 5 g Vaseline; and (3) 25% v/b Javanese turmeric: 1.25 mL paste + 5 g Vaseline.

2.6 DM Induction

The rats were DM-induced with a single dose of 40 mg/kg body weight streptozotocin (STZ) by intraperitoneal injection with 0.1 M citric acid (pH 4.5) as the solvent after a 12-hour fasting period. Research results stated that rats with more than 200 mg/dL blood glucose level after 7 days of STZ injection can be considered diabetic (Arokiyaraj *et al.*, 2011). Seven days after STZ injection, the blood glucose level was measured with a glucometer and every rat with more than 200 mg/dL blood glucose was considered diabetic (Winarsih *et al.*, 2012). After injection, every rat was given 5% glucose solution for 24 hours in order to prevent death by hypoglycemia.

2.7 Diabetic Ulcer Induction

The rats were anesthetized with 25 mg/kg body weight ketamine hydrochloride intra peritonial injection. The ventral hair on a 5 x 3 cm area was shaved and the shaved area was disinfected with 70% alcohol. A 1.5 x 1.5 cm incision wound was introduced in the shaved area (Li *et al.*, 2011).

2.8 Diabetic Ulcer Treatment

Wound treatment progressed for 14 days using sterile technique and a secondary dressing of sterile gauze to prevent infection. Control groups were treated with Vaseline and the treatment groups were treated with Javanese turmeric ointment, based on their respective group. The diabetic ulcer was treated once a day (Lodhi *et al.*, 2013).

2.9 Histopathology Preparation Procedure

The histological staining was based on Lodhi, *et al.* (2013). Briefly, all specimens from skin tissue were fixed in 4% buffer formalin for less than 24 hours, embedded in paraffin, sectioned into 4-6 μm thick slices, and stained with hematoxylin and eosin (Ijaz *et al.*, 2021).

2.10 Fibroblast Enumeration and Assessment of Granulation

Fibroblasts were observed in the skin dermis layer using an Olympus XC10 series light microscope with OlyVIA (Viewer for Imaging Application) software. The observations were made at 400x magnification in every observation field. Five observation fields were taken from each slide and the average was taken. Fibroblasts were counted manually (Melo *et al.*, 2011). Tissue granulation was assessed by measuring the granulated tissue from the wound surface to the lower dermis where fibroblast proliferation stopped and fibrocytes were first observed as purple cells by HE staining. The thickness was measured from the lower edge to the upper edge of the wound with a sequential mark every 2 mm. The values were averaged to determine the mean granulated tissue thickness. HE-stained slides were scanned with OlyVIA software by competent personnel (single-blinded study), then magnified by 40x on the screen, and analyzed using AutoCAD software (Kusuma *et al.*, 2016).

2.10 Blood Vessel Density Measurements

The blood vessel density was measured by the average of the vessel in each specimen. Blood vessels were shown by erythrocyte cells within the vessels (Yuhernita, 2014). The observation was done under Olympus microscope 400 magnification, then scanned using OlyVia software. Every specimen was observed ten times in different areas including in the skin wound and surrounding area (Melo *et al.*, 2011).

2.11 Wound Contraction Measurements

Diabetic ulcer healing was assessed by a physical parameter, namely wound contraction. This parameter was based on the progressive difference in the wound area, excluding not including the day of wound induction, and was measured by the following formula (Bairy *et al.*, 2012).

$$\%\ Contraction = \frac{Initial\ wound - Wound\ at\ n\ day}{Initial\ wound} \times 100\%$$

AutoCAD was used to measure the wound area as it is more precise for obtaining quantitative data (Ashkani-Esfahani *et al.*, 2012; Wibawani *et al.*, 2016) The wound area was measured by clicking the polyline and then making a line corresponding to the wound area. The area, in mm^2, was calculated after right-clicking on the line in the property tab.

2.12 Data Analysis

Data analysis used SPSS 21 for windows. The statistical tests included the Shapiro-Wilk normality test and Levene's homogeneity test. After that, one-way ANOVA and the Tukey HSD post hoc tests were performed to determine significance compared to other variables. A p-value below 0.05 was considered significant. A double linear regression test was performed to determine the relationship between the dependent and independent variables.

3. Results

3.1 The effect of Javanese turmeric extract on fibroblast number.

Javanese turmeric extract had a significant effect on the number of fibroblast ($P < 0.05$) in the wound tissue of diabetic rats based on the one-way ANOVA (Figure 1 and 2). The fibroblast number was significantly higher in the treatment groups compared to the control groups on day 14 of treatment. Fibroblast in negative control (11.68 ± 2.03); positive control (6.48 ± 1.64); 15% Javanese turmeric treatment (15.12 ± 1.20); 20% Javanese turmeric treatment (22.64 ± 1.51); and 25% Javanese turmeric treatment (23.64 ± 3.36). The dose of Javanese turmeric (25%) has the highest fibroblast.

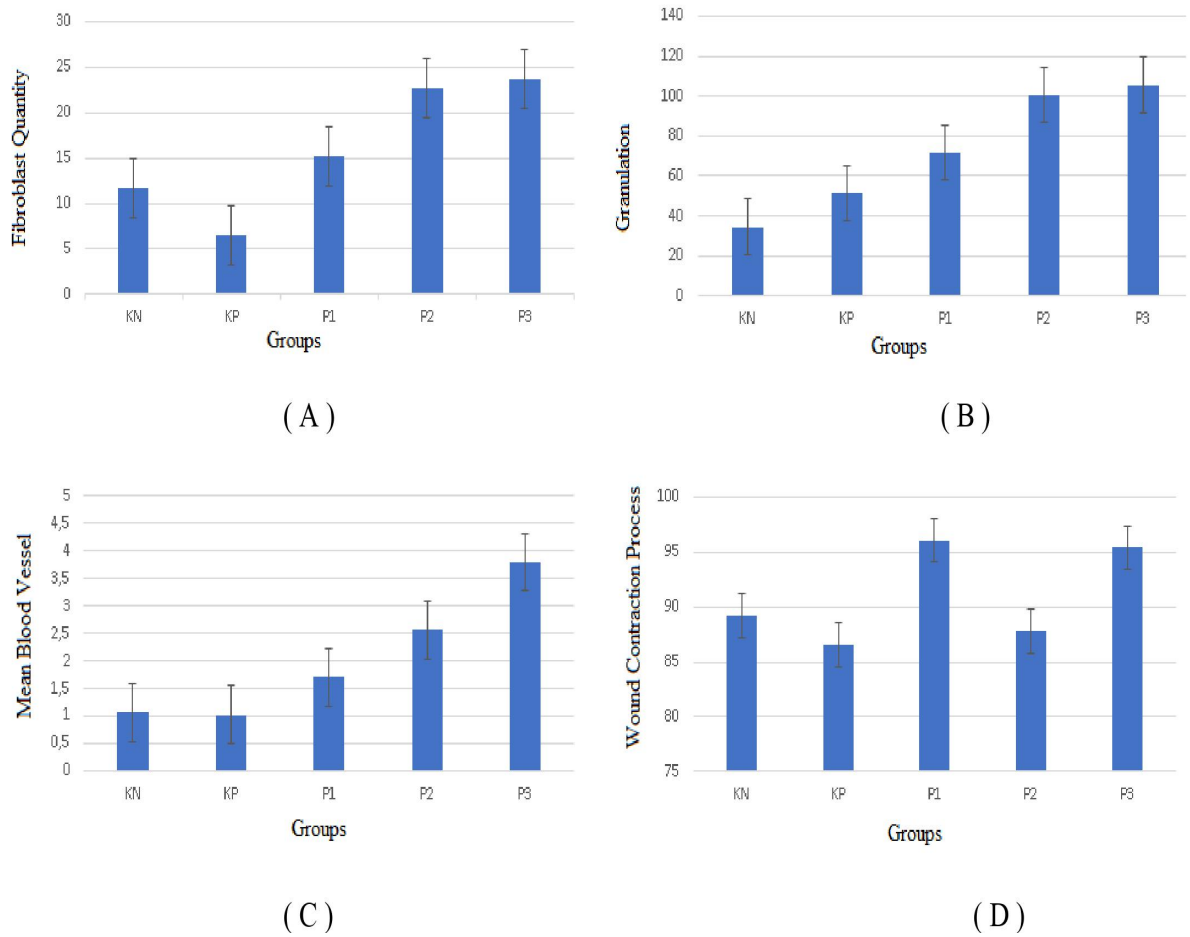

Fig. 1. Mean fibroblast (A); Mean granulation (B); Mean blood vessel (C); Mean wound contraction (D). KN: negative control; KP: positive control; P1: 15% Javanese turmeric treatment; P2: 20% Javanese turmeric treatment; and P3: 25% Javanese turmeric treatment.

3.2 The effect of Javanese turmeric extract on granulation.

One-way ANOVA revealed that *Curcuma xantorrhizza Roxb* treatment had a significant effect on wound tissue granulation compared to untreated wounds ($P < 0.05$). The treated groups had significantly more granulation than the control group (figure. 1 and figure. 2). Granulation thickness in negative control (51.21 ± 1.74); positive control (34.50 ± 3.69); 15% Javanese turmeric treatment (71.93 ± 21.86); 20% Javanese turmeric treatment(100.45± 14.86); and 25% Javanese turmeric treatment (105.607 ± 17.12). The dose of Javanese turmeric (25%) has the highest granulation thickness.

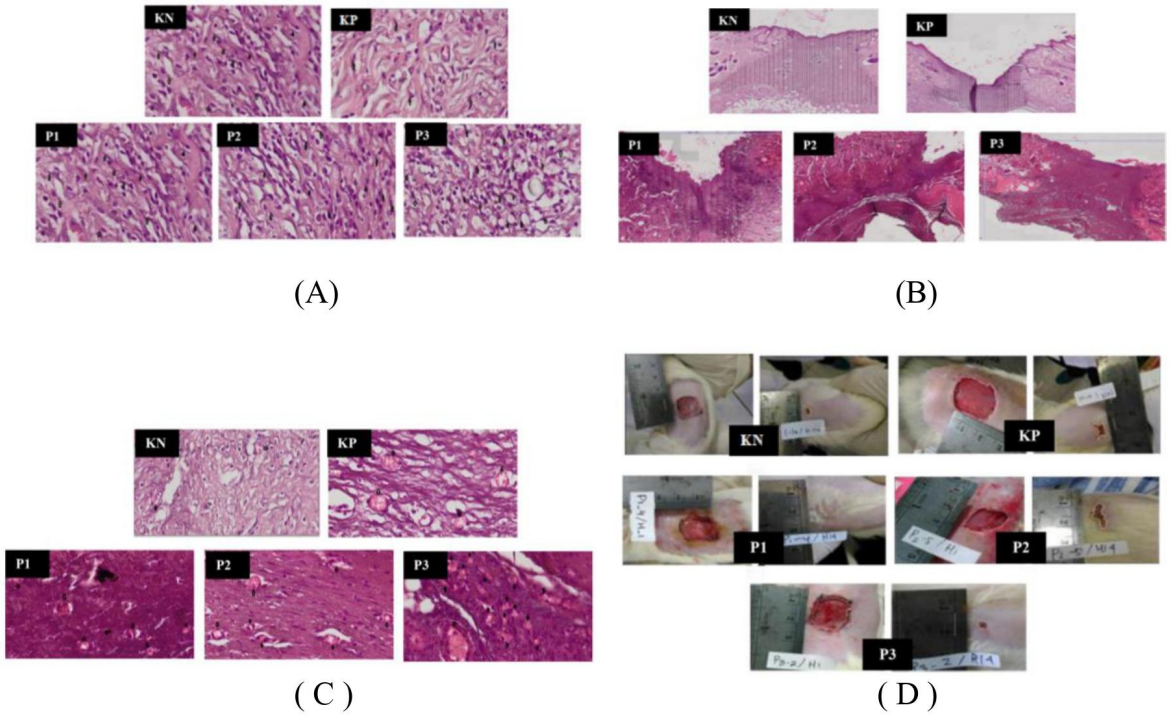

Fig. 2. Scanning results of each observational field in HE staining and 400x magnification. (A) Fibroblast (dark cells) quantity difference of each group; (B) Granulation tissue thickness; (C) Blood vessels are marked by black arrows; (D) AutoCAD 2010 analysis on diabetic ulcer area. KN: negative control; KP: positive control; P1: 15% Javanese turmeric treatment; P2: 20% Javanese turmeric treatment; and P3: 25% Javanese turmeric treatment.

3.3 The effect of Javanese turmeric extract on blood vessel density.

The blood vessel density is determined by vessel quantity. Javanese turmeric extract significantly increased blood vessel formation in the wounded tissue based on the statistical analysis ($P < 0.05$). The control groups had significantly fewer blood vessels compared to the treated groups on day 14 of treatment (Figure 1 and 2). Blood vessels in negative control (1.06 ± 0.54); positive control (1.02 ± 0.31); 15% Javanese turmeric treatment (1.70 ± 0.41); 20% Javanese turmeric treatment (2.56 ± 0.79); and 25% Javanese turmeric treatment (3.80 ± 0.78). The dose of Javanese turmeric (25%) has the highest density of blood vessels.

3.4 The effect of Javanese turmeric extract on wound contraction.

Javanese turmeric extract significantly increased the wound contraction rate compared to the control groups ($P < 0.05$). The wound contraction process was significantly faster in the treated group than that in the control group on day 14 of treatment (Figure 1 and 2). Wound contraction analysis revealed that wound contraction in negative control (89.22 ± 5.92); positive control (86.51 ± 6.09); P1: 15% Javanese turmeric treatment (96.07 ± 2.99), ; P2 20% Javanese turmeric treatment(87.76 ± 3.08); and P3 25% Javanese turmeric treatment (95.42 ± 1.15). The dose of Javanese turmeric (15%) has the highest wound contraction.

3.5 The relationship between fibroblast number, granulation, blood vessel density, and wound contraction during diabetic ulcer healing

All data from the three variables were analyzed regarding their relationships with each other. Double linear regression to all variables revealed a significant relationship between fibroblast number, granulation, blood vessel density, and wound contraction rate ($P < 0.05$). Correlation and regression analyses for fibroblast number, granulation, blood vessel density, and wound contraction rate in relation to the dose of Javanese turmeric extract were also done (Table 1).

Table 1. Correlation and Regression analysis of all variables to Javanese turmeric doses

Variable	r	R^2	P *value*
Fibroblast Blood vessel Granulation	0.959	0.919	0.000

Correlation and regression analysis on fibroblast number, blood vessel density, and granulation revealed that Javanese turmeric ointment explained 91.9% of the changes in fibroblasts, blood vessel density, and tissue granulation, while the other 8.1% was explained by other unobserved variables. In other words, all of the assessed variables could explain 91.9% of the dose variable. A requirement for double linear regression is significant. So, the regression model was considered significant for predicting the dose variable. The wound contraction variable had a p-value of 0.67 in the coefficient table. So, it was not used for double linear regression. The analysis resulted in the following equation:

$$\text{Dose} = 11.93 + 0.710\ (\text{fibroblast}) + 2.149\ (\text{blood vessel}) + 0.108\ (\text{granulation})$$

The equation explains that every additional fibroblast will increase the required dosage by 0.710 after controlling the blood vessel density and granulation variables. Every increase in blood vessel density will increase the required dosage by 2.149 after controlling fibroblast number and granulation. Every increase in tissue granulation will increase the required dosage by 0.108 after controlling blood vessel density and fibroblast number. Fibroblasts had the greatest influence on the required dosage, based on the value of 0.473 in the beta column of the coefficient.

4. Discussion

The number of fibroblasts was significantly different in each group. The positive control group had the fewest fibroblasts. This may be the effect of a high glucose content in the blood. The positive control group and P1 did not show any significant differences, possibly because a low dose of Javanese turmeric (15%) had a small effect on normal wound healing process.

During the normal wound healing process, homeostasis occurred. The blood vessel density in the positive and negative control groups was relatively similar. It was slightly lower in the positive control group due to the high blood glucose content, indicating a diabetic condition (Abdennabi *et al.*, 2016). The diabetic condition induced proinflammatory agent release and led to oxidative stress with the production of ROS and TNF-α (Luc *et al.*, 2019). Oxidative stress decreases vascular endothelial growth factor (VEGF) production and inhibits angiogenesis (Tahergorabi *et al.*, 2012). The highest dose of Javanese turmeric (25%) was associated with the highest density of blood vessels. Unfortunately, this condition can lead to excessive tissue granulation (hypergranulation) and eventually produce scars in the wounded area due to continuous collagen synthesis and catabolism. Wound contraction was significantly faster in P1 than in P2. Although the P1 wound closure percentage was higher than that of P3, the mean was not significantly different. 15% Javanese turmeric extract gave a better effect than the higher doses (20% and 25%), supported by the macroscopic observation that the wound was starting to close on day 12.

The inflammatory phase of wound healing was identified from tissue granulation from day 1 until day 10 (Gantwerker *et al.*, 2012). The proliferation phase was indicated by fibroblast proliferation and new granulation tissue characterized by a newly-formed extracellular matrix (collagen) and angiogenesis. An adequate level of oxygen and nutrition is paramount for the formation of healthy granulation tissue and preventing bleeding in the wound area. After that, the epithelialization process continued from day 4 to day 24 (Abdennabi *et al.*, 2016).

Angiogenesis was initiated on day 3 after wound induction and reached a peak on days 3 to 7 (Ram *et al.*, 2016). Angiogenesis occurred on days 3 to 7 after wound induction and ceased by day 13. The peak of angiogenesis was at day 5 (Prasetyo *et al.*, 2010). In the same pattern, angiogenesis declined at day 15 (Ferdinandez *et al.*, 2013). Other studies have shown that angiogenesis starts on day 1 after wound induction, peaks at day 5, and declines from day 7 to day 14 (Setiawan *et al.*, 2015). At the end of the proliferation period, the maturation period began, marked by contraction at the edge of the wound, a decline in vascularity, and an increase in tensile strength (Gantwerker *et al.*, 2012).

Javanese turmeric ointment was observed to have a positive effect on wound contraction in diabetic ulcers. Xanthorrizol, curcumin, flavonoids, and tannins in Javanese turmeric may play a role in this process, as these compounds are known to possess antimicrobial (Ray *et al.*, 2021), anti-inflammatory and antioxidant properties (Kuntorini *et al.*, 2018). Antioxidant activity and wound healing were indicated by increased collagen formation. Collagen is the pivotal extracellular matrix in the proliferative phase of wound healing. The more collagen formed in the wounded tissue, the faster it pulls the fibroblasts to the edge of the wound. Fibroblasts will differentiate into myofibroblasts, which are responsible for the wound contraction process (Kusuma *et al.*, 2016; Vermolen & Van Rijn, 2012). Based on the data of this study, 15% Javanese turmeric extract treatment had positive effects in the homeostasis phase. Higher doses of Javanese turmeric extract (20% and 25%) showed significant differences compared to the control groups. Further research can test pure contents having the most significant effect on wound healing in patients with diabetes mellitus.

5. Conclusion

Javanese turmeric extract has positive effects on the wound healing process of diabetic ulcers. The effects include a higher number of fibroblasts, increased wound tissue granulation, higher blood vessel density, and faster wound contraction in treated diabetic rats.

ACKNOWLEDGMENTS

The researchers would like to thank the diabetes wound research group, Department of Nursing, Faculty of Health Science, Universitas Brawijaya for the support.

References

Abdennabi, R., Bardaa, S., Mehdi, M., Rateb, M. E., Raab, A., *et al.*(2016). Phoenix dactylifera L. sap enhances wound healing in Wistar rats: Phytochemical and histological assessment. *International journal of biological macromolecules,* **88,** 443-450.

Arokiyaraj, S., Balamurugan, R. & Augustian, P.(2011). Antihyperglycemic effect of Hypericum perforatum ethyl acetate extract on streptozotocin–induced diabetic rats. *Asian Pacific journal of tropical biomedicine,* **1,** 386-390.

Ashkani-Esfahani, S., Emami, Y., Esmaeilzadeh, E., Bagheri, F. & Namazi, M.(2012). Glucosamine enhances tissue regeneration in the process of wound healing in rats as animal model: a stereological study. *J Cytol Histol,* **3,** 150.

Atlas, D.(2015). International diabetes federation. *IDF Diabetes Atlas, 7th edn. Brussels, Belgium: International Diabetes Federation*.

Bairy, K., Kumar, M. S., Savin, C., Kumar, N. K. & Avinash, M.(2012). Effect of different formulations of silver sulphadiazine cream on experimentally induced burn wound healing. *Research Journal of Pharmaceutical, Biological and Chemical Sciences,* **3,** 884-889.

Caley, M. P., Martins, V. L. & O'toole, E. A.(2015). Metalloproteinases and wound healing. *Advances in wound care,* **4,** 225-234.

Fatmawati, D.(2008). *Pola Protein dan Kandungan Kurkuminoid Rimpang Temulawak (Curcuma xanthorriza Roxb)* IPB.

Ferdinandez, M. K., Dada, I. K. A. & Damriyasa, I.(2013). Bioaktivitas ekstrak daun tapak dara (Catharantus roseus) terhadap kecepatan angiogenesis dalam proses penyembuhan luka pada tikus wistar. *Indonesia Medicus Veterinus,* **2,** 180-190.

Gantwerker, E. A. & Hom, D. B.(2012). Skin: histology and physiology of wound healing. *Clinics in plastic surgery,* **39,** 85-97.

Harding, J. L., Pavkov, M. E., Magliano, D. J., Shaw, J. E. & Gregg, E. W.(2019). Global trends in diabetes complications: a review of current evidence. *Diabetologia,* **62,** 3-16.

Hinkle, J. L. & Cheever, K. H. (2018). *Brunner and Suddarth's textbook of medical-surgical nursing,* Philadelphia, Wolters Kluwer India Pvt Ltd.

Huang, D., Refaat, M., Mohammedi, K., Jayyousi, A., Al Suwaidi, J., *et al*.(2017). Macrovascular complications in patients with diabetes and prediabetes. *BioMed research international,* **2017**.

Ijaz, H., Ishtiaq, S., Rubab, F. & Munir, A.(2021). Effect of Trianthema triquetra Rottl. ex Willed (Aizoaceae) on ethanol induced gastric ulcers in experimental rats and assessment of various ulcer parameters. *Kuwait Journal of Science*.

Kesumayadi, I., Almas, A. I., Rambe, I. N. H. & Hapsari, R.(2021). Effect of Curcuma xanthorrhiza Gel on Methicillin-Resistant Staphylococcus aureus-Infected Second-Degree Burn Wound in Rats. *Natural Product Sciences,* **27,** 1-9.

Kristianto, H., Nurachmah, E. & Gayatri, D.(2013). Peningkatan Ekspresi Transforming Growth Factor Beta 1 Pada Luka Diabetes Melitus Melalui Balutan Modern. *Jurnal Keperawatan Indonesia,* **13**.

Kuntorini, E. M., Astuti, M. D. & Milina, N.(2018). Struktur Anatomi dan Kerapatan Sel Sekresi serta Aktivitas Antioksidan Ekstrak Etanol dari Rimpang Temulawak (Curcuma Xanthorrhiza Roxb) Asal Kecamatan Pengaron Kabupaten Banjar Kalimantan Selatan. *Bioscientiae,* **8**.

Kusuma, R. F., Ratnawati, R. & Sli, D. D.(2016). Pengaruh perawatan luka bakar derajat II menggunakan ekstrak etanol daun sirih (Piper betle Linn.) terhadap peningkatan ketebalan jaringan granulasi pada tikus putih (Rattus norvegicus) jantan galur Wistar. *Majalah Kesehatan FKUB,* **1,** 86-94.

Labban, L.(2014). Medicinal and pharmacological properties of Turmeric (Curcuma longa): A review. *Int J Pharm Biomed Sci,* **5,** 17-23.

Laksmi, I. A. A., Kristianto, H. & Suharsono, T.(2020). Application of Levine's Model in Nursing Care of Patient with Diabetic Foot: A Case Study. *Journal of a Sustainable Global South,* **4,** 6-9.

Lazzarini, P. A., Pacella, R. E., Armstrong, D. G. & Van Netten, J. J.(2018). Diabetes-related lower-extremity complications are a leading cause of the global burden of disability. *Diabetic Medicine,* **35,** 1297-1299.

Li, K., Diao, Y., Zhang, H., Wang, S., Zhang, Z., *et al*.(2011). Tannin extracts from immature fruits of Terminalia chebula Fructus Retz. promote cutaneous wound healing in rats. *BMC Complementary and Alternative Medicine,* **11,** 1-9.

Lodhi, S. & Singhai, A. K.(2013). Wound healing effect of flavonoid rich fraction and luteolin isolated from Martynia annua Linn. on streptozotocin induced diabetic rats. *Asian Pacific Journal of Tropical Medicine,* **6,** 253-259.

Luan, S. & Wang, C.(2020). Hyaluronic Acid-Povidone-Iodine Compound Facilitates Diabetic Wound Healing in a Streptozotocin-Induced Diabetes Rodent Model. *Plastic and Reconstructive Surgery,* **145,** 454e-455e.

Luc, K., Schramm-Luc, A., Guzik, T. & Mikolajczyk, T.(2019). Oxidative stress and inflammatory markers in prediabetes and diabetes. *J. Physiol. Pharmacol,* **70,** 809-824.

Mavrogenis, A. F., Megaloikonomos, P. D., Antoniadou, T., Igoumenou, V. G., Panagopoulos, G. N., *et al*.(2018). Current concepts for the evaluation and management of diabetic foot ulcers. *EFORT open reviews,* **3,** 513-525.

Melo, V. A. d., Anjos, D. C. S. d., Albuquerque Júnior, R., Melo, D. B. & Carvalho, F. U. R.(2011). Effect of low level laser on sutured wound healing in rats. *Acta Cirurgica Brasileira,* **26,** 129-134.

Musfiroh, I., Muchtaridi, M., Muhtadi, A., Diantini, A., Hasanah, A. N., et al.(2013). Cytotoxicity studies of xanthorrhizol and its mechanism using molecular docking simulation and pharmacophore modelling. *Journal of Applied Pharmaceutical Science,* **3,** 7.

Oh, H.-I., Shim, J.-S., Gwon, S.-H., Kwon, H.-J. & Hwang, J.-K.(2009). The effect of xanthorrhizol on the expression of matrix metalloproteinase-1 and type-I procollagen in ultraviolet-irradiated human skin fibroblasts. *Phytotherapy Research,* **23,** 1299-1302.

Pizzino, G., Irrera, N., Cucinotta, M., Pallio, G., Mannino, F., *et al*.(2017). Oxidative stress: harms and benefits for human health. *Oxidative medicine and cellular longevity,* **2017**.
Prasetyo, B. F., Wientarsih, I. & Priosoeryanto, B. P.(2010). Aktivitas sediaan gel ekstrak batang pohon pisang ambon dalam proses penyembuhan luka pada mencit. *Jurnal veteriner,* **11,** 70-73.

Prompers, L., Schaper, N., Apelqvist, J., Edmonds, M., Jude, E., *et al*.(2008). Prediction of outcome in individuals with diabetic foot ulcers: focus on the differences between individuals with and without peripheral arterial disease. The EURODIALE Study. *Diabetologia,* **51,** 747-755.

Rahmat, E., Lee, J. & Kang, Y.(2021). Javanese Turmeric (Curcuma xanthorrhiza Roxb): Ethnobotany, Phytochemistry, Biotechnology, and Pharmacological Activities. *Evidence-Based Complementary and Alternative Medicine,* **2021,** 9960813.

Ram, M., Singh, V., Kumawat, S., Kant, V., Tandan, S. K., *et al*.(2016). Bilirubin modulated cytokines, growth factors and angiogenesis to improve cutaneous wound healing process in diabetic rats. *International Immunopharmacology,* **30,** 137-149.

Ray, R. R., Lahiri, D., Nag, M., Dey, S. & Dutta, B.(2021). Phytocompounds of Curcuma longa extract are more effective against bacterial biofilm than pure curcumin only-an in-vitro and in-silico analysis. *Kuwait Journal of Science,* **48,** 1-14.

Rukayadi, Y. & Hwang, J.-K.(2013). In Vitro Activity of Xanthorrhizol Isolated from the Rhizome of Javanese Turmeric (Curcuma xanthorrhiza Roxb.) Against Candida albicans Biofilms. *Phytotherapy Research,* **27,** 1061-1066.

Setiawan, M. R., Dewi, N. & Oktaviyanti, I. K.(2015). Ekstrak ikan haruan (Channa striata) meningkatkan jumlah neokapiler pada penyembuhan luka (Extract of haruan (Channa striata) increases neocapillaries count in wound healing process). *Dentofasial,* **14,** 1-5.

Singh, S., Pai, D. R. & Yuhhui, C.(2013). Diabetic foot ulcer–diagnosis and management. *Clin Res Foot Ankle,* **1,** 120.

Stoekenbroek, R., Santema, T., Legemate, D., Ubbink, D., Van Den Brink, A., *et al*.(2014). Hyperbaric oxygen for the treatment of diabetic foot ulcers: a systematic review. *European journal of vascular and endovascular surgery,* **47,** 647-655.

Tahergorabi, Z. & Khazaei, M.(2012). Imbalance of angiogenesis in diabetic complications: the mechanisms. *International journal of preventive medicine,* **3,** 827.

Vermolen, F. & Van Rijn, O. (2012). A Mathematical Model for Wound Contraction and Angiogenesis. *Tissue Regeneration-From Basic Biology to Clinical Application.* IntechOpen.

Vibha, S., Kulkarni, M. M., Ballala, A. K., Kamath, A. & Maiya, G. A.(2018). Community based study to assess the prevalence of diabetic foot syndrome and associated risk factors among people with diabetes mellitus. *BMC endocrine disorders,* **18,** 43.

Wibawani, L., Wahyuni, E. S. & Utami, Y. W.(2016). Pengaruh Pemberian Ekstrak Etanol Daun Melati (Jasminum sambac L. Ait) secara Topikal terhadap Peningkatan Kontraksi Luka Bakar Derajat II A pada Tikus Putih (Rattus norvegicus) Galur Wistar. *Majalah Kesehatan FKUB,* **2,** 196-206.

Winarsih, W., Wientarsih, I. & Sutardi, L. N.(2012). Aktivitas salep ekstrak rimpang kunyit dalam proses persembuhan luka pada mencit yang diinduksi diabetes. *Jurnal Veteriner,* **13,** 242-250.

Yan, Y., Liu, X., Zhuang, Y., Zhai, Y., Yang, X., *et al*.(2020). Pien Tze Huang accelerated wound healing by inhibition of abnormal fibroblast apoptosis in Streptozotocin induced diabetic mice. *Journal of Ethnopharmacology,* **261,** 113203.

Yuhernita, J.(2014) Pengaruh pemberian gel dari ekstrak metanol daun jarak Tintir (Jatropha multifidi L) terhadap kepadatan serabut kolagen dan jumlah angiogenesis dalam proses penyembuhan luka. Prosiding Seminar Nasional dan Workshop Perkembangan Terkini Sains Farmasi dan Klinik IV, 2014 Jakarta. 47-55.

Submitted: 19/07/2021
Revised: 13/02/2022
Accepted: 07/04/2022
DOI: 10.48129/kjs.15261

The effectiveness of Proteolytic bacteria isolated from effluent of Modjo tannery for their application in the leather and detergent industry

Tayachew Desalegn[1], Ketema Bacha[1], MesfinTafesse[2, 3], Chandran Masi[2, 3*]

[1]*Dept.of Biology, Jimma University., Ethiopia*
[2]*Dept. of Biotechnology, College of Biological and Chemical Engg*
Addis Ababa Science and TechnologyUniversity, Addis Ababa, Ethiopia
[3]*Center of Excellence, Biotechnology and Bioprocess,*
Addis Ababa Science and TechnologyUniversity, Addis Ababa, Ethiopia.

**Corresponding Author: chandran.chandran@aastu.edu.et*

Abstract

Protease also called proteinase or peptidase is a digestive enzyme that is categorized under proteolytic enzymes and it has great potential in industrial application. Extracellular proteases are used in a variety of industries because they exhibit practically all of the characteristics needed for biotech applications such as detergent, bioremediation, food, and leather processing.In the synthesis of all three major types of acidic, neutral, and alkaline proteases, microbial sources have dominated an unbeatable area. Alkaline proteases are a large group of industrial enzymes formed by a wide variety of species, including animals, fungi, and bacteria. The fermentation method serves to make bacteria, fungi, and yeast alkaline proteases. Proteases are produced in large quantities by Gram-positive bacteria, especially those belonging to the *Bacillus genus*. Following standard procedures, the bacterial isolates PMOJ-01 and PMOJ-05 with the prominent zone of clearance and efficient enzyme development were further characterized to the genus level. Moreover, the growth conditions for the highest protease production were optimized with different pH, temperatures, and NaCl concentrations, in the results of PMOJ-01 and PMOJ-05 pH (7 and 8), temperatures 45^{o}C, and 1% NaCl Concentrations both cases respectively. The proteases activities from PMOJ-01, *Pseudomonas aeruginosa,* and PMOJ-05, *Bacillus subtilis* were most active at pH7.0 and pH8.0 and temperature at 35^{o}C and 45^{o}C, respectively. The enzyme activity and the total solid protease sample of the crude enzyme of *Pseudomonas aeruginosa* and *Bacillus subtilis* were 0.299 U/ mL and 0.289 U/ mL, 1.37±0.14 U/mg, and 1.199 U/mg respectively. The effect on dehairing, distaining, and scum removal revealed that the purified protease enzyme of PMOJ-01 and PMOJ-05 can be used in detergent and leather industries.

Keywords: Bioremediation; concentration;dehairing; detergent; extracellular proteases.

1. Introduction

Enzyme technology is well established and used in many industrial applications in the modern era of biotechnology. A better understanding of and functionality of enzymes suggests numerous new applications for these catalytic activities and a constant discovery with new R&D properties

(Amar, 2001; Najafi *et al*.,2005). Enzymes are used in many environmentally-friendly industries such as food, dairy, leather, etc. since they are efficient, selective, accelerate and accelerate reactions through the forming with its substrate of transition state complexes, which reduce the energy of activation of the reaction (Bayoudh *et al.,* 2000; Madan *et al.,*2000). Proteases or proteolytic enzymes catalyze the cleavage of peptide bonds in proteins. Protease is one of the most common types of industrial enzymes, accounting for more than 65 percent of all industrial enzymes (Pastor *et al.,* 2001; Belma *et al.,* 2002). In contrast to their behavior, the wide variety of proteases has drawn international attention and concentrated on exploiting physiological and biotechnologies (Rao *et al.,* 1998;Chandran *et al.,* 2014a; Hatem *et al.,* 2018). Proteases are also expected to play an important role in the advancement of environmental innovations and bioremediation processes (Singh *et al.,* 2001; Masi *et al.,* 2014b). In a large number of industries, one of thebiggest industrial enzymes (Protease) is commonly used:- in detergent, leather manufacturing, meat processing, milk product, organic fertilizer preparation, digestive aid, silk industry, and silver recovery from X-ray films used (Sudha *et al.,* 2010; Chandran *et al.,* 2014b).

Microbial origins have dominated an invincible domain in the development of all three major acidic, neutral, and alkaline protease forms. Alkaline proteases, a broad group of industrial enzymes, are generated by a wide variety of species, including animals, fungi, and bacteria. Alkaline proteases are produced by bacteria, fungi, and yeast using the fermentation process (Takami *et al.,* 1989; Masi *et al.,* 2014c). Gram-positive bacteria are considered a major commercial producer of proteases, in particular the *Bacillus* genus (Thangam *et al* 2002;Masi *et al.,* 2015). Gupta *et al.,* (2002) reported *Bacillus licheniformis, Bacillussubtilis, Bacillus acidophilus, Bacillus lentus*, etc., are important industrial alkaline protease producers. Alkaline proteases are one of the most essential classes of enzymes used as detergents, pharmaceutical products, leather, meat-treating products, protein hydrolysates, dairy products, and even waste processing products in various industrial processes (Masi *et al.,*2016a; Thangam *et al.,* 2016).

Alkaline proteases have a large share of the enzyme market, despite having just a two-thirds share of the detergent industry. They're also used in industries like leather, food, textiles, organic synthesis, and waste-water treatment (Wang *et al.,* 2007: Masi *et al.,* 2016b). Microbial proteases account for nearly 60% of total global enzyme sales, with 25% of total global alkaline protease enzyme sales (Madan *et al.,*2000; Masi *et al.,* 2014b). The important applications of the enzymes have been authenticated in this present study.Protease is usually produced from bacteria such as Teredinobacterturnirae, *Bacillus sp., Pseudomonas sp*. and also from other fungal species (Isiaka & Agbaje, 2016;Masi *et al.,* 2021). Bacterial species can be isolated from various industries' effluents(Sudha *et al.,* 2010; Masi *et al.,* 2017). Protease production conditions are optimized and the highest protease producing environments with optimized nutrient sources, pH, and temperature were determined to get maximum protease from each bacterium (Takami *et al.,* 1989; Masi *et al.,* 2018). Bacterial species can be isolated from the effluents by the serial dilution method. A normal agar medium can be used to isolate various numbers of colonies. Each species have a different potential for producing protease. By comparing the protease activities of different strains that were isolated from the effluents; the maximum protease yielding bacteria can be obtained (Gopinath,2002; Thangam *et al.,* 2002).

Bacterial proteases have recently been noted as a viable alternative to the bioremediation and use of tannery-rich protein waste for rawhide treatment by substituting dangerous chemicals that are particularly involved in the soaking, dehairing, and tanning of hides before tanning, for quality leather production without pollution (Takami *et al.,* 1989;Masi *et al.,* 2018). Even though proteases have been identified in several areas and many have been used in industry and biotechnology, the proteases now in use are insufficient to suit all biotechnological needs. As a result, the goal of this research was to identify and characterize possible proteolytic bacteria from Modjo Tannery Waste, as well as to assess their potential for use in detergent and leather industries.

2. Materials and methods

2.1 Screening for protease production

A total of six samples were taken from more than 50 years of accumulated sludge. The samples were transported to the Microbiology Laboratory at Addis Ababa Science and Technology University, where 1.0 g was transferred into 10 mL sterilized normal distilled water in a 250 mL conical flask and agitated at 100 rpm in a water bath shaker at 37^{o}C for 15 min. Nutrient agar was used to dilute and spread the soil suspension. After 24-hour incubation in 37^{o}C and using separate bacterial colonies, the capacity of their proteolytic enzyme was screened on Petri plates containing skim milk agar medium (Skin Milk Powder 2.8 g, Casinenzymichydrolysates 500 mg, Yeast extract 250 mg, Dextrose 100 mg, and agar 1.5 g powder with 100 mL of distilled water to maintaining pH 8).The inoculated plate was then incubated for 48 hours at 37°C, looking for clearance zones that indicated bacterial isolate proteolytic activity.Five isolates with the potential to produce protease in the primary screening were chosen based on the diameter of the clearance zone, and they were further screened to find the most potent isolates among them based on incubation time, clearance zone size, and production (the ratio of the clearance zone diameter to the colony diameter) (Belma *et al* 2002;Chandran *et al.,* 2014a).

2.2 Proteolytic isolates identification

The proteolytic isolates were identified based on biochemically (citrate utilization, triple iron sugar test, Urease, VP tests, catalase, indole starch hydrolysis, and oxygen requirements) and morphological (Gram staining, motility test, and endospore staining) features and then the identified isolates were subjected to the methods suggested in Bergey's Manual, which showed prominent clearances in the sky-milk agar medium. (Masi *et al.,* 2014c).

2.3 Characterization of protease producing isolates

By inoculating the species to nutrient broth supplemented with skim milk agar, the effects of NaCl concentration, pH, and temperature on bacterial growth and activity were investigated.

2.4 Protease assay

For protease assay, the method adopted by Takami *et al.,* (1989) was used. To establish a standard curve, a 0.2 mg/mL L-tyrosine standard solution was prepared. Five test tubes containing 0.2, 0.4, 0.6, 0.8, and 1.0 mL of standard solution, but no standard blank, were prepared. Then, using

distilled water and a blank, it was rendered up to 2mL. Following the addition of 5mL of Na_2CO_3, 0.5mL of Folin and Ciocalteu's reagent was applied to each vial. The blue color produced was measured at A660 nm using a UV-visible spectrophotometer after 30 min of incubation at 37^oC. Casein acts as a substratum in this test. When we test the protease for digester casein, the amino acid tyrosine is liberated along with other amino acids and peptide fragments. Folin&Ciocalteo Phenol interacts mainly with free tyrosine to create blue-colored chromospheres, which can be quantified and calculated as an absorbent value on a spectrophotometer at 660nm.

2.5 Estimation of total protein

The total protein content of the samples was measured using a slightly modified method of Lowry's process. Lowery *et al.,*(1951) used Egg Albumin as a protein standard. In the test tube, different dilutions of egg albumin solutions were made by mixing one mg of egg albumin and one ml of water. Each of the test tubes had a final volume of 5ml. The solution's concentration ranged from 0.05 to 1 mg per mL. A 0.5ml protein solution was taken from each of these dilutions and 5 ml of lowery reagent D was applied to each test tube. This solution was incubated for 10 minutes at room temperature. After that, each tube received 0.5 mL of FolinCiocalteu reagent (responsible solutions) and was incubated for 30 minutes.

2.6 Purification of protease enzyme

Around 10 ml of solution-free cell enzymes (supernatants) were taken from parent isolates by and adding 80 percent saturation of ammonium sulfate. The solutions of the enzyme were agitated for 1 hour at 4^oC after the ammonium sulfate interacted with protein to form precipitous. The precipitated proteins were extracted by centrifugation at 6,000 rpm for 30 min at 4°C. To obtain a concentrated suspension of the injectable enzyme, the pellets were re-dissolved in 10ml Tris-Hcl buffer, vol. 0.05M, pH 7.5 (Masi *et al.,* 2015).

2.7 Characterization of protease activity

The two test isolates were subjected to different temperatures (25°C, 35°C, 45°C, 55°C,and 65°C) and pH levels (4 to 12) to determine the optimal conditions for protease activity.

2.8 Experiments to evaluate commercial applications of proteases

Removing a bloodstainrequired soaking a clean piece of cloth in blood and allowing the blood cloth to dry. The cloth was cut into equal pieces and incubated with the purified protease for 5 min at 45°C. The control underwent the same process as the experimental group, except for incubation with the enzyme solution. Using enzymes as a detergent ingredient to remove egg albumin protein stain: On pieces of white cotton cloth (5 x 5 cm) stained with egg yolk, the use of enzymes as a detergent additive was investigated (rich in protein).Skin dehairing: - sheepskin was sliced into 5cm 2 pieces and treated in 50 mMTris-HCl (pH 8) at 50^oC with the purified protease. At different incubation times, the skin was examined for hair eradication (Najafi*et al.,* 2005).

2.9 Analytical Statistics:

Origin 2019 was used to draw the graph and conduct analyses of the data at which the optimum point were calculated

3. Results

3.1 Isolation, screening, and identification

The sludge samples obtained from the Modjo Tannery industry yielded a total of 20 distinct bacteria. Only 12 of them were effective in forming clear zones in 24 hours on 1.0 percent skim milk agar. Only two protease-producing isolates were chosen after primary and secondary screening based on their incubation time, clearance zone size (Figures 1 and 2), and efficiency (the ratio of the diameter of the clearance zone to colony diameter) in 24 hours (Table 1). These were PMOJ-01 and PMOJ-05 and were subjected to further study (P- Protease, MO - Modjo Tannery industry, J - Jimma University).

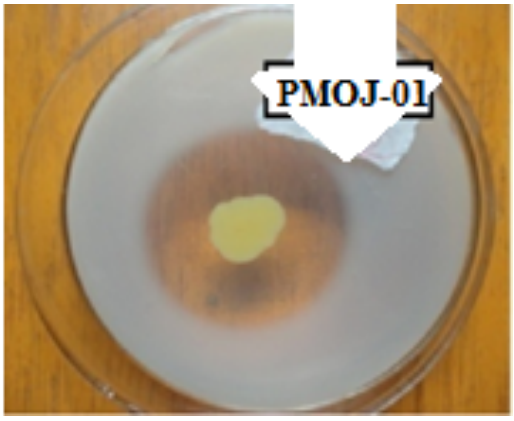

Fig. 1. Clear zone (Protease producing bacteria) formed by isolate PMOJ-01

Fig. 2. Clear zone (Protease producing bacteria)formed by isolate PMOJ-05

Table 1. Screening of protease producing bacterial isolates using zone of inhibition methods

Isolates	The efficiency of Diameter (in mm)
PMOJ-01	22.3
PMOJ-02	8.6
PMOJ-03	9.15
PMOJ-04	2.1
PMOJ-05	14.05

Further species identification (Biochemical Test and microscopic examination) of isolates was performed at the microbiology lab at AddisAbaba Science and Technology and isolate in PMOJ-01 was identified as *Pseudomonas aeruginosa* while PMOJ-05 was identifiedas *Bacillus subtilis* (Table 2).

Table 2. Microscopic examination and biochemical characterization of growing colonies of the isolate PMOJ-01 and PMOJ-05

	Isolate PMOJ-01	Isolate PMOJ-05
Pigment	Yellow	White
Margin	Convex with an entire margin	Circular form and flat elevation
Gram reaction	-	+
Spore	-	+
Motility	-	+
Catalase	++	++
Oxygen requirement	Facultative	facultative
Triple sugar iron test	+ (very less)	+
MR	+	-
VP	-	+
Indole	-	-
Citrate	-	+
Mannitol utilization	-	-
Starch hydrolysis	-	+
Nitrate test	+ (less)	+(less)
Growth in 0%NaCl	+	+
Growth in 2%NaCl	+	+
Growth in 5%NaCl	-	+
Growth at 0^0C	-	-
Growth at 20^0C	+	+
Growth at 37^0C	++	++
Growth at 65^0C	-	+(less)
Urease test	+	-
Identified as	*Pseudomonas aeruginosa*	*Bacillus subtilis*

3.2 Characterization of bacterial isolates

Maximum cell density for *Pseudomonas aeruginosa* (PMOJ-01) and *Bacillus subtilis*(PMOJ-05) was observed when growth temperature was 45^{0}C with the highest Optical Density (OD) measurement of 0.429±0.001 and 0.488±0.004, and the least cell density was recorded at 5^{0}C with mean OD 0.142±0.002 and 0.127±0.007 respectively (Figure 3). The highest cell growth was recorded at pH 7 with 0.659±0.013 OD and pH 8 with 0.694±0.001 OD of PMOJ-01 (*Pseudomonas aeruginosa*), and PMOJ-05 (*Bacillus subtilis)* respectively (Figure 4). The maximum growth of PMOJ-01(*Pseudomonas aeruginosa*), was obtained at 1% NaCl with cell density (OD) of 1.31±0.035 but isolated PMOJ-05(*Bacillus subtilis)* also its OD measurement of 0.71±0.035 was obtained at 1 % concentrations of NaCl as shown high (Figure 5).

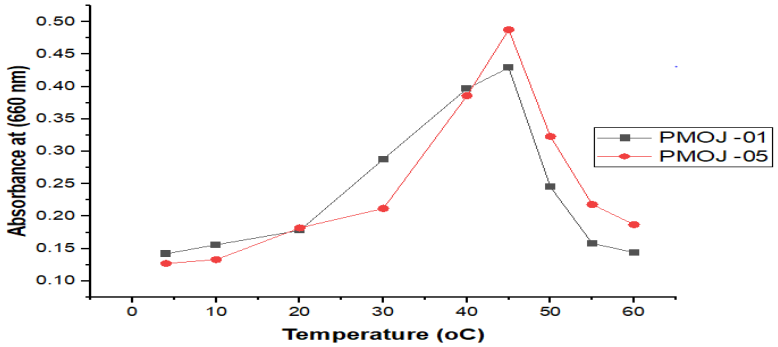

Fig.3. Effect of temperature on microbial growth of the selected two isolates

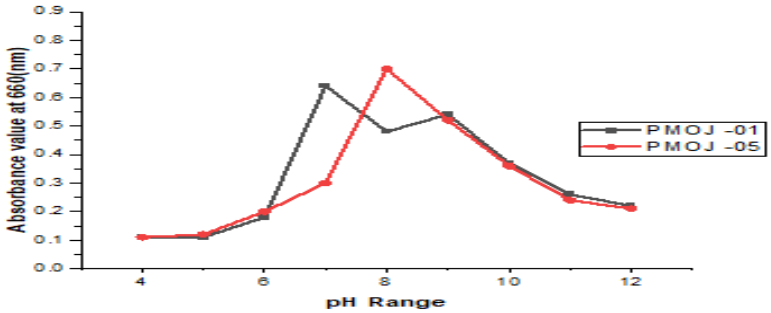

Fig. 4. Effect of pH on the growth pattern of the selected two isolates at 37ºC

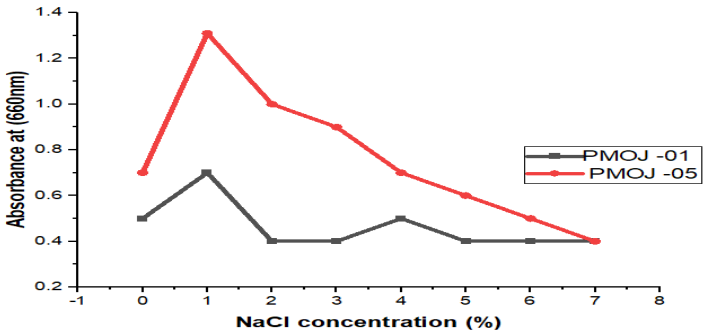

Fig. 5.Growth pattern of the selected two potent isolates under differentsalt concentrations at 37ºC

3.3 Protease assay

The concentration for PMOJ-01 (*Pseudomonas aeruginosa*) and PMOJ-05 (*Bacillus subtilis*) was 0.544µmole and 0.526 µmole and crude enzyme activity was calculated as 0.299 U/ mL and 0.289 U/mL, respectively. Furthermore, the enzyme activity of the partially purified enzyme of PMOJ-01(*Pseudomonas aeruginosa*) and PMOJ-05(*Bacillus subtilis*) was 0.242 U/ mL and 0.231 U/ mL, respectively. The total solid protease sample was 1.37 U/mg for PMOJ-01 (*Pseudomonas aeruginosa)* whereas 1.199 U/mg PMOJ-05 (*Bacillus subtilis)*. The total solid protease of a partially purified enzyme of PMOJ-01 and PMOJ-05 was 2.05 U/mg and 1.55 U/mg respectively. One unit of proteolytic enzyme activity is classified as the amount of enzyme that generated an absorbance difference per milliliter of crude or distilled extract solution after a 10-min incubation at 37°C.

3.4 Characterization of protease enzyme

Protease production increased in both species as pH increased (Figure 6). *Pseudomonasaeruginosa*and *Bacillussubtilis* produced the most proteases at pH 7 and 8, respectively. *Pseudomonas aeruginosa*produced more protease when the temperature was raised to 35ºC. (PMOJ-01) But, the protease production started decreasing then after till the end of work with the lowest protease production obtained at the temperature of 65ºC. But the protease production of *Bacillus subtilis* (PMOJ-05) is maximum growingat 45ºC (Figure 7).

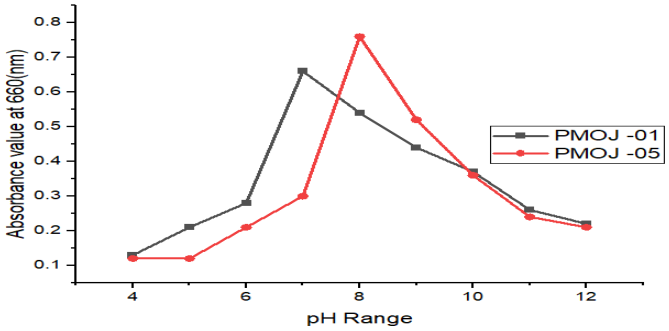

Fig. 6. Effect of different pH on Proteases activities produced by *Pseudomonas aeruginosa* - PMOJ-01 and *Bacillus subtilis*- PMOJ-05

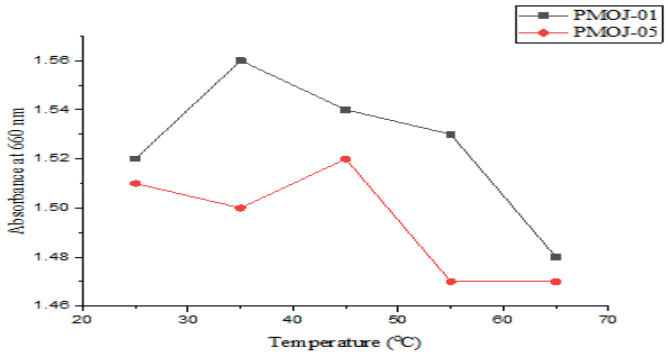

Fig. 7. Effect of temperature on Protease activities produced by *Pseudomonas aeruginosa* - PMOJ-01 and *Bacillus subtilis*- PMOJ-05

3.5 Application of protease in industries

The result of the bloodstain removal study (Figure 8) and egg albumin removal study (Figure 9) revealed that protease from isolate PMOJ-05(*Bacillus subtilis)* is a promising additive for the detergent industry as such applications are well established by the related study conducted. Thus, the enzyme produced by our isolate could be a choice for the commercially available enzymes.In the present dehairing study, incubation of protease with sheepskin for hair (Figure 10) and 12 hrs.showed removal scum (Figure 11) very easily without affecting the skin quality as compared to skin treated with buffer only. However, the skin quality was damaged in the chemically treated skin. Under similar conditions, the control skin incubated in distilled water showed no signs of Scum removal.

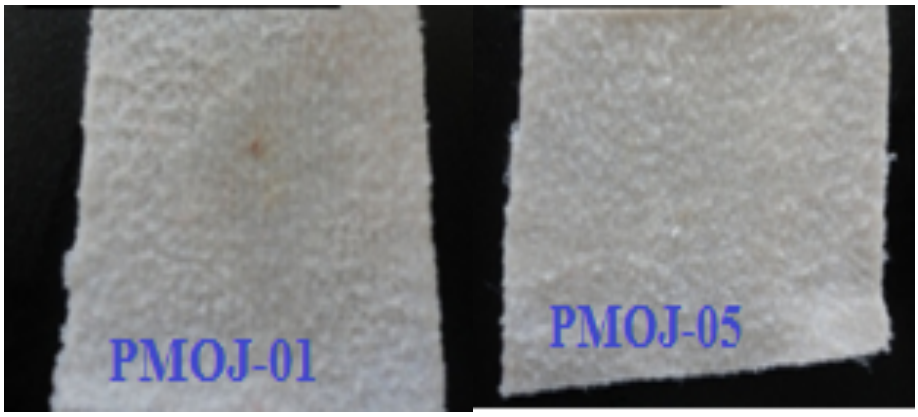

Fig. 8. Effects of distilled water, Alcohol, Enzyme of PMOJ-01(*Pseudomonas aeruginosa)*, Enzyme of PMOJ-05 *(Bacillus subtilis)* on blood-stained clothes after 30 minutes incubation.

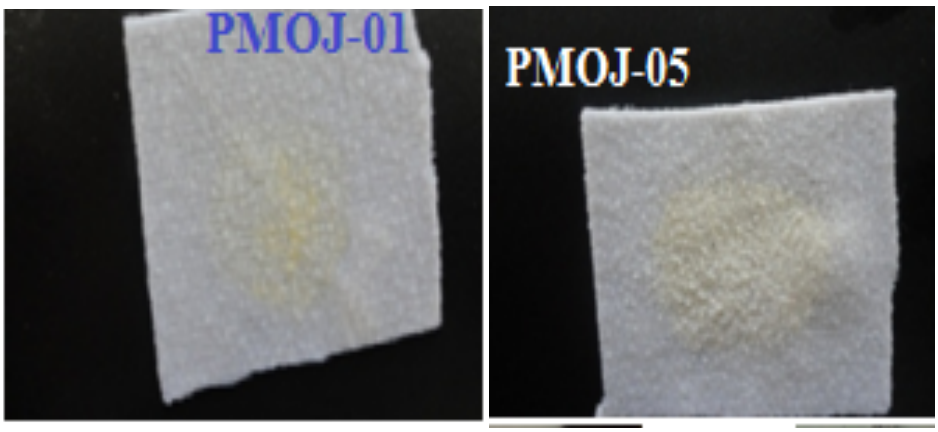

Fig. 9. Effects of distilled water, Alcohol, Enzyme of PMOJ-01(*Pseudomonas aeruginosa)*, Enzyme of PMOJ-05*(Bacillus subtilis)* on prepared egg-stained clothes after 30 minutes incubation.

Fig. 10. De-hairing effect PMOJ-01(*Pseudomonas aeruginosa)* enzyme and PMOJ-05 *(Bacillus subtilis)*enzyme after 12 hours incubation

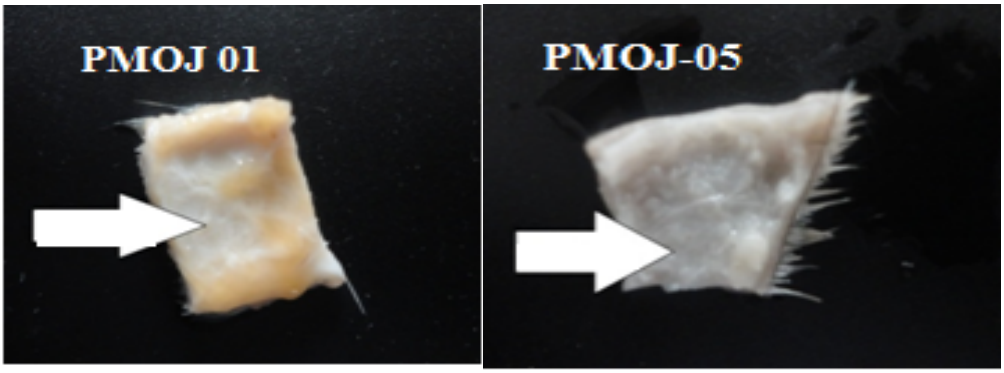

Fig. 11. Scud removal effect of PMOJ-01(*Pseudomonas aeruginosa)* enzyme and PMOJ-05*(Bacillus subtilis)* enzyme after 12 hours incubation

4. Discussion

During the screening, isolation, and production of protease from marine microbes, Guravaiah *et al.,*(2010) reported that bacteria that form a large clear zone on skim milk agar were found in the highly proteolytic zone. After the evaluation of the entire morphological and biochemical test, the two most promising isolates in this study were identified as *Pseudomonas aeroginosa* and *Bacillus subtillis*. High-yielding isolates such as *Bacillus sp*., *Alcaligenes faecalis*, *Pseudomonas fluorescent*, and *Aeromonashydrophilia* contain microbial proteases (Isiaka & Agbaje, 2016;Yu *et al.,* 2017). *Bacillus sp*., for example, is one of the most common classes of bacteria used in the enzyme industry, and this bacterium is also known to produce efficient proteolytic enzymes (Chandran *et al.,* 2014b). As per the observation by Gopinath (2002), the predominant bacterial genera in tannery sludge were *Pseudomonas, Vibrio, Bacillus,* and*Micrococcus*.

The most commercially important proteases come from *Bacillus species*. Their ability to secrete large amounts of proteases with high proteolytic activity and stability at extremely high pH and temperatures is well known (Gupta *et al.,* 2002). Another research looked at the development of alkaline protease from soil samples and found that 27 of the 40 bacteria isolated belonged to the genus *Bacillus* (Guravaiah *et al.,* 2010). In the current study, the predominant isolates were *Bacillus*, followed by *pseudomonas.*When Amar (2001) looked at the microflora in tannery effluent, he

discovered that *Bacillus* was the most common species, followed by Coryneformes, Vibrio, Micrococcus, *Pseudomonas*, and *Acinetobacter*. Furthermore, the importance of this enzyme has been emphasized by various researchers due to the rapid growth rate and improved genetic manipulation production in *Bacillus species* (Morita *et al.,* 1998).

The enzyme activity of the partially purified enzyme of PMOJ-01 and PMOJ-05 was 0.242U/ mL and 0.231 U/ mL and the total solid protease of the partially purified enzyme of PMOJ-01 and PMOJ-05 was 2.05 U/mg and 11.55 U/mg, respectively. According to Kumar (2002),*Bacillus pumilus* had a maximum enzyme activity of 0.065 U/ml, and *Staphylococcus auricularis* had a maximum enzyme activity of 0.038 U/ml at optimum temperature, pH, and nutrient availability. *Bacillus pumilus* and *Staphylococcus auricularis* enzymes were found to have high activity in leather processing and biofilm degradation.About this, enzymes from the current isolates are much better in their activities.

The effect of pH on protease activities of our isolates was consistent with (Gupta *et al.,* 2002) protease development findings, in which the optimum temperature and pH of partially purified *Bacillus species* protease were found to be 40°C and pH 7 respectively. In a Flavobacterium population, the optimal pH for protease development was 7.4(Masi *et al.,* 2014a; Dewi *et al.,* 2018). In *Bacillus polymyxa*, however, protease development was best at pH 9. In different *Bacillus species*, the optimal pH for protease development was between 7 and 10 (Holt *et al.,* 1994). *Pseudomonas* protease development is best at pH8 (Thangam *et al.,* 2002).

The leather industry generates many pollutants that are environmentally detrimental, including sulfides and chromate. There have been many reports of goat/beef dehairing using cleansed and semi-cleansed protease (Nadeem *et al.,* 2006). The spark removal of protease activity has generated the interest of researchers as well as the improvement of leather quality as a chemical methodology due to a significant reduction in toxicity (Najafi *et al.,* 2005; Masi *et al.,* 2014a). In support of the above observations, the current study confirmed the scum removal activity of protease from our isolates with promising potential applications in the leather industry (Longo *et al.,* 1999). Furthermore, blood removing study revealed that protease from PMOJ-05 (*Bacillus. sp)* was a promising additive for the detergent industry in agreement with the well-established practices reported by many authors including Nadeem *et al.,* 2006. They studied the high capacity of bloodstain removal by *Bacillus licheniformis*N-2 and *Bacillus subtilis.*Surprisingly, our findings revealed that the isolates' proteolytic enzyme performed better than some commercially available enzymes. Protein stains, such as grass, blood, egg, and human sweat, are easily removed with proteases, which are commonly used in the detergent industry (Isiaka & Agbaje,2016; Masi *et al.,* 2021).

5. Conclusion

The PMOJ-01(*Pseudomonas aeruginosa)* and PMOJ-05 (*Bacillus subtilis)* bacterial strains are very powerful sources for the production of protease enzymes. Leather making can produce leather with the most softness with the aid of protease enzymes and eliminate the use of pollutant substances such as sodium, lime, and solvents. It is, therefore, reasonable to assume the promising nature of

this enzyme for commercial applications in the detergent industry since they can degrade animal blood and egg albumin in 30 min. so these two bacterial strains (*Pseudomonas aeruginosa*and *Bacillus subtilis)* are very potential protease enzyme-producing. These two bacteria strain references to detergent and leather industries.

ACKNOWLEDGMENT

We appreciate the assistance of the College Dean, Head of Department, and Lab Coordinator from the Department of Biotechnology, College of Biological and Chemical Engineering, Addis Ababa Science and Technology with this research work.

References

Amar, B. (2001). Fermentation of prawn shell waste and application of its products as a dietary ingredient for the Indian white prawn, Penaeusindlcus (H.Milne Edwards). Ph.D. thesis, Cochin University of Science and Technology, India.

Bayoudh, A., Gharsallah, Chamkha, M., Dhouib, A., Ammar, S.,& Asri, M. (2000). Purificationand characterization of an alkaline protease from *Pseudomonas aeruginosa* MNI. J. of Industrial Microbiology & Biotechnology. 24: 291-295.

Belma, A., Zehra, N. Y. & Yavuz, B.(2002). Determination of PHB growth quantities of certain *Bacillus species* isolated form soil. Turkish Elect. J. Biotechnol. Special issue, 24-30.

Chandran,M., M. Fazil, A.& N. Parthasarathi (2014a). A Comparative Study on The Protease Producing Bacteria Isolated From Dairy Effluents of Chennai Region, Identification, Characterization and Application of Enzyme in Detergent Formulation, Asian Journal of Microbiology, Biotechnology and Envimental science. 16 (1):41- 46.

Masi, C., Pandian, A. A. S., Thiruvengadam, S., & Parthasarathy, N. (2014b). Enrichment and Immobilizaiton of *Enterococcus hirae* In Various Matrices to Study their Protease Production Efficiency. Journal of Pure and Applied Microbiology, 8(5), 3747-3754.

Chandran, M., Duraipandi, V., Yuvaraj, D., Vivek, P., & Parthasarathy, N. (2014b). Production and extraction of bacterial pigments from novel strains and their applications. RJPBCS, 5(6), 584-593.

Masi, C., Vivek, P., Sowmya, V., Sindhuja, V., & Parthasarathi, N. (2014c). Production and process optimization of protease using various bacterial species–a review. Int J ChemTech Res, 6(9), 4268-4275.

Masi, C., Balaji, E., Vigneshwar, J., Chandramohan, C., Ahmed, M. F., & Parthasarathy, N. (2014a). Isolation and Production of Proteolytic Enzyme by Bacterial Strains by Using Agrowates as Substrate. Asian Journal of Chemistry, 26(7), 2182 -2184.

Masi, C., Vivek, P., Kotteshwari, J., Mithun, C., Uma Maheswaran, A., & Parthasarathi, N. (2015). Cloning, expression and characterization of serine proteasegene from *Entrococcus hirae*. BioTechnol: Indian J, 11(9), 328-334.

Masi, C., Balaji, E., Vigneshwar, J., & Parthasarathy, N. (2016a). Application of response surface methodology (RSM) for protease production from *Enterococcushirae* and using algae as substrate. Bio Technology: An Indian Journal, 12(3) :145 - 155.

Masi, C., Kumar, N. K., & Umesh, R. (2016b). Media Optimization, Production, Purification and Characterization of Alkaline Protease Enzymes from *Pseudomonas aeruginosa*. Research Journal of Pharma, Biological and Chemical Sciences, 7(4), 716-729.

Masi, C., Kumar, N. K., Raja, G. N., & Umesh, R. (2017). Immobilization of alkaline protease enzyme from *Pseudomonas aeruginosa* on surface functionalized magnetic iron oxide nanoparticles. Research Journal of Pharmaceutical Biological and Chemical Sciences, 8(6), 153-161.

Masi, C., Chandramohan, C., & Ahmed, M. F. (2018). Immobilization of the magnetic nanoparticles with alkaline protease enzyme produced by *Enterococcus hirae* and *Pseudomonas aeruginosa* isolated from dairy effluents. Brazilian Archives of Biology and Technology, 60. DOI:10.1590/1678-4324-2017160572

Masi, C., Gemechu, G., & Tafesse, M. (2021). Isolation, screening, characterization, and identification of alkaline protease-producing bacteria from leather industry effluent. Annals of Microbiology, 71(1), 1-11. https://doi.org/10.1186/s13213-021-01631.

Dewi,S.Z., YusroN.F.& Agustinus R. U. (2018). Identification of Protease-Producing Bacteria Isolated from Banyuwedang, Bali, and Characterization of its Protease. Squalen Bulletin of Marine and Fisheries Postharvest and Biotechnology, 13 (3):101-108.

Gopinath, S.(2002). Phosphatases from bacteria isolated from Arabian Sea and Cochin Estuary. PhD Thesis, Cochin University of Science and Technology, India.

Gupta, R., Beg, Q.K.& Lorenz, P.(2002). Bacterial alkaline proteases: molecular approaches and industrial applications. Appl. Microbiol. Biotechnol. 59(1): 15-32.

Guravaiah, M., Prabhakar, T., Prameela, C.H., Santhoshi,K., C.H. & Guravaiah M.V.(2010). Screening, Isolation and Production of Protease by Marine *Actinomycetes*. Advanced Biotech, 10(2): 07-13.

Hatem,R., Nadia, Z. J., Fares, G., Wacim,B., FakherF., Najah,J., Samir, B., &BassemJ. (2018). Purification and biochemical characterization of a novel detergent-stable serine alkaline protease from *Bacillus safensis strain* RH12. BIOCHEMPHYS-01. 2(4).

Holt, J. G., Krieg, N. R., Sneath, P. H. A., Stately, J. T. &William, S. T.(1994). Bergey's Manual of Determinative Bacteriology, 9th Ed., Williams and Wilkins, Baltimore, Maryland, USA. 559.

Isiaka, A. &Agbaje,L. (2016). Keratinases: emerging trends in production and applications as novel multifunctional biocatalysts, *Kuwait J. Sci.* 43 (3) pp. 118-127, 2016.

Kumar, C.G. (2002). Purification and characterization of a thermostable alkaline protease from alkaliphilic *Bacillus pumilus*. Lett. Appl. Microbiol. 34: 13-17.

Longo, M.A., Novella, L.S., Garcia, L.A.& Diaz, M. (1999). Comparison of *Bacillus subtilis* and *Serratiamarsescenes* as protease producers under different operating conditions. J. Biosci. Bioeng. 88: 35-40.

Lowery, O.H., Rosebrough, N., Farr, A.L. & Rondall, R.L. (1951). Protein measurement with the folin phenol reagent. J. Biol. Chem. 193: 265-273.

Madan, M., Dhillon, S.& Singh, R.(2000). Production of alkaline protease by a UV- mutant of *Bacillus polymixa*. Ind. J. Microbiol. 40: 25-28.

Morita, Y., Hasan, Q., Sakaguchi, T., Murakami, Y., Yokoyama, K. & Tamiya, E.(1998). Properties of a cold active protease from psychrotrophicFlavo bacterium baustinum P104. Appl. Microbiol. Biotechnol. 50: 669-675.

Nadeem, M., Shahjahan, B., Syed Q. A. & Qazi, J. I.(2006). Microbial production of alkaline proteases by locally isolated *Bacillus subtilis* PCSIR-5. Pak J.Zool., 38: 109-114.

Najafi, M. F., Deobagkar, D. & Deobagkar, D., (2005). Potential application of protease isolated from *Pseudomonas aeruginosa*PD100. Electronic J. Biotechnol., 8: 197-203.

Pastor, M. D., Lorda, G. S. & Balatti, A. (2001). Proteases production using *Bacillus subtilis*-3411 and amaranth seed meal medium at different aeration rate.Brazilian J. Microbiol., 32: 6-9.

Rao, M.B., A.M. Tanksale, M.S. Ghatge, & Deshpande, V.V. (1998). Molecular and biotechnological aspects of microbial proteases. Micro biol. Mol.Biol.Rev. 62: 597-635.

Singh, J., Vohra, R.M. & Sahoo, B.K.(2001). Purification and characterization of two extracellular alkaline protease from a newly isolated obligate alkaliphilic *Bacillus sphaericus.* J. Ind. Microbiol. Biotechnol. 26: 387 - 393.

Sudha, J., Ramakrishnan, V., Madhusudhanan, N., AsitBaranMandal& Gurunathan, T.(2010). Studies on industrially significant haloalkaline protease from *bacillus sp*. Jsgt isolated from decaying skin of tannery. Adv. Lab. Res. Biol. 1(1): 60-67.

Takami, H., Akiba, T.& Horikoshi, K. (1989). Production of extremely thermo stable alkaline protease from *Bacillus* sp. no. AH 101. Appl. Microbiol. Biotechnol, 30: 120-124.

Thangam, E. B., Nagarajan, T., Suseela, R. G.& Chandrababu, N. K. (2001). Application of alkaline protease isolated from *Alcaligenesfaecalis* for enzymatic un-hairing in tanneries. J. Ind. Leather.37: 215-222.

Thangam, E.B. & Rajkumar, G.S.(2002). Purification and characterization of alkaline protease from *Alcaligenesfaecalis*. Biotechnol. Appl. Biochem. 35: 149-154.

Wang, H. Y., Liu, D. M., Liu Y., Cheng, C. F., Ma, Q. Y., Huang, Q. &Zhang, Y. Z.(2007). Screening and mutagenesis of a novel *Bacillus pumilus* strain producing alkaline protease for dehairing. Letters in Appl. Microbiol. 44: 1-6.

Yu, Z., Wei, Z., Jian, N., Ting-Ting, X., Ling, W., Lu-E, S.& Zhen-Xing, T.(2017). Evaluation of partial characteristics of the strain *Enterococcus faecalis* P3 isolated from peacock feces*in vitro, Kuwait J. Sci.* 44 (1) pp. 91-98.

Submitted: 28/06/2021
Revised: 03/01/2022
Accepted: 07/01/2022
DOI: 10.48129/kjs.14053